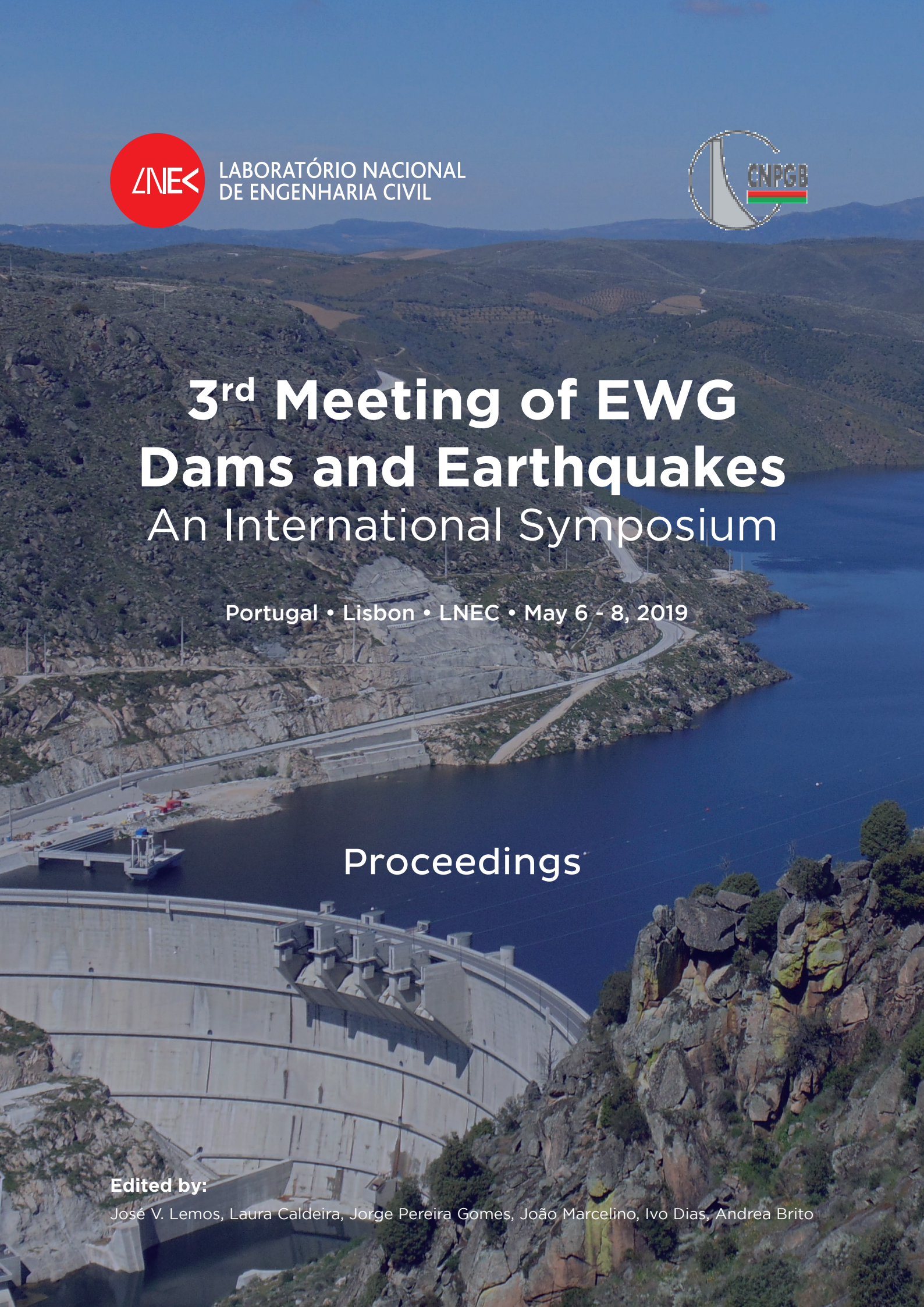

LABORATÓRIO NACIONAL
DE ENGENHARIA CIVIL

CNPGB

3rd Meeting of EWG Dams and Earthquakes

An International Symposium

Portugal • Lisbon • LNEC • May 6 - 8, 2019

Proceedings

Edited by:

José V. Lemos, Laura Caldeira, Jorge Pereira Gomes, João Marcelino, Ivo Dias, Andrea Brito

LABORATÓRIO NACIONAL
DE ENGENHARIA CIVIL

3rd Meeting of EWG Dams and Earthquakes

An International Symposium

Portugal • Lisbon • LNEC • May 6 - 8, 2019

Proceedings

Edited by:

José V. Lemos, Laura Caldeira, Jorge Pereira Gomes, João Marcelino, Ivo Dias, Andrea Brito

Divisão de Divulgação Científica e Técnica
AV DO BRASIL 101 • 1700-066 LISBOA
e-e: livraria@lnec.pt
www.lnec.pt

Publisher: LNEC

Collection: National and international meetings

Série: RNI 105

1st. edition: 2019 (pdf)

Descriptors: Seismic response of structures / Concrete dams / Embankment dams / Monitoring / Dams safety / / International congress

Descritores: Solicitação sísmica de estruturas / Barragens de betão / Barragens de aterro / Monitorização / Segurança de barragens / Congresso internacional

CDU 627.82.042.7(063)(100)
ISBN 978-972-49-2308-6

Preface

The 3rd meeting of the ICOLD European Club Working Group "Dams and Earthquakes" took place at LNEC, Lisbon, Portugal, on 6-8 May 2019. Following the very successful events in St. Malo and Rome, this meeting brought together a group of international experts to discuss the multiple challenges that earthquakes pose to dams. Recent advances on dynamic monitoring techniques coupled with new developments in material and structural modelling are making available to engineers powerful tools that need to be tested, validated and widely disseminated. The digital proceedings contain a collection of papers that reflect the state-of-the-art on the analysis and safety assessment of concrete and embankment dams under seismic actions. We would like to acknowledge our appreciation to the authors for their effort in preparing these contributions and their willingness to share their research accomplishments. We would also like to express our gratitude to the members of the Scientific Committee who reviewed these papers.

The Organizing Committee

Themes

- Definition of seismic hazard for dams
- Measurements of response of concrete or embankment dams under earthquakes
- Dynamic monitoring and testing of dams
- Comparison of numerical models with dynamic field measurements
- Qualification of equipment under seismic loading

Organizing Committee

José V. Lemos
Laura Caldeira
Jorge Pereira Gomes
João Marcelino
Ivo Dias
Andrea Brito

Scientific Committee

Jean-Jacques Fry (EWG Dams & Earthquakes, Chairman)
José Rocha Afonso (CNPGB, Portugal)
Carlos Pina (CNPGB, Portugal)
Bernard Tardieu (CFBR, France)
Giovanni Ruggeri (ITCOLD, Italy)
Ignacio Escuder (SPANCOLD, Spain)
Martin Wieland (ICOLD, Switzerland)
Norihisa Matsumoto (JCOLD, Japan)
Pierre Léger (E.P. Montréal, Canada)
D. Silva Matos (EDP, Portugal)
A.L. Batista, J. Bilé Serra, Telmo Jeremias, A. Campos Costa (LNEC, Portugal)

Index

KEYNOTE LECTURES

SEISMIC ACTION

CONCRETE DAMS

EMBANKMENT DAMS

Earthquakes records on concrete dams: benefits, difficulties and proposal of an international database

Emmanuel Robbe

EDF CIH Le Bourget du Lac 73 373 Cedex, France
E-mail: emmanuel.robbe@edf.fr

Keywords: Dams; Concrete; Seismic hazard; Dynamic monitoring

Abstract. *In the same way as the monitoring of dams under static loads allows engineers to build and calibrate numerical models that offer a better understanding of the static behavior of dams and assess their safety, earthquake recordings on dams are highly valuable for understanding their dynamic behavior.*
In 2013, the French committee on large dams (CFBR) started collaborating with the Japanese committee (JCOLD) about seismic analyses on dams. During these exchanges, JCOLD provided 602 sets of records on 257 dams, including 135 concrete gravity dams and 22 concrete arch dams. The keynote lecture will highlight analyses of these records for evaluating the dynamic properties of the structure and for assessing and improving finite element analysis methods for the seismic assessment of concrete dams. The benefits and difficulties of the use of earthquake records for such purposed will be discussed.
Outside of Japan, an increasing number of recordings of the behavior of dams under earthquake are available, but they remain rare and isolated and are generally not shared with the community. Analyses of such recordings can also be particularly time-consuming for engineers not always specialized in this field and require specific post-processing tools. This keynote lecture will be an opportunity to introduce the DamQuake project. The aim of DamQuake is to create an international database of earthquake recordings on dams. The database's user interface will allow easy navigation through the data and the possibility of performing specific analyses to better evaluate a dam's response under earthquake. Such analyses can be particularly useful for comparing several dams' responses or the responses of a single dam under several earthquakes. Evaluation and improvement of safety assessment methods might also be facilitated in the process.

Seismic response of earthfill and rockfill embankment dams

Stavroula Kontoe[1], Bo Han[2], Loizos Pelecanos[3] & Lidija Zdravković[1]

Imperial College London
South Kensington Campus, London, UK
E-mail: stavroula.kontoe@imperial.ac.uk

Keywords: embankment dams; numerical modelling; nonlinear analysis

Abstract. *The seismic design of earthfill and rockfill dams routinely relies on methods of analysis, which adopt simplifying assumptions regarding the dam geometry, soil behaviour and the dynamic interaction of the fluid and solid phases within the dam body. This paper explores such simplifying assumptions, which are typically used for the numerical modelling of earthfill and rockfill embankment dams, within the context of two case studies. First a clay core dam, the La Villita dam in Mexico, is considered focusing mainly on the implications of 2D plane strain approximation in the case of dams built in relatively narrow canyons. In the second case study, of the rockfill Yele dam in China, the importance of hydro-mechanical coupling is explored by parametrically varying the permeability of the materials.*

1. INTRODUCTION

The seismic response of earthfill and rockfill dams has been extensively studied over the years with several well-established methods of analysis, such as the pseudo-static, the shear beam and the dynamic finite element (FE) methods. Significant progress has been made in FE modelling; the use of advanced constitutive models has allowed for accurate modelling of the deformation characteristics of embankment dams under seismic excitations for two-dimensional (2D) plane strain conditions (e.g. Rampello et al. 2009, Elia et al. 2010, Pelecanos et al. 2015). However, the rigorous simulation of the nonlinear soil response through the use of advanced constitutive models, increases the computational cost and as a result three-dimensional models are not commonly used.

Apart from the constitutive models, realistic predictions of the dynamic response of dams also require the appropriate treatment of other aspects of the computational model, such as time integration (Kontoe et al 2008), boundary conditions (Kontoe et al 2009) and hydro-mechanical (HM) coupling between the fluid and the solid phases (Han et al 2016). The latter is required to compute the development and dissipation of pore water pressures, and account for their impact on the response of earth and rockfill dams (e.g. Lacy and Prevost, 1987; Elia et al., 2011, Pelecanos et al 2015, Han et al 2016). The adoption of a HM coupled formulation is usually more critical for the accurate simulation of the dynamic behaviour of rockfill materials due to their large permeability. In rockfill dams, depending on the range of permeability and loading duration, consolidation can occur during the dynamic loading and therefore the response cannot be considered as drained or undrained. Given the complexity of

[2] Formerly Imperial College London, Shandong University, bo.han@sdu.edu.cn
[3] Formerly Imperial College London, University of Bath, L.Pelecanos@bath.ac.uk

the numerical modelling of embankment dams, there is a need for well-documented case studies to properly validate the assumptions and processes involved in dynamic FE analysis.

This paper explores several issues related to the numerical modelling of earthfill and rockfill embankment dams within the context of two case studies. First a clay core dam, the La Villita dam in Mexico, is considered focusing mainly on the implications of 2D plane strain approximation in the case of dams built in relatively narrow canyons. In the second case study, of the rockfill Yele dam in China, the importance of HM coupling is explored by parametrically varying the permeability of the materials.

2. CASE HISTORY 1: LA VILLITA DAM, MEXICO

2.1 Description of the dam

La Villita is a 60m high zoned earth dam built in Mexico, with a crest about 420m long, founded on a 70m thick alluvium layer. The dam cross-section is composed of a central clay core of very low permeability, with sand filters and rockfill shells. Alluvial deposits beneath the clay core were grouted below the dam, while a concrete cut-off wall controls seepage through the alluvium below the dam. Figure 1 (a) shows a schematic representation of the transverse cross section of the dam, whereas part (b) shows a longitudinal section.

A summary of the adopted material properties is given in Table 1, based on the investigation of Elgamal (1992). The maximum shear stiffness, G_{max}, for all the materials in the dam embankment varies in the range of 140-260 MPa from top to bottom, whereas the foundation alluvium was assumed to have a constant value of 200 MPa.

The dam was built in 1967, the reservoir was impounded over a 6-month period in 1969 and it operated safely until the major seismic event in 1975. It experienced six major seismic events during the period between 1975 and 1985, which resulted in some permanent deformations. The earthquake motions were recorded by three accelerometers, installed at the crest (shown as C in Figure 1), at the downstream berm, i.e. the small embankment on the downstream side of the dam (shown as B in Figure 1) and at the right rock bank (shown as R in Figure 1). However due to instrument malfunction only two seismic records (denoted herein as EQ2 and EQ5, see Table 2) are of sufficient quality to be useful for numerical analysis (Elgamal 1992), (see Pelecanos et al 2015 for more details on the instrumentation).

Table 1: Summary of material properties of La Villita dam

No	Material	Mass density ρ (kg/m^3)	Poisson ratio ν	Cohesion c′ (kPa)	Angle of shearing resistance φ'(deg)	Angle of dilation ψ (deg)
1	Clay core	2000	0.49	5	25	0
2	Sand filters	2180	0.33	0	35	0
3	Inner rockfill	2080	0.33	5	45	0
4	Outer rockfill	2080	0.33	5	45	0
5	Alluvium	2080	0.33	5	35	0

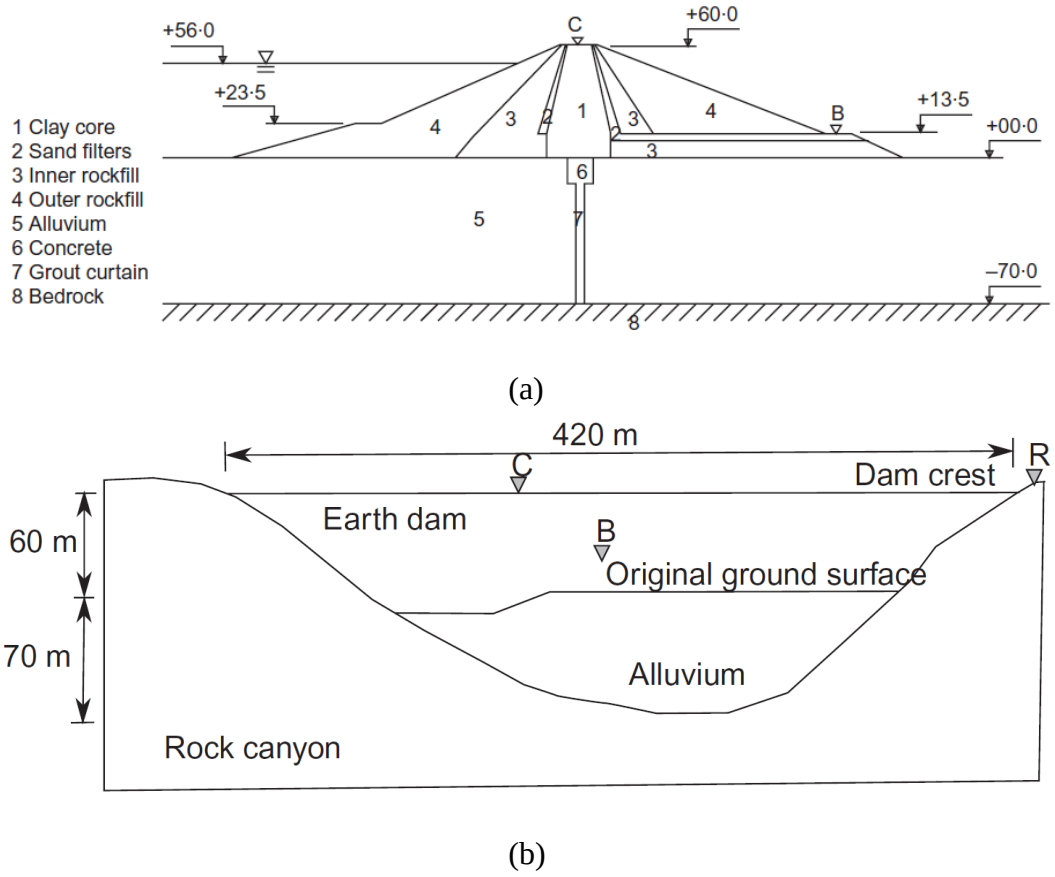

Figure 1: Geometry of La Villita dam in Mexico (not to scale): (a) cross-sectional view, (b) longitudinal view.

Despite the intense seismic activity during the period 1975-1985, the dam performed well without any major damage. The seismic events resulted in some permanent displacements which were recorded at various locations on the dam body, but which did not disrupt its operation (Elgamal 1992). Due to the scarcity of dam case studies with publically available recorded seismic motions, this dam has been extensively investigated with a variety of numerical models, with studies focusing on simulating the recorded acceleration response (Elgamal 1992, Pelecanos 2013, Pelecanos et al. 2015), on the recorded permanent displacements (Elgamal et al. 1990, Succarieh et al 1993, Gazetas & Uddin 1994), on dam-canyon interaction (Papalou & Bielak, 2001; 2004) and on dam-reservoir interaction (Pelecanos et al 2018).

Table 2: Seismic events considered for the analysis of La Villita dam

No	Date	Ms	Epicentral distance	Max Rock acc. (g)	Max Berm acc. (g)	Max Crest acc. (g)
EQ2	15/11/1975	5.9	10	0.04	0.08	0.21
EQ5	19/09/1985	8.1	58	0.12	-	0.76

2.2 Numerical model

All the analyses presented in this study were carried out in plane-strain conditions, in the time domain, using the bespoke FE code ICFEP (Imperial College Finite Element Program) (Potts & Zdravković 1999). It should be noted that the full description of the numerical model of La Villita can be found in Pelecanos et al (2015) and only its main features are summarised herein. The time-integration scheme employed was the Generalised-alpha method of Chung and Hulbert (1993) which is able to optimise the induced numerical damping to selectively

filter high frequencies (here, the spectral radius at infinity used, ρ_∞= 9/11, see Kontoe et al. 2008). For all sets of analyses the dynamic hydro-mechanically coupled (u-p) formulation of ICFEP was used for the clay core and the alluvium foundation layer, with permeability values of 10^{-10} m/s and 10^{-7} m/s respectively. The remaining materials were assumed to behave in a drained manner. The reservoir domain was not modelled explicitly and hence the impact of hydrodynamic pressures was neglected. Pelecanos et al (2013) found the impact of hydrodynamic pressures to be minor on the overall acceleration response for earthfill dams. Pelecanos et al (2018) though recognised that the hydrodynamic pressures can lead to stress concentration on the upstream face of the dam and thus to potentially larger localised plastic deformations.

Prior to the dynamic analysis the full stress history of the dam (including layered embankment construction, reservoir impoundment and consolidation) was simulated in all considered cases. The static model was able to predict very well the recorded settlements (see Pelecanos et al 2015) and to therefore establish a realistic in-situ stress distribution for the subsequent time-domain dynamic analyses. The employed constitutive model was a cyclic nonlinear-elastic (CNL) model, which adopts a logarithmic function to describe the backbone curve (Puzrin & Burland, 2000; Taborda, 2011), coupled with a Mohr-Coulomb plastic model. The logarithmic relation dictates the degradation of shear stiffness, G, and the increase of damping, ξ, with cyclic shear strain, γ. Due to the lack of experimental data, the CNL is calibrated against empirical relations (Vucetic & Dobry, 1991; Seed, et al., 1986; Rollins, et al., 1998). The constitutive equations, parameters, associated calibration, boundary conditions and other FE model details are described in detail by Pelecanos et al. (2015) and therefore, for brevity, are not repeated herein. The acceleration motions EQ2 and EQ5 (see Table 2) recorded at the rock abutment were used as the input excitation at the base of the alluvium layer.

2.3 Effect of canyon geometry

Figure 2 compares the computed response spectra with the recorded data for both considered seismic excitations (i.e. EQ2 and EQ5) at the crest of the dam (point C in Figure 1). For EQ2 the predicted response is significantly smaller than the recorded one for the entire period range, while for EQ5 the spectral accelerations are smaller than the recorded ones in the small period range, T<1.3s with the trend reversing for T>1.3s. This comparison implies that the computed response of the dam is softer than the recorded one.

It is long known (Ambraseys, 1960; Dakoulas & Gazetas, 1987) that dams built in narrow canyons exhibit a stiffer response than dams built in wide canyons. In this case, La Villita, is a 60m high dam founded on a 70m alluvial deposit and its crest length is about 420m. Therefore, the canyon length over height, L/H ratio is equal to 420/(60+70) = 3.2. Based on this, canyon effects could be significant and a 2D analysis would be inappropriate as the real problem is stiffer than the corresponding 2D plane strain model. Such a 2D analysis would be suitable for a wide canyon (L/H > 4) (Ambraseys, 1960). In order to overcome this soft response of a 2D analysis, the stiffening effect of the canyon geometry is taken into account by increasing the material stiffness of the dam. A parametric study was carried out to determine the ratio of the new updated shear stiffness over the initial stiffness, which would provide the best match between the calculated and recorded response spectra. It was found that the shape of the response spectrum (and therefore the fundamental period of the dam) is improved if the shear modulus, $G_{max}(z)$ is increased by 3.5 times. Therefore, the updated value of the maximum shear stiffness, G^*_{max} for all the materials in the dam embankment is 490-910 MPa, and 700 MPa for the alluvium. Because the calibration of the CNL model depends on the value of G^*_{max}, a new calibration was carried out for the updated stiffness values.

Figure 3 plots the response spectra at the crest of the dam computed with the revised shear stiffness showing a much better agreement with recorded response. The use of an

increased material stiffness appears to be effective as a simplified way to account for the stiffening effect of a narrow canyon. Dakoulas & Gazetas (1987) showed that the ratio of the fundamental period of vibration of a dam built in a narrow canyon, T_n, over that of a dam built in an infinitely wide canyon, T_w, for a L/H = 3.2 and for various shapes of the canyon ranges, T_n/T_w = 0.6 ~ 0.75. In the present study, the updated value of the shear modulus is taken as G^*_{max}= 3.5 G_{max} which leads to a T*=0.54T. The ratio of 0.54 is reasonably close to the range suggested by Dakoulas & Gazetas (1987) for various canyon shapes, considering the differences in the adopted assumptions (idealised geometry of earth dam and canyon geometries, and linear soil material behaviour in Dakoulas & Gazetas 1987). The small discrepancy could be also attributed to the uncertainty associated with the original material properties that were based on the literature (Elgamal, 1992).

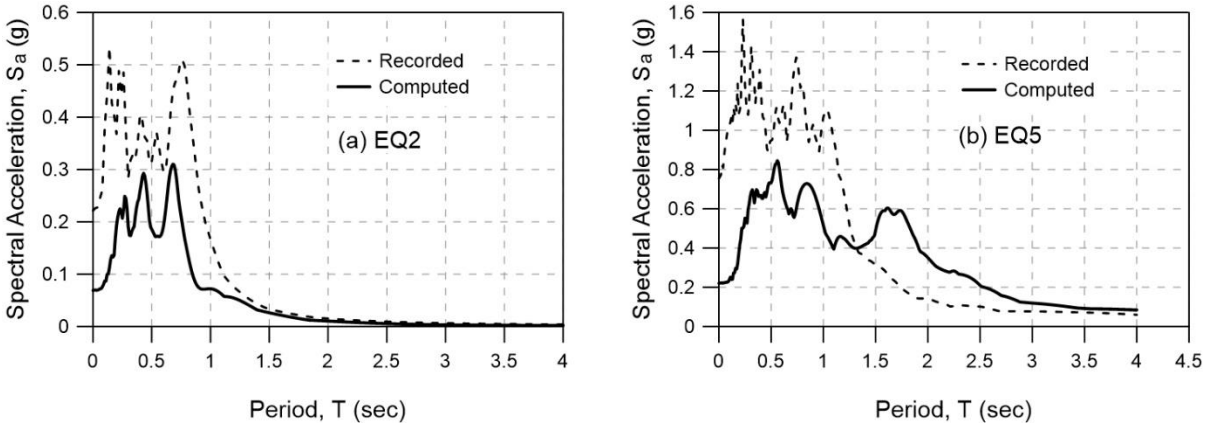

Figure 2: Comparison of computed acceleration response spectra (ξ=5%) and recorded data at the crest of the dam for (a) EQ2 and (b) EQ5.

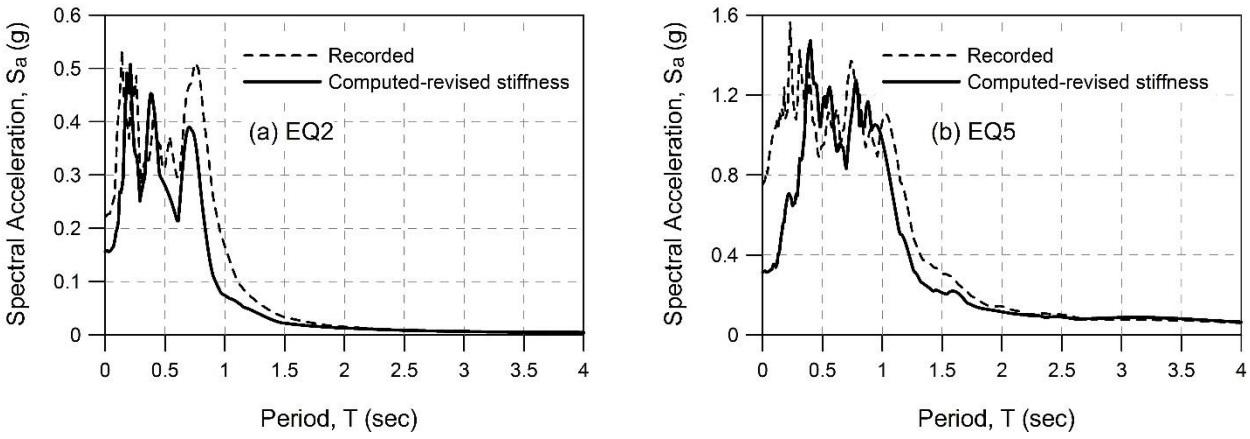

Figure 3: Comparison of computed acceleration response spectra (ξ=5%) with revised stiffness properties and recorded data at the crest of the dam for (a) EQ2 and (b) EQ5

2.4 Asymmetry in the acceleration response

The comparison of the numerical prediction with the field response for EQ5 is overall satisfactory (see Figure 3b), but it does reveal a high frequency (low period) part of the motion which is not captured by the numerical analysis. The recorded high acceleration values in the high frequency range are believed to originate from notable asymmetric peak values in the recorded ground motion at the crest of the dam for EQ5 (shown in Figure 4b). It is interesting

to note that the acceleration response at the rock abutment (Figure 4a), which was used as the input motion, is symmetric and that the asymmetry is only observed in the crest response.

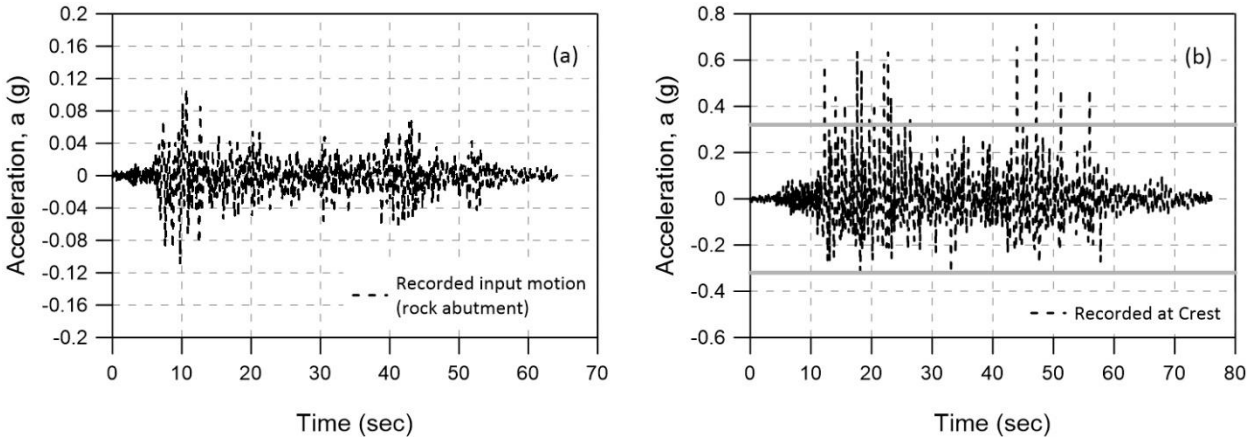

Figure 4: Acceleration time history for EQ5 recorded at (a) rock abutment and (b) dam crest.

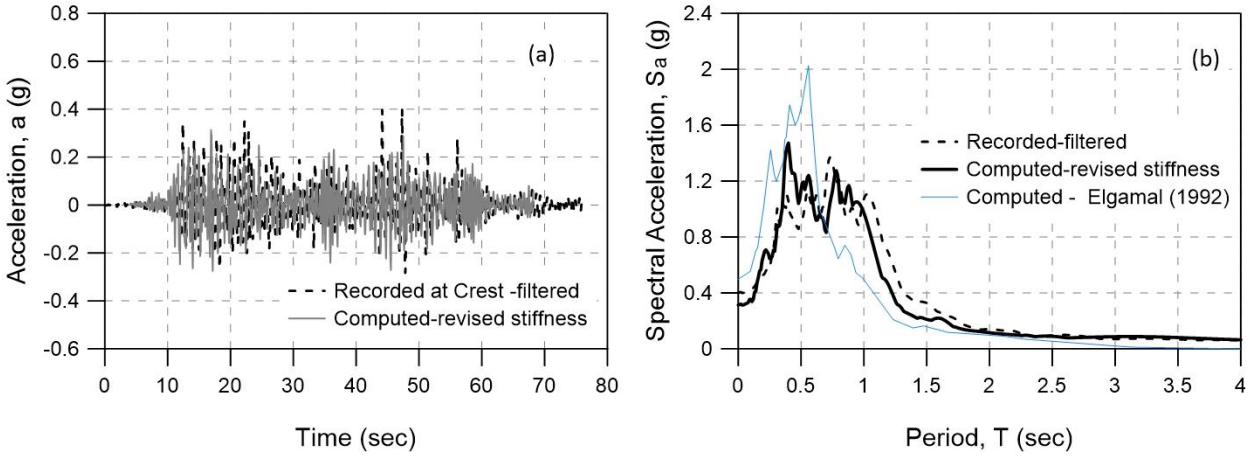

Figure 5: Comparison of computed response with filtered recorded data for EQ5 in terms of (a) acceleration time history and (b) response spectra (ξ=5%).

This asymmetry in the crest record is believed to be due to a localised slope failure, as suggested by previous researchers, which was not predicted by the FE analysis in this study. The work of Gazetas & Uddin (1994), which included interface elements to model a small zone of localised weakness, has shown some acceleration asymmetry and indicated that a localised discontinuity existed in the upstream dam rockfill. The present model does not include any pre-defined weak zones, as this aspect was addressed in the work of Gazetas & Uddin (1994), and attempts a more direct prediction of the response. If the high frequencies are filtered from the recorded accelerations at the crest, a better agreement is obtained between the recorded and the calculated response. Indeed, Figure 5a shows a comparison between the filtered recorded accelerations at the crest for EQ5 and those calculated in this work, whereas Figure 5b shows the associated response spectra. The filtering was performed using SeismoSignal (Antoniou & Pinho, 2004), adopting a 4th order Bandpass Butterworth filter for frequencies higher than 4 Hz (i.e. periods smaller than 0.25s). The frequency for the filtering was obtained after a parametric study and was taken as the value for which the high values of peak acceleration (due to the localised slip failure) vanish, rendering the record symmetric and consequently representative of the overall dynamic behaviour of the dam structure. The

filtering does not eliminate the predominant frequency of the input motion which is around 1.8Hz. The reason behind the filtering is that by eliminating the high values of peak accelerations (due to the localised slip) the remaining record shows the dynamic behaviour of the dam and this is used to check whether the vibration characteristics (e.g. fundamental period of vibration) have been predicted well by the adopted model. Moreover, the EQ5 response spectrum of the crest response predicted by Elgamal (1992) is included in Figure 5b for comparison. It is evident that the computed response in this work is in better agreement with the recorded one than the response calculated by Elgamal (1992). The response spectrum of Elgamal (1992), obtained from a 3D shear beam analysis has a narrower frequency content and higher amplifications at the significant frequencies, whereas the broader frequency content of the spectrum from the present study matches better the low frequency spectral ordinates.

3. CASE HISTORY 2: YELE DAM, CHINA

3.1 Description of the dam

The Yele dam is an asphaltic concrete core rockfill dam located at the Nanya River in Sichuan Province, China. The dam body consists of several filling zones, i.e. an asphaltic concrete core, transition layer, filter layer, coffer dam, cap dam and rockfill zone, as shown in Figure 6. The dam foundation consists of an alluvium layer of varying thickness, of mainly gravelly and silty soils, with an average depth of approximately 53m. The filter and transition layers of the dam are composed of fine sands to discharge seeping water and to accommodate any differential deformations between the core and the outer rockfill (Xiong 2009). The soil properties of all dam materials are summarised in Table 3 (He et al., 2006), obtained from in-situ and laboratory tests.

Table 3: Summary of material properties of Yele dam

Material	Mass density ρ (kg/m^3)	Shear wave velocity, Vs (m/s)	Cohesion c′ (kPa)	Angle of shearing resistance φ′(deg)	Permeability, k (m/s)
Foundation layer	2300	800	80	38	1.0E-8
Core	2400				
Grouting curtain	2400				
Transition layer	2300	224	0	45	1.0E-5
Filter layer	2300	224	0	45	1.0E-5
Rockfill	2300	365	0	50	1.08E-3
Coffer dam	2300	365	0	50	1.08E-3
Cap dam	2300	365	0	50	1.08E-3

The construction of the dam started in October 2003 and was completed in November 2005, reaching a height of 124.5m. The reservoir impounding started in January of 2005, while the dam was still under construction and had reached a height of 75m, and the power plant started to generate electricity in November 2005 (He et al. 2006). On the 12th of May 2008, the Wenchuan earthquake (Ms=8.0) struck west China, damaging approximately 391 dams at a varying degree, including 4 large-scale ones (heights exceeding 100m) (Xu, 2009). Among all these dams, only the seismic monitoring equipment of the Yele dam (258km from the epicentre) was in good working order. Eight seismometers recorded the multi-directional

ground motion at different locations on the dam, providing valuable monitoring data for a detailed investigation of its seismic response. The dam performed well during the strong motion, sustaining only some minor damage which did not disrupt the normal operation of the power plant (Cao et al 2010). Before the occurrence of the Wenchuan earthquake, the reservoir level was at its minimum (at 75m) due to a dry season and this might have contributed to its satisfactory performance.

3.2 Numerical model

A two-dimensional plane strain model of the Yele dam was analysed with the FE code ICFEP (Potts & Zdravković 1999) under static (to simulate the construction sequence and operation prior to the earthquake) and bi-directional dynamic conditions. A hydro-mechanically coupled (u-p) formulation was used for all the materials, employing the permeability values reported in Table 3. The adopted numerical model is discussed in detail in Han et al. (2016) and only a brief summary of its main features is included herein.

For the static and dynamic analyses of the Yele dam, a cyclic nonlinear model, i.e. the Imperial College Generalised Small Strain Stiffness model (ICG3S model, Taborda & Zdravković (2012); Taborda et al. (2016)) coupled with a Mohr-Coulomb failure criterion was employed to simulate the elasto-plastic soil behaviour of the dam and foundation materials. This model is based on the hyperbolic model by Kondner and Zelasko (1963) and the modified hyperbolic model by Matasovic and Vucetic (1993), but it involves additional rules to account for important aspects of soil behaviour, such as the independent simulation of shear and volumetric deformation mechanisms, spatial variation of soil stiffness and simulation of material damping at very small strain levels. The independent simulation of shear and volumetric deformation is very important for the undertaken bi-directional analyses which consider both the horizontal and the vertical component of the ground motion, with the latter imposing significant compressional loading. It should be noted that the asphalt concrete core and the grouting curtain are assumed to behave as linear elastic materials due to their large stiffness.

The ICG3S model was calibrated against site-specific shear modulus degradation and damping curves for the rockfill material, which were derived from laboratory cyclic triaxial tests, detailed in Xiong (2009) (Figure 7). As there was no site-specific information available for the remaining materials and the rockfill was sourced and processed near the dam site, it was assumed that the foundation materials are characterized by the same stiffness degradation and damping curves. Furthermore, due to the lack of laboratory data for the constrained modulus degradation and damping curves, identical model parameters are employed for the calibration related to the compressional deformation. The only exception was made for the constitutive parameter which controls the constrained modulus degradation. Based on the findings of Han (2014) and Han et al. (2016b) from back-analysis of downhole array seismic data, the constrained modulus has a wider linear plateau but its degradation appears to be slightly steeper afterward, than that of the shear modulus.

The constitutive equations, parameters, associated calibration, boundary conditions and other FE model details are described in Han et al. (2016) and therefore, for brevity, are not repeated herein. From the eight installed seismometers usable monitored data were obtained from 3 seismometers; one at the crest, a second at the base of the downstream slope at the maximum transverse section and a third in the grouting gallery at the left bank. It should be noted that the grouting gallery was constructed just above the bedrock at the left bank and therefore the data monitored by this seismometer can be considered as the bedrock motion. Both the EW and the vertical (UD) components of the bedrock were applied uniformly at the base of the mesh, as indicated in Figure 6, while the available ground motion data are summarised in Table 4.

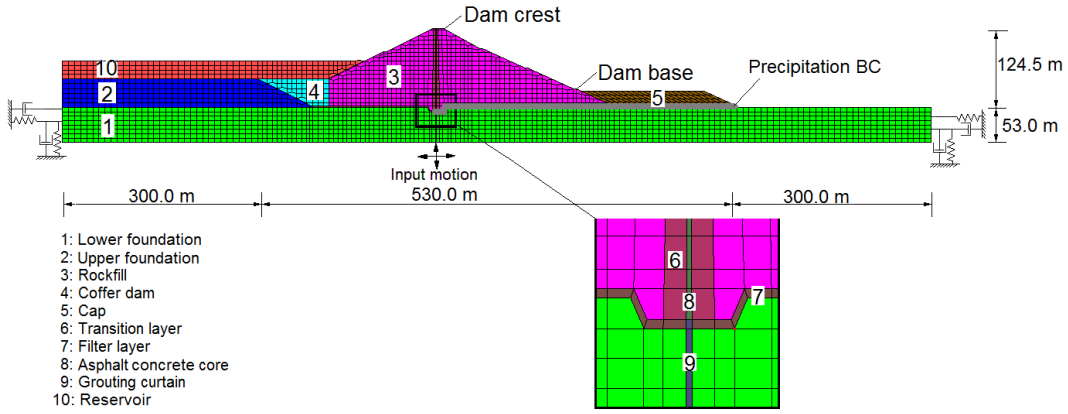

Figure 6: FE mesh and boundary conditions for the dynamic analysis of the Yele dam.

Table 4: Summary of the ground motion data

Monitoring positions	EW direction			UD direction		
	Bedrock	Base	Crest	Bedrock	Base	Crest
PGA (g)	0.007	0.035	0.044	0.012	0.020	0.032
Amplification factor	0.102	0.499	0.622	0.102	0.173	0.275
Predominant frequency (Hz)	0.348	0.355	0.260	0.510	0.319	0.340
Fundamental frequency (Hz)	$f_{crest/bedrock}$= 2.48 $f_{crest/base}$= 1.64			$f_{crest/bedrock}$= 3.45 $f_{crest/base}$= 3.31		

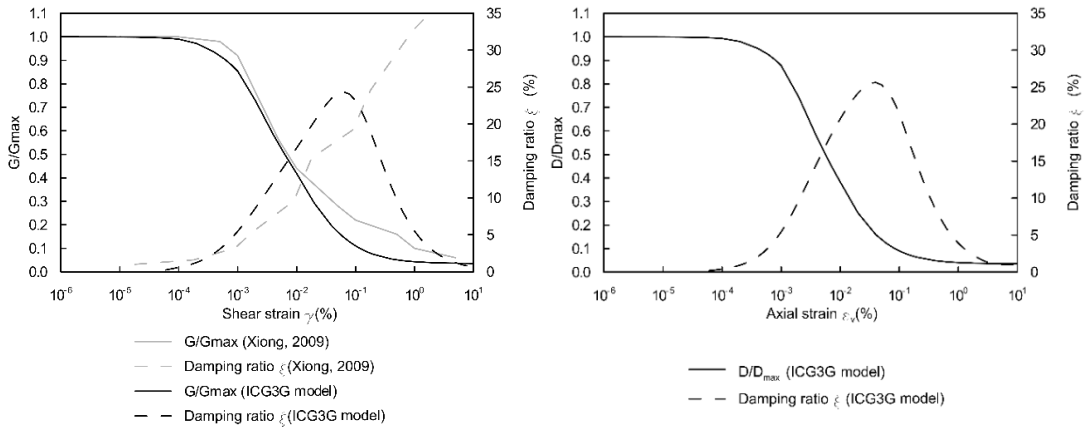

(a): Shear modulus degradation and damping curves

(b): Constrained modulus degradation and damping curves

Figure 7: Calibration of the ICG3S model for the Yele dam materials.

3.3 Bi-directional seismic response of Yele dam

The computed seismic response of the Yele dam is compared with the recorded data in both directions in Figures 8 and 9 for the crest and the base of the dam respectively, showing overall good agreement. The predicted horizontal and vertical response spectra at the dam crest and dam base match well with the monitored response both in terms of frequency content and amplitude. A small overestimation of the vertical response at the dam base is observed, which

is probably due to the low damping assumed for compressional deformation in the small strain range (see Figure 7b).

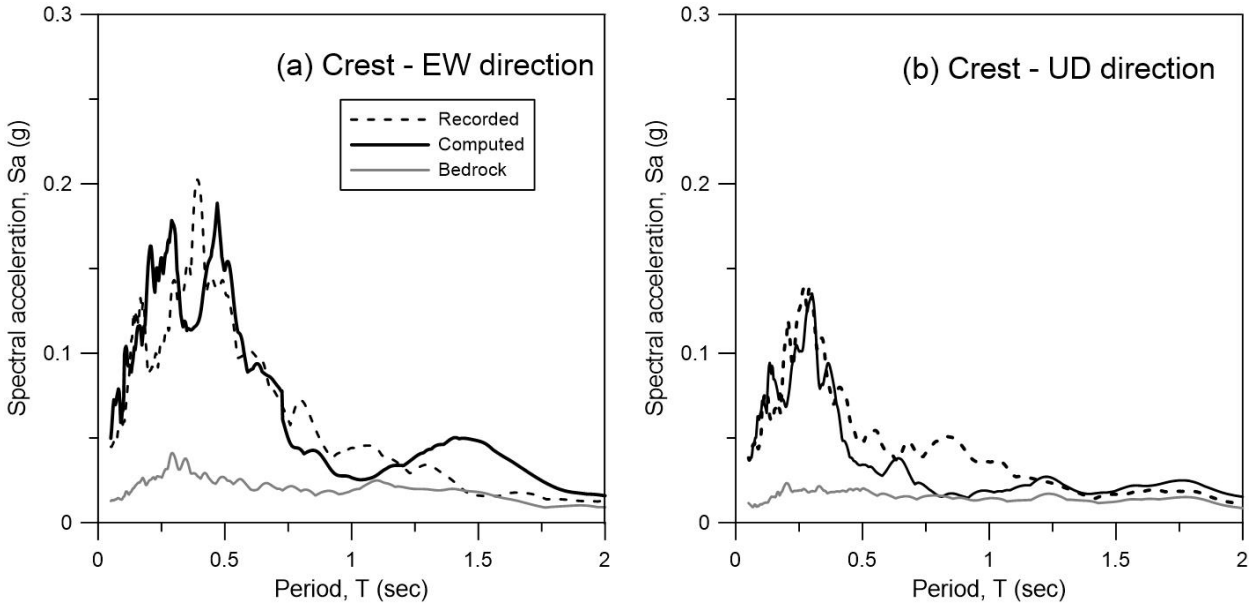

Figure 8: Acceleration response spectra (ξ=5%) of motions recorded or computed at the crest of the dam (a) EW direction (b) UD (vertical) direction.

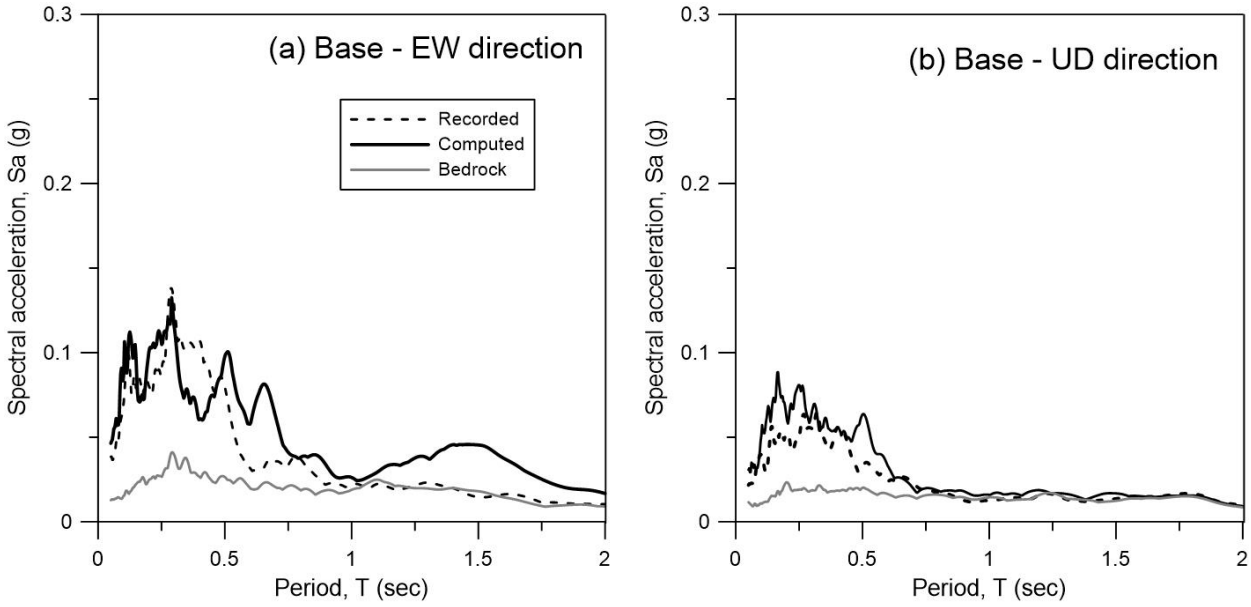

Figure 9: Acceleration response spectra (ξ=5%) of motions recorded or computed at the base of the dam (a) EW direction (b) UD (vertical) direction.

The impact of hydromechanical coupling was also examined by varying the permeability of the dam materials. The reference analysis (which adopted the properties listed in Table 3 was repeated adopting a very low permeability, k=1.0E-8 m/s, which is essentially equivalent to performing an undrained analysis. The comparison of the response spectra at the crest of Figure 10 shows that the permeability significantly affects the numerical predictions in both directions, as the low permeability analysis (k=1.0E-8 m/s) overestimates the response. This is more pronounced in the vertical (UD) direction which can be attributed to the influence of the fluid-induced viscous damping, discussed in Han et al. (2017) and Han et al. (2018). In particular, for low permeability soils subjected to vertical motions, lower or no viscous

damping is introduced as there is very little or no interaction between the solid and pore fluid phases, leading to larger vertical dynamic response. However, larger horizontal response is also predicted by the analysis employing the lower permeability values, which reflects the coupling effects between the responses in the two directions. Clearly the impact of the HM formulation on the seismic behaviour of dams depends on the permeability of the materials consisting the dam body. This impact is expected to be more significant for large permeability materials which are typically encountered in rockfill dams.

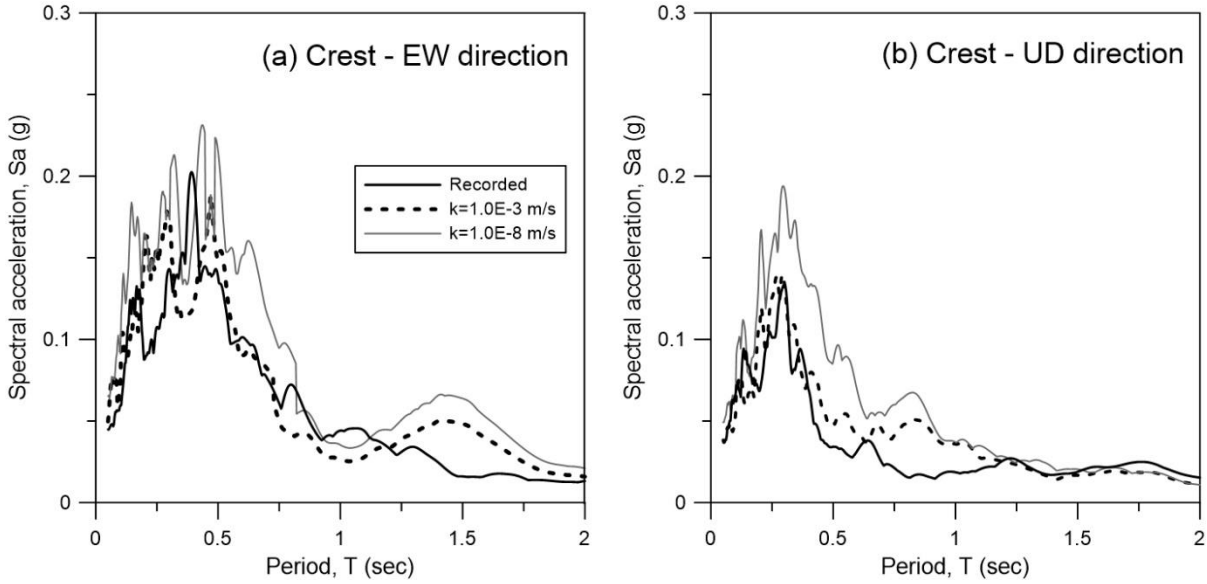

Figure 10: Impact of permeability on the computed acceleration response spectra (ξ=5%) of motions recorded at the crest of the dam (a) EW direction (b) UD (vertical) direction.

4. CONCLUSIONS

This paper explored issues related to the numerical modelling of earthfill and rockfill embankment dams within the context of two well-documented case studies. For the considered case studies there is available information relating to the dam geometry, material properties as well as field records of the dams' seismic response.

First, a clay core dam, La Villita dam in Mexico, was analysed under two seismic excitations of distinct intensity, considering nonlinear elasto-plastic soil behaviour. The developed numerical model was successful in (a) predicting the overall dynamic behaviour of the dam structure for two earthquakes of different magnitude, duration and frequency content; and (b) demonstrating (indirectly by careful filtering of the record) the validity of the assumption taken from the studies by previous researchers that the observed acceleration asymmetry and large displacements have likely resulted from localised failure near the measuring instrument. It is also shown that increasing the stiffness of the dam materials in a 2D analysis, using a carefully designed parametric study, is an acceptable approximate way to take account of the stiffening effect of the 3D canyon. The degree of stiffening agrees reasonably well with previous linear analytical solutions (Dakoulas & Gazetas, 1987) and therefore the developed numerical model may be considered as a further verification of these analytical solutions.

The second case study, considered the rockfill Yele dam in China which experienced the Ms=8.0 2008 Wenchuan earthquake. A good agreement was observed between the numerical results and the recorded ground motion at two points, at the dam crest and base, in terms of acceleration response spectra. The importance of HM coupling for the rigorous modelling of

rockfill dams was also investigated. The analysis with the assumption of undrained behaviour for all dam materials severely overestimated the response, particularly in the vertical direction, while the analysis with the more appropriate permeability values showed good agreement with the field measurements.

REFERENCES

[1] Ambraseys, N. N. (1960) On the shear response of a two-dimensional truncated wedge subjected to arbitrary disturbance. B. Seismol. Soc. Am., 50 (1), 45-56.

[2] Antoniou, S. & Pinho, R. (2004) SeismoSignal: A computer program for signal processing of strong-motion data. Technical Report 4.0.0, SeismoSoft.

[3] Cao, X., He, Y., Xiong, K. & Liu, B. (2010). The dynamic response of Yele dam under Wenchuan earth-quake (in Chinese). Rock & Soil Mechanics, 31(11) 3542-3548.

[4] Chung, J. & Hulbert, G. M. (1993). Time integration algorithm for structural dynamics with improved numerical dissipation: the generalized-α method. J. Appl. Mech., 60 (2) 371-375.

[5] Dakoulas, P. & Gazetas, G. (1987) Seismic lateral vibration of embankment dams in semi-cylindrical valleys. Earthq. Eng. Struct. D., 13(1) 19-40.

[6] Elgamal, A. W., 1992. Three-dimensional seismic analysis of La Villita dam. J. Geotech. Eng. -ASCE, 118(12) 1937-1958.

[7] Elgamal, A. W., Scott, R. F., Succarieh, M. F. & Yan, L. (1990). La Villita dam response during five earth-quakes including permanent deformations. J. Geotech. Eng.-ASCE, 116(10) 1443-1462.

[8] Elia, G., Amorosi, A., Chan, C. & Kavvadas, M. J. (2010), Fully coupled dynamic analysis of an earth dam, Géotechnique 61(7), 549–563.

[9] Gazetas, G. & Uddin, N. (1994), Permanent deformation on pre-existing sliding surfaces in dams, J. Geotech. Eng. 120(11), 2041–2061.

[10] Han B., Zdravković L., Kontoe S. & Taborda D.M.G. (2016) Numerical investigation of the response of the Yele rockfill dam during the 2008 Wenchuan Earthquake. Soil Dyn. Earthq. Eng., 88, 124-142

[11] Han B., Zdravković L., Kontoe S. and Taborda D.M.G. (2017). Numerical investigation of multi-directional site response based on KiK-net downhole array monitoring data. Comput. Geot., 89, 55-70.

[12] Han, B., Zdravković, L. and Kontoe, S. (2018) Analytical and numerical investigation of site response due to vertical ground motion Géotechnique, 68 (6) 467-480, doi: 10.1680/jgeot.15.P.191.

[13] He, S., Hu, Y. & Liu, J. (2006). The asphalt concrete core rockfill dam in Yele hydraulic project (in Chi-nese). Hydraulic stations design, 22(2), 46-53.

[14] Kondner, R. L. & Zelasko, J. S. (1963). A hyperbolic stress-strain formulation for sands. The Proceedings of the 2nd Pan American Conference on Soil Mechanics and Foundations Engineering, Brazil, 1: 289-324.

[15] Kontoe, S., Zdravković, L. & Potts, D. M (2008) An assessment of time integration schemes for dynamic geotechnical problems. Comput. Geot. 35 (2) 253-264.

[16] Kontoe, S., Zdravković, L., Potts. D. M. (2009) An assessment of the domain reduction method as an advanced boundary condition and some pitfalls in the use of conventional absorbing boundaries, Int. J. Num. Anal. Meth., 33, 309-330.

[17] Matasovic, N. & Vucetic, M. (1993). Cyclic characterization of liquefiable sands. J. Geotech. Eng.-ASCE, 119(11), 1805–22.

[18] Papalou, A. & Bielak, J. (2001). Seismic elastic response of earth dams with canyon interaction. J. Geotechn. Geoenviron., 127(5), 446-453.

[19] Papalou, A. & Bielak, J. (2004). Nonlinear seismic response of earth dams with canyon interaction. J. Geotech. Geoenviron., 130(1), 103-110.
[20] Pelecanos, L., 2013. Seismic response and analysis of earth dams, London, United Kingdom: PhD thesis, Imperial College London.
[21] Pelecanos, L., Kontoe, S. & Zdravković, L. (2013). Numerical modelling of hydrodynamic pressures on dams. Comput. Geot., 53, 68-82.
[22] Pelecanos, L., Kontoe, S. & Zdravković, L. (2015). A case study on the seismic performance of earth dams. Géotechnique, 65(11), 923-935.
[23] Pelecanos, L., Kontoe, S. & Zdravković, L. (2016). Dam-reservoir interaction effects in the elastic dynamic response of concrete and earth dams. Soil Dyn. Earthq. Eng. 82, 138-141.
[24] Pelecanos, L., Kontoe, S. & Zdravković, L. (2018). The Effects of Dam–Reservoir Interaction on the Nonlinear Seismic Response of Earth Dams. J. Earthq. Eng. doi: 10.1080/13632469.2018.1453409
[25] Potts, D. M. & Zdravković, L. (1999). Finite element analysis in geotechnical engineering: theory. London: Thomas Telford.
[26] Puzrin, A. M. & Burland, J. B. (2000). Kinematic hardening plasticity formulation of small strain behav-iour of soils. Int. J. Num. Anal. Meth., 24(9), 753-781.
[27] Rampello S., Cascone E. & Grosso N. (2009) Evaluation of the seismic response of a homogeneous earth dam, Soil Dyn. Earthq. Eng. 29, 782–798.
[28] Rollins, K., Evans, M., Diehl, N. & Daily, W. (1998). Shear modulus and damping relations for gravel. J, Geotech. Geoenviron. 124(5), 396-405.
[29] Seed, H. B., Wong, R. T., Idriss, I. M. & Tokimatsu, K. (1986). Moduli and damping factors for dynamic analyses of cohesionless soils. J. Geotech. Eng.-ASCE, 112(11), 1016-1032.
[30] Succarieh, M. F., Elgamal, A. W. & Yan, L. (1993). Observed and predicted earthquake response of La Villita Dam. Eng. Geol., 34(1-2), 11-26.
[31] Taborda, D. (2011). Development of constitutive models for application in soil dynamics, London, United Kingdom: PhD Thesis, Imperial College London.
[32] Taborda, D. M. G. & Zdravković, L. (2012). Application of a Hill-Climbing technique to the formulation of a new cyclic nonlinear elastic constitutive model. Comput. Geot., 43, 80-91.
[33] Taborda, D. M. G., Potts, D. M. & Zdravković L. (2016). On the assessment of energy dissipated through hysteresis in finite element analysis, Comput. Geot., 7, 180-194.
[34] Vucetic, M. & Dobry, R. (1991). Effects of soil plasticity on cyclic response. J. Geotech. Eng.-ASCE, 117(1), 87-107.
[35] Xiong, K. (2009). Seismic observations on Yele dam during the 2008 Wenchuan earthquake (in Chinese). Wuhan University. Government Report.
[36] Zienkiewicz, O. C., Clough, R. W. and B., S. H. (1986), Earthquake analysis procedures for dams - state of the art, Technical Report Bulletin 52, International Committee on Large Dams.

PSHA testing against historical seismicity across the border between France and Italy

Pierre Labbé[1], Umberto Sopranzi[2]

Ecole Spéciale des Travaux Publics
28, Avenue du Président Wilson, Cachan, France
pierre.labbe@estp.fr

Keywords: Seismic hazard map, PSHA testing, Historical seismicity, Fragility curves

Abstract. *In order to test PSHA outputs against historical seismicity data, the seismic risk is first introduced in terms of annual probabilities of occurrence of given damage degrees for vulnerability class B buildings (EMS98 scale). Then the risk is calculated by two methods. The first one considers historical earthquakes of epicentral Intensities I_0 = VI to IX, and statistics of affected areas. The second one is based on convolution of seismic hazard and fragility curves. Seismic hazard is described by the SHARE map, considered in the aimed area across the border between France and Italy. Fragility curves are described in the form of a log-normal distribution of the probability of exceedance of a given damage versus the PGA, according to the recent results of the SYNER-G European research program. The risk calculated on the basis of the SHARE map and fragility curves is tremendously higher, by a factor larger than 10, than the historically observed risk. Some tracks are discussed on the origin of this gap and on ways to bridge it.*

1 INTRODUCTION

Probabilistic seismic hazard assessment (PSHA) is a more and more popular technique for establishing hazard maps at the scale of a country or even at larger scale. In 2015, a seismic hazard map of Europe was proposed as an output of the European research program SHARE [1] [2] (Figure 1). The purpose of this paper is to discuss the consistency of the SHARE hazard map against historical seismicity, taking also into account the more recent developments on fragility curves resulting from the SYNER-G European research program [3]. This assessment is carried out on an about 95,660 km² area across the border between France and Italy presented in Figure 2, designated hereunder as the Region. The methodology applied in this paper was already applied and tested for the French Metropolitan Territory [4].

When testing PSHA outputs against historical seismicity, a general feature of those methods proposedin literature is that, at a given moment, it is necessary to translate macroseismic observations into accelerations (generally PGA). This is not the case for the method that we present in this paper, which is based on seismic risk assessment. The seismic risk is defined as the probability that a vulnerability class B building (representative of conventional masonry building) experiences a damage grade D according to the definitions of the European Macroseismic Scale (EMS98) [5]. Consistently with the seismic risk exposure in the Region, damage grades 2 to 4 (D=2, 3,4) are considered.

[2] Polytecnico di Milano, umberto.sopranzi@mail.polimi.it

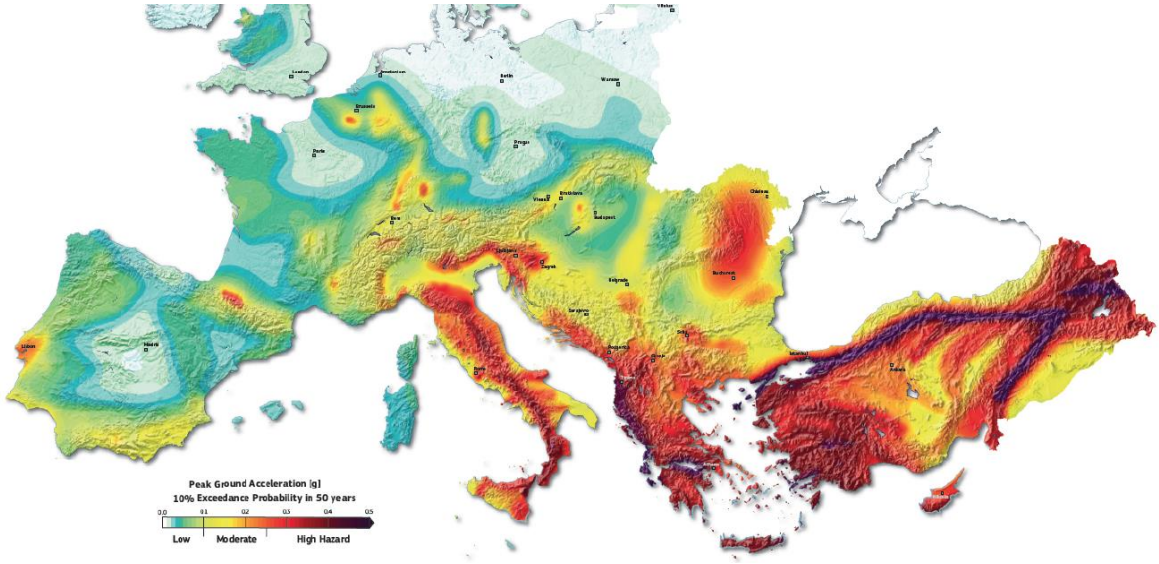

Figure 1: South part of the SHARE map

In this context, the core of the method consists of calculating the seismic risk by two different approaches:

- The first one derives the risk from historical seismicity. It is based on a statistical analysis of both earthquakes felt in the Region and isoseismical radii.
- The second one calculates the risk by convolution of hazard maps and fragility curves.

Eventually the two risk estimates are compared and conclusions are drawn about consistency of the SHARE hazard map with historical seismicity in the Region.

2 SEISMIC RISK BASED ON HISTORICAL SEISMICITY

2.1 Areas yearly affected by a given intensity

2.1.1. Principle of calculation

We consider a territory with a seismic activity homogeneous (in space) and stationary (in time). Taking the example of intensity VI, we denote A_{VI} the average area of this territory yearly affected by intensity equal to or larger than VI. Conceptually, would we have at our disposal comprehensive macro-seismic data on a very long period of time (T years), calculating A_{VI} would be easily achieved as follows: For every event i, occurring during the period of time T, we denote $\mathcal{A}_{i,VI}$ the area affected by an intensity larger than or equal to VI. Then

$$A_{VI} = \mathcal{A}_{VI}/T \quad \text{with} \quad \mathcal{A}_{VI} = \Sigma\, \mathcal{A}_{i,VI} \tag{1}$$

Practically we do not have at our disposal the above-mentioned ideal comprehensive information. However, we can build on historical data as follows: We denote

- n_{I0} ($I_0 \geq$ VI) the number of events of epicentral intensity I0, felt in the Region during a reference period of time T, in the present case 1895-2004 (110 years).
- $A_{I0,VI}$ the average area affected by an intensity larger than or equal to VI for an event of epicentral intensity I_0.

Then an estimate of $\mathcal{A}_{VI}$ is given by Eq. (2). It can be introduced into Eq.(1) to get an estimate of A_{VI} . Other A_I can be estimated similarly.

$$\mathcal{A}_{VI} = \Sigma\, n_{I0}\, A_{I0,VI}, \quad I_0 = \text{VI to IX} \tag{2}$$

NB a) We do not consider epicentral intensities smaller than VI because, by definition, they do not cause any damage of grade 2 or more on Class B vulnerability buildings.
NB b) In the following intensities are designated by Arabic numbers; for instance, I=6.5 stands for I= VI-VII.

Figure 2: The considered Region across the border between France and Italy

2.1.2 Application to the Region

Historical seismicity is well documented in France [6] as well as in Italy [7]. The Italian and French historical catalogues, respectively SisFrance and CPTI15, have been exploited in order to define the historical seismicity of the area. Duplicate values have been filtered out and a total of 100 events, with an effect in the Region greater than or equal to 6, have been retained (Table 1).

Table 1: Number of events ($I_0 \geq$ VI) felt with I ≥ VI in the Region on 1995-2004

Epicentral Intensity, I_0	6	6,5	7	7,5	8	8,5	9
Nb events, n_{I0}	47	17	22	12	0	1	1

Regarding areas affected by a given intensity for a given epicentral intensity, employment of isoseismal maps is still active in France and they are still drawn either automatically or manually from instrumental databases. The complete catalogue developed within the Sigma project, in partnership EDF and BRGM, provided all the information concerning isoseismal lines and their main features (extension, location, epicentral coordinates, confidence index). This atlas, based on the SisFrance catalogue reports all the earthquakes that occurred in the last century in metropolitan France with intensity greater than 6 [8].

In Italy this practice has decayed with time in favour of instrumental recordings information only. In this case, the information concerning macroseismic effects is solely discrete. The Italian database DBMI15 provides this kind of information. As a first attempt, isoseismal lines in the Italian territory have been manually traced and integrated to the existing French isoseismal maps. Processing French and Italian data result in the affected areas presented in Table 2.

Table 2: Average area affected by an intensity ≥VI for a given epicentral intensity

Epicentral Intensity, I_0	6	6,5 & 7	7,5 & 8	8,5 & 9
Average affected area (km²)	59	664	1512	5 066
Inside the Region	55	383	1271	1662

Applying formulas (1) and (2) with data included in the Tables 1 and 2 leads to: A_{VI} = 378 km²/year in the Region. The same procedure leads to results presented in the second line of the Table 3 for other intensities.

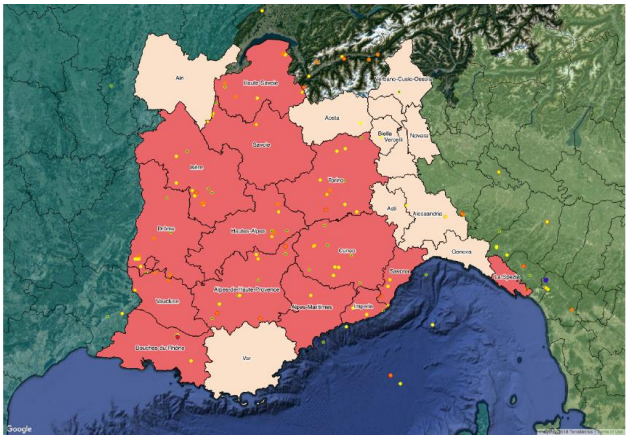

Figure 3: Subdivision into Zone 1 (in red) and Zone 2

2.1.3. Variability of seismic activity in the Region

On the basis of the activity rate calculated as the number of events per square kilometre, it is possible to split the Region into a zone of higher seismicity (Zone 1, representing 70% of the Region) and a zone of lower seismicity (Zone 2, 30%), as illustrated in Figure 3. Annual affected areas per zone are also presented in the Table 3.

Table 3. Average annual areas (km²) affected by a given intensity (or higher) according to historical seismicity

Intensity	6	7	8	9
In the Region, 95,660 km²	328	69	2.6	0.5(*)
In Zone 1, 67,160 km², 70 % of the Region	293	61	2.3	0.5 (*)
In Zone 2, 28,500 km², 30 % of the Region	35	7.4	0.3	0
(*) Postulated value in the absence of historical data.				

2.2 Annual probability of damage grade 2 to 4 for vulnerability class B buildings

The EMS98 scale [5] classifies types of buildings according to their sensitivity to seismic input motion and introduces a definition of damage grades. According to this scale, and considering the vulnerability class B, the proportion of buildings that undergo grade 2 to 4 damage is related to the intensity as reported in Table 4. Definitions of terms *a few*, *many* and *most* are based on fuzzy set techniques. They lead to quantify the terms as follows: *a few* is equivalent to 8%, *many* to 35% and *most* to 80%.

Table 4 : Damage rate *vs* Intensity for vulnerability class B buildings according to EMS 98

Intensity	6	7	8	9
D=2 (damage grade 2)	a few	many	*most*	*all*
D=3 (damage grade 3)	/	a few	many	*most*
D=4 (damage grade 4)			a few	many
In italic: interpretation of EMS 98 macroseismic scale				

For calculating the probability that a building undergoes a given damage grade, the probability it is exposed to a given intensity should first be established. This probability is directly derived from data presented in Table 3. For instance, the annual probability that a building located in Zone 1 is exposed to an intensity VII or higher is calculated as 66,3 / 67 160 = 9,87 10^{-4}.

Eventually, the annual probability that a class B vulnerability building experiences a given damage grade is calculated. Results are presented in the Table 5.

Table 5 : Annual probability that a vulnerability class B building undergoes a damage grade 2 to 4 ($D \geq 2, 3, 4$) on the basis of historical seismicity data

	$D \geq 2$	$D \geq 3$	$D \geq 4$
In the Region	5,54E-04	7,14E-05	4,00E-06
In Zone 1	7,05E-04	9,14E-05	5,37E-06
In Zone 2	1,98E-04	2,42E-05	7,83E-07

3 SEISMIC RISK BASED ON HAZARD MAPS AND FRAGILITY CURVES

3.1 Methodology

3.1.1 Principle of calculation

It is assumed that seismic hazard is described in the form of a map providing Peak Ground Acceleration (PGA) values, a_{ref}, associated to a given return period, T_{ref}. On any site of the territory, the annual probability that the observed PGA is greater than a is denoted $P_e(a)$. Consequently, the annual probability that a PGA with a value comprised between a and a+da occurs on this site is equal to $p_e(a)\,da$, so that:

$$p_e(a)\,da = -P_e'(a)\,da\,. \qquad (3)$$

Regarding a given type of buildings, its fragility is described by the probability it suffers a damage of degree D (or larger) in case it undergoes a seismic input motion whose PGA equals to a. This conditional probability is denoted $P_{f,D}(a)$. The annual probability that a building of the considered type suffers a damage of degree D (or larger) is derived as follows:

$$p_D = \int_0^{\infty} p_e(a)\, P_{f,D}(a)\, da\,. \tag{4}$$

3.1.2. Forms of P_e et $P_{f,D}$ functions

It is generally accepted that, at a given location in the territory, return periods, T, and associated PGAs, a, are linked by a function of the form given by Eq. (5), where T_{ref} is the return period selected for establishing the considered hazard map and a_{ref} the corresponding PGA at the considered location.

$$T/T_{ref} = (a/a_{ref})^n \tag{5}$$

Additionally, $P_e(a)$ is linked to the return period by $P_e(a)=1–\exp(-1/T(a))$, which results in the approximate $P_e(a) \approx 1/T(a)$ for relatively rare events. Consequently, a good approximate of $P_e(a)$ reads as per Eq. (6), this formula being not applicable for relatively small a values. A simple derivation leads to the $p_e(a)$ expression presented in Eq. (7). In practice the selected return period is 475 years, and consequently $P_e(a)$ takes the form of Eq. (6').

$$P_e(a) = \frac{1}{T_{ref}} \left(\frac{a_{ref}}{a} \right)^n \tag{6}$$

$$p_e(a) = \frac{n}{T_{ref}} \frac{1}{a} \left(\frac{a_{ref}}{a} \right)^n \tag{7}$$

$$P_e(a) = \frac{1}{475} \left(\frac{a_{475}}{a} \right)^n \tag{6'}$$

It is also generally accepted that building fragility is log-normally distributed. It means that the population of PGAs generating a damage grade greater than or equal to D is log-normally distributed; its median value is denoted a_D and β_D the standard deviation of its natural logarithm.

$$P_{f,D}(a) = \Phi\left[\frac{1}{\beta_D} \mathrm{Ln}\left(\frac{a}{a_D} \right) \right] \qquad \text{with} \quad \Phi(u) = \frac{1}{\sqrt{2\pi}} \int_{-\infty}^{u} \exp(-t^2/2)\, dt \tag{8}$$

3.1.3. Risk analytical formula

On the basis of these assumptions, it is possible to calculate an analytical formula of p_D given by Eq. (9), which in practice takes the form of Eq. (9').

$$p_D = \frac{1}{T_{ref}} \left(\frac{a_{ref}}{a_D} \right)^n k_D \quad , \quad k_D = \exp \frac{n^2 \beta_D^2}{2} \tag{9}$$

$$p_D = \frac{1}{475} \left(\frac{a_{475}}{a_D} \right)^n k_D \quad , \quad k_D = \exp \frac{n^2 \beta_D^2}{2} \tag{9'}$$

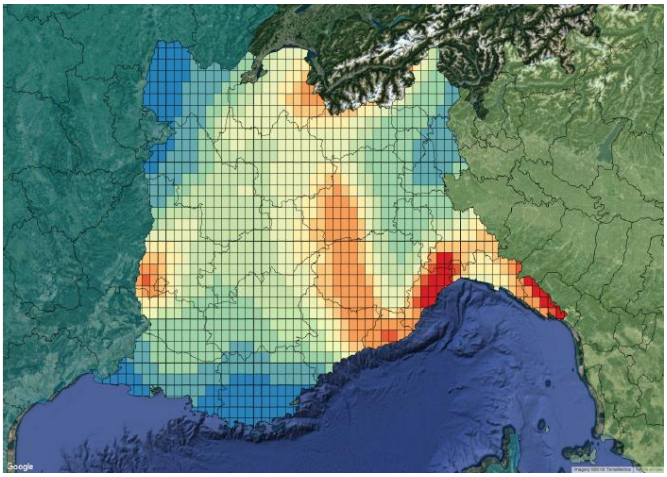

Figure 4: Share map on the Region

3.2 Application to the Region

3.2.1. Hazard data

The hazard map (Figure 4) and hazard curves have been downloaded from the SHARE web site [2], and the Region has been split into ten areas according to a_{475}, starting with a_{475} < 0.06 g for area 10 up to a_{475}.> 0.22 g for area 1, with a 0.02 g range per area. Regarding n, it varies from 2 for area 10 up to 3.5 for area 1.

For the sake of comparison with historical seismicity, the Region has been split into two zones that correspond to 70% and 30% of the Region area. It results in Zone 1' where a_{475} ≥0.09 g, and Zone 2' where a_{475} <0.09 g, presented in Figure 5. There are some differences compared to Zone 1 and Zone 2.

The SHARE map provides PGA values in rock conditions. It should therefore be taken into account that in our mountainous Region most buildings are built in valleys where rocky site conditions are not met. We have not taken this phenomenon into account; the point is discuss in the conclusions.

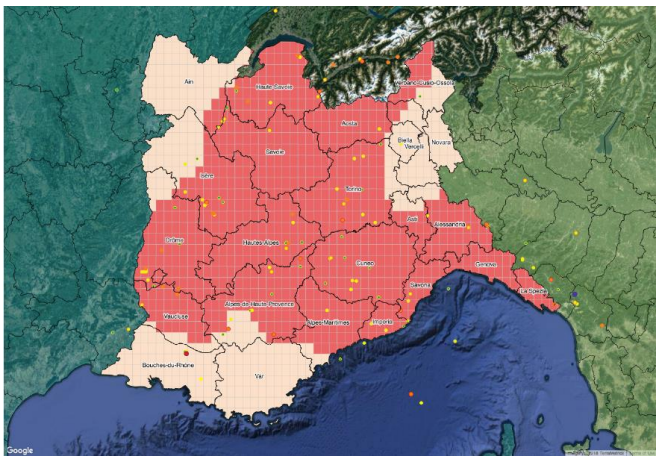

Figure 5: Subdivision of the Region into Zone 1'(in red) and Zone 2'

3.2.2. Fragility data

In section 2.2, the seismic risk was calculated for buildings of the vulnerability class B. Therefore, in order to obtain a reliable comparison with the output of historical seismicity approach, the fragility curve of class B buildings should now be selected for convolution with the seismic hazard. According to Lagomarsino and Cattari [9] two possible sets of fragility curves can be used, depending on the in-field experience feedback processed either by Murphy and O'Brien [10] (source 1) or more recently by Faccioli and Cauzzi [11] (source 2). Every set includes three curves corresponding to D=2, 3 and 4, whose a_D and β_D values are reported in the Table 6.

Table 6 : a_D and β_D values for vulnerability class B

	D=2		D=3		D=4	
	a_D (g)	β_D	a_D (g)	β_D	a_D (g)	β_D
Source 1, [9] & [10]	0.118	0.62	0.204	0.61	0.355	0.63
Source 2, [9] & [11]	0.145	0.54	0.240	0.54	0.390	0.56

3.2.3. Calculated risk

Eventually the risk is calculated according to Formula (9') in the Region and in Zones 1' and Zone 2'. Final outputs are presented in Table 7.

Table 7: Annual probability that a vulnerability class B building undergoes a damage grade 2 to 4 (D=2, 3, 4) on the basis of the SHARE map and fragility data

	Source 1, [9] & [10]			Source 2, [9] & [11]		
	$D \geq 2$	$D \geq 3$	$D \geq 4$	$D \geq 2$	$D \geq 3$	$D \geq 4$
Region	$3.14\ 10^{-2}$	$4.45\ 10^{-3}$	$7.85\ 10^{-4}$	$8.89\ 10^{-3}$	$1.61\ 10^{-3}$	$3.57\ 10^{-4}$
Zone 1'	$4.37\ 10^{-2}$	$5.95\ 10^{-3}$	$1.03\ 10^{-3}$	$1.19\ 10^{-2}$	$2.11\ 10^{-3}$	$4.57\ 10^{-4}$
Zone 2'	$2.42\ 10^{-3}$	$5.29\ 10^{-4}$	$1.34\ 10^{-4}$	$9.83\ 10^{-4}$	$2.59\ 10^{-4}$	$7.56\ 10^{-5}$

4 COMPARISONS AND CONCLUSIONS

Comparison of Tables 5 and 7 leads to the conclusion that the seismic risk calculated on the basis of the SHARE map and fragility curves overestimates the historically observed risk by a factor of the order of 50! Several reasons could be put forward in order to explain such a large gap and tracks could be investigated in order to try to bridge the gap.

- Risk evaluation on the basis of historical seismicity could be underestimated in case the last century has been an unusually quiet period for seismic activity. Very large earthquakes that occurred in the past could be put forward and a way found so as to take them into account. Researches are currently carried out on the subject at the scale of Continental France on the basis of the mathematics of extreme. The conclusion trend to be that there is no evidence that some correcting factor should be introduce in order to compensate for those large events that occurred in the past.
- Translation of intensity data into probabilities of damage on the one hand, and fragility curves on the other hand have been carefully selected so that they are consistent, corresponding in both cases at the same vulnerability class, namely Class

B. The same exercise has been run with other vulnerability classes (namely A and C), whose results are very similar.

- There is a significant variability in fragility curves. In order to better capture the sensitivity of the output to them, other fragility curves have been tested [12] [13]. It results that, depending on the selected fragility curve, the calculated risk may vary by a factor of the order of 2 or 3, which is significant, but still very far from providing a track to bridge the observed gap with risk assessment based on historical seismicity
- The SHARE map is the input data that should be regarded as the main cause of the discrepancy between the two risk calculations. Keeping in mind that the risk is dominated by the contribution of the most active areas, we may consider that an effective n=3 value is representative of the Region. In such condition, Formula (9) shows that dividing the hazard by a factor 2 results in dividing the risk by a factor 8. It leads to the conclusion that the seismic hazard presented by SHARE could be overestimated by a factor 2 or more. This conclusion is consistent with recent seismic hazard re-evaluation that were carried out in Switzerland [14] and Germany [15]. For instance, the SHARE map indicates that the 475-year return period PGA is comprised between 0.25 and 0.30 g at Basel city, while Swiss and German experts conclude independently that it should be 0.1 g.
- Regarding the site coefficients that have been disregarded in the convolution approach (see hereabove section 3.2.1), taking them into account would result in an increase of the calculated risk. It means that the gap between the two approaches would be even larger than presented in this paper.

In conclusion, in the light of the observed historical seismic risk, the SHARE map tremendously overestimates the seismic hazard in the Region, by a factor 2 or more. This conclusion is consistent with the most recent seismic hazard assessments carried out in Switzerland and Germany.

REFERENCES

[1] J. Woessner et al. *The 2013 European Seismic Hazard Model: key components and results*, BEE, Dec. 2015, Vol. 13, Issue 12, pp 3553–3596

[2] Giardini D. et al., (2013), Seismic Hazard Harmonization in Europe (SHARE): Online Data Resource, DOI: 10.12686/SED-00000001-SHARE, 2013. www.share-eu.org

[3] Pitilakis K, Crowley H, Kaynia AM (2014): *SYNER-G: Typology Definition and Fragility Functions for Physical Elements at Seismic Risk*, Springer.

[4] Labbé P (2010): PSHA outputs versus historical seismicity; Example of France. *14th European Conference on Earthquake Engineering*, Ohrid, FYROM.

[5] Grunthal G (1998): European Macrosismic Scale, *Cahiers du Centre Européen de Géodynamique et de Séismologie, vol 15*, Luxembourg.

[6] SisFrance (2013). *Catalogue des séismes français métropolitains*, BRGM, EDF, IRSN, www.sisfrance.net

[7] DISS Working Group (2018). Database of Individual Seismogenic Sources (DISS), Version 3.2.1: A compilation of potential sources for earthquakes larger than M 5.5 in Italy and surrounding areas. http://diss.rm.ingv.it/diss/, Istituto Nazionale di Geofisica e Vulcanologia; DOI:10.6092/INGV.IT-DISS3.2.1.

[8] J. Lambert; D. Monfort, O. Bouc (2015): Catalogue of isoseismal areas for xxth century French historical earthquakes (Io > VI). SIGMA report – Ref SIGMA-D1-148.

[9] Lagomarsino S, Cattari S (2014) *Fragility Functions of Masonry Buildings*, in *SYNER-G: Typology Definition and Fragility Functions for Physical Elements at Seismic Risk*, Springer.

[10] Murphy JR, O'Brien LJ (1977) The correlation of peak ground acceleration amplitudes with seismic intensity and other physical parameters. BSSA, 67:877-915.

[11] Faccioli E, Cauzzi C (2006). Macroseismic intensities for seismic scenarios, estimeted from instrumentally based correlations. *First European Conference on Earthquake Engineering and Seismology*, Geneva.

[12] Rota M., Penna A., Magenes G., A methodology for deriving analitycal fragility curves for masonry buildings based on stochastic nonlinear analyses. J. Engineering Structures, 32 (2010), 1312-1323.

[13] Risk-UE (2002). The European Risk-UE project: An advanced Approach to Earthquake Risk Scenarios with application to Different European Towns. 12th ECEE, London 2002, Special session.

[14] Swiss Seismological Service (2016). *Seismic Hazard Switzerland*, http://www.seismo.ethz.ch/en/knowledge/seismic-hazard-switzerland/index.html

[15] GFZ (2016), *Seismic Hazard Germany*, *http://www-app5.gfz-potsdam.de/d-eqhaz16/index.html*

Input motion transfer by linearization technique for seismic qualification of dam equipment

Pierre Labbé[1], Thuong Anh Nguyen[2]

Ecole Spéciale des Travaux Publics
28, Avenue du Président Wilson, Cachan, France
pierre.labbe@estp.fr

Keywords: Dam seismic response, linearization technique, frequency domain, damage, plasticity, transfer function, equipment

Abstract. *The widely used to model nonlinear responses under strong earthquakes, the concept of linearization is systematically re-examined by carrying out time-response analyses of non-linear oscillators. The considered non-linear constitutive relationships cover all the possible combinations from purely plastic to purely damage model, with hardening modulus in the range 0-20% of the elasticity modulus. The considered ductility demand varies from 1 to 20. The dynamics of the system covers cases where the natural frequency of the oscillator is lower than, close to or larger than the central frequency of the seismic input motion. The seismic input motion variability is taken into account by simulating 1000 accelerograms corresponding to a given spectral density. A total of 750,000 time-responses of non-linear oscillators are carried out and analyzed. For every case, the equivalent linear oscillator (effective frequency and effective damping) most appropriate for transferring the seismic input motion is identified through comparison of its transfer function with the non-linear response translated into the frequency domain. The approach is illustrated by comparison of spectra transferred through linear, equivalent linear and nonlinear oscillators. In conclusion, the satisfactory of the transferred signal through a non-linear oscillator by mean of the proposed equivalent linearization allows to apply this method to the case of dams under strong motions.*

1 INTRODUCTION

In order to assess dam response under strong seismic input motion, an engineering practice consists in running nonlinear time response analyses. Such calculations require huge CPU time and memory and raise convergence problems. In lieu of nonlinear analyses an option could be that equivalent linear models are employed. In the field of geotechnics, the concept of equivalent linearization was developed by Seed and Idriss (1970) [1], who introduced the concept of shear modulus degradation curve and associated damping ratio increase curve, both versus soil shear strain. This widely used engineering method enables, in its validity domain, to cope with nonlinear behaviour by implementing an iterative procedure, without running nonlinear transient analyses.

[2] Géodynamique et Structure 106, Av. Marx Dormoy, Montrouge, France ; anh.nguyen@geodynamique.com

For concrete structures, many authors have investigated this concept (Gulkan and Sozen 1974 [2]; Iwan 1980 [3]; Kennedy 1984 [4]; Chopra and Goel 1999 [5], Priestley et al. 2007 [6]) for different nonlinear constitutive relationships. Most of the proposed linearization concepts are based on the response in terms of maximum displacement of a single degree of freedom (sdof) system in order to determine an associated equivalent linear oscillator. Then, the equivalent frequency and damping ratio are expressed in terms of the maximum displacement, which is often translated into the concept of ductility demand defined as the ratio of maximum displacement X_{max} over the yield X_y such that $\mu = X_{max}/X_y$. A widely used approach consists in calculating the equivalent stiffness as equal to the secant stiffness corresponding to X_{max}. Concurrently, the equivalent damping ratio is generally estimated from the dissipated energy in the hysteretic loop corresponding to the same X_{max}.

In this global picture, few has been done concerning transferred signals through the nonlinear structures. Politopoulos and Feau (2007) [7] presented an equivalent linearization based on the modulus of the power spectral density (PSD) in acceleration.

This paper deals with the equivalent linearization through a systematic analysis using the complex frequency response function (FRF) as equivalence criterion. Filtered white noise signals are considered as input motions, described in the section 2. In section 3, various canonical constitutive relationships, mix of elasto-plasticity and damage models are introduced. They are used in section 4 to equip oscillators, so that 75 different configurations of oscillators are considered. Section 5 introduces equivalent linearization by minimization in the frequency domain, resulting in identification of equivalent frequency ratio f_{eq}/f_0 (f_0 is the natural frequency of the oscillator) and equivalent damping ratio ξ_{eq} versus ductility demand, μ, for the 75 configurations. In section 6, we present the performance of the proposed equivalent linearization for transferred seismic motions.

2 SEISMIC INPUT SIGNALS

Given that the response of a nonlinear structure is determined by a direct transient calculation, acceleration time histories are used. Generated signals can all be regarded as samples of a common stochastic process, namely a filtered white noise. The filter consists of a Kanai-Tajimi filter [8] and a high-pass filter described for instance by Clough and Penzien [9]. Numerical values of parameters are presented in Table 1. One thousand samples of this process are generated, designated by $\{g_j(t), j=1\ldots1000\}$. The time-envelope curve of α-type in the definition of Jennings et al. (1968) [10] is used. A sample of time-envelope curve is presented in Figure 1-a, and a sample of input signals in Figure 1-b.

Regarding the frequency content of the generated input signals, their central frequencies and non-dimensional bandwidth were calculated. The descriptive statistics are presented in Table 2. According to the calculated bandwidth values, the input signals are of large band type.

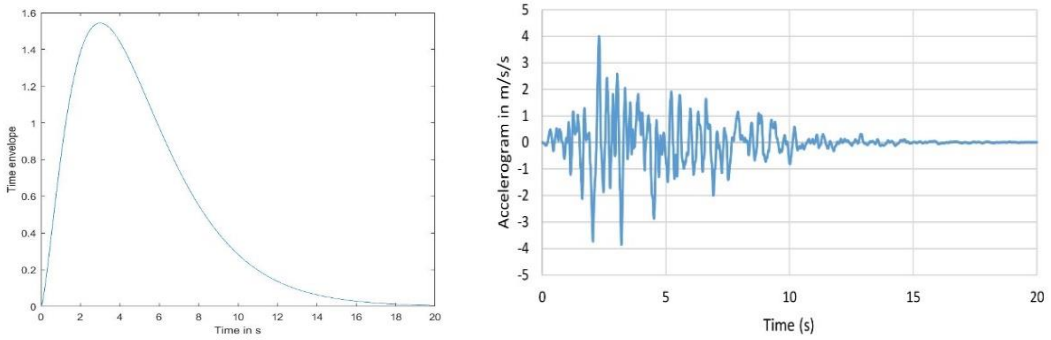

Figure 1: Example of time-envelope curve (1-a, left) and sample of input signals (1-b, right)

Table 1: Numerical parameters for generating input signals

Parameter	Notation	Value	Unit
Frequency step	Δf	0.05	Hz
Number of cosines	k_{max}	1000	
Frequency range	f_{min}-f_{max}	0.05-50	Hz
Filter Kanai-Tajimi,	f_{kt}	2.5	Hz
	β_{kt}	50	%
High-pass filter	f_{cp}	0.125	Hz
	β_{cp}	100	%
Low-pass filter	f_{bf}	10	Hz
	β_{bf}	100	%
Time-envelope curve α-type	a_1	1.33	
	a_2	2.50	
	a_3	0.50	

Table 2: Descriptive statistics of the 1000 generated input signals

	Central frequency in Hz	Non-dimensional bandwidth
Mean	3.38	0.63
Median	3.32	0.63
Standard deviation	0.22	0.03
Min	2.77	0.53
Max	4.18	0.73

3 CONSTITUTIVE MODELS

Two most-considered models (or constitutive relationships) in earthquake engineering are: elastoplastic model represented in Figure 2-a and damage model in Figure 2-b. The damage model was introduced by Mazars (1986) [11] for representation of concrete behaviour and continuously developed by this author. The internal variables are the plastic displacement at the instant t, noted $x_p(t)$, for the elastoplastic model and the maximum value reached at the instant t, noted Y(t), for the damage model, both exemplified in Figure 3.

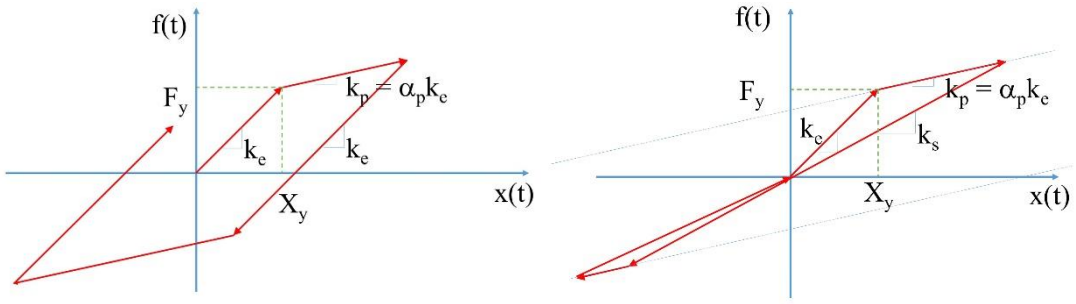

Figure 2: Elastoplastic behaviour with kinematic hardening (2-a, left) and Damage behaviour (2-b, right)

We introduce a Hybrid model, which consists of an assemblage in parallel of elastoplastic and damage models, with respective weights χ for the elastoplastic model and 1-χ for the damage model. In addition, we assign the same k_e, k_p and X_y values to both models. It implies that the elastic response of the Hybrid model, and consequently the natural frequency of an oscillator equipped with such a Hybrid model, does not depend on χ.

In practice, it is expected that concrete dams exhibit a behaviour that could be represented by $\chi = 0$ as it is the case for unreinforced concrete structures. Embankment dams are more of the type $\chi = 1$, as confirmed when outputs of the here presented approach are compared to those obtained from a conventional engineering approach based on degradation curves.

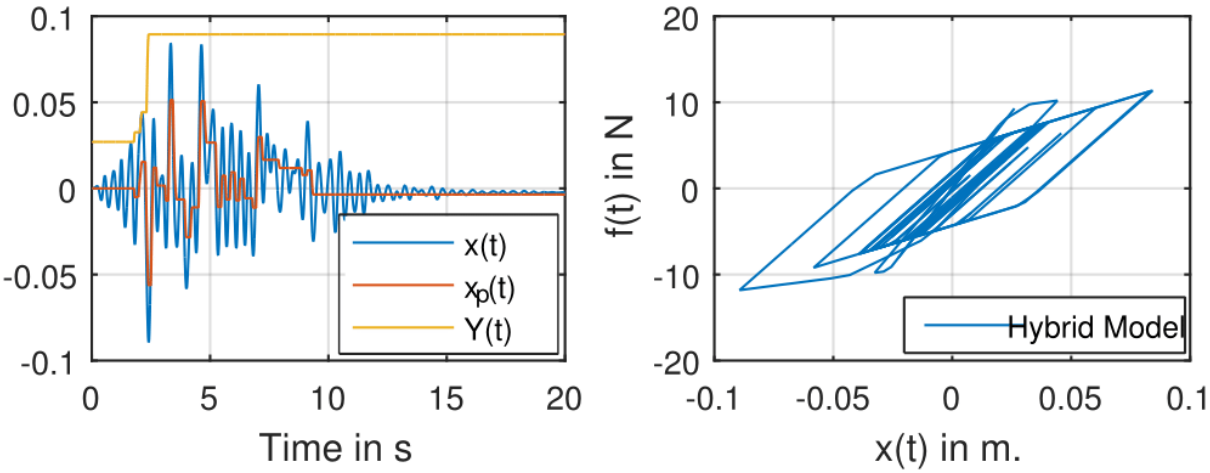

Figure 3: Example of response of Hybrid model for { f_0/f_c; α_p; χ} = {1.0; 10%; 0.5}, ξ_0 = 5%, μ = 3.31. For all axe labels, displacements x(t), $x_p(t)$ and Y(t) in m and force in N.

Such a Hybrid oscillator, whose an example of response is displayed in Figure 3, is characterized by five parameters:

- natural frequency, f_0,
- damping ratio, ξ_0,
- yielding displacement, X_y,
- second stiffness ratio, $\alpha_p = k_p/k_0$,
- hybridity index, χ.

4 NUMERICAL PARAMETRIC ANALYSIS

4.1 Configurations of Hybrid oscillators

When establishing the inelastic response spectrum for the NRC, Newmark & Hall (1978) [12] observed a frequency dependence of the seismic response of elastoplastic oscillators. Later on, evidences were more precisely given about the role of the ratio between the natural frequency of the oscillator and the central frequency of the input motion (Gantenbein and Hoffmann 1986 [13]; Labbé 1994 [14]). Therefore, instead of reasoning on f_0, we consider the ratio f_0/f_c. For a given system, this parameter reflects the high/low frequency content of the seismic input motion.

Consequently, in the performed numerical experiments, we first calculate the central frequency, $f_{c,j}$, of every input signal $g_j(t)$. For every input signal, five linear oscillators $\{f_{0,j}; \xi_0\}$ are considered such that:

- f_{0j}/f_{cj} takes values 0.1; 0.5; 1.0; 1.5; 2.0,
- ξ_0 is fixed to 5%.

For every elastic oscillator $\{f_{0,j}; \xi_0\}$, we calculate its response $x_{e,j}(t)$ to the input signal $g_j(t)$. Then we assign its maximum response to the yield displacement:

$$X_{y,j} = \max\left| x_{e,j}(t) \right| , j = 1....1000 \quad (1)$$

Afterwards, associated to every elastic oscillator, 15 different Hybrid models are considered resulting from the combination of α_p and χ where:

- α_p takes values 0.0; 0.1; 0.2,
- χ takes values 0.00; 0.25; 0.50; 0.75; 1.00.

In the following, a configuration, denoted $\{f_0/f_c; \alpha_p; \chi\}$ is a set of Hybrid oscillators that have in common the same values of these three parameters. There are in total 5 x 3 x 5 = 75 configurations.

4.2 Investigation of non-linear responses

Once $X_{y,j}$ has been calibrated, we increase the level of the input signal by applying on it a factor λ, such that it becomes $g_{\lambda,j}(t) = \lambda g_j(t)$. The amplification factor λ ranges between 1 and λ_{max}, the retained value of λ_{max} corresponding to the case when the median value of ductility demand is equal to 20.

Once λ_{max} is established, ten intermediate values of λ are considered, evenly distributed between 1 and λ_{max}.Then, for each level of input signal $g_{\lambda,j}(t)$, we carry out nonlinear time-response calculations (using the β -Newmark scheme, with $\beta = ¼$ et $\gamma = ½$) in order to calculate the response $x_{\lambda,j}(t)$ of the Hybrid oscillator under consideration, as well as its derivatives with respect to t.

Eventually, for a given configuration, we get 10,000 time-responses $\{x_{\lambda,j}(t), \lambda=1\ldots\lambda_{max}, j = 1\ldots1000\}$. For every of them we derive:

- the ductility demand defined as $\mu_{\lambda,j} = \max|x_{\lambda,j}(t)| / X_{y,j}$,
- the experimental complex FRF defined as $H_{ex,\lambda,j} = \ddot{X}_{\lambda,j}(\omega)$,/ $\Gamma_{\lambda,j}(\omega)$,

where $\ddot{X}_{\lambda,j}(\omega)$ and $\Gamma_{\lambda,j}(\omega)$ are the Fourier transform of the nonlinear response in relative acceleration and of the input motion. The Fourier transform is obtained through the fast Fourier transform operator of Matlab software. It results in two sets of

- 10,000 ductility demands: $\{\mu_{\lambda,j}, \lambda = 1\ldots\lambda_{max}, j = 1\ldots1000\}$,

- 10,000 complex FRFs: $\{H_{ex,\lambda,j}\ ,\ \lambda = 1\ldots\lambda_{max},\ j = 1\ldots1000\}$.

5 EQUIVALENT LINEAR FREQUENCY RESPONSE (ELFYR)

5.1 Principle

For every time response of a Hybrid oscillator, the principle is to identify an equivalent linear oscillator, $\{f_{eq},\ \xi_{eq}\}$, whose FRF is the closest to the FRF of the considered Hybrid oscillator according to the ELFYR method introduced in section 5.2.

As an output of the ELFYR method, we derive two sets of 10,000 equivalent frequency and damping values:

- $\{f_{eq,\lambda,j}\ ,\ \lambda = 1\ldots\lambda_{max},\ j = 1\ldots1000\}$,
- $\{\xi_{eq,\lambda,j}\ ,\ \lambda = 1\ldots\lambda_{max},\ j = 1\ldots1000\}$.

From the 10,000 couples $\{\mu_{\lambda,j}\ ,\ f_{eq,\lambda,j}\}$, we establish by regression, as presented in section 5.3, an empirical relationship between μ and $f_{eq,}/f_0$; and similarly between μ and ξ_{eq}. These relationships are presented for some of the 75 configurations.

5.2 Determination of equivalent characteristics by minimization in frequency domain

According to the procedure of minimization in the frequency domain, we determine the equivalent linear oscillator of $\{f_{eq,\lambda,j};\ \xi_{eq,\lambda,j}\}$ that minimizes the "difference" between the "experimental" complex FRF $\left(H_{ex,\lambda,j}\right)$ and the "theoretical" one $\left(H_{th,\lambda,j}\right)$ of the equivalent elastic oscillator with $\{f_{eq,\lambda,j};\ \xi_{eq,\lambda,j}\}$. This procedure is entirely performed by nonlinear least square regression approach. In other words, the $\{f_{eq,\lambda,j};\ \xi_{eq,\lambda,j}\}$ values are determined by minimizing the function introduced in Equation (2), where Re (.) and Im (.) denote the real and imaginary parts of complex number.

$$J\left(f_{eq,\lambda,j};\ \xi_{eq,\lambda,j}\right) = \sum_{f_{min}}^{f_{max}} \left(\left(\mathrm{Re}(H_{ex,\lambda,j} - H_{th,\lambda,j})\right)^2 + \left(\mathrm{Im}(H_{ex,\lambda,j} - H_{th,\lambda,j})\right)^2\right) \qquad (2)$$

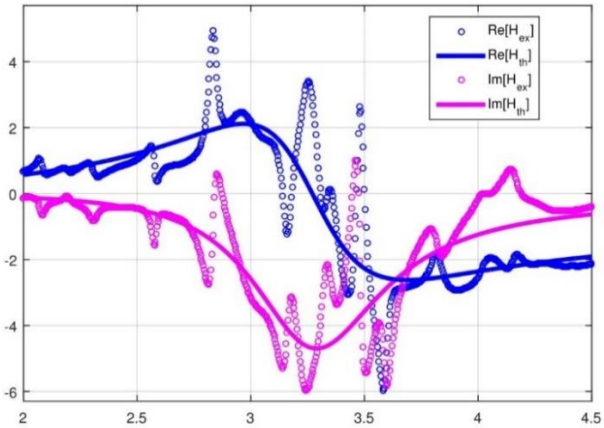

Figure 4: Example of minimization for $\{f_0/f_c;\ \alpha_p;\ \chi\} = \{1.0;\ 10\%;\ 1.0\}$

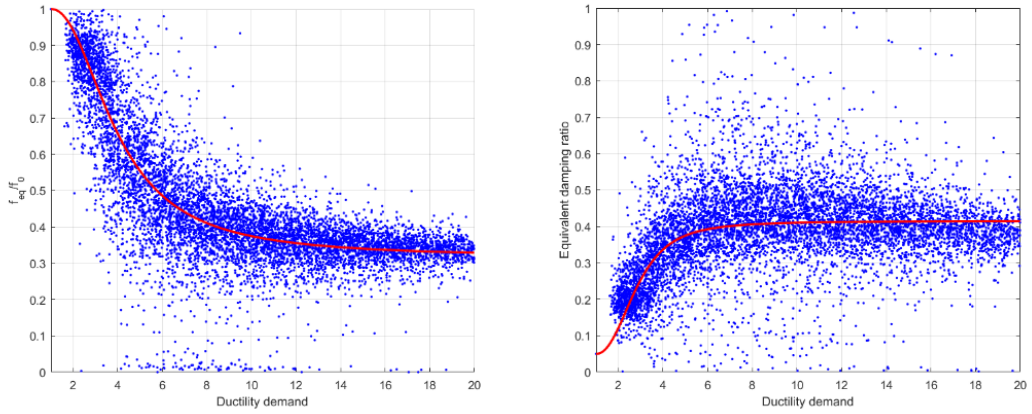

Figure 5: Equivalent frequency ratio f_{eq}/f_0 (left) and equivalent damping $\xi_{eq,}$ versus ductility demand, μ, for $\{f_0/f_c; \alpha_p; \chi\} = \{0.1; 10\%; 1.0\}$ (elastoplastic model).

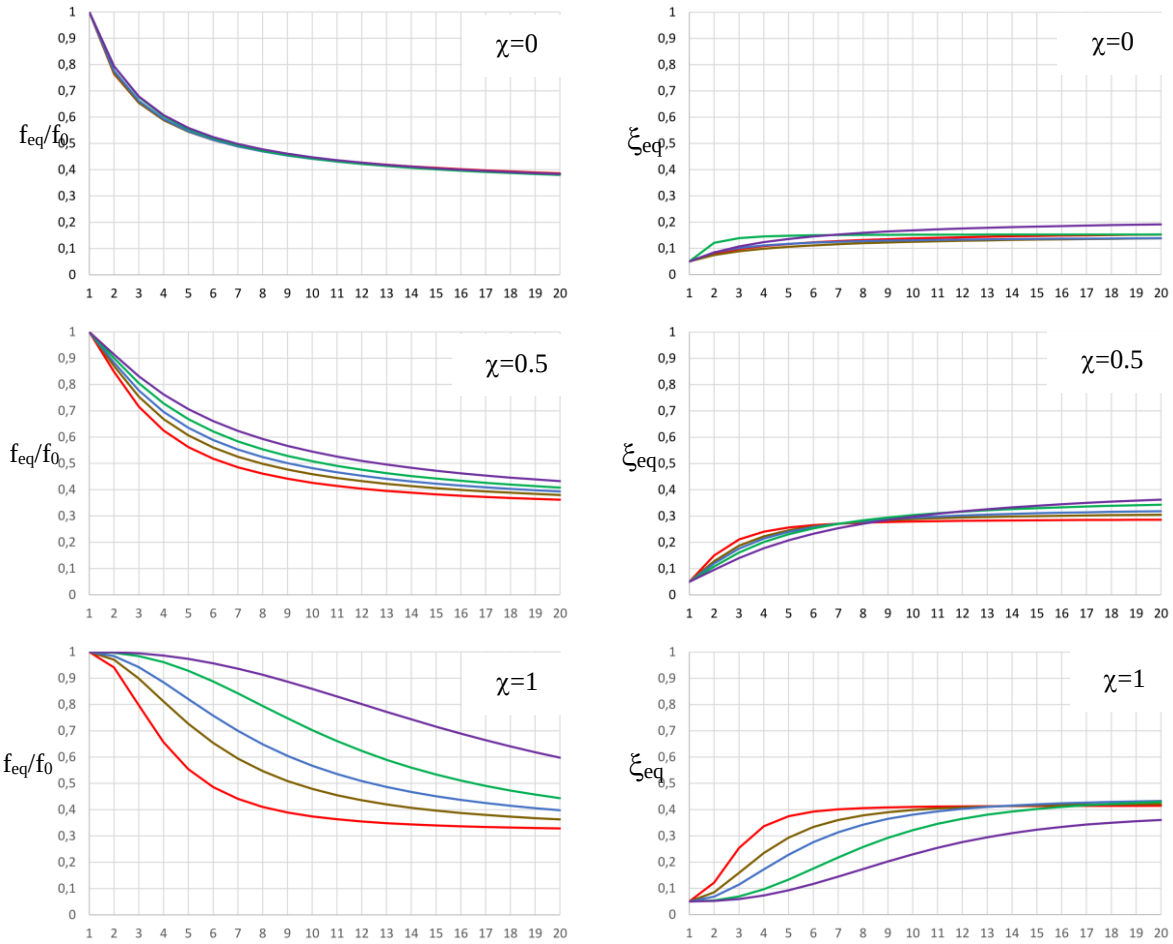

Figure 6: f_{eq}/f_0 and ξ_{eq} versus ductility demand, μ in abscissa for $\alpha_p = 0.1$ and three χ values.
Color legend: $\frac{f_0}{f_c}$= 0.1; $\frac{f_0}{f_c}$= 0.5; $\frac{f_0}{f_c}$= 1.0; $\frac{f_0}{f_c}$= 1.5; $\frac{f_0}{f_c}$= 2.0.

For example, in Figure 4, we present the minimization of $\{f_{eq,\lambda,j}; \xi_{eq,\lambda,j}\}$ determined for $\lambda = 2$ and $j = 1$ in the configuration $\{f_0/f_c; \alpha_p; \chi\} = \{1.0; 10\%; 1.0\}$. The yielding displacement $X_{y,1} = 0.021$ m is determined by the linear analysis of the elastic oscillator

$\{f_0; \xi_0\} = \{3.35 \text{ Hz}, 5\%\}$. The equivalent oscillator is characterized by $\{f_{eq,2,1}; \xi_{eq,2,1}\} = \{3.27 \text{ Hz}, 13.6\ \%\}$ and the ductility demand is equal to 1.87.

5.3 Outputs of numerical parametric analysis

For every configuration, we have to process the two scatter plots of $\{f_{eq,\lambda,j}$ vs $\mu_{\lambda,j}\}$ and $\{\xi_{eq,\lambda,j}$ vs $\mu_{\lambda,j}\}$. Examples of scatter plots are shown in Figure 5 for a case of elastoplastic model: $\{f_0/f_c; \alpha_p; \chi\} = \{0.1; 10\%; 1\}$. The blue dots are the 10,000 couples of $\{f_{eq,\lambda,j}; \mu_{\lambda,j}\}$ and $\{\xi_{eq,\lambda,j}; \mu_{\lambda,j}\}$ for the considered configuration, and the red line is the regression process result.

Outputs of the regression process are presented in Figure 6 for 15 configurations corresponding to $f_0/f_c = \{0.1; 0.5; 1.0; 1.5; 2.0\}$; $\alpha_p = 0.1$ and $\chi = \{0.0; 0.5; 1.0\}$. This result highlights the following points:

- Opposite of the damage model, the relations $\{f_{eq}/f_0$ vs $\mu\}$ and $\{\xi_{eq}$ vs $\mu\}$ strongly depend on the f_0/f_c ratio for elastoplastic model. For the later, the larger f_0/f_c, the larger the equivalent frequency ratio f_{eq}/f_0.
- Curves $\{f_{eq}/f_0$ vs $\mu\}$ present a $\sqrt{\alpha_p}$ asymptote. Regarding the plastic model, this asymptotic value is approached under small ductility demands in case of small f_0/f_c ratio, and conversely, under very large ductility demands in case of large f_0/f_c ratio.
- For the damage behaviour, the f_{eq}/f_0 ratio is the same as established by Chopra and Goel (1999) [5] on the basis of the secant stiffness. However, the damping ratio is much less than the value proposed by these authors. This result confirms that an oscillator whose equivalent frequency is equal to the secant one does not present a damping ratio corresponding to the dissipated energy through the loop at maximum displacement.

6 ASSESSMENT OF TRANSFERRED SEISMIC MOTIONS

As it is based on the transfer function, an expected advantage of the ELFYR method is that the resulting equivalent linear system should appropriately transfer the seismic input motion. To substantiate the point, response spectra obtained through equivalent systems are hereunder compared to those obtained through their father non-linear systems, considering both absolute acceleration (SA) and relative displacement (SD) response spectra.

For this purpose, we focus on a limited number of configurations defined as follows: for all of them we select: $\xi_0 = 5\%$, $\alpha_p = 10\%$ and a typical moderate ductility demand $\mu = 4$. Then we examine the nine cases defined by the combination of $f_0/f_c = \{0.1; 1; 2\}$ and $\chi = \{0; 0.5; 1\}$. Oscillators are qualified as flexible for $f_0/f_c = 0.1$, resonant for $f_0/f_c = 1$ and stiff for $f_0/f_c = 2$.

SA median spectra are compared in Figure 7, where the response spectrum calculated in linear regime is also plotted; and similarly for SD in Figure 8. It draws to some conclusions:

- There is a generic trend that response spectra in nonlinear regime are significantly reduced as compared to those obtained under linear assumption. This is visible on the SD spectrum for flexible oscillators and on the SA spectrum for resonant and stiff ones.
- For elastoplastic flexible oscillators, the frequency shift is visible. However, it has a limited effect on the SA spectrum, which is dominated by the input motion frequency content. The nonlinear effect is very clear on the SD spectrum.

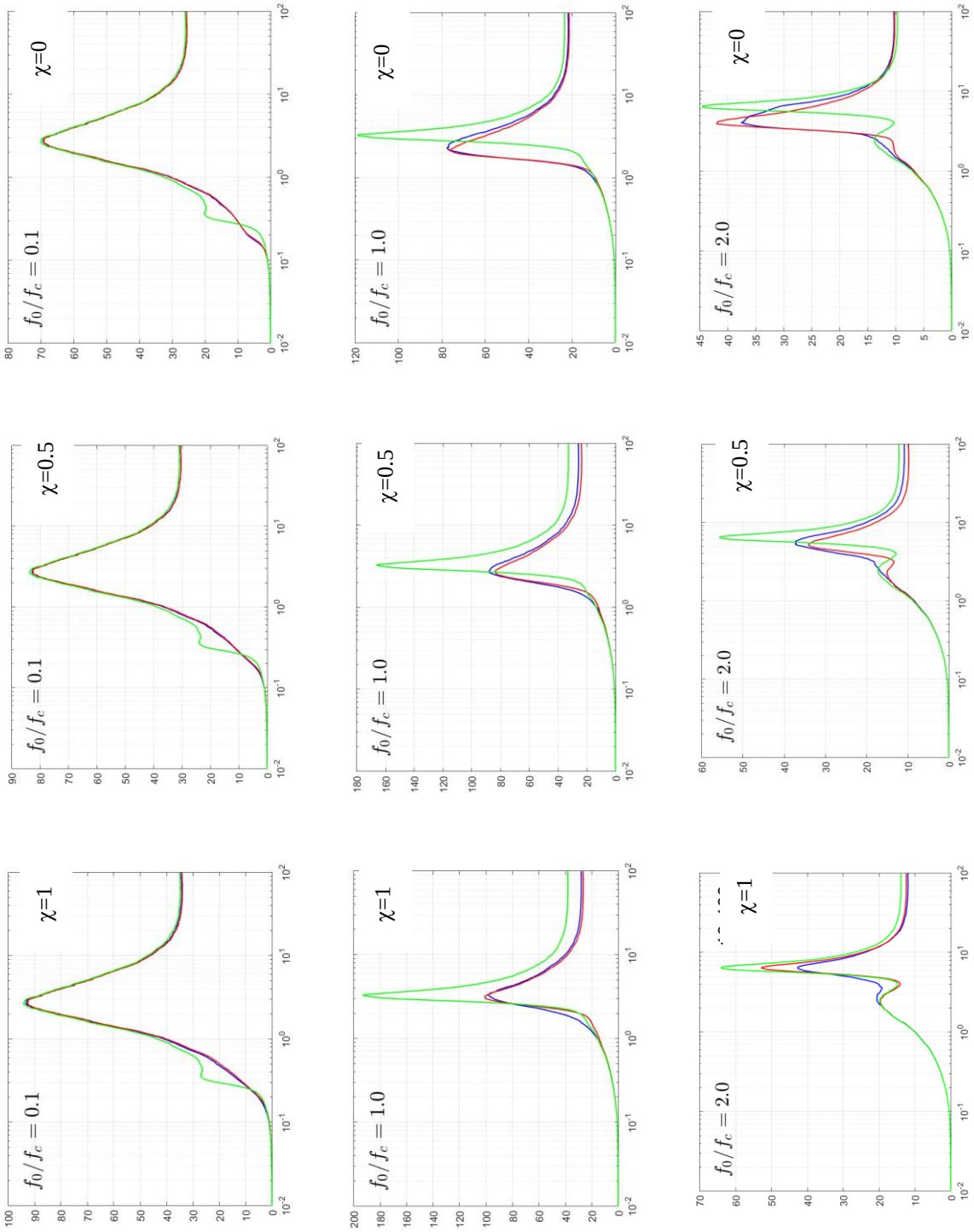

Figure 7: Response spectra in absolute acceleration (SA in m/s² in ordinate) as function of frequency (from 0.01 to 100 Hz in abscissa).
Colour legend: linear oscillator $\{f_0;\ \xi_0\}$; equivalent linear oscillator; nonlinear oscillator.

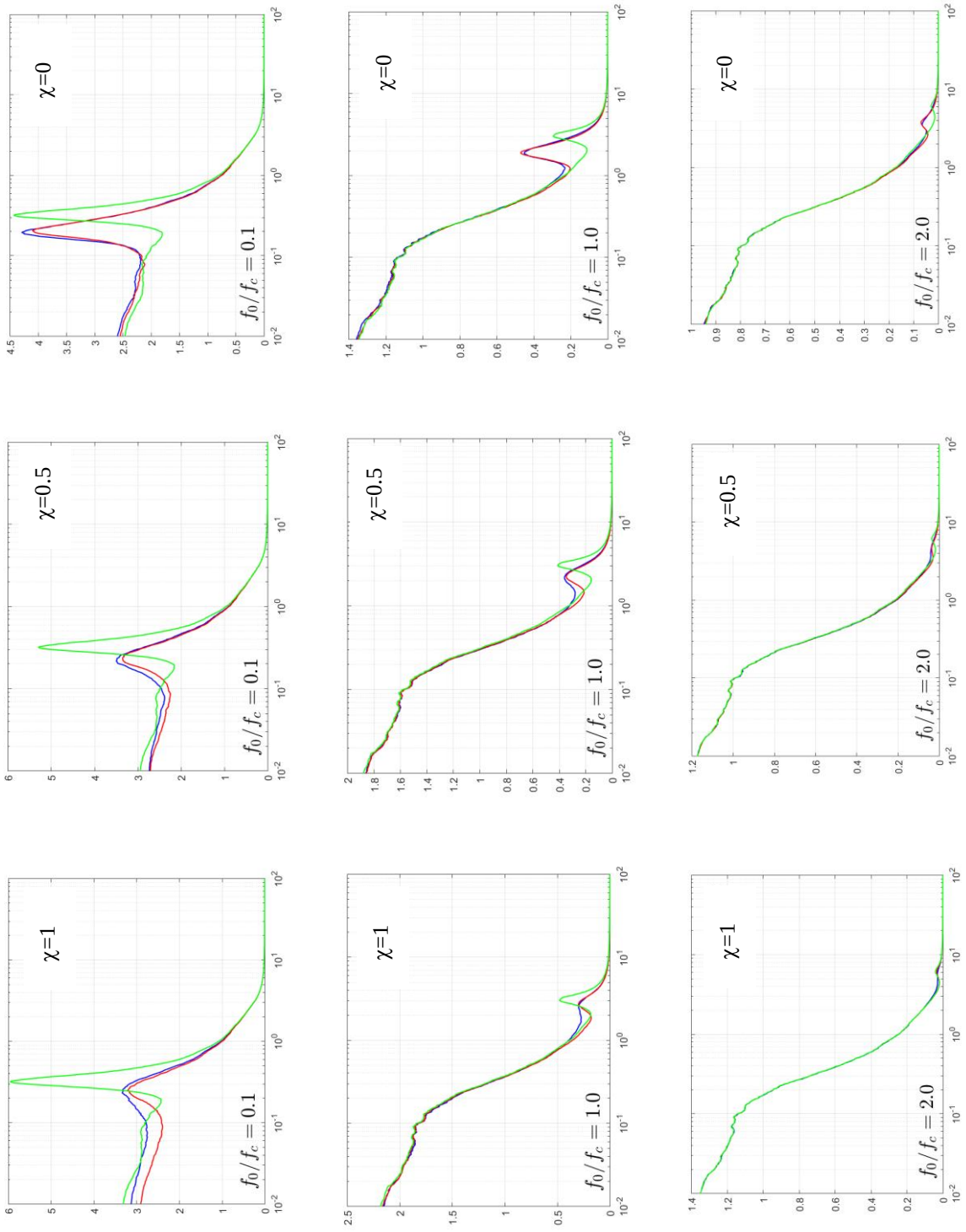

Figure 8: Response spectra in displacement (SD in m in ordinate) as function of frequency (from 0.01 to 100 Hz in abscissa).
Colour legend: linear oscillator $\{f_0;\ \xi_0\}$; equivalent linear oscillator; nonlinear oscillator.

- For elastoplastic resonant and stiff oscillators, the frequency shift is tiny if not negligible; the nonlinear effect is expressed through damping which results in a remarkable decrease of the spectrum peak magnitude.
- For damage oscillators, the frequency shift is very visible either on the SD spectrum (flexible oscillators) or on the SA spectrum (resonant and stiff oscillators). The effect on peak amplitude is limited due to the relatively small equivalent damping.
- Regardless the type of constitutive relationship, the SA peak response spectrum of the resonant oscillator is significantly reduced. This result reflects that the oscillator is detuned as soon as it enters the nonlinear regime.
- Response spectra delivered by the ELFYR method constitute a very good approximation of those that are derived from nonlinear calculations, as confirmed hereunder by the Anderson's criterion [15].

In order to assess the similarity between two signals of acceleration, Anderson introduced ten criteria, including criterion C8 dedicated to quantify the similarity of acceleration response spectra [15]. According to Anderson, a note between 8 and 10 means that an excellent fit is obtained. The similarity in term of SA between the nonlinear and equivalent linear systems were quantified by using the C8 Anderson's criterion for the nine cases under consideration, in the 0.01-100 Hz frequency range. The nine obtained notes were larger than 9.6, substantiating the very good performance of the ELFYR approach for spectrum transfer.

7 CONCLUSIONS

This work proposes an equivalent linearization method (abbreviated by ELFYR) using the complex FRF as equivalence criterion. The concept is applied to 75 canonical systems that cover a wide range of oscillators stiffness (controlled by f_0/f_c), equipped with constitutive relationships that range from elastic-plastic model to damage model (controlled by hybridity index χ) with a second stiffness that ranges from 0 to 20 % (controlled by α_p). Noticeable outputs regarding the dependence to the constitutive relationship are:

- For the damage behaviour ($\chi = 0$), which is deemed to be representative of concrete dams, the equivalent stiffness is equal to the secant stiffness, but the equivalent damping is much less than frequently indicated in literature on the basis dissipated energy in a cycle of the underwent maximum displacement.
- For the elastoplastic behaviour ($\chi = 1$), deemed to be representative of embankment dams, the equivalent stiffness is generally much larger than the one corresponding to the secant stiffness. In case of large ductility demand, around 10, the equivalent damping is in the order of magnitude of the one derived from the dissipated energy in a cycle of the underwent maximum displacement.
- Equivalent stiffness and damping are not dependent on the frequency content of the seismic input motion for $\chi=0$ (concrete dams), while they are very dependent on it for $\chi=1$ (embankment dams).

A significant advantage of the ELFYR concept is that the obtained equivalent linear oscillator can be used to calculate transferred signals, which is not the case with other techniques of equivalent linearization.

After the study presented is this paper has established the ELFYR proof of concept, next coming steps will consist in examining the concept robustness when considering i) actual recorded seismic strong motions in lieu of artificial ones and ii) multimodal structures.

Acknowledgements The authors thank EDF- DIPNN for its support.

REFERENCES

[1] Seed, H. B. & Idriss, I. M., 1970. *Soil moduli and damping factors for dynamic response analyses*. EERC 70-10.

[2] Gulkan, P. & Sozen, M. A., 1974. *Inelastic responses of reinforced concrete structure to earthquake motions*. Earthquake Spectra, Vol. 71, No. 12, pp. 604-610.

[3] Iwan, W. D., 1974. *A model for the dynamic analysis of deteriorating systems*. Proceedings of the Sixth World Conference on Earthquake Engineering, Vol.2, pp 1094-1099.

[4] Kennedy, R. P. et al., 1984. *Engineering characterization of ground motion. Task I. Effects of characteristics of free-field motion on structural response*, NUREG/CR-3805.

[5] Chopra, A. K. & Goel, R. K., 1999. *Capacity-demand-diagram methods for estimating seismic deformation of inelastic structures : SDF systems*. PEER1999/02.

[6] Priestley, M. J. N., Calvi, G. M. & Kowalsky, M. J., 2007. *Displacement-based seismic design of structures*. Pavia, Italy: IUSS Press.

[7] Politopoulos, I. & Feau, C., 2007. *Some aspects of floor spectra of 1DOF nonlinear primary structures*. Earthquake Engineering & Structural Dynamics, Volume 36, pp. 975-993.

[8] Tajimi, H., 1960. *A statistical method of determining the maximum response of a building structure during an earthquake*. Proc. 2nd World Conf. on Earthquake Eng. pp. 781-797.

[9] Clough, R. W. & Penzien, J., 1975. *Dynamics of Structures*, McGraw-Hill, 1975.

[10] Jennings, P. C., Housner, G. W. & Tsai, N. C., 1968. *Simulated earthquake motions.* California Institute of Technology.

[11] Mazars, J., 1986. *A description of micro-and macroscale damage of concrete structures*. Engineering Fracture Mechanics, 25(5-6), 729-737

[12] Newmark, N. M., & Hall, W. J. (1978). *Development of criteria for seismic review of selected nuclear power plants*. NUREG/CR-0098.

[13] Gantenbien, F. & Hoffmann, A., 1986. *Effect des seismes sur la structre - Contribution a la prise en compte de la ductilite*. CEA-DEMT 86-199 Internal report.

[14] Labbé, P. B., 1994. *Ductility demand and design of piping systems.* 10th European Conference of Earthquake Engineering (pp. 2689-2693).

[15] Anderson, J. G. (2004, August). *Quantitative measure of the goodness-of-fit of synthetic seismograms*. The 13th world conference on earthquake engineering conference proceedings, Vancouver, Canada, Paper (Vol. 243).

Seismic Action to be considered at the hydroelectric scheme of Foz Tua site

A. Carvalho and F. T. Jeremias

Laboratório Nacional de Engenharia Civil
Av. Brasil, 101, 1700-066 Lisboa
E-mail: xana.carvalho@lnec.pt

Keywords: Strong ground motions; Maximum design earthquake, Foz Tua

Abstract. *The hydroelectric scheme of Foz Tua is located on Tua river and includes a concrete arc dam. Seismological studies carried out aimed to define the design earthquakes. For this purpose, different approaches for definition of design earthquakes were analysed and the OBE (operating basis earthquake) and the MDE (maximum design earthquake) were defined. The application of the methodology adopted required a previous review of geological and seismological data of the area, mainly focused on regional active faults and on earthquake data recorded at vicinity of dam site. Seismic motions for the MDE were evaluated through a stochastic methodology which take into account fault geometry, rupture heterogeneities and characteristics of seismic wave propagation media.*

1 INTRODUCTION

The seismic actions that should be considered in the design of large dams are well defined in ICOLD (International Commission of Large Dams) Bulletins and also in Portuguese dam safety regulations, foreseeing the use of the Operating Basis Earthquake (OBE), the Maximum Credible Earthquake (MCE) or the Maximum Design Earthquake (MDE).

The definition of the mentioned earthquakes required a previous review of geological and seismological data of the area, mainly focused on regional active faults and on earthquake data recorded at vicinity of dam site. However, the methodologies to be used in the seismological studies to characterize the seismic ground motion of those earthquakes are not so well established, mainly for the MCE or MDE, earthquakes of higher magnitudes.

Two approaches, probabilistic seismic hazard analysis (PSHA) and deterministic seismic analysis (DSHA) are widely used in deriving the ground motion parameters for design purposes. However, for both approaches there are significant weaknesses affecting the seismic input at the dam site and the definition of the design earthquake for a dam site should be based on finite-fault modeling. This mentioned methodology was applied to assess the MDE for Foz Tua hydropower project.

2 DEFINITION OF THE SEISMIC HYPOTHESIS

Given the features of the region where the dam site is located and taken into account the low seismicity of the surrounding area, it was considered adequate to assume for the earthquake source zone a circle area with a radius of 100 km long centered in the dam site (Figure 1). This zone is characterized by a diffuse seismicity where an equiprobable maximum earthquake of magnitude M5.0 in any point inside of this area may be assumed.

Considering that the operating basis earthquake relates to the maximum earthquake with a high probability to occur during the lifetime of the dam, it was assumed that a maximum

earthquake M = 5.0 constituted a credible seismic hypothesis for the determination of OBE, which was characterized accordingly by (magnitude, distance, depth):

OBE: M = 5.0; D = 10 km; d = 10 km

The historical maximum magnitude recorded MHME = 5.7 seems to be not related to any particular fault. Therefore, it was adopted for the maximum designed earthquake a majored magnitude MDE = MHME + 0.5. Accordingly, MDE was characterized by:

MDE: M= 6.2; D = 10 km; d =10 km

It must be stressed that, in this case, the prediction of the maximum earthquake on the basis of the concept of the maximum credible earthquake it is not a more advantageous way to deal with the uncertainty related to the prediction of the maximum earthquake. In fact, the consideration of the MCE implies the formulation of hypotheses concerning the Vilariça fault segmentation and the length of an eventual co-seismic rupture at surface, being the prediction of those parameters merely speculative.

However, and given the importance attributed to the Vilariça fault as a seismic source, it was considered convenient to assume a second hypothesis for the MDE, which correspond to the hypothesis of the Vilariça fault reactivation, according to paleoseismicity studies [1]. Despite the doubts raised by the conclusions of that study, namely concerning the maximum earthquake adopted, a second MDE hypothesis was characterized by:

MDE: M= 7.25; D = 25 km; d =10 km

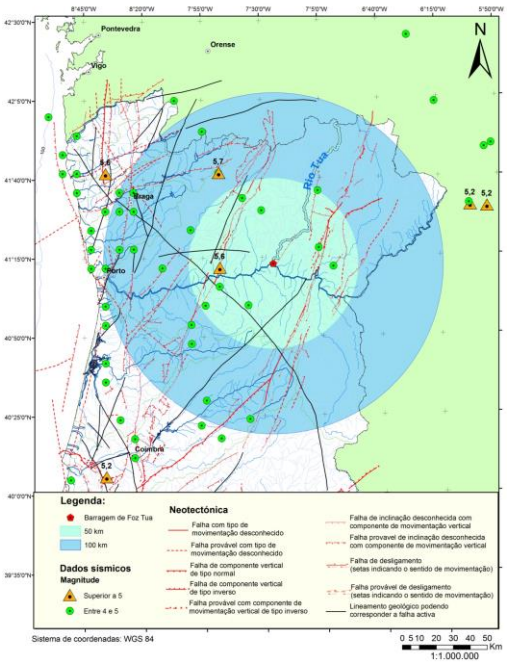

Figure 1: Earthquakes occurred in the circle areas centered in Foz Tua dam site, considering radius 50 and 100 km long

3 METHODOLOGY

For a realist and feasible ground motion prediction it is important to use a set of assumptions about the earthquake source spectrum, effects of path and site conditions. To make allowance for these effects, the methodology applied for ground motion characterization combines:

(i) the finite-earthquake-source modelling technique [2] that includes a fault discretized into several elements (sub-faults), a nucleation point (initial point of the rupture), a heterogeneous slip distribution, a rupture velocity and the summing at the site of the contribution of each element lagged in time. The ground motion at an observation point is obtained by summing the contributions over all sub faults (Figure 2, left). An element triggers when the rupture reaches its centre. The contributions from all elements are lagged and summed at the receiver, the time delay for an element being given by the time required for the rupture to reach the element, plus the time for shear wave propagation from the element to the receiver. The duration of motion comes from the source duration plus the path duration.

(ii) the source-point stochastic model [3]: each element of the fault is modelled as a stochastic omega-square point source, the amplitude of the acceleration Fourier spectrum for each subfault is calculated as a product of the spectrum produced by the source at a certain distance and filtering functions representing the effects of path attenuation and site response (Figure 2, right).

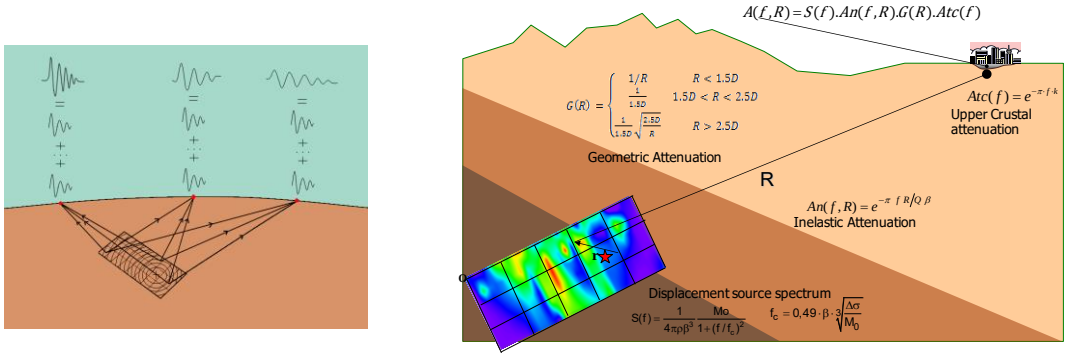

Figure 2: Left: Summing process ; Right: Schematic view of the stochastic model

Finite-fault simulations require that the fault-plane geometry (length, width, strike, dip, number of subfaults considered and depth to the upper edge), the source parameters (seismic moment, slip distribution, stress drop, nucleation point, rupture velocity), the crustal properties of the region (geometrical spreading coefficient and anelastic attenuation) and the site-specific soil response information be previously specified.

The model parameters calibration has been obtained with a dataset that includes horizontal components of ground acceleration records (at rock sites) obtained by the Portuguese digital accelerometer network and from independent studies. Validation, by comparing synthetic seismograms against recorded ones, were done entirely in terms of 5% damped pseudo absolute response spectra for acceleration [4].

To account for the uncertainty in model parameters, and to estimate upper bound for the seismic input it is important to perform a large number of runs for the same fault. The effects of aleatory uncertainty is considered expressing random variability in the parameter from one ground motion realization to another. Each key parameter (length, width and strike of the fault, stress drop, upper crustal attenuation and geometric-spreading coefficient) is treated as a probability distribution (truncated normal or uniform distributions, depending on the parameter which is being modelled).

4 MDE ASSESSMENT

While seismic motions for the OBE were evaluated considering either the deterministic approach and two different attenuation laws [5][6] or the probabilistic approach for a 145 years return period - 50% of exceedance probability for a 100 years lifetime - (Figure 3), MDE was assessed considering the stochastic methodology described in the previous section. For that, fifteen random trials were realized, each run with a different combination of the set of parameters (Table 1), according to the probabilistic distribution of each one, considering a random distribution of the slip and a random initiation point of rupture so that it was possible to capture directivity effects. Results were presented in terms of response spectral amplitudes (Figure 4).

Table 1: Seismic source parameters, and their variability, considered to MDE assessment

Magnitude, *M*	6.2	7.25
Fault Length x width [km]	12-5 x 5-8	65-76 x 13-16
Strike (medium value)	0 – 90º (N24ºE)	N20ºE-N30ºE (N24ºE)
Dip (º)	0º - 90º	90º
Velocity of rupture Vr [*km s^{-1}*]	2.50	
Slip	random	

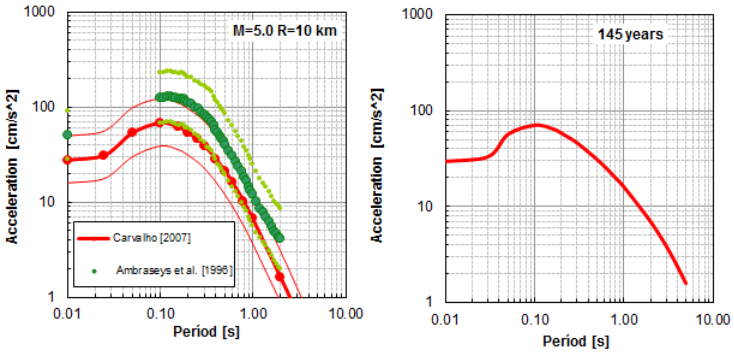

Figure 3: OBE assessment. Left: Deterministic approach. Right: probabilistic approach, for a 145 years return period

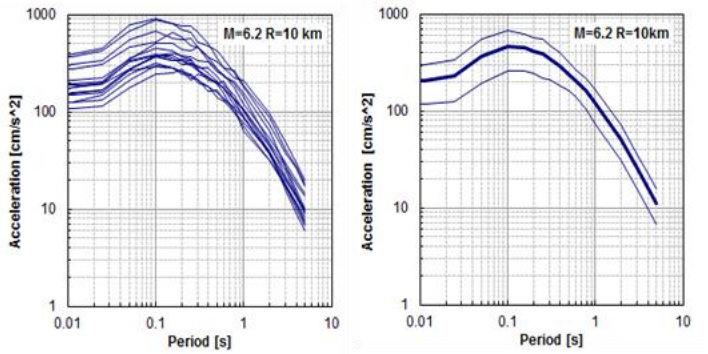

Figure 4: MDE=6.2 assessment. Left: 15 response spectra, corresponding to the random trials simulated. Right: mean and the mean plus and minus one standard deviation spectra

5 CONCLUSIONS AND FINAL REMARKS

Results, considering peak ground acceleration, are summarized in Table 2.

Table 2: Final peak ground acceleration (PGA), considering OBE and MDE, for Foz Tua dam site (in brackets it is shown PGA values plus 1 standard deviation)

		Peak Ground Acceleration (cm.s^{-2})			
Earthquake		Deterministic Approach		Stochastic methodology	Probabilistic Approach T = 145 years
		Ambraseys et al, 1996	Carvalho, 2007		
OBE	M=5.0 R=10 km	51 (90)*	29 (49)*	–	29
MDE	M=6.2 R=10 km			200 (267)*	
	M=7.25 R=25 km			231 (340)*	

Well-founded physical models must be used as the basis for the predictions of strong motion in Portugal. The finite-fault model, when a fault is known, will generate more accurate ground-motion time histories for a future earthquake at a site near the fault, since it incorporates average directivity effects and provides the correct ground motion based on fault rupture time. Being so, it is emphasized in this paper that the MDE should be synthesize by stochastic finite fault methods, as there are major obstacles when using seismic hazard commonly used approaches such as PSHA and DSHA.

The stochastic finite fault methodology was applied for the first time to assess MDE for Portuguese dams.

REFERENCES

[1] Rockwell, J. Fonseca, C. Madden, T. Dawson, L. A. Owen, S. Vilanova, P. Figueiredo, Palaeoseismology of the Vilariça Segmento of the Manteigas-Bragança Fault in northeastern Portugal, in Reicherter, K., Michetti, A.M. & Silva, P. G. (eds) Palaeoseismology: Historical and prehistorical Records of Earthquake Ground Effects for Seismic Hazard Assessment. The Geological Society of London, Special Publications, 316, 237-258 (2009).

[2] I.A Beresnev, G.M. Atkinson, *FINSIM - a FORTRAN program for simulating stochastic acceleration time histories from finite fault*, Seism. Res. Lett., 69, pp. 27-52 (1998).

[3] D.M. Boore, *Simulation of ground motion using the stochastic method*, Pure Appl. Geophys. 160, 635-676 (2003).

[4] A. Carvalho, G. Zonno, G. Franceschina, J. Bilé Serra, A. Campos Costa, A, Earthquake shaking scenarios for the Metropolitan Area of Lisbon. Soil Dynamics and Earthquake Engineering 28, 347-364, (2008).

[5] N.N. Ambraseys, K.A. Simpson, J.J. Bommer, J.J., *Prediction of horizontal response spectra in Europe*. EESD 1996; 25, pp. 371-400 (1996).

[6] A. Carvalho, *Modelação estocástica da ação sísmica em Portugal Continental*. Dissertação de doutoramento, IST, Lisboa (2007)

Seismic hazard on the territory of yeghvard reservoir dam

Karapetyan S.S.,[1] Mkrtchyan G.A.[2] and Karapetyan J.K.[3]

Institute of Geophysics and Engineering Seismology after A. Nazarov NAS RA
V.Sargsyan 5, Gyumri, Armenia
e-mail: iges_ra@mail.ru

Keywords: Armenia; dams, earthquake; seismic hazard; soil; prevailing periods; seismic impact;

Abstract. *We have set forward the task of determining the quantitative values of expected seismic hazard on the territory of Yeghvard reservoir designed on Qasakh river. To solve this problem, we have carried out the following comprehensive research works. A catalog of earthquakes on the Yeghvard reservoir and adjacent territories was compiled. Active faults in the area were observed. The seismicity for R=150km area was studied resulting in the assessment of baseline seismic hazard on the territory of the reservoir for the mid class soils (II class-[3]soil conditions (first stage-DSZ). We have identified main engineering geological areas characterizing the study area and determined maximum values of seismic intensity expected in typical ground conditions in parts of g. We calculated and constructed Fourier spectra, and determined prevailing patterns of seismic fluctuations in different ground conditions. Based on the results of the two stages, the seismic micro-zoning 1: 2000 scale map for the reservoir area was compiled with the corresponding expected acceleration values (second stage - SMZ).*

INTRODUCTION

Hydrotechnical structures and facilities such as reservoirs, dams, tunnels, canals, etc., are extremely important for the economics of each country - its ecology and social sphere. Violations during operation period can lead to accidents, environmental and social disasters. The damage caused by the destruction of each structure can be huge. Therefore, we should pay attention to the reliability and safety of these structures. Security activities should be performed starting from the design stage. When designing exactly reservoir dams, one should take into account the degree of seismic hazard on its territory that will help reduce seismic risk for both the structure and neighboring settlements.

This work relates to the assessment of seismic hazard on the territory of Yeghvard reservoir. Yeghvard reservoir is one of the most important hydraulic structures in Armenia. It is located in the central part of the Republic of Armenia near the town of Yeghvard. Within the framework of "Improvement of the Yeghvard reservoir irrigation system in Armenia" project preparation, carried out under financial support of the Japan International Cooperation Agency (JICA), large-scale geological-geophysical, seismological, engineering-

[2] IGES NAS RA, e-mail: mkrtchyan201056@yandex.ru
[3] IGES NAS RA, e-mail: iges@mail.ru

seismological detailed studies were carried out aimed at determining the expected seismic hazard on the proposed Yeghvard reservoir.

The work was performed in two stages. At the first stage, detailed seismic zoning (DSZ) of the territory of the Yeghvard reservoir was performed; the maximum expected horizontal acceleration of PGA (in parts of g) is determined in the dam territory for the original middle-class soils by seismic properties.

At the second stage of work based on comprehensive engineering-geological and instrumental studies, seismic micro-zonation (SMZ) of the dam areas was carried out. Zones with the most vivid geotechnical and seismic characteristics are identified. Moreover, the expected PGA maximum horizontal seismic effects in g parts are determined for these zones.

1. SEISMIC HAZARD ASSESSMENT

1.1 Detailed seismic zoning (DSZ)

We performed detailed seismic zoning on the R=150km radius area around designed Yeghvard reservoir to determine the expected seismic hazard on baseline ground conditions (II class soils). To implement this work we have prepared a catalog of earthquakes happened in the study area, which includes the main data of earthquakes from prehistoric period up to 2015 including also paleo-earthquakes [17,25]. The seismological data of the IGES NAS RA electronic database was used to create catalogs, which include all the seismic statistical materials of all regional catalogs [8÷19,25].

Figure 1 shows the spatial distribution of epicenters of M≥5 magnitude earthquakes in the R=150 km radius of the reservoir and the existing active fault system in the area. Locations of 5 paleo earthquakes are shown in (fig.1), two of which are in the source zone of Spitak earthquake happened in the 3-2 and 23-17 millenniums B.C., another 2 paleoearthquakes are dated by the 1-st and 5-4 millennium B.C. in Tsghut source zone and 782 B.C. Khonarasar earthquake [17,25]. Above mentioned distribution denotes to the fact that designed reservoir area in located on active faults which are of great significance from regional point of view, moreover have been a source of strong historical earthquakes. However, Dvin earthquake group is directly neighboring the designed reservoir (M=5.2 in 851, M=5.2 in 863, M=5.0 in 869, M=6.5 in 893, M=5.7 in 906), Garni in 1679, M=6.5 and Tsaghkadzor in 1827, M=5.0 magnitude earthquakes. Due to the analysis of epicenter spatial distribution it was revealed that strong earthquake sources in the study area are distributed group by group on the active faults [26,27,28]. Some of them are Spitak on the north (fig.1 - ①, PSSF), Ani from north-west (fig.1-②, AF), Dvin on the south spreading parallel to each other (fig.1-③, PDF), Ararat (fig.1- ④, IF-DF) and Van-Chaldiran (fig.1-⑤, CF), Gyanja on the east (fig.1-⑥ PSSF3) and Syunik from south-east (fig.1-⑦ PSSF4) source groups.

Hence seismic effect quantitative values of the strongest earthquakes occurred on mentioned source groups were calculated, when assessing seismic effect in the reservoir location area. The calculations of initial seismic effect is carried out using well known empiric dependences [21,22,23,24]. All results are shown in table 1. The results show that the Dvin 893 and Garni 1679 earthquakes are the most dangerous for the Yeghvard reservoir construction

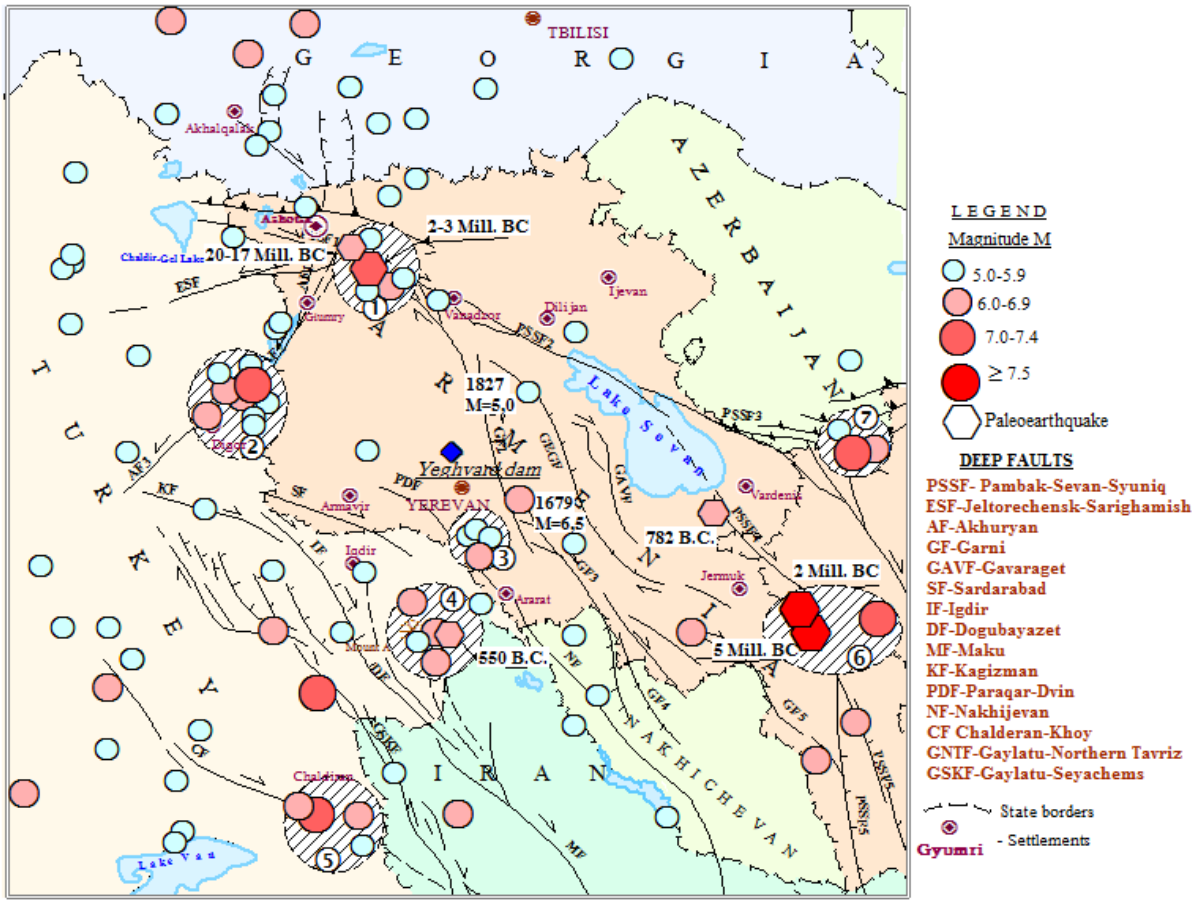

Figure 1. Map of sources of strong earthquakes (M≥5.0) and active faults in the adjacent territories of Yeghvard dam area R=150km

Table 1:Estimated maximum horizontal accelerations caused by sources of strong earthquakes

№	Earthquakes	Magnitude M	Depth H (km)	PGA (in g's) by					
				Boor-Joyner [23]	Campbell & Bozorgia [22]		K.Sadikh [21]		F.Aptikayev [24]
					For I class ground	For II class ground	For I class ground	For II class ground	
1.	5-4 mill. B.C. Tskhuk	7,5	15	0,08	0,2	0,267	0,097	0,1	0,05
2.	893 Dvin	6,5	10	0,17	0,26	**0,36**	0,14	0,16	0,101
3.	1064 Ani	7	13	0,12	0,18	0,24	0,12	0,13	0,07
4.	1679 Garni	7	15	0,23	0,25	0,32	0,19	0,22	0,23
5.	1827 Tsakhkadzor	6,5	9	0,2	0,2	0,24	0,164	0,2	0,16
6.	1840 Ararat	6,9	14	0,085	0,14	0,188	0,09	0,093	0,04
7.	1976 Van-Chaldiran	7,1	17	0,06	0,137	0,186	0,07	0,07	0,03
8.	1988 Spitak	7	12	0,15	0,21	0,27	0,14	0,16	0,109

site, the obtained maximum horizontal acceleration values of which are PGA(g)=0.33g and PGA(g)=0.32g calculated according to Campbell-Bozorgia seismic effect quantitative damping model for II class ground conditions [22]

Relying on obtained results ***we can conclude that the assessed initial seismic hazard for the territory of Yeghvard designed reservoir is PGA=0.36g for mid (II class) ground conditions.***

2. EXPECTED SEISMIC HAZARD ASSESSMENT IN THE AREA (SEISMIC MICROZONATION)

2.1 General geological conditions

The designed reservoir is located in the western part of the Yeghvard volcanic plateau at an altitude of 1200-1400 meters above sea level. The length of the plateau is 4.5 km, the width is 3.5 km and the entire surface of the area is about 1000 hectares. The hydrological network in the study area is very poor. The study area is characterized by a very dry continental climate, hot summer up ot + 40^0C and fairly cold winter up to -25^0 C. The vegetation can be characterized as semi-desert and steppe.

The study of geological structure of Yeghvard plateau, as well as geo-geological investigations had been carried out by various organizations and specialists in the last century [7]. The research on the projected reservoir resumed in 2015 by Sanyu Consultant and "Hidrogeoshin" LLC.

2.2 General Geology of Dam-site

Practical geologic basement of Yeghvard Reservoir area is a sedimentary rock formation belonging to Miocene, usually called as “Hrazdan Suite,” which is consisted of sandstones, clays and marls. The Suite forms impei-vious basement in this area, hydrogeologically. Upper surface of the Miocene sediments near around the reservoir area inclined from east to west, and the maximum inclination of the basement is shown just near the dam-site. On a significant scale, the surface of Miocene was dissected and heavily covered by many volcanic formations emerged from the Aragats and Arailrer Volcanos in Pleistocene age. Volcanic activities of these volcanos were quite heavy' throughout Pliocene and continued to the almost end of Pleistocene, Quaternary age. The oldest volcanic formation in this area is Dacites (series ⑰ see legend in fig.2) in late Miocene, covering the Miocene sediments (Hrazdan Suite) but dissected strongly so as merely cropping out on some gentle hill tops. Covering the oldest Dacites, several volcanogenic formations together with a few sedimentary formations, were accumulated in the high land between the Kassakh and the Hrazdan rivers. Among them, Olivine-basaltic Andesites in middle Pliocene (series ⑬) formed the framework of southern bank, and younger Olivine-basaltic Andesites in middle Quaternary (series ⑤) flowed down as lavas formed the main body of the northern bank of reservoir area. And, directly covering the Andesite lava, characteristic red-brown Scoria or Welded Tuffs are distributing (series ④). The formation changes its facies from hard rock to rather soft scoria, and pyroclastic flow deposits looking like sand-and-gravels. The low-land of planned reservoir was an enormous dissected valley in lower Quaternary and buried several volcanogenic and alluvial deposits through upper Quaternary to Holocene. It is striking that the last large scale volcanic activities had happed in late Pleistocene near around the site, and thick basaltic Andesite lavas flowed down (series ⑤) and further covered by pyroclastic, welded tuffs, and scoria (series ④) with chai-acteristic brick-red color as mentioned above. Notably, the tuffs show quite high gamma-ray radiation. At the end of Pleistocene, huge volumes of moraine deposits were left in northwest bank of the reservoir area (series ②). The deposits were consisted of huge basalt blocks, boulders, cobles, pebbles, sand and gravels, without selection, and they are diverted as an embankment materials in these day. Moraine deposits are now covered by recent alluvial and diluvia

sediments (series 2a) thinly, but it is rather difficult to distinguish in the site. Recent Aeolian diluvial - proluvial formations (series ① and 1^a) cover almost all of the central portion of the reservoir area, represented by gray Sandy Loam or Loamy Sand with comparatively impervious property. Thin sand or clay layers are intercalated. Thickness of the formation is said from 35 to 40m in the central portion. However, the total thickness of relatively impervious layers including Lower to Lower-middle Quaternary - Lacustrine -alluvial deposits (series ⑥ to ⑧) should be beyond 120m in the central portion.

2.3 Engineering-geological zonation of the area

Engineering-geological zoning map, which serves as a base for seismic microzonation map, was compiled taking into consideration engineering-geological, hydrogeological materials about the study area, as well as criteria determining physico-mechanical properties of grounds and seismic features (table 2), also considering engineering-geological cross sections in the dam body. Using existing engineering-geological materials, a map of engineering-geological zoning for the reservoir area is compiled (fig. 2).

According to the results, the central part of the reservoir is composed of mainly second-lass ground conditions.

The sections of the dams correspond to I class ground conditions. However, a little part of the first dam and a small area of the second dam correspond to the second class (fig.2, fig.3, fig.4). Thus, instrumental observations were carried out to determine real properties of above mentioned sections.

Table 2: Physico-mechanical properties of ground varieties in Yeghvard reservoir area

Grounds category	N according Fig. 2	Ground type	Density ρ g/sm^3	Porosity coefficient (E)	Cohesion C kg/sm^2 (natural)	Natural humidity W %	Filtration coefficient K_f m/day	Friction angle φ^0 (natural)	Number plasticit W_n	Consistency index I_L
I	4	Welded tuff (Pink)	1.74	-	-	6	13	55	-	-
	10	Welded tuff (Black)	1.94	-	-	5	17	65	-	-
	5, 13, 15	Basaltic Andesite lava	2.23	-	-	5	23	70	-	-
	14	Volcanic Breccia	2.08	0.3	-	13	4-5	23	-	-
II	1	Sandy Loam and Loamy Sand	1.65	0.48	13	18-22	0.4-0.5	24	4.5-5.5	<0
	2	Surface Gravel	1.8	-	0.02	16	1.66	27	-	-
	3	Moraine Deposit (gravel)	1.90	-	-	-	-	-	-	-
	7	Sand and Loamy Sand	1.70	0.5	-	10	1,5	30	-	<0
	9	Lithoidal Pumice	1.45	0.42	-	-	-	-	-	-
	11	Scoria Tuff	1.85	0.36	-	-	-	-	-	<0
	12	Piroclastic Flow	1.8	-	-	-	-	-	-	-
	17	Sandstone, Clay, Marls (Hrazdan Suite)	1.80	0.5	0.68	-	0.28	18	3.6	0.25

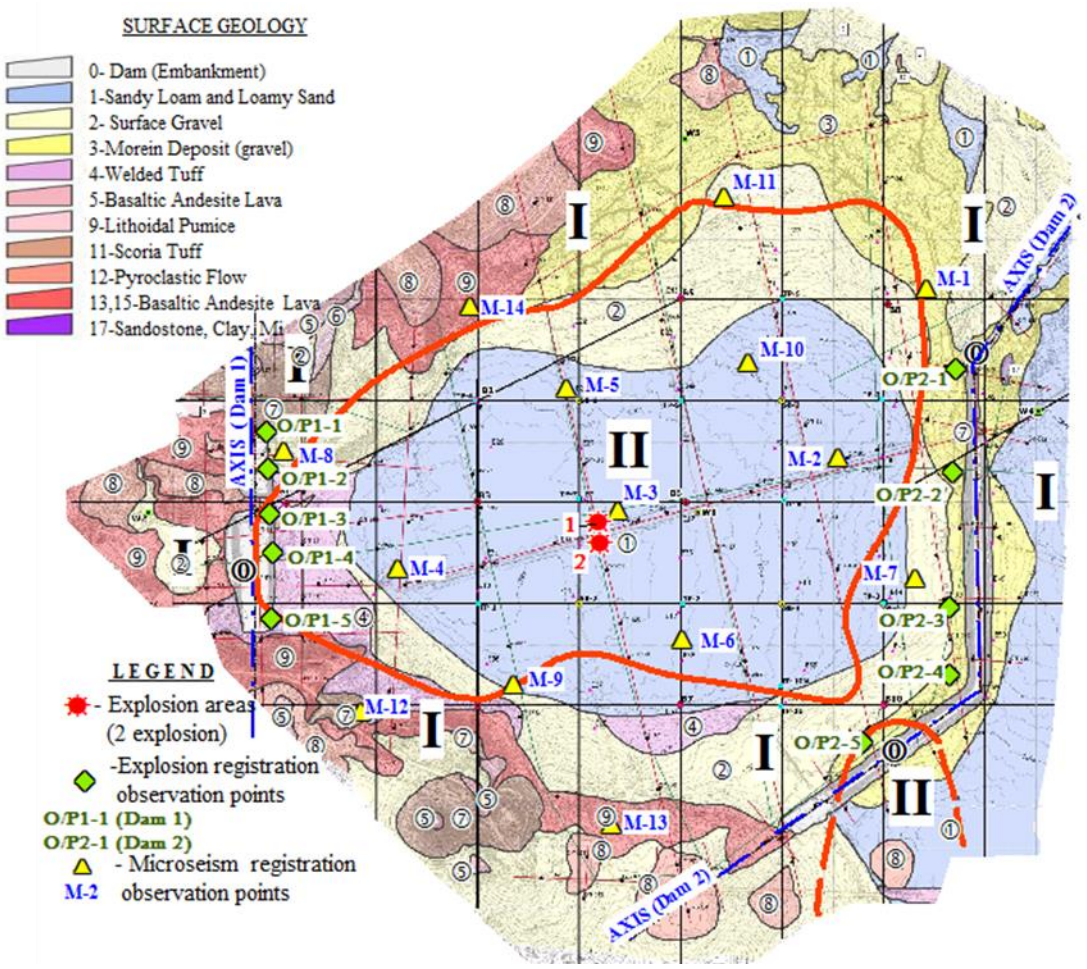

Figure 2: Geophysical observation deployment scheme on engineering-geological zoning map of Yeghvard reservoir area

2.4 Instrumental observations

Seismic properties of varieties ground conditions representing the territory of the Yeghvard reservoir were determined using the methods of seismic explosion and high-frequency microtremors (microseism).

As a recording device, a new generation storage system with a hard memory and with SM-3 seismic receivers was chosen. To record the explosions, the sites were selected according to the following logic:

- In engineering-geological respect they should be typical.
- If possible, should have identical distances from the epicenter of the explosion.

Based on the above, the recordings are made in nearby areas, covering the territory of the reservoir dam.

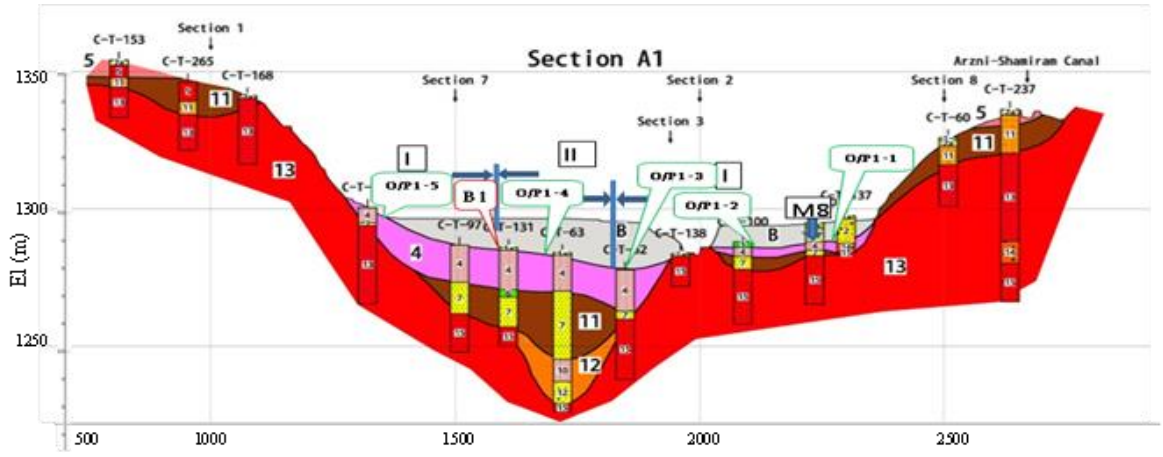

Figure 3: The cross section in the base of the first dam and the location of the observation point

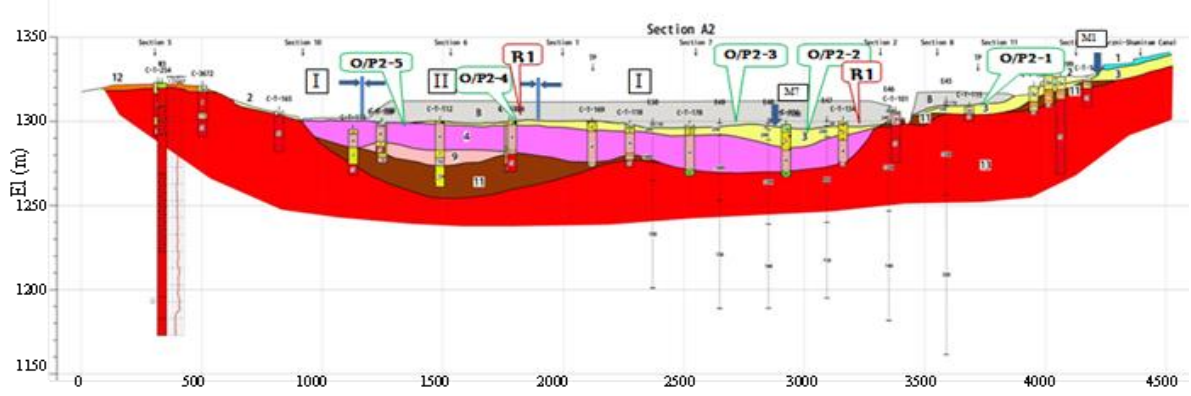

Figure 4: The cross section in the base of the second dam and the location of the observation point

Two explosion were implemented. The first explosion was aimed at studying the small dam (fig.2. dam 1), and the second explosion to study the large dam (fig.2. dam 2). For the explosion in the center of the designed reservoir, two wells each 5 meters depth were drilled. Device installation schemes and explosion points are presented on the scheme of the actual material (fig.1) and also on sections of the dam foundations (fig.3, fig.4). We have observed the engineering-geological 30m capacity cross sections of both dam bases. The cross section of the first dam is composed of up to 4 meters capacity cracked, weathered red tuff, below within 14 capacity black color weak cracked tuffs are bedded, under which about 3.5 meter capacity are strongly weathered red tuff sands, below these up to 30 m depth, with 8.5 meter capacity are fine-grained alluvial sands and loamy sand layers. The capacity of fine-grained sands with loamy sand layer gradually decreases on the left of central part and disappears abruptly to the right of it. The observation points O/P1-3 and O/P1-4 (fig.3) are located in this section. Given that, explored area lacks in pure second-class ground conditions according seismic properties, so O/P1-1 is accepted as a etalon or baseline with Basaltic Andesite Lava pure first class ground conditions. Figure 4 shows the cross section of the second dam. The main composition of this section is Moraine Deposit gravel with a capacity of about 3 m, located on andesite-basaltic soils with a capacity of more than 50 meters. As with the first dam, ground conditions of a purely second category are also lacking here by seismic properties. Therefore, the ground conditions at the O/P2-1 were also considered the initial or baseline for the second dam. According to the BCRA norms when shifting from second-class ground conditions to first-class the value of the initial seismic intensity will be PGA=0.36g*0.8=0.288g=0.29g: where PGA=0.36g is the value of initial seismic intensity, obtained at the first stage of investigation.

According to the records of explosions and using the formula of S.V. Medvedev [1] seismic intensity increments are determined O/P1-1 and O/P2-1 for the first and second dams respectively.

Using the obtained records, the values of the prevailing periods for each observation point are also calculated. The results of the calculations are shown in table 3. Microtremor observations were carried out in different parts of the study area at 14 points, including all possible ground types. Fourier spectra were built according to microtremor recordings, using which prevailing periods were determined. The research results showed that in the study area, the background of microtremors is characterized by a rather wide range of prevailing periods of grounds T_0=0.1÷0.5 sec, whereas the calculated according to BCRA II 6.02-2006, 5.3.3 [3] is $T_0 \cdot 1.3 = 0.13 \div 0.65$ sec (table 4). For both ground types, according to their engineering geological properties the following prevailing periods are distinguished;

- for the I class it is T=0.1 ÷0.25 sec (calculated 0.13÷0.32 sec)
- for the II class it is T=0.3 ÷ 0.5 sec (calculated 0.4 ÷0.65 sec).

Table 3: Results obtained from two explosions

Observation Point O/P	Registration amplitude A_{max}	Seismic intensity increase in units of bal (ΔI)	Seismic intensity increase in units of g	Expected seismic intensity PGA(g)	Prevailing periods values T_0 (sec)
first explosion, first dam					
O/P-1	24,99	0	0	0.29	0,25
O/P -2	26,94	0,1	0.01	0.3	0,2-0,26
O/P -3	29,07	0,2	0.02	0.31	0,25, 0,35
O/P -4	35,24	0,5	0.05	0.34	0,2, 0,3
O/P -5	28,04	0,2	0.02	0.31	0,21
second explosion, second dam					
O/P2-1 (Etalon)	35,03	0	0	0	0,23-0,3
O/P2 -2	37,94	0,11	0,011	0,27	0,2-0,3
O/P 2-3	36,07	0,043	0,0043	0,26	0,25, 0,3
O/P 2-4	37,18	0,083	0,0083	0,27	0,2-0,3
O/P2 -5	44,22	0,33	0,033	0,29	0,25, 0,32

2.5 Seismic hazard assessment for Yeghvard reservoir dam installation area (Seismic microzoning map)

Seismic micro-zoning for Yeghvard reservoir dam installation area was carried out by seismic micro-zoning implementation general rules [2,4,5,6]. Moreover, seismic hazard degree in the sections with different type grounds was determines using two methods; engineering-geological analogies and instrumental explosion recordings.

Table 4: Results obtained from microseism observation

O/P	Geographic coordinates		Elevation above sea level (m)	Ground category according seismic properties	Prevailing periods T_0 (sec)	
	Latitude	Longitude			Actually registered	According RABC II-6.02–2006 5.3.3
M-1	40.319521^0	44.456384^0	1305	I	0.12	0.17
M-2	40.312182^0	44.453224^0	1295	II	0.3-0.33	0.4-0.43
M-3	40.309550^0	44.440125^0	1290	II	0.4-0.5	0.52-0.65
M-4	40.307121^0	44.427654^0	1289	II	0.32-0.38	0.41-0.5
M-5	40.315172^0	44.437394^0	1292	II	0.3	0.4
M-6	40.304065^0	44.444222^0	1289	II	0.32	0.42
M-7	40.306839^0	44.457756^0	1299	I	0.2	0.26
M-8	40.311769^0	44.421561^0	1297	I	0.15-0.2	0.2-0.26
M-9	40.303859^0	44.433933^0	1291	I-II	0.2-0.3	0.26-0.39
M-10	40.316415^0	44.447944^0	1296	II	0.3-0.4	0.39-0.52
M-11	40.323395	44.446743^0	1310	I	0.2-0.25	0.26-0.32
M-12	40.300765^0	44.425595^0	1320	I	0.16-0.2	0.21-0.26
M-13	40.295843^0	44.440188^0	1317	I	0.12-0.15	0.16-0.2
M-14	40.318823^0	44.432754^0	1318	I	0.1-0.12	0.13-0.16

Table. 5 Expected seismic intensity values of Yeghvard reservoir

Section Name	Ground category	Dominant periods T_0(sec.)	Acceleration by g according to		Expected maximum acceleration values by g
			Eng.-geol.analogy	seismic-explosions	
The central part of the reservoir	II	0.2-0.4 (0.26-0.52)	0.36	-	0.36
The right side of the first dam	II	-	0.36	0.32	0.32
The left side of the first dam	I	0.15-0.2 (0.2-0.26)	0.29	0.29	0.29
A part of the right side of the second dam	II	-	0.36	0.31	0.31
The rest of the second dam	I	0.12-0.2 (0.17-0.26)	0.29	-	0.29
Other areas of the reservoir	I		0.29	-	0.29

Using high frequency microtremor methods, the prevailing periods for different type ground conditions were determined. When determining prevailing periods by Fourier spectra seismic explosion recordings were also used. The final degree of seismic hazard was determined by the analysis of the intensity values obtained by these methods. The central part of the reservoir, which was previously assessed as second-class ground by its seismic properties, was estimated at PGA = 0.36g. More attention was paid to the dam deployment areas. According to engineering, geological, and instrumental researches, there are both first and second class grounds in these sites. It should be noted that the second class sites identified on the dam according to their physical and mechanical properties and dynamic parameters exceed the norms of the Second Class Grounds.

As a result of explosions the following acceleration values were obtained: for the first dam it is PGA=0.32g and PGA=0.31g for the second dam (table 5). The rest of the reservoirs

area is composed of first-class ground conditions and the degree of assessed seismic hazard is PGA = 0.29g.

Based on obtained results, the map of the expected seismic hazard or seismic micro-zoning (fig. 5) has been compiled. Summarizing obtained results for all the sections of the dams as the expected seismic hazard value PGA = 0.32g acceleration value is accepted.

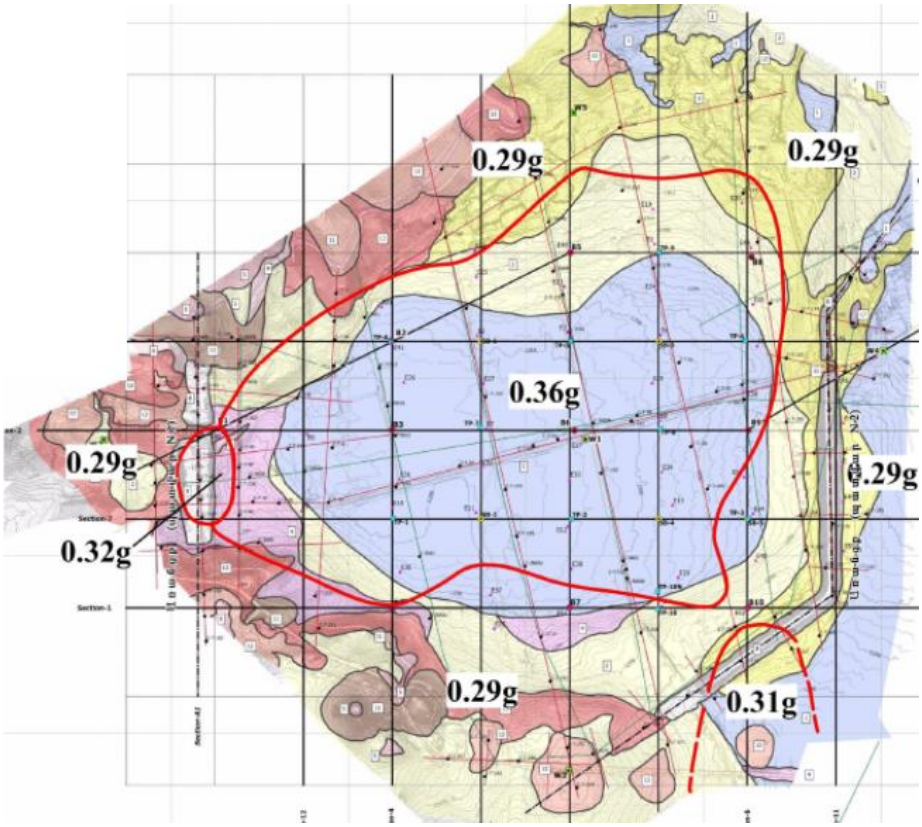

Figure 5. Seismic microzonation map

3. CONCLUSIONS

First stage conclusions

- For the accurate assessment of initial seismic hazard on the territory of Yeghvard designed reservoir (according to seismic properties for mid II class ground conditions [3] detailed seismic micro-zoning (DSZ) as well as geologic-geophysical, seismic tectonic and seismological investigations were carried out on R=150km radius area. Based on the results obtained, the baseline seismic hazard on the Yeghvard reservoir area was assessed PGA = 0.36g middle (II class) ground conditions.

Second stage conclusion

- The main engineering-geological sites, characterizing the study area are distinguished. Major attention was paid to the dam site.
- In both cases, geological sections corresponding to O/P-1 observation points were selected as initial or baseline. It is >30 meter Basaltic Andesite Lava for the first dam. For the second it's about three meters thick Moraine Deposit (gravel), which is located on Basaltic Andesite Lava with> 50 meter thickness (fig. 4). For both sections, the baseline seismic intensity is evaluated according to the BC RA norms [3], $PGA(g) = 0.36g \cdot 0.8 = 0.29g$.
- Using the method of engineering-geological analogies as well as recording obtained due to explosions expected seismic increment and corresponding intensity values were

determined. By combining them, the largest values of seismic intensity expected in typical ground conditions were determined. For the second-class ground conditions of the first dam, it is PGA=0.32g. For the second-class ground conditions of the second dam the obtained value is PGA=0.31g.

- The value of the expected seismic intensity for the ground conditions in the installation site of both dam PGA = 0.32g was accepted.
- Recordings of microtremors were made at 14 points in different areas of the study area. Based on these, Fourier spectra were calculated and built by determining the prevailing periods of seismic fluctuations in different ground conditions. The results obtained are presented in Table 3, Table 4.
- The seismic micro-zoning 1:2000 scale map of the reservoir area was compiled with corresponding acceleration values.

REFERENCES

[1] S.V. Medvedev, *Engineering Seismology*, Nauka, Moscow, Russia (1973).

[2] S.V. Medvedev, *Seismic microzonation*, Nauka, Moscow, Russia (1984).

[3] RA BC II-6.02-2006, *Earthquake Resistance Requirements, Building Codes*, Yerevan, Armenia (2006)

[4] *Recommendations for seismic microzonation in engineering surveys for construction*, Rosstroy USSR, Glavstroy Project, PNIIIS, Moscow, Nauka, (1985).

[5] T.O. Babayan, S.S. Karapetyan. *Development of seismic microzoning and the behavior of the soil-structure system*. Gituitun, NAS RA Yerevan, (2013).

[6] J.Karapetyan, E. Geodakyan, H. Hovhannisyan, S. Karapetyan, G. Mkrtchyan. *Assessment of the expected seismic effects on the territory of Yeghvard reservoir.* Scientific and technical report, IGES NAS RA Funds, Gyumri, Armenia (2016) (in arm. and eng.).

[7] *Engineering-geological and hydrogeological conditions.* State Design Institute "ARMGIPROVODKHOZ" Natural conditions, book1, 2, ("Reservoir on the Hrazdan River (Yeghvard reservoir)", volume IV, Ministry of Meloriation and Water Management of the USSR, Leading Organization "SOYUZVODPROEKT", Yerevan, (1985).

[8] *Regional catalog IGES NAS RA, Gyumri, Armenia.*

[9] *Regional catalog NSSZ, Gyumri, Armenia.*

[10] A.Godzikovskaya, *Database Catalog of Caucasus earthquakes from M≥4.0 (K≥11.0) from ancient times to 2000.* Geophysical Center Russian Academy of Sciences. Moscow, Russia http://zeus.wdcb.ru/wdcb/sep/caucasus/catrudat.html

[11] *Database of the European Mediterranean Seismic Center* (EMSC). https://www.emsc-csem.org.

[12] N.V. Kondorskaya and N.V. Shebalin, *New Catalog of Strong Earthquakes in USSR From Ancient Times Trough, (1977)*. World Data Center A for Solid Earth Geophysics, Boulder, Colorado, USA, July 1982.

[13] T.O. Babayan. *Atlas of Strong earthquakes of the Republic of Armenia, Artsakh and Adjacent Territories From Ancient Times Through 2003*.Gyumri, Armenia, (2006).

[14] M. Berberian. *Natural hazards and the first Earthquake Catalogue of Fram.Vol.1;Historical Hazards in Iran Prior to 1900*. UNESCO, IIEES, JDNDR. Iran (1994).

[15] M. Berberian. *Seismic Sources of the Transcaucasian Historical Earthquakes, map M 1:1000000,* Najarian Associates Engineers, Planners, Scientists Surveyors, New Jersey, Kluwer Ac. Pub. (1996).

[16] N.V. Shebalin and R.E. Tatevosian. *Catalog of large historical of the Caucasus.Historical and Prehistorical Earthquakes in the Caucasus*. Kluwer Academic Publishers, (1997).
[17] S.A. Pirousian et al. *The Catalog of strong earthquakes in the territory of Armenia and adjacent regions.* Historical and Prehistorical Earthquakes in the Caucasus. Kluwer Ac. Pub. (1997).
[18] N.N. Ambraseys and C.P. Melville. *A History of Persian Earthquakes*, Cambridge University Press, London, (1982).
[19] Ergin Kazim and Guglo Ugur, *A Catalog of Earthquakes for Turkey and Surrounding Area (11 A.D. to 1964 A. D) ve Zeki Uz*, Istanbul, (1967).
[20] Ergin Kazim, *A Catalogue of Earthquakes of Turkey and Surrounding Area, (1965-1970)*, EPhE, Istanbul, (1971).
[21] K. Sadich et al. *Attenuation relationships for Shallow crustal earthquakes based on California strong motion data*. Seismol. Res. Lett 68. (1997).
[22] K. Camptell And Bozorgia. *Near-Source attenuation of peak acceleration from worldwide accelerograms recorded from 1957 to 1993*. Procudings Fifth National Conference on Earthguake Engineering EERI.3. (1994).
[23] W. Joyner and D. Boore. *Measurement, characterization and preduction of strong ground motion.* Proc. Earth. Eng. and Soil Dyn.Div. ASSE. vol II GT. (1988).
[24] F.F. Aptikaev. *Strong ground motions during earthquakes*. PhD Dissertation abstract Moscow, (2001).
[25] A.S. Karakhanian, R.A.Haroutiunyan, V.S. Balasanyan, A.O. Assatryan. *Cataloge of strong historical earthquakes in the Armenian Upland.* Georisk, Scientific Research Company Armenia (1998).
[26] A.S. Karakhanian, R.T. Djrbashian, V.G. Trifonov, H. Philip, S. Arakelian, A.V.Avagian,. *Holocene-historical volcanism and active faults as natural risk factor for Armenia and adjacent countries.* Journal of Volcanology and Geothermal Research. (2002).
[27] A.S. Karakhanian, V.G. Trifonov, H. Philip, A.Avagyan et al. *Active faulting and natural hazards in Armenia, Eastern Turkey and north-western Iran*. Tectonophysics (2004).
[28] J.-F. Ritz, A. Avagyan, M. Mkrtchyan, H. Nazari, P.-H. Blard, A. Karakhanian et al. *Active tectonics within the NW and SE extensions of the Pambak-Sevan-Syunik fault: Implications for the present geodynamics of Armenia.* ARTICLE IN PRESS. Quaternary International xxx, (2015).

Seismic design and safety aspects of dams subjected to aftershocks and multiple earthquakes

Martin Wieland[1] and Sanaz Ahlehagh[2]

[1] Chairman, ICOLD Committee on Seismic Aspects of Dam Design,
Poyry Switzerland Ltd., Herostrasse 12, CH-8048 Zurich, Switzerland
e-mail: martin.wieland@poyry.com

Keywords: Dams; Multiple earthquakes, Aftershocks, Ground motion model, Earthquake safety of dams, Seismic analysis of dams

Abstract. *Depending on local geological and tectonic conditions, strong aftershocks may occur after a major earthquake and the seismicity in the region may remain high for days or months. Besides main shock and aftershocks, dams may be subjected to several earthquakes during their long service life, especially in regions of high seismicity. The seismic design aspects of large dams subjected to strong aftershocks, or multiple earthquakes are discussed. In the case of a dam weakened by an earthquake, when there are threats of aftershocks or when there are doubts about the seismic safety of a dam, the safety can be increased by lowering of the reservoir. In the analysis of aftershocks and multiple earthquakes the time between events may play an important role as rainfall after an earthquake may reduce the static stability of cracked embankment dams or due to blockage of the drainage or damage of the grout curtain the full uplift pressure may develop under a concrete dam, reducing the static safety of the dam and increasing the earthquake vulnerability. Moreover, the rockfall or landslide hazard may increase, if an aftershock occurs during or after a period of extensive rainfall. The focus of this paper is on ground shaking. In general, aftershocks are a problem, when the static safety has decreased after the main shock. In this case the seismic safety check may consist of two separate analyses, i.e. one for the main shock and the second for the main aftershocks, taking into account decreased strength properties. When no static safety deterioration has taken place after the first shock then effects of aftershocks and multiple earthquakes can be accounted for in the dynamic analyses by simply extending the duration of strong ground shaking of the safety evaluation earthquake. This extended acceleration time history is a model of the ground shaking and not a real one, but using such a model the damage accumulated by the main and aftershocks or multiple earthquakes can be determined. Finally, the seismic safety aspects of dams built in areas, where strong earthquakes have occurred in the past, are discussed.*

1 INTRODUCTION

Depending on local geological and tectonic conditions, strong aftershocks may occur after a major earthquake and the seismicity in the region may remain high for days or months. Besides main shock and aftershocks, dams may be subjected to several earthquakes during their long service life, especially in regions of high seismicity. The seismic design aspects of

[2] Senior Engineer, Poyry Switzerland Ltd. Tehran Branch, Tehran, Iran
e-mail: sanaz.ahlehagh@poyry.biz

large dams subjected to strong aftershocks, or multiple earthquakes are discussed. In the case of a dam weakened by an earthquake, when there are threats of aftershocks or when there are doubts about the seismic safety of a dam, the safety can be increased by lowering of the reservoir. In the analysis of aftershocks and multiple earthquakes the time between events may play an important role as rainfall after an earthquake may reduce the static stability of cracked embankment dams or due to blockage of the drainage or damage of the grout curtain the full uplift pressure may develop under a concrete dam, reducing the static safety of the dam and increasing the earthquake vulnerability. Moreover, the rockfall or landslide hazard may increase, if an aftershock occurs during or after a period of extensive rainfall. However, in this paper the focus is on ground shaking.

In general, aftershocks are a problem, when the static safety has decreased after the main shock. In this case the seismic safety check may consist of two separate analyses, i.e. one for the main shock and the second for the main aftershocks, taking into account decreased strength properties. When no static safety deterioration has taken place after the first shock then effects of aftershocks and multiple earthquakes can be accounted for in the dynamic analyses by simply extending the duration of strong ground shaking of the safety evaluation earthquake. This extended acceleration time history is a model of the ground shaking and not a real one, but using such a model the damage accumulated by the main and aftershocks or multiple earthquakes can be determined.

In dams and other structures, the damage generally depends on the duration of strong ground shaking or the number of relevant load cycles. For example, the damage of reinforced concrete or steel structures can be described by low-cycle fatigue models. In this case the aftershocks or multiple earthquakes increase the number of equivalent load cycles and thus contribute to the low cycle fatigue damage. A similar situation is encountered when trains are crossing a steel bridge, where the number of train passages contributes to the fatigue damage. This well established concept can be used for the seismic safety assessment of dams, which is discussed in this paper.

2 OVERVIEW ON SEISMIC DESIGN AND PERFORMANCE CRITERIA FOR LARGE DAMS

2.1 Overview on current seismic analysis aspects

In this Section an overview on the different seismic analysis aspects are given, which represent the current state-of-the-art for large storage dams. The basis is ICOLD Bulletin 148 “Selection of Seismic Parameters for Large Dams” [1]. The design criteria are the prerequisites for any dynamic analysis and the performance criteria and the analysis of failure modes are required for the safety assessment of dams under different types of design earthquakes. Today, the dynamic analyses of dams are carried out in the time domain using acceleration time histories as an input. Various assumptions have to be made in obtaining such time histories, therefore, they are not real earthquake ground motions but models of the ground motion, a concept usually used for civil structures subjected to different live load scenarios [2]. The methods of dynamic analyses, the finite element modelling of the dam-reservoir-foundation system and the different material models are not discussed as they are the same for main shock-aftershock analyses.

It should also be pointed out that seismic safety assessments must be carried out repeatedly during the long lifespan of dams, as all items discussed in the following Sections may change with time and new earthquake data etc. may become available.

2.2 Seismic design criteria

According to [1] two levels of earthquakes have to be considered for the design of large storage dams, i.e.:

- Operating Basis Earthquake (OBE): The OBE may be expected to occur during the lifetime of the dam. No damage or loss of service must happen. It has a probability of occurrence of about 50% during the service life of 100 years. The return period is taken as 145 years [1]. The OBE ground motion parameters are estimated based on a probabilistic seismic hazard analysis. The mean values of the ground motion parameters of the OBE can be taken.
- Safety Evaluation Earthquake (SEE): The SEE is the earthquake ground motion a dam must be able to resist without uncontrolled release of the reservoir. The SEE is the governing earthquake ground motion for the safety assessment and seismic design of the dam and safety-relevant elements (gates and valves of spillways and bottom outlets, motors, emergency power supply, hydraulic pistons, etc.), which have to be functioning after the SEE in order to control the water level in the reservoir.

For the safety evaluation of existing dams, only the SEE ground motion is used.

2.3 Seismic performance criteria for large dams and safety-critical elements

In the past, when the pseudo-static analysis method was used and the earthquake ground motion was characterized by a seismic coefficient – this method is obsolete and shall no longer be used for large dams [2] - the main performance criteria for concrete dams were allowable stresses and sliding and overturning safety factors and for embankment dams it was the sliding stability of critical slopes [3] [4]. Today, the seismic performance criteria of dams are given in a rather general way for both the OBE and SEE, which are very different from those used in the past. This creates problems to engineers, who were used to work with well-defined allowable stresses and sliding and overturning safety factors.

The following criteria apply for the OBE:

(i) Dam body and foundation: No structural damage in dam is accepted; the safety-relevant elements must remain functioning.

(ii) Safety-relevant components and equipment (gated spillways, bottom outlets) shall be fully operable after the OBE and therefore should behave elastically during the OBE.

The following criteria apply for the SEE:

(i) Dam body and foundation: The reservoir must be retained safely, structural damage (cracks, deformations, leakage etc.) are accepted as long as the stability of the dam is ensured and no large quantities of water are released from the reservoir causing flooding in the downstream region of the dam.

(ii) After the SEE the reservoir level must be controlled and it must be possible to release a moderate flood by the spillway or low level outlet(s), which must remain functioning.

(iii) After the SEE it should be possible to lower the reservoir for repair of earthquake damage, and/or to increase the safety of a dam, if there are doubts about its static or seismic safety after an earthquake or other incidents.

(iv) Safety-relevant components and equipment (gated spillways, bottom outlets) must be fully operable after the SEE. Minor distortions and damage (e.g. leakage of seals of gates) are accepted as long as they have no impact on the proper functioning of the components and equipment. This means that all gates, valves, motors, control units, power supply and emergency power generators

for the spillway and low level outlets must withstand the SEE ground motions and they must be functioning after the SEE, i.e. the equipment shall be properly anchored etc. This is a new requirement of ICOLD [1], which concerns hydro-mechanical and electro-mechanical engineers, who may not have been fully aware of their importance in the seismic safety of dams.

The OBE performance criteria can be verified by dynamic linear-elastic stress and deformation analyses - usually time history analyses -, and by rigid body sliding (and overturning) stability analyses using the peak acceleration acting in the centre of gravity of the sliding mass [3]. The safety criteria are given in terms of allowable stresses, deformation (e.g. crack width) and allowable sliding stability safety factor for the OBE load combination. The safety criteria are basically the same as those used in pseudo-static analyses, however, the pseudo-static method has been replaced by a linear dynamic analysis, and the seismic coefficient has been replaced by the peak acceleration acting on the moving mass.

The SEE performance criteria for the dam body will require a nonlinear dynamic analysis as discussed in the subsequent Section. These analyses must all be done in the time domain, requiring the seismic input in the form of acceleration time histories. The main results required for the safety checks are the inelastic deformations of the dam after the earthquake. The basis of the safety checks are the failure modes of embankment and concrete dams as discussed below.

2.4 Seismic failure modes of concrete and embankment dams

The main seismic failure modes of embankment dams are as follows [3] [4]:

- Overtopping of rockfill dam due to (i) malfunction or blockage of spillway gates (overtopping will occur after the earthquake), (ii) excessive seismic settlements of embankment dams, causing overtopping, or (iii) mass movements into the reservoir, causing impulse waves and overtopping of the dam crest.
- Internal erosion due to (i) insufficient protection of core of earth core rockfill dams, (ii) sliding movements of slopes or fault movements in the dam footprint that exceed the thickness of the fine sand filter, or (iii) damage of the contact between the core, abutment rock, concrete structures or conduits through the dam body (due to settlements, poor compaction etc.).

For concrete gravity dams and buttress dams the main seismic failure modes due to ground shaking are as follows [3]:

- Sliding of concrete block along discontinuities in foundation rock or along the dam-foundation contact (sliding in downstream direction).
- Local sliding stability of concrete blocks near the dam crest (sliding in downstream direction along lift joints).

For concrete arch and arch-gravity dams the main failure modes due to ground shaking are as follows [3]:

- Global sliding of dam or different blocks along discontinuities in foundation rock or along the dam-foundation contact (sliding in downstream direction).
- Local sliding stability of concrete blocks near the dam crest (sliding in upstream direction along lift joint; due to the dam geometry, block sliding movements are larger for empty reservoir than for full reservoir).
- Crushing of concrete in thin arch dams under high seismic compressive stresses in arch direction (spalling of concrete and loss of bearing capacity in arch direction).

For other types of dams, other failure modes have to be considered. This applies mainly to earth dams, concrete face rockfill dams, asphalt core or asphalt surface dams, dams on soil foundation, dams on problematic foundations (dissolution of material, liquefaction, etc.).

The main structural failure modes can be checked based on dynamic stability analyses of slopes of embankment dams, sliding blocks of concrete dams or wedges in the dam abutments.

2.5 Ground motion models for seismic analysis of dams

For the seismic analysis and safety checks, time history analyses are needed, which require the seismic input in form of acceleration time histories. These time histories are not physically correct earthquake records but are models of the earthquake ground motion as discussed by Wieland [5].

According to [1], the following aspects of the 'design acceleration time histories' should be considered:

- The three components of the spectrum-matched acceleration time histories must be statistically independent.
- The acceleration time histories of the horizontal earthquake components may be assumed to act in along river and across river directions. No modifications in the horizontal earthquake components are needed if they are applied to other directions, i.e. directivity effects can be neglected.
- The duration of strong ground shaking shall be selected in such a way that aftershocks are also covered, i.e. records with long duration of strong ground shaking shall be selected.
- In the case of dams that are susceptible to damage processes, which are governed by the duration of strong ground shaking such as, e.g., the build-up of pore pressures, earthquake records with long duration of strong ground shaking shall be used. The duration of strong ground shaking depends on the magnitudes of the worst case earthquake scenarios for a particular dam site. Empirical relations or recommendations in seismic codes or guidelines may be used as a reference.
- For the safety check of a dam at least three different earthquakes shall be considered for the SEE ground motion.

Moreover, in the seismic analysis, spatial variation of the ground shaking is neglected, as no such information is available for most dam projects in the foreseeable future.

Using ground motion models will result in a safe dam design. It is important that this is also understood by earth scientists involved in seismic hazard studies for large dams.

The concept of ground motion models is the basis for the practical assessment of the seismic safety of dams subjected to strong aftershocks or multiple earthquakes. The main factor being the duration of strong ground shaking as discussed in the subsequent Section.

3 SEISMIC DAMAGE OF CONCRETE AND EMBANKMENT DAMS

Several dams have been damaged by strong earthquakes. Concrete dams have experienced cracking and joint movements and embankment dams have experienced inelastic deformations and different types of cracking as shown in Fig. 1.

Sliding movements of concrete dams may damage the grout curtain and drainage system causing changes in the uplift pressures along sliding surfaces. Damage of waterstops and cracks will allow water seeping into joints and cracks at the upstream dam face etc. Open cracks in embankment dams may be subject to water infiltration during rainfall after an earthquake.

These may be some of the important changes, which may take place between the time of the earthquake and the largest aftershocks or between two subsequent earthquakes.

Figure 1: Crack in Sefid Rud buttress dam caused by the 1990 Manjil earthquake in Iran (left) and cracks in embankment dam covered by plastic sheets following the 2008 Wenchuan earthquake in China (right)

4 GROUND MOTION MODEL FOR AFTERSHOCKS OR MULTIPLE SEISMIC EVENTS

As discussed in the previous Section, water may cause changes in the pore pressure distribution and uplift forces in dams, which experienced inelastic deformations and cracking during strong earthquake. Moreover, the strength properties along sliding surfaces may decrease and approach residual strength values, depending on the size of movements.

These are the main physical changes that may take place after an earthquake. If no changes occur in the water regime within the dam, the effect of aftershocks and multiple earthquakes can accounted for in the seismic analysis and safety assessment of a dam, by simply extending the duration of strong ground shaking in the seismic ground motion model discussed in Section 2.5. It is assumed conservatively that the acceleration response spectra of the aftershock and multiple seismic events are the same as that of the main earthquake. In the case of the main aftershocks, whose magnitude is about 0.5 to 1.0 smaller than that of the main shock, the duration of strong ground shaking of the aftershock will be shorter than that of the main shock. This duration of strong ground shaking is then added to that of the main shock. This can be considered as a conservative assumption.

In the case where between the main shock and aftershock or between multiple seismic events physical changes are anticipated, then independent analyses for all events would be needed. Again, ground motion models should be used for the conservative analysis of such scenarios.

As water has a negative effect on the seismic safety of a damaged dam, it is necessary to lower the reservoir, if low level outlets are provided, and to cover open cracks by plastic sheets as shown in Fig. 1. Covering of cracks, will prevent intrusion of surface water and lowering of the reservoir will increase the safety of the dam and will reduce the amount of water that could be released in the case of the accidental failure of a dam. Therefore, the provision of low level outlets is an effective mean to reduce the seismic risks of dams.

5 EXAMPLE: DYNAMIC SLIDING STABILITY OF GRAVITY DAM

To illustrate the effect of aftershocks and multiple earthquakes, the sliding movements of a gravity dam for different seismic scenarios are calculated. In this analysis the following assumptions are made:

(i) only the horizontal earthquake component is considered,
(ii) the sliding movement will occur along the dam-foundation contact,
(iii) the reservoir is full and the grout curtain is working at the time of the main shock,
(iv) residual shear strength with zero cohesion is assumed along the sliding surface with a friction coefficient of 0.7, and
(v) the duration of strong ground shaking of the aftershock is taken as 1/3 of that of the main shock, i.e. 7 s.

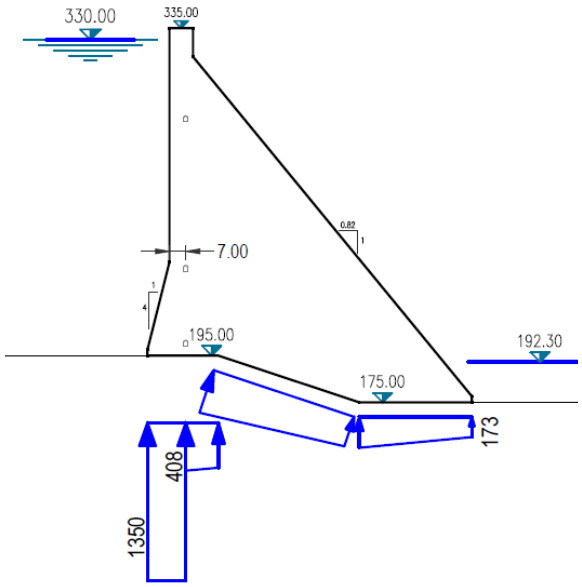

Figure 2: Cross-section of gravity dam used in dynamic sliding stability analysis with uplift pressure in kPa and elevations in m

The analysed scenarios of main shock-aftershock and multiple earthquakes are as follows:

1. Main shock-aftershock scenario with extended duration of strong ground shaking without uplift and residual friction coefficient of 0.7.
2. Main shock-aftershock scenario with extended duration of strong ground shaking with normal uplift (residual friction coefficient of 0.7).
3. Main shock with normal uplift followed by 7 s long aftershock with normal uplift (residual friction coefficient of 0.7).
4. Main shock with normal uplift and residual friction coefficient of 1.0 followed by 7 s long aftershock with uplift increased by 50% and residual friction coefficient of 0.7.
5. Main shock followed by other main shock without uplift and residual friction of 0.7
6. Main shock followed by other main shock with normal uplift and residual friction of 0.7.
7. Main shock with normal uplift and residual friction of 1.0 followed by another main shock with uplift increased by 50% and residual friction of 0.7.

The scenarios 4 and 7 with the uplift increased by 50% after the main shock represent the possible damage of the drainage system due to sliding movements.

The main shock-aftershock scenarios 1 and 2 are applicable, if the aftershock occurs within a short period after the main shock and the uplift pressure in concrete dams or the water pressure in embankment dams affected by rainfall (see Fig. 1 with protection of cracks by plastic sheets to prevent infiltration of rain water in the cracked dam) will remain unchanged.

Figure 2 shows the geometry of the gravity dam with the distribution of the uplift pressure at the dam-foundation contact. In this figure the reservoir water level and the tail-water level are also shown. The effects of the grout curtain and drainage system are taken into account, assuming an efficiency of 70%, which is usually assumed in the design.

The sliding movements of the dam are analysed with computer program RS-DAM [6].

The analysed load combination includes dead load of the dam, hydrostatic pressure for full reservoir and earthquake ground motion. The hydrodynamic pressure is represented by an added mass according to Westergaard, assuming incompressible water in the reservoir.

The acceleration time histories applied to the base of the dam, according to the scenarios 1 to 7 discussed above, are illustrated in Figs. 3 to 5. The peak ground acceleration (PGA) of the main shock is 0.67 g the duration of the earthquake is 35 s. The effects of the aftershock are idealized by a 7 s long record of strong ground shaking taken from another acceleration time history with the same characteristics (acceleration response spectrum) as the main shock. The second main shock in the multiple earthquake scenarios is also assumed to have the same dynamic characteristics (acceleration response spectrum and duration) as the main shock.

It is important to note that these earthquake time histories are not ground motions from real earthquakes. They represent idealized models of ground motions, which are used by dam engineers for the evaluation of the seismic safety of the dam. For that purpose, there is no need to calculate the dynamic behaviour of the dam accurately. Of importance is the analysis of the worst case failure scenario of the dam, which is the sliding stability. In the present example only the sliding movement along the dam-foundation contact is analysed, however, sliding movements of detached concrete blocks close to the dam crest are more critical than the base sliding as discussed in [7].

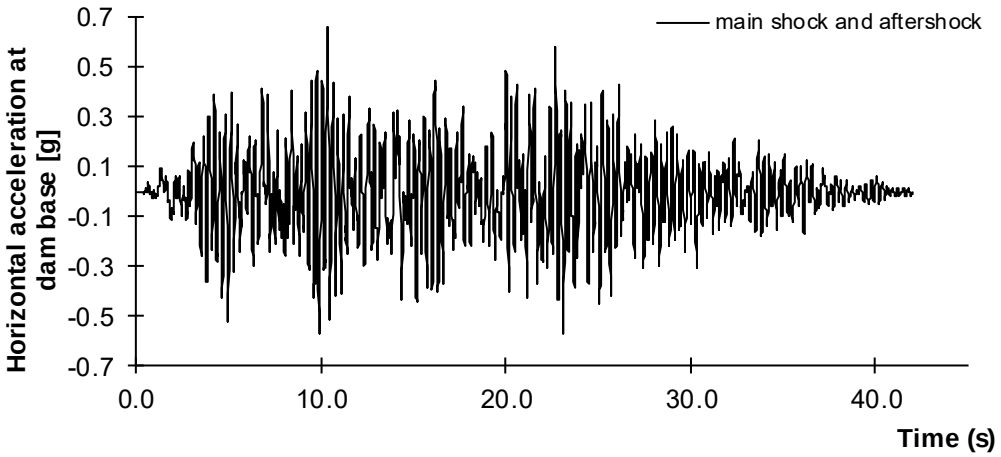

Figure 3: Horizontal acceleration time history at dam foundation: Duration of strong ground shaking extended by 7 s to account for aftershock

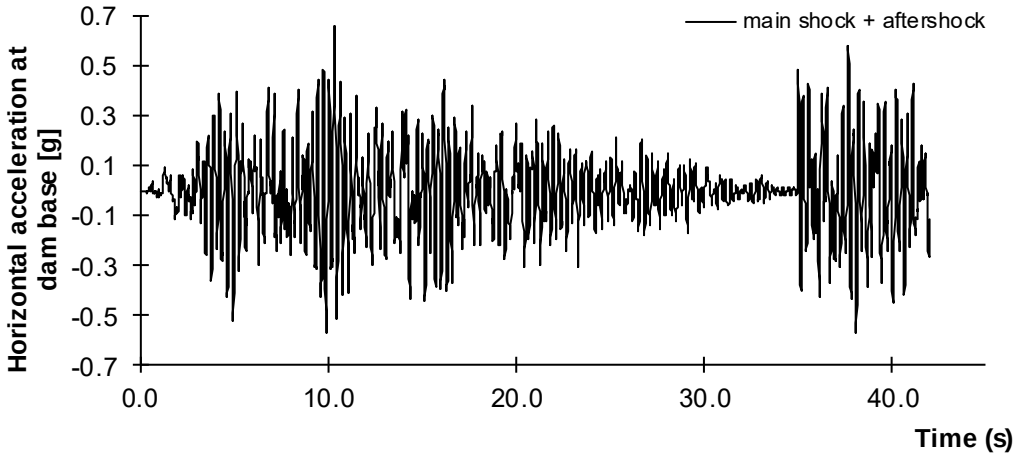

Figure 4: Horizontal acceleration time history at dam foundation: Idealized aftershock represented by 7 s of strong ground shaking inserted after the main shock

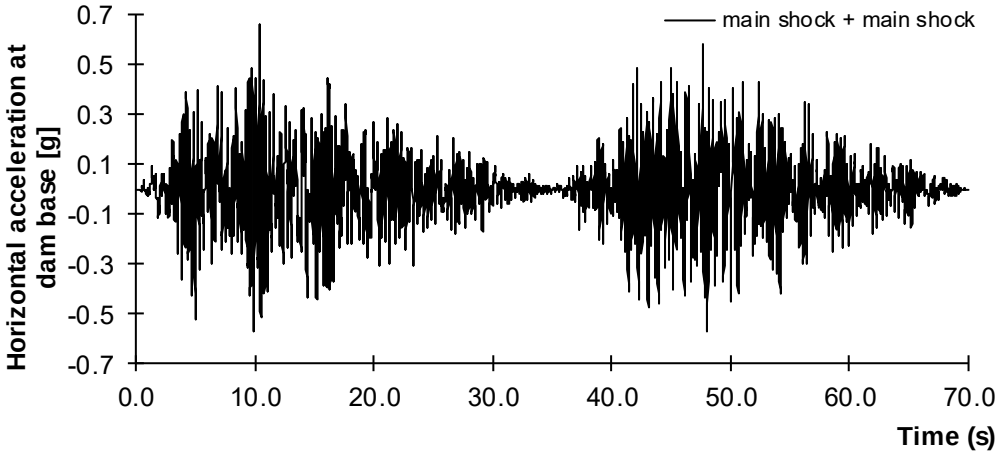

Figure 5: Horizontal acceleration time history at dam foundation: Multiple earthquakes idealized by two main shocks following each other

Time histories of cumulative sliding displacements of the gravity dam are shown in Figs. 6 and 7 for earthquake scenarios 1 to 4 and 5 to 7, respectively.

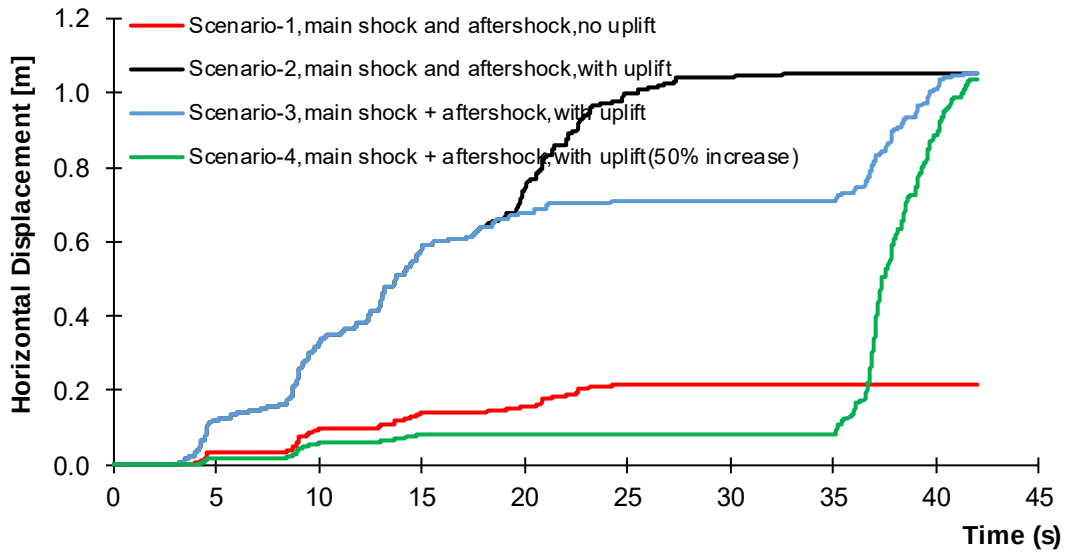

Figure 6: Sliding displacement of gravity dam for main shock-aftershock scenarios 1 to 4

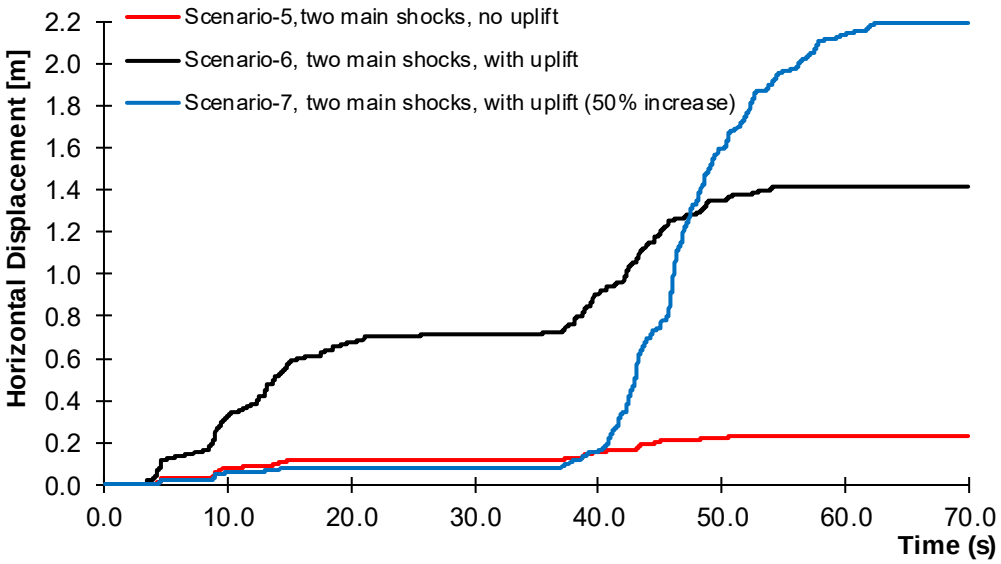

Figure 7: Sliding displacement of gravity dam for scenarios 5 to 7: Two main shocks following each other

The sliding displacements of the seven earthquake scenarios shown in Figs. 5 to 7 are given in Table 1. It is obvious that when the uplift pressure is increased or the friction coefficient is decreased, the cumulative sliding movement of the gravity dam in downstream direction is increased. The sliding movements would become very large, if the static sliding stability safety factor is approaching 1.0.

A sensitivity analysis is performed on the amount of increase in uplift pressure during the second main shock. Normal uplift with friction coefficient of 1.0 is assumed for the first main shock. In the second main shock residual friction coefficient of 0.7 is considered and uplift is increased by 0%, 25%, 50% and 75%. The resulting residual displacement are 0.8 m, 1.25 m, 2.2 m and 5.15 m, respectively. In this analysis by 25% increase in uplift, residual displacement increases by about 60% which shows the significant effect of uplift on dam stability.

The dynamic sliding stability analyses were carried out for one set of earthquakes, however, for the safety assessment of dams according to ICOLD [1], at least three different earthquakes shall be analysed for each of the 7 scenarios discussed above. But as the main objective of this paper is to discuss the effect of different earthquake scenarios on the sliding movement, the analysis of three different earthquake records is not required.

Table 1: Summary of sliding movements for different earthquake scenarios (Normal uplift means uplift pressure distribution according to Fig. 2)

	Main shock		Aftershock/2nd main shock		Sliding displacement (m)		
	uplift	Friction coefficient	uplift	Friction coefficient	Total	end of first main shock	due to aftershock or second main shock
Scenario-1	without	0.7	without	0.7	0.217	-	-
Scenario-2	with (Normal)	0.7	with (Normal)	0.7	1.052	-	-
Scenario-3	with (Normal)	0.7	with (Normal)	0.7	1.054	0.712	0.342
Scenario-4	with (Normal)	1.0	with (50% increase)	0.7	1.038	0.082	0.957
Scenario-5	without	0.7	without	0.7	0.227	0.120	0.107
Scenario-6	with (Normal)	0.7	with (Normal)	0.7	1.419	0.713	0.707
Scenario-7	with (Normal)	1.0	with (50% increase)	0.7	2.198	0.082	2.116

6 CONCLUSIONS

Based on the discussions made in this paper, the following conclusions can be made regarding the analysis of the effects aftershocks and multiple earthquakes on the safety of dams:

1. Aftershocks may have dynamic characteristics that are different from those of the main shock and the magnitude of the strongest aftershock may 0.5 to 1.0 magnitudes less than that of the main shock.
2. Aftershocks following strong earthquakes or multiple earthquakes that have not caused any important cracks or sliding movements, the effect of these earthquakes can be accounted for in the seismic analysis and conservative seismic safety assessment of dams by extending the duration of strong ground shaking. For aftershocks the duration of strong ground shaking should range from 5 s to about 1/3 of the duration of strong ground shaking of the main shock.
3. The downstream sliding displacement of the gravity dam is increased, when the uplift pressure is increased or the friction coefficient is decreased.
4. The sliding movements would become very large, if the static sliding stability safety factor is approaching 1.0.
5. The dynamic sliding stability analysis of a gravity dam can be carried out by a simple rigid body analysis.
6. The modelling of the aftershock by extending the duration of strong ground shaking of the main shock by about 1/3 provides conservative displacement values, when the uplift and friction properties remain unchanged. If these values are different in the time of the aftershock main shock and the idealized aftershock must be analysed separately.
7. For multiple earthquakes the same assumptions apply as in item 5 above when the uplift and friction properties remain unchanged. This is the usual situation as two main shocks may occur with a large time gap. If the dam is damaged, then the damage could be repaired or the reservoir could be lowered to increase the safety of the damaged dam. Lowering of the reservoir will also reduce the effects of aftershocks if time is sufficiently long between the main shock and the strongest aftershocks.

These conclusions and recommendations are made from the engineering point of view and apply to new and existing dams, where for the safety checks models of earthquake ground motion are used, which are not real earthquake ground motions, but allow a proper safety assessment of the dam as used in standard practice in the design of civil structures subjected to variable live loads [5]. This means that an accurate model of the aftershock acceleration time history is not required by the dam engineer.

REFERENCES

[1] ICOLD (2016) Selecting seismic parameters for large dams, Guidelines, Bulletin 148, Committee on Seismic Aspects of Dam Design, International Commission on Large Dams (ICOLD), Paris.

[2] Wieland, M. (2018) Application of pseudo-static sliding stability analysis in seismic design and safety evaluation of embankment dams, Proc. 16th European Conf. on Earthquake Engineering, Thessaloniki, Greece, June 17-21.

[3] Wieland, M. (2019) Seismic design and performance criteria for large dams and methods of dynamic analysis, Proc. International Dam Safety Conference – 2019, Bhubaneswar, Odisha, India, 13-14 February 2019

[4] Wieland, M. and Brenner, R.P. (2015) Performance criteria for rockfill dams subjected to multiple seismic hazards, Q98, R.16, Proc. 25th Int. Congress on Large Dams, ICOLD, Stavanger, Norway, June 13-20.
[5] Wieland, M. (2018) Models of earthquake ground shaking used in seismic design and safety checks of large dams, Int. Journal of Civil Engineering, doi.org/10.1007/s40999-018-0339-3, June 2018
[6] Leclerc, M., Leger, P. and Tinawi, R. (2002) RS-DAM user's manual, University of Ecole Polytechnique of Montreal, Canada, Nov. 2002, www.struc.polymtl.ca/rsdam/
[7] Wieland, M. and Ahlehagh, S. (2013) Dynamic stability analysis of a gravity dam subject to the safety evaluation earthquake, Proc. 9th Symposium of ICOLD European Club IECS2013, Venice, Italy, April 10-13, 2013

ICOLD benchmark workshops to compare models for seismic analyses

Guido Mazza'[1], Gerald Zenz[2], Massimo Meghella[1], Edwin Staudacher[2]

Ricerca sul Sistema Energetico S.p.A.
Via Rubattino, 54, Milan, Italy
E-mail: guido.mazza@rse-web.it

Keywords: Dams; FEM analysis; Concrete; Seismic hazard; Dynamic monitoring.

Abstract. ICOLD in 1988 decided to appoint the Committee *Computational Aspects of Analysis and Design of Dams* with the aim to contribute to the diffusion of computer software in the field of dam engineering and to fill the gap existing between the specialists of mathematical modelling and dam designers, authorities, and managers. As a matter of fact, numerical modelling represents nowadays a key tool for dam engineers to perform efficiently the design making process, the construction stage as well as the whole operational dam life until the possible decommissioning phase. The activities of the Committee have contributed to make fully accepted the numerical models in the engineering practice. The present paper, after a general introduction on the benchmark workshop activities, focuses on a case-study proposed and analyzed during the 12th benchmark held in Graz (Austria).

1 INTRODUCTION

When ICOLD, the International Commission on Large Dams, appointed in 1988 the *ad hoc* Committee *Computational Aspects of Analysis and Design of Dams*, converted as a permanent Technical Committee in 2005 with the aim to fill the gap existing between the specialists of mathematical modelling and dam designers, authorities, and managers and to contribute to the diffusion of computer software in the field of dam engineering.

Today and future activities of the Committee are oriented towards:

- Creating a stronger link between the observed dam behavior and the modelling process with the aim to contribute to the preservation and maintenance of existing dams;
- Promoting mathematical modelling improvements to approach safety-related problems that cannot at present be properly analyzed;

- Issuing guidelines to be used for educational purposes in the current practice. The Committee is strongly committed to contribute in the process of a suitable transfer of experience, skill and knowledge across generations.

[2] Graz University of Technology - Austria, e-mail: gerald.zenz@tugraz.at

The work done by the Committee during its long activity has given rise to the issuing of three Technical Bulletins [1][2][3].

Moreover, the Committee has promoted the organization of benchmark-workshops (BWs), with the aim to guide dam engineers in the correct use of computer programs and the interpretation of results obtained using numerical modelling. The benchmarking program started in Bergamo (Italy) in 1991, continued up to 2017 with the 14th workshop held in Stockholm and will be continued with the 15th benchmark under organization in Milan, 9th – 11th September 2019.

The benchmarking activities represent a reference for the whole dam community, and in particular for young engineers engaged in the challenging task of dam safety assessment and design. Such examples can be taken as part of the master education program at the universities. The problem description together with input data and a concluding report written by the formulator after the benchmark - about individual results and their comparison - is available for further discussions.

Several examples of benchmark workshops deal with seismic induced loading of dam structures. Many of those more recently examined have considered concrete dams. During the benchmark workshops BW10 (2009, Paris), BW12 (2013, Graz), BW13 (2015, Lausanne), BW14 (2017, Stockholm) the following examples related to seismic aspects of analyses of dams were discussed:

BW10 - Theme A: Initial strain and stress development in a thin arch dam considering realistic construction sequence

BW12 - Theme A: Fluid structure interaction arch dam - reservoir at seismic loading

BW13 - Theme A: Seismic Safety Assessment of the Luzzone Arch Dam

BW14 - Theme B: Static and seismic analysis of an arch-gravity dam

In the next paragraph, a focus on a study-case proposed and analyzed during the 12th Benchmark Workshop held in Graz (Austria) in 2013 is deeply discussed.

2 ICOLD BENCHMARK 2013 – FLUID STRUCTURE INTERACION

Theme A, titled “Fluid Structure Interaction, Arch Dam – Reservoir at Seismic Loading” [4] was one of the four themes devoted to the seismic response of an arch dam considering hydrodynamic effects of water in the reservoir due to fluid structure interaction (FSI).

The aim of this example was to gain further knowledge regarding the effects of the different modelling techniques for FSI. Hence, a linear model of a symmetric arch dam with a simplified geometry has been provided to the contributors, to focus on the results of the different modelling approaches, which can be classified in two general types:

- Added mass approach according to Westergaard [5] or Zangar [6].
- Discretisation of the fluid domain using acoustic or fluid finite elements which are coupled to the structural domain.

If the fluid domain is modelled with the above-mentioned types of finite elements, further boundary conditions have to be applied, such as zero pressure at the free surface of the water body as well as reflecting or non-reflecting boundary conditions at the bottom and at the back end of the reservoir. Therefore, the engineers have to make some assumptions related to these additional boundary conditions.

The formulators defined the geometry and two meshes (a coarse and fine) of a 220 meters high arch dam, the foundation body and reservoir, as shown in Figure 1. Furthermore, material parameters, acceleration time histories together with general specifications regarding damping, applied loads and boundary conditions have been defined.

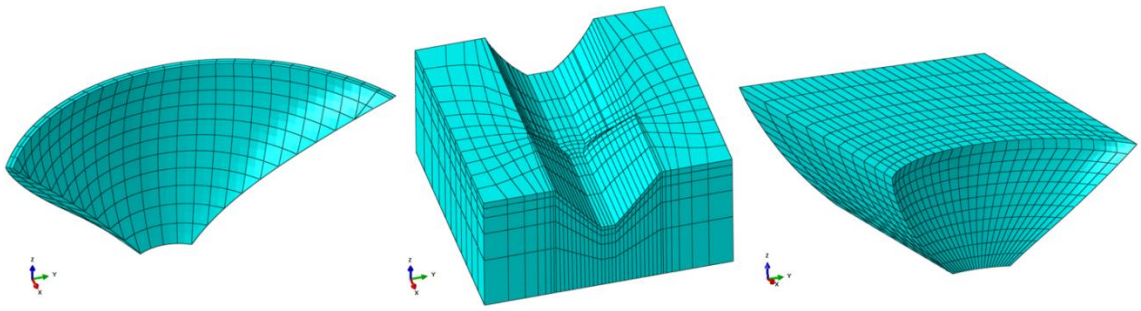

Figure 1: Provided mesh (coarse) of the dam, foundation and reservoir

The contributors were asked to conduct analyses such as evaluating the first ten natural frequencies and corresponding mode shapes as well as the minimum and maximum envelopes over time of displacements and stresses for static and dynamic load cases, at three different cross sections of the arch dam (

Figure 2).

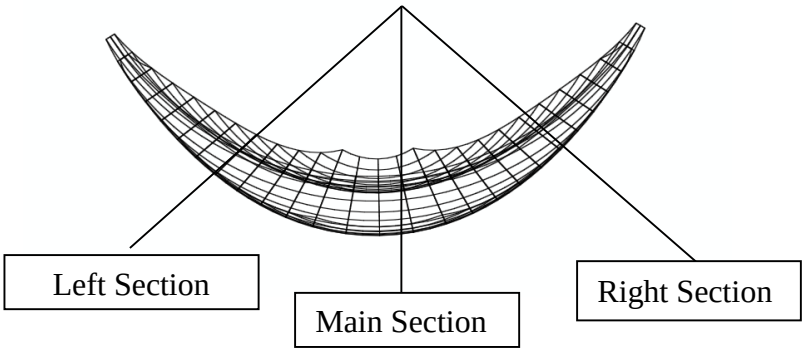

Figure 2: Plan view on dam structure and indication of evaluation sections

Finally, 11 participants presented their results in Graz, which were later on compared to each other and to the reference solution provided by the formulators. In total seven different, commercial and open - source finite element software packages were used to obtain the requested results. Four of the participants used the added mass approach according to Westergaard or Zangar, the other participants modelled the FSI by using acoustic elements to discretize the fluid domain.

2.1 Discussion of results

In general it can be said that the comparison of the natural frequencies showed a good agreement, especially for the lower frequencies of the first two modes, with slightly lower

frequencies in the cases were the added mass approach has been used. Beginning with the third mode, deviations of some results can be noticed.

The comparison of deformations and stresses along the upstream and downstream surfaces in the defined cross sections, showed that there is a significant spread of the individual results, especially when the results of static and dynamic loads are superimposed. One reason can be found in the fact that some participants accounted for several construction stages dead weight in the calculation of the static load case.

The way how the hydrodynamic effects in the seismic load case are accounted for, significantly influences the results of this loading situation. If the added mass approach is considered in the numerical model, the hydrodynamic effects are overestimated which leads to more conservative results. If Westergaard's approach is used in its fully frequency dependent formulation, the results show good agreement to those which are obtained by using more elaborated methods.

Even in case of acoustic of fluid elements usage, the results are not closely matching because some additional assumptions are required, like the dampening along the outer boundaries of the acoustic or fluid domain, for instance, the reflection coefficient at the bottom of reservoir and the absorption at the end of the reservoir.

Another factor which influences the results are specific calculation methods, especially for dynamic loading. In this example two participants used the Hybrid Frequency-Time Domain Method (HFTD-Method) which accounts for frequency dependent properties of the fluid domain.

Figure 3 and Figure 4 exemplarily show the results of the hoop (arch) stresses for the main section of the dam plotted against the height of the dam. Letters A to K indicates one of the participant and REF stands for the reference solution. There are three groups of lines, where the ones on the left and right refer to the min. and max. values of the time histories. The group of lines in the middle correspond to the results of the static load case (dead weight and hydrostatic pressure)

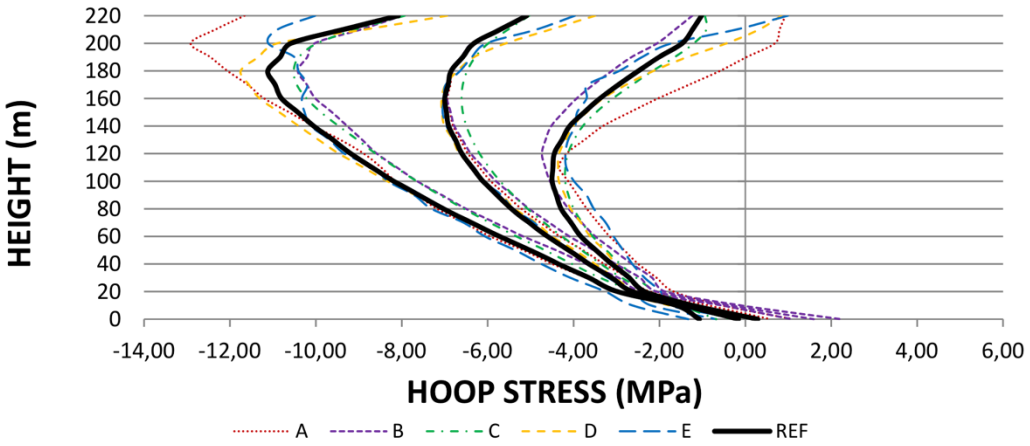

Figure 3: Hoop (arch) stresses at the main section of the dam (upstream) for participants A to E, REF corresponds to the reference solution

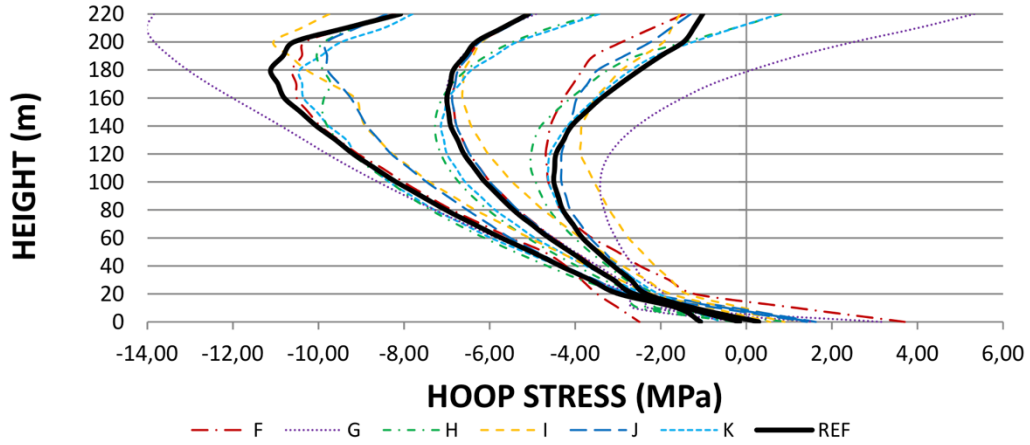

Figure 4: Hoop (arch) stresses at the main section of the dam (upstream) for participants F to K

2.2 Some remarks

Although the geometry of the provided model was idealized (symmetric dam and foundation conditions), the boundary conditions (no non-linearities), material parameters, loads were given for all participants, the individual results varied in a broad range. The reason for these deviations can be found in the different assumptions (e.g. FSI, added mass, reflecting or no reflecting boundary), which have to be made by the engineer who conducts the calculations.

Therefore, the outcomes of this theme, but also of all other themes of past and future Benchmark Workshops, are a valuable contribution for more detailed discussions within the dam engineering community on further modelling assumptions.

3 CONCLUSIONS

During the meetings of the Technical Committee on *Computational Aspects of Analysis and Design of Dams* the following further needs should be formulated and could be included in the next benchmark workshops:

- Especially for **Embankment Dams,** the applicability of material behaviour under dynamic excitation need improvement. Additionally, in the analyses pore water pressure accumulation, seepage and stability analyses need to be coupled.

- For **Concrete Dams,** the simultaneous excitation produces too conservative results. Therefore the system and radiation damping under high acceleration need to be better accounted for in the numerical models. Nonlinear system analysis in the time domain requires more appropriate modelling of the energy radiation behaviour.

From the requirements pointed out above, many formulated benchmark examples and future needs have to be related to simulate the seismic behaviour of dams. Therefore a common workshop with the Committee on Seismic Aspects of dam design was recently held during the ICOLD Congress in Vienna [7]. The e-book and ICOLD Bulletins [7] ÷ [12] deal with design, hazard as well as analysis aspects. The observed dam behaviour during

earthquake together with recorded acceleration time histories are valuable information to carry out back analyses to verify the numerical procedure.

To facilitate the accessibility and critically review the proceedings related to the 14 BWs held so far, a capitalization activity of the tremendous amount of data at disposal has been recently started. The preparation of a new Bulletin to provide a synthesis of the BWs results and comments on the progresses achieved on the numerical modelling methods and the strategies to be used to tackle most of the dam engineering problems is foreseen for the end of 2019.

REFERENCES

[1]. ICOLD -Bulletin-94 (1994): "Computer Software for Dams. Validation".
[2]. ICOLD-Bulletin-122 (2001): "Computational Procedures for Dam Engineering".
[3]. ICOLD-Bulletin-155 (2013): "Guidelines for use of Numerical Models in Dam Engineering".
[4]. M. Goldgruber and G. Zenz, Fluid Structure Interaction, Arch Dam – Reservoir at Seismic loading – Results Comparison. Proceedings of the ICOLD – 12th International Benchmark Workshop on Numerical Analysis of Dams, Austrian National Committee on Large Dams, Graz (2014).
[5]. H.M. Westergaard, *Water Pressure on Dams during Earthquakes*. Transactions of the American Society of Civil Engineers, Vol. 98, Issue 2, 418–472 (1933).
[6]. C.N. Zangar, *Hydrodynamic Pressures on dams due to horizontal earthquake effects*. U.S. Department of the Interior - Bureau of Reclamation, Engineering Monographs No. 11, Denver, Colorado (1952).
[7]. Hydro Engineering Symposium (2018): "Book of Extended Abstracts", ISBN (e-book) 978-3-85125-614-7.
[8]. ICOLD-Bulletin-120 (2001): Design features of dams to effectively resist seismic ground motion
[9]. ICOLD-Bulletin-123 (2002): Earthquake design and evaluation of structures appurtenant to dams
[10]. ICOLD-Bulletin-137 (2011) Reservoirs and seismicity (reservoir-triggered seismicity)
[11]. ICOLD-Bulletin-148 (2016): Selecting seismic parameters for large dams Design Criteria
[12]. ICOLD- Bulletin 166 (2016): Inspection of dams following earthquakes

Machine learning based seismic stability assessment of dams with heterogeneous concrete

F. Salazar[1] and M. A. Hariri-Ardebili[2]

International Centre for Numerical Methods in Engineering (CIMNE)
Gran Capitán s/n, Barcelona, Spain
E-mail: fsalazar@cimne.upc.edu

Keywords: Dams; Seismic Analysis; Probabilistic Risk Assessment; Machine Learning; Random Forests; Random Fields

Abstract. *Nowadays, the probabilistic risk assessment (PRA) is one of the standard tools for safety evaluation of the existing dams. Although many factors are involved in risk-informed condition assessment of infra-structures, a detailed numerical simulation plays the key role. A comprehensive numerical model usually includes the interaction of the dam with foundation and reservoir, nonlinearity of the concrete, and appropriate seismic wave propagation. Often, the concrete is assumed to be a homogenous material which facilitates the transient simulations. However, in reality, the mass concrete has a heterogeneous nature especially in the case of old dams suffering from aging and deterioration.*
The objective of this joint contribution is to evaluate the seismic response of a typical gravity dam with heterogeneous concrete material. Since the simulations are cast in the context of probabilistic methods, a relatively large number of analyses are required to fully understand the impact of concrete random field on the structural responses (i.e. displacements, and stresses). Therefore, a Random Forest (RF) meta-model is adopted in order to reduce the computational burden of the probabilistic simulations. RF is an effective technique in the regression analyses of the systems with large number of inputs, and can provide a measure of input variables' importance. This technique is useful to identify the critical areas within the dam body which deterioration may affect the seismic stability of the dam and jeopardize its integrity.

1 INTRODUCTION

Probabilistic risk assessment (PRA) is widely used as a standard technique in safety evaluation of the existing dams. Different factors are involved in PRA; however, the detailed numerical simulation plays the key role. Most of the current applications simplify the finite element model by assuming the mass concrete as an isotropic homogenous material. Nevertheless, in reality the concrete shows anisotropic and heterogeneous behavior in micro-, meso- and macro-scales. The harsh environmental conditions (e.g. aging and deterioration) intensify the degree of heterogeneity in large-scale infra-structures such as dams and bridges.

In the physical level, the non-destructive tests can provide useful information about the quality of materials, potential damages, and mechanical properties. Methods such as impact-echo, spectral analysis of surface waves, and ultrasonic pulse velocity tomography can be used [1]. Figure 1 shows modulus of elasticity tomograms for three cross sections of

[2] University of Colorado, Boulder, USA. moha2643@colorado.edu

Seminoe Dam. As seen, distribution of the properties in these images is heterogeneous with the cross section as well as along the canyon.

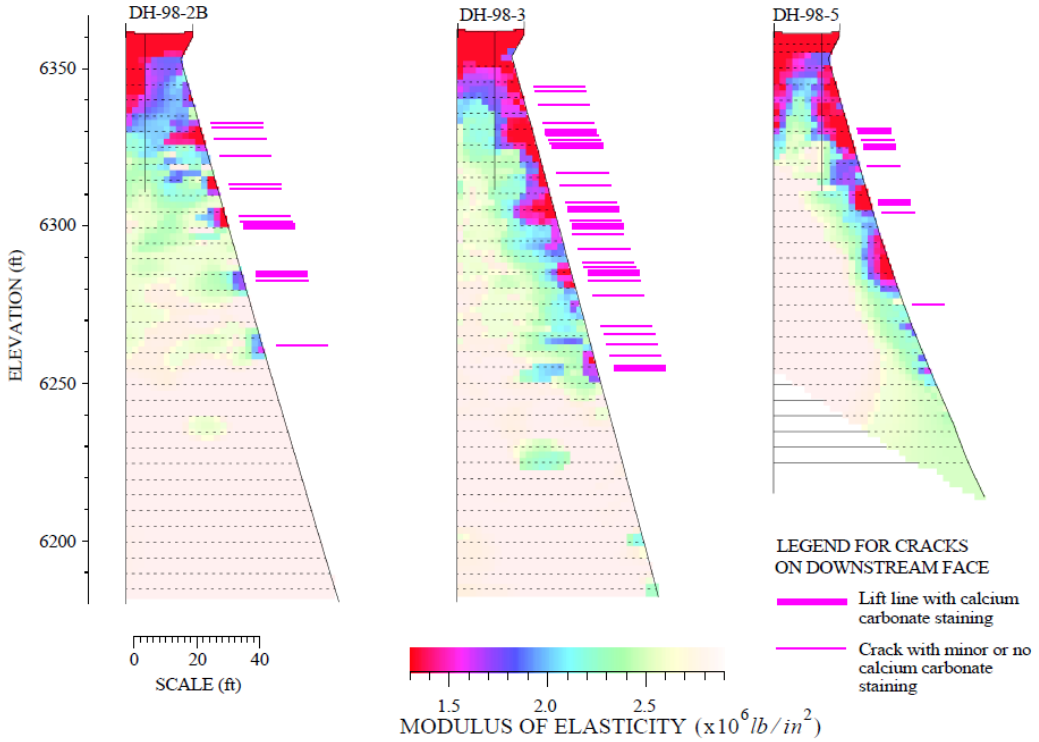

Figure 1: Modulus of elasticity tomograms for the three cross sections adopted from [2]

To obtain such a realistic distribution within the concrete dams either a series of detailed (and so expensive) field tests, or numerically generated random patterns are required. The former one can be used only for the existing dams. However, the latter one is suitable for both the existing dams and those to be built in future. Since the random patterns vary case by case, a Monte Carlo Simulation (MCS) is usually required to cover all the potential distributions.

Random field is one of the numerical techniques which accounts for randomness of the material properties within the domain of interest. Random fields are used to propagate the uncertainty in space though finite element codes. Application of random fields in concrete dams is very limited. Zhong *et al.* [3] and Tang et al. [4] studied the failure of gravity dams with heterogonous material based on the Weibull distribution law and damage plasticity. They found when concrete heterogeneity is considered, the stress distribution is no longer smooth, which therefore better reflects the real-world situation. Altarejos-García *et al.* [5] proposed a strategy to analyze failure of dam-foundation interface in concrete dams including the consideration of the local strength parameters as random variables. Hariri-Ardebili *et al.* [6] studied the linear elastic seismic response of gravity dams with random concrete material. Impact of correlation length, single vs. double random material, 1D vs. 2D uncertainty propagation were all studied. More recently, Hariri-Ardebili *et al.* [7] generalized the random field theory in order to quantify the vibration response of high arch dams in the context of system identification. An analytical model is proposed for mean and variation of the multi-modes as a function of geometry, material properties and spatial distribution.

This paper aims to evaluate the seismic response of a typical gravity dam with heterogeneous concrete material. Since the simulations are cast in the context of probabilistic methods, a relatively large number of simulations are performed. To reduce the computational burden, a Random Forest (RF) based meta-model is proposed for probabilistic simulations. It can

provide a measure of input variables' importance. This technique is useful to identify the critical areas within the dam body which deterioration may affect the seismic stability of the dam and jeopardize its integrity.

2 METHODS

2.1 Random Fields

An efficient random field generator is used based on covariance matrix decomposition as well as a midpoint discretization method. The generator relies on a uniformly-distributed random field obtained by means of transformation from normally-distributed, homogeneous and isotropic random fields [8]; Latin Hypercube Sampling (LHS) is also used to reduce the total number of simulations compared to the crude MCS. Details of its application can be found in [6] where a time-independent random field is first discretized into a mean value and a fluctuating component. The former one is a deterministic function, while the latter one is a random function with zero mean and an auto-covariance of predictors:

$$C_{aa}(\xi, \sigma_0) = \sigma_0^2 \rho_{aa}(\xi) \tag{1}$$

where $\xi = |\boldsymbol{u} - \boldsymbol{u}'|$ is the distance between any two arbitrary locations ($\boldsymbol{u}$ presents the position vector), σ_0 the (constant) standard deviation, and ρ_{aa} the auto-correlation function.

The square exponential auto-correlation function is used in this paper [9]:

$$\rho_{aa}(\xi) = e^{-\left(\frac{\xi}{l_{corr}}\right)^2} \tag{2}$$

where l_{corr} is the correlation length and represents the distance over which the quantities exhibit strong correlation.

2.2 Random Forests

Random forests (RF) are non-parametric data-based models. No a priori assumptions are made about the type of relationship between input variables (i.e. modulus of elasticity in the mesh elements) and the system response (i.e. displacement, stress).

RF models estimate the value of the target variable from the average prediction of a large number (usually several hundreds) of simple decision tree models. The description of the theoretical basis can be found in various sources (e.g., [10]), as well as in the seminal article by Breiman [11]. The advantages of RF models over other machine learning algorithms include:

- They are robust against outliers and uninformative predictors
- They require little pre-processing and variable selection
- They are less prone to overfitting
- They provide a realistic estimate on prediction accuracy based on the training data (Out-of-bag error - OOB).

Although the interpretation of RF models is not straightforward, there are tools that allow extracting useful information on the behavior of the system. The main tool for interpreting RF-based models is the variable importance index [11]: Once the model has been fit, each of the predictor variables is randomly permuted and the new prediction error is calculated. The difference between the accuracy of the original model and that obtained with the permuted input is taken as the importance of the corresponding variable. It is based on the idea that the model accuracy is insensitive to the permutation of the values of variables with low association to the system response, and vice versa. This measure has been shown to be

biased when categorical variables are involved [12], but has offered useful results when all inputs are numerical [13], as in this work.

Information can also be extracted from the model using partial dependence plots [14]: For each predictor variable, a set of values evenly distributed along its range is selected. For each of these values, the mean of the model prediction is calculated considering the real values of the rest of the predictors:

$$\hat{f}(\boldsymbol{x}) = \frac{1}{n}\sum_{i=1}^{n} f(\boldsymbol{x}, \boldsymbol{x_C}) \tag{3}$$

where $\boldsymbol{x}$ is the variable whose effect is to be evaluated, n is the number of samples in the training set and $\boldsymbol{x_C}$ represents the rest of the variables. For example, if $\boldsymbol{x}$ is the Young modulus of element #1, a set of p equispaced values is defined along its range of variation x_j, $j=1...p$. First, the original values are replaced by a constant $x=x_1$. The prediction of the model is calculated keeping the rest of variables ($\boldsymbol{x_C}$) at their original value, and the average of these predictions is computed. The process is repeated for each x_j. This results in a series of points that show the average effect of the variation of $\boldsymbol{x}$ on the response of the model.

RF models have been previously applied in dam safety assessment based on monitoring data [15]. Other examples of applications in dam engineering include the estimation of discharge curves in labyrinth spillways [16] and the identification of the factors affecting the response of double-curvature arch dams [17].

3 NUMERICAL EXAMPLE

3.1 Finite Element Simulations

Koyna Dam has been selected as a case study. The dam height is 103 m, and its thickness at its base and the crest are 70.2 m and 14.8 m, respectively. Figure 2 shows the cross-section of the tallest non-overflow monolith, including the reservoir and the foundation. The finite element method was used to perform the transient analyses by implicit time integration. The 2D plane strain quadratic elements are used for both the dam and foundation. Since many transient analyses are required in this paper, a medium-dense mesh is selected for dam body with 336 elements. Pressure-based fluid elements are placed in the reservoir domain, and the fluid-structure interaction is modeled by Eulerian-Lagrangian approach. Loads consist of: self-weight, hydrostatic pressure (full reservoir), bottom sediment (wave reflection coefficient for the reservoir bottom materials assumed to equal 0.75), and seismic loads.

The foundation is assumed to be a homogeneous material. The mean concrete properties are: modulus of elasticity (E_c) 30 GPa, mass density 2643 kg/m^3, and tensile strength 2.2 MPa. According to Dam Safety Office (DSO) [2], the modulus of elasticity is the only random field in this paper with standard deviation, σ_0 , of 0.5, and the upper and lower bounds of [22, 38] GPa. Furthermore, the correlation length, l_{corr}, is assumed to be 10 m in this paper. It corresponds to about 8% of the largest length, l_{max}, in the dam. In practice, other correlation length also should be studied for a completeness of the case which is skipped in this paper.

The coupled system is excited with both horizontal and vertical components from Koyna Dam recordings. Duration of the shaking is limited to 10 s. Since Δt = 0.01 s for this signal, the outputs are vectors of length 1,000. Results are extracted in terms of displacement and stress time histories for some of the target points (e.g., crest and base), as well as the stress envelopes within the whole dam body. These results are then used (along with the input random field for modulus of elasticity) for prediction purposes.

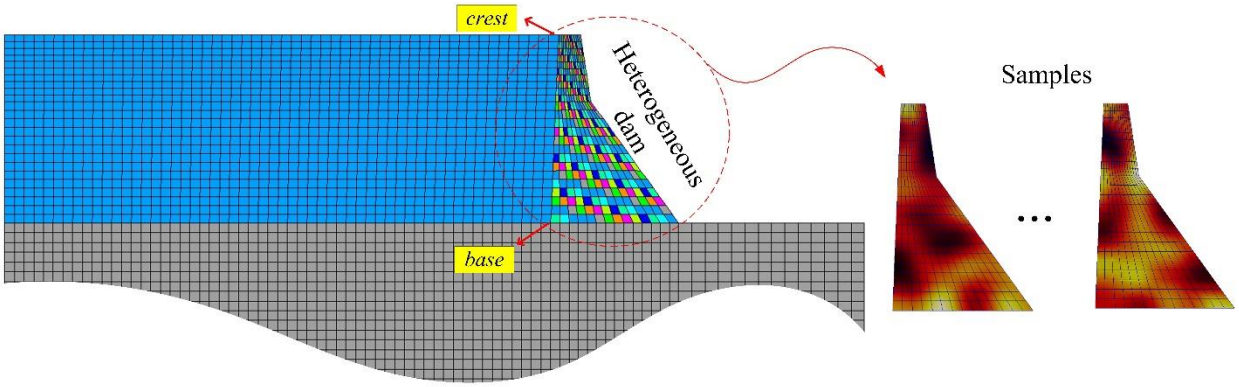

Figure 2: Finite element model of the coupled dam-reservoir-foundation system, including two sample realization of a heterogeneous dam with correlation length of 10 m

3.2 Prediction Tasks

Two separated RF models were fitted to predict: 1) maximum crest displacement (*CDmax*), and 2) maximum stress at the base (*SBmax*). In both cases, the values of the modulus of elasticity for each element in the mesh, normalized to bring all values into the range [0, 1], were considered as inputs. The 100 cases run were randomly separated into a training set (70 cases) and a test set (30 cases). Both sets have 336 inputs (mesh elements) and one output (i.e. *CDmax* or *SBmax*) for each model.

In such setting, with more inputs (336) than samples in the training set (70), some machine learning algorithms are prone to overfitting and poor generalization accuracy. On the contrary, RFs have shown to be appropriate in these conditions [18]. Accuracy was computed in terms of Mean Absolute Error (MAE) and Mean Absolute Percentage Error (MAPE).

We then repeated the analysis by adding to the input variables the maximum stress and the displacements at crest and neck for time step #27 (out of 1,000) of the transient analysis, where the first relative maximum acceleration is recorded. Adding variables to the modulus of elasticity of the mesh elements complicates the interpretation of the model. On the contrary, the precision in the prediction is increased with a low computational cost, i.e., only 27 time steps need to be computed in finite element analysis to estimate the maximum values registered in a period of 1,000 time steps. The same approach was followed with the results at step #197, when the second relative maximum (higher than the first one) was recorded.

The *randomForest* library was used [19], with the default training parameters. All the models were repeated 20 times to observe the effect of the random component selection in the algorithm.

4 RESULTS

4.1 Prediction Accuracy

Table 1 shows the results in terms of the model accuracy for different settings analyzed. The mean and the standard deviation for the 20 model repetitions are included. Some conclusions can be drawn from these results:

- Model accuracy for the test set is similar to that for training (even better for models C and E). This proves the absence of over-fitting and the reliability of the OOB error computed by the training algorithm.
- Incorporating the results at time step #27 as inputs allows reducing the error by about 50% for both the outputs.

- Incorporating the results at time step #197 did not result in higher accuracy. This suggests that the additional input does not provide relevant information regarding the system response. Since the computational cost is higher (by more than 7 times compared to step #27), this option was not further analyzed.

Table 1: Mean (standard deviation) accuracy of the RF models. Training accuracy is computed from the OOB error.

Inputs	Output	Model ID	MAE-Train	MAE-Test	MAPE-Train	MAPE-Test
E_c	*CDmax* (mm)	A	1.39 (0.011)	1.47 (0.017)	3.95 (0.032)	4.15 (0.046)
	SBmax (MPa)	B	21.08 (0.21)	23.57 (0.26)	2.13 (0.020)	2.42 (0.027)
E_c, results* at #27	*CDmax* (mm)	C	0.67 (0.014)	0.66 (0.015)	1.90 (0.040)	1.82 (0.042)
	SBmax (MPa)	D	8.71 (0.32)	10.71 (0.32)	0.88 (0.032)	1.11 (0.033)
E_c, results at #197	*CDmax* (mm)	E	0.72 (0.014)	0.70 (0.017)	2.01 (0.040)	1.93 (0.047)
	SBmax (MPa)	F	11.05 (0.12)	12.56 (0.17)	1.11 (0.012)	1.29 (0.018)

* The results considered as inputs include displacement at crest, neck and base, as well as stress at the base

4.2 Variable Importance

The importance of the variables has been calculated, which in the first model is equivalent to that of the elements of the mesh. The results are shown on the geometry of the model, so that it can be interpreted as an indicator of the areas whose modulus of elasticity is more influential on the studied response variables.

Figure 3 shows that the elements whose strength has the greatest influence on *CDmax* are located around the neck. As for *SBmax*, the most relevant areas are the heel and the toe. These findings are consistent with the physics of the problem in which the Koyna Dam's displacement response is highly affected by the strength of the material around the neck. The dam has very long and unusual neck shape which makes this area vulnerable. On the other hand, a gravity dam is usually overstressed (in linear elastic analysis) around the heel and toe subjected to dynamic excitation. Thus, they are the most sensitive areas to the first principal stress.

Figures 4 and 5 show the 10 most important input variables in each model. As mentioned earlier, 20 repetitions of each case were generated to evaluate the random component of the training algorithm. The results of the 20 repetitions are plotted in the form of boxplots for the 4 versions resulting from combining the two response variables (*CDmax* and *SBmax*), and two sets of predictor variables (modulus of elasticity only, and modulus of elasticity plus the results in time step #27).

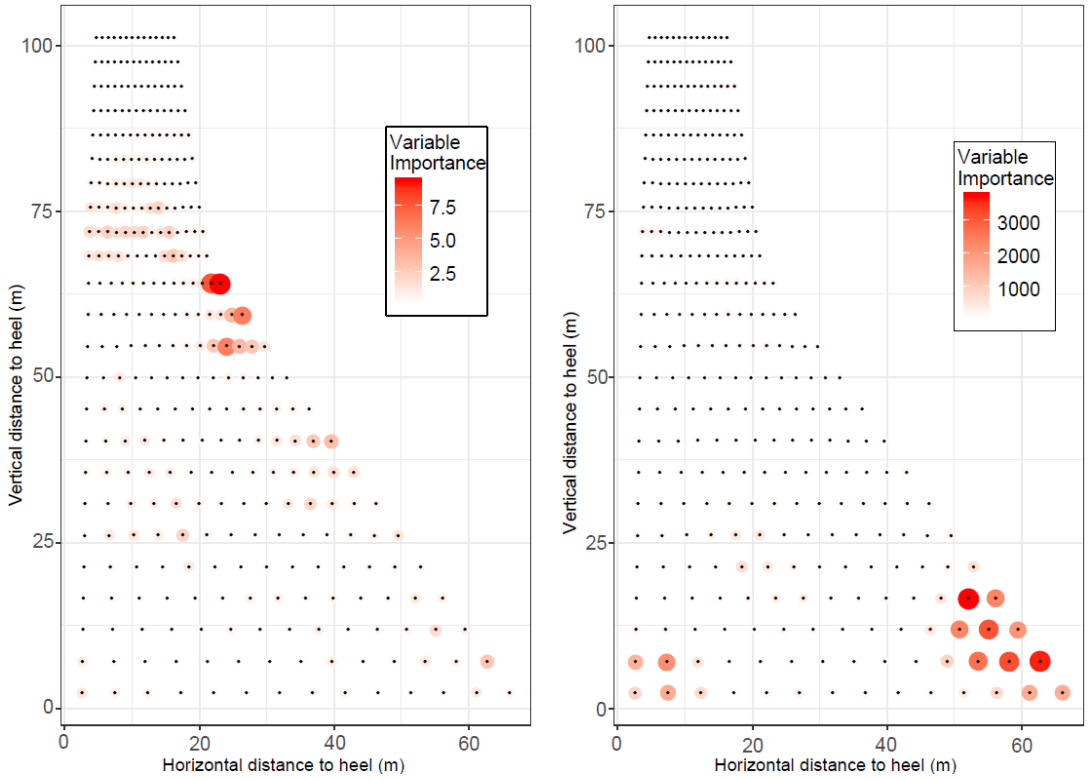

Figure 3: Variable importance of mesh elements on the maximum crest displacement (left) and maximum stress at the base (right). Average results for 20 models solely based on modulus of elasticity (Models A and B).

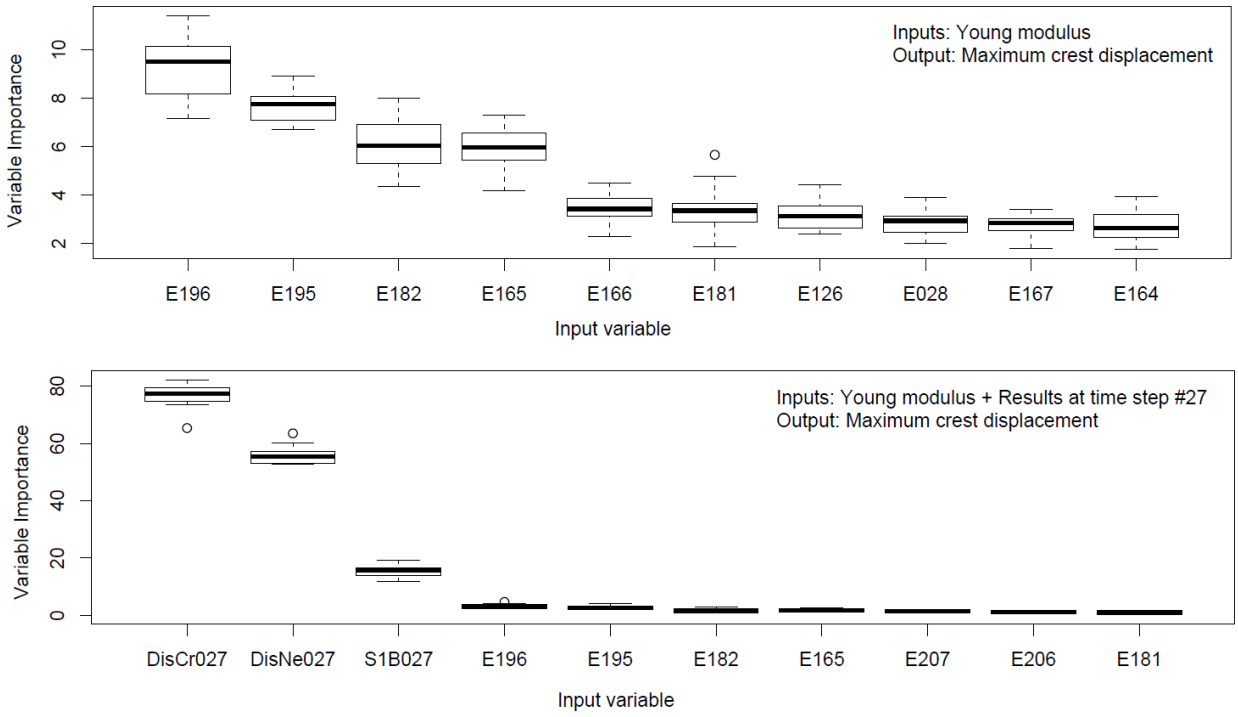

Figure 4: Variable importance for the 10 most relevant inputs for models A (top) and C (bottom). Results for 20 repetitions of each model. Note: DisCr027: crest displacement at #27, DisNe027: neck displacement at #27, S1B027: base first principal stress at #27.

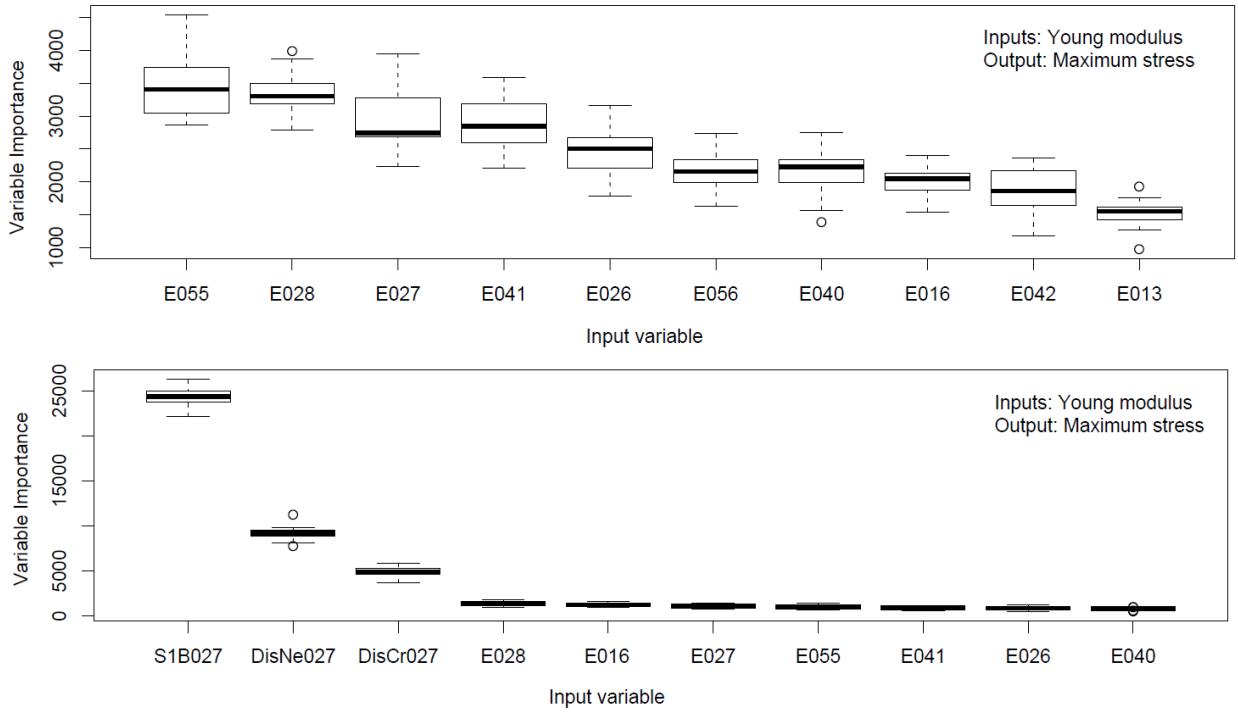

Figure 5: Variable importance for the 10 most relevant inputs for models B (top) and D (bottom). Results for 20 repetitions of each model. Note: DisCr027: crest displacement at #27, DisNe027: neck displacement at #27, S1B027: base first principal stress at #27.

As expected, the results for time step #27 are more associated to the response than the elemental modulus of elasticity, except for the displacement at the base. However, if these same results are shown in the format of Figure 3, *i.e.* if only the importance of the elements is considered and they are drawn on the dam body, the results are very similar, as can be seen in Figure 6. This means that even when partial results are added to the values of the modulus of elasticity of the elements, the algorithm is able to classify the importance of the elements in terms of their influence on the dam response; the increase in the prediction capacity does not imply a reduction in the possibilities of identification of the most vulnerable zones.

4.3 Relative Influence

The average effect of the 9 more influential variables is plotted in Figures 7 and 8. In Model A, Figure 7, only the elemental modulus of elasticity are considered as inputs. The effect of all the most relevant elements is similar; i.e., low values are associated with higher displacements, and vice versa. The change in dam response occurs abruptly in most variables. For example, for the most important variables (E196 and E195), a sudden change is observed around 0.5. This change occurs for different values in other elements, as for example in E28, which is located next to the downstream toe.

In Model C, Figure 8, whose output is also displacement, but which considers the results in time step #27, the effect of the modulus of elasticity is smaller. Here it is observed because the same elements have a similar effect in shape but with smaller magnitude. Note the vertical scale of the common variables between Figures 7 and 8 (e.g. E195 and E196).

In the same model, the effect of the results in time step #27 is somehow proportional to the entire transient analysis: Higher values of displacements at the crest (*DisCr027*), neck (*DisNe027*), and stress at the base (*S1B027*) all in time step #27 are proportional to the maximum absolute response of the system during the whole dynamic analysis (note that this is a linear elastic system). This can be interpreted as meaning that the "weakest" models

(according to the distribution of the modulus of elasticity), which register high displacement at the crest in the first relative maximum (time step #27), are also those with the greatest absolute displacement during the complete transient analysis.

The analysis of predictive models of *SBmax* gives similar results (not shown in this paper). The most noticeable difference is the shape of the E016 graph: High values of its modulus of elasticity are associated with higher values of *SBmax*. This is because the element is located next to the dam heel, while the rest of the most influential elements are close to the downstream toe.

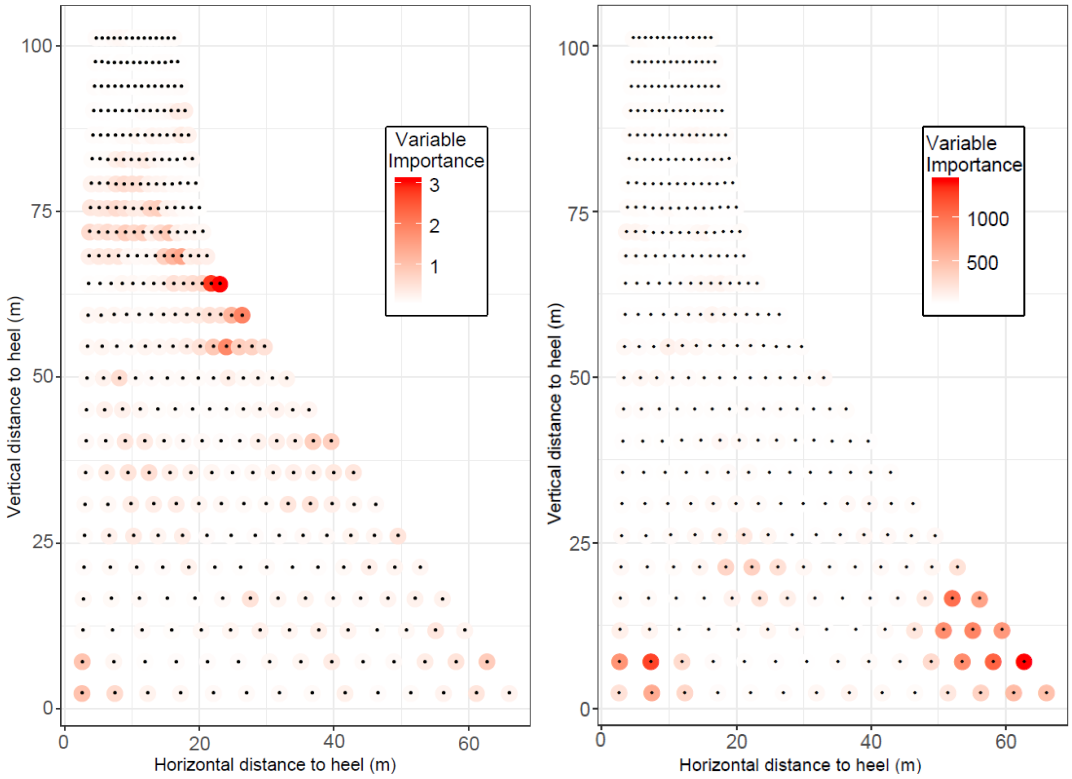

Figure 6: Variable importance for the mesh elements in the RF models that include results at step #27, to predict *CDmax* (left) and *SBmax* (right). Average value of 20 models. (Models C and D)

5 CONCLUSIONS

In this paper, the results of the random finite element simulations are combined with a machine learning technique (i.e. random forest) to predict the most vulnerable locations of a gravity dam under heterogeneous material distribution and seismic excitation. The results suggest that RF models might be useful in reducing computational cost in seismic probabilistic risk assessment.

With a base of 100 realizations of the random fields, the RF models allow to estimate the variables of interest exclusively from the values of random modulus of elasticity with relatively small correlation length, with a precision of 4% for the maximum displacement at the crest, and of 2% for the maximum principal stress at the base.

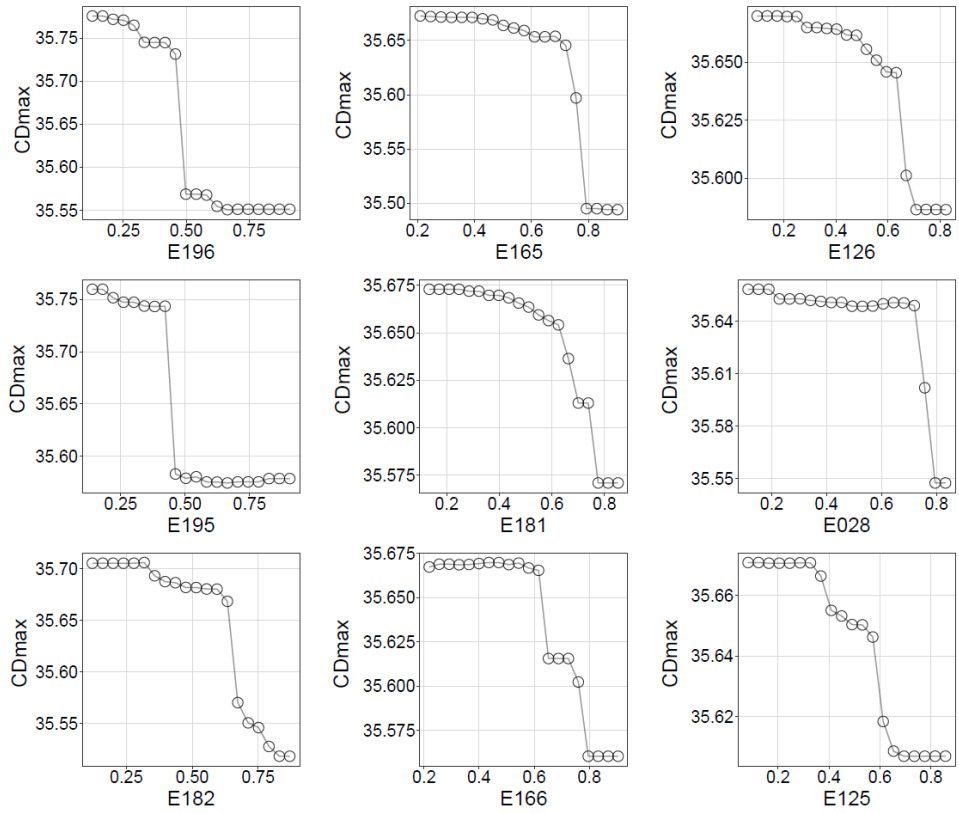

Figure 7: Partial dependence of *CDmax* for the most influential inputs. Model A.

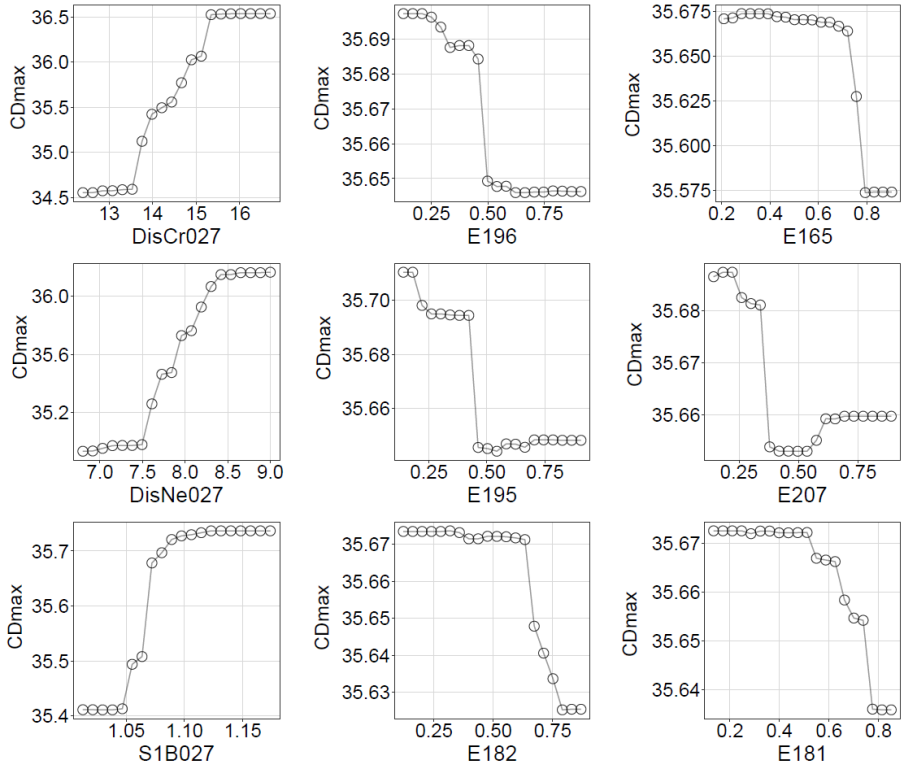

Figure 8: Partial dependence of *CDmax* for the most influential inputs. Model C.

If the results of the calculation in a relative maximum of the ground motion acceleration are also considered as inputs, the mean error is reduced to 1.8 and 1.1%, respectively. Although this second option implies a higher computational cost with respect to

the former one, it also allows an important saving of computational time with respect to the finite element simulations. In the example, the calculation time is reduced with respect to the complete model by 97% (only 27 of the original 1,000 time steps need to be executed). If we consider that the absolute maximum occurs after 350 time steps, the real saving is higher than 90%.

Although the obtained accuracy can be adequate for certain analyses, it may not be enough in other cases, where low probability failure scenarios are studied. This aspect should be considered when applying this approach. Partial dependence plots also provide useful information on the effect of modulus of elasticity for each of the regions considered.

Additionally, the analysis of the importance of the variables that is automatically calculated when fitting RF models allows identifying the areas of the dam body whose modulus of elasticity have the largest impact on the variables of interest. The results are in agreement with the engineering intuition, since the neck is the critical zone for crest displacements, while the strength of the downstream heel/toe is more associated to the maximum stress at the dam-foundation interface. This result is considered an interesting example of the possibilities of data-driven algorithms: The case is relatively simple, and the result only confirms what can be deduced from engineering knowledge. However, in other problems with more variables involved, where it is not possible to have a reliable intuition about the most important variables, this analysis can provide essential information to better understand the behavior of the system.

6 ACKNOWLEDGEMENT

The second author would like to appreciate the technical advice by Dr. Jerzy Salamon from US Bureau of Reclamation.

REFERENCES

[1] L.J. Bond, W.F. Kepler, and D.M. Frangopol, Improved assessment of mass concrete dams using acoustic travel time tomography. Part I-theory. *Construction and Building Materials*, 14(3), (2000), 133-146.

[2] Dam Safety Office (DSO), Seismic Tomography of Concrete Structures Report No. DSO-02-03, Tech. Report, Department of the Interior, Bureau of Reclamation, US, (2002).

[3] H. Zhong, G. Lin, X. Li and J. Li, Seismic failure modeling of concrete dams considering heterogeneity of concrete, *Soil Dynamics and Earthquake Engineering* 31(12), (2011), 1678-1689.

[4] X. Tang, Y. Zhou, C. Zhang and J. Shi, Study on the heterogeneity of concrete and its failure behaviour using the equivalent probabilistic model, *Journal of materials in civil engineering* 23(4), (2010), 402-413.

[5] L. Altarejos-García, I. Escuder-Bueno and A. Morales-Torres, Advances on the failure analysis of the dam-foundation interface of concrete dams. *Materials*, 8(12), (2015), 8255-8278.

[6] M.A. Hariri-Ardebili, S.M. Seyed-Kolbadi, V.E. Saouma, J. Salamon, and B. Rajagopalan, Random finite element method for the seismic analysis of gravity dams. *Engineering Structures*, 171, (2018), 405-420.

[7] M.A. Hariri-Ardebili, S.M. Seyed-Kolbadi, V.E. Saouma, J.W. Salamon, and L.K. Nuss, Anatomy of the vibration characteristics in old arch dams by random field theory. *Engineering Structures*, 179, (2019), 460-475.

[8] G. A. Fenton and D. V. Griffiths, Risk assessment in geotechnical engineering, Wiley, (2008).
[9] A. Olsson and G. Sandberg, Latin hypercube sampling for stochastic finite element analysis, *Journal of Engineering Mechanics* 128(1), (2002), 121-125.
[10] T. Hastie, R.Y. Tibshirani and J. Friedman, The elements of statistical learning - Data mining, *Inference and Prediction.* Springer, 2nd edition (2009).
[11] L. Breiman, Random forests, *Machine learning* 45(1), (2001), 5-32.
[12] C. Strobl, A.L. Boulesteix, T. Kneib, T. Augustion, A. Zeileis, Conditional variable importance for random forests. *BMC Bioinformatics*, (2008), 9:307
[13] F. Salazar, M.A. Toledo, E. Oñate and B. Suárez, Interpretation of dam deformation and leakage with boosted regression trees. *Engineering Structures*, 119, (2016), 230-251.
[14] J.H. Friedman, Greedy function approximation: a gradient boosting machine. *Annals of Statistics*, 29, (2000), 1189-1232.
[15] F. Salazar, M.A. Toledo, E. Oñate and R. Morán, An empirical comparison of machine learning techniques for dam behaviour modelling. *Structural Safety*, 56, (2015), 9-17.
[16] F. Salazar, and B.M. Crookston, A performance comparison of machine learning algorithms for Arced Labyrinth spillways. *Water*, 11(3), (2019), 544.
[17] F. Salazar, M.A. Toledo and D.J. Vicente, A systematic assessment of the influence of geometry and materials properties on the performance of arch dams. International Benchmark Workshop on Numerical Analysis of Dams. Stockholm, Sweden (2017).
[18] R. Díaz-Uriarte and S.A. De Andres, Gene selection and classification of microarray data using random forest. *BMC bioinformatics*, *7*(1), (2006), 3.
[19] A. Liaw and M. Wiener, Classification and Regression by random Forest. *R News* 2(3), (2002), 18-22.

Towards the seismic capacity assessment of concrete dams

L. Furgani[1], M. A. Hariri-Ardebili[2] and M. Meghella[3]

Mott MacDonald
8-10 Sydenham Road, Croydon CR0 2EE, United Kingdom
E-mail: luca.furgani@mottmac.com

Keywords: Dams; Concrete; Seismic assessment; Capacity curves; Damage

Abstract. *The purpose of this joint contribution is to estimate the maximum earthquake the concrete dams can withstand. The so called "seismic capacity curve" for these infra-structures seems now technically and commercially feasible thanks to modern finite element techniques, hardware capabilities and positive experiences collected so far. The key topics faced during the seismic assessment of the dams are also discussed using different point of views and examples, which include: the selection of seismic parameters, the progressive level of details for the numerical simulations, the implementation of the non-linear behaviours, and definition of the service and collapse limit states. The approaches adopted by local institutions and engineers on the subject of dam capacity curves will be discussed using the authors' experiences and an overview of time and resources will be outlined to help decision makers. Finally, the paper is wrapped up with a list of suggestions for analysts, the application limits and further studies.*

1 INTRODUCTION

Special efforts have been devoted in recent years on the seismic assessment of large dams. High seismicity countries went through or are still facing reassessment programmes for their dams. These extensive studies are required for the lack of seismic checks in older dams, updated seismic hazard parameters and new seismic standards. Despite the opportunities offered by modern technologies, it is sometimes difficult to select a cost-effective procedure for the seismic assessment of dams which makes the decision makers or even the public opinion confident of the outcomes. It is understandable that the complex analyses make the stakeholders feel uncomfortable. For this reason, in the author's opinion is vital to find a new procedure to balance the numerical simulations with the comprehensive outcomes. As the technical literature shows, the seismic behaviour of dams involves different key aspects to be considered. The seismic analyses of the large dams must consider the following aspects: specific seismic hazard assessment, step-by-step analysis approach, soil-structure interaction, fluid-structure interaction and the system's non-linear behaviour. It is a common opinion that the dams are unique prototypes each having their own behaviour. Even more so, it is generally expected that the seismic response of the dams must be considered with an opportune degree of distinction between different case studies. Previous experiences on the application of capacity curves [1] demonstrated that using certain classification rules,

[2] University of Colorado Boulder, X-Elastica LLC, moha2643@colorado.edu
[3] Ricerca Sistema Energetico RSE, massimo.meghella@rse-web.it

the overall seismic behaviour of concrete dams may be similar especially towards the failure point. This aspect should exhort the scientific community and the best practice of the sector to consider capacity curves as a way forward.

The current paper tries to share some experiences gained by the authors on capacity curves. This will be accomplished using the examples showing the advantages and limits of this approach. It has been also discussed a summary of the typical procedures available to extract the capacity curves. These have been applied with a certain confidence in the buildings industry. Special attention will be offered for the Endurance Time Analysis (ETA) method [1]. A technical discussion will be presented on the benefits that capacity curves can add to the dam's industry and public interests.

1.1 Seismic Assessments and Risk Management

Following a period in which the lack of rules permitted to design and build the dams without (or with too simplified) seismic design principles, it is now well recognized the necessity to cope with the safety reassessment of these dams, and to select the right method to evaluate their performance during the earthquake event. Despite the variety of seismic safety approaches in dam engineering, the concept of "risk assessment" is, implicitly or explicitly, present in all the technical codes used in most of the developed countries (e.g., ICOLD bulletins, European Standards, USBR, and CDA guidelines).

In Switzerland, which recently is undertaking the task of re-assessing the dams [3], some outlines are provided on the framework and efforts required to manage the dams' portfolios. After 10 years required to assess 208 dams, important outcomes and lessons learned have been collected by the Swiss experience. It is worth to note that the cases appeared to be non-compliant with the standards were generally dams with problems also in static conditions or with unusual design concepts.

Other European countries are following the example of Switzerland for the seismic assessment of their dams. For instance, recently adopted dam safety regulations introduce risk concepts such as the residual safety margin of the dam against seismic actions, a kind of qualitative evaluation of the dam's capacity. Despite this, it is still necessary to bridge the gap between the seismic response determined for the target seismic levels, mainly collapse and serviceability limit states, and the dams' ultimate capacity. Considering this, it appears clear where the so called "capacity curves" may play their role.

1.2 Overview on Seismic Assessment Procedures

To evaluate what may be called the "failure or critical earthquake" of a concrete dam, it is necessary to put in place a numerical model and a seismic assessment procedure allowing to consider the most important aspects involved. Considering advancements in computer science, the idea to investigate the non-linear behaviour of concrete dams towards collapse is becoming more common between researchers and engineers. The technical literature shows different authors [4] performing non-linear analysis to evaluate the capacity or fragility curves of dams. Despite the excellent work done or planned to be done in the future, the greatest obstacle for non-linear analysis and capacity curves is the formal definition of acceptable damages against the different limit states used in the modern structural codes. At the current stage, we can simulate the structural performance decay of these structures, but we have no practical guidelines to indicate their expected behaviour is acceptable other than subjective engineering judgement.

In the buildings sector, the capacity curves are used to demonstrate the design target and the actual ductility of the structures are met. A similar route can be expected for dams, with appropriate procedures, the definition of "failure modes" and "limit states". An

important aspect to be considered is the confidence with the methods used to produce the capacity curves. In the buildings sector, the use of non-linear static push-over analysis is considered common practice. Predefined load patterns are used to reproduce the effects produced by earthquakes. This loading pattern is then increased through a scale factor to produce the damages of the main structural elements until the point of collapse. From the author's experience, it is not possible to use the same procedure for dams. This is due to the different way the dam and the surrounding domains, soil and water, react against the seismic actions. For this reason, it is more reasonable to use a bespoke dams sector approach. This may consist of non-linear dynamic analysis procedures where all the mechanism involved in the response can be included and properly captured without limits associated with standardised and increasing pseudo static forces.

A capacity curve determined for a concrete dam under seismic forces is always associated with concurrent actions, namely dead weight, thermal loading and water hydrostatic pressure, applied to the dam before the seismic action is applied. In addition to this, the seismic actions are characterized by their spatial variation using the three directions of the seismic action and concurrency factors. The numerosity of the combinations suggests capacity curves cannot be developed for all of them. A procedure is then necessary to perform a screening of the most critical combinations. The proposed approach is to start with simplified linear pseudo static procedures to move then to linear dynamic analysis and finally non-linear dynamic analysis. This approach is also giving assurance on the validity of the analysis methods while more detailed aspects are introduced, concept already introduced within technical guidelines.

Capacity curves require numerical models able to consider the main non-linear behaviours of dams during earthquakes. For gravity dams the sliding at the base, or at the weaker joints, is the main failure mode expected. This phenomenon can cut off the seismic action acting as a seismic isolator. The reduction of stresses above the sliding plane is obtained at the cost of a residual displacement, captured by jumps in the force displacement diagrams.

Slips occurring over joint are also important for arch dams but are not governing the global response of these structures. On the other way, the right representation of joint openings and closures are essential for arch dams to represent the different behaviour of these dams under seismic actions acting in different directions.

For both gravity and arch dams, cracking behaviour is required to consider the effects produced by the reduction of concrete properties along the dam body and the associated change in the way dam deforms. These effects are represented by the slope change in the capacity curve. The non-linear model used should be also selected based on the data necessary to evaluate damages and the associated relationship with limit states.

Another aspect to be considered for large models is the management of computation time as already mentioned. This is highly dependent on modelling techniques and assumptions. If a numerical model is considered in its most effective condition, mesh and time steps are key aspects in this sense, the only way to reduce the computational time required for the analysis is the selection of alternative seismic inputs. The ETA method introduced in the following paragraphs is proposed to significantly reduce the computational effort.

2 CAPACITY ESTIMATION TECHNIQUES

In the following paragraphs, it is reported a summary of the procedures available for the estimation of the capacity curves and the seismic assessment procedures in general.

The "Seismic Capacity Function" is defined as the relationship between an external (or internal) parameter affecting the capacity of the structure, also referred to as a "stressor" and "response" of the system at the macro level [5].

Stressor (S): can be 1) an incrementally-increasing monotonic, cyclic or time-dependent load (or displacement, acceleration, pressure); 2) an incrementally-decreasing resistance parameter or degradation in strength properties; and 3) a discrete increasing/decreasing critical parameter in a system leading to failure. Stressor is typically called an intensity measurement (IM) parameter [6] in earthquake engineering. In the present paper; however, S is more generally defined and refers to any quantity whose variation (continuous or discrete) may lead to progressive system failure and its ultimate collapse.

Response (R): is representative of the system behaviour under the varying stressor. It is depicted in either an absolute or relative sense. R may be: 1) a single damage variable (DV), such as drift or energy dissipation; 2) a combination of several DVs in terms of damage index (DI); and 3) any safety monitoring index. In the field of earthquake engineering, R is typically called an engineering demand parameter (EDP) [6]. EDPs and DIs for dams have been discussed by the authors in previous publications (see [7] and [8]).

2.1 Incremental Dynamic Analysis (IDA)

The seismic capacity function can be obtained using real ground motion. Single-record IDA (SR-IDA) is the most basic technique. In this method, single ground motion is used for the nonlinear time history analysis of the coupled system. Let $\ddot{\boldsymbol{x}}_g$ be the "as-recorded" (unscaled) acceleration time history. To consider both the stronger and weaker scenarios, ground motion can be scaled uniformly using a factor λ_{SF}. The scaled ground motion will be: $\ddot{\boldsymbol{x}}_g^{\lambda} = \lambda \ddot{\boldsymbol{x}}_g$. This should be represented by a monotonic scalable IM (e.g., peak ground acceleration (PGA), or the 5% damped spectral acceleration at the first-mode period ($S_a(T_1,\zeta$=5\%))). With these scaled ground motions, the nonlinear time history analysis should be performed in each case. Let's assume that the response of the nonlinear system to the scaled signal is $\boldsymbol{R}^{\lambda}$. The response parameter can be any general monitoring item in dams, such as deformation, stress, uplift or even DI.

Multi-Record IDA is a collection of several records, "*n*", for the same structural system. The required ground motion records are usually obtained from a Probabilistic Seismic Hazard Analysis (PSHA) conducted at the site. The number of required records typically varies given the dispersion among them and the code requirements. The order of *n* for framed structures is about 30-50, while for concrete dams (with high computational effort), it is around 12-20.

Single-intensity measure but multi records: This is the most common format of an IDA plot in the IM-EDP coordinate system. Figure 1a presents the raw data obtained from multi record IDA. This figure also shows the capacity functions resulting from *n*=40 ground motion based on the spline interpolation technique. Considering the record-to-record (TRT) variability in the capacity functions, they should be summarized using some central values like mean, median, 16% and 84% fractiles.

Multi-EDP multi record IDA analysis: The IDA curves are plotted in <EDP_1, EDP_2, IM> coordinates with two EDPs. This type of 3D plot is useful when two EDPs have a strong correlation, i.e. joint opening/sliding, Figure 1 b.

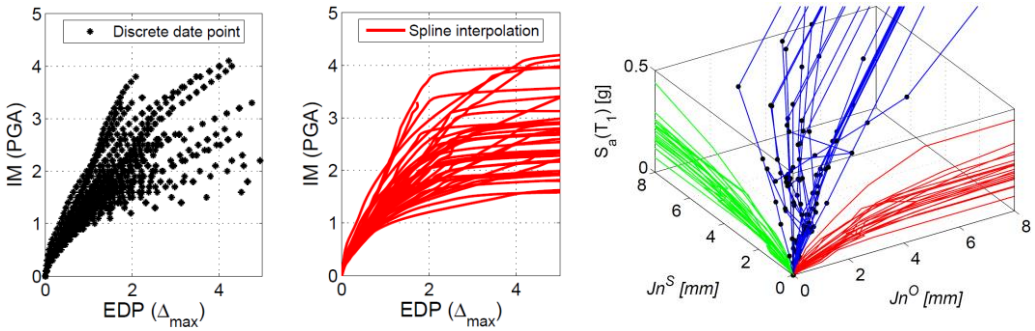

Figure 1: Multi-Record IDA capacity functions for concrete dams. (a) SIM-MR-IDA. (b) MEDP-MR-IDA.

2.2 Cloud Analysis (CLA)

CLA is a numerical procedure in which a structure is first subjected to a set of (un-scaled or as-recorded) ground motions and analysed numerically. If the ground motion records are extracted from a bin, they can represent an earthquake scenario defined by (M_{bin}, R_{bin}), i.e. the magnitude and distance representative of the bin. From these results, EDP vs. IM are then determined and form the so-called cloud response. The CLA method is normally used in conjunction with probabilistic seismic demand analysis (PSDA) [9]. It is now well accepted that the discrete data points resulting from CLA have a linear trend on the logarithmic scale, thus implying a power curve on the arithmetic scale. A sample CLA-based capacity curve for a gravity dam is shown in Figure 2 where the EDP is selected to be crest displacement.

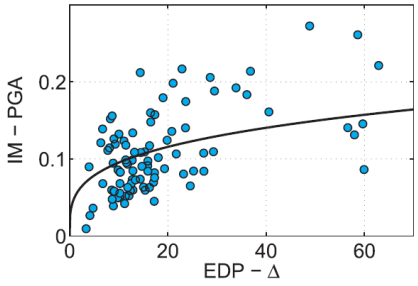

Figure 2: Cloud-based data power-form capacity function for concrete gravity dams.

2.3 Endurance Time Analysis (ETA)

ETA is a dynamic pushover procedure used to estimate the seismic performance of structures when subjected to pre-designed intensifying excitation [10]. The simulated acceleration functions are intended to shake the structure from a low excitation level - with a structural response in the elastic range - to a medium excitation level - where the structure experiences some nonlinearity - and ultimately to a high excitation level causing failure. All these response ranges are experienced in a single time history analysis.

The challenging part of this method lies on generating the endurance time excitation functions (ETEF). Recent advances in the simulation of ETEFs can be found in Mashayekhi et al. (2018) [11] where the functions are optimized in time and frequency domains accounting for the acceleration and displacement response spectra, as well as the nonlinear displacement, absorbed hysteretic energy, etc.

The ETEF is an artificially designed intensifying acceleration time history, where the response spectra of the ETEF linearly increases with time. Ideally, the profile of the acceleration time history and response spectrum increase linearly by time. Figure 3 shows

a sample ETEF and its response spectra at three different times (i.e. 5, 10, and 15 sec). As seen, the spectrum at t=10 sec is nearly twice the one at t=5 sec and the spectrum one at t=15 sec is three times the one at t=5 sec. In this technique, the seismic performance is determined by the duration the structure can endure the dynamic input.

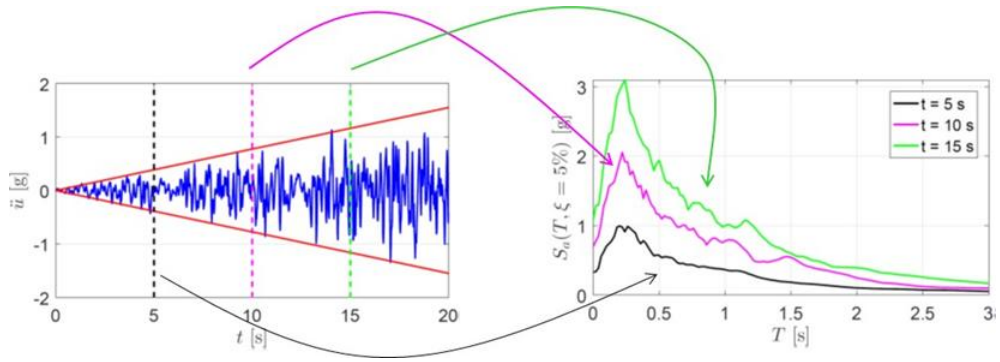

Figure 3: Sample ETEF, its acceleration profile, and time-dependent response spectra.

In order to retrieve a capacity function, the "ETA curve" should first be derived (See Figure 4a). This curve is a diagram, whose the vertical axis refers to the maximum absolute values of EDP during the time interval from 0 to *t*, and the horizontal axis is time. Finally, the "time" parameter is converted to IM (this can be easily performed due to the direct relation between time and acceleration, Figure 3), and the EDP-IM coordinate is flipped to IM-EDP. The resulting stepwise capacity function can be smoothed later, Figure 4b. Although this procedure is applicable only with a single ETEF, in order to reduce the uncertainty (due to its random nature), the mean of three ETEFs typically is used.

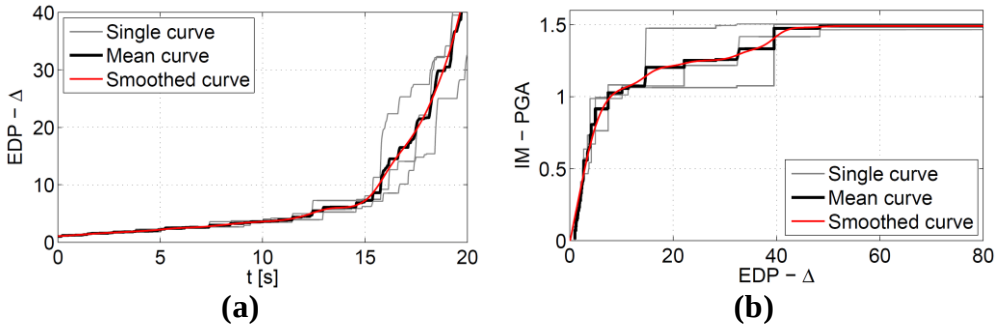

Figure 4: ETA-based capacity function generation for concrete gravity dams. (a) ETA curve. (b) Capacity function.

From the engineering practice point of view, the ETEFs can be considered as synthetic signals and for this reason their application may not be permitted by legislations (as oppose to IDA and CLA). From a capacity function evaluation point of view, this procedure appears to be the most effective way. One of the concerns in this technique includes the rate of the energy released to the structure. The signal is always increasing with no off-peak stages, this may affect the natural development of damages. Important upgrades have been proposed in recent papers (e.g. [11]) on this matter and further improvements are expected in the following years.

3 CASE STUDIES AND CAPACITY FUNCTION EXAMPLES

According to the historical records collected in the ICOLD Bulletin 120, concrete dams performed relatively well during earthquakes. From previous experiences, it has been confirmed the key role of their geometry. For gravity dams, the use of narrowing sections at the neck are generally associated with cracking problems while for arch dams a large "U" shape of the valley rift can affect negatively the overall seismic resistance of the dam. These typical aspects of dams' seismic vulnerability have been confirmed by post-earthquake inspections and the structural analysis. Some examples of capacity curves are reported below. The outcomes have not been discussed in detail deliberatively to allow the reader to focus on the concept behind the use of capacity curves.

3.1 Concrete Gravity Dams

Koyna gravity dam is selected as a case study. It has 103 m height; the thicknesses at the base and at the crest are 70.2 m and 14.8 m, respectively for the central non-overflow monoliths. Figure 5a shows the cross-section of the tallest non-overflow monolith including the mesh. The numerical model includes the reservoir and the foundation. The mesh is refined around the neck and dam-foundation interface to capture all the potential failure modes precisely. Pressure-based fluid elements are used in the reservoir domain. The fluid-structure interaction (FSI) is applied according to the Eulerian-Lagrangian approach where the pressure in the fluid domain is coupled with the solid domain's displacements. The massless foundation might lead to slightly different response distribution in dams, particularly for relatively soft rocks, because the radiation damping is ignored. Applied loads on the system are: dam's self-weight, hydrostatic pressure, bottom sediment, and seismic loads.

Figure 5: a) Finite element model of the gravity dam-foundation-reservoir system, b) Geometry of four arch dams considered in this study

3.2 Concrete Arch Dams

Four arch dams are considered in the following paragraphs to introduce the key aspects associated with their seismic response towards global failure. Together they represent a reasonable representation of concrete arch dams with heights ranging from 59m to 111m [1]. For each dam the interaction with the foundation is considered using the mass-less approach, which for high intensity level earthquakes represent a major limitation. The fluid structure interaction is considered directly modelling the fluid domain with acoustic elements adding a non-reflection condition at the far end and wave reflection coefficient at the bottom end. The non-linear behaviour of vertical and horizontal joints separating the different blocks of the dam have been modelled to reproduce both joint slips and openings. The non-linear

behaviour of concrete has been considered using the Lee and Fenves Damage Plasticity Model. The results reported in the following paragraphs are associated with the full reservoir seismic combination (dead weight, water pressure and winter thermal condition).

3.3 Progressive Collapse of a Gravity Dam

This section explains the damage response of the gravity dam subjected to a single 15-sec ETEF. The failure mechanism is based on the concrete smeared crack model based on the rotating crack model and can simulate the cracking in three orthogonal directions as well as crushing. Figure 6(a) shows the variation of the crest horizontal displacement normalized with respect to the total dam height (i.e. 103 m). As seen, the first large horizontal jump occurs for PGA of about 0.78g (which corresponds to about 12 sec of ETEF). Moreover, the variation of three cracks and the crushing is shown in Figure 6(b) using the concept of DI. This is defined as a ratio of the damaged area (in a particular cracked or crushed direction) to the total dam cross-sectional area. Finally, the damage profile of the dam at two different time steps corresponding to two (relatively) big changes at pre-failure and failure stages are shown in Figure 6(c) and 6(d). The progressive collapse can be tracked in these two set of plots, especially for crack-2 and crack-3 directions.

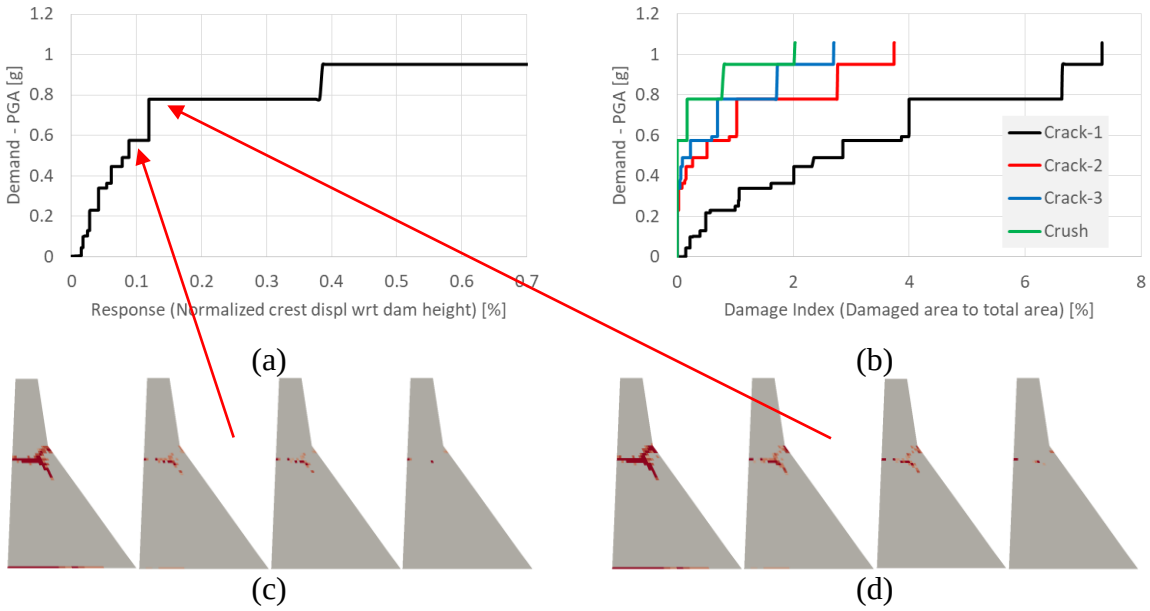

Figure 6: ETA-based capacity function for gravity dam with smeared crack model. (a) Displacement-based capacity curve. (b) Damage index-based capacity curves. (c) Damage at t = 9 sec, PGA = 0.57 g. (d) damage at t = 12 sec, PGA = 0.78 g (crack profile: left to right: crack 1, crack 2, crack 3, and crushing)

The results confirm the typical failure modes for the Koyna dam, widely investigated by different authors using traditional accelerograms also through seismic testing on the scale model. If numerical methods for non-linear behaviour are left out, the capacity curve is offering important information on the development of response parameters and DI over increasing seismic actions.

It is worth to note that the results shown have been obtained using a single simulation exploiting the advantages of the ETA method. The advantage of computational time also unlock opportunities over parametric analysis. With these procedures, it may be possible to establish the capacity curves associated with typical geometries of concrete gravity dams and define a classification of dams for their seismic performance. DI curves can be defined as

well, like those indicated, to understand the most critical failure mode and the associated limit of acceptance.

With the global and local measure of the seismic response of dams under non-linear behaviour, it is also permitted in principle to follow the example of the buildings sector on the definition of the so-called "structure or behaviour factor". This will allow the analysts to perform linear analysis with seismic spectra properly scaled down to consider the accepted level of damages.

3.4 Assessment of an Arch Dam Portfolio

Figure 7 represents the relationship between the seismic action demand against the post-processed response. For more details on the developments behind these curves refer to the paper presented by the 1st and 3rd authors during the 13th ICOLD Benchmark [1]. Additional curves have been provided for other relevant EDPs in a separate paper [8].

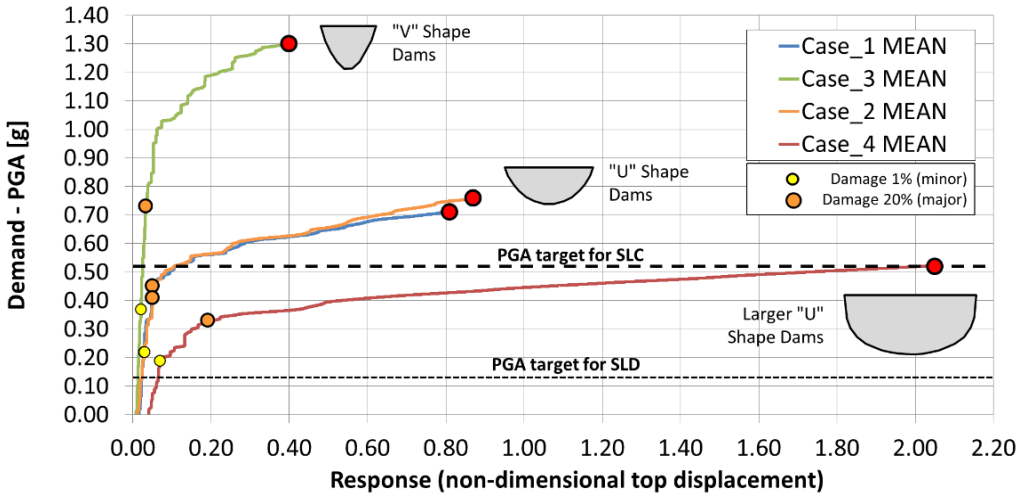

Figure 7: Capacity curves for Dams 1 to 4 with damage points, dotted lines represent indicative limit states.

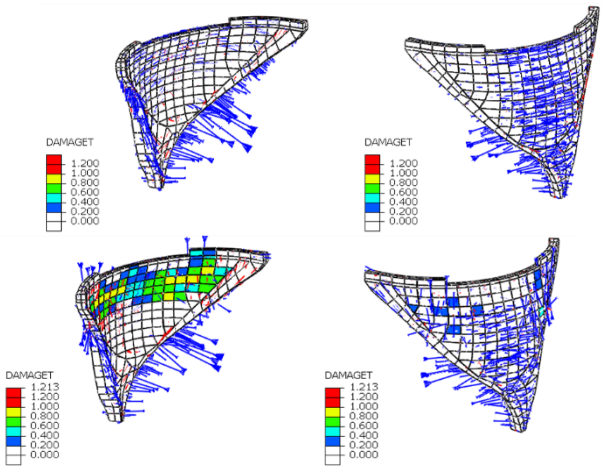

Figure 8: Damage state for Dams 3 under seismic forces (PGA 0.13g) at the SLS limit state (deformed shape x 200) and at the force (PGA 0.52g) at ULS limit state (deformed shape x 10).

According to the results obtained in this study, larger "U" shaped dams, result to be the most vulnerable, while "V" shaped dams provide higher seismic resistance. Each of the curves also shows key points associated with damages of the upstream and downstream faces of 1% and 20% considered respectively minor and major damages. The relationship between

these points and the associated serviceability and collapse limit states, represented by dotted lines, give an idea of the safety factor often translated in D/C ratios. As mentioned previously, these ratios should be widely investigated and discussed to establish what can be defined as acceptable in terms of overall seismic safety. If these criteria cannot be defined considering the bespoke nature of this type of dams, the proposed method can be used as a tool to compare qualitatively the dynamic response of different structures or to have a better understanding of the impact of model assumptions over the seismic response.

For instance, one of the most controversial issues on this regard is the well know "foundation massless" approach, which is the method widely adopted for practical seismic safety assessment of dams so far. Nevertheless, it has been extensively demonstrated that such method provides over-conservative and misleading dam response. To properly consider such effects a drastic increase in size and density of FEM domains is required [12]. Capacity curves, being able to represent the dam vulnerability in just one synthetic picture, can help to identify a critical PGA value beyond which the massless approach is no longer valid to achieve a consistent and realistic dam response (see Figure 9).

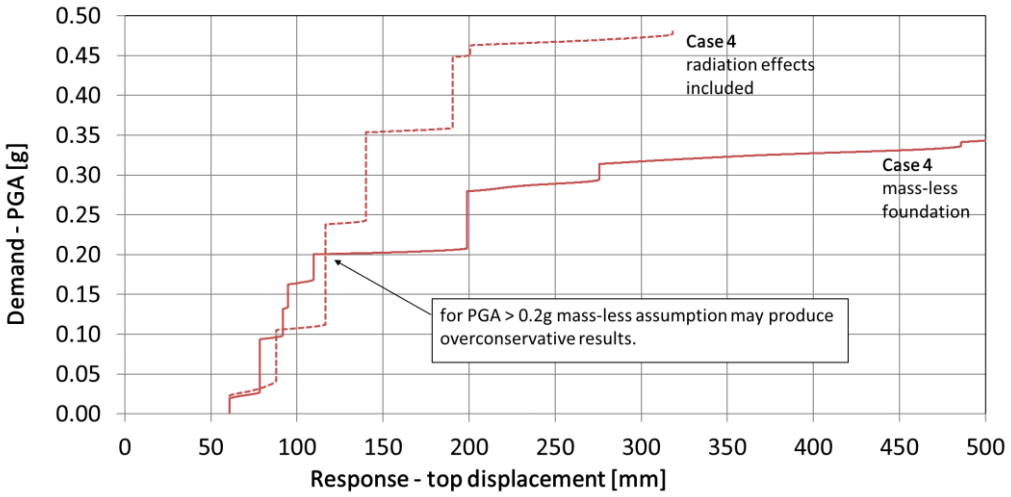

Figure 9: Capacity functions for Dams 4: Sensitivity analysis performed using ETEF 2 and two alternative assumptions for the model, introduction of mass and damping in the foundation (hidden line) and behaviour of the concrete purely linear (dotted line).

Moreover, the wide range of uncertainty affecting the model parameters cannot always be reduced by means of experimental investigations (e.g. concrete non-linear parameters, MCE equivalent loadings, scale effects, etc.), but can be numerically evaluated only through the execution of significant amount of sensitivity analyses, which are very expensive and not practical when using time history analysis. The capacity curves proposed can instead ease and drastically shorten the amount of time requested for a full sensitivity analysis allowing a quick identification of the most important parameters affecting the dam response, on which possibly focus the resources for experimental investigations.

4 PRESENT AND FUTURE OPPORTUNITIES OFFERED BY CAPACITY FUNCTIONS

The most advanced (or latest) regulations and guidelines regarding the seismic assessment of existing dams are very demanding in terms of methods, resources and time needed for its accomplishment. Moreover, even if properly executed, the analyses are significantly affected by uncertainty, particularly when strong earthquakes have to be considered and strong nonlinear effects on construction joints and concrete are expected to

occur. In this light, the information provided by the "capacity functions" before described, can be very useful to make balanced decisions about the modelling assumptions.

The capacity functions are also crucial to judge the safety factor available against failures for existing structures. This graphical form of the seismic response of the dams may help decision makers to drive economic efforts for advanced studies or retrofitting techniques.

It is worth mentioning that standardised seismic functions such those used in the ETA method may resolve major issues associated with the arbitrary selection of natural accelerograms. It is intuitive that it is hard to compare the seismic response of dams in the non-linear field if the time history used are different. It is worth to note that according to the experience of some of the authors, legislators are reluctant to the use of synthetic signals. This may represent a major obstacle for the ETA method and other similar methods.

5 CONCLUSIONS

Capacity functions are recognized in the buildings sector as tools to judge their non-linear behaviour. The advantages of their application seem remarkable and may be crucial within the seismic assessment procedures for concrete dams. A brief introduction to their use and the theoretical background have been shown in the paper using some examples.

Despite the implementation of the procedures is still in a preliminary stage, the capacity curves may represent a powerful tool to meet some of the key requirements introduced by modern technical codes. The ETA method represents a good choice to determine the capacity curves with reasonable computational time. More recent studies on the generation of ETEF functions are addressing the main concerns received by the sector on their validity.

It is the authors' opinion that capacity curves in the form of standardized procedures will be available in the next future. Their comparison on a large scale will highlight crucial information of the seismic response of dams characterized by similar geometries and conditions.

AKNOLEDGMENTS

The first author would like to thank the Mott MacDonald BSE Professional Excellence lead for funding the attendance to the symposium clarifying that most of the work presented has been developed outside Mott MacDonald.

REFERENCES

[1] M. Meghella, L. Furgani, *Endurance Time Analysis for the Seismic Vulnerability of Arch Dams*, 13th International Benchmark on the Numerical Analysis of Dams 9-11 , pp. 251-258, Lausanne, (2015).

[2] H.E. Estekanchi, A. Vafai and M. Sadeghaza, *Endurance Time Method for Seismic Analysis and Design of Structures*, Scientia Iranica, Vol. 11, No. 4, 361-370, Sharif University of Technology, (2004).

[3] G. R. Darbre, M. Schwager and R. Panduri, *Seismic safety evaluation of all large dams in Switzerland: Lessons learned*, 26th International Congress on Large Dams, Vienna, (2018).

[4] A. Andonov, A. Iliev and K. S. Stoev, *Towards Displacement-Based Seismic Assessment of Concrete Dams Using Non-linear Static and Dynamic Procedures*. Structural Engineering International, (2013).
[5] M.A. Hariri-Ardebili and V.E. Saouma, *Single and multi-hazard capacity functions for concrete dams*, Soil Dynamics and Earthquake Engineering, 101, 234-249, (2017).
[6] D. Vamvatsikos and C. A. Cornell, *Applied incremental dynamic analysis*, Earthquake Spectra, 20(2), 523-553, (2004).
[7] M.A. Hariri-Ardebili and V.E. Saouma, *Quantitative failure metric for gravity dams*, Earthquake Engineering & Structural Dynamics, 44(3), 461-480, (2015).
[8] M.A. Hariri-Ardebili, L. Furgani, M. Meghella and V.E. Saouma, *A new class of seismic damage and performance indices for arch dams via ETA method*, Engineering Structures, Volume 110, Pages 145-160, (2016).
[9] Shome, N., *Probabilistic seismic demand analysis of nonlinear structures*, PhD Dissertation, Stanford University, (1999).
[10] M.A. Hariri-Ardebili and V.E. Saouma and K.A. Porter, *Quantification of seismic potential failure modes in concrete dams*. Earthquake Engineering & Structural Dynamics, 45(6), 979-997, (2016).
[11] M. Mashayekhi, H.E. Estekanchi, H. Vafai and S.A. Mirfarhadi, *Development of hysteretic energy compatible endurance time excitations and its application*. Engineering Structures, 177, 753-769, (2018).
[12] A. Lokke, A.K. Chopra "*Direct finite element method for nonlinear analysis of semi-unbounded dam-water-foundation rock systems*", Earthquake Engineering & Structural Dynamics, 46(8), 1267-1285, (2017).

Dynamic behavior of high arch dams under recorded seismic accelerograms Study on the influence of reservoir water level

André Alegre[1], Sérgio Oliveira[2], Margarida Espada[3] and Romano Câmara[4]

Laboratório Nacional de Engenharia Civil (LNEC), Concrete Dams Department
Av. do Brasil 101, Lisbon, Portugal
E-mail: andrefalegre92@gmail.com

Keywords: Seismic response of high arch dams, Recorded accelerograms, Reservoir water level.

Abstract. *In this paper the seismic response of a large arch dam (290 m high), located in a high seismicity region, is analysed. The goal is to study the influence of the reservoir water level in the dam's dynamic response under recorded seismic accelerograms. The numerical calculations are carried out using a 3D finite element program (DamDySSA3.0), developed in MATLAB, for linear dynamic analysis of arch dams. The 3DFEM model is based on a formulation in pressures and displacements, considering a state space approach to solve the coupled eigenproblem with damping, while the seismic response is computed by means of direct integration in time domain using the Newmark method. The dam-reservoir-foundation system is discretized using cubic 3D finite elements with 20 nodal points. The seismic analysis of the dam is performed for the Jiashi earthquake (April5, 1997), using the recorded seismic accelerogram as input, and considering two different reservoir water levels, a massless foundation and a global damping of about 5%. The main numerical results are presented, including displacement and acceleration time histories, as well as the hoop and cantilever stresses envelopes.*

1 INTRODUCTION

Most of the major arch dams currently in operation, under construction or in the design phase, are located in seismic regions, as is the case of several of the new large dams under construction in China. Due to the high potential risk associated with large dams, it is fundamental to develop adequate methodologies to evaluate their behaviour under seismic events [1] and to support safety control activities [2]. With this aim, Seismic and Structural Health Monitoring (SSHM) systems have been installed in several large dams, allowing to control the evolution of the modal parameters over time [3] and to characterize the structural effects due to seismic events, provided that they include appropriate software to manage and analyse monitoring data and to perform the comparison between experimental and numerical results [3, 4, 5]. Nonetheless, important challenges still arise in the seismic analysis of arch dams in both monitoring and modelling, given that the structural response of the dam is strongly influenced by the water-structure dynamic interaction, by damping effects related with reservoir pressure waves radiation, by

[2] Laboratório Nacional de Engenharia Civil, soliveira@lnec.pt
[3] Laboratório Nacional de Engenharia Civil, marga.espada@gmail.com
[4] Laboratório Nacional de Engenharia Civil, romano@lnec.pt

movements of contraction joints and cracks and, of course, by the seismic vibrations at the foundation and at the dam body. Regarding the influence of the reservoir water level in the dynamic response of dams, which is to be studied in this paper, it is important to remind that the full reservoir condition is generally assumed in seismic calculations. However, the oscillatory movements of greater amplitude can occur for non-full reservoir conditions, as shown in recent works [6].

In this context, the importance of performing reliable numerical simulations (Fig. 1) in order to predict the seismic behaviour of arch dams should be highlighted. These studies are off great use in the scope of SSHM of dams, namely for the comparison between the measured response during earthquake events and the corresponding seismic response computed with 3DFEM models, considering the real reservoir water level and the measured acelerogramas at the rock mass foundation during the seismic event as inputs to the numerical models.

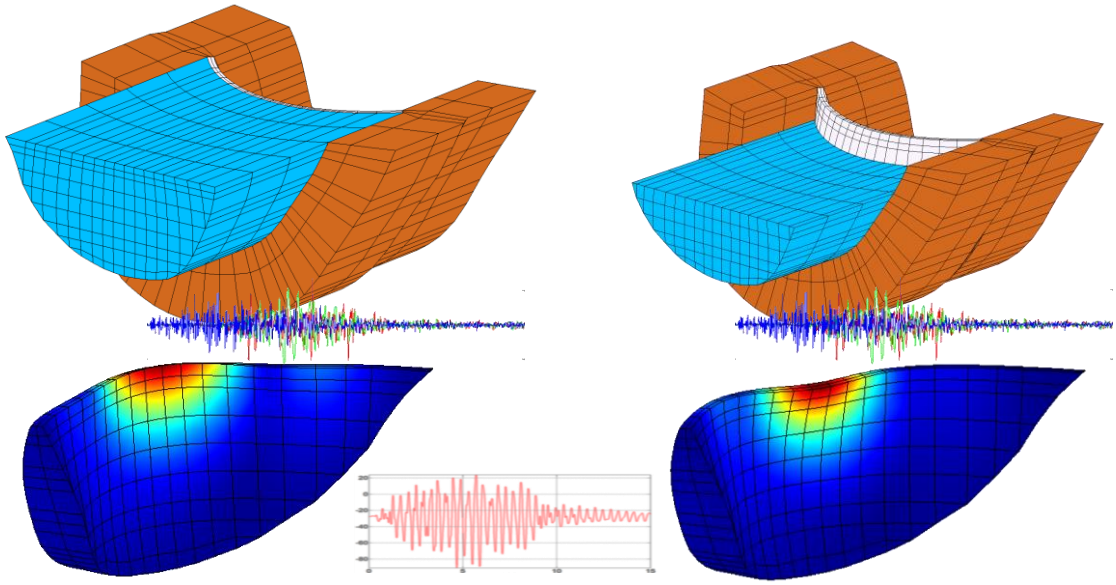

Figure 1: Numerical analysis of the seismic response of an arch dam for different reservoir water levels.

2 MODELING THE SEISMIC BEHAVIOR OF ARCH DAMS

For the simulation of the dynamic response of dams under seismic loading it is essential to use reliable numerical models, based on robust mathematical formulations and using adequate simplifying hypotheses. Here we present some considerations regarding the numerical modelling of dam-foundation-reservoir systems and the 3DFEM model implemented in the program DamDySSA3.0, used to carry out the seismic calculations.

2.1 Dam-foundation-reservoir systems. Water-structure dynamic interaction

For simulating the dynamic behaviour of dam-reservoir-foundation systems and the solid-fluid dynamic interaction, several formulations and models can be used, aiming at reproducing the measured response of dams under real seismic events as accurately as possible. In the numerical models, different hypothesis can be assumed, namely in what concerns the water-structure motion coupling [7, 8], the geometry of the dam and reservoir [9], the coupled system's global damping [4] and other hydrodynamic and foundation effects [10, 11].

For dynamic analysis of arch dams using Finite Element Method (FEM) based formulations [12] (Fig. 2)., it is common to use classic added water mass models based on Westergaard's solution [7] to simulate the hydrodynamic pressures in a simplified way. These

models, although very useful and easy to implement, present limitations in the simulation of the dam-reservoir dynamic interaction. Therefore, more sophisticated models can be used, namely coupled models [8, 12], based on FEM formulations in displacements and pressures that enable to simulate the propagation of the pressure waves in the water by means of a FE discretization of the reservoir. As regards the calculation of the seismic response in time domain, the coupled problem can solved using a state space approach, in complex modal coordinates, or by direct time integration, in general coordinates.

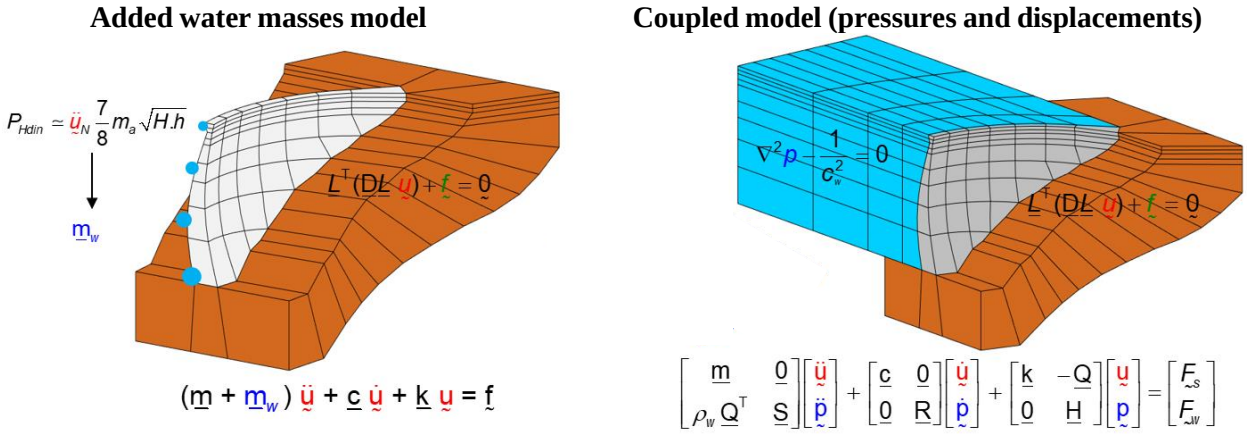

Figure 2: FEM based numerical models to simulate the water-structure dynamic interaction.

2.2 Developed MATLAB code: DamDySSA3.0

The numerical calculations were performed with DamDySSA3.0, a program developed in LNEC, using MATLAB, for linear dynamic analysis of arch dams. The dam-reservoir-foundation system is modelled using a coupled model [8], based on a FEM formulation in displacements and pressures [12]. The implemented coupled formulation enables to simulate the solid-fluid dynamic interaction, considering the propagation of pressure waves along the reservoir. For the solid domain the hypothesis of proportional or non-proportional damping can be assumed, while in the fluid domain the damping effect is associated with the energy loss by radiation of the hydrodynamic pressure waves. The foundation is simulated as an elastic, massless substructure. Also, the contraction joints are assumed to have linear behaviour. The dynamic calculations are performed for the coupled dam-reservoir system: the seismic response in displacements (dam) and pressures (reservoir) is computed by direct time integration using the Newmark Method.

DamDySSA3.0 includes an interactive and versatile graphical interface, developed in MATLAB (Fig. 3), which presents high quality graphical representations to facilitate the analysis and interpretation of the results obtained in the numerical calculations. As outputs, the program provides 3D representations of the dam-foundation-reservoir model, the natural frequencies and modal configurations of the main vibration modes, and the main results of the seismic analysis, including acceleration and displacement histories in certain nodes, as well as the displacement and stress fields in the dam body for specific time instants when the maximum displacements occur.

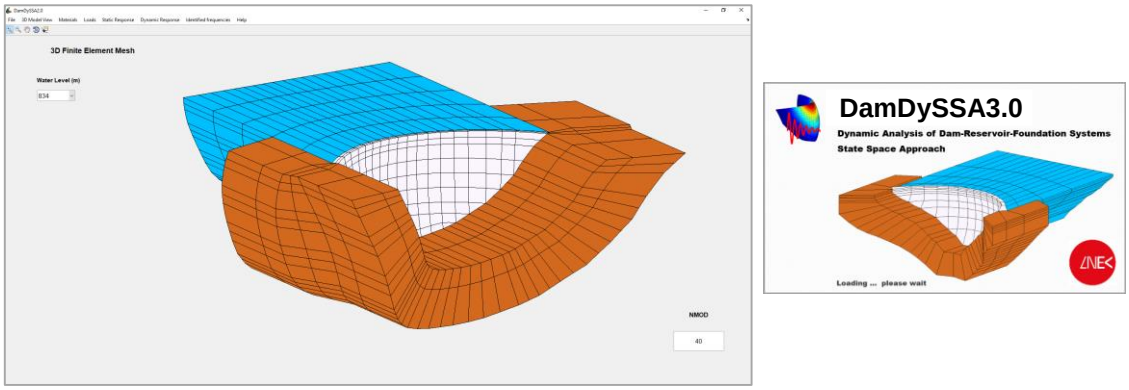

Figure 3: DamDySSA3.0. A 3DFE program for dynamic analysis of arch dams.

3 SEISMIC RESPONSE OF A 290 m HIGH ARCH DAM

The numerical results are presented in this section for the chosen case study, a large arch dam (Fig. 4) located on a tributary of the Yangtze River in Southwest China. The dam has been under construction since 2008 and is expected to go into operation in 2021. It is a double-curvature arch dam with a maximum height of 290 m above the foundation. The arch at the crest presents a development of 710 m between banks. The minimum thickness is of 14 m at the crest and the maximum of about 64 m at the insertion.

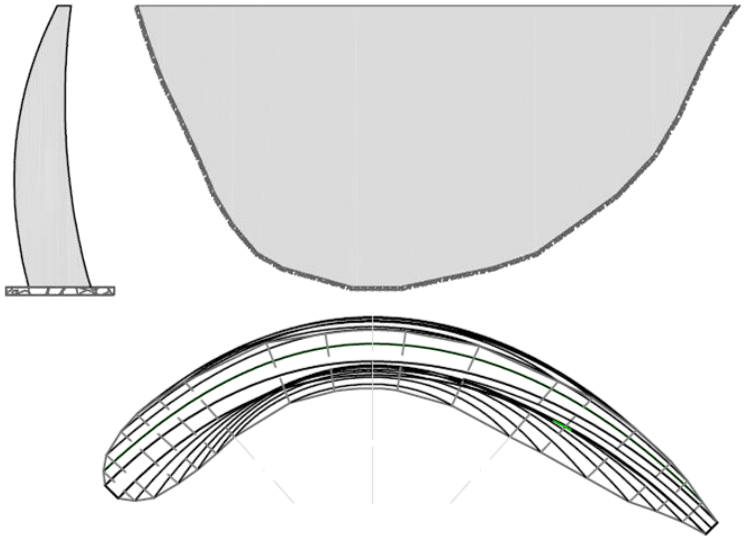

Figure 4: Arch dam, 290 m high. Cross section, front view and plan view.

The main results of the present work, regarding the study of the seismic behaviour of the abovementioned arch dam, which were computed with DamDySSA3.0, are presented herein. The aim is to evaluate the influence of the reservoir water level variations in the dam's response under earthquake motion, namely for a real accelerogram with a peak acceleration of about 0.23g, recorded during the Jiashi earthquake, China, on April 5, 1997, The numerical calculations are performed for two water levels: full reservoir (H_w=834 m) and a non-full reservoir, considering the water level at 34 m below the crest (H_w=800 m).

3.1 Seismic response for full reservoir

First, the numerical study of the dam's seismic response was carried out considering a full reservoir (Fig. 6) and using the referred Jiashi earthquake accelerogram as input to the

numerical model In this case, despite the asymmetry of the dam, the modal configurations are symmetric for modes 1, 3 and 4, and antisymmetric for mode 2 (Fig.7). For a seismic analysis, it is important to know the natural frequencies in order to evaluate the frequency content of the seismic load.

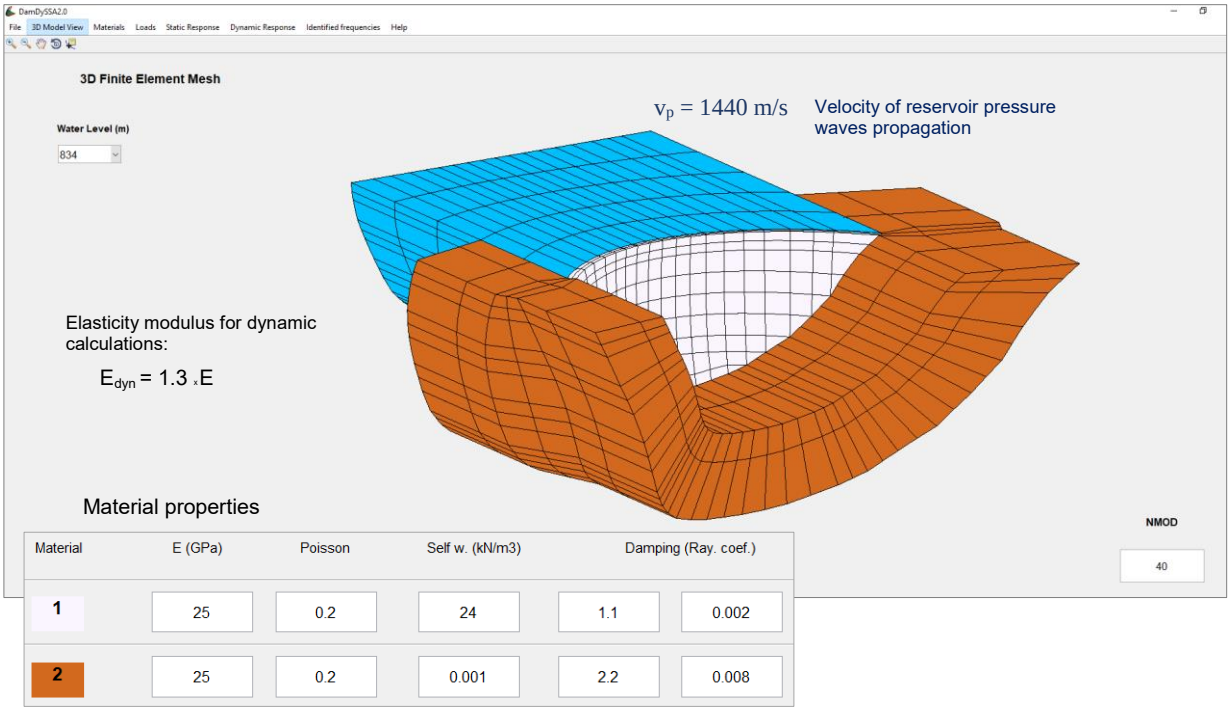

Figure 6: Dam-reservoir-foundation system with full reservoir. 3DFE discretization (cubic FE, 20 nodes), and material properties

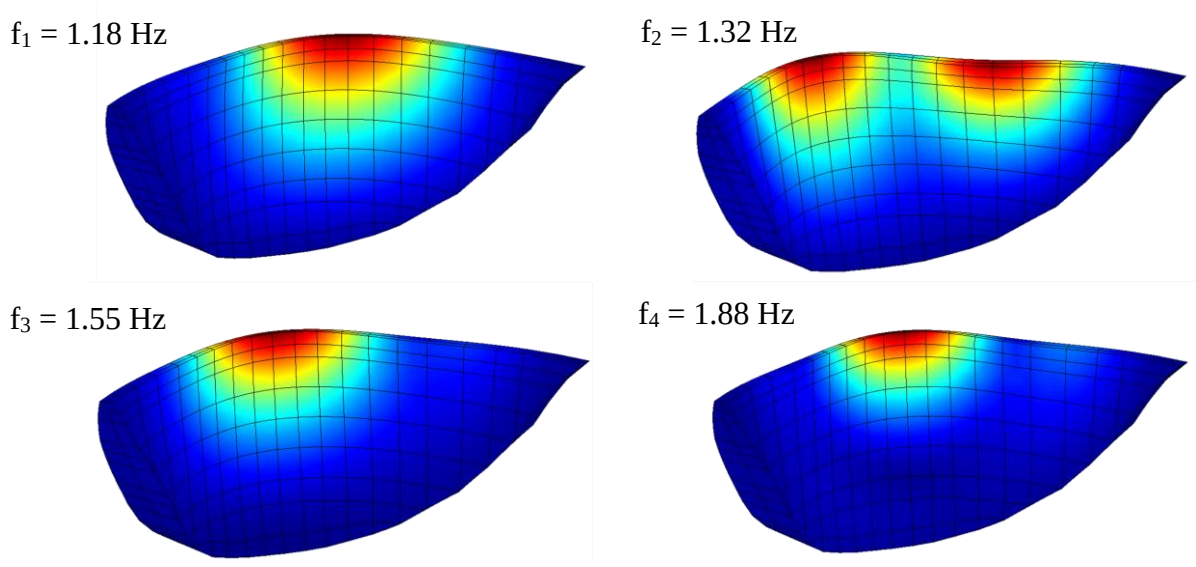

Figure 7: Vibration modes and natural frequencies for full reservoir.

The dam's seismic response is shown in Fig. 8, considering only the application of the seismic load. For full reservoir, it should be noted that the main natural frequencies do not coincide with the largest peaks of the seismic acceleration Fourier spectrum. Concerning the accelerations at the control node, located at the top of the central cantilever, a peak acceleration of about 16 m/s^2 was calculated in the upstream-downstream direction, which represents an

amplification of about 7 times in relation to the seismic acceleration applied at the base. The maximum radial displacement due to the seismic load occurs in the upper central zone, to the left of the central cantilever, and corresponds to an oscillatory movement with a half-amplitude of about 100 mm. The principal stresses, computed at the time instant when the maximum downstream displacement occurs, are also presented: high tensile ($\sigma \approx 3.3$ MPa) and compressive hoop stresses ($\sigma \approx -4.6$ MPa) occur in the upper central zone at the upstream face).

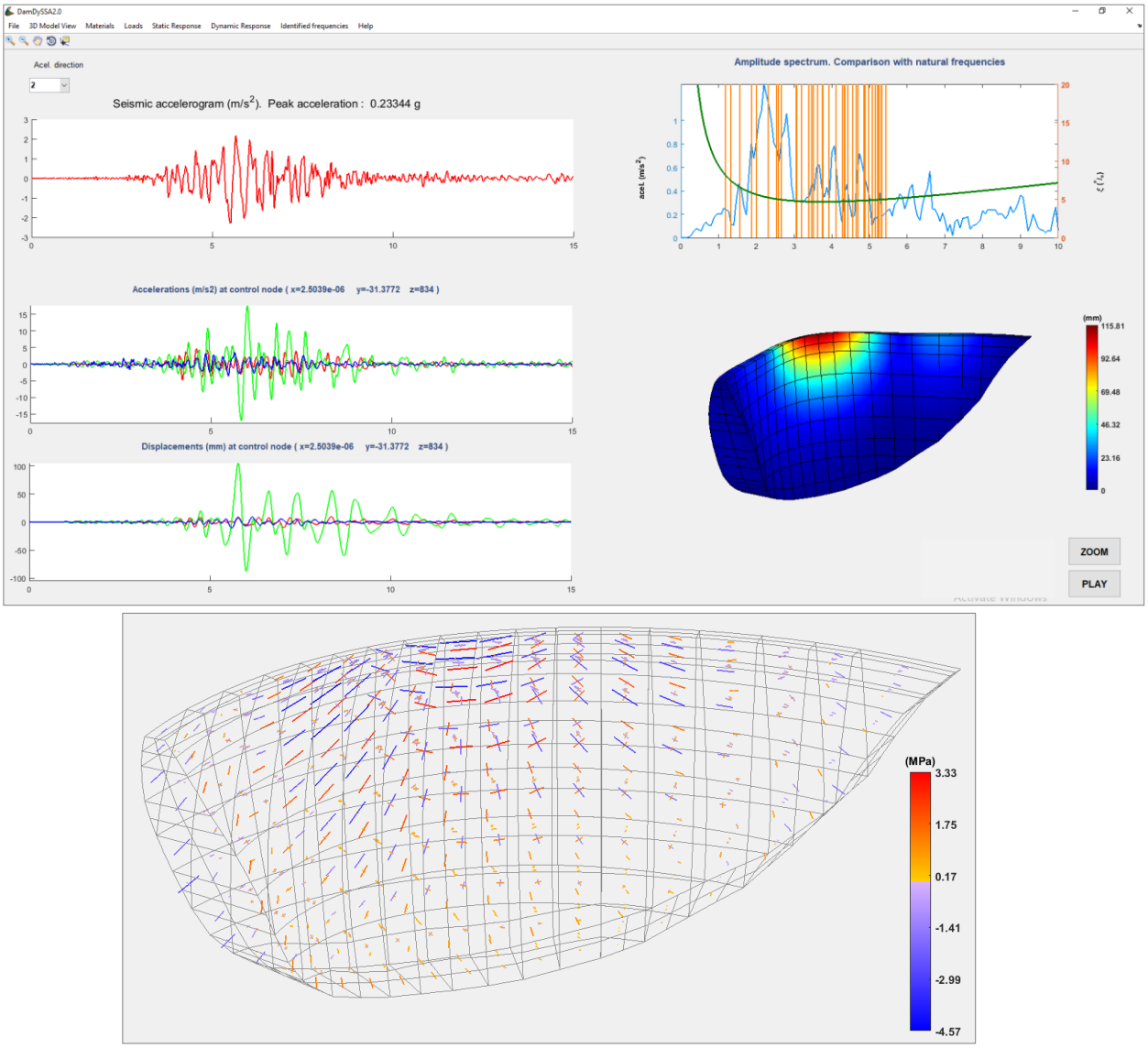

Figure 8: Seismic response for full reservoir. Accelerogram in the upstream-downstream direction and Fourier spectrum (with Rayleigh damping law and the main dam natural frequencies); history of accelerations and displacements at the top of the central cantilever; and displacement field and principal stresses at the instant the maximum downstream displacement occurs.

Fig. 9 shows the hoop and cantilever stress envelopes at the central cantilever for a dynamic load combination involving the self-weight (SW), the hydrostatic pressure for full reservoir (HP290) and the seismic acceleration (applied at the base): SW+HP290+Earthquake. The highest hoop compressions are of $\sigma \approx -11$ MPa (in both faces, upstream and downstream), in the upper zone; tensions in the hoop direction do not arise and the minimum hoop stresses are inferior to - 1 MPa, near the insertion. Regarding the cantilever compressions, the

maximum values are around σ ≈ - 5 MPa at the downstream face, close to the base. For this earthquake, even when the largest seismic upstream displacements occur, which might result in significant hoop tensions (or, alternatively, cause the contraction joints to open), the dam remains generally under compression due to the static compressive stresses. In summary, no tensions occur for full reservoir, which means that the opening of the contraction joints is not expected.

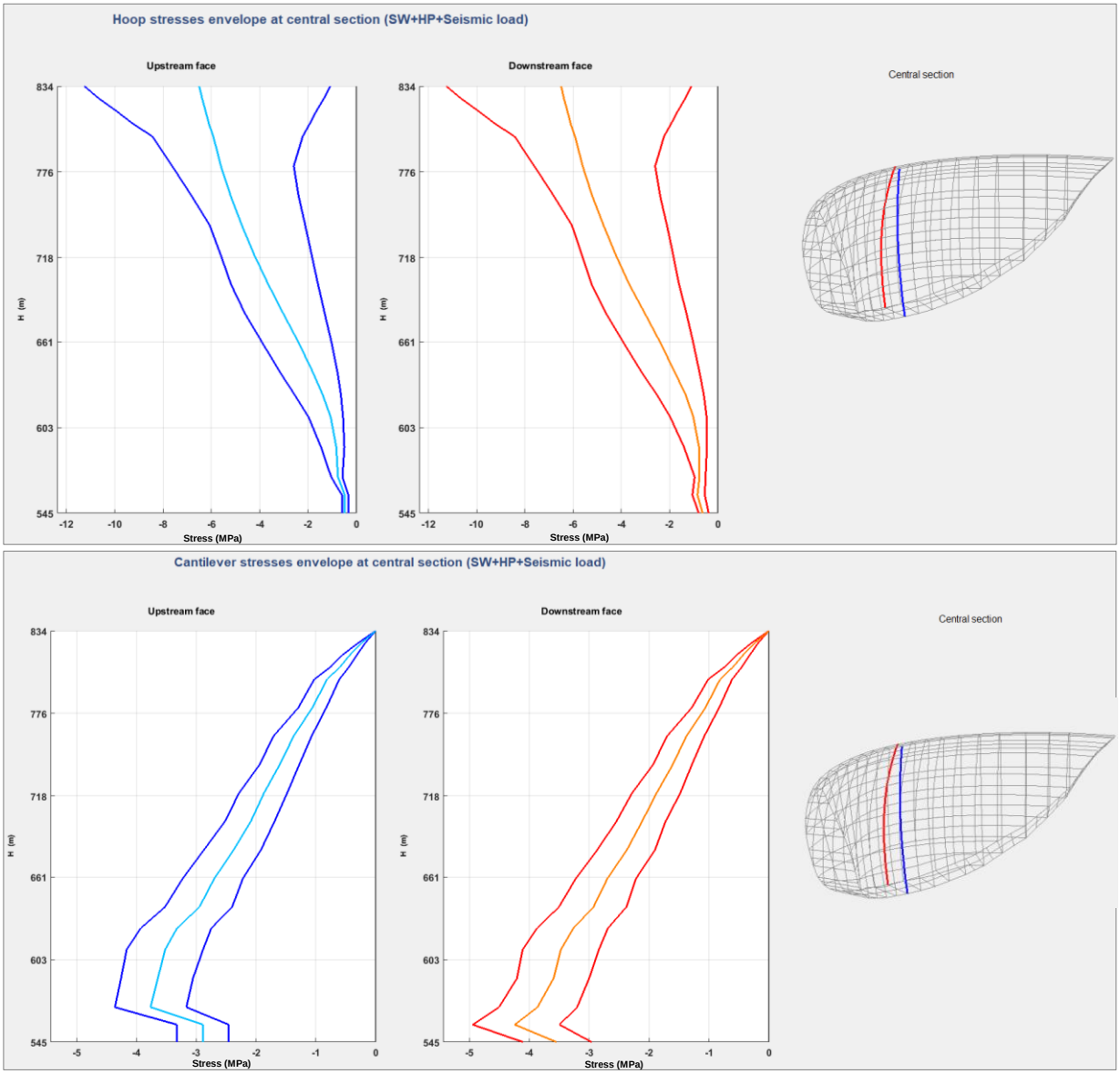

Figure 9: Seismic response for full reservoir. Results for the combination SW + HP290 + Earthquake. Hoop and cantilever stresses envelopes in the central section.

3.2 Seismic response for non-full reservoir (water level at 34 m below the crest)

In this section are presented the numerical results of the dam seismic response considering the reservoir water level 34 m below the crest (Fig. 10) and the same Jiashi earthquake accelerograms. As expected, with a lower water level, the mass of the global coupled system is reduced and thus the natural frequencies increase, while the modal configurations are similar to those obtained for a full reservoir model (Fig. 11).

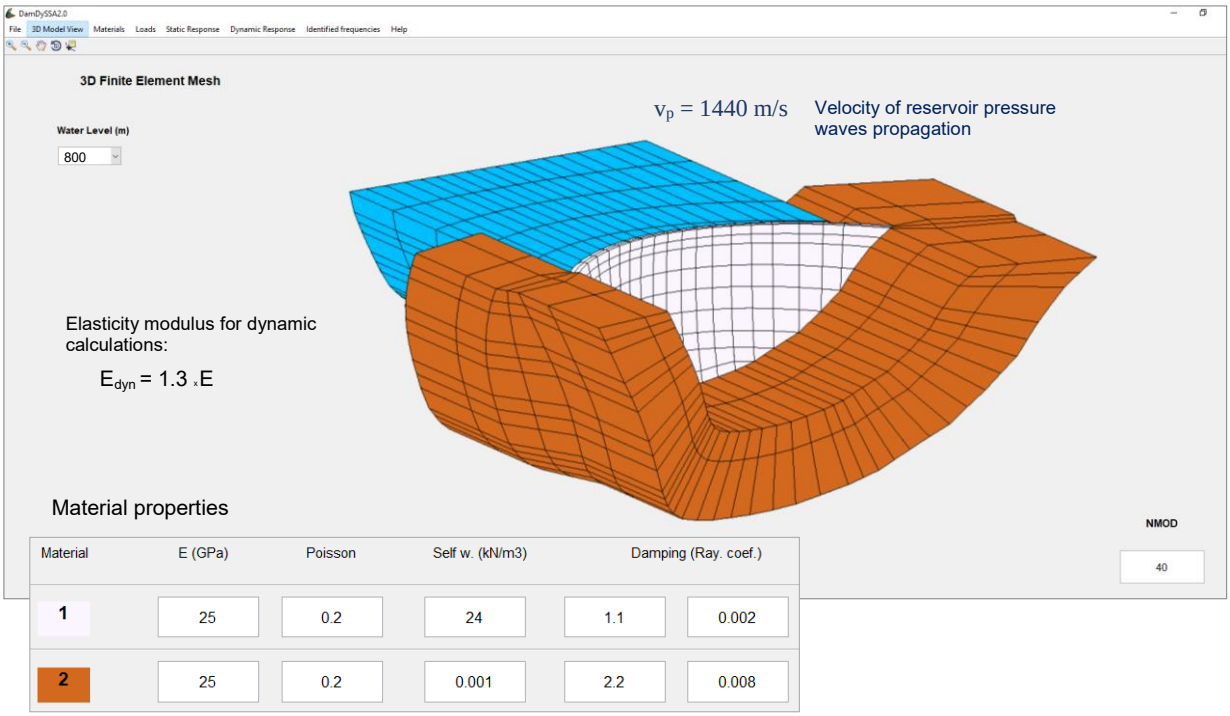

Material	E (GPa)	Poisson	Self w. (kN/m3)	Damping (Ray. coef.)	
1	25	0.2	24	1.1	0.002
2	25	0.2	0.001	2.2	0.008

Figure 10: Dam-reservoir-foundation system with non-full reservoir: water level 34 m below the crest. 3DFE discretization (cubic FE, 20 nodes), and material properties.

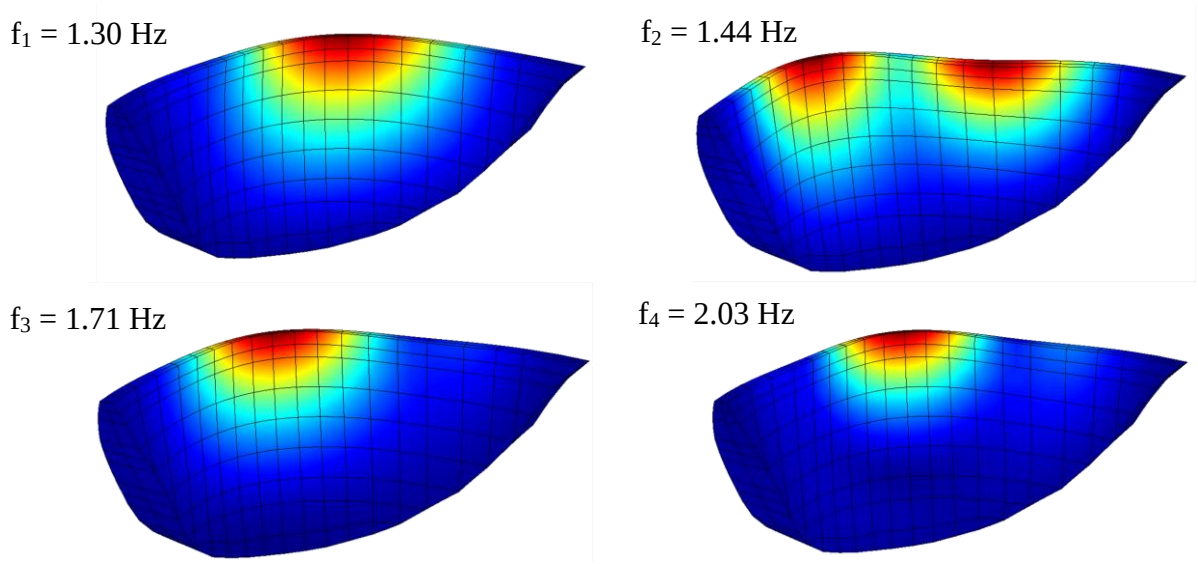

Figure 11: Vibration modes and natural frequencies for non-full reservoir: water level 34 m below the crest.

The dam's seismic response under the seismic load is shown in Fig. 12. In what concerns the accelerations at the top of the central cantilever, a peak acceleration of about 22 m/s^2 was computed in the upstream-downstream direction, representing an amplification of around 9 in comparison with the seismic peak accelerations at the base. Again, the maximum radial displacement solely under seismic loading were computed in the upper central zone, resulting in an oscillatory motion with a 100 mm half-amplitude. As in the calculation for full reservoir, the higher tensions and compressions arise in the hoop direction at the upper zone (upstream face). However, due to the lower water level a decrease in the maximum tensions and an increase in the maximum compressions is obtained.

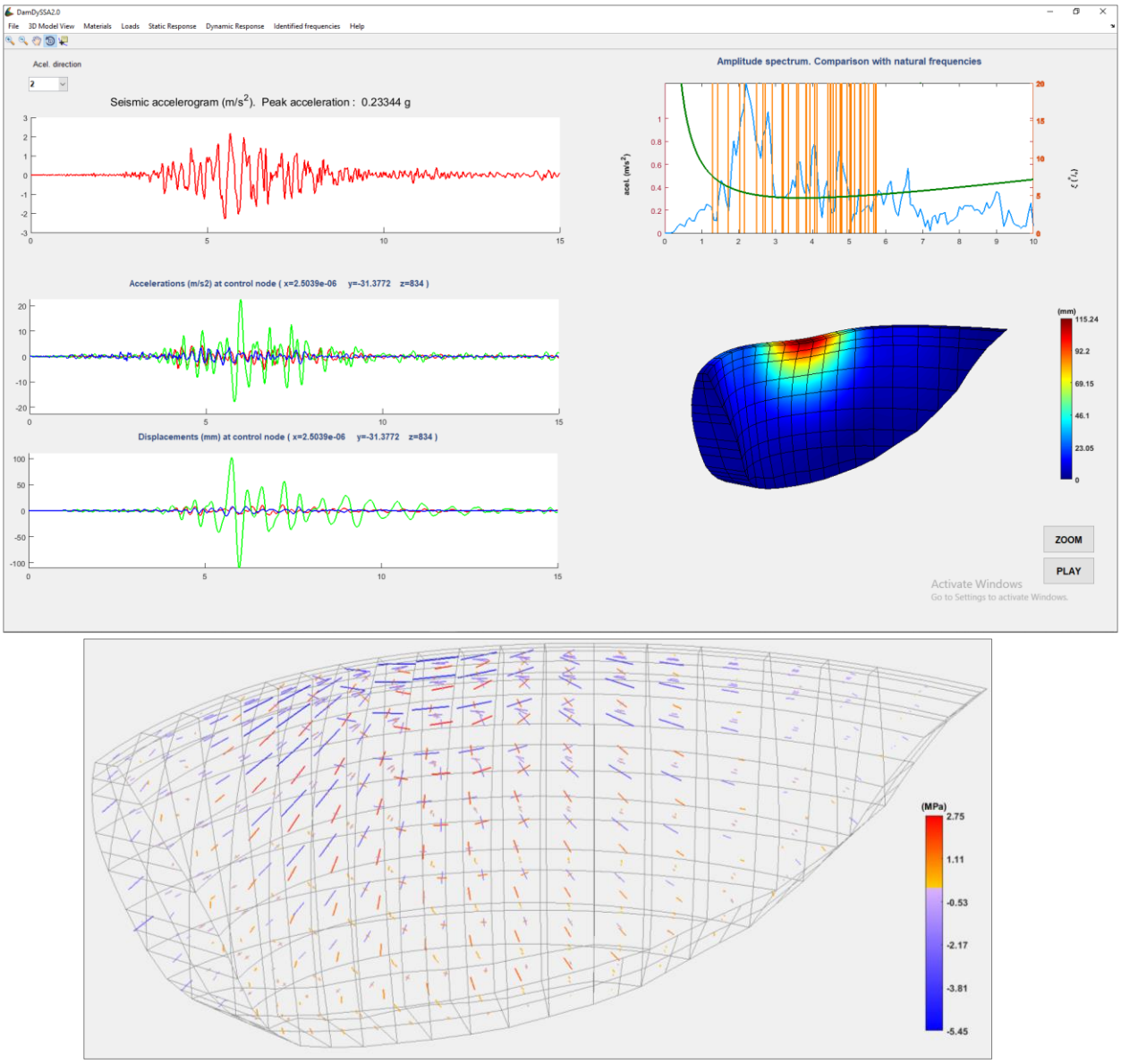

Figure 12: Seismic response with non-full reservoir: water level 34 m below the crest. Accelerogram in the upstream-downstream direction and Fourier spectrum (with Rayleigh damping law and the main dam natural frequencies); history of accelerations and displacements at the top of the central cantilever; and displacement field and principal stresses at the instant the maximum downstream displacement occurs.

The stress envelopes at the central section for the load combination SW+HP256+Earthquake are presented in Fig 13. The maximum hoop compressions, ($\sigma \approx$ - 7.5 MPa) are calculated in both upstream and upstream faces at the upper zone; once more, tensions in the arch direction do not arise. The minimum hoop stresses are inferior to - 1 MPa and are calculated near the dam base. In relation to the cantilever compressions, the higher stress values are around $\sigma \approx$ - 5 MPa at the downstream face, near the insertion. In comparison with the stress fields computed for the seismic calculations with full reservoir, one can note that the cantilever stresses envelopes are quite similar, while for the hoop stresses envelopes, a decrease in the maximum and minimum compressions at the upper zone of the central cantilever was obtained. In resume, no tensions arise for the combination with the water level at 34 m below the crest even when the largest seismic upstream displacements occur, hence the contractions joints are not expected to open, as for the previous load combination with full reservoir.

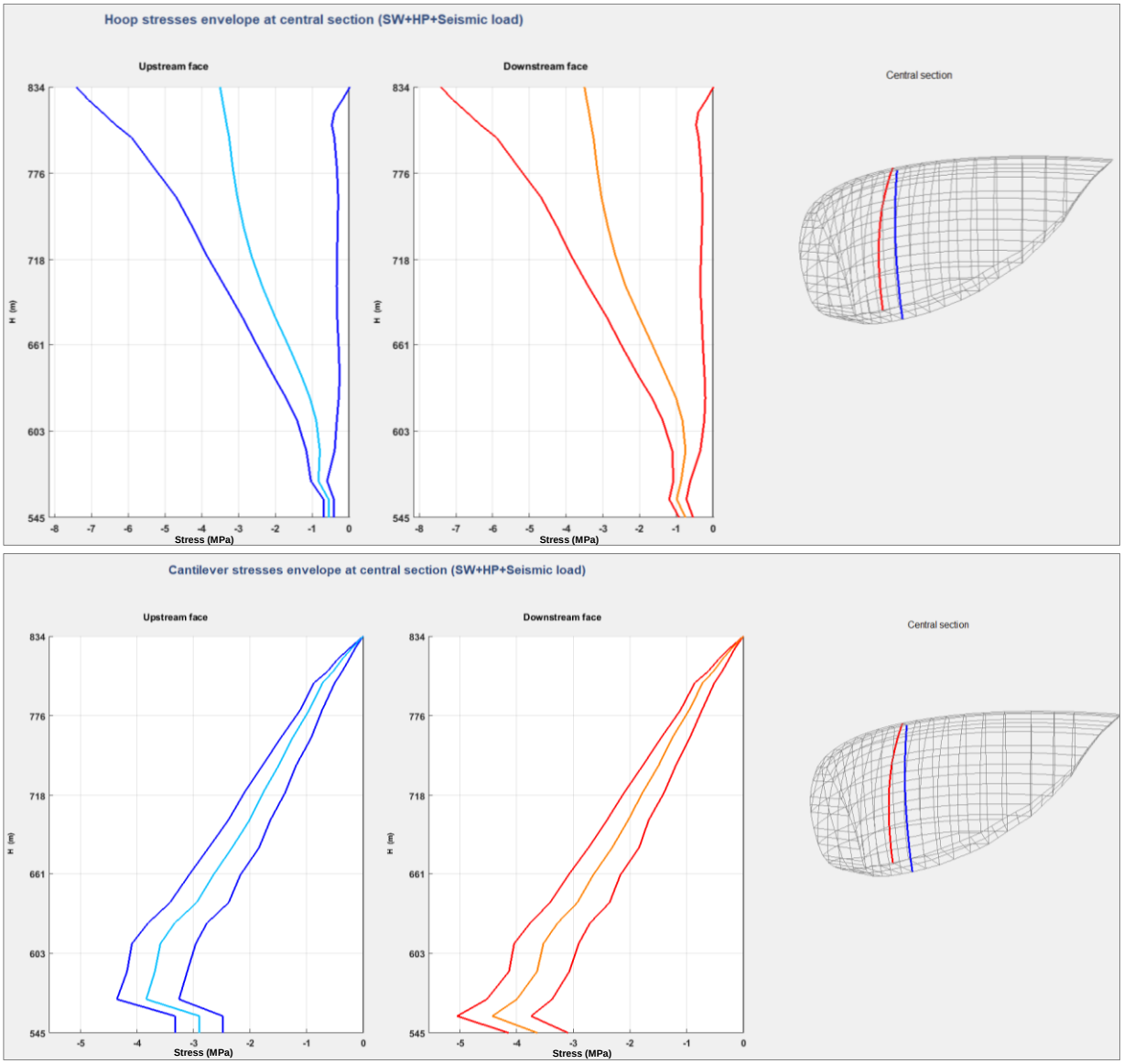

Figure 13: Seismic response for the reservoir water level at 34 m below the crest. Results for the combination SW+HP256+Earthquake. Hoop and cantilever stresses envelopes in the central section.

4 CONCLUSIONS

In this work the program DamDySSA3.0, developed at the Concrete Dams Department in LNEC for linear dynamic analysis of arch dams, was used to study the seismic behaviour of a 290 m high arch dam, considering two reservoir conditions: full reservoir and a reservoir water level at 34 m below the crest. The numerical calculations were carried out using a coupled formulation to simulate the dam-reservoir dynamic interaction, considering the propagation of pressure waves in the reservoir. The seismic analysis is performed for a recorded accelerogram from the Jiashi earthquake (April 5, 1997) with a peak acceleration of 0.23g and considering Rayleigh damping with a damping ratio of about 5% for the frequencies of the main dam vibration modes.

The presented results show that only compressive hoop stresses occur in the upper central zone for the full reservoir combination (SW+ HP290 + Earthquake), which indicates that there will be no opening of the contraction joints. For the combination with the reservoir water level at 34 m from the top (SW+PH256+Earthquake), if the same damping law is used, one can note

that the greatest hoop compressions occur in the upper central zone, at the time instant when the maximum downstream displacements downstream; also, the maximum compression values are clearly inferior than those obtained for full reservoir. In both cases, even when the maximum displacements occur, the contraction joints are not expected to open, given that no tensile hoop stresses arise (if that were to be the case, tensile stresses would be computed at the locations of the contraction joints opening, given that the implemented model does not incorporate joints).

ACKNOWLEDGEMENTS

The authors wish to acknowledge the funding association, Fundação para a Ciência e Tecnologia, Portugal (FCT) for the PhD grant SFRH/BD/116417/2016.

REFERENCES

[1] M. Wieland and R.P. Brenner (2008). Current seismic safety requirements or large dams and their implication on existing dams. Proc. Int. Symposium on Operation, Rehabilitation and Upgrading of Dams, 76th Annual ICOLD Meeting, Sofia, Bulgaria.
[2] Dam Safety Regulation (2018). Decree-law Nº 21/2018 of March 28 (in Portuguese).
[3] S. Oliveira and A. Alegre (2018). Vibrations in large dams. Monitoring and modelling. 26th Congress and 86th Annual Meeting. 1st-7th July, Vienna, Austria.
[4] J. Proulx, G.R. Darbre and N. Kamileris (2004). Analytical and experimental investigation of damping in arch dams based on recorded earthquakes. 13th World Conference on Earthquake Eng., Vancouver, B.C., Canada.
[5] A.K. Chopra and J. Wang (2012). Comparison of recorded and computed earthquake response of arch dams. 15th World Conference on Earthquake Eng., Lisbon, 2012.
[6] A. Alegre, S. Oliveira, R. Ramos and M. Espada (2018). Seismic response of arch dams. Numerical study on the influence of the reservoir water level. Encontro Nacional de Betão Estrutural (BE2018), 7-9 Nov., LNEC (in Portuguese).
[7] H.M. Westergaard (1993). Water pressures on dams during earthquakes. Transactions (ASCE), 98:418-472.
[8] O.C. Zienkiewicz and P. Bettess (1978). Fluid-structure dynamic interaction and wave forces. An introduction to numerical treatment. Int. J. Numer. Meth. Eng., 13:1-16.
[9] M.A. Millán, Y.L. Young and J.H. Prévost (2007). The effects of reservoir geometry on the seismic response of gravity dams. Earthquake Eng. Struct. Dyn., 36:1441-1459.
[10] A.K. Chopra and S. Gupta (1981). Hydrodynamic and foundation interaction effects in earthquake response of a concrete gravity dam. J. Struct. Div. ASCE, 107(8):1399-1412.
[11] G. Fenves and A.K. Chopra (1983). Effects of reservoir bottom absorption on earthquake response of concrete gravity dams. Earthquake Eng. Struct. Dyn., 11:809-829.
[12] O.C. Zienkiewicz, R.L. Taylor and J.Z. Zhu (2005). The Finite Element Method: Its Basis and Fundamentals: 6th Ed., Elsevier Butterworth-Heinemann.

Baixo Sabor concrete arch dam: dynamic monitoring and numerical damage simulation

Sérgio Pereira[1], Jorge Gomes[2], José V. Lemos[3], Filipe Magalhães[4] and Álvaro Cunha[5]

Contruct-ViBest, Faculty of Engineering of the University of Porto (FEUP)
Rua Dr. Roberto Frias 4200-465, Porto, Portugal
E-mail: pereira.sergio@fe.up.pt

Keywords: Concrete arch dam; Continuous dynamic monitoring; Numerical modelling; Simulation of damage

Abstract. *The nowadays-available dynamic monitoring equipment integrating very sensitive low noise sensors creates an opportunity to implement continuously operating dynamic monitoring systems in dams and validate the suitability of these systems to monitor such massive structures with the goal of detecting damage. The detection of abnormal structural behaviour, that may indicate the occurrence of damage, can be based on control charts and is associated with shifts in the modal parameters values that are not explained by other physical phenomena but a change in the structure's stiffness. To test these statistical tools, modal parameters obtained from real field measured time series may be contaminated with simulated damages.*

In this context, this paper describes the continuous dynamic monitoring of Baixo Sabor arch dam, which has been carried out by both ViBest/FEUP (Laboratory of Vibrations and Structural Monitoring) and LNEC (National Laboratory for Civil Engineering). Moreover, it is presented the simulation of a set of plausible damage scenarios and their influence in the dam dynamic properties, namely the natural frequencies, with the aim of testing the ability of the said control charts to identify the emergence of abnormal structural behaviour. For this, a numerical model of the dam developed at LNEC's Concrete Dams Department has been used.

1 INTRODUCTION

The Baixo Sabor hydroelectric development, which is fully operating since 2016, is one of the most recent plants in Portugal, and it is strategically located, taking into account that the water used to produce energy in Baixo Sabor will find four other power plants located downstream, in Douro River. With the aim of studying Baixo Sabor arch dam dynamic properties and their evolution over time, in order to assess the dam's structural health and the effect of exceptional events in its behaviour, a continuous dynamic monitoring of the dam is being carried out by ViBest-FEUP and LNEC. The monitoring takes into account the variation of ambient and operational conditions, as well as the possible evolution of material mechanical properties.

Integrated monitoring systems considering real time data directly obtained from structures, such as the one implemented in Baixo Sabor dam, are very important to the long-

[2] National Laboratory for Civil Engineering (LNEC), jgomes@lnec.pt
[3] National Laboratory for Civil Engineering (LNEC), vlemos@lnec.pt
[4] Construct-ViBest, Faculty of Engineering of University of Porto (FEUP), filipema@.up.pt
[5] Construct-ViBest, Faculty of Engineering of University of Porto (FEUP), acunha@.up.pt

term management of large civil infrastructures [1]. Though health monitoring systems are historically associated with static data, vibration-based systems have already been successfully implemented in different structures such as bridges [2], wind turbines [3], stadia roofs [4] or bell-towers [5]. Such vibration-based health monitoring systems rely on operational modal analysis to continuously identify the structures modal properties, which can be used as monitoring features to evaluate the structures health condition evolution over time. Statistical tools such as control charts can be used to detect the occurrence of damage associated with shifts in the modal parameters values that are not explained by other physical phenomena but a change in the structure's stiffness. To test these statistical tools, modal parameters obtained from real field measured time series may be contaminated with simulated damages.

In this sense, this paper presents a brief description of the dynamic monitoring system installed in Baixo Sabor arch dam, the results obtained during the first six months of continuous dynamic monitoring, between 01/12/2015 and 31/05/2016, and a short introduction to the minimization of the effects of operational and environmental conditions on modal properties. Additionally, the numerical model of the dam developed by LNEC is presented along with the damages scenarios that were simulated using this model, in order to test in the future the suitability of control charts to detect damage with data from Baixo Sabor arch dam.

2 CONTINUOUS DYNAMIC MONITORING OF BAIXO SABOR ARCH DAM

2.1 Instrumented dam and monitoring system

The Baixo Sabor hydroelectric development is located in Sabor river, a tributary of Douro river in the northeast of Portugal. This 123 m high double-curvature concrete arch dam, with a crest at 236 m of elevation, is 505 meters long and its arch is composed by 32 concrete blocks, separated by vertical contraction joints, including six horizontal visit galleries. The reservoir created by the dam has a capacity of 1095 hm^3 at exploration level (234 m of elevation), which corresponds to a flooded area of about 2819 ha .The left part of Figure 1 shows an aerial picture of the dam and the reservoir, referring to May 2016, after the monitoring had started.

In order to identify the dam's dynamic characteristics and their evolution over time, taking into account the variation of ambient and operational conditions, as well as the possible evolution of the materials mechanical properties, a vibration-based health monitoring system has been working in the dam since December 2015, right after it started operating. The continuous dynamic monitoring system consists of 20 uniaxial accelerometers that have been radially disposed in the dam's three upper visit galleries, whose synchronization is achieved using GPS antennas. The right part of Figure 1 shows the position of the accelerometers installed in the dam, marked with red dots in a picture of the structure. The dynamic monitoring system is configured to continuously record acceleration time series with a sampling rate of 50 Hz and a duration of 30 minutes at all instrumented points, thus producing 48 groups of time series per day.

A monitoring software developed at ViBest/FEUP called DynaMo [6] was adapted to process to continuously process the data collected by the monitoring system. Besides backing up the original data samples, this monitoring software performs the pre-processing of the acceleration time series, through trend elimination, filtering and re-sampling, it characterizes vibration levels and it performs the identification of the dam modal properties through automatic operational modal analysis.

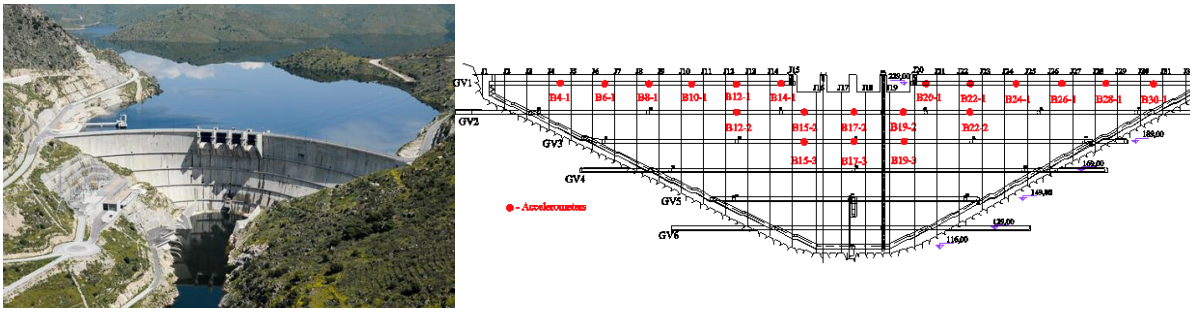

Figure 1 – Baixo Sabor arch dam: a) aerial view (on the left) [7]; b) position of accelerometers marked with red dots (on the right).

2.2 Operational Modal Analysis

The six months of data were processed following the steps described in the previous section. The first five modes of vibration were identified and natural frequencies, modal damping values and modal configurations were obtained. The three-dimensional representations of the identified modal configurations are presented in Figure 2, in which the dashed line represents the dam's original geometry and the modal configuration is represented in red. The first, third and fifth modes are approximately symmetric and the second and fourth are antisymmetric.

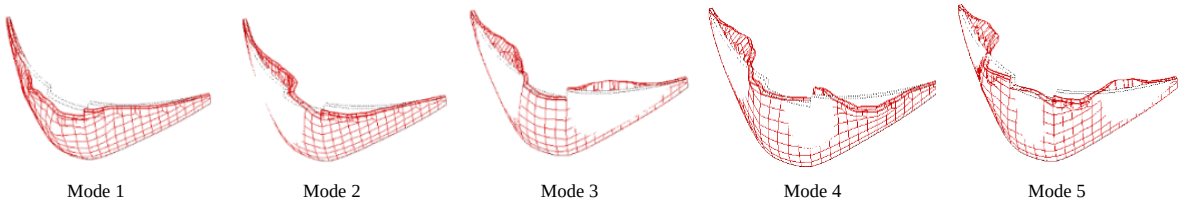

Mode 1 Mode 2 Mode 3 Mode 4 Mode 5

Figure 2 – Modal configuration of the first five modes of Baixo Sabor arch dam.

Modal estimates corresponding to the first five modes are resumed in Table 1. Minimum, maximum, mean and standard deviation frequencies (f) and damping values (d) were obtained and presented for the studied period. It is important to notice the significant difference between minimum and maximum frequencies for each vibration mode (even after the elimination of outliers), which is reflected in the standard deviation values as well, indicating significant oscillations during the evaluation period.

Table 1: Modal Parameters

Mode	$f_{[min;max]}$ [Hz]	f_{mean} [Hz]	f_{std} [Hz]	$d_{[min;max]}$ [%]	d_{mean} [%]	d_{std} [%]	Description
1	[2.43;2.75]	2.53	0.10	[1.16;3.16]	1.50	0.23	Symmetric
2	[2.57;2.92]	2.68	0.12	[0.85;2.11]	1.42	0.15	Antisymmetric
3	[3.33;3.85]	3.51	0.17	[0.55;3.00]	1.67	0.25	Symmetric
4	[3.92;4.50]	4.12	0.18	[0.92;1.82]	1.36	0.16	Antisymmetric
5	[4.78;5.34]	4.99	0.18	[0.75;2.66]	1.88	0.30	Symmetric

However, since the evolution of modal properties is easier to understand when graphically depicted, the evolution over six months of the natural frequencies estimates of the first five modes of vibration of the structure is characterized in Figure 3 – (on the left part of the figure), where each point corresponds to a 12-hour average. Small blank spaces with no

representation correspond to periods of system failure or maintenance, for which no data is available, and each colour represents one vibration mode. As 12-hour averages were calculated, two values are presented per day, leading to a figure visually cleaner, without losing accuracy in the characterization of the modal parameters fluctuations, since their variations are quite slow in very massive structures such as this. Major frequency variations occurred in January due to intense rains and a fast increase in the level of water in the reservoir.

On the other side, the right part of Figure 3 presents the temporal evolution of the first five modal damping ratios using 12-hour averages, with colours corresponding to those in the representation of frequencies. The level of water in the reservoir shows to influence as well the damping ratios, whose values increased as well in January, period after which a higher stability is verified. As observed in other monitoring applications the modal damping estimates present a much higher scatter than the observed in the natural frequencies.

These experimental results obtained during the first filling of a dam reservoir are quite unique and very relevant for the tuning of numerical models that take into account the influence of the water level in the dynamic behaviour of dams.

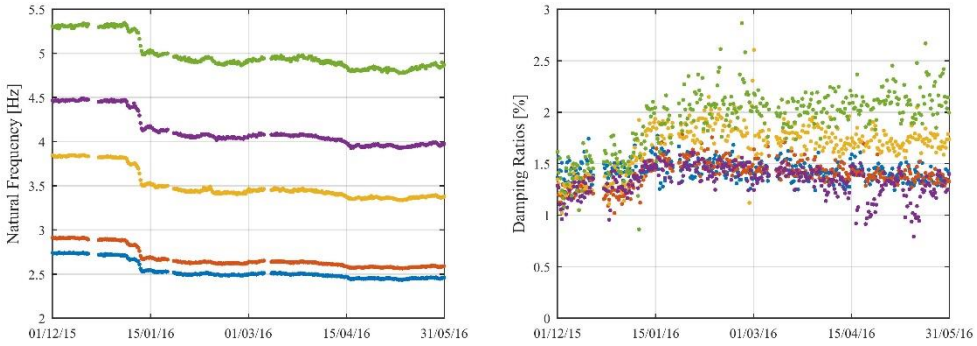

Figure 3 – Time evolution of natural frequencies (on the left) and damping values (on the right) 12-hour average.

2.3 Minimization of Operational and Environmental Conditions

In order to detect small variations of the natural frequencies of the structure motivated by structural alterations, which may be associated with the occurrence of damages, it is important to minimize the effects of environmental and operational factors, such as reservoir water level and temperature. In this sense, the evolution of the level of water in the reservoir and the ambient temperature verified between 01/12/2015 and 31/05/2016 are presented in Figure 4. The water level is rising almost continuously over time, which was expected since the first filling of the reservoir occurred during the studied period. The variation of water level was particularly important in January, during a period of intense rains. In turn, ambient temperature suffers high daily amplitudes, but its daily average is more or less constant until early March, when its values start rising.

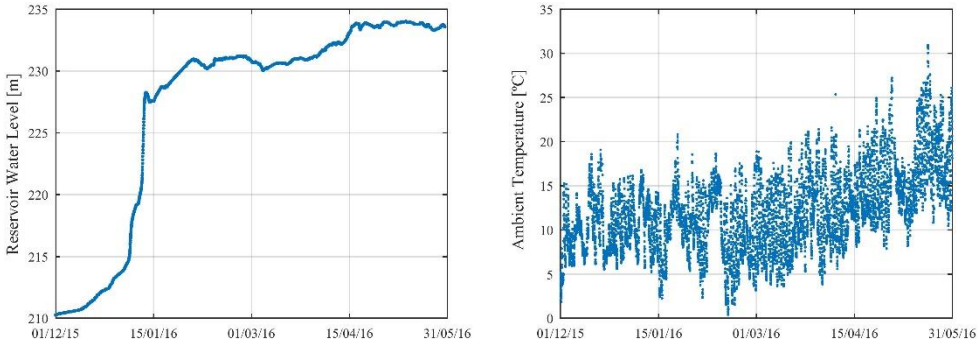

Figure 4 – Time evolution of reservoir water level (on the left) and ambient temperature (on the right)

Since the factor that more strongly affects natural frequencies is the water level, statistical relationships between all the vibration frequencies of the structure and the water level in the reservoir were developed. The representation of the relation between these two variables is presented in Figure 5 (left part of the figure), using the first vibration mode. The obtained quadratic regressions are generally of high quality, presenting values for the determination coefficient of the order of 0.95. It is also important to note that there is much more data for the highest and lowest levels of water in the reservoir during the observation period compared to those in the intermediate zone of the figures due to the intense rains that took place in January, leading to a sudden rise of the water level.

The statistical relations obtained were then used to mitigate the effect of water level in the values of natural frequencies. The standard deviation of each modes frequency during the studied period was drastically reduced. However, there still some variability that could possibly be explained by the variation of temperature. In this sense, the process previously described was repeated, now using the values of natural frequencies corrected from the effect of water level. In this case linear regressions were obtained between ambient temperature and natural frequencies, indicating frequency values increase with the rising of temperature. Lower determination coefficients were obtained, with values between 0.3 and 0.5, depending on the studied vibration mode. The relation between ambient temperature and the frequency of the first vibration mode corrected by the effect of water level is presented in the right part of Figure 5.

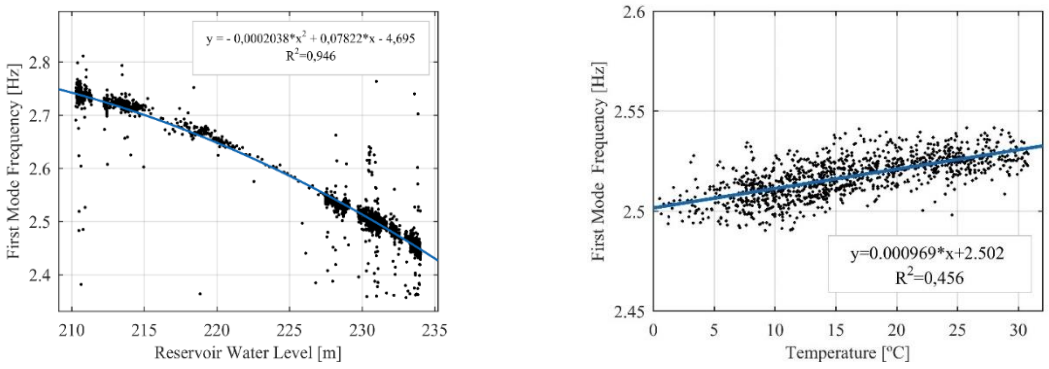

Figure 5 – Correlation between the first natural frequency and reservoir water level (on the left); correlation between the corrected first natural frequency and ambient temperature

Afterwards, this effect was mitigated from the values of the frequencies that had been already corrected for the effect of water level, resulting in the evolution of frequencies in time represented in Figure 6, side by side with the evolution of frequencies that had been obtained before the correction of operational and environmental effects. This new set of natural

frequencies shows great stability over the six months and can now be used as reference features for the detection of novel structural behaviour.

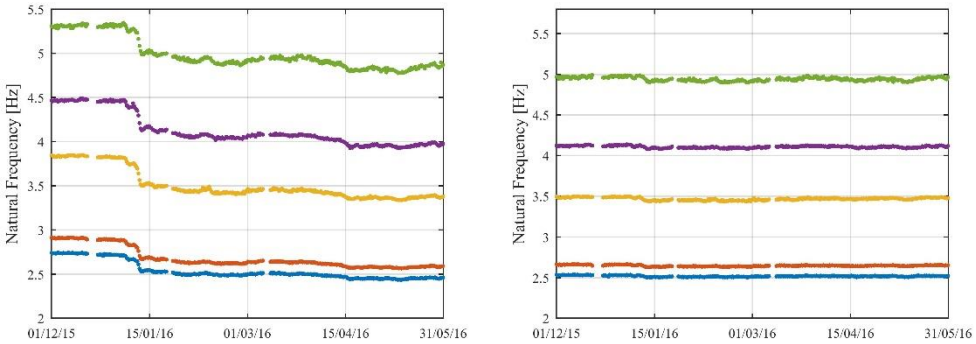

Figure 6 - Time evolution of natural frequencies' 12-hour averages before (on the left) and after the mitigation of operational and environmental effects (on the right)

Table 2 presents the standard deviation for the daily mean frequencies of each vibration mode before and after the process of removing the effects of environmental and operational conditions. For the first five modes, the normalization process resulted in a decrease on the standard deviation of 85%, or higher, thus attesting the model efficiency.

Table 2: Decrease in natural frequencies standard deviation

Mode	$f_{std\_initial}$ [Hz]	f_{std_final} [Hz]
1	0.100	0.008
2	0.115	0.016
3	0.169	0.023
4	0.183	0.016
5	0.181	0.031

3 NUMERICAL MODELLING

3.1 Introduction

In order to study the static and dynamic behaviour of Baixo Sabor arch dam, the Concrete Dams Department of the National Laboratory for Civil Engineering developed a numerical model of the dam. This model, based on discrete and finite elements, takes into account the dam's contraction joints, the deformability of the foundation and the reservoir [8]. The body of the dam was modelled with 32 vertical blocks which were discretized in isoparametric 20-node brick finite elements. A simplified representation of the reservoir and foundation was used, which was intended to allow a preliminary comparison with the experimental data.

The dynamic dam-reservoir interaction was simulated with Westergaard's added mass technique, for the nodal points of the model located in the upstream face below the reservoir level. The masses had to be scaled since, it is known that in arch dams, Westergaard's method overestimates the hydro-dynamic effects [9]. The model was calibrated for several water levels varying from 210 to 234 m, therefore a set of different scaling factors were used to match the first natural frequency estimated with both the results from a forced vibration test performed on the dam [8] and from the continuous dynamic monitoring [10]. Both these experimental and numerical results are presented in Table 3. In turn, Figure 7 presents the representation of the

used scaling factors as a function of reservoir water level, which shows a strong quadratic relation, with a determination coefficient of 0.99.

The deformability of the foundation was achieved through an elastic joint on the dam's surface of insertion, with stiffness parameters calibrated to provide an approximate deformability of a rock mass with a Young's modulus of 35 GPa, obtained from field tests. The adopted material parameters are presented in Table 4 and two different views of the numerical model are presented in Figure 8.

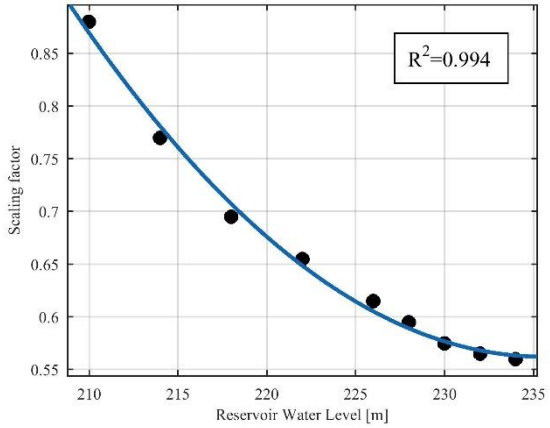

Figure 7 – Relation between water level and scaling factors for Westergaard's added masses

Table 3: Comparison between experimental and numerical results

Mode	Continuous monitoring [Hz]	Forced vibration test [Hz]	Numerical model [Hz]
1	2.45	2.44	2.44
2	2.57	2.57	2.67
3	3.34	3.34	3.56
4	3.93	3.93	4.03
5	4.78	4.78	4.81

Table 4: Main parameters of the numerical model

Concrete		Dam contraction joints		Foudation joint	
Young's modulus	35.0 Gpa	Normal stiffness	50.0 GPa/m	Normal stiffness	12.5 GPa/m
Poisson ratio	0.20	Shear stiffness	20.8 GPa/m	Shear stiffness	5.2 GPa/m
Density	2400 kg/m^3				

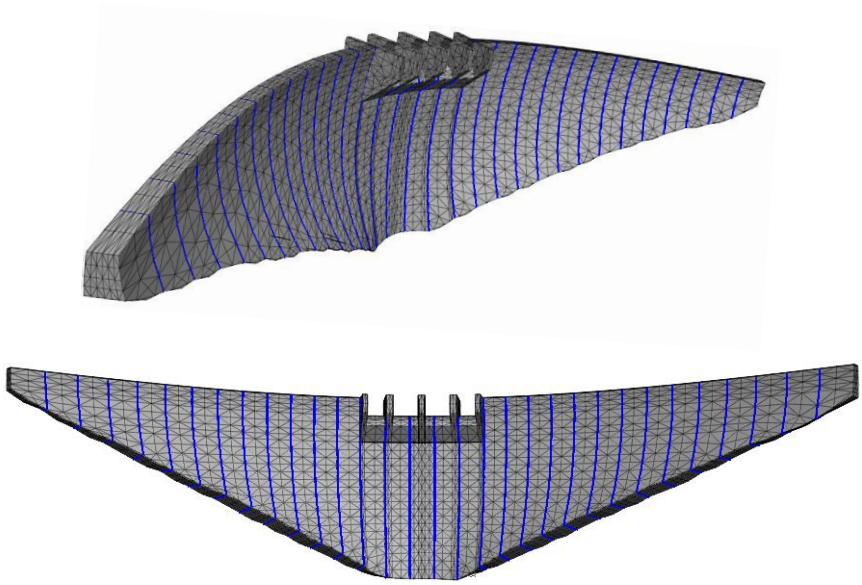

Figure 8 - Two views of the numerical model of Baixo Sabor dam; representation of blocks separated by contraction joints

3.2 Damage simulation

In section 2 it was shown that it is possible to largely reduce the effects of operational and environmental factors on the identified natural frequencies of an arch dam, to a degree that allows the detection of small shifts in their values. To detect such frequency variations, sensitive statistical tools may be used. With the aim of testing the ability of these statistical tools to identify realistic frequency variations, small damages were simulated with the finite model of the dam presented in the previous section.

Damage in dams may stem from a diversity of occurrences, as for instance vibrations due an earthquake, foundation sliding, or concrete deterioration due to cracking or chemical reactions. The accurate numerical modelling of damage scenarios directly motivated by the referred causes would require the development of very complex non-linear models and a large number of assumptions. As these models would provide only approximate results, and the construction of very sophisticated models is not the main focus of this work, a simpler approach was followed. The likely consequences of extreme events or of structural ageing are modelled in a simplified manner by reductions of inertia in a few dam components, such as part of concrete blocks or the contraction joints.

In this manner, four different damage scenarios were considered, D1, D2, D3 and D4. The location and extent of each damage considered is presented in Figure 9. The first damage scenario (D1) corresponds to the decrease of the Young's modulus value in a group of 11 elements in the central part of the dam, at an elevation of 200 m above sea level. Only elements in the most upstream layer were considered, which corresponds to a part of the structure that is stress sensitive and may be subjected to cracking. The second damage scenario (D2) is equivalent to the first one, with similar extent, though only 5 elements were damaged in this case, and it is located between the abutment and the central part of the dam, also at 200 m above sea level. The third scenario (D3) correspond to a more confined damage in the central part of the structure, but it goes from upstream to downstream, through the three layers of elements of the dam model, between 185 and 205 m above sea level. In this case, 18 elements were damaged. Finally, in the fourth damage scenario (D4) both the normal and shear stiffness of the six central contraction joints were reduced. Damages D1, D2 and D3 were represented in Figure 9 with light blue and damage D4 was represented with red.

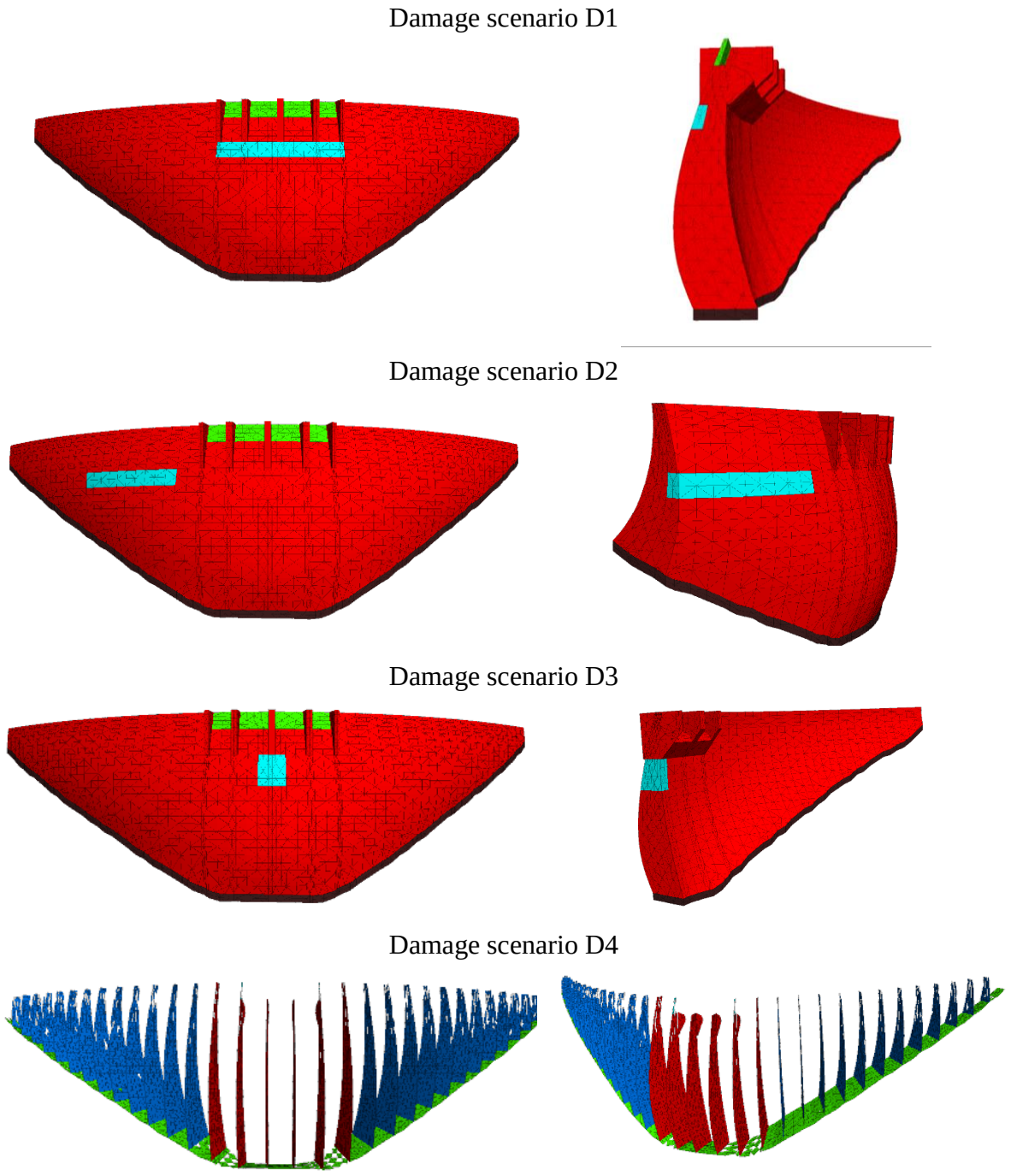

Figure 9 – Location, extent and type of simulated damage scenarios

The natural frequencies obtained with the numerical model for the first five vibration modes were used as reference values for comparison with the natural frequencies obtained after the introduction of each damage. Results were obtained for several reservoir water levels between 210 and 234 m, but small differences were found between them. Moreover, five levels of damage intensity were considered, which consisted in the reduction of Young's modulus of selected elements (or normal and shear stiffness in the case of joints) in 10, 30, 50, 70 and 90 %. Major differences were observed between the results obtained with the five damage intensities.

The results obtained with a level of water in the reservoir of 234 m and damage intensities of just 10 %, which is the most challenge scenario to test the damage detection tools, are

presented in Table 5. Frequency reductions between 0.015 and 0.181 % were verified. However, frequency reductions increase to values between 0.1 and 1% when damage intensities rise to 50 %, and to values between 1 and 4 % when 90 % damage intensities are considered. Furthermore, in each damage scenario different frequency reductions were verified for each vibration mode, indicating the possibility of locating damage through the study of the relation of the effect of damages between modes.

Table 5: Natural frequencies (in Hz) associated with damage scenarios D1, D2, D3 and D4 (10% of damage intensity) compared with the numerical reference values (Ref) with a water level of 234 m

		D1		D2		D3		D4	
Mode	Ref	freq.	Δ freq. [%]	freq.	Δ freq. [%]	freq.	Δ freq. [%]	freq.	Δ freq. [%]
1	2.45372	2.44928	-0.181	2.45337	-0.014	2.45065	-0.125	2.45186	-0.076
2	2.68436	2.68276	-0.059	2.68297	-0.052	2.68235	-0.075	2.68259	-0.066
3	3.58254	3.58199	-0.015	3.57815	-0.122	3.58189	-0.018	3.58085	-0.047
4	4.05438	4.05196	-0.060	4.05131	-0.076	4.05312	-0.031	4.05269	-0.042
5	4.84020	4.83624	-0.082	4.83665	-0.073	4.83662	-0.074	4.83820	-0.041

4 CONCLUSIONS

The dynamic monitoring system installed in Baixo Sabor dam was described and the main results obtained between December 2015 and May 2016 were presented. During its first 6 months of operation, the monitoring system has been functioning properly, producing very relevant data. Even though facing a challenging application, the processing routines produced good results, being able to identify the structure modal properties. The structure modal properties for the first five vibration modes were obtained. The high variability presented by natural frequencies during the filling period is mostly due to the variation of operational and environmental conditions, namely the reservoir water level and temperature.

Quadratic regressions were developed between the values of natural frequencies and the correspondent levels of water in the reservoir that showed a close correlation between these two variables. After correcting the effect of the water level, linear regressions were also developed between the previous corrected natural frequencies and ambient temperature and the effect of temperature was removed. The corrected natural frequencies present much lower variability than the ones that first resulted from the identification process, with standard deviation values five to ten times smaller than the original ones. Presently, multivariate regression models are being tested to minimize the effect of external conditions on modal properties and other variables such as the concrete temperature are being considered. Additionally, the processing of a larger database, containing entire annual cycles of temperature variation will certainly permit to achieve even better results.

The numerical model of Baixo Sabor arch dam developed by LNEC was presented along with its calibration for different reservoir water levels, using Westergaard's added masses. Furthermore, four damage scenarios were simulated using this model and frequency variations corresponding to the effect of each simulated damage in the structure were obtained, comparing the natural frequencies of the first five modes in the damaged model with the reference frequencies from the model of the healthy dam. Five damage intensities were considered for each water level. Frequency reductions in the order of 0.1 % were generally obtained across the four scenarios, considering the lower damage intensity. These results will be used in the future to test the capability of detecting damage with control charts.

ACKNOWLEGMENTS

This work was financially supported by: UID/ECI/04708/2019- CONSTRUCT - Instituto de I&D em Estruturas e Construções funded by national funds through the FCT/MCTES (PIDDAC); PTDC/ECM-EST/0805/2014|16761 – DAM_AGE - Advanced Online Dynamic Structural Health Monitoring of Concrete Dams, funded by FEDER funds through COMPETE2020 - Programa Operacional Competitividade e Internacionalização (POCI) – and by national funds through FCT - Fundação para a Ciência e a Tecnologia; FCT PhD Scholarship SFRH/BD/100587/2014 provided to the first author. The authors would like also to acknowledge all the collaboration and support provided by EDP Produção.

REFERENCES

1. Gomes, J.P., J. Palma, F. Magalhães, S. Pereira, G. Monteiro, and D. Silva Matos. Seismic monitoring system of baixo sabor scheme for structural dynamic behaviour monitoring and risk management. in 26th International Congress on Large Dams, 2018. 2018.
2. Magalhães, F., A. Cunha, and E. Caetano, Vibration based structural health monitoring of an arch bridge: From automated OMA to damage detection. Mechanical Systems and Signal Processing, 2012. 28: p. 212-228.
3. Oliveira, G., F. Magalhães, Á. Cunha, and E. Caetano, Development and implementation of a continuous dynamic monitoring system in a wind turbine. Journal of Civil Structural Health Monitoring, 2016. 6(3): p. 343-353.
4. Martins, N., E. Caetano, S. Diord, F. Magalhães, and T. Cunha, Dynamic monitoring of a stadium suspension roof: Wind and temperature influence on modal parameters and structural response. Engineering Structures, 2014. 59: p. 80-94.
5. Ubertini, F., G. Comanducci, and N. Cavalagli, Vibration-based structural health monitoring of a historic bell-tower using output-only measurements and multivariate statistical analysis. Structural Health Monitoring, 2016. 15(4): p. 438-457.
6. Magalhães, F., S. Amador, Á. Cunha, and E. Caetano. DynaMo - Software for vibration based structural health monitoring. in Bridge Maintenance, Safety, Management, Resilience and Sustainability - Proceedings of the Sixth International Conference on Bridge Maintenance, Safety and Management. 2012.
7. EDP. Energias de Portugal. [cited 2018 21/09/2018]; Available from: http://www.a-nossa-energia.edp.pt/centros_produtores/.
8. Gomes, J. and J.V. Lemos, Characterization of the dynamic behavior of an arch dam by means of forced vibration tests, in 1st Meeting of EWG Dams and Earthquakes. 2016, Balkema: Saint Malo, France.
9. Priscu, R., A. Popovici, D. Stematiu, and C. Stere, Earthquake engineering for large dams. John Wiley & Sons. 1985, New York.
10. Pereira, S., F. Magalhães, J.P. Gomes, Á. Cunha, and J.V. Lemos, Dynamic monitoring of a concrete arch dam during the first filling of the reservoir. Engineering Structures, 2018. 174: p. 548-560, DOI: 10.1016/j.engstruct.2018.07.076

Fluid structure displacement based interaction models for the dynamic behaviour of an arch dam

N. Monteiro Azevedo[1], M. Braga Farinha[2], N. Schclar[3], and R. Câmara[4]

National Laboratory for Civil Engineering (LNEC)
Av. Brasil 101 1700-066 Lisboa,Portugal
E-mail: nazevedo@lnec.pt

Keywords: Arch dams; Fluid-structure interaction; Lagrangian models; Dynamic analysis

Abstract. *This paper presents the application of a fluid displacement based formulation for the modelling of dynamic dam-reservoir interactions. This approach requires the introduction of a constraint penalty term multiplier that should be as high as necessary to enforce rotational constraint, but small enough to avoid numerical ill-conditioning and overly stiff responses. A maximum design earthquake and a forced vibration numerical analyses of an arch dam are carried out. The performance of two different displacement based finite elements are compared against each other and against known forced vibration experimental results on an arch dam, for a given reservoir level. The influence of the penalty term, of the free surface motion and of the type of finite element are assessed.*

1 INTRODUCTION

Whenever the reservoir is present, the dynamic dam-reservoir interaction should be considered when performing seismic analysis or when modelling *in situ* forced vibration tests. The fluid-structure interaction was initially modelled using the added mass approach through analytical/experimental based expressions, first proposed by Westergaard for vertical upstream faces [1] and later by Zangar for inclined upstream surfaces [2]. The classical added-mass approach is still being used, due to its simplicity and given its advantages within explicit solution procedures, even though it is well known that the added mass approach can be too conservative, leading to an overestimate response. For example, in a recent international ICOLD fluid-structure interaction benchmark [3] some of the participants still considered this type of modelling. Recently several authors have proposed the introduction of correction factors to the added mass values computed by Westergaard equation in the order of 50% to 70% which leads to better estimates of the arch dam dynamic behaviour [4, 5].

The dam-reservoir interaction can also be addressed using the finite element method (FE). Two different numerical approaches are usually adopted for the reservoir: i) Euler pressure based FE models [6, 7] and ii) Lagrange displacement based fluid models [6,8,9,10,11, 12]. The Euler approach based on acoustic media simplification was adopted by a large number of participants in the recent ICOLD benchmark workshop [3], whereas no research group adopted a Lagrangian approach. This is mainly due to the fact that the Euler approach is computationally efficient, numerically stable and several known commercial

[2] LNEC, lbraga@lnec.pt
[3] LNEC, nschlar@lnec.pt
[4] LNEC, rcamara@lnec.pt

programs have this formulation implemented and readily available, including the interaction with solid media.

In this study a fluid displacement based formulation is used. This type of approach allows a perfect match between the solid and the fluid domains, which has, when compared with fluid pressure based formulations, computational advantages for explicit algorithms such as the centred difference. Two different finite elements can be adopted for the fluid modelling: i) the traditional 8 node cubic fluid element with reduced integration (8N-1GP) [8, 9, 10, 11, 12]; ii) 8 node cubic mixed discretization fluid element based on the average behaviour of two independent 5 tetrahedra overlay (MDE) [12, 13, 14, 15].

The 8N-1gp Lagrangian fluid finite element accurately predicts the analytical responses especially when regular plane/brick meshes are adopted [9, 10, 11], namely the theoretical eigenvalues of a fluid within a tank and also the Westargaard hydrodynamic pressures in 2D and 3D. The 8N-1gp Lagrangian fluid finite element has also been applied to the seismic analysis of concrete arch dams, predicting reasonable responses and showing that the Westergaard added mass concept cleary overly estimates the seismic response [8, 9, 10, 11, 12].

Nevertheless, especially in 3D applications and for refined less regular brick meshes, the model behaviour should be further validated, either against experimental data obtained by monitoring the dynamic behaviour during earthquakes, or by data registered from ambient vibration or by data recorded during forced vibration tests or by comparing the predicted response with the responses obtained using an Euler approach.

A maximum design earthquake and a forced vibration numerical analyses of an arch dam are carried. The influence of the penalty term, of the free surface motion and of the type of finite element are assessed. The performance of the adopted FE fluid models are compared against each other, and against known forced vibration experimental results on a arch dam for a reservoir level 2m below the crest of the dam [16].

2 LAGRANGE DISPLACEMENT FLUID FORMULATION

In the Lagrangian approach the fluid is considered to be linearly elastic, inviscid and irrotational. The constitutive relationship under small displacement amplitude is given by [8]:

$$\mathrm{p} = \mathrm{K_v}\ \varepsilon_v \tag{1}$$

where p is the fluid pressure, ε_v is the fluid volumetric strain and $\mathrm{K_v}$ is the fluid bulk modulus given by $K_v = \rho\, c^2$, where ρ is the fluid mass density and c is the sound wave speed. In order to ensure the irrotational nature of the fluid it is necessary to include the following irrotational condition [8,9,10,11,12]:

$$\left\{\hat{p}_x \quad \hat{p}_y \quad \hat{p}_z\right\}^t = \lambda\, \mathrm{K_v} \left\{\hat{\varepsilon}_{rx} \quad \hat{\varepsilon}_{ry} \quad \hat{\varepsilon}_{rx}\right\}^t \tag{2}$$

where $\hat{p}_x$, $\hat{p}_y$ and $\hat{p}_z$ are the rotational stresses, λ is the rotational constraint penalty term fluid bulk modulus multiplier, $\hat{\varepsilon}_{rx}$, $\hat{\varepsilon}_{ry}$ and $\hat{\varepsilon}_{rz}$ are the rotations about, respectively, the global x, y and z axis, given by:

$$\left\{\hat{\varepsilon}_{rx} \quad \hat{\varepsilon}_{ry} \quad \hat{\varepsilon}_{rx}\right\}^t = \left\{\frac{1}{2}\left(\frac{\partial u_z}{\partial y} - \frac{\partial u_y}{\partial x_z}\right) \quad \frac{1}{2}\left(\frac{\partial u_x}{\partial z} - \frac{\partial u_z}{\partial x}\right) \quad \frac{1}{2}\left(\frac{\partial u_y}{\partial x} - \frac{\partial u_x}{\partial y}\right)\right\}^t \tag{3}$$

The constraint penalty term multiplier (λ) should be as high as necessary to enforce rotational constraint, but small enough to avoid numerical ill-conditioning and overly stiff responses. In 3D modelling the eight node hexahedral brick element with reduced integration (8N-1gp), Figure 1a), is usually adopted for the fluid model [8, 9, 10, 11], and the penalty term (λ) is generally taken as 1000 K_v [8, 9, 10 11]. Note that the optimal constraint parameter may change with the material properties, with the geometry and with the type of problem that is being modelled.

The fluid domain can also be discretized with 8 node cubic fluid mixed discretization element given by the average behaviour of two independent 5 tetrahedra overlay (8N-MDE) [12], Figure 1b). Pedro [13] proposed, at the early stages of FE modelling, the simulation of an hexahedron brick through the averaging of two independent five tetrahedra composition. In order to increase the accuracy of the element under plastic deformation the volumetric deformation in each tetrahedra overlay should be taken as the average volumetric strain rate of each tetrahedron [14]:

$$\dot{\varepsilon}_v^{overlay} = \frac{\sum_{k=1}^{5} \dot{\varepsilon}_v^k V^k}{\sum_{k=1}^{5} V^k} \tag{4}$$

where $\dot{\varepsilon}_v^k$ and V^k are, respectively, the volumetric deformation and the volume of each tetrahedron. The tetrahedron strain-rate tensor components ($\dot{\varepsilon}_{ij}^k$) of a given tetrahedra are then calculated using:

$$\dot{\varepsilon}_{ij}^k = \dot{\eta}_{ij}^k + \frac{\dot{\varepsilon}_v^{overlay}}{3} \delta_{ij} \tag{5}$$

where $\dot{\eta}_{ij}^k$ is the deviatoric strain rate tensor of a given tetrahedron and δ_{ij} is the Kronecker symbol. It is known that the 8N-MDE solid element is able to predict accurate results under high plasticity deformation, avoiding stress locking and overly stiff responses [14]. This behaviour gives an indication that the element may also perform well under a Lagrangian fluid finite element formulation. It has been shown that the 8N-MDE fluid element predicts well the Westergaard hydrodynamic pressures for a regular mesh [15]. In [12] the MDE formulation has been extended in order to be able to reduce the influence of zero energy spurious nodes. A nonzero rotational constraint has been added, following a similar concept to the volumetric averaging approach. The rotation rates about each global axis are averaged on each overlay:

$$\hat{\dot{\varepsilon}}_{ri}^{overlay} = \frac{\sum_{k=1}^{5} \hat{\dot{\varepsilon}}_{ri}^k V^k}{\sum_{k=1}^{5} V^k} \tag{6}$$

In [12] it was found that a small value of 0.001 K_v for the penalty stiffness multiplier needs to be included in the 8N-MDE model in order to guarantee the irrotational nature of the fluid.

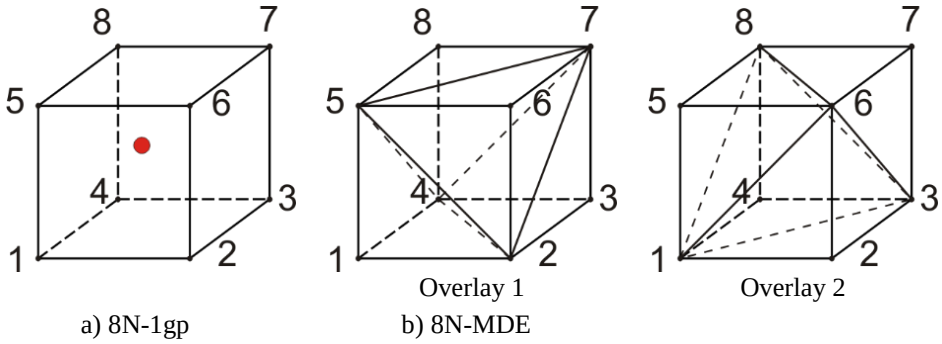

Figure 1: 3D based Lagrangian fluid finite elements

The effect of surface waves and sloshing behaviour should also be taken into account. With this purpose an elastic support with a spring value equal to $\rho\, g$ is added to the free surface nodes. The free surface pressure field is then given by:

$$p = \rho\, g\, u_s \tag{7}$$

where u_s is the vertical displacement at the free surface, ρ is the fluid mass density and g is the acceleration due to gravity.

3 CASE STUDY

3.1 Introduction

The dynamic behaviour of Alto Lindoso dam, under seismic loading and forced vibration loading is studied, Figure 2. The dam is located in the North of Portugal and is a double curvature concrete arch dam with a maximum height of 110 m, a thickness of 21 m at the base of the crown cantilever and of 4 m at the crest. Figure 3 presents the adopted numerical models, see also Table 1. With the exception of the foundation model, wich has two elements in thickness the MDE numerical model, both numerical models are similar. Given that the run times of the FV analysis is extremely high the adopted foundation numerical model was intentionally reduced to a minimum size.

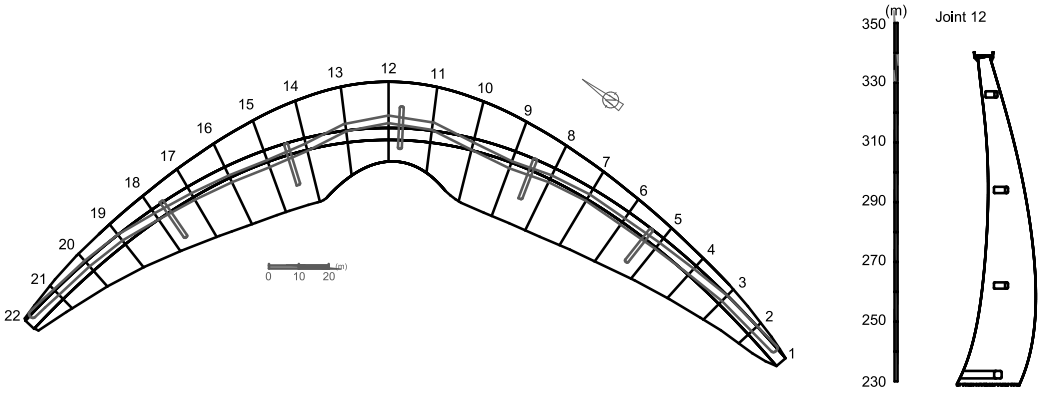

Figure 2: Alto Lindoso dam. General view and geometric definition [17]

Table 2 presents the material properties adopted for the dam body and the dam foundation. The Young's modulus values are taken as 1.25 times the static values that were

found to give a good agreement with the observed *in situ* response of the dam [17]. Table 3 presents the adopted interface material properties. As indicated in Table 3, for the solid/fluid interactions only the normal spring stiffness is considered guaranteeing that the interaction will only occur in the perpendicular direction of the fluid surface. For the fluid displacement based finite elements a bulk modulus of 2.0 GPa and a mass density of 1.0 ton/m^3 are adopted. The concrete material properties are in close range with the properties adopted in [16] that produce an excellent agreement for the transfer functions, namely the first and second experimental resonance where a 0.8% modal damping was adopted for both the dam and foundation.

Table 1: Finite element models.

Model	Nodal points	Brick elements	Interface plane elements
MDE loading	14924	3212	901
Forced vibration	12651	2396	901

Table 2: Material properties

	Dam	Foundation		
		Z1	Z2	Z3
Young's modulus (GPa)	40.0	18.0	37.5	50.0
Poisson's ratio	0.20	0.20	0.20	0.20
Mass density (ton/m3)	2.40	2.6	2.6	2.6

Table 3: Interface joint elastic properties

	Dam/ Foundation	Solid/Fluid
Normal stiffness k_n (GPa/m)	80.0	2.0 or 4.0
Shear stiffness k_s (GPa/m)	32.0	0.0

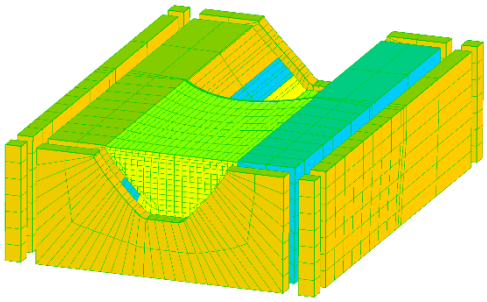

a) MDE – Full model including free-field

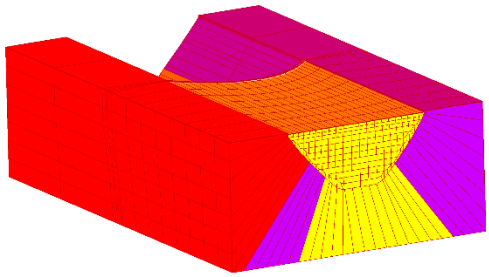

b) FV – Full model

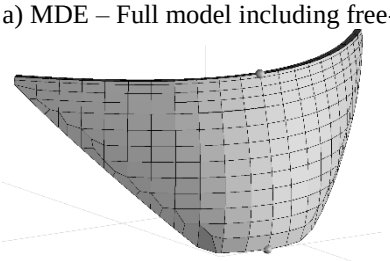

c) MDE – Dam body including control points

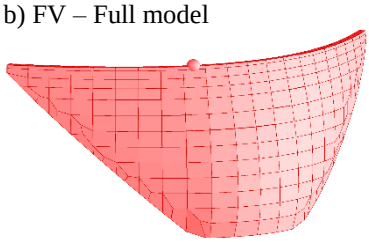

d) FV – Dam body including control point

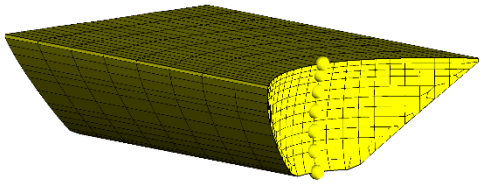

e) MDE – Fluid model including control points

Figure 3: Adopted MDE and forced vibration numerical models

3.2 Maximum design earthquake (MDE)

The MDE analysis is carried out in to loading stages. Firstly, the static permanent loads are applied to the model, dead-weight and the hydrostatic pressure at the dam upstream face and foundation upstream interface (added mass approach). At the end of the static loading, the supports are replaced by the equivalent static reactions. Secondly, the seismic action is considered. This action is represented by plane waves, propagating upwards from a model base with a non-reflecting character, using a viscous boundary formulation [18]. The dynamic boundary conditions of the 4 lateral boundaries of the model are obtained by performing independent free-field calculations, subject to the same base motion (Figure 3a). For each side of the model, a 2D free-field mesh is created, each one having its own 1D free-field meshes at the sides [18]. Two acceleration records with approximately 5 seconds length were adopted for the upstream/downstream and vertical MDE components [12]. They were defined based on a numerical stochastic fault rupture model for a peak ground acceleration of 0.34 *g* [19]. In this work, in a simplified manner, the vertical seismic component is given by scaling with a factor of 2/3 the vertical component acceleration record.

Mass-proportional Rayleigh damping was adopted in all domains (2.0% at the second resonance frequency obtained in the forced vibration tests [16]. The analysis was carried out using an explicit solution algorithm based on the central difference method [12]. Figure 4 shows the fluid pressure distribution 15 seconds after the end of the MDE loading. It can be seen that both the adopted finite element fluid models, 8N-1gp and 8N-MDE, return to the initial static pressure loading distribution, as long as the correct constraint penalty terms are adopted, $\lambda = 1000\ K_v$ for the 8N-1gp and $\lambda = 0.001\ K_v$ for the 8N-MDE.

Figure 5 shows the fluid pressure time history at different elevations, Figure 3e), in the vicinity of the upstream face of the dam. It can be seen that both fluid finite elements predict a similar response. Nevertheless, at the dam base the 8N-1gp response is slightly different

and includes a very low frequency response that requires almost 20 seconds to be attenuated. Figure 5 also shows that the pressure wave amplitude returns to the initial static value faster in the 8N-1gp fluid finite element. Figure 6 shows the vertical dynamic stress at the dam base close to the upstream face for both adopted fluid finite elements and for the Westergaard added masses with a correction factor of 0.7. It is shown that both fluid models predict similar response at the dam body, even as shown in Figure 5, the fluid dynamic pressure distribution can be slightly different. It can also be verified that even with a 0.7 correction factor the Westergaard approach is still conservative when compared with the values predicted with both fluid finite elements.

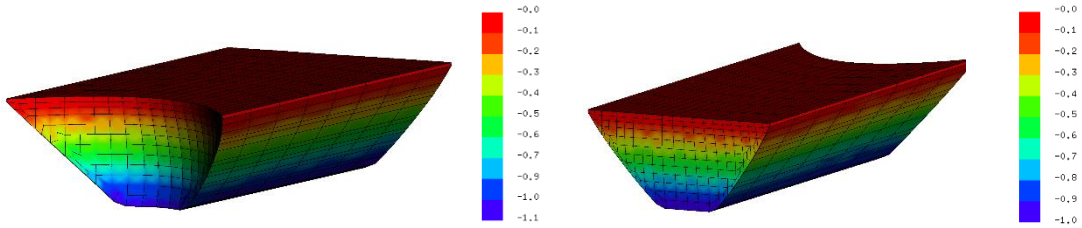

a) 8N-1gp b) 8N-MDE

Figure 4: Static loading fluid pressure distribution after MDE loading – Nonzero constraint penalty term

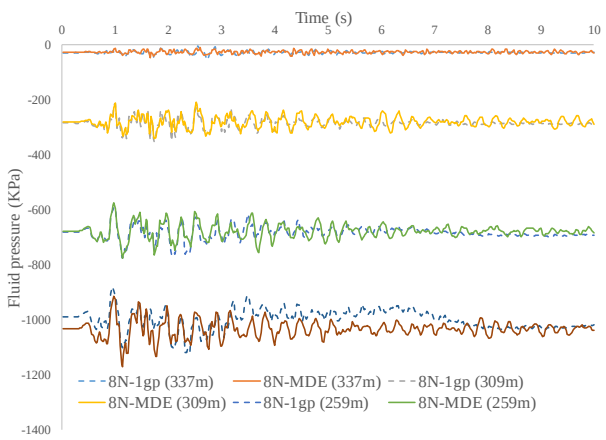

Figure 5: Fluid pressure close to the upstream face of the dam at different elevations.

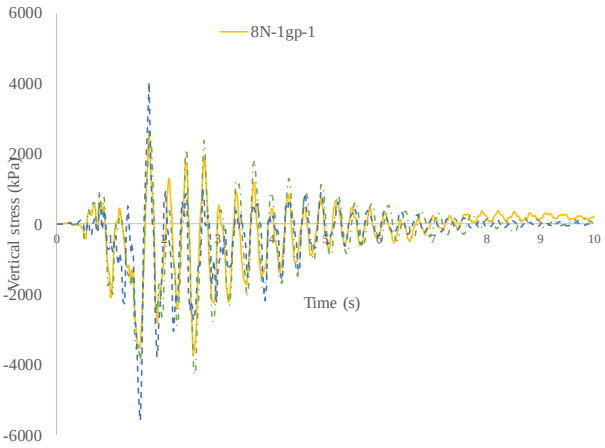

Figure 6: Vertical dynamic stress at the dam base close to the upstream face of the dam.

Figure 7 shows the dynamic fluid pressure at the base close to the dam foundation interface for both fluid finite elements. It can be seen that with the 8N-1gp fluid finite element is used the response when the rotational penalty stiffness is included (8N-1gp-1) greatly differs from the response obtained when no rotational penalty stiffness is considered, Figure 7a). It is also shown that the predicted response including the influence of the surface waves (8N-1gp-1) is slightly different from the response when this phenomenon is not considered. Figure 7 b) shows that with the 8N-MDE fluid finite element the response when the rotational penalty stiffness is included (8N-MDE-1) just slightly differs from the response obtained when no rotational penalty stiffness is included (8N-MDE-2), Figure 7a). The study carried out shows that the response including the influence of the surface waves (8N-MDE-1) is very similar to that predicted when this phenomena is not considered adopting an 8N-MDE fluid element.

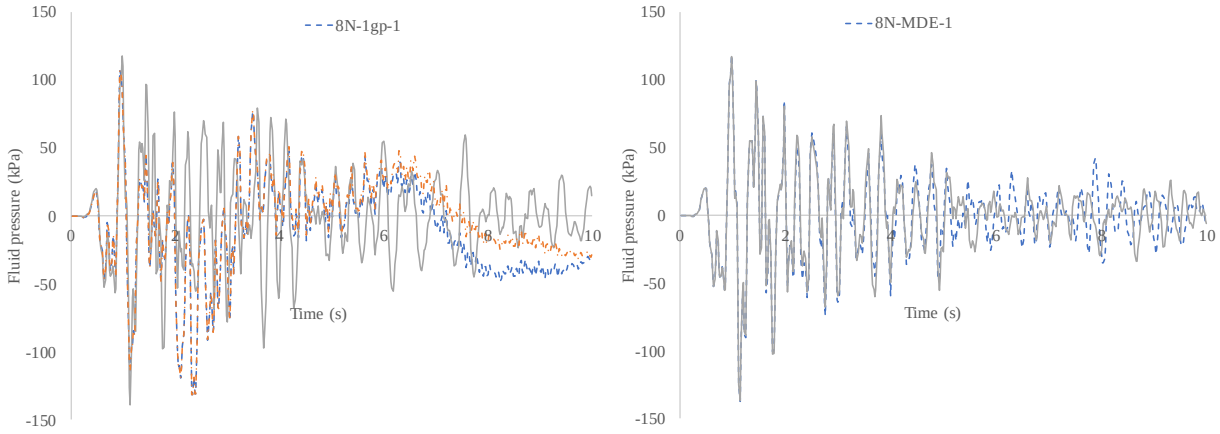

a) 8N-1gp b) 8N-MDE

Figure 7: Fluid pressure at the upstream face of the dam at the dam base close to the dam/foundation interface.

3.3 Forced vibration testing

The *in situ* forced vibration dynamic tests are usually performed in order to characterize current dam operational conditions. A sinusoidal force is applied within a given range of frequencies, usually with components in both the upstream/downstream and left/right bank directions. In each frequency value, the displacement and the velocity time history in some selected points are registered (Figure 3c)). This procedure allows the vibration eigenvalues which are given by peaks of the load transference force/displacement curves, to be characterized in an indirect way.

In [16] forced vibration tests that were carried out with the water level in the reservoir 2m below the crest arch were analysed and compared with the numerical results following an Euler approach for the fluid. The computed transfer functions from shaker forces to radial displacements were shown to fit well the experimental data in terms of frequencies and peak amplitude for the lower resonances.

Numerically, a unitary vibration force is applied at the dam crest, at the point highlighted in Figure 3c), with frequencies ranging from 2.5 to 5.5 Hz adopting a 0.1 Hz increment. In each frequency loading a 35 s time history simulation is performed, that guarantees the stabilization of the numerical response. A Newmark integration implicit procedure with 0.5% damping at the second experimental fundamental frequency (3.45 Hz) only at the dam body was adopted. At the vertical model boundary upstream from the dam a non-reflecting boundary, using a viscous boundary formulation is adopted for the fluid elements [18]. Given that the FV tests are computational intensive the foundation model is simplified with only one finite element (Figure 3b).

Figures 8a) and 8b) show the load transfer functions for the radial displacement when adopting the 8N-1gp fluid element for two different fluid/solid interface normal stiffness values. The same also show the load transfer functions obtained with a Westergaard added mass approach using a correction factor of 0.7. It can be seen that both the rotational penalty stiffness and the normal interface stiffness play an important role in the measured response. Without the penalty constraint, the peak values occur at slightly different frequencies, the number of recorded peak values and the peak amplitudes can also be different. It is also shown that a high value of interface normal stiffness can lead to different responses. Note that the dam body is simulated using 20 node hexahedra bricks and the fluid is simulated with 8 node hexahedra bricks and the final coupled deformation requires some adjustment at the dam/reservoir interface.

Figures 8 c) and 8 d) show the load transfer obtained using the 8N-MDE with penalty constraint (8N-MDE-1) and without penalty constraint (8N-MDE), the response are closer when compared with the 8N-1gp response, with and without the penalty term. Nevertheless, differences can be found as different peaks can be predicted, similar peaks can occur in slightly different frequencies and the peak amplitudes can also be slightly different.

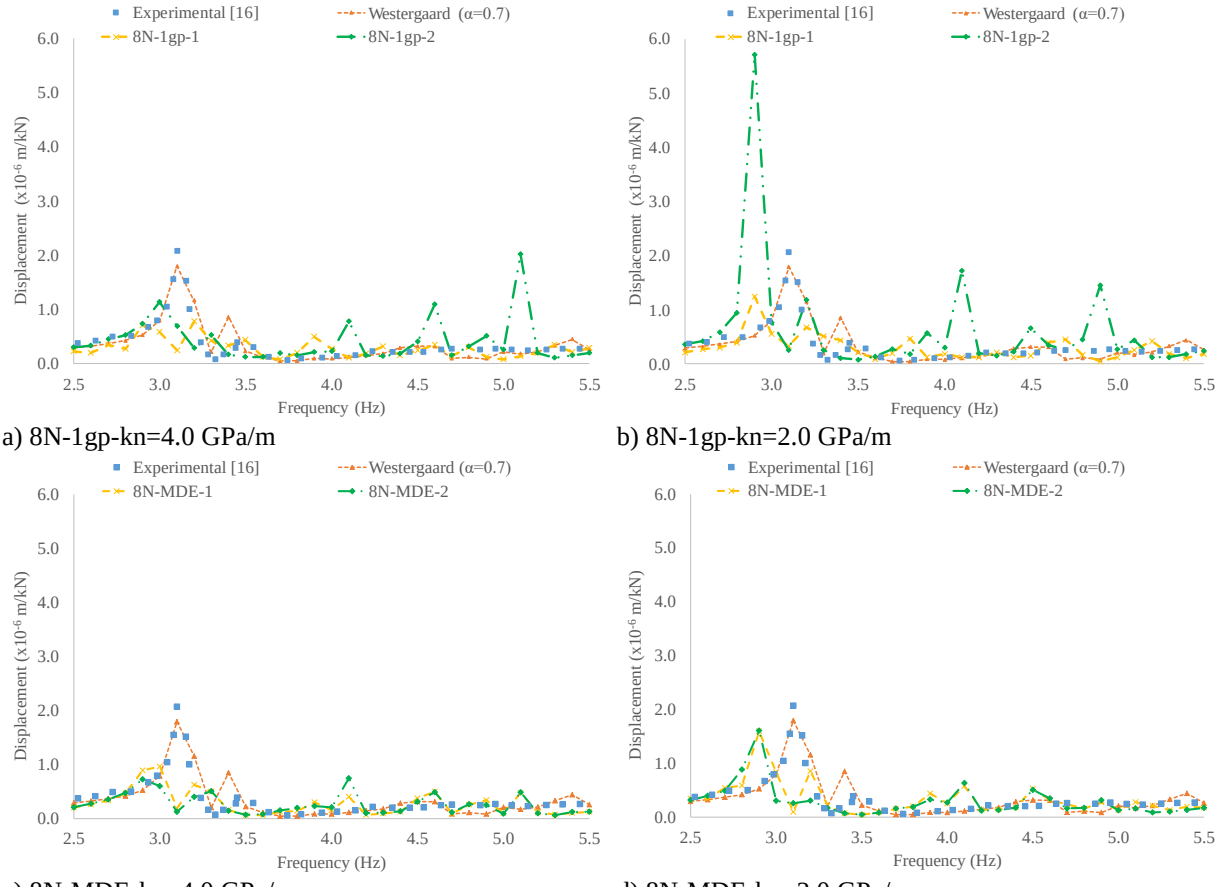

a) 8N-1gp-kn=4.0 GPa/m

b) 8N-1gp-kn=2.0 GPa/m

c) 8N-MDE-kn=4.0 GPa/m

d) 8N-MDE-kn=2.0 GPa/m

Figure 8: Load transfer functions for the radial displacement at highlighted point (Figure 3b)

Figures 9a) and 9b) show the load transfer functions for the radial displacement when adopting both fluid elements when the material properties are defined as 1.43 of the static values adopted in [17]. It can be seen that with the 8N-MDE finite element including the rotational penalty term (8N-MDE-1) both the first (3,10 Hz) and the second (3.45 Hz) experimental resonance values can be predicted. It can also be seen that the increase in the model stiffness has little influence on the numerical results obtained with the 8N-1gp finite

element model with penalty term. In fact the the change in the predicted response is almost negligible.

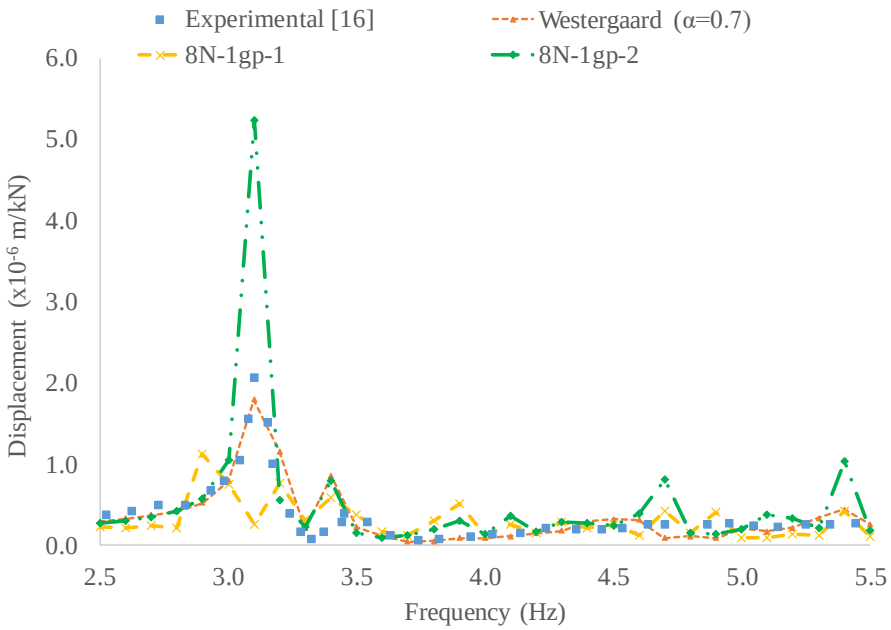

a) 8N-1gp-kn=2 GPa/m, 1.43 static values [17]

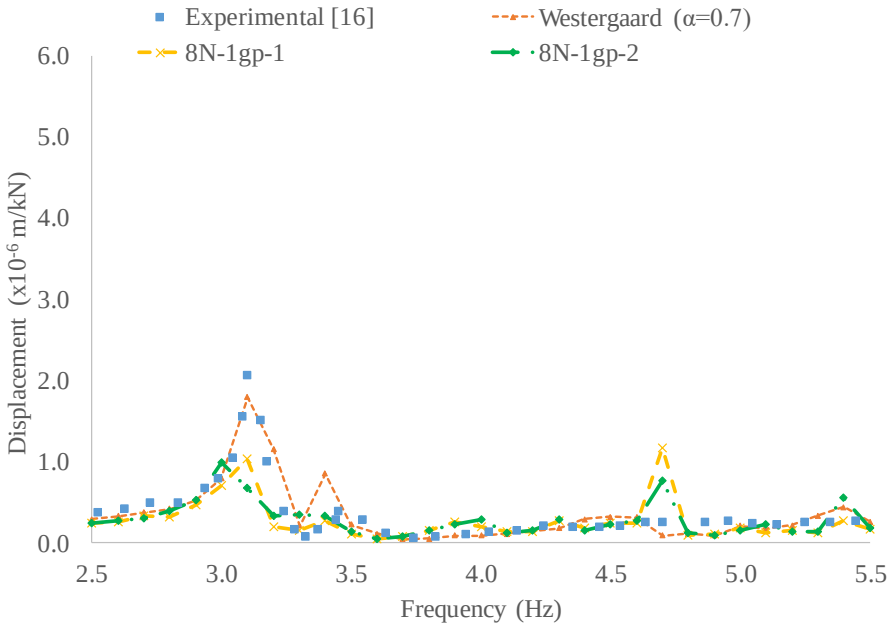

b) 8N-1gp-kn=2, 1.43 static values [17]

Figure 9: Load transfer functions for the radial displacement at highlighted point (Figure 3b) for recalibrated elastic properties

4 CONCLUSIONS

Two different Lagrangian fluid based displacement FE elements valid for small amplitudes that can be applied to fluid/structure dynamic analysis are presented. It is shown that for a less regular brick finite element model the 8N-1gp and 8N-MDE predict similar responses for MDE loading. The slight differences in the predicted fluid dynamic pressure have little effect on the overall dam body response. Comparison with Euler based methods needs to be carried out in order to assess which finite model predicts a response closer to that obtained with other methods. It is also shown that the rotational penalty term has an influence on the final response, as expected, being more relevant when the 8N-1gp finite element is used, as it requires a higher penalty term value.

The forced vibration analysis that is carried out also shows that the rotational penalty term influences the numerically obtained load transfer function in both finite elements, slightly different peak values for similar modes can be obtained, different peak values can also occur and different peak amplitudes can be obtained. It is also shown that the adopted interface normal stiffness at the dam/reservoir interface influences the predicted response, a lower value predicts a response closer to that obtained experimentally. As mentioned, the adopted normal stiffness value cannot be too high because it has to be low enough in order to guarantee the compatibilization between the deformation that occurs with the 20 node hexahedra mesh adopted in the dam body with the 8 node cubic fluid elements, with an approximate linear field.

It is shown that with the 8N-MDE finite element it is possible to obtain a load transfer function that leads to results closer to those obtained experimentally in the lower resonances. Before the application of this type of models to MDE loading it is important to calibrate the interface stiffness parameter using known forced vibration records, taking into account both frequencies and peaks amplitudes.

The results that are here presented show that the 8N-MDE finite element model including the rotational term is a promising finite element model that can be adopted for nonlinear explicit analysis including gravity effects. Further studies need to be carried out in order to assess whether the Lagrangian based models are able to predict correct responses for refined distorted fluid meshes.

ACKNOWLEDGMENTS

The study presented here is part of the research project “DAMFA: Cutting-edge solutions for sustainable assessment of concrete dam foundations” which has been supported by LNEC with the main purpose of developing a numerical multiphysic integrated tool for the sustainable assessment of concrete dam foundations, taking into account the interaction between the mechanical, hydraulic and thermal behaviours.

REFERENCES

[1] H. Westergaard, *Water pressures on dams during earthquakes*, Transactions of the American Society of Civil Engineers, Vol. 1835, pp. 418-433 (1931).

[2] C.N. Zangar, *Hydrodynamic pressures on dams due to horizontal effects*, U.S. Department of Interior, Bureau of Reclamation Engineering Monographs, n. 11 (1952).

[3] Theme A – Fluid Structure Interaction Arch Dam – Reservoir at Seismic loading (2013). Proc. of the 12th ICOLD International Benchmark Workshop on Numerical Analysis

of Dams (eds. G. Zenz and M. Goldgruber), Austrian National Committee on Large Dams, pp. 13-188, Graz, Austria (2014).

[4] C. Houqun, *Seismic safety of high concrete dams*, In Chincold, Seismic safety of dams in China, pp 1-54, (2014).

[5] A. Alegre, S. Oliveira, M. Espada, R. Câmara, J. Lemos, *Hydrodynamic pressures on arch dams: Numerical and experimental results*, Revista Portuguesa de Análise Experimental de Tensões, Vol 28, pp. 55-62 (2017) (in Portuguese).

[6] O.C. Zienkiewicz and P. Bettess, *Fluid-Structure dynamic interaction and wave forces. An introduction to numerical treatment*, International Journal for Numerical Methods in Engineering, vol. 13, 1-16 (1978).

[7] M. Cervera, J. Oliver and R. Faria, *Seismic evaluation of concrete dams via continuum damage models*, Earthquake Engineering and Structural Dynamics, Vol. 24, pp. 1225-1245 (1995).

[8] E. Wilson, M. Khalvati, *Finite elements for the dynamic analysis of fluid-solid systems*, International Journal for Numerical Methods in Engineering, Vol. 19, pp. 1657-1668 (1983).

[9] Y. Calayir and A. Dumanoglu, *Static and Dynamic Analysis of Fluid and Fluid-Structure Systems by the Lagrangian method*, Computers and Structures, Vol. 49, pp. 625-632 (1993).

[10] E. Greeves and C. Taylor, *The use of displacement type fluid finite elements for the analysis of dam reservoir interaction*, Dam engineering, Vol. III, pp. 169-200 (1992).

[11] M. Akkose, S. Adanur, A. Bayraktar, A. Dumanoglu, *Elasto-plastic earthquake response of arch dams including fluid-structure interaction by the Lagrangian approach*, Applied Mathematical Modelling, Vol. 32, pp. 2396-2412 (2008).

[12] N. Monteiro Azevedo, and R. Câmara, *Dynamic analysis of concrete dams: fluid structure displacement based interaction models*, Dam Engineering, Vol XXV (4), pp. 113-132 (2015).

[13] J.O. Pedro, *Three dimensional structural analysis using the finite element method*, 2as Jornadas Luso-Brasileiras de Engenharia Civil, pp. 1-13, (1967).

[14] J. Marti and P. Cundall, *Mixed discretization procedure for accurate modelling of plastic collapse*, International Journal for Numerical and Analytical Methods in Geomechanics, Vol. 6, pp. 129-139 (1982).

[15] N. Monteiro Azevedo, R. Câmara and J. Lemos, *Numerical modelling of fluid-solid interaction using a finite element displacement formulation*, LNEC report 54/2008 – DBB/NMMF (2008) (in Portuguese).

[16] R. Câmara and S. Oliveira, *Dynamic behavior of an arch dam-foundation-reservoir system:Experimental and numerical study*, In Structural dynamics – Eurodyn 96, (eds. Augusti, Borreli and Spinelly), Balkema, Rotterdam, pp. 703-709 (1995).

[17] N. S. Leitão, *Environmental thermal actions – Thermal analysis of Alto Lindoso dam*, In 6th International Conference on Dam Engineering (eds. Pina, Portela & Gomes), Balkema, Rotterdam, pp. 11 (2011).

[18] J.V. Lemos, *Discrete element analysis of dam foundations*, in Distinct Element Modelling in Geomechanics (eds. Sharma, Saxena & Woods), Balkema, pp. 89-115 (1999).

[19] A. Carvalho, *Modelação estocástica da ação sísmica em Portugal continental*, Ph.D Thesis, Instituto Superior Técnico, Portugal (2007).

Determination of material parameters using numerical models and field measurement data

E. Staudacher[1] and G. Zenz[1]

Institute of Hydraulic Engineering and Water Resources Management / Graz University of Technology
Stremayrgasse 10/II, Graz, Austria
E-mail: edwin.staudacher@tugraz.at

Keywords: Dams; Concrete arch dam; Field measurements; Modal analysis; Material parameters; Numerical methods

Abstract. *For the structural safety assessment of dams several material parameters have to be defined in the analysis, in case of concrete dams these parameters are mainly related to materials such as concrete, rock as well as water. Essential parameters of materials are elastic modulus or Young's modulus (E), compression and tensile strength and Poisson's ratio (ν). For dynamic load cases these parameters can significantly differ, in comparison to static loading. The linear elastic dynamic material properties can be calibrated by using numerical models, based on results of dynamic in-situ test at existing structures.*
In Austria, such in-situ tests have been performed at the 131 m high Schlegeis double-curvature arch-gravity dam, at two different reservoir water levels. As result of the measurements, the significant natural frequencies for each situation were determined.
This study presents modal analyses using finite element (FE) method were parameter studies have been performed to back-calculate the dynamic parameters of concrete and rock.

1 INTRODUCTION

The structural safety assessment of large structures like dams is of high interest because of the potential of losses in case of a structural failure. Therefore, dams are designed for different kinds of static loads and furthermore for dynamic loads like earthquakes. For a critical assessment the knowledge of eligible material parameters is essential for static and dynamic load cases.

This paper presents a way to obtain dynamic material parameters by using the finite element (FE) method in combination with results from in-situ vibration tests. Schlegeis double-curvature arch-gravity dam (maximum height 131 m) is discretized using ANSYS Mechanical finite element software to estimate the dynamic material properties like Young's modulus and Poisson's ratio. The first five natural frequencies of the dam gained from in-situ tests are the benchmark in the optimization process in ANSYS DesignXplorer module. A Multiple-Objective Genetic Algorithm (MOGA) calibrates the above mentioned material parameters so that the computed natural frequencies fit to the measured ones within a certain tolerance.

[1] Institute of Hydraulic Engineering and Water Resources Management / Graz University of Technology, gerald.zenz@tugraz.at

2 SCHLEGEIS DAM

Schlegeis dam (constructed from 1967 to 1972) is part of the Zemm-Ziller pumped storage hydropower scheme which is located in the Tyrolian part of the Austrian Central Alps. With its maximum height of 131 m, crest length of 725 m and concrete volume of 980000 m^3 it impounds the Schlegeis reservoir which acts as upper reservoir of the Roßhag power station. In terms of the total storage capacity of 129 million m^3 it is the third largest reservoir in Austria. The active storage capacity of 126.5 million m^3 is defined by the maximum operating water level at 1782.0 m a.s.l. and the minimum operation water level at 1680.0 m a.s.l.. [1]

The dam is founded on competent rock (Gneiss) in a relatively wide unsymmetrical U-shaped glacial valley. An optimization of the dam's volume led to a double curvature arch-gravity dam type with a crest width of 9 m and a maximum base width of 34 m. The geometry is based on elliptical horizontal sections, the principal axis of the ellipse is parallel to the valley. This design results in larger radii at the abutments and in contrary to smaller radii in the central part of the dam. Therefore, the load transfer to the foundation is similar to gravity dams for blocks at the lateral portion of the dam, at the central blocks an arch effect is triggered. [2]

Figure 1: Aerial photo of Schlegeis dam (Photo: Verbund Hydro Power GmbH (VHP))

Schlegeis dam has been numerically investigated twice during former ICOLD Benchmark Workshops, once within Theme A ("Uplift pressure and Stress Analysis of an Arch Dam and Foundation") of the Fifth Benchmark Workshop in Denver [3], a second time two years later in 2001 in Salzburg as part of Theme C named "Interpretation of Measurement Results"[4].

3 IN-SITU TESTS AT SCHLEGEIS DAM [5]

Vibration tests were conducted in 1981 and 1992/93, the results of the later ones are used as benchmark for the numerical analyses presented in this paper.

3.1 Setup of the tests in 1992/93

In total three measurement campaigns were performed between September 1992 and May 1993 at reservoir water levels as shown in Figure 2 as well in Table 1, values in parentheses relate to the difference of water level during testing to max. operation water level of the reservoir.

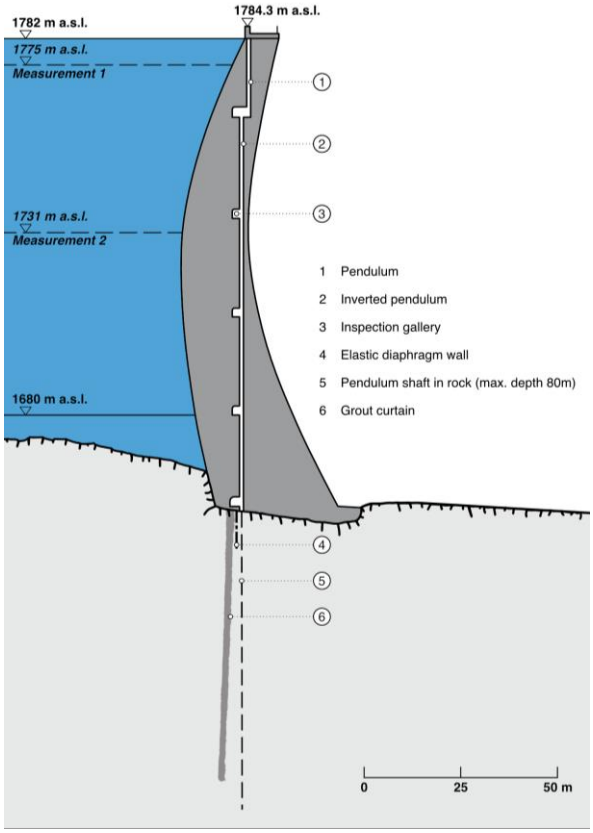

Figure 2: Cross section at the main section of Schlegeis dam, reproduction from [5]

The tests in 1981 clearly showed that the induced vibrations of the exciter can trigger all relevant mode shapes of the dam, if it is placed at crest level of block 2 (Figure 3). The exciter produced a horizontal directed sinusoidal varying force (max. amplitude 25 kN) in radial and tangential directions to the main dam axis.

Table 1: Key data of in-situ measurements

Measurement	Average Water level [ma.s.l.]	Direction of excitation
1	1775 (-7 m)	Radial
2	1731 (-51 m)	Radial
3	1730 (-52 m)	Tangential

With a computer controlled setup it was possible to perform frequency sweeps in the range from 0 to 10 Hz. Along the crest as well as in the inspection galleries numerous sensors

have been installed to capture the response of the structure. Table 2 summarizes the first five identified natural frequencies ω_n of each measurement campaign.

Table 2: Natural frequencies of the three in-situ measurements

Mode Nr.	Measurement 1 (1775 m a.s.l.)	Measurement 2 (1731 m a.s.l.)	Measurement 3 (1730 m a.s.l.)
	ω_n [Hz]	ω_n [Hz]	ω_n [Hz]
1	1.91	2.21	2.22
2	2.04	2.34	2.35
3	2.47	2.75	2.76
4	2.93	3.22	3.24
5	3.54	3.83	3.86

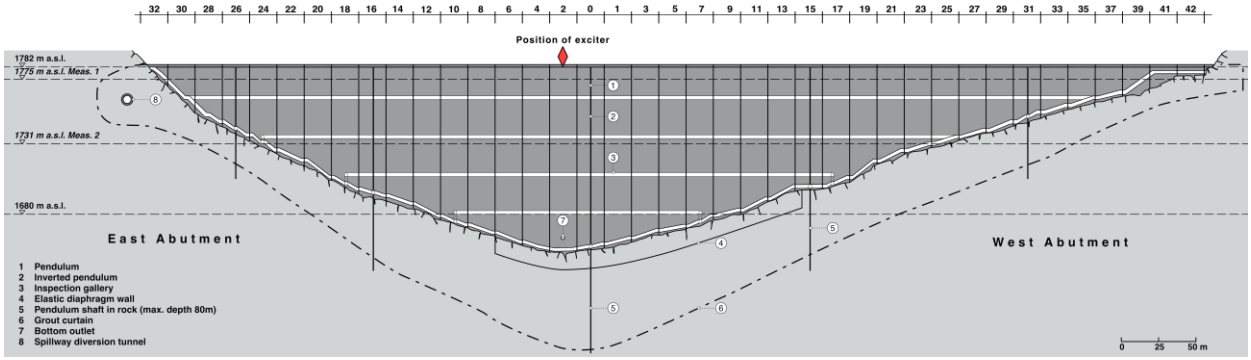

Figure 3: Longitudinal section of Schlegeis dam, reproduction from [6]

4 NUMERICAL ANALYSIS

The in-situ measurements were performed at certain reservoir water levels and therefore the influence of the dam's interaction with the water has to be considered in the finite element analysis. The reservoir is discretized with acoustic elements which are coupled to the dam to consider the fluid structure interaction (FSI) in the analyses. For the identification of dynamic material parameters of concrete and rock, two finite element models have been set up with the corresponding reservoir water levels in the fluid domain.

4.1 Discretization of the geometry

The main dimensions of the geometric domain measure 1500 m each in horizontal directions and approximately 500 m in vertical direction, the crest level defines also the top level of the foundation block. The shortest dimension of the fluid domain in streamwise direction, measured from the apex of the dam's main axis to the end of the reservoir is approximately 760 m.

The structural domains together with the fluid domain were meshed by using the ANSYS MultiZone meshing method to generate a pure hexahedral mesh. With this method it was possible to reduce the number of elements and nodes compared to a mesh with tetrahedral elements. The aim of this procedure was to generate a higher quality mesh compared to a tetrahedral mesh and to reduce the solving time of the analyses.

The final mesh of the model that discretizes the situation of the first in-situ measurement with higher water level in the reservoir (1775 m a.s.l.) consists of approximately 18300 elements and 84600 nodes as shown in Figure 4. The number of elements and nodes in the second model is lower due to the smaller fluid domain which represents the situation of the second measurement campaign at reservoir water level 1731 m a.s.l..

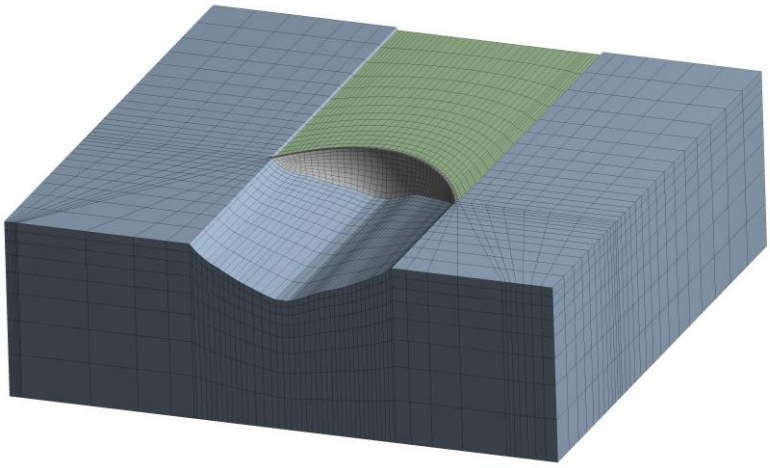

Figure 4: Geometry and finite element mesh that represents the situation of the first in-situ measurement

In both models the structural domain is discretized by SOLID186 higher order elements (quadratic displacement behavior) with 20 nodes each, and so-called uniform reduced integration that prevents volumetric mesh locking. The higher order FLUID220 20-node acoustic element type with pressure as the only degree of freedom is used for those regions of the fluid domain that are not in the first layer at the interaction interface to the structure. Those acoustic elements that are connected to the FSI interface, displacement degrees of freedom are solved in addition to the pressure degree of freedom.

4.2 Model setup

The displacement degrees of freedom of the structural and fluid domains are coupled at the FSI interface by using the bonded type (no separation) of the Multi-Point constraint (MPC) approach, this leads to a two-way, matrix coupled FSI problem. At the top of the fluid domain a zero pressure boundary condition is applied to the acoustic elements.

It is assumed that the dam body cannot separate from the foundation block, therefore, the bonded MPC coupling is used as well at this interface. Linear elastic behavior was assumed for both parts of the structural domain (concrete and massless foundation). Thus, a linear system is solved in the modal analyses of the parameter study.

Constant material parameters have been defined in preliminary modal analyses to investigate the mesh sensitivity on the calculated natural frequencies of the dam to obtain the optimum number of elements with respect to the computation time.

4.3 Dynamic material properties - parameter study

The natural frequencies gained from the in-situ test at Schlegeis dam (Table 2) are the reference for the numerical parameter studies to obtain values for the dynamic material properties of concrete and rock. The difference between the obtained natural frequencies of the

second and third measurement are marginal therefore, the frequencies of the second measurement are considered as input in the numerical study with water level 1731 m a.s.l..

ANSYS DesignXplorer module offers different tools for parameter studies or design optimization, one of these tools that has been used is called Direct Optimization which uses the Multiple-Objective Genetic Algorithm (MOGA) method to solve the optimization problem. More detailed information can be found in [7]. Basically, the investigations in this paper are the optimization (variation) of material properties of the finite element modal analysis so that the first five calculated natural frequencies match the measured ones within a tolerance threshold (Pareto criterion). Table 3 gives an overview about the chosen properties and their ranges in case of variation.

Table 3: Input material properties for modal analyses

Property	**Unit**	**Concrete**	**Rock**	**Fluid**
Density (ρ)	kg/m^3	2400	massless	1000
Speed of sound (c)	m/s	-	-	1440
Poisson's ratio (ν)	-	0.15 - 0.20	0.25 (const.)	-
E-modulus (E)	GPa	25 - 40	20 - 25	-

Table 4 shows the results of the computed dynamic parameters that are found after several iterations in the optimization process, with the best fit to the first measurement which is related to the higher water level in the reservoir. A comparison of the natural frequencies in Table 5 shows very good agreement of the measured and computed frequencies for the case of the higher reservoir water level.

Table 4: Material parameters gained from parameter studies

		Water level 1775 m a.s.l.	
Property	**Unit**	**Concrete**	**Rock**
Poisson's ratio (ν)	-	0.15	0.25
E-modulus (E)	GPa	38.9	24.2

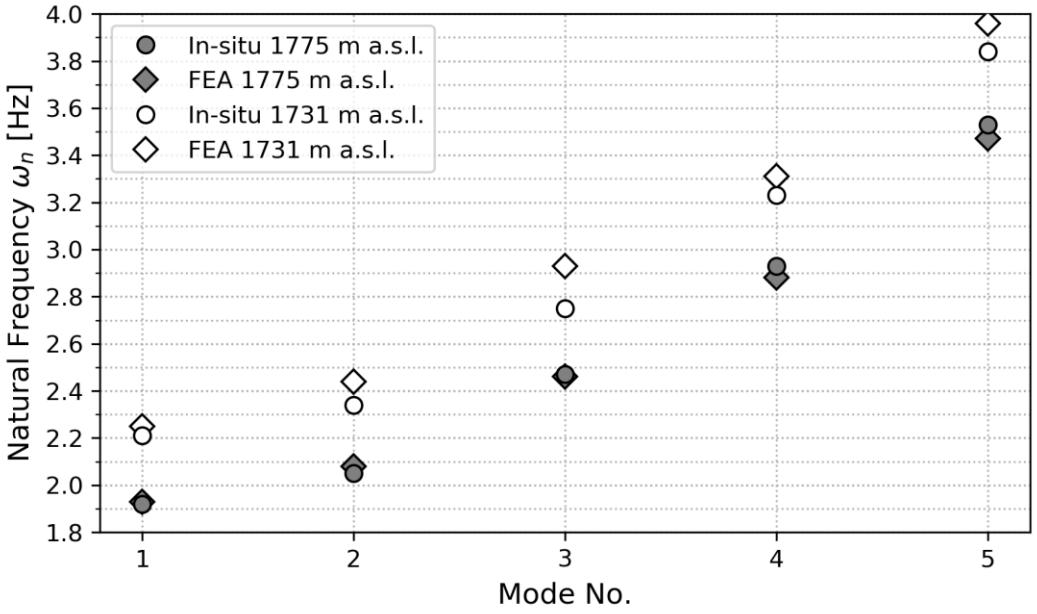

Figure 5: Natural frequencies from in-situ measurements from [5] and finite element analyses (FEA)

If the gained material parameters from the analysis that corresponds to the higher water level in the reservoir, are used as input for the modal analysis of the second model (water level 1731 m a.s.l.) the computed natural frequencies differ more significant (see Figure 5 and Table 5). The reason for this deviation may be explained due to nonlinear effects such as partial opening of the block joints for lower water levels which was captured by the in-situ measurements but is not considered in the numerical model due to its linear nature.

Table 5: Natural frequencies from in-situ measurements from [5] and finite element analysis (FEA)

Mode no.	Reservoir water level 1775 m a.s.l.			Reservoir water level 1731 m a.s.l.		
	In-situ	FEA	Deviation	In-situ	FEA	Deviation
	ω_n [Hz]	ω_n [Hz]	Δ [%]	ω_n [Hz]	ω_n [Hz]	Δ [%]
1	1.91	1.93	1.0	2.21	2.25	1.8
2	2.04	2.08	2.0	2.34	2.44	4.3
3	2.47	2.46	-0.4	2.75	2.93	6.5
4	2.93	2.88	-1.7	3.22	3.31	2.8
5	3.54	3.47	-2.0	3.83	3.96	3.3

5 DYNAMIC MATERIAL PROPERTIES

During seismic events variable loads act within short time periods on the dam as well as foundation rock, with strain rates $\dot{\epsilon}$ of $10^{-4} - 10^{-1}\ s^{-1}$ [8]. Several investigations e.g. like U.S. Bureau of Reclamation [9], showed that dynamic material parameters of concrete and rock such as e.g. Young's modulus E and Poisson ratio ν differ from their static values. U.S. Bureau of Reclamation did intense dynamic material testing on more than hundred concrete

cores taken from several dams to quantify the ratio of dynamic to static values of concrete properties like compression and tensile strengths, Young's modulus, Poisson's ratio, etc..

The Young's modulus can be computed based on the compressive strength $f_{ck(t)}$ at a certain age *t* of concrete by using the following relationship [10]:

$$E_{(t)} = 22 \cdot \left(\frac{f_{ck(t)}}{10}\right)^{0.3} \quad (1)$$

Using Equation 1 together with the measured compressive strength of 12 year old concrete cores taken from Schlegeis dam, leads to a static elastic modulus $E_{12yrs} = 31.6\ GPa$. The corresponding compressive strength $f_{ck(12yrs)} = 33.0\ MPa$, together with conversion formulas to consider the effect of specimen size are provided in [11]. In [2] the static Young's modulus of the foundation rock is given as 20 GPa, as a result of several in-situ and laboratory tests.

By comparing the above mentioned static properties to the results gained by the numerical investigations, ratios of dynamic to static parameters of concrete and rock are calculated as shown in Table 6.

Table 6: Static and dynamic Young's moduli of concrete and rock

Property	Unit	Static	Dynamic	Ratio dyn./stat.
E concrete	GPa	31.6	38.9	1.23
E rock	GPa	20.0	24.2	1.21

According to [9] the average ratio of dynamic to static Poisson's ratio is 1.09 with a variation coefficient of 0.29. Due to this scatter of these results it is recommended to use the static Poisson's ratio of concrete which is in the range between 0.15 to 0.20. Therefore, results shown in Table 6 are based on static values of Poisson's ratio of concrete. Furthermore this assumption has been devolved to the Poisson's ratio of rock in the numerical analyses.

Finally, the dynamic/static ratio of 1.23 for Young's modulus of concrete which was calculated in this study, lies within the span of values that are provided in several standards and guidelines for dam engineering. A comprehensive summary of these numbers can be found in [11].

6 CONCLUSION

Dams are structures with a high risk potential. Therefore, intensive and critical structural safety assessment in the design phase for static and dynamic load cases is essential. The responsible engineers rely on material parameters from testing in the laboratory and if possible from in-situ tests of already build structures.

In the present study a numerical investigation with the aim to calculate dynamic material properties of concrete and rock has been undertaken for the Schlegeis double-curvature arch-gravity dam in Austria, based on already published results of in-situ measurements at this dam. Modal analyses using the finite element method were carried out to study the influence of varying material parameters on the natural frequencies of the dam. Natural frequencies measured at the prototype were used as benchmark to identify values of dynamic Young's moduli for concrete and rock. A comparison with dynamic material parameters which are

provided in international standards and guidelines for dam engineering, shows a good agreement of the gained results of this study. The result can be improved even further by creating a more detailed FE model of the foundation.

In conclusion, the results of in-situ measurements in general, and in this case at the Schlegeis dam, are a valuable basis for engineers that are in charge of assessing the structural safety of dams and other hydraulic structures, by adapting the material parameters in the model to values that were gained from similar structures.

REFERENCES

[1] F. G. Pikl, E. Staudacher, and W. Richter, in *Pumped storage hydropower in Austria*, G. Zenz, Ed. Graz: Verlag der Technischen Universität Graz, 2018.
[2] R. Widmann, J. Schlosser, and H. Stäuble, 'Die Bogengewichtsmauer Schlegeis', *ÖZE*, vol. 25, no. 10, pp. 395–404, 1972.
[3] G. Zenz and E. Aigner, 'Uplift pressure and stress analysis of an arch dam and foundation', in *Proceedings of the 5th ICOLD International Benchmark Workshop on Numerical Analysis of Dams*, Denver, CO, 2000, pp. 17–26.
[4] 'Proceedings of the 6th ICOLD International Benchmark Workshop on Numerical Analysis of Dams', Austrian Committee On Large Dams (ATCOLD), Salzburg, 2001.
[5] J. Riezinger and R. Flesch, 'Dynamische Untersuchungen an der Gewölbesperre Schlegeis', Technische Universität Wien und BVFA - Arsenal (Abt. Dynamik und Akustik), Vienna, 1994.
[6] F. Huber, E. Huber, R. Meisinger, and M. Hanzl, Eds., *Dams in Austria*. Vienna: Austrian National Committee on Large Dams, 1991.
[7] *Help System, Design Xplorer*. ANSYS® Academic Research, Release 19.2.
[8] E. Brühwiler, 'Fracture of mass concrete under simulated seismic action', *Dam Engineering*, vol. 1, no. 2, pp. 153–176, 1990.
[9] U.S. Bureau of Reclamation, 'Dynamic Properties of Mass Concrete Obtained from Dam Cores', *ACI Materials Journal*, vol. 97, no. 3, 2000.
[10] *EN 1992-1-1:2004: Eurocode 2: Design of concrete structures - Part 1-1 : General rules and rules for buildings*. 2004.
[11] 'Bulletin 145: The physical properties of hardened conventional concrete in dams', ICOLD, 2009.

Response of Scandarello Dam to the 2016-2017 seismic sequence in Central Italy

Matteo Sbarigia[1], Rosella Caruana[1], Angelica Catalano[2], Armando Lanzi[2]

[1] Enel Green Power S.p.A. – Dams & Civil Infrastructures Safety
Viale Egeo 150, Rome, Italy
E-mail: matteo.sbarigia@enel.com

Keywords: Gravity dams; Concrete; Seepages; Statistical Model; Dynamic monitoring

Abstract. *From August 2016 until the beginning of 2017, a long seismic sequence affected Central Italy, particularly between the cities of Macerata and L'Aquila. Scandarello Dam is located in the municipality of Amatrice and only 7 km far from the epicenter of the first shock occurred on August 24th (Accumoli). Post-earthquake controls and inspections didn't show significant damages neither to the dam body nor on the banks or on the appurtenant structures. The static monitoring system of the dam recorded some anomalies, although they were found to be of limited importance if compared to the overall behavior of the dam. This paper describes the post-earthquake measured response of the dam and compares it with historical data. Results suggest the importance of providing dams with automatic, static and dynamic monitoring systems.*

1 INTRODUCTION

On 24th August 2016 at 3:36 a.m. a 6.0 Magnitude earthquake hit the Central Apennines, only 7 km far from Scandarello Dam.

This paper describes the seismic sequence in terms of hazard and effects on the territory and on the Scandarello Dam. It will be shown that the dam underwent no significant damage, contrary to other types of structures and infrastructures in the area. Some small evidences were observed only on the crest with an accentuation of the existent cortical cracking pattern and slight damages on the parapets.

Furthermore, the paper deals with the response of the dam in terms of its fundamental measurements and their variations in relationship with the historical seasonal behaviour.

Finally, the conclusions put in evidence the good response of the dam to the earthquakes happened also the importance of historical surveillance and information as well as a reliable monitoring system, in order to express a judgement almost immediately after the earthquake. For this reasons both of an automatic monitoring system of the fundamental magnitudes and a dynamic monitoring system with accelerometers were installed as soon as possible after the earthquake.

[2] Ministry of Infrastructures and Transport – Directorate-General for dams, hydraulic and electrical infrastructures

2 THE CENTRAL SEISMIC SEQUENCE

Between August 2016 and January 2017, four major earthquakes occurred in Central Italy. The first event, with M6.0, took place on 24 August 2016, the second one (M5.9) on 26 October, the third one (M6.5) on 30 October 2016 and the forth one (M5.5) on 18th January 2017.

As shown in Figure 1, this earthquake sequence occurred in a gap between two earlier damaging events, the 1997 M6.1 Umbria-Marche earthquake to the north-west and the 2009 M6.1 L'Aquila earthquake to the south-east.

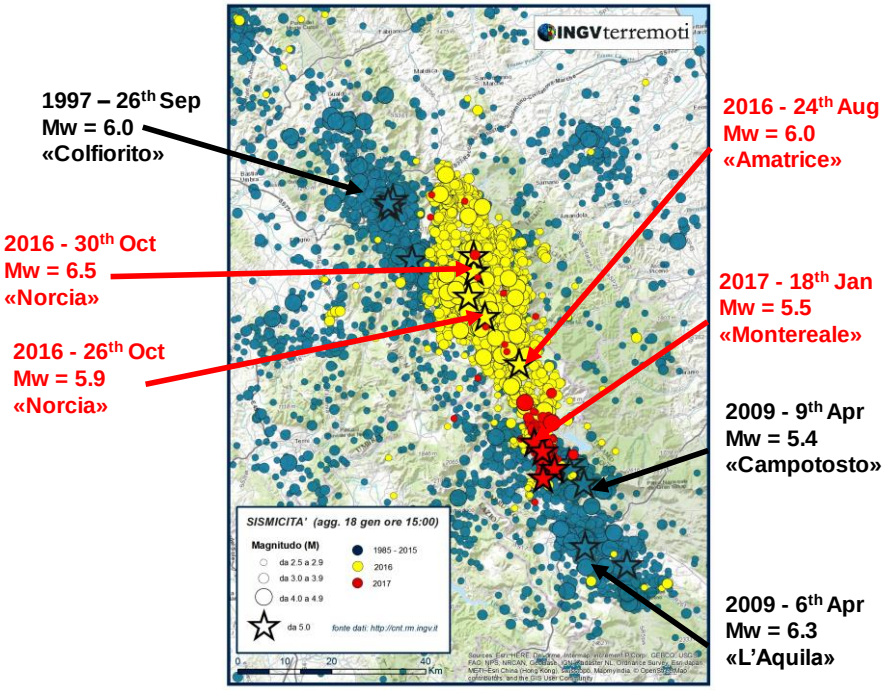

Figure 1: Seismic main events in the last 20 years in the interested area.

These events occurred along the spine of the Apennine Mountain range on normal faults and had rake angles ranging from -80 to -100 deg., which corresponds to normal faulting. Each of these events produced substantial damage to local towns and villages.

2.1 Effects on territory

The 24th August event caused massive damages to the following towns: Arquata del Tronto, Accumoli, Amatrice, and Pescara del Tronto. In total, there were 299 fatalities, generally from collapses of unreinforced masonry dwellings (fig. 2). The October events caused significant new damage in the villages of Visso, Ussita, and Norcia, although they did not produce fatalities, since the area had largely been evacuated.

Furthermore, several important coseisimic effects was recorded (i.e. Monte Vettore slip of about 1 m), as well as many rockfalls and landslides. One of the most relevant was the Nera River Landslide, a 300 meter-high wedge-type translational slide that became a large rockfall that dammed the river below and closed the highway (fig. 3).

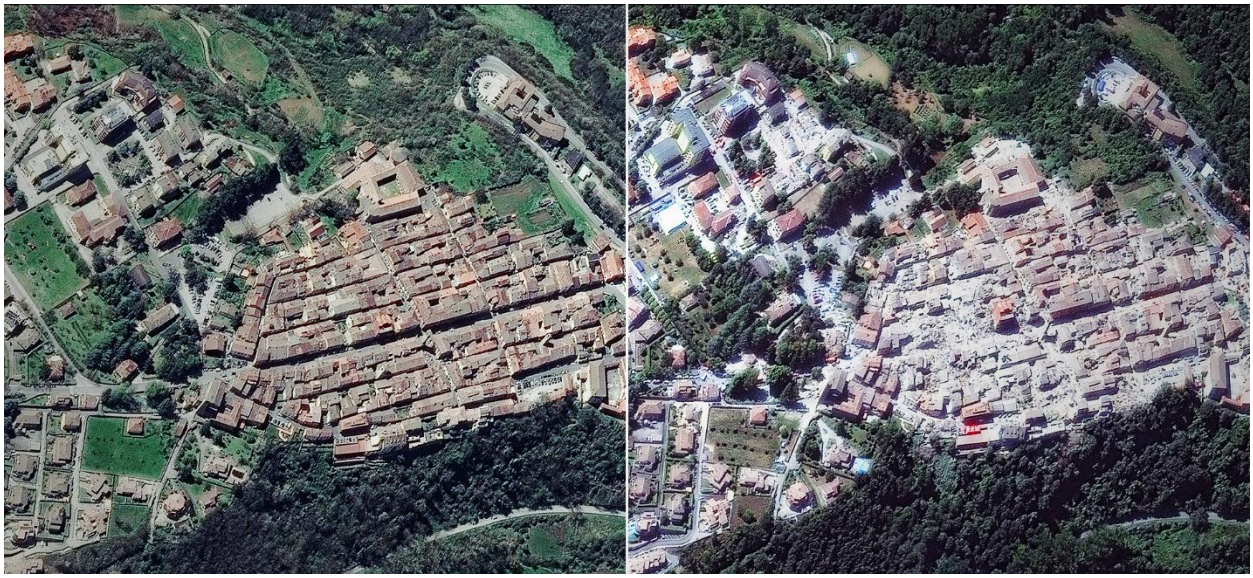

Figure 2: Amatrice town before and after 24th August Mw 6.0 earthquake.

Figure 3: The Nera River Landslide that dammed the river below and closed the highway.

At Scandarello dam, starting from 24th August 2016 until January 2017, more than 50 shocks with a PGA evaluated at the site above 0.04 g [3] were felt. But the most important earthquake was the first shock (Amatrice M6.0), located only 7 km from the dam, with a PGA evaluated at the site about 0.25 g [2]. On the contrary, the PGA recorder by the AMT Station (located closer to the dam, but in Amatrice Town) was definitely greater and equal to 0.43g, certainly affected by amplification due to the alluvial substratum.

[3] *PGA = (*F. Sabetta e A. Pugliese, *1996) estimation of the horizontal component of the maximum free-field acceleration at the dam site (as a percentage of the gravity acceleration).*

3 SCANDARELLO DAM

Scandarello Dam is a 45.15 m high gravity concrete dam, located in the Municipality of Amatrice (Rieti Province), along Rio Scandarello, a tributary of Tronto River, built between 1921 and 1927.

The reservoir, with a capacity of 12.5 Mm^3, is managed by Enel for hydroelectric power generation in a plant at the foot of the dam. However, the reservoir is also very important as a summer reserve providing water for the above Tronto Valley.

The dam has a curved layout, with a radius of the arch equal to 150m. The crest of the dam, 6m wide and over 200 m long, reaches an elevation of 876.5m a.s.l.

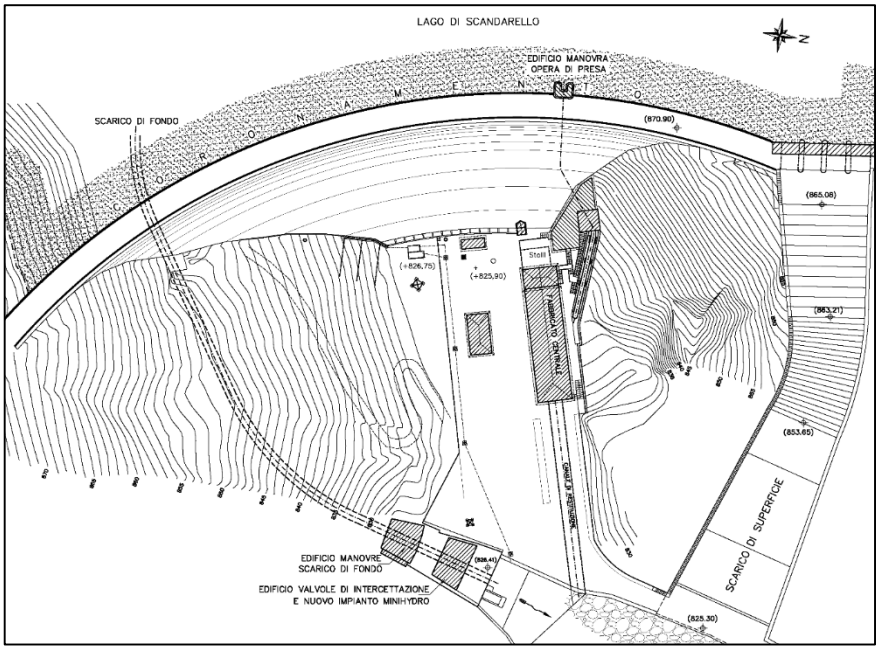

Figure 4: Scandarello dam - Layout

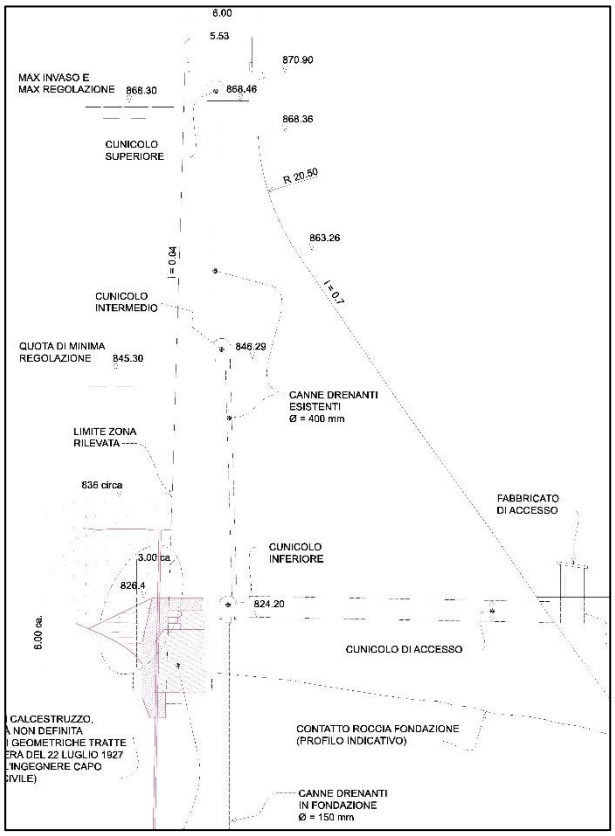

Figure 5: Scandarello dam - Main cross-section

The core is monolithic without vertical joints and the base has a thickness of about 40m. The foundation substratum is comprised of sandstone and marlstone in a mixed layers succession, different from right and left abutments.

4 EFFECTS ON THE DAM

4.1 Evidences from inspections

Following each of the 54 earthquakes with magnitude $M_w > 4$, visual inspections were carried out, without recording significant effects either on dam body or on the banks or on the appurtenant structures. Some small evidences of damage were observed after the 24th August M6.0 earthquake only on the crest with an accentuation of the existent cortical cracking pattern and slight damages on the parapets.

Furthermore, some fissures were observed on three structures: the small building on the crest containing the penstock head gate controls, the dam warden's house and the power plant. The latter was interested by important cracks and damages on the highest wall of the control

room. These damages were speedily repaired, so that the wall could resist without significant damages the 30th October 6.5 Mw earthquake.

4.2 Instrumental evidences

The monitoring system of Scandarello dam generally showed no relevant anomalies in the dam behavior.

However, after 24th August earthquake, Enel increased the frequency of measurements, especially pendulum displacements, uplift pressures (piezometers) and seepages through dam body, foundation and right abutment, that registered some variations.

In the following, considerations about these significant measures are expressed, based on statistical models carried out starting from the historical database.

The other measurements, as rotations of the foundation, joint displacements, didn't show any significant variations after earthquakes.

4.2.1 Pendulums

Scandarello dam is provided of two pendulums in order to measure both the radial (downstream-upstream) and tangential (right-left) displacements of the crown cantilever, in a movable point located at the bottom gallery floor. The measurements are made in respect to two fixed points: one located 50 cm under the crest (direct pendulum) and the second one in the foundation (16 m under the floor).

For both pendulums statistical models were developed, calibrated considering as a reference the period between 1st October 2009 (last day of the 2009 L'Aquila Seismic sequence) and 4th August 2016 (latest day of measurements before the Amatrice 6.0M earthquake).

In term of variations only the downstream-upstream components are significant, showing a very good correlation coefficient (R^2 both over 0.87), with the driving factors (seasonal temperatures for both, only hydraulic level of the reservoir for inverted pendulum).

As shown in the diagrams of figures 6 and 7, for both pendulums, the day-after-24thAugust measurements (blue line) deviate from the model (red line), showing millimetric downstream displacements. On the contrary, the day-after-30th October measurements recorded comparable upstream displacement, bringing themselves back almost overlap the model line.

After that, the seasonal behavior seems regular, in good agreement with the model.

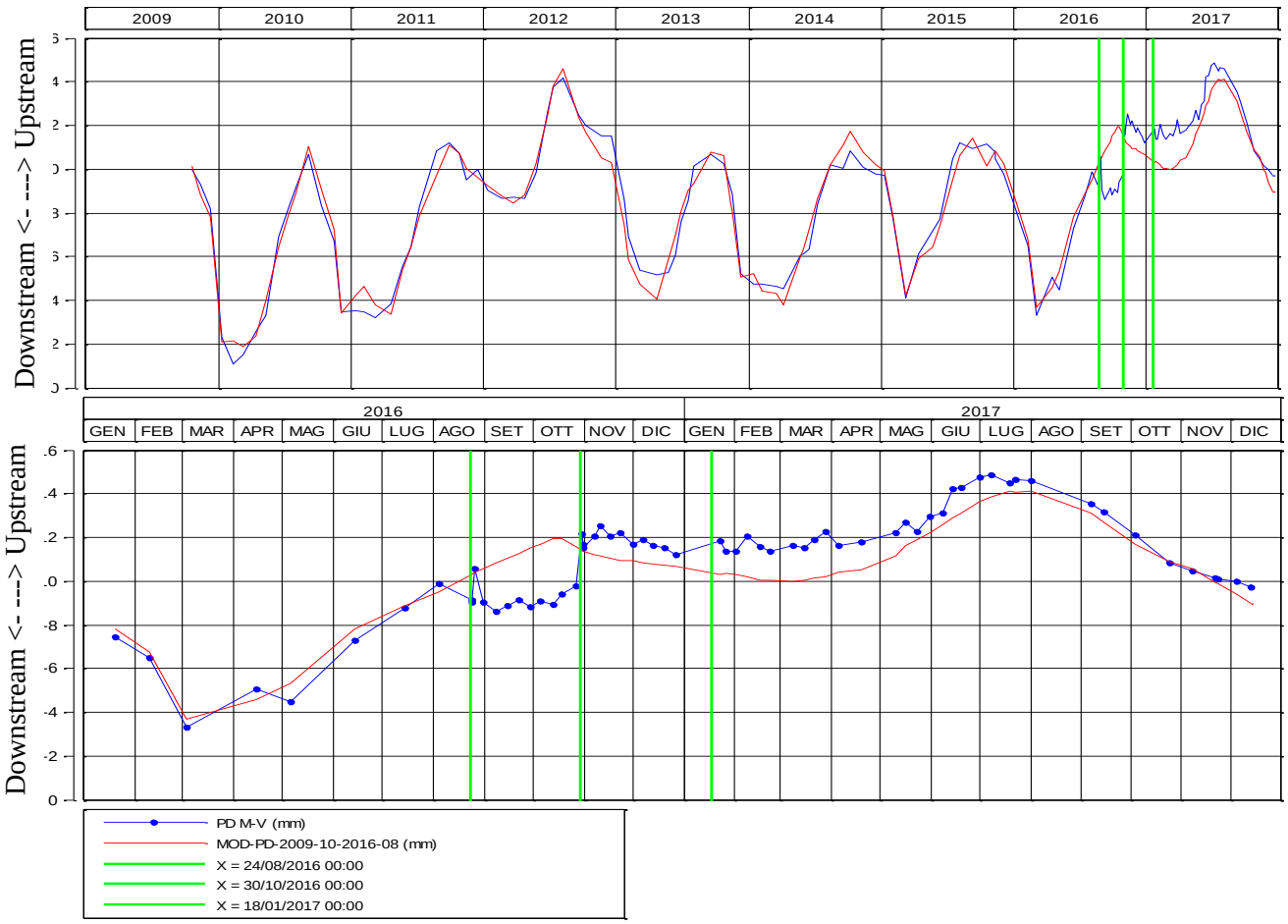

Fig. 6 Direct pendulum – downstream-upstream displacements. The measurements are blue dots-lines; the models are the red lines.

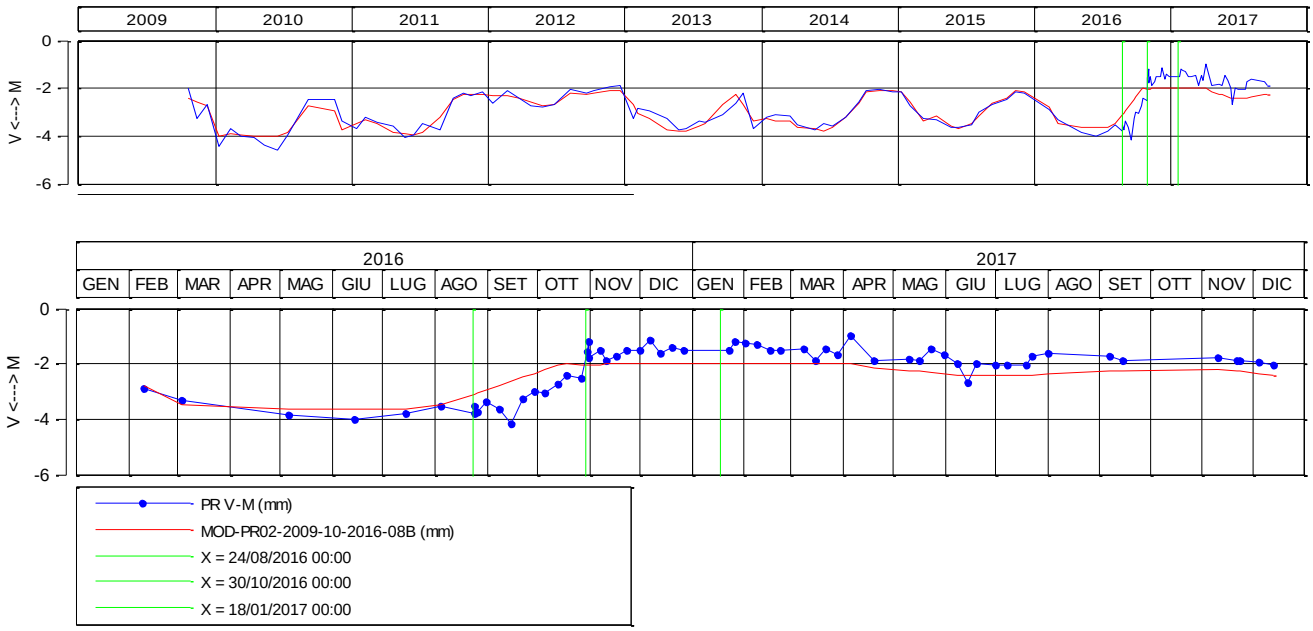

Fig. 7. Inverted pendulum – downstream-upstream displacements. The measurements are blue dots-lines; the models are the red lines.

4.2.2 Seepages

Since it was built, Scandarello dam has always been interested by a significant seepages pattern, especially through the foundation and right abutment. No deep grouting was carried out in the foundation rock before dam construction.

At the first impounding, underseepages over than 100 liters per second occurred, caused by the dam heel being too shallow. A supplementary hell wall was constructed, but it did not prove successful. Therefore, in 1927 a grout curtain was realized in order to reinforce and connect the wall to the foundation rock, made of strongly fractured sandstone and marlstone in a mixed layers succession. The seepages decreased down to 4-5 l/s, measured at the end of the bottom gallery.

At the end of 2002, in order to effectively reduce the uplift pressures, a new drainage system into the foundation was realized in addition to the original one in the dam body.

This chimney drain resulted very efficient, but caused an increase of seepages, up to 10-12 l/s at maximum water level.

A statistical model of the total amount of seepages was developed, considering for calibration a reference period between 1st October 2009 (last day of the 2009 L'Aquila Seismic sequence) and 4th August 2016 (latest day of measurements before the Amatrice 6.0M earthquake). The cause magnitude influencing the measurements is only the hydraulic level with a very good correlation coefficient ($R^2 = 0.93$).

As shown in the diagram of figure 8, the day-after-24thAugust measurements (blue line) deviate from the model (red line), pointing out an important increase (about 8 l/s), partially due to the efficiency of the drainage system. After earthquake, following the reservoir emptying, the seepages decreased with a higher rate than the model, trying to recover a normal behavior. The 30th October 6.5M earthquake caused another slight increase of seepages (about 3.5 l/s), which slowly reduced during the next months.

Seepages increased again after in 2017 the reservoir was partially re-impounded. However, the deviation between measurements and model prevision decreased during summer, reaching values about 3.5 l/s. This difference has remained constant until today, despite the higher reservoir water level.

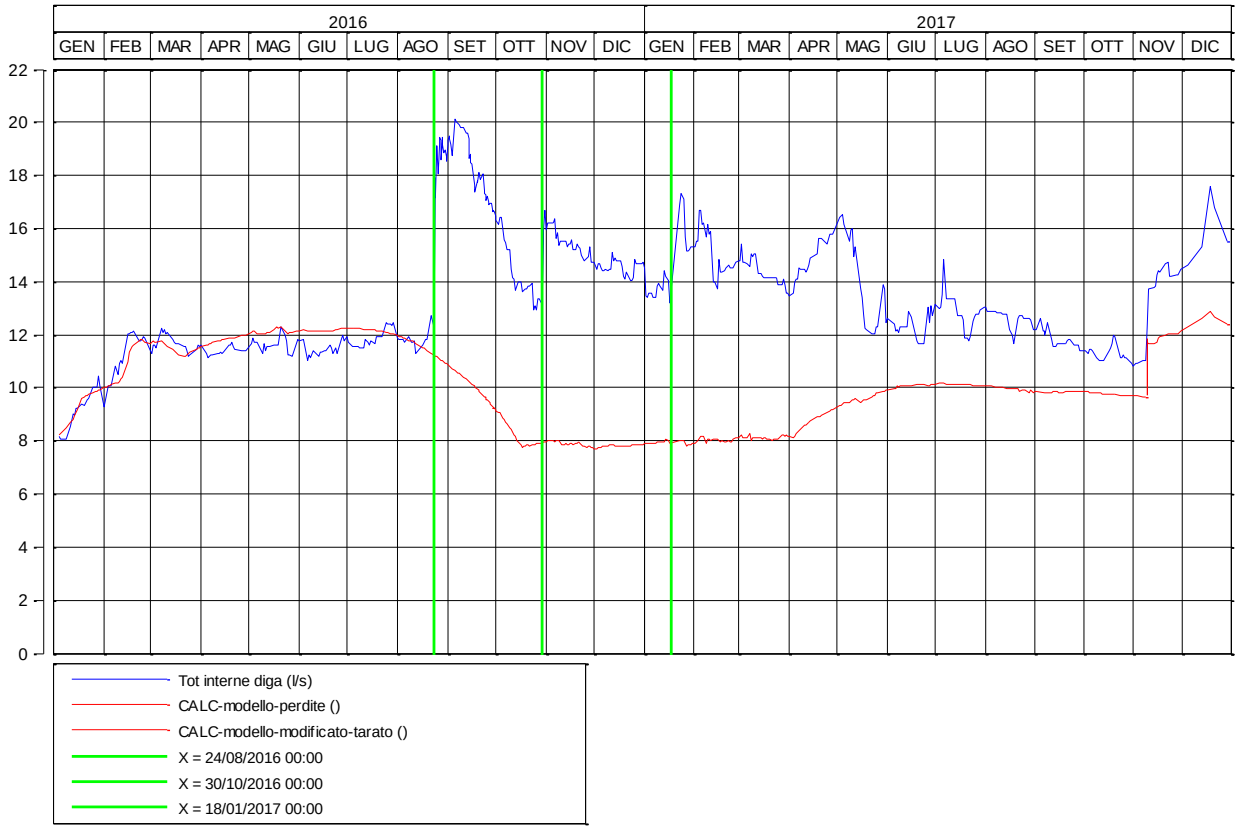

Fig. 8. Seepages. The measurements are blue lines; the models are the red lines.

4.2.3 Uplift pressures

Together with the realization of the new drains into the foundation, three piezometers were installed into the longitudinal bottom gallery and another two piezometers in the downstream right abutment, in order to evaluate the reduction of the uplift pressures.

All piezometers were provided with sensors put into an open standpipe with a 2-meters windowed section located at the contact between dam and foundation rock.

The analysis are made on the two most significant piezometers, one located into the bottom gallery, named PZS1, and the other one in the low part of the downstream right abutment, named PZV1.

The normal historical reduction of the uplift pressures, evaluated in respect to the contact dam/foundation, for these two piezometers, depends from the reservoir water levels, but is about 80-85% for PZS1 and 84-88% for PZV1, showing a very good efficiency of the drainage system.

For both instruments, statistical models were developed, considering for calibration a reference period between 1st October 2009 (last day of the 2009 L'Aquila Seismic sequence) and 4th August 2016 (latest day of measurements before the Amatrice 6.0M earthquake). The main factor influencing the measurement of PZS1 is only the hydraulic level, which shows a good correlation coefficient (R^2 = 0.86). The PZV1 is also influenced by the seasonal temperature variations (R^2 = 0.89).

As shown in the diagram of figures 9 and 10, the day-after-24thAugust measurements (blue line) deviate from the model (red line), pointing out a small uplifts increase (about 0.5-0.7 m) and confirming the efficiency of the drainage system. After that, both piezometers measurements decreased and no additional increase was recorded after 30th October 6.5M earthquake (when reservoir was almost at the minimum level). In 2017 the measurements,

especially for PZV1, recovered a regular behavior in good agreement with the models. The PZS1 showed values lower than the model, so that Enel decided to update all the piezometers sensors (see Par. 5.1). Now, measurements are stable on the values before earthquakes.

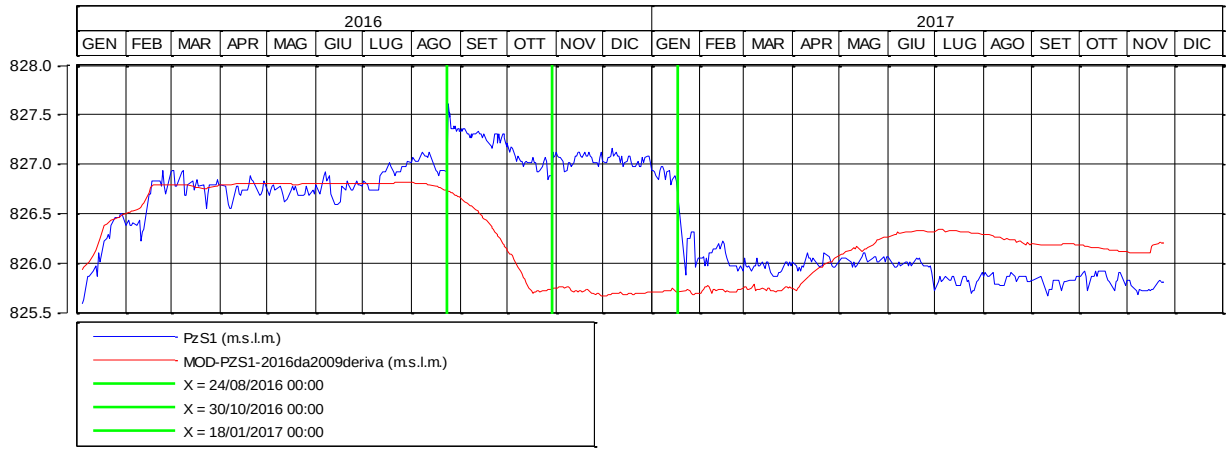

Fig. 9. Uplifts (piezometer PZS1). The measurements are blue lines; the models are the red lines

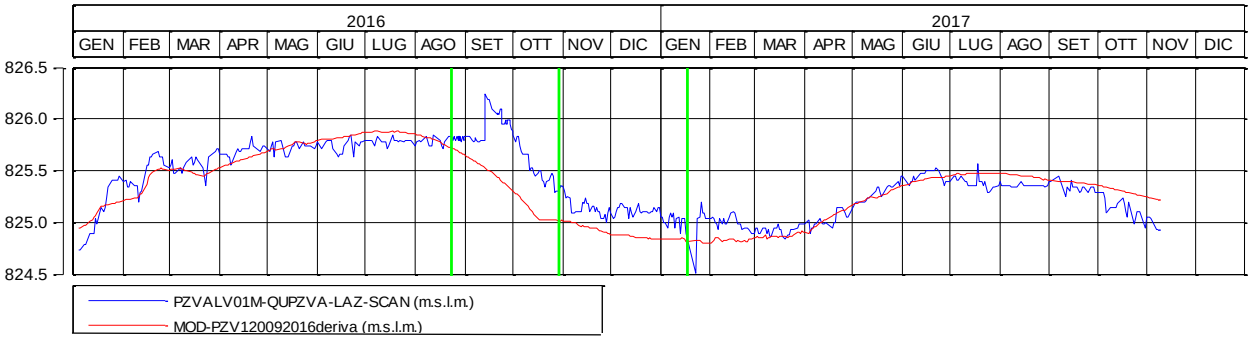

Fig. 10. Uplifts (piezometer PZV1). The measurements are blue lines; the models are the red lines

5 PROJECTS IN PROGRESS

5.1 Automatic monitoring system

Some months after earthquakes, an automatic monitoring system was installed in order to measure the most important magnitudes (laser sensor to measure downstream-upstream displacement of the pendulum weirs, magnetostrictive level sensors for seepages and pressure sensors for uplift) in real time and remotely. This is an important target in order to have information immediately available, especially after significant earthquakes.

5.2 Improvement of the foundation sealing

In order to definitively solve the filtration problem that characterize the dam since it was built, Enel is designing an important improvement of the foundation sealing. It will consist, as shown in figure 11, in a new deep grout curtain in the foundation rock, both in the right and central part, that is responsible of over than 90% of the seepages.

The curtain, made with a stable grout mix with micro-cements, will extend more than 50 meters below the foundation, and will be composed with two parallel lines in order to obtain a strong barrier to the filtration.

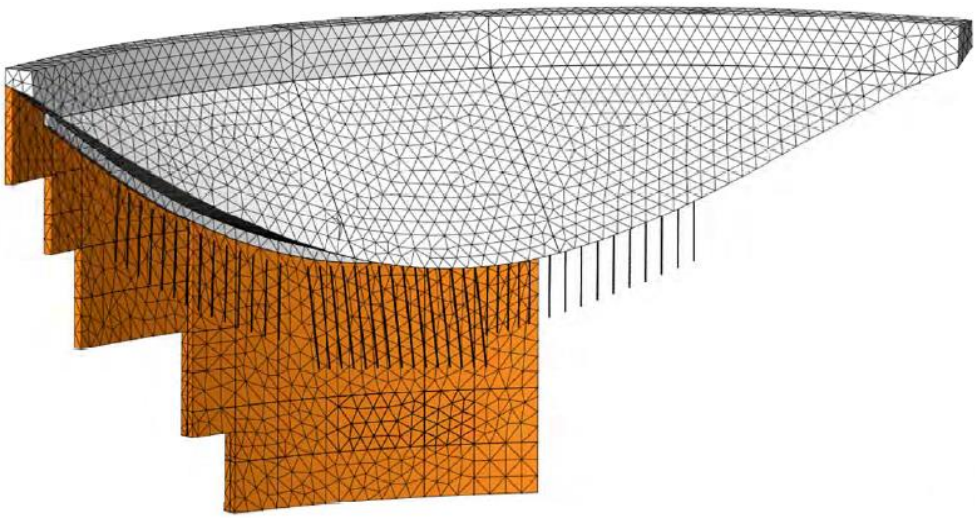

Fig. 11. Grout curtain into the foundation. Design in progress.

6 SEISMIC MONITORING OF THE DAM

In February 2017, about six months after the August 24th main shock, the Civil Protection Department (DPC), in collaboration with the national dam authority (Directorate-General for dams, hydraulic and electrical infrastructures or DGD) and with the support of ENEL, equipped Scandarello dam with a dynamic monitoring system.

The system is made of three force-based, 3-axial acceleration sensors, cable-connected to a central data acquisition unit responsible for sensor control, basic signal processing and remote transmission of measured data. All the instruments are sheltered because they are installed inside the dam's body: two in the top gallery and one in the base gallery. The instrument layout is shown in Figure 12: sensor "C" and "S" are located in the top gallery, the former at the crown cantilever, the latter at the right quarter; sensor "B" is placed at the base of the dam, in the bottom gallery at the crown cantilever.

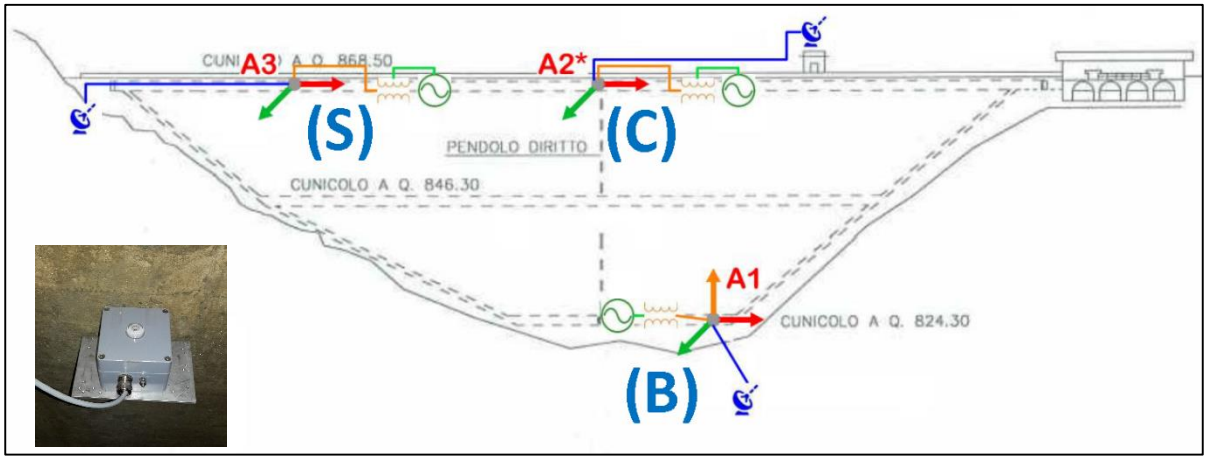

Fig. 12. Layout of the seismic monitoring system installed in February 2017.

The seismic monitoring system of Scandarello dam is part of a larger project named *Italian structural seismic monitoring network* (OSS) [7], developed and managed by DPC, aimed at collecting and analyzing seismic data recorded by many critical structures and infrastructures equipped with seismic monitoring systems. The OSS network is automatized

so that, after an earthquake with magnitude larger than 4.0, the recorded data and some basic parameters of the motion are readily available for download from the OSS website.

After installation of the seismic monitoring system on Scandarello dam in February 2017, a number of low-to-moderate magnitude earthquakes, all belonging to the sequence started August 24th, affected the region close to the dam. The data presented hereafter was recorded from ten earthquakes with local magnitude between 3.0 and 4.2, occurred from February 2017 to March 2018. The source-to-site distance of the ten earthquakes ranges from a minimum of 3.0 Km to a maximum of 23.5 Km. Free-field *PGA* values, recorded by the national strong motion network (RAN), range from 0.3% to 13% of the gravitational acceleration *g*.

Peak acceleration values recorded by the dam monitoring system are shown in the scatter plot of Figure 13. For each record, peak accelerations at the crest (sensors C and S) are plotted against the peak acceleration at the base (sensor B). Data for both stream (M-V) and cross-stream (S-S) directions are included, and data are grouped into three data sets: (1) crown cantilever section (sensor C), stream direction; (2) right quarter section (sensor S), stream direction; (3) cross-stream direction, including both data from C and S sensors. Standard linear regression has been used to provide a best-fit of the three data sets.

Analysis of the plot in Figure 13 leads to the following results:

- Large amplification of the base motion is registered in the stream direction, both for the crown and the quarter section. Amplification factors vary from 1 to 10.
- The response in the stream direction of the crown cantilever is well described by a linear pattern ($R^2 = 0.85$), with an amplification factor of about 5.7.
- On the contrary, data points for the quarter section are more scattered ($R^2 = 0.56$), and the best-fit amplification factor, equal to 6.2, is slightly greater than the one computed for the crown section.
- Much smaller amplification is registered in the cross-stream direction, with similar values for the crown and the quarter sections. Data points show a very good linear correlation, characterized by an amplification factor of about 1.7. This is a result of the higher stiffness of the dam for such modes.

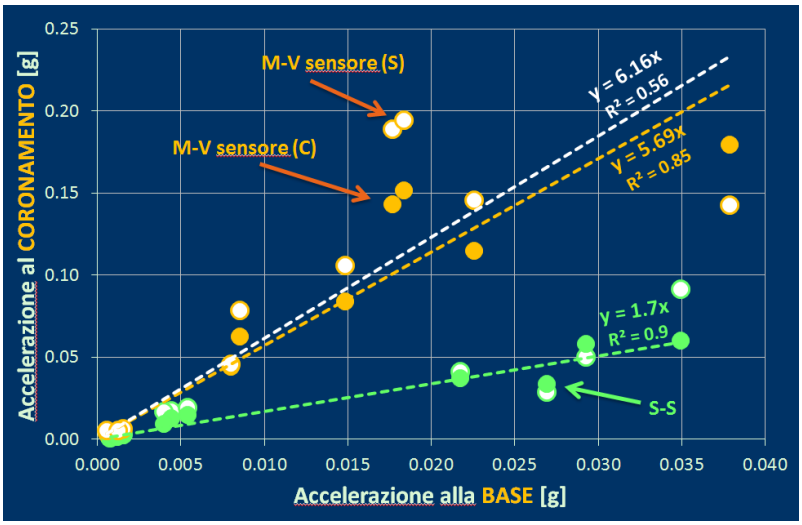

Fig. 13. Scatter plot of the peak accelerations recorded by the seismic monitoring systems during 10 low-magnitude earthquakes (M = 3.0 – 4.2) occurred in 2017-2018. Acceleration at the crest of the dam (C and S sensors) versus acceleration at the base of the dam (sensor B): data points and regression lines.
Stream (M-V) and cross-stream (S-S) directions. The plot is excerpted from [8].

7 CONCLUSIONS

Scandarello Dam, located in the municipality of Amatrice only 7 km far from the first 24th August Mw=6.0 earthquake epicentre, showed a comforting behaviour in response to the 2016-2017 seismic sequence in Central Italy. The numerous controls and inspections didn't show any significant effects either on the dam body or on the banks or on the appurtenant structures. The monitoring system, even if it didn't show overall relevant anomalies in the behaviour of the dam, recorded some variations in the measurements.

For the most important magnitudes characterizing dam behaviour, those variations were compared with statistical models developed starting from the historical seasonal measurements.

Significant concentrated displacements with deviations with respect to the models were recorded only by pendulums in the downstream-upstream direction. These millimetric deviations have partially gone back and measurements are regular in good accordance with models. The seasonal behavior during reservoir re-impounding didn't show anomalies with respect to the past.

Piezometers recorded a slight increase of the uplifts, especially after the first 24th August 6.0M earthquake. In any case, in the following months they returned to a regular behavior, in good agreement with the statistical models.

Seepages through the foundation showed the greatest difference after the first 24th August 6.0M earthquake, with an increase of more than 50% of the expected values. Despite the others earthquakes occurred, during the following months about half of the increase has been recovered. Nevertheless, considering that filtration phenomena were the critical element of Scandarello Dam since it was built, Enel is designing a new deep grout curtain to be realized in the next years.

Finally, automatic and dynamic monitoring systems were implemented in order to provide better quality data on the dam behaviour, immediately available after an earthquake.

REFERENCES

[1] ANIDEL, 1951. *Associazione Nazionale Imprese Distributrici di Energia Elettrica, Milano. Le dighe di ritenuta degli impianti idroelettrici italiani*, Vol. 5.

[2] Department of Civil Protection (DPC): *Website of the Italian Civil Protection Department* - Presidency of the Council of Ministers.

[3] INGV: *Website of Istituto Nazionale di Geofisica e Vulcanologia*. http://www.ingv.it/it/

[4] Paolo Zimmaro and Jonathan P. Stewart. *Engineering Reconnaissance of the 24 August 2016 Central Italy Earthquake. Version 2*. Geotechnical Extreme Events Reconnaissance Association Report No. GEER-050B. 22 November 2016

[5] Paolo Zimmaro and Jonathan P. Stewart. *Engineering Reconnaissance following the October 2016 Central Italy Earthquakes. Version 2*. Geotechnical Extreme Events Reconnaissance Association Report No. GEER-050D. 08 May 2017.

[6] Sabetta F., Pugliese A. *Estimation of response spectra and simulation of non stationary earthquake ground motion*. Bull. of Seismological Society of America, vol.86, No. 2, 1996

[7] M. Dolce et Al. *Osservatorio sismico delle strutture: the Italian structural seismic monitoring network*. Bull Earthquake Eng., vol.15, Issue 2, Febraury 2015.

[8] A. Lanzi, *Monitoraggio sismico delle dighe – Obiettivi, stato dell'arte e prime osservazioni.* Presented at the joint meeting between the Department of Civil Protection (DPC) and the Directorate-General for dams (DGD), Rome, 28 March 2018.

Seismic and structural health monitoring of Cabril dam

Sérgio Oliveira[1], André Alegre[2]

Laboratório Nacional de Engenharia Civil (LNEC), Concrete Dams Department
Av. do Brasil 101, 1700-066 Lisboa, Portugal
E-mail: soliveira@lnec.pt

Keywords: Modal Identification, Ambient and seismic measured vibrations, Experimental and numerical results, Cabril dam.

Abstract. *This paper is focused on the Portuguese experience regarding the development and operation of continuous vibrations monitoring systems in large concrete dams. The goal is to emphasize the importance of the combined use of monitoring data and numerical models for Seismic and Structural Health Monitoring (SSHM) of Dams. The case study is Cabril arch dam (132 m high), the highest dam in Portugal, in which a pioneer SSHM system has been in operation since 2008. This system, installed by LNEC, was designed for measuring accelerations in the dam body and near the base (dam-foundation interface), using 16 uniaxial and 3 triaxial accelerometers. Appropriate software has been developed to integrate and complement the monitoring system, aiming to automatically process and analyse the recorded data, including tools for simplified study of monitoring results and for automatic comparison with numerical results from 3DFE models. The main experimental results obtained for Cabril dam are presented, namely the evolution of natural frequencies over time, mode shapes and the measured seismic response to an earthquake event. A comparison with results from numerical modelling is presented, using a coupled 3DFE model based on a formulation in displacements and pressures, considering a state space approach to simulate the dynamic behaviour of the dam-reservoir-foundation system and the Newmark method to compute the seismic response.*

1 INTRODUCTION

Nowadays, the installation of monitoring systems for continuously measuring vibrations is being proposed for most of the new large dams and for some of the older dams, given that these are civil engineering structures of great relevance and that are associated with high potential risk in case of collapse [1]. Thus, the safety control of large concrete dams tends to rely on Seismic and Structural Health Monitoring (SSHM) systems, aiming to study the dynamic response of dams both under seismic events and ambient or operational excitations (usually sampling frequencies of about 50 Hz are used, however, for seismic monitoring it may be useful to adopt higher sampling frequencies, e.g. up to 1000 Hz). In Portugal [2] (Fig. 1), the structural health monitoring of large concrete dams using systems for continuously measuring vibration started in 2008, when LNEC and Electricidade de Portugal (EDP) decided to install a pioneer SSHM system for monitoring the dynamic behaviour of Cabril dam over time, under ambient/operation excitations and/or seismic events [3]. This system was designed and implemented in the scope of a LNEC research program, supported by EDP and the

[2] LNEC – DBB, sbmoliveira@gmail.com

Portuguese Foundation for Science and Technology (FCT). Following the success achieved with the system installed in Cabril dam, considering the important results obtained in several studies [4,5,6,7] EDP made the decision to install similar complete monitoring systems in other dams, namely in Baixo Sabor dam (2015) and Foz Tua dam. Other systems for measuring seismic vibrations in dams are installed in Alqueva dam, Alto Ceira II dam and Ribeiradio dam.

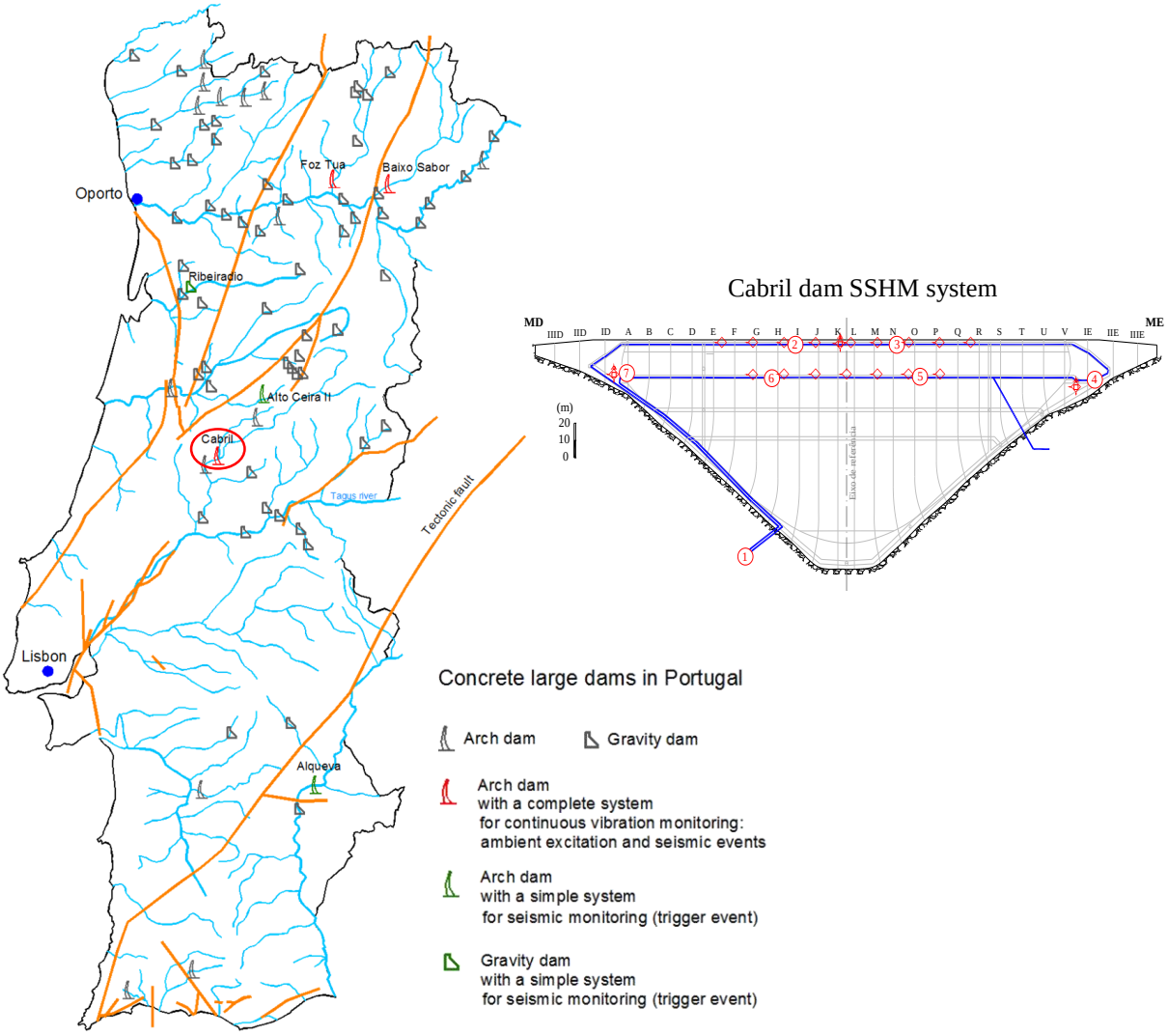

Figure 1: Concrete dams in Portugal and seismic faults. Indication of dams with monitoring systems installed for measuring vibrations under ambient/operation excitations and/or seismic events.

2 DYNAMIC MONITORING OF LARGE DAMS. HARDWARE AND SOFTWARE.

For large concrete dams, the installation and operation of SSHM systems for continuous dynamic monitoring aims to measure physical quantities (e.g. accelerations) in the dam body and in the foundation, using the latest technology for automatic data acquisition. Nevertheless, besides the need for the installation of quality hardware (transducers, data acquisition and transmission, etc.), the efficiency and accuracy of these systems depend heavily on the use of sophisticated software to process, manage and analyse the recorded data. Currently, this is one of the main issues regarding the successful operation of monitoring systems, given that the equipment suppliers only deliver the specific software for data acquisition. Therefore, in order

to improve the efficacy of the new SSHM systems, it has become necessary to develop appropriate software adapted and optimized to each dam thus enabling to carry out interactive and/or automatic analysis of monitoring data and to perform the comparison with numerical results from 3DFEM models [4], as has been done in LNEC in recent years [2]. In this way, important results can be provided for engineers/technicians responsible for dam safety control and health monitoring [4,5,6,7], to study the dynamic behaviour for ambient and operational excitations (e.g. to study the evolution of natural frequencies and mode shapes over time in order to characterize the effects of water level and/or seasonal variations, and in order to detect structural changes due to material deterioration), and to evaluate the structural response under seismic loading (for earthquakes with different peak accelerations and different frequency content). This data is also of great use to calibrate and validate the developed numerical FE models used to predict the seismic response of dams.

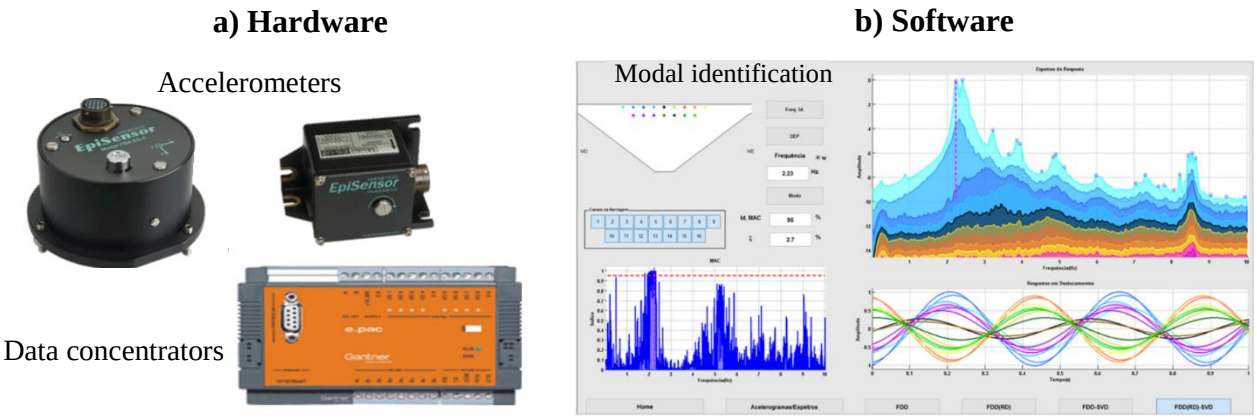

Figure 2: SSHM monitoring. Hardware components and software for modal identification.

3 CABRIL DAM. SEISMIC AND STRUCTURAL HEALTH MONITORING:

Cabril dam (Fig. 3a), the highest dam in Portugal, is located on the Zêzere river and has been in operation since 1954. This is a double curvature arch dam, founded on a granite mass rock foundation, with the particularity of presenting a greater thickness in the crest. The dam has a maximum height of 132 m above the foundation and the crest, which reaches an elevation of 297m, is about 290 m long. The central cantilever has a maximum width of 20 m at the base and a minimum width of 4.5 m below the crest. In this dam, a significant horizontal cracking phenomenon occurred near the crest (at the height 280-290 m) during the first filling of the reservoir. Also, a concrete swelling process has been detected in the late 90's. As for the reservoir, the water surface level usually ranges from a minimum of about 265 m to the maximum storage level of 294 m (the maximum flood level is 296.3 m) throughout the year.

As mentioned previously, in the framework of LNEC research activities regarding monitoring and modelling the dynamic behaviour of dams, a pioneer SSHM system was installed in Cabril dam in 2008 [3] (Fig. 3b). The installation of the hardware components was carried out by the Scientific Instrumentation Centre, while the software presented in this work was developed in the Concrete Dams Department. The goal was to implement a system with high dynamic range, capable of a continuous and accurate measurement of the dam's response for ambient/operation excitations or earthquakes of various magnitudes. The system was designed to continuously measure accelerations in the upper zone of the dam body and near the base, thus including 16 uniaxial and 3 triaxial accelerometers. The outlined configuration was based on experience gathered in LNEC over the years, from both monitoring data and numerical results. The uniaxial accelerometers (measure vibrations in a radial direction) are distributed in the upper part of the dam by two galleries, above and below the cracked zone.

As for the triaxial accelerometers, one is positioned in the central cantilever (upper gallery), while the other two are installed near the insertion of the dam base, in both banks. The accelerometers are connected to a modular system composed by acquisition/digitalization units, which in turn are controlled by 4 data concentrators that receive the recorded data. This data is sent through a local optical fibre network (intranet) to a computer in the observation and control station (OCS), located at the dam power station. In total, 25 accelerograms are recorded and stored every hour, continuously, at a sampling rate of 1000 Hz. Storage and management of the collected data is carried out at the server located in the OCS using appropriate software developed in LNEC. The data can be accessed remotely via internet (a smartphone can be used to explore the collected data with the referred software).

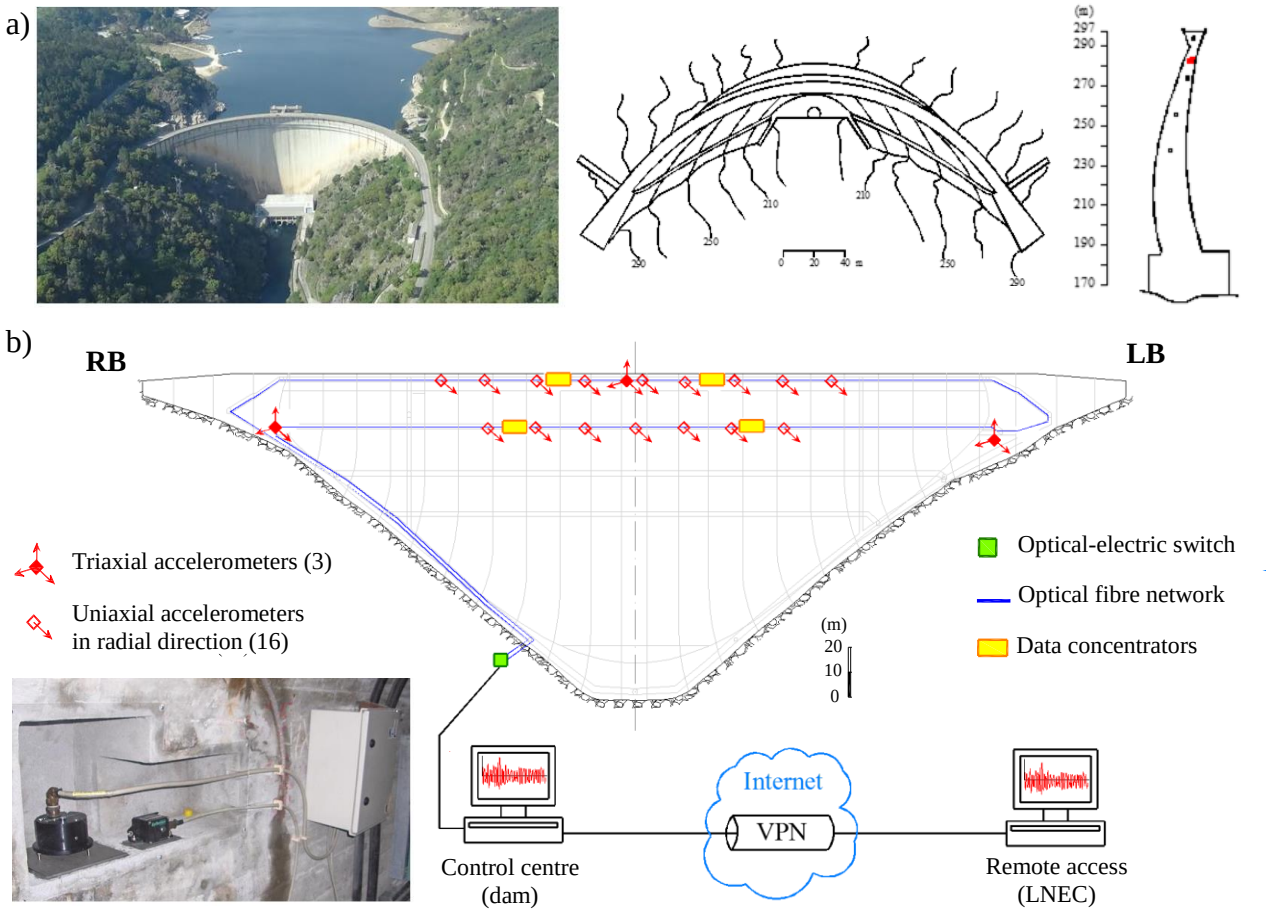

Figure 3: Cabril dam: a) aerial view, plan view and central cantilever cross section; b) front view and SSHM system (main hardware components)

The SSHM system installed in Cabril dam integrates two computational modules (developed using MATLAB): i) **DamModalID1.0**, for interactive monitoring data analysis; and ii) **DamModalID_Auto1.0**, for automatic analysis of data measured over time. The natural frequencies and mode shapes are estimated from acceleration records measured on site, using the Frequency Domain Decomposition (FDD) method for modal identification [8], which is based on the Singular Value Decomposition (SVD) of the Power Spectral Density (PSD) Matrix, using a technique for automatic identification of spectral peaks specifically developed in LNEC.

Regarding **DamModalID_Auto1.0**, this software performs automatic signal processing and modal identification of natural frequencies and mode shapes from large datasets of acceleration time series measured continuously over time, based on parameters defined in

advance by the user. With the goal of facilitating the analysis and interpretation of several months or even years of experimental data, the program generates files with a synthesis of the most important results as well as graphical representations that show the evolution of the natural frequencies over time (Fig. 4). This type of results is very important for engineers/technicians responsible for structural health monitoring, namely, to analyse the influence of the water level and/or seasonal thermal variations in the dynamic response of dams and to detect eventual structural changes due to concrete deterioration or seismic loading.

With **DamModalID1.0** (Fig. 5), the user can chose a data file, with measured accelerations, for any 'hour-day-month-year'. The measured water level is showed and an interactive graphical user interface allow the visualization of all the acceleration records. A modal identification can be easily performed for several parameter sets. The developed user interface includes several menus, where the following outputs are presented: a) the acceleration records for each accelerometer installed in the dam and the corresponding auto-spectral density functions; b) graphical representations of the singular values spectra; and c) the estimated natural frequencies and the respective mode shapes (2D configurations and harmonic waves that represent the oscillatory movement in each measured point). The modal identification results are presented in order to be immediately available for a simple comparison with results from numerical models.

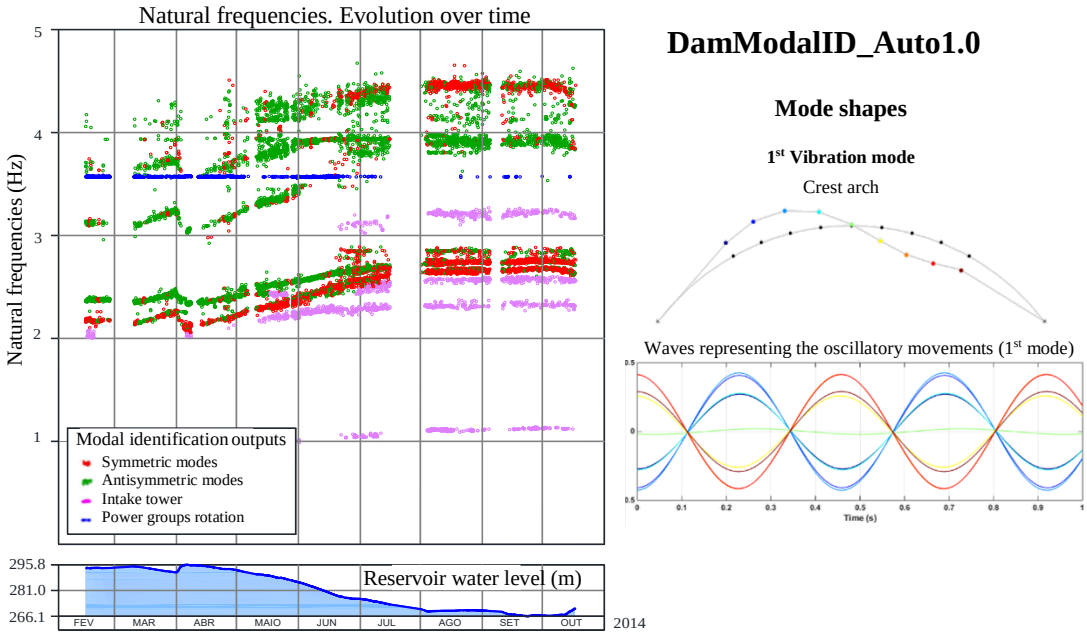

Figure 4: Modal identification software developed for Cabril dam's SSHM system. Results from **DamModalID_Auto1.0**, for automatic monitoring data analysis.

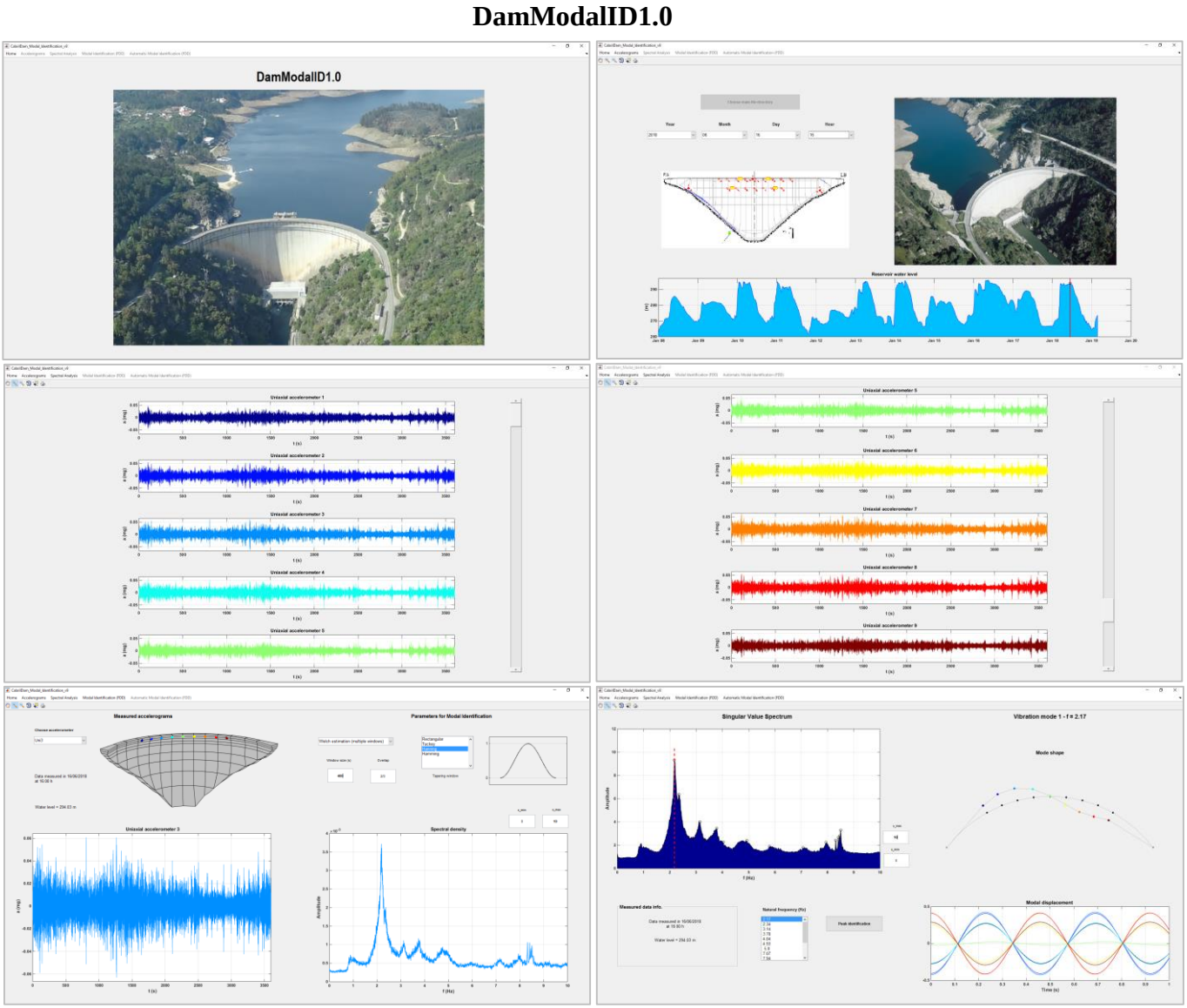

Figure 5: Modal identification software developed for Cabril dam's SSHM system. Results from **DamModalID1.0**: interactive monitoring data analysis, including modal identification using FDD-SVD.

4 DYNAMIC BEHAVIOUR OF CABRIL DAM. EXPERIMENTAL AND NUMERICAL RESULTS

The dynamic analysis of Cabril dam under ambient/operational excitations and under seismic events is presented in this section, based on the combined use of experimental and numerical modelling results. The goal is to contribute in improving knowledge regarding the dynamic response of Cabril dam, as well as to demonstrate the potential of the developed software to study the dynamic response of arch dams and support seismic and structural health monitoring.

The numerical calculations were carried out with **DamDySSA3.0**, a 3DFEM program developed in LNEC, using MATLAB, for linear dynamic analysis of arch dams with generalized (non-proportional) damping. The dam-reservoir-foundation system is simulated using a coupled model based on a Finite Element Method (FEM) formulation in displacements and pressures [10]. The dam-reservoir dynamic interaction is modelled considering the solid-fluid motion coupling at the dam-water interface and the pressure waves propagation

throughout the reservoir, which is a semi-infinite domain terminated by a radiation boundary. The foundation is simulated as an elastic massless substructure: only its flexibility is computed and incorporated into the dam-foundation interface. A state space formulation with two state matrices and complex modal coordinates is used to solve the damped eigenproblem of the system and thus compute the natural frequencies (eigenvalues) and mode shapes (eigenvectors). The seismic response is calculated by direct time integration in global coordinates using the Newmark method, considering seismic accelerograms applied at the base.

A 3DFE model of the dam-reservoir-foundation system (Fig. 6), comprising 626 FE and 3914 nodes (106 elements in dam body), was used. For concrete, the Young's modulus is $E = 25\ GPa$ and Poisson's ratio $\nu = 0.2$. In the dynamic calculations it was used for concrete $E_{dyn} = 1.25 \times 25\ GPa$. For the reservoir it was considered a pressure waves propagation velocity of $c_w = 1440\ m/s$.

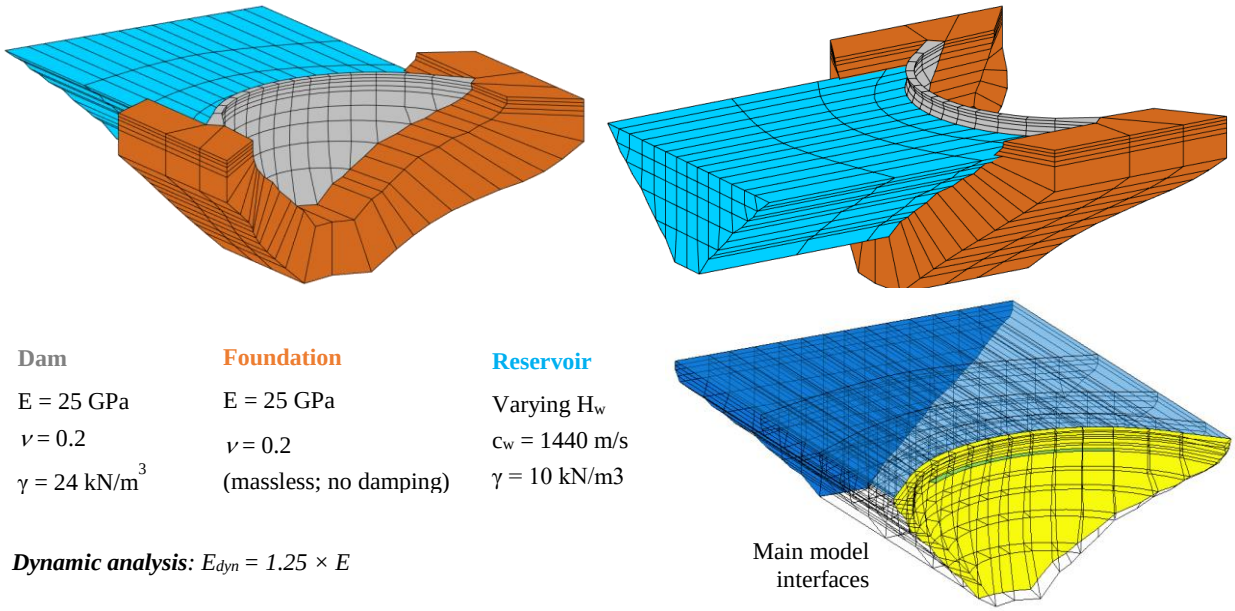

Figure 6: Cabril dam: 3DFE model and material properties.

4.1 Dynamic behaviour: natural frequencies and mode shapes

Initially the analysis is focused on the natural frequencies and mode shapes estimated from the measured acceleration records in the dam body, using interactive (**DamModalID1.0**) and automatic (**DamModalID_Auto1.0**) software. Modal identification is performed using the FDD-SVD method: the PSD matrix is computed using Welch method, considering 400 s long data segments (overlap: 2/3) and Hanning tapering windows. The natural frequencies are estimated from the PSD matrix first singular value spectrum, by automatically selecting the main spectral peaks. The corresponding mode shapes are obtained from the singular vectors of the PSD matrix. For Cabril dam, the identification of natural frequencies should take into account that some values of the dam natural frequencies could be near from the natural frequencies of the intake tower and from the power groups rotation frequencies. It is necessary to implement methodologies that allow to distinguish properly the frequencies of the dam, the tower and the power groups.

Fig.7 shows the evolution of the automatically estimated dam natural frequencies (green and red circles), using acceleration time series recorded from February to October 2014 (water level variation: from 296 to 266 m). The coloured lines represent the correspondent evolution of dam natural frequencies, numerically computed with DamDySSA3.0. In Fig.8, the natural

frequencies and mode shapes identified in June 16, 2018 (acceleration records measured between 4 and 5 p.m.) are presented, as well as the correspondent modes and natural frequencies computed numerically. The water level was 294.03 m (3 m below the crest). The first mode is antisymmetric, the second and third modes are symmetric, and the fourth is also antisymmetric.

From the presented study, one can note that a very good agreement between modal identification outputs and 3DFE numerical results was achieved, for different reservoir water levels, regarding the evolution of natural frequencies and the modal configurations (particularly for the first three modes). It is also worth highlighting that the coupled model with generalized damping enables the computation of non-stationary vibration modes, as can be measured in situ. Finally, it is relevant to state that such promising results could not be achieved using classic added water mass models based on Westergaard's solution [5, 6].

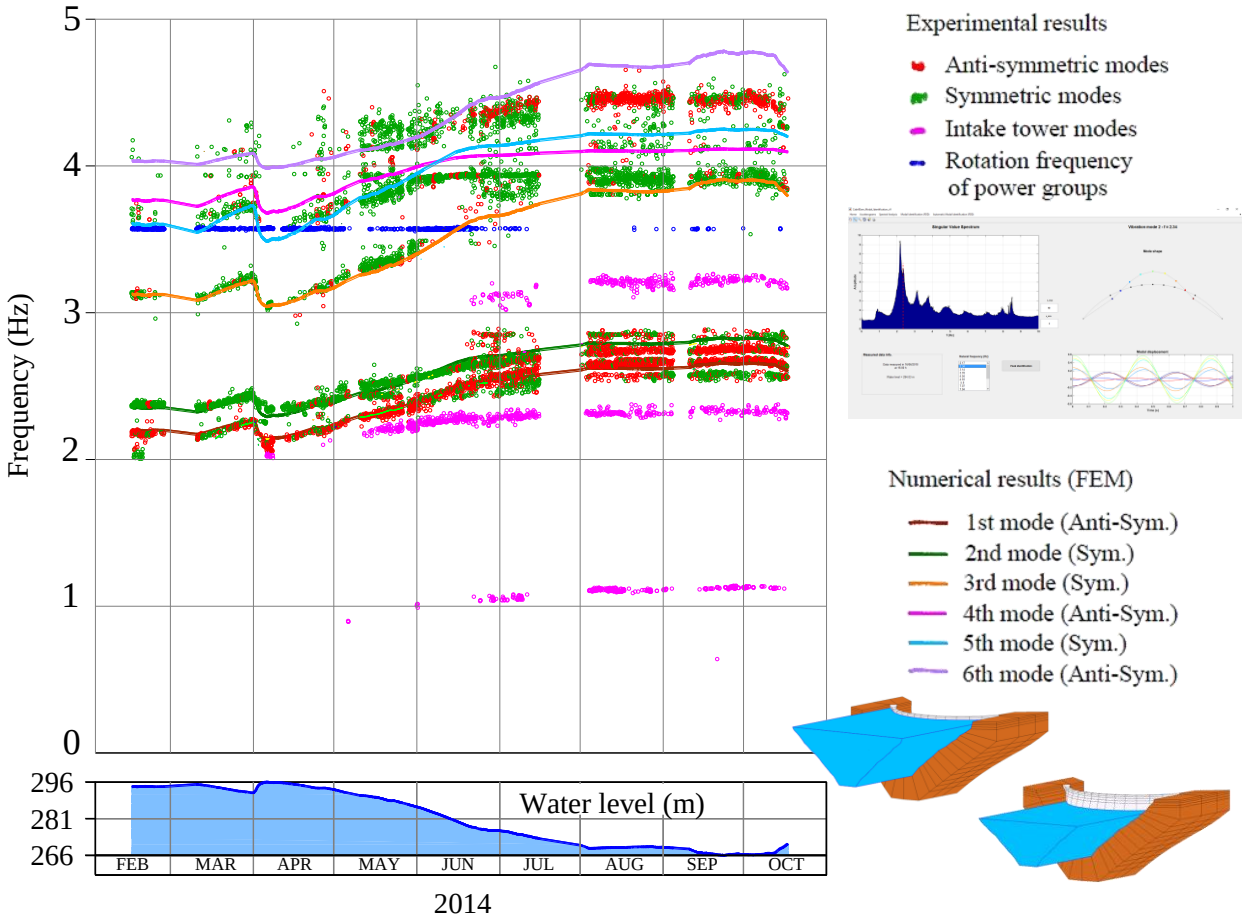

Figure 7: Cabril dam: evolution of natural frequencies over time. Comparison between automatic modal identification outputs (data from February to October 2014) and numerical results from **DamDySSA3.0**.

DamModalID1.0 results
Data measured in June 16, 2018; 4 to 5 p.m.;
Water level: 294.03 m

Numerical modelling results
Water level: 293.5 m

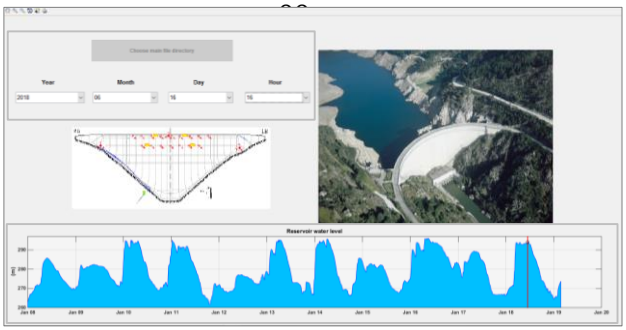

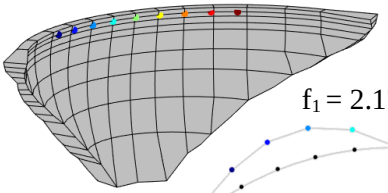

f_1 = 2.17 Hz

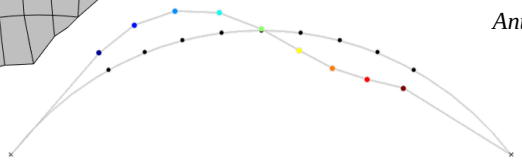

Antisymmetric

f_1 = 2.16 Hz

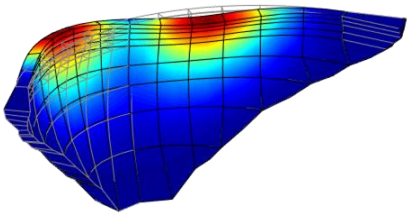

f_2 = 2.34 Hz

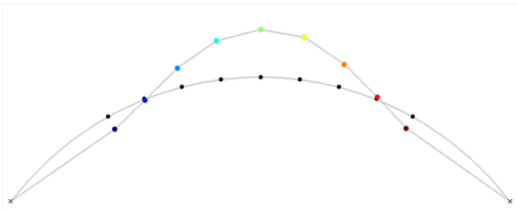

Symmetric

f_2 = 2.31 Hz

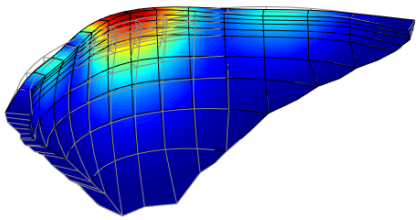

f_3 = 3.14 Hz

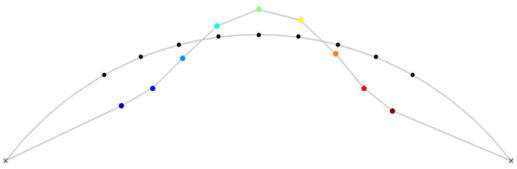

Symmetric

f_3 = 3.11 Hz

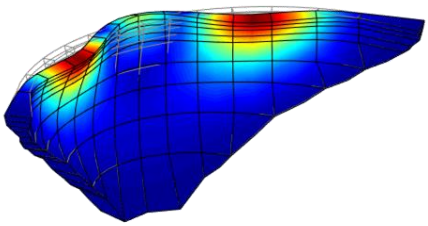

f_4 = 3.78 Hz

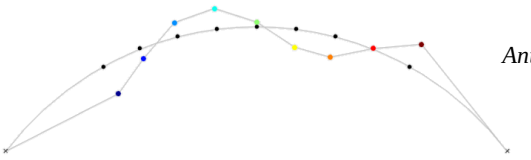

Antisymmetric

f_4 = 3.52 Hz

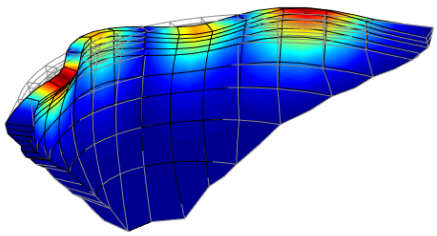

Figure 8: Cabril dam: Natural frequencies and mode shapes. Comparison between modal identification outputs (June 16, 2018, 4 to 5 p.m.) and 3DFE results (**DamDySSA3.0**).

4.2 Seismic response

Using Cabril dam's SSHM system, it has been possible to automatically identify earthquake events and to measure the accelerations close to the foundation and in the dam body, thus allowing to study the dynamic response of the dam under seismic loading. One of the main goals is to analyse the accelerations amplification factor between the base and the top of the dam, for different earthquakes measured on Cabril dam.

In this section, the seismic response of Cabril dam is studied for an earthquake of magnitude 4.6 on the Richter scale, measured on site on September 4, 2018 (Fig. 9). The epicentre was in Peniche abyssal region, at a distance of around 200 km from the dam and the reservoir water level at the time was 281.2 m (15.8 m below the crest). The acceleration time histories recorded with the triaxial accelerometer located in the right bank (RB_{xyz}) are shown: the peak accelerations near the base were of 2.16 mg in the cross-valley direction, 1.39 mg in the upstream-downstream direction and 1.23 mg in the vertical direction.

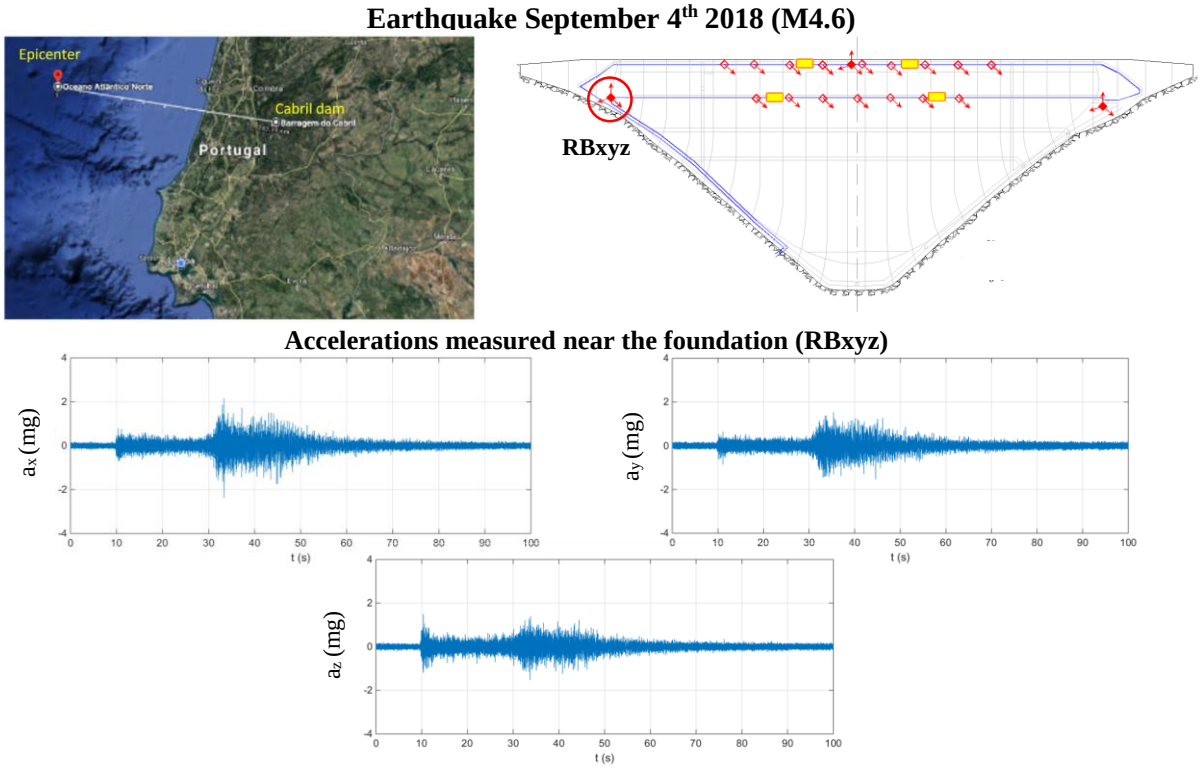

Figure 9: Cabril dam. Earthquake event on September 04, 2018: measured accelerations near the base.

Next, the measured seismic response of Cabril dam (Fig. 10) is compared with the response computed numerically, considering a reservoir water level of 280 m and using the seismic acelerogramas measured at the dam-foundation interface (RB_{xyz}) as inputs to the reference 3DFE coupled model. In this study, in order to analyse the amplification of the accelerations from the insertion to the top of the central cantilever, the average peak accelerations, calculated as the mean value of the ten highest peaks of the acceleration time series, are considered.

Regarding the measured response, let us focus on the acceleration time series recorded with the accelerometer KL294, at a height of 294 m, in the upper gallery of the central cantilever (block KL). An average maximum acceleration of 2.69 mg was recorded, which corresponds to a base (RBxyz) to top acceleration amplification of about 2.5 times. For comparison, the radial acceleration time histories are computed for nodal point 140 (in blue), at a height of 293.5 m, chosen to be located as near as possible to the real position of the sensor

KL294. The average peak acceleration is of about 2.94 mg, resulting in a base to top amplification of about 2.7 times.

Finally, it can be noted that a very good agreement has been achieved between measured and calculated acceleration time histories, but only when a global (dam and foundation) damping ratio of about 20% was assumed in the model. Although this is a surprisingly high value, in comparison with standard values (1 to 5 % in the dam) used when studying the seismic behaviour of large dams, analogous conclusions have been drawn by other researchers in similar studies [10] (as mentioned, this might be related to the averaging of the input seismic accelerograms along the dam-foundation interface).

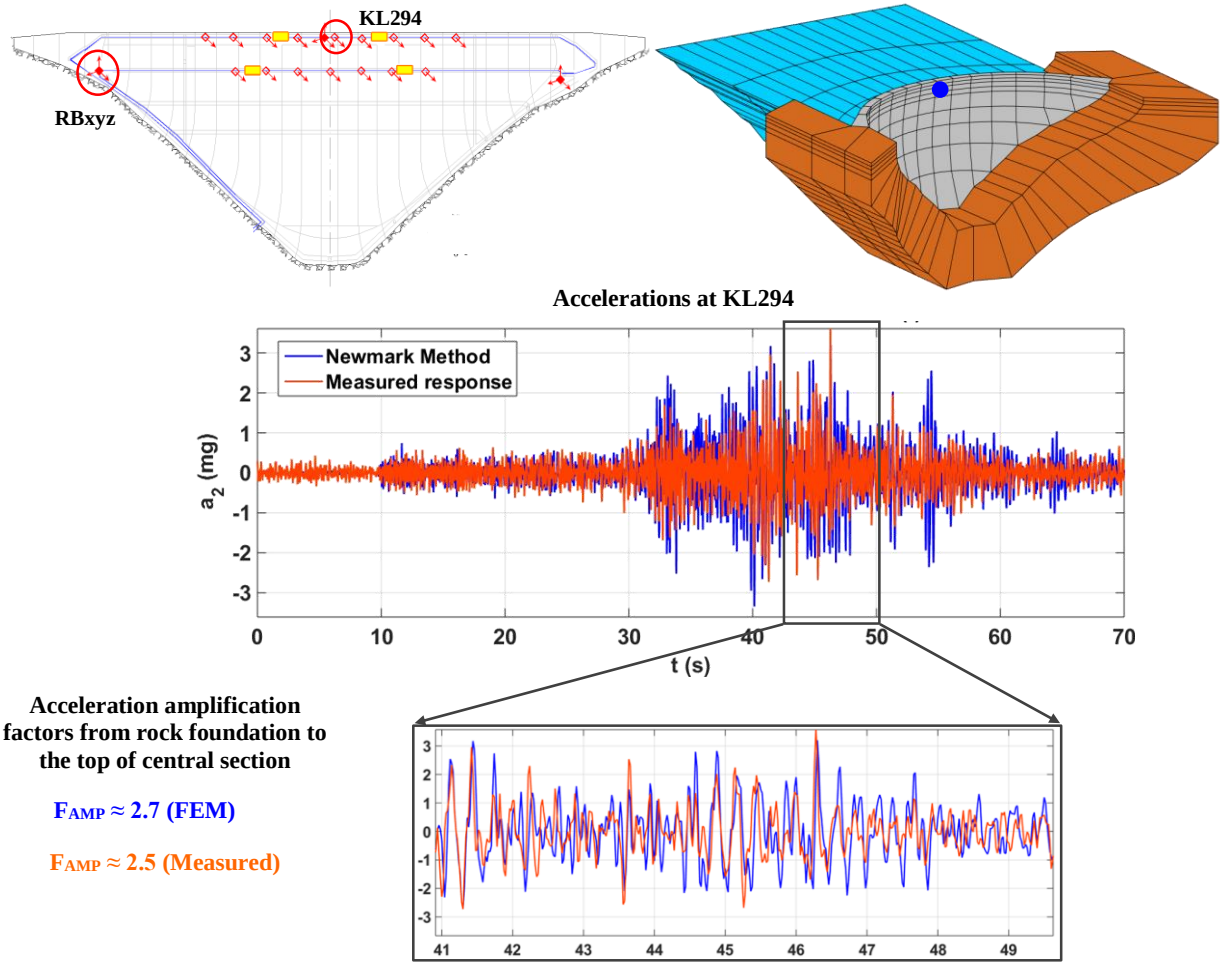

Figure 10: Cabril dam. Earthquake event on September 04, 2018. Measured and computed seismic response.

5 CONCLUSIONS

In this paper it was presented the software developed in LNEC to integrate the SSHM system installed in Cabril dam, namely the programs **DamModalID1.0** and **DamModalID_Auto1.0**, for interactive and automatic analysis of acceleration records. The obtained monitoring results were used to study the dam's dynamic behaviour under ambient/operational excitations, aiming to estimate the natural frequencies and mode shapes for several reservoir water levels, and the response under seismic loading, by analysing the accelerations at the top of the central section. The experimental outputs were compared with numerical results obtained with a 3DFE coupled model, considering generalized damping and a massless foundation. Based on the presented results, one can note that it was possible to

achieve a good agreement between the measured dynamic response of Cabril dam and the response predicted in the numerical calculations.

This paper has shown the potential of the developed software for SSHM systems to study the dynamic behaviour of arch dams over time based on acceleration records (continuously acquired), as well as the importance of the combined use of experimental and numerical results for supporting seismic and structural health monitoring studies.

ACKNOWLEDGEMENTS

The authors wish to acknowledge Electricidade de Portugal (EDP) and Fundação para a Ciência e Tecnologia, Portugal (FCT) for supporting the installation of Cabril dam's SSHM system (REEQ/815/ECM/2005), and to the latter also for the PhD grant SFRH/BD/116417/2016.

REFERENCES

[1] Dam Safety Regulation (2018). Decree-law Nº 21/2018 of March 28 (in Portuguese).
[2] S. Oliveira and A. Alegre (2019). Seismic and Structural Health Monitoring of Dams in Portugal. In *Seismic Structural Health Monitoring,* M.P. Limongelli and M. Celebi (Eds.), Springer, Chapter 4.
[3] S. Oliveira (2002). Continuous monitoring system for the dynamic performance assessment of arch dams. Sub-program D, in "Study of evolutive deterioration processes in concrete dams. Safety control over time". National Program for Scientific Re-equipment funded by FCT, REEQ/815/ECM/2005, LNEC-FEUP (in Portuguese).
[4] S. Oliveira, I. Ferreira, A. Berberan, P. Mendes, J. Boavida and B. Baptista (2010). Monitoring the structural integrity of large concrete dams. The case of Cabril dam, Portugal. Hydro2010, Lisbon.
[5] S. Oliveira, P. Mendes, A. Garret and O. Costa (2011). Long-term dynamic monitoring systems for the safety control of large concrete dams. The case of Cabril dam, Portugal. 6th Int. Conference on Dam Engineering, LNEC, Lisbon.
[6] S. Oliveira, M. Espada and R. Câmara (2012). Long-term dynamic monitoring of arch dams. The case of Cabril dam, Portugal. 15th World Conference on Earthquake Engineering, Lisbon.
[7] S. Oliveira and A. Alegre (2018). Vibrations in large dams. Monitoring and modelling. 26th Congress and 86th Annual Meeting. 1st-7th July, Vienna, Austria.
[8] R. Brincker and C. Ventura (2015). Introduction to Operational Modal Analysis. John Wiley & Sons.
[9] O.C. Zienkiewicz, R.L. Taylor and J.Z. Zhu (2005). The Finite Element Method: Its Basis and Fundamentals: 6th Ed., Elsevier Butterworth-Heinemann.
[10] J. Proulx, G.R. Darbre and N. Kamileris (2004). Analytical and experimental investigation of damping in arch dams based on recorded earthquakes. 13th World Conference on Earthquake Engineering, Vancouver, B.C., Canada.

Seismic monitoring system of Baixo Sabor hydroelectric power scheme

Gilberto Silva Monteiro[1], Jorge Pacheco Neves[2], Jorge Pereira Gomes[3]

EDP, Gestão da Produção de Energia S.A
R. Ofélia Diogo Costa nº 39, 4149-022 Porto, Portugal
E-mail: gilberto.monteiro@edp.com

Keywords: Dams; Concrete; Seismic hazard; Safety; Dynamic monitoring

Abstract. *The Baixo Sabor hydroelectric scheme is located at northeast of Portugal and creates a reservoir with a storage capacity of 630 million m^3 of water. The dam is a concrete double-curvature arch dam with 123 m high. According to the Portuguese legislation and considering the seismic risk of the dam construction zone, a Seismic Monitoring System (SMS) need be provided. In their most extensive configuration, these systems may incorporate remote stations along the reservoir for studying the propagation of seismic waves and to detect eventual induced reservoir seismicity.*
So, for the observation of the seismic activity on the surrounding area of the reservoir, to characterize the seismic action and the corresponding structural response of the dams, an observation system based on triaxial accelerometers was designed and installed. This system has been in continuous operation since its installation, and the data of the recorded earthquake records has been analyzed and processed. This article presents a brief description of the regional geological and tectonic setting including the stratigraphic and lithological unit's description, the main geological faults, tectonic history resume, and the local geological surface characterization of the seismic exterior stations. Also, the paper describes the main features of the seismic monitoring system that was installed in the Hydropower Scheme of Baixo Sabor, constructed and owned by EDP Produção a company of EDP - Energias de Portugal Group, and presents some of the main results obtained during the first period of operation of the dam.

1 INTRODUCTION

The Baixo Sabor Hydropower Scheme is situated in the north-eastern of Portugal in the lower part of the Sabor river, that is a tributary of the right bank of the Douro river. This global area has a moderate seismic risk, but the existence of the Vilariça fault near the scheme had considered. So, an exhaustive seismological study was developed in order to predict the characteristics of the seismic actions. These actions were considered in the dam's design to assure adequate safety conditions.

According to the current Portuguese legislation and considering the seismic risk of the dam construction zone, a Seismic Monitoring System (SMS) was provided, incorporating instrumentation to characterize the seismic action induced in the dams and the corresponding structural response. In this context, and for all new large dams, the implementation of an SMS is mandatory. In their most extensive configuration, these systems may incorporate remote

[2] EDP Produção, Gestão da Produção de Energia S.A, jorgepacheco.neves@edp.com
[3] LNEC, Laboratório Nacional de Engenharia Civil, Lisboa, jgomes@lnec.pt

stations along the reservoir for studying the propagation of seismic actions and to evaluate the induced reservoir seismicity.

The hydropower scheme of Baixo Sabor is composed of two dams, namely the upstream Baixo Sabor dam and the downstream Feiticeiro dam (Figure 1), located about 12.6 km and 3.3 km far from the confluence of the Sabor with the Douro river, respectively. Reversible units were installed in the powerhouses associated to each dam to enable the water pumping from the upper zone of the Douro river to the large reservoir of the upstream dam. Both dams were studied and designed by EDP Produção.

The Baixo Sabor arch dam is a 123m high structure, with a total crest length of 505 m and a total concrete volume of 670 000 m^3. For the full storage level water located at elevation (234.0) the reservoir capacity is of 1 095 million cubic meters. A controlled surface spillway is located at the central part of the dam crest with a discharge capacity of 5 000 m^3/s, including four spans controlled by radial gates and provided of a downstream plunge pool. The underground power house, located in the right bank, has two reversible units of 81 MW each.

Figure 1: Aerial views of Baixo Sabor and Feiticeiro dams

The Feiticeiro dam is a concrete gravity structure, with a rectilinear layout, a maximum height of 45m, and a total crest length of 315m. The controlled spillway is located in the central part of the dam also designed for a maximum flood of 5 000 m^3/s. It is provided of four spans controlled by radial gates and a downstream roller bucket for the water energy dissipation. Two independent tunnels connect the reservoir to the two reversible power units which, are installed into two shafts situated in the right bank, downstream the dam. The reservoir has a capacity of 30 million cubic meters of for the full storage level located at elevation 138 m.

For continuous dynamic monitoring behaviour of the two dams, when subjected to seismic action, a seismic monitoring system (SMS) was installed in the Baixo Sabor Scheme. This system has been developed as an active system, operating permanently and guaranteeing the recording of the dams and their soundings vibrations when earthquakes occur.

Characterization of the dynamic response is essential for structures located in seismic regions. Furthermore, the monitoring of the dynamic behaviour of concrete arch dams is increasingly viewed as an important component of safety assessment procedures to envisaging the risk associated to the prediction of dam's behaviour. The evolution of the dynamic characteristics may also help to detect the initiation, or development, of damage phenomena throughout the structure lifetime. Ambient vibration monitoring is nowadays often used for these purposes. In this context, a continuous dynamic monitoring system was also installed in the Baixo Sabor dam with sophisticated automatic tools based on operational modal analysis to continuously evaluate the dynamic parameters of the dam along the time.

2 GEOLOGICAL AND TECTONIC SETTING

The Baixo Sabor dam is located in a 1 km long, NE-SW orientated valley segment (Figure 2), with a deep, narrow and slightly asymmetrical transversal profile, 25m wide at the base and 440m at the crest level. The dam is founded in a granitic rock mass that intruded the phyllite-greywacke metassediments of the Douro-Beiras Group during the 3rd phase of the Hercynian orogeny, approximately 300 m.yr. ago (K/Ar dating) [1]. From a petrographic point of view, this rock corresponds to a medium to coarse grained, biotitic-muscovitic, porphyroid granite.

The oldest rocks in this region originated from a thick Cambrian turbiditic sequence of marine sandy-argillaceous sediments (greenish colors in Figure 2 that were deformed during the Caledonian orogeny (~490-390 m.yr.) by epyrogenic movements and a compression phase with formation of large open folds and NE-SE to ENE-WSW and sin-sedimentary thrust faults. The posterior Ordovician sandy-quartzitic and argillaceous sediments were deposited during this orogeny in costal to distal marine and, in some cases, euxinic environments [1].

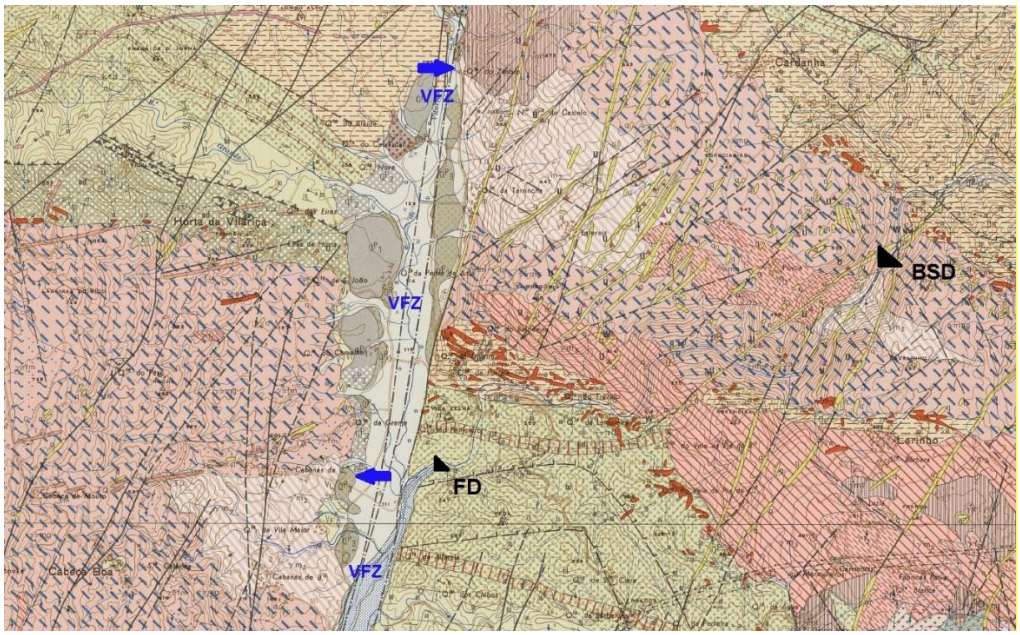

Figure 2: Baixo Sabor dam geological setting (adapted from [1]).
BSD – Baixo Sabor dam; FD – Feiticeiro dam; VFZ – Vilariça fault zone (the space between arrows corresponds to the horizontal accumulated displacement)

During the Hercynian orogeny (~370-270 m.yr.), these lithologies were intensely folded, metamorphized and intruded by large granitic batholiths (pinkish colors in Figure 2). There were 3 Hercynian deformation phases, the 1st one being the responsible for the main NW-SE mega and meso-scale folds with formation of an axial plane schistosity. The 2nd phase originated overthrust and thrust faults and a crenulation (microfolds) cleavage [1].

Several granitic batholiths were implanted during and immediately after the 3rd phase of this orogeny. Isoclinal folds and an axial plane schistosity were also formed, transposing the 1st phase schistose cleavage.

A brittle fracture regime was established in final Hercynian times and later, with formation of large NNE-SSE to NE-SW sinistral strike-slip faults and 2nd order WSW-ENE

dextral conjugated faults. Many of these faults were intruded by thick quartz or aplitic-pegmatitic veins and sometimes micro-gabbros, during the post-tectonic distensive phase.

This region main tectonic feature is the Vilariça fault (Figure 2 and Figure 3) which is located 6.5 km and 0.5 km, in a straight line, to the west of the Baixo Sabor and Feiticeiro dam sites, respectively. It is a late Hercynian NNE-SSW strike slip fault, with an accumulated horizontal sinistral displacement of approximately 6.5 km and a length of more than 200 km, extending from Sanábria region (Spain) to Serra da Estrela region, in the center of Portugal.

This fault was reactivated several times since the end of the Hercynian orogeny and presently, is classified as active [2]. A distensive phase, with a vertical component of movement developed in the secondary subparallel faults, initiated in the Miocenic, and contributed to the formation of an echelon *graben* [1] with an elevation difference of more than 300m between the upper and the lower blocks, preserving the Quaternary torrential piedmont deposits (*rañas*) and the posterior fluvial deposits inside this tectonic basin.

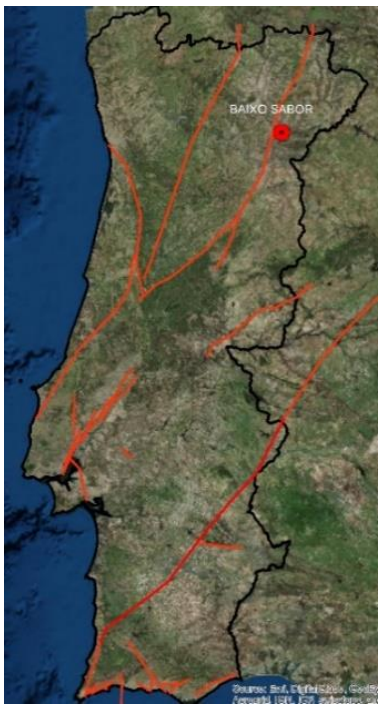

Figure 3: Localization of Baixo Sabor dam and of the main Portuguese geological faults

The region where the Baixo Sabor Hydropower Scheme is located presents diffuse seismicity of moderate to low intensity, which is characteristic of an intra-plate zone.

The proximity of the Vilariça fault zone to the Baixo Sabor and Feiticeiro dams led to the development of a geomorphologic and paleoseismological study [3] during the design phase. This study included the detailed mapping geological (Figure 4) of trenches located on the Vilariça fault trace, sediment sampling and dating using Optical Stimulated Luminescence technics and allowed the estimation of a slip rate of 0.2-0.3 mm/yr. The long return period (~9000 years) obtained for the Maximum Credible Earthquake (MCE) on Vilariça fault, with an estimated magnitude of 7.25, reflects the above mentioned intraplate seismotectonic setting of this region. The most striking feature visible in Figure 4 is the one related with the fault N15ºE, 85ºSE, that puts in contact the Cambrian phyllites (Pi) and the Quaternary alluvium (Qoa) and, also affects the Quaternary colluvium (Col2), proving the activity of the Vilariça fault in this geological period (< 1.6 m.yr.).

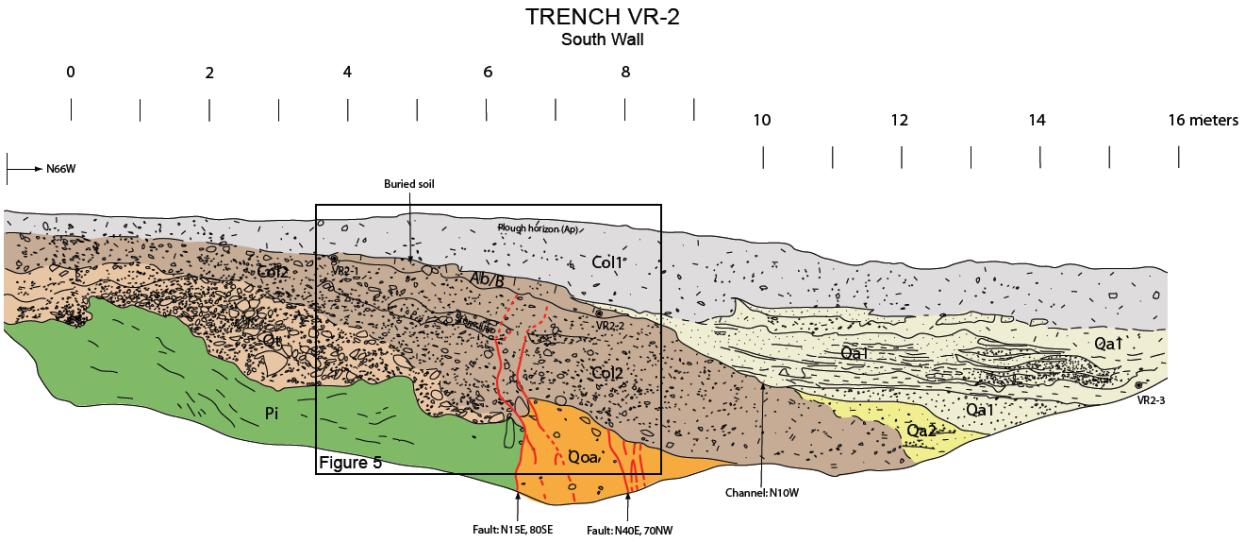

Figure 4: Detailed geological mapping of the south wall of trench VR2 (adapted from [3]).
Pi – Chloritic phyllite (Cambrian); Qoa – Older alluvium; Qt – river terrace; Col2 – Older colluvium; Qa2 – Intermediate alluvium; Qa1 – Younger alluvium; Col1 – Younger colluvium

Other nearby faults, also considered active in the published literature [2], are the Ribeira de Zacarias fault, a 20 km long, N-S reverse fault that crosses the dam reservoir approximately 8.5 km upstream and a 4 km long, NNE-SSW fault, near the village of Felgar.

The current Alpine orogeny, with a NW-SE to NNW-SSE maximum compressive stress orientation [4] in the NE region of Portugal, is the responsible for stress accumulation and the reactivation of ancient faults like the Vilariça and other faults, that have implications in the Baixo Sabor area seismicity. So, considering the tectonic setting in the Baixo Sabor area, the dam height (123m) and the reservoir dimensions, the tectonic and the reservoir induced seismicity had to be monitored. The selection of locations for the seismic monitoring remote stations (Table 1 and Figure 5) was performed during the design phase, taking into account this seismotectonic framework.

Table 1: Remote seismic monitoring stations

Remote Station		Foundation	Nearby fault
Designation	Localization		
SR 1	Adeganha	Coarse grained granite (W3-4)	Vilariça
SR 2	Felgar	Coarse grained granite (W3)	Felgar
SR 3	Meirinhos	Phyllite (W3)	Ribeira de Zacarias
SR 4	Sendim	Greenish phyllite (W3-4)	Ribeira de Zacarias
SR 5	Baixo Sabor dam	Fine to medium grained granite (W4)	Vilariça
SR 6	Feiticeiro dam	Greyish phyllite (W3)	Vilariça

In the construction phase, these locations were slightly adjusted, also considering the foundation geotechnical characteristics.

3 SEISMIC STUDIES AND DESIGN SCENARIOS

According to Portuguese Regulations for Dams Safety [6] and to the Portuguese Dam Design Recommendations (PDDR) [7], two types of scenarios must be considered when checking the dam structural safety, namely the exploitation and the failure scenarios.

For the most frequent scenarios that can occur to be considered in the exploitation scenarios, the dam must be able to support these actions without, or with minor damages. On

the other hand, the failures scenarios deal with extreme actions that can cause important damages in the dam. Examples of failure scenarios are ruptures in the dam foundation or in the dam structure, they need to be pointed out. For failure scenarios, overall dam stability has to be assured and uncontrolled reservoir water release can't occur.

Earthquake loading, due to seismic activity is one of the important actions that have to be considered in the design of dams. In addition to a set of complete geological and geotechnical studies, seismic studies are essential to estimate the dynamic loadings that can appear. For these issues, the statements of PDDR are very similar to the ICOLD (International Commission on Large Dams) standards.

The seismic studies are based mainly in the local and regional geological settings, and in the area seismic history. In this frame, the seismotectonic studies, which include the identification of the possible active faults, are a major issue.

In accordance with PDDR (1993), the seismic studies should define the seismic actions in terms of intensity, frequency content and duration of the seismic vibrations in the dam site. During the design phase, the following design earthquakes types were considered:

- The maximum credible earthquake (MCE), which must be evaluated using a deterministic procedure or a probabilistic approach, and should have a long return period;
- The maximum design earthquake (MDE), which for dams with high potential risk hazard should be considered as the MCE;
- The operating basis earthquake (OBE), less intensive than the MDE, and with an assumed return period related to the involved estimated risks, and that is determined by probabilistic approaches.

According to ICOLD (1989) [8], the OBE is an earthquake with significant probability of occurrence during the dam life, and it only can cause minor damage in the dam. So, a 50% probability of not being exceeded in 100 years is usually adopted for OBE estimation. In this frame, for dam design and for dam safety analysis, the OBE must be considered as an action included in the exploitation scenarios. In addition, a more severe earthquake with a return period of about 1000 years Base Design Earthquake (BDE) is also used to check structural dam behaviour in these scenarios.

The MDE must be estimated rather by deterministic procedures, considering local and regional seismotectonics conditions. Probabilistic approaches, considering long return periods, can also be applied for MDE estimation, and are often used for comparison purposes. So, the MDE should be considered a failure scenario, concerning dam design or structural safety assessment purposes.

In addition, Reservoir-Induced-Earthquake (RIE), that represents the ground motions capable of being triggered at the dam site by the presence of the reservoir, should be taken into account, and so, the effects of faults susceptible to give rise to induced seismicity should be properly evaluated. Depending on the dam location and on seismotectonics conditions the RIE may represent motions less than, equal to, or greater than the OBE, but should in no case be greater than the MDE [8].

Given the importance and the potential risks associated to the Baixo Sabor dam, and in line with the adopted in the design of other EDP dams, a 50% probability of not being exceeded in 100 years was adopted for the Operating Basis Earthquake. According to the studies carried out [5] this seismic action has a peak ground acceleration of 0,084 g.

Relying on the same seismological study, which takes in account the importance of the Vilariça geologic fault near to the dam's, the peak ground acceleration of 0,522 g (corresponding to a return period of about 10 000 years) was estimated as maximum design earthquake (MDE). The seismological studies also gave information about intensity, frequency

content and duration of the seismic vibrations loads that are probable to occur in the dam site, which have supported the dynamic dam behaviour analysis for this extreme scenario.

The faults classified as active in the Neotectonic Map or Portugal [2] that cross the Baixo Sabor reservoir (Ribeira de Zacarias and Felgar faults) have a maximum length of approximately 20km, thus it is estimated that these faults may not produce an induced earthquake with an acceleration greater than the OBE value at the dam site.

4 DESCRIPTION OF THE SEISMIC MONITORING SYSTEM

The structural response analysis requires a correct characterization of the seismic action induced to the dam, so, the SMS allows the characterization of the seismic action, but also its propagation along the rock mass from different directions and characterize the induced seismicity associated to the large reservoir. According to these objectives the SMS of the Baixo Sabor scheme was defined with the following composition layout (Figure 5):

Baixo Sabor dam:

- 1 station placed near the Vilariça fault;
- 3 stations located around the Baixo Sabor dam reservoir;
- 1 station placed next to the Baixo Sabor dam (upstream the dam);
- 6 stations installed inside the galleries of Baixo Sabor dam;

Feiticeiro dam:

- - 1 station next to the Feiticeiro dam;
- - 2 stations installed inside the galleries of Feiticeiro dam.

A computer unit for managing the data transmission process for collecting data from all stations, and subsequently organizing and processing it.

Each station consists of a triaxial accelerometer (GeoSIG, Model: GMSplus, full scale: ± 2g) equipped with the associated equipment for data acquisition and data transmission to the central unit. All the stations have local memory for long term autonomous work. Since real time data transmission is not required, because the data segments of interest may be sent with some time delay. The 3G/GPRS service was considered adequate for the communication process with remote stations, while an Ethernet network with TCP/IP protocol was installed for connecting the central unit to the stations inside each dam.

Each station is permanently measuring and when an earthquake event occurs, identified by acceleration(s) higher than a pre-defined trigger value, a call to the central unit (alert) is issued and data is automatically stored in local memory, within an interval from a pre-event to a post-event time, at a given sampling frequency [10]. After receiving an alert, the central unit initiates a process of gathering the data stored in all stations sequentially, one by one.

If any remote station is temporarily unavailable, the central unit will contact it later repeatedly. Whenever ordered by the central system, each data acquisition unit should be able to retrieve the registered data of specified intervals from pre-trigger to post-trigger limits.

The time synchronization is essential to achieve the objectives of this system, because it is necessary that all stations be constantly collecting data in accurate and same instants of acquisition, with GPS time synchronization facility used for that purpose [11].

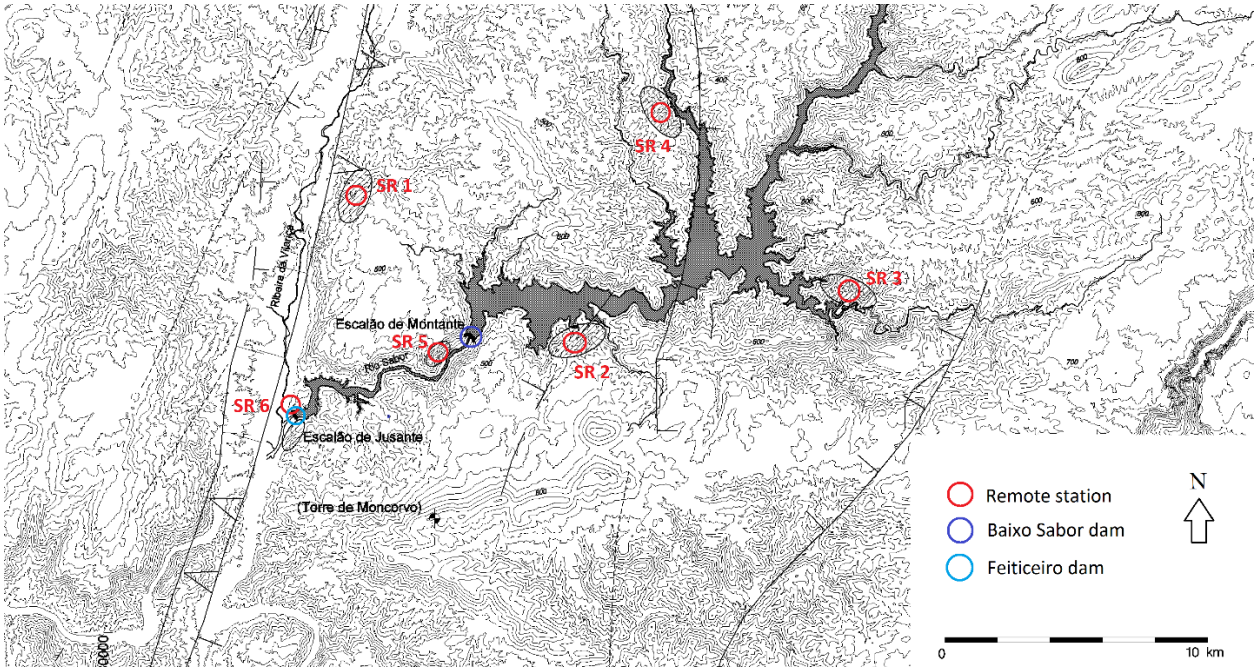

Figure 5: Location of remote stations on Baixo Sabor scheme

The remote stations are normally implanted in locals without mains power supply, so it is necessary to provide a system with a photovoltaic panel and accumulators for energy storage. The remote stations are implanted in a 15x5 m^2 area (Figure 6a)). This area is protected with a metal net fence, and has two small masonry cabinets, for protection of equipment from aggressive environmental actions (solar radiation, wind, heat, rain, atmospheric discharges). One cabinet contains the measurement equipment and the other the components of power supply, data transmission and GPS time synchronization (Figure 6b)c)). The proximity of masts or poles to the measurement units should be totally avoided in order to preserve measurements from artificially induced background noise.

a

b

c

Figure 6: Remote station of Baixo Sabor scheme: a) global view ; b) inside view of one cabinet showing a seismometer installed on a concrete block; and c) a view of the other cabinet with a photovoltaic pannel on the rooftop and the location of accumulators

In the Baixo Sabor dam, 6 remote stations were installed, consisting of triaxial accelerometers, distributed through the galleries of the dam. In the drainage gallery was installed a station in the bottom of the valley, and a station in the upper part of the left and right banks. Other 3 stations were installed in the galleries of the dam structure near the crest (Figure 7).

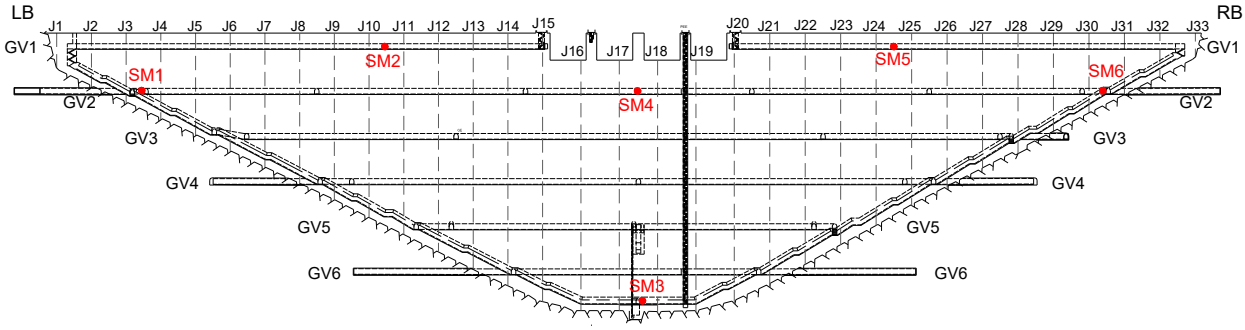

Figure 7: Location of the seismic stations inside Baixo Sabor dam

In the Feiticeiro dam two seismic stations were installed, one at the top and other at the foundation of the central block (Figure 8). In Figure 9 is presented a view of the seismic stations inside the dams.

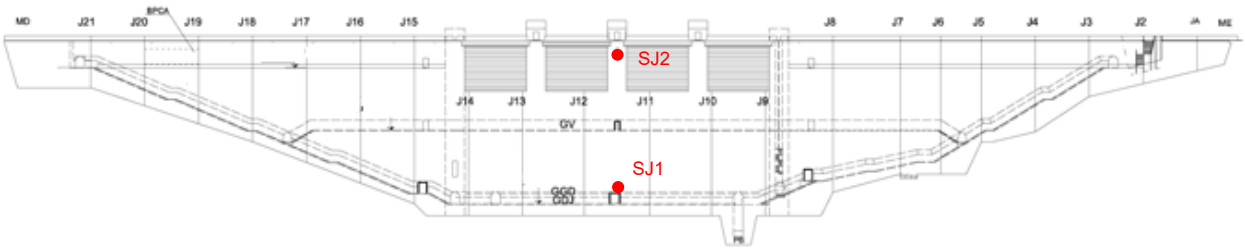

Figure 8: Location of the seismic stations in Feiticeiro dam

Figure 9: Seismic station in dam's galleries

The Figure 10 shows the general layout scheme of the entire seismic network.

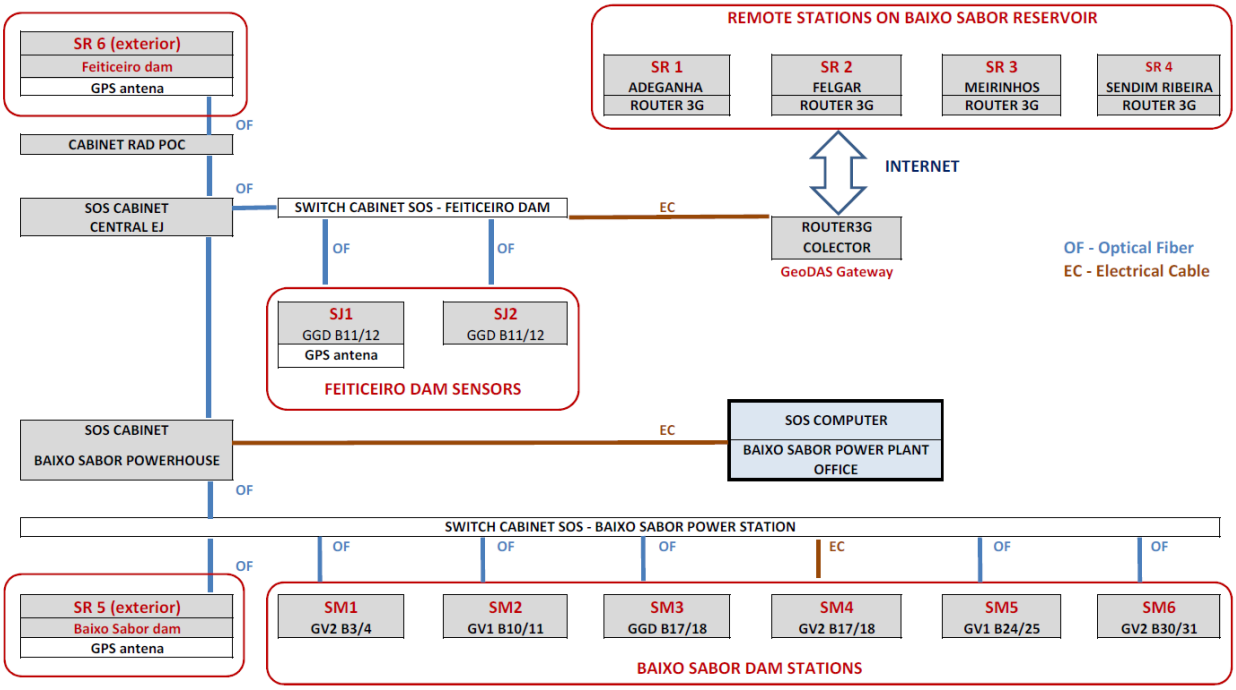

Figure 10: Baixo Sabor seismic monitoring system layout

The time series from the remote stations are used in the Seisan software to determine the event characteristics [12] and in the future these records will be integrated in the Portuguese seismic network. The installation of this system was finalized in June of 2017 and is fully operational.

5 MAIN RESULTS DURING THE FIRST PERIOD OF OPERATION OF BAIXO SABOR DAM

During the first months of operation the system registered three seismic events, characterized in the Figure 11 and Table 2.

The maximum value record was 8.6 mg in the radial direction for the station SM5, located in the gallery GV1 in the right bank (Table 3). Figure 12 presents the records in radial direction for the event with the epicenter in Torre de Moncorvo, occurred in 2017/08/03 09:17. It is visible the amplification motivated by the dam, of the accelerations recorded in the foundation when compared with the dynamic structural response in the crest.

With the seismic records of the six tridimensional points in the dam, the natural frequencies of the dam were calculated applying output only modal identification techniques. The length of these records is only about 60 s and the duration of the seismic event is near 5 seconds. This small duration may be a problem for the correct identification of the dynamic parameters, but it is compensated by the amplitude values of the accelerations. The values of the first 5 natural frequencies for the events occurred in Torre de Moncorvo are presented in the Table 4.

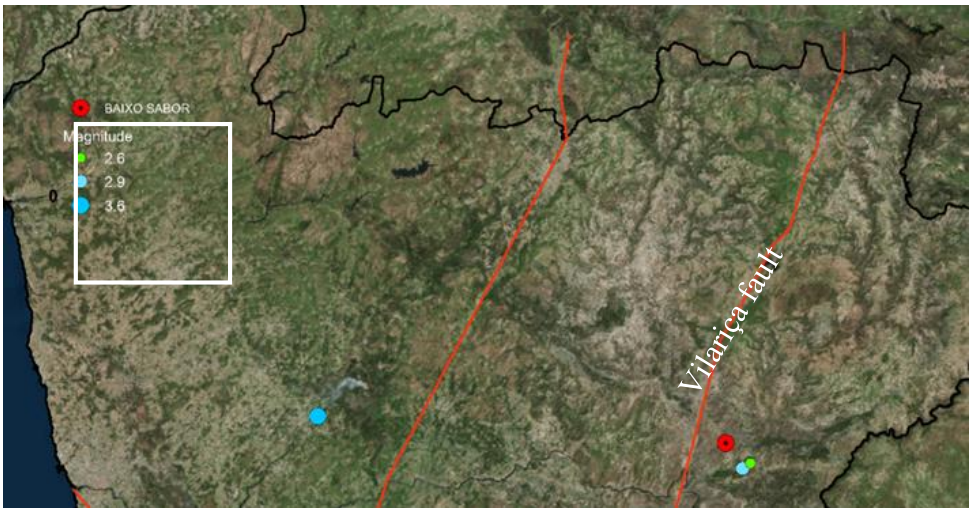

Figure 11: Seismic events registered with the SMS in relation to the principal Portuguese north faults

Table 2: Seismic event registered with the SMS

Date		Magnitude	Localization of the event	Distance to the Baixo Sabor dam
Day	Time			
2017/06/06	16:03	3.6	Amarante	≈ 115 km
2017/08/03	09:17	2.9	Torre de Moncorvo	≈ 8 km
2017/08/03	14:57	2.6	Torre de Moncorvo	≈ 10 km

Table 3: Maximus values of accelerations registered in the SMS (mg) in the Baixo Sabor dam stations

	Stations	Events date		
		2017/06/06 16:03	2017/08/03 09:17	2017/08/03 14:57
Dam	SM2r	2.72	7.51	5.35
	SM2t	1.61	4.36	2.64
	SM2z	0.76	5.77	2.48
	SM4r	1.66	3.79	3.33
	SM4t	1.15	4.20	2.61
	SM4z	1.22	4.37	2.80
	SM5r	3.08	8.60	6.01
	SM5t	1.12	8.14	6.01
	SM5z	0.99	5.69	3.58
Foundation	SM1r	0.38	4.74	2.86
	SM1t	0.79	2.85	1.93
	SM1z	0.52	2.84	1.88
	SM3r	0.66	6.42	3.15
	SM3t	0.69	2.83	1.87
	SM3z	0.50	2.69	1.48
	SM6r	0.61	3.04	1.50
	SM6t	0.62	5.12	3.70
	SM6z	0.52	3.04	2.20

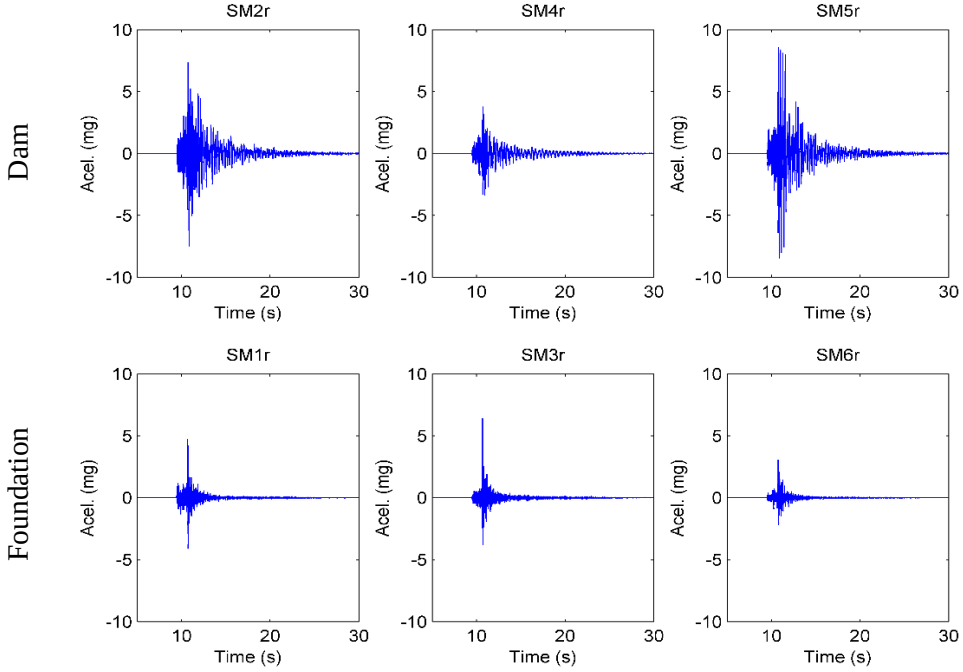

Figure 12: Radial seismic records (acceleration) in the Baixo Sabor dam for the event of 2017/08/03 09:17

Table 4: Dynamic parameters calculated for the two Torre de Moncorvo events by modal identification (SSI).

Mode	Mode type	Events			
		2017/08/03 09:17		2017/08/03 14:57	
		Freq [Hz]	ξ [%]	Freq [Hz]	ξ [%]
1	Symmetric	2.54	1.32	2.55	0.96
2	Antisymmetric	2.66	0.77	2.67	0.99
3	Symmetric	3.48	1.70	3.50	1.79
4	Antisymmetric	4.10	2.06	4.11	1.34
5	Symmetric	4.95	2.50	4.94	2.01

To ensure a good characterization of the dynamic behaviour of the Baixo Sabor dam a continuous dynamic monitoring system (CMDS) was installed. 20 uniaxial accelerometers were radially installed along the three upper galleries of the dam. In the GV1 gallery, 12 accelerometers are divided in two groups of six, disposed on each side of the spillway. Each of these groups of six is connected to a digitizer, which is linked to a field computer. In turn, the eight accelerometers on the two lower galleries are connected to a different set of two digitizers. All the equipment is connected by optic fibre and the synchronization of the data recorded by each digitizer is assured with GPS antennas.

The dynamic monitoring system is configured to continuously record acceleration time series with a sampling rate of 50 Hz and a duration of 30 minutes at all instrumented points, thus producing 48 groups of time series per day [13].

The data continuously collected by the dynamic monitoring system is independently processed by ViBest/FEUP and LNEC, this paper presents the processing developed by ViBest/FEUP, which is accomplished with a monitoring software developed at ViBest/FEUP called DynaMo [14].

The first six months of data were processed, and the first modes of vibration were identified and natural frequencies, modal damping values and modal configurations were obtained [18]. The three-dimensional representations of the modal configurations are presented in Figure 13. The first, third and fifth modes are approximately symmetric and the second and fourth are antisymmetric.

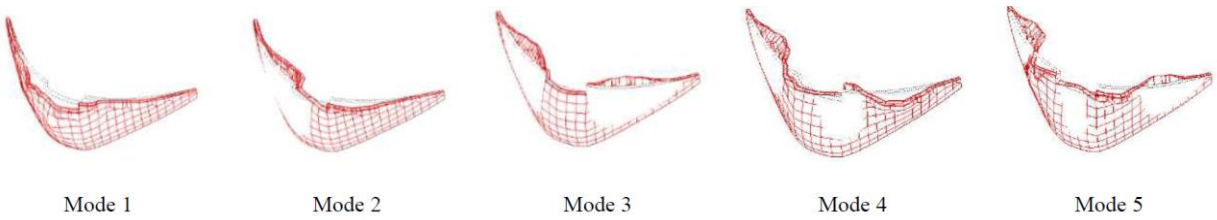

Figure 13: Modal configuration of the first five modes of Baixo Sabor arch dam.

Estimations of the modal parameters by the CDMS system for the first five modes are resumed in Table 5, where minimum, maximum, mean and standard deviation frequencies and damping values are presented. Notice the significant difference between minimum and maximum frequencies for each vibration mode, even after the elimination of outliers, which is reflected in the standard deviation values as well, indicating significant oscillations during the evaluation period. Additionally, the damping values present slightly higher mean values for the symmetric modes.

Table 5: Modal Parameters obtained by SMC for Baixo Sabor dam

Mode	Mode type	$f_{[\text{Min}\,;\,\text{Max}]}$ [Hz]	f_{mean} [Hz]	f_{std} [Hz]	$\xi_{[\text{Min}\,;\,\text{Max}]}$ [%]	ξ_{mean} [%]	ξ_{std} [%]
	Symmetric	[2.43 ; 2.75]	2.53	0.10	[1.16 ; 3.16]	1.50	0.23
2	Antisymmetric	[2.57 ; 2.92]	2.68	0.11	[0.85 ; 2.11]	1.42	0.15
3	Symmetric	[3.33 ; 3.85]	3.51	0.17	[0.55 ; 3.00]	1.67	0.25
4	Antisymmetric	[3.92 ; 4.50]	4.12	0.19	[0.92 ; 1.82]	1.36	0.16
5	Symmetric	[4.78 ; 5.34]	4.99	0.18	[0.75 ; 2.66]	1.88	0.30

These results are consistent in the results obtained by the seismic monitoring system and by the continuous dynamic monitoring system are reliable.

6 CONCLUSIONS

Baixo Sabor dam is the second highest dam in Portugal, its reservoir is the second in volume and its monitoring system is one of the most complexes implemented in Portugal, combining traditional measurements instruments with the most advanced technologies applied in dynamic monitoring.

Both dynamic monitoring systems installed in the Baixo Sabor Hydroelectrical Scheme, SMS and CDMS, are operational and integrate automatic procedures that make then fully autonomous, providing useful outputs for the safety control of these important structures. The features implemented in both systems revealed excellent efficiency and demonstrated a perfect suitability. The results showed an expect and direct relation with the variation of seismic and dynamic loads.

The results of the observation systems are being compared with the ones obtained with numerical models that were calibrated with the results provided by the forced vibration tests that were performed in the dam, both for empty [19] and [20], and full reservoir [21] situations.

These systems proved already to be extremely useful to evaluate the behaviour of these structures during seismic events and to provide relevant information for the development of numerical models including new behaviour models. So, they demonstrate to be a very important tool concerning dam safety control and seismic risk management.

REFERENCES

[1] Ferreira da Silva, A., Rebelo, J.A. and Ribeiro, M.L., *Carta geológica de Portugal na escala 1/50000. Notícia explicativa da folha 11-C (Torre de Moncorvo)*, Serviços Geológicos de Portugal, Lisboa, Portugal (1989).

[2] Cabral, J. and Ribeiro, A., *Carta Neotectónica de Portugal. Escala 1:1000000*, Serviços Geológicos de Portugal, Lisboa, Portugal (1988).

[3] Rockwell, T., Madden, C. and Gath, E., Fault trenching investigation to assess the potential seismic hazard of the Vilariça fault – Northeastern Portugal (unpublished report), ECI-Project Report no. 2505, Earth Consultants International, EUA (2005).

[4] Heidbach, O. (head) et al., *Stress map of Central Europe and Mediterranean 2016*, http://dataservices.gfz-potsdam.de/wsm/showshort.php?id=escidoc:1809897

[5] CPPE, “Aproveitamento Hidroeléctrico do Baixo Sabor”. Project, 2005, (in Portuguese).

[6] Portuguese Regulations for Safety of Dams, 2007, (in Portuguese).

[7] Portuguese Dam Design Recommendations, 1993, (in Portuguese).

[8] ICOLD, Bulletin 72: Selecting seismic parameters for large dams, 1989.

[9] Davies A., IRM GPRS & 3G Security Overview: What are GPRS and 3G, 2007.

[10] GEOSIG. GMS Measuring System: Features, Applications, 2012.

[11] GEOSIG. GMS – GPS Receiver, 2012.

[12] SEISAN - The Earthquake/Seismic Analysis Software, 2012.

[13] LNEC, FEUP, and Ambisig, "Upstream step dam of Baixo Sabor hydroelectric power plant. Characterization of the dam's dynamic behaviour through continuous monitoring. Installation Report." (in Portuguese), 2015.

[14] Magalhães, F., Amador, S., Cunha, A. and Caetano, E., "Dynamo - software for vibration based Structural Health Monitoring", 6th Int. Conf. on Bridge Maintenance, Safety and Management, IABMAS 2012, Vila Erba, Lake Como, Italy, 2012.

[15] MATHWORKS, "Matlab. R2016a.," ed, 2016.

[16] Magalhães, F. and Cunha, A., "Explaining Operational Modal Analysis with data from ana arch bridge", Mechanical Systems and Signal Processing, Invited Tutorial Paper, Volume 25, Issue 5, pp. 1431-1450, 2011.

[17] Magalhães, F., Cunha, A. and Caetano, E. “Online automatic identification of the modal parameters of a long span arch bridge”, Mechanical Systems and Signal Processing, Vol.23, Issue 2, pp. 316-329, 2009.
[18] VIBEST/FEUP, "Dynamic Monitoring System Baixo Sabor Dam. Results of May 2016." (in Portuguese).
[19] LNEC, “Upstream dam of the Baixo Sabor hydroelectric scheme. Characterization of the dynamic behavior by performing a forced vibration test in january 2015”, 2016, Lisboa, (in Portuguese).
[20] Gomes, J.P.; Lemos, J.V. “Characterization of the dynamic behavior of an arch dam by means of forced vibration tests”. 1st meeting of the EWG “Dams and Earthquakes”, September 2016, Saint-Malo, France.
[21] LNEC, “Baixo Sabor dam. Characterization of the dynamic behaviour by performing forced vibration tests in May 2016, with the reservoir water at 234,0 m elevation”, 2017, Lisboa, (in Portuguese).
[22] Vilanova, S.P.; Fonseca, J.F.B.D.; Guerreiro, L.M.C.; Oliveira, C.A.S. "Estudo sismológico do sítio da Barragem do Baixo Sabor", julho, 2005.
[23] IST, Instituto Superior Técnico, “Estudo sismológico do sítio da barragem do Baixo Sabor – Relatório Final”, Relatório ICIST – EP nº 48/05, Lisboa (2005)

Identification of dynamic soil properties of dam materials by in-situ testing with seismic geophysical methods

Thomas M. Weber[1] and Lorenz Keller[2]

Studer Engineering GmbH
Thurgauerstrasse 56, 8050 Zurich, Switzerland
E-mail: thomas.weber@studer-engineering.ch

Keywords: Identification of dynamic soil properties, geophysical testing, case study

Abstract. *After Swiss regulations, all existing large dams in Switzerland had to be assessed in respect of earthquake safety for revised design criteria by the year 2013. The present paper documents the case study of Marmorera embankment dam in Switzerland of 91 m height in respect of parameter identification for numerical earthquake assessment. In order to obtain in-situ dynamic properties of the dam, seismic geophysical measurements had been performed to measure shear wave velocities of the dam body and the foundation. The paper gives an introduction to the structure of the dam and presents the geophysical testes performed and their results. The measured shear wave velocities are compared to experience from other studies taken from literature. Further, it is shown how the initial shear modulus G_{max} of the dam material was derived and implemented in the numerical model for linear equivalent analysis of earthquake behaviour.*

1 INTRODUCTION

According to the guidelines of the Federal Office of Energy - Section Dams [1], all dams in Switzerland were inspected for their earthquake safety under federal supervision by 2013. This also applies to the Marmorera embankment dam operated by the ewz (Electricity Works Zurich). The dam is located in Graubunden in the Surses region below the Julier Pass in the Swiss Alps The dam is classified as large dam of category I. Construction work started in year 1949 with the first impounding in year 1954.

The Marmorera dam is a zoned earth fill dam with core sealing, filter layer and supporting shell. Only local earth materials consisting of moraine, landslide material and suspended debris were used for the dam body. During the construction of the dam in the late 1940's early 1950's, the sealing core was compacted with sheep foot compaction rollers and the supporting body was washed in with high-pressure water jets [2]. On the upstream side, a protective layer of coarse block material against wave impact was applied. The downstream side of the dam is covered with humus and is greened. The dam foot areas are stabilized with blocks of rock. An aerial photograph and the main cross-section at profile +226 are shown in Figure 1 and Figure 2 respectively.

With a maximum dam height of 91 m and a reservoir volume of approximately 60 million m^3, the Marmorera dam belongs to large dams of category I according to Swiss regulations [1]. Table 1 provides an overview of the key figures for the dam. Due to the size of the dam, increased requirements need to be fulfilled in respect to earthquake safety and the

[2] roXplore gmbh, Oberfeldstrasse 6, 8514 Amlikon-Bissegg, Switzerland, e-mail: roxplore@roxplore.ch

verification of dam safety. This includes, for example, the requirement for measurements of dynamic soil parameters and the verification of the dam using numerical methods with time history analysis [1].

Figure 1: Areal view of Marmorera dam

Table 1: Characteristics of Marmorera dam

Characteristics	Value
dam type	zoned earth fill dam with core sealing
maximum dam height	91 m
crest length	400 m
crest elevation	1684.40 masl
foundation elevation	1593.40 masl
width at crest	12 m
width at foundation	400 m
slope inclination upstream	variable min. 1 V : 2.1 H
slope inclination downstream	variable min. 1 V : 1.63 H
dam body volume	2.7 Mm^3
reservoir level	1680.00 masl
volume of reservoir	ca. 60 Mm^3

For the majority of geotechnical soil parameters, extensive investigations from the construction as well as from the operation period of the dam are available. For the dynamic soil parameters, the earthquake testing focuses on specifically performed field tests with geophysical measurements of the dam. By means of seismic tomography, a spatial model of the shear wave velocity distribution of the dam and of the foundation is developed. The present article deals with the geophysical measurements of the dam and describes the calibration of the dynamic shear modulus for the numerical calculation model of the dam.

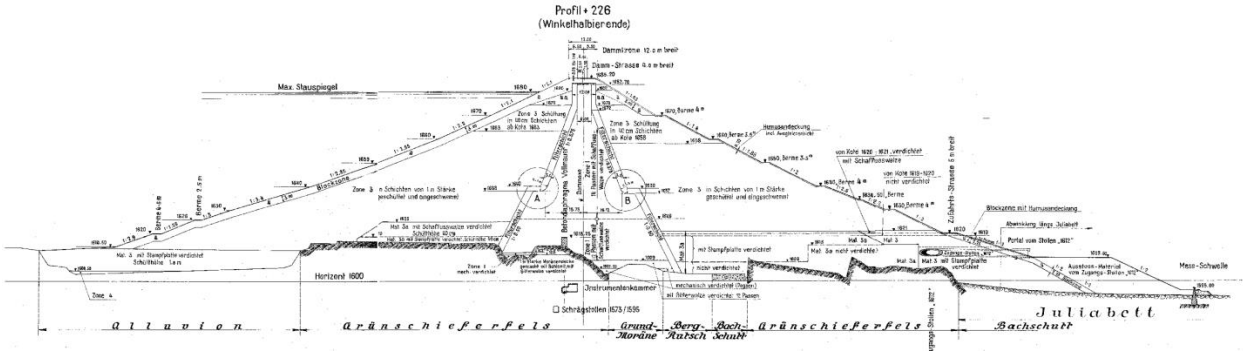

Figure 2: Main cross section of Marmorera embankment dam at profile +226

2 GEOPHYSICAL MEASURING PROGRAM

Already in the 1940's, geophysical investigations by means of P-wave seismic refraction were carried out to determine the rock horizon and the thickness of the soil. However, the old measurement results are hardly meaningful for the required earthquake analysis. For this reason, roXplore gmbh carried out a comprehensive seismic-geophysical investigation program in 2012 [3]. Seismic refraction and MASW (Multichannel Analysis of Surface Waves) from the dam surface, tomography measurements from the dam surface to the inspection galleries inside the dam and H/V measurements on the dam surface were carried out. An overview of the measurement profiles is shown in Figure 3. Figure 4 shows parts of the geophone layout on the dam crest and in the inspection galleries as well as the shaker for excitation of harmonic shear wave sweeps.

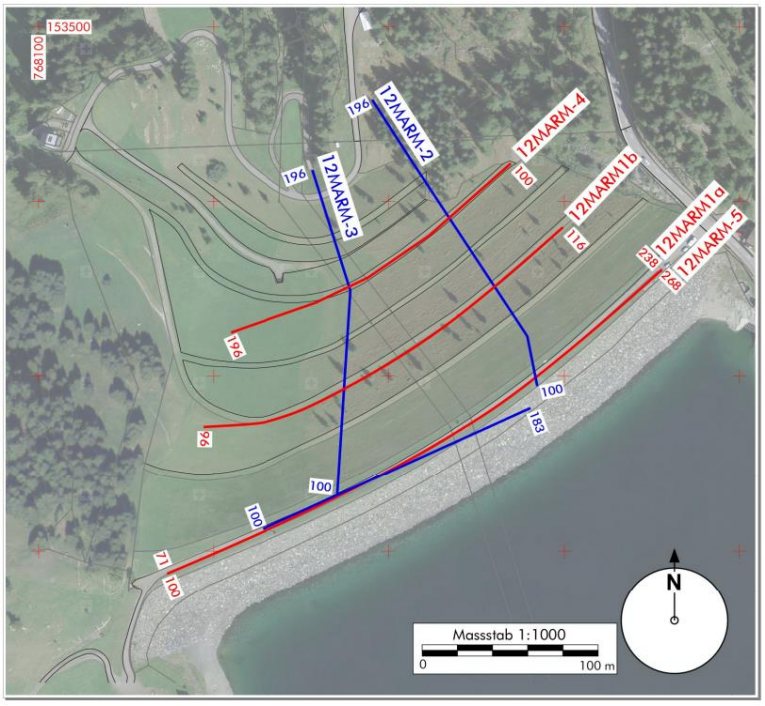

Figure 3: Layout of measurement profiles [1], red - arrays on dam surface, blue arrays in inspection galleries in the inner dam body

Figure 4: Seismic geophysical measurements, left: excitation of shear waves on the dam crest with shaker and part of geophone array mounted on a landstreamer system; right: geophone array in the inspection gallery in the inner dam body [3]

2.1 Seismic tomography

A total of 4 tomographic profiles were recorded, two profiles in the dam axis and two profiles in the dam cross section. The tomographic measurements are possible because the dam in the dam axis and on the downstream side perpendicular to the dam axis has several inspection galleries. The inspection galleries run in the floor plan according to the measuring profiles 12MARM-1a, 12MARM-2 and 12MARM-3, as shown in Figure 3. The wave excitation was performed at the dam surface, while the receivers were arranged in the inspection galleries (see Figure 4). Selected results of the tomography measurements are shown in Figure 5 to Figure 7.

The two tomographic profiles in the dam cross-section (Figure 5 and Figure 6) show a relatively homogeneous structure of the dam body. The shear wave velocities vary between 500 m/s and 800 m/s. Figure 5 clearly shows the bedrock surface with a shear wave velocity of approx. 2500 m/s, as this inspection gallery of the cross-section 12MARM-2 runs exclusively under the dam body in the bedrock. The tomography also provides indications of a geological disturbance in the rock due to reduced shear wave velocities.

There is one issue noticeable about the results of the tomographic cross section measurements. In the shear wave velocity distributions of the downstream dam body (e.g. see Figure 6), there is no obvious difference in shear wave velocity for dam core material and the shell material. This phenomenon can be mainly explained by the similar geological origin and characteristics of the moraine and slope debris material used and the similar construction process. A comparison of the grain size distribution shows that all materials have a well graded grain size distribution and only the core zone has a slightly larger proportion of fine content. The general well graded grain structure with sand, gravel and stones is quite similar for core and shell material. The relative densities of all materials are high due to the compacted placement. The in-situ densities show only minor differences between materials.

Figure 7 shows the tomographic longitudinal section of the dam along the dam crest (12MARM-1a in Figure 3). The measured shear wave velocities show relatively consistent values compared to the tomographic cross-sections. The bedrock surface on the east side of the dam body (Figure 7 left area) cannot be reliably determined due to layout of the inspection gallery and the limited space for the geophone array.

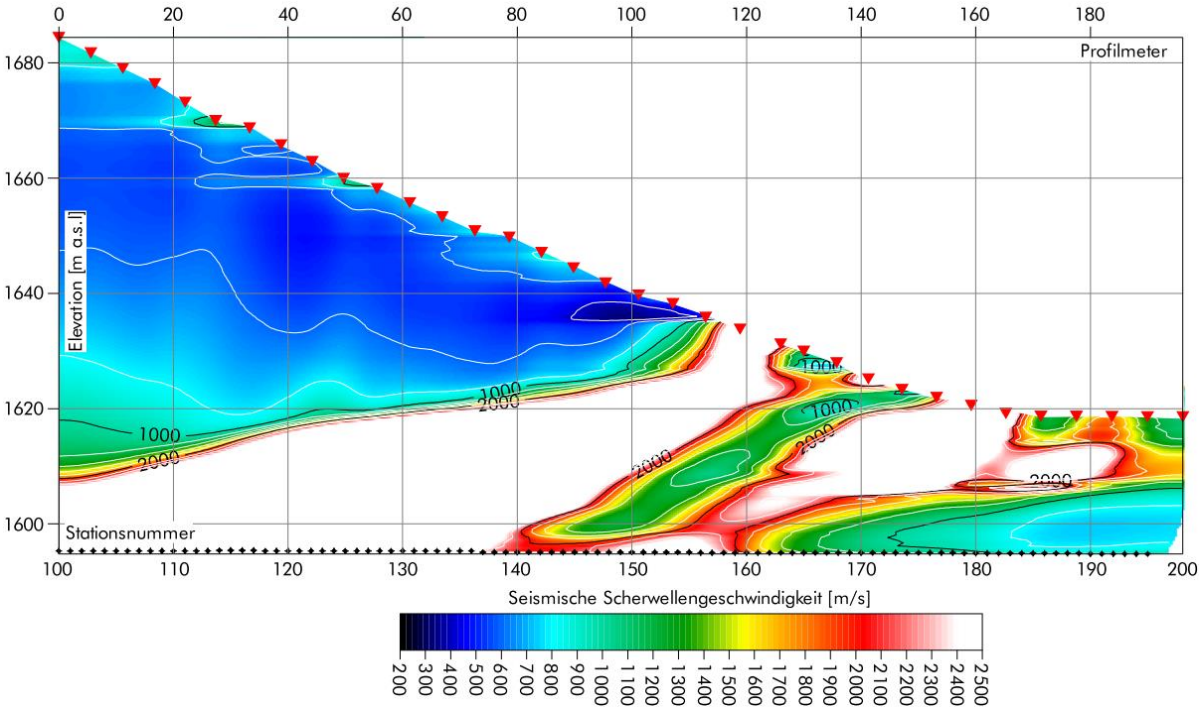

Figure 5: Tomography results: shear wave velocity distribution on the downstream side in section 12MARM-2 (see Figure 3) with excitation on the dam surface and measurements in the inspection gallery at elevation 1595 masl located in the bed rock [3]

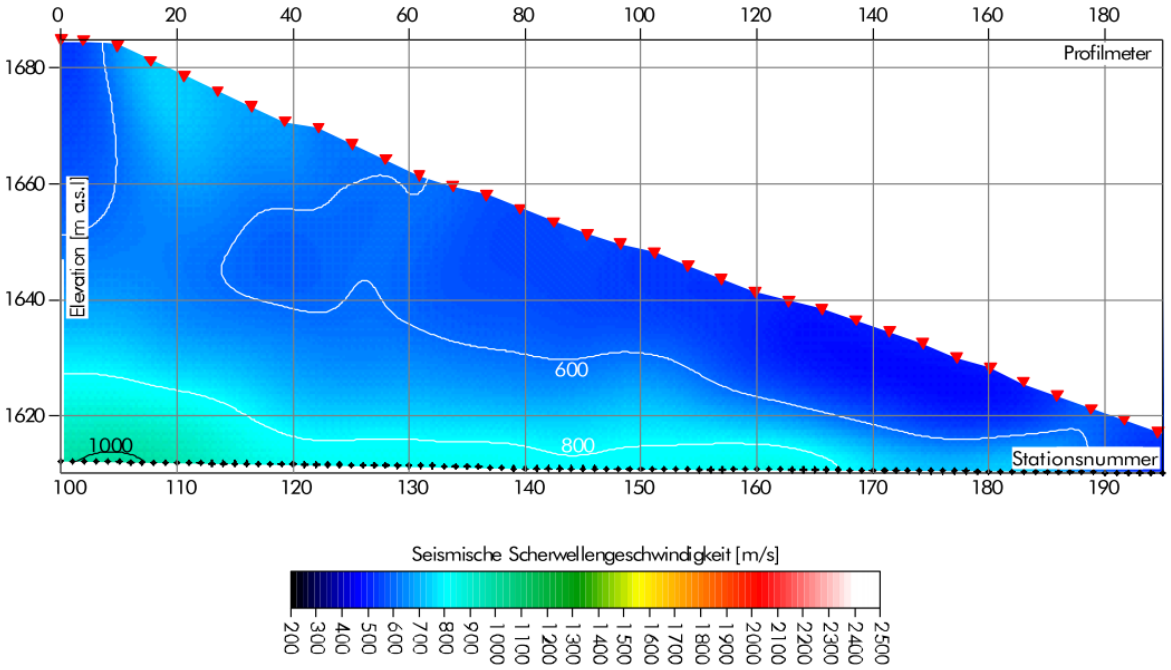

Figure 6: Tomography results: shear wave velocity distribution on the downstream side in section 12MARM-3 (see Figure 3) with excitation on the dam surface and measurements in the inspection gallery at elevation 1615 masl [3]

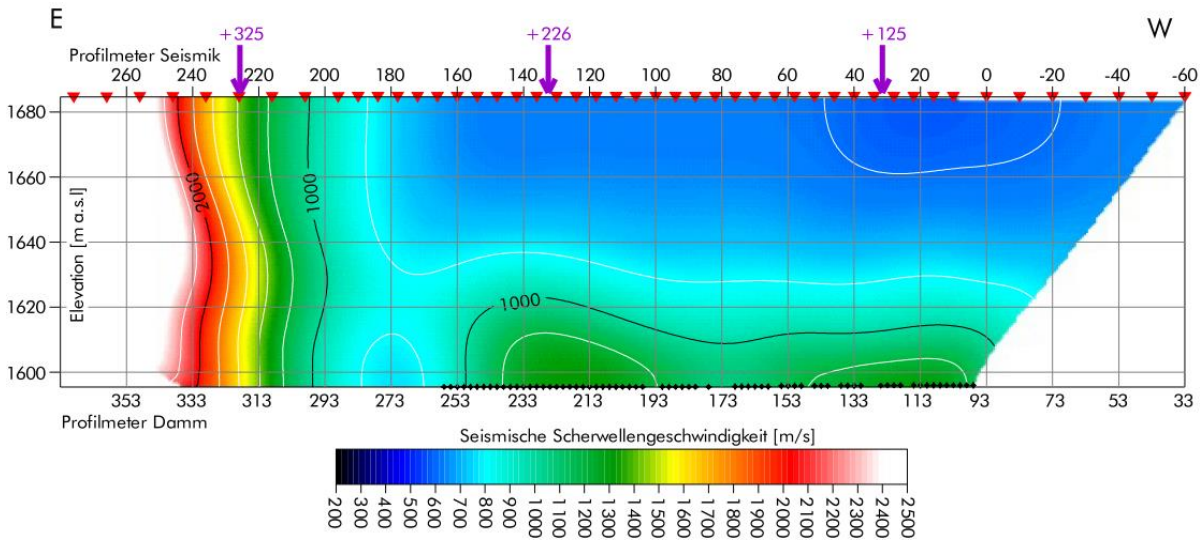

Figure 7: Tomography results: shear wave velocity distribution in dam axis in section 12MARM-1a (see Figure 3) with excitation on the dam crest and measurements in inspection gallery at elevation 1595 masl [3]

2.2 Seismic refraction

The results of seismic refraction are summarized in Figure 8 and Figure 9. The shear wave velocities of the dam body are in the range between 300 m/s and 1000 m/s. During the measurement on the berm at elevation 1640 (Figure 9), the bedrock surface with shear wave velocities of approx. 2000 m/s is clearly visible. From seismic refraction, the shear wave velocity of the core material along the dam axis measured from the dam crest at elevation 1684 masl is smaller as the shear wave velocity of the shell material measured froim the berm at elevation 1640 masl.

The lower measured shear wave velocities of seismic refraction at the dam surface compared to the results of the tomography measurements are due to the higher resolution of seismic refraction near the surface.

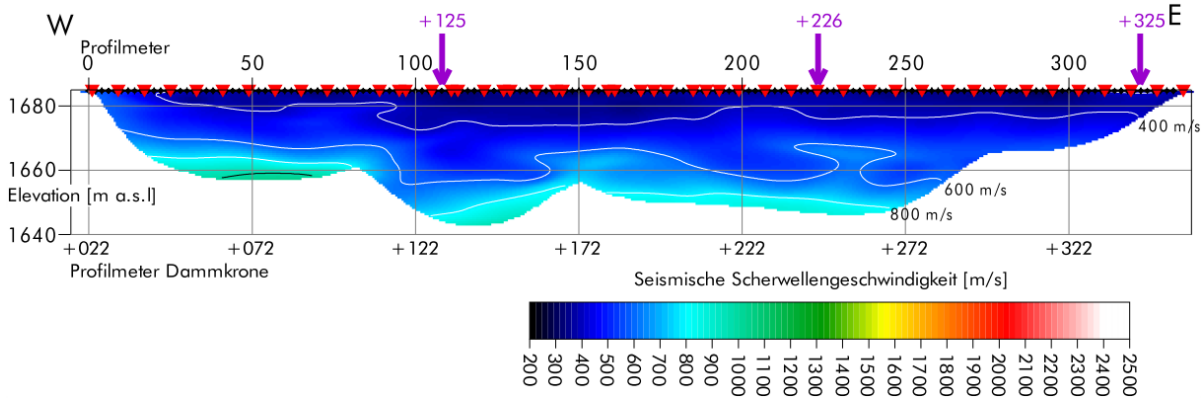

Figure 8: Results from seismic refraction: shear wave velocity distribution with measurements on the dam crest at elevation 1684 masl along the dam axis (section 12MARM-5 in Figure 3) [3]

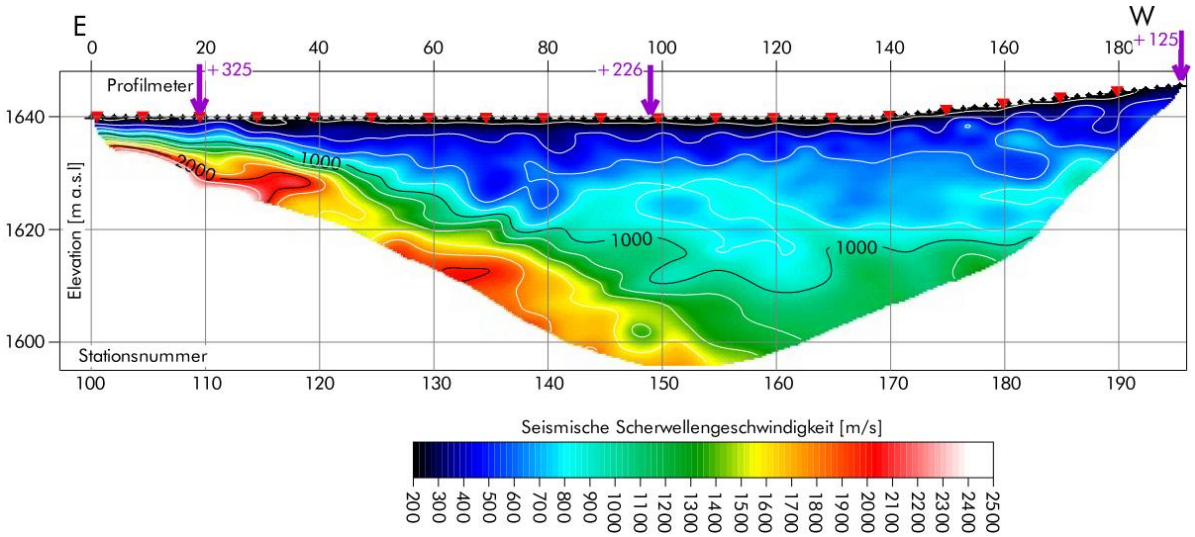

Figure 9: Results from seismic refraction: shear wave velocity distribution with measurements parallel to the dam axis on berm at elevation 1640 masl (section 12MARM-4 in Figure 3) [3]

2.3 MASW measurements

The following Figure 10 and Figure 11 give selected results of MASW measurement on the dam crest at elevation at 1684 masl and on the berm at elevation at 1640 masl respectively. The results also from other measuring stations show some variability with a tendency to high shear wave velocities. The values of v_{s30} range between 580 m/s to 660 m/s. Based on MASW measurement the core and shell material show no obvious difference in shear wave velocity. The values in depth below 20 m reaches values of v_s up to 1000 m/s and above with shear stiffness comparable to rock. The v_s results from MASW measurements are higher than from seismic refraction.

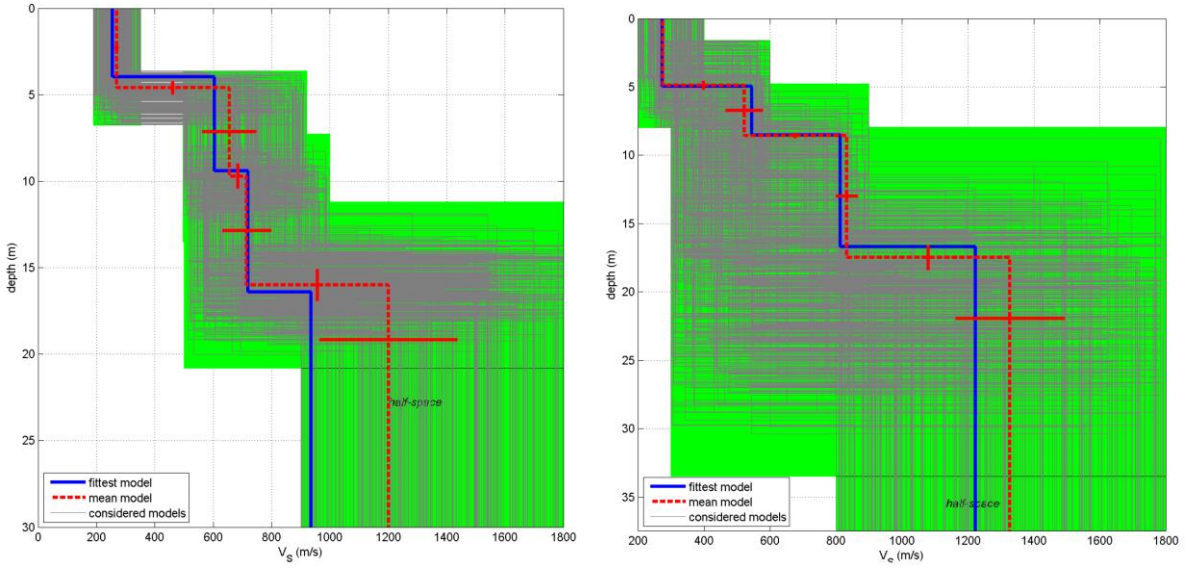

Figure 10: MASW measurements on dam crest al elevation 1684 masl: left - station 173 (v_{s30} = 614 m/s); right - station 176 (v_{s30} = 629 m/s) [3]

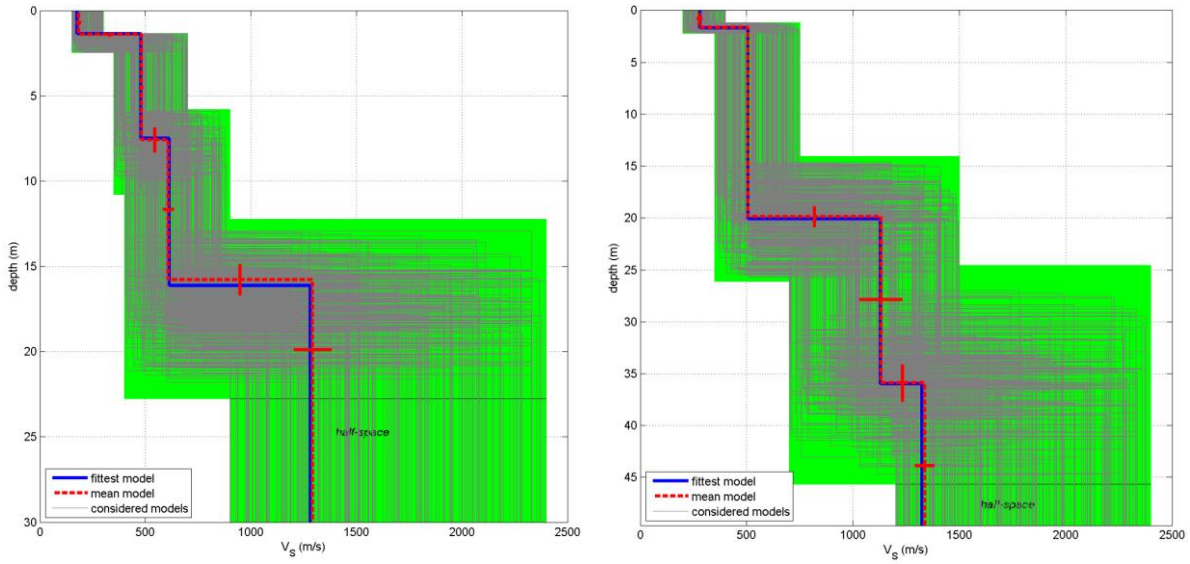

Figure 11: MASW measurements on berm at elevation 1640 masl: left - station 167 (v_{s30} = 661 m/s); right - station 189 (v_{s30} = 587 m/s) [3]

3 COMPARISON OF SHEAR WAVE VELOCITIES TO OTHER DATA

The geophysical investigations were used to measure the shear wave velocities of the dam body and the bedrock on the downstream side of Marmorera dam. The measurements generally show consistent results. Based on the results from seismic refraction, the shear wave velocities at 20 m depth are about $v_s \approx 600$ m/s and based on the tomography measurement at 80 m depth about $v_s \approx 900$ m/s.

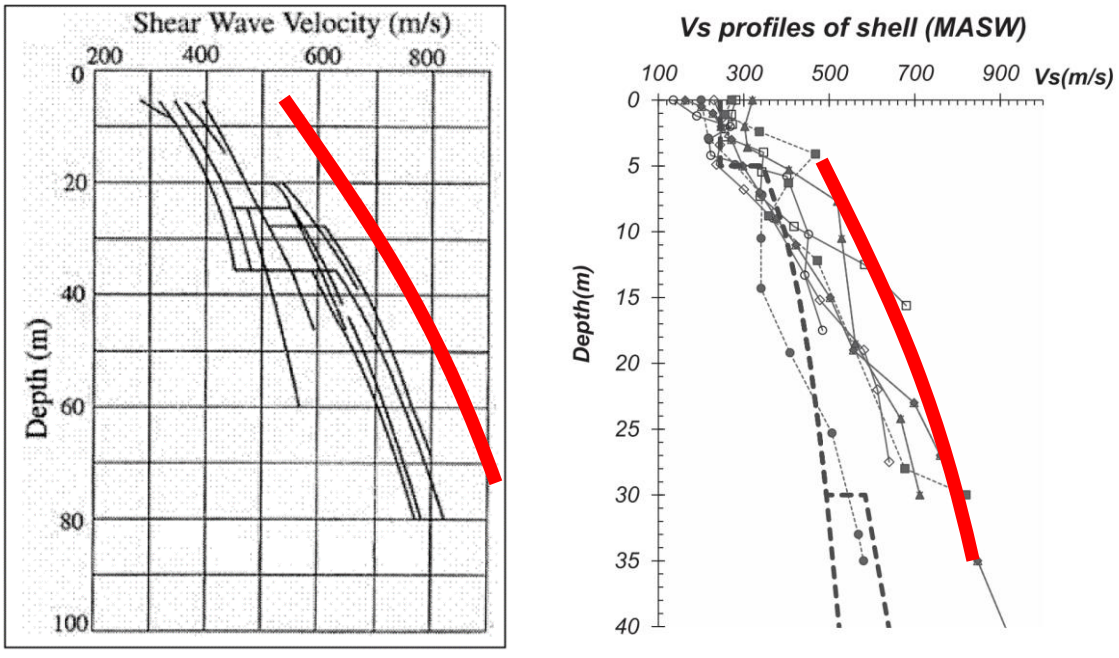

Figure 12: Shear wave velocities of dams, left from [4] and right from [5] in comparison to Marmorera data in red

The shear wave velocities of Marmorera dam body are higher than the upper bound of shear wave velocities documented by Sawada & Takahashi [4] based on Japanese data. The Marmora measurements correlate nicely with measurements by Park & Kishida [5] from 28

Korean embankment dams. They commented, that the Japanese data from Sawada & Takahashi [4] underestimate the shear wave velocities of dam shell material. This conclusion can be supported from the measurements of Marmorera dam. The comparison of data from Marmorera dam to data from the other authors is shown in Figure 12.

4 H/V MEASUREMENT

Here, it should be noted that the H/V measurements on the dam surface did not yield any reasonable results. The measured H/V maxima could not be assigned to any eigenperiod of the dam gained from numerical analysis, even considering the directivity of wave orientation in the dam body. The measured eigenperiods are too large, by a factor of 3 to 5. The method H/V according to Nakamura [6] applies to horizontally layered half-space. It is assumed that the correlation of H/V measurement results is poor to dam eigenperiods due to the topography of the dam. Based on experience from Marmorera, the favourable H/V method cannot be transferred to dam structures for easy eigenperiod measurements.

5 CALIBRATION OF MAXIMUM SHEAR MODULUS

The maximum shear modulus G_{max} and the shear wave velocity v_s are directly related with the influence of density:

$$G_{max} = v_s^2 \cdot \rho \quad (1)$$

Here it is assumed that the shear strains caused by shear waves from geophysical measurements excitation are in a very small strain range ($\gamma < 10^{-6}$). According to geotechnical reports, the density of the dam body materials at Marmorera dam averages around 2300 kg/m^3.

According to Seed and others [7], [8], the maximum shear modulus G_{max} can be represented as a function of the mean effective stress σ_m'. The correlation is given as follows:

$$G_{max} = 220\ K_2\ (\sigma_m')^{0.5} \quad [kN/m^2] \quad (2)$$

The parameter K_2 is calibrated by means of the shear wave velocity from geophysical measurement results and stress analysis. Based on the analysis of the initial stress condition of the dam with elastic-plastic material behaviour (Mohr-Coulomb), the distribution of the mean effective stresses σ_m' in the dam body is shown in Figure 13. The red rectangle corresponds to the tomography measurement in Figure 6. This results in stress state σ_m' of approx. 900 kN/m^2 to 1000 kN/m^2 for the effective stress with an empty reservoir in the middle of the dam at a foundation level of approx. 80 m depth. Based on the stress analysis with the Finite-Element-Method (Figure 13) and the distribution of the shear wave velocity (e.g. Figure 6 and Figure 8), a value of $K_2 = 240$ was determined (z = 20 m - σ_m' = 240 kN/m^2 - v_s = 600 m/s; z = 80 m - σ_m' = 970 kN/m^2 - v_s = 850 m/s). A higher weight is given to results from seismic refraction than to MASW. Figure 14 shows the mean effective stress σ_m', shear wave velocity v_s and the maximum shear modulus G_{max} in the dam body as a function of the depth z under the dam crest according to the formulation of Seed & Idriss [7] for a value $K_2 = 240$. This K_2 value is consistent from laboratory test result in Switzerland for dense alpine moraine material, see [9].

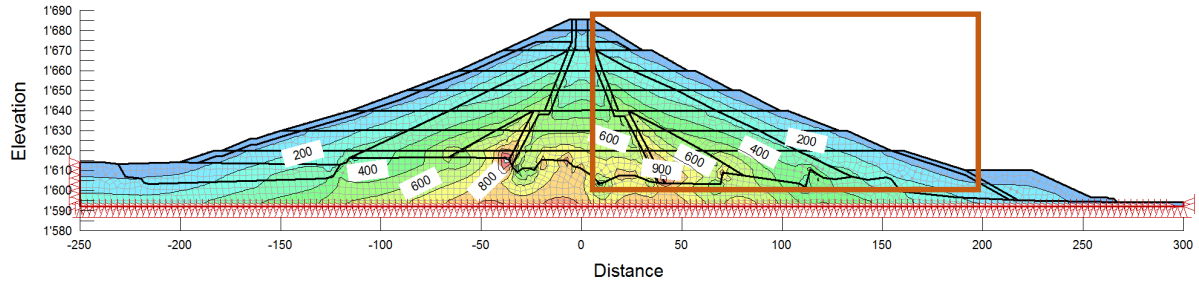

Figure 13: Numerical stress analysis with FEM [9], initial stress state in the dam body before impounding, mean effective stress σ_m' [kN/m^2], red marked area of seismic tomography measurements Figure 6

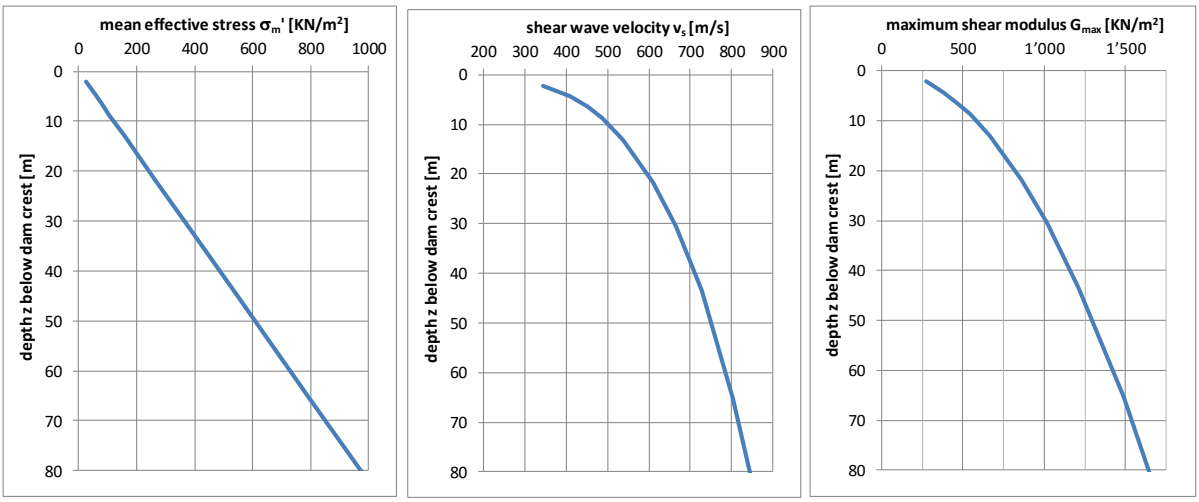

Figure 14: Mean effective stress σ_m', shear wave velocity v_s and maximum shear modulus G_{max} in the dam body depending on depth from dam crest

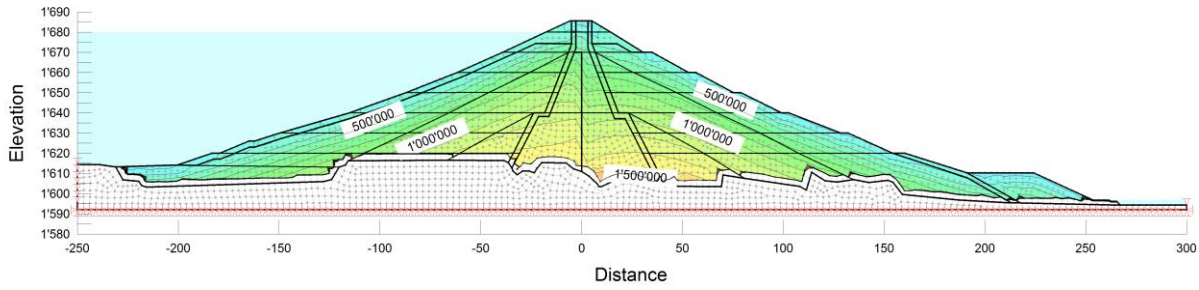

Figure 15: Distribution of maximum shear modulus G_{max} [kN/m^2] in the dam body before earthquake time history analysis [10]

The stress dependence of the maximum shear modulus G_{max} is defined in the numerical model for the initial state of the dynamic analysis. Figure 15 shows the distribution of the maximum shear modulus G_{max} at the beginning of the earthquake time history analysis using the program QUAKE/W of the software system GeoStudio 2012. For a comprehensive earthquake assessment, further dynamic soil parameters need to be defined. These include the strain-dependent linear-equivalent parameters of shear modulus and damping ratio for soil and rock. For the determination of the normalised strain dependent shear modulus curves, which are attached to the maximum the shear modulus G_{max}, and the corresponding damping curves, values are taken from literature, [9] and [11] since no specific cyclic laboratory tests were performed for Marmorera dam.

6 CONCLUSION

By means of seismic-geophysical measurements, such as tomography, seismic refraction and MASW, the distribution of the shear wave velocity in the dam body of the Marmorera dam was examined in more detail. Based on the shear wave velocity distribution, the stress dependent maximum shear modulus G_{max} was correlated. As a result, the shear wave velocities of the dam body material at Marmorera dam are consistent on the higher side compared to values from the literature and thus the dam has a high initial shear stiffness.

The initial shear modulus has a large influence on the earthquake behaviour of the dam, as it decisively influences the amplification of the earthquake excitation in the dam body from the foundation to the crest. The geophysical measurements performed are very well suited to determine the maximum shear modulus of the dam materials. This knowledge reduces the uncertainty in numerical earthquake calculations of soil materials. Measurements of H/V ratio even with consideration of wave field orientation did not gain reasonable results to determine fundamental dam periods.

In summary, it is recommended to measure the shear wave velocities of dam materials of existing dams with geophysical methods in order to specify the dynamic characteristics of G_{max} for numerical calculations. Also for new to be build dam, geophysical measurements can be performed after construction in order to verify numerical analysis performed and assumptions made initially.

ACKNOWLEDGEMENTS

The authors would like to thank Andreas Siegfried and Patrick Saudan from ewz - Electricity Works Zurich - for the very good cooperation and the permission to publish the data. Special thanks goes to Jan Laue from the Technical University Lulea Sweden for his support and cooperation in the project. Finally, Jost A. Studer, who unfortunately was not able to experience the completion the project, is remembered here.

REFERENCES

[1] BWG (2003) Sicherheit der Stauanlagen. Basisdokument zum Nachweis der Erdbebensicherheit, Federal Office for Water and Geology, Switzerland.

[2] Zingg, W. *Der Staudamm Castiletto des Juliawerkes Marmorera*. Schweizerische Bauzeitung, 71(33): 470-475 (1953).

[3] Keller, L. *Projekt Stauanlage Marmorera, Bericht zu den geophysikalischen Untersuchungen im Zusammenhang der Erdbebenüberprüfung*. roXplore gmbh, Amlikon-Bissegg, Switzerland, November (2012).

[4] Sawada, Y. & Takahashi, T. *Study on the material properties and the earthquake behaviors of rockfill dam*, Proc. of 4th Japan Earthquake Engineering Symposium, pp. 695-702 (1975).

[5] Park, D.S. & Kishida, T. *Shear wave velocity profiles of fill dams*. Soil Dynamics and Earthquake Engineering, Vol. 104, pp. 250-258 (2018).

[6] Nakamura Y. *A method for dynamic characteristics estimation of subsurface using micro-tremor on the ground surface*. Quarterly Report Railway Tech. Res. Inst., 30-1: 25-30 (1989).

[7] Seed, H.B. & Idriss, I.M. *Soil moduli and damping for dynamic response analysis*. Report No. EERC 70-10, Berkeley CA (1970).

[8] Seed, H.B., Wong, R.T., Idriss, I.M & Tokimatsu, K. *Moduli and Damping Factors for Dy-namic Analysis of Cohesionless Soils*. Report No. UCB/EERC-84/14, University of California Berkeley (1984).
[9] Studer, J.A., Laue, J. & Koller, M.G. *Bodendynamik, Grundlagen, Kennziffern, Probleme*, 3. edition, Springer-Verlag, Berlin, Germany (2007).
[10] Weber, T.M., Studer, J.A. & Laue, J. *Stauanlage Marmorera, Nachweis der Erdbebensicherheit*. Studer Engineering GmbH, unpublished report 6301-01, May (2018).
[11] Towhata, I. *Geotechnical Earthquake Engineering*. Springer-Verlag, Berlin, Germany. (2008)

Laboratory investigation on nonlinear dynamic properties of core materials of Italian dams

G. Lanzo[1], A. Pagliaroli[2], G. Scasserra[3] and A. Di Giulio[4]

Dpt. of Structural and Geotechnical Engineering, Sapienza University of Rome
Via A. Gramsci 53, Rome, Italy
E-mail: giuseppe.lanzo@uniroma1.it

Keywords: Italian earth-core rockfill dams; Core material; Modulus reduction curve; Damping ratio curve; Laboratory investigation

Abstract. *This paper presents the results of a series of laboratory investigations into the dynamic properties of core materials of Italian earth-core rockfill dams. All tests have been performed on specimens of undisturbed samples reconsolidated in a wide range of effective confining stresses. Most of the data were obtained from cyclic simple shear tests and few data from resonant column tests. It is shown that the shifting of the G/G_0-γ_c and D-γ_c curves with plastic index and effective confining stress is not as significant as it is well established for natural fine-grained soils. Generic literature curves do not predict properly the dynamic behaviour of the core materials, especially in the small-to-medium strain range. The importance of conducting site-specific measurements in order to accurately model the behaviour of core materials for dynamic analyses of embankment dams is therefore highlighted.*

1 INTRODUCTION

A peculiarity of the infrastructural heritage of Italian dams is that most of them were built before or shortly after the middle of the last century. That means most of them are more than 50 years old. As the chance to build new dams in Italy is rather limited, consequently there is a strong need for the seismic re-evaluation of existing ones. In addition to their age, this need is dictated by other important reasons. The dams were generally designed using seismic design criteria and methods of analysis (e.g. pseudo-static method) that are considered not suitable today, especially under specific local circumstances (e.g., liquefaction). After the release in 2004 of the updated hazard map of the Italian territory [1], many dams may be nowadays located in areas of higher seismicity as compared to the seismicity considered at the time of their construction. A recent National Code on Dams [2], hereafter referred as NTD2018, has been issued very recently, which dedicates a specific section to the assessment of seismic safety of existing dams.

Different methods can be used for the seismic re-evaluation of existing dams, including pseudo-static, simplified (Newmark) and advanced dynamic analyses. These latter nowadays became extremely common in geotechnical earthquake engineering practice. However, these

[2] Università di Chieti-Pescara, Pescara, Italy, alessandro.pagliaroli@unich.it
[3] Ground Engineering srl, Rome, Italy, ground.eng@gmail.com
[4] Istituto di Geologia Ambientale e Geoingegneria (IGAG), CNR, Rome, Italy, addigiulio@gmail.com

analyses still suffer from several uncertainties that can compromise the results, and consequently, possible intervention strategies. Among these, it is worth to mention the knowledge of: i) history of the dam, especially under earthquake actions ii) material properties under static as well as dynamic conditions iii) input motion and iv) the confidence on the limits of the methodology used.

In this paper, attention is focused on one of the source of uncertainties above mentioned, explicitly related to the dynamic behaviour of the core material of embankment dams. Basic fundamental parameters required for performing advanced analyses are the nonlinear deformation properties, that is the variation of normalized shear modulus reduction (G/G_0) and damping ratio (D) with the cyclic shear strain amplitude (γ_c), G_0 being the maximum shear modulus. Experimental data based on laboratory investigations carried out on samples retrieved from the core of zoned Italian dams are analysed and discussed.

2 ITALIAN EARTH-CORE ROCKFILL DAMS

Six earth-core rockfill Italian dams are considered in this study. These dams are generally constituted by a central core of fine-grained material protected by shells of sand and gravels on both sides.

Table 1 shows the list of the dams examined, the construction period and the maximum height. The dams are aged between 30 and 60 years since their construction. Maximum height is comprised between about 20 and 65 m, the only exception being San Pietro in Villa (H_{max}=6.3 m). The location of the dams is illustrated in Figure 1, superimposed to the hazard map of the Italian peninsula referred to the return period T_R=475 years. The values of maximum acceleration PGA for return periods of 475 and 1950 years are also reported in Table 1. For all dams, PGA for T_R=475 years is larger than 0.15g; more specifically, for Angitola $PGA_{TR=475yrs}$ =0.27g whereas for the other dams $PGA_{TR=475\ yrs}$ is comprised between 0.18 and 0.22g.

The experimental data presented in this study are obtained from different sources. Data of Angitola, Montedoglio, Polverina and San Pietro in Villa dams derive from the consultant activity of one of the Authors (Ground Engineering srl), data of San Pietro dam were taken from the literature [3] whereas data of Penne dam have been derived from tests carried out on a sample provided from a consultant engineering company (see acknowledgments).

Table 1: Italian earth-core rockfill dams considered

#	Dam name	Region	Construction period	H_{max} (m)	$PGA_{475\ yrs}$ (g)	$PGA_{1950\ yrs}$ (g)
1	Angitola	Calabria	1960-1966	22.6	0.270	0.468
2	Montedoglio	Toscana	1977-1986	64.3	0.217	0.346
3	Penne	Abruzzo	1966-1969	35.7	0.182	0.294
4	Polverina	Marche	1964-1965	27.5	0.196	0.309
5	San Pietro	Campania	1958-1964	49	0.211	0.395
6	San Pietro in Villa	Toscana	1980-1993	6.30	0.221	0.353

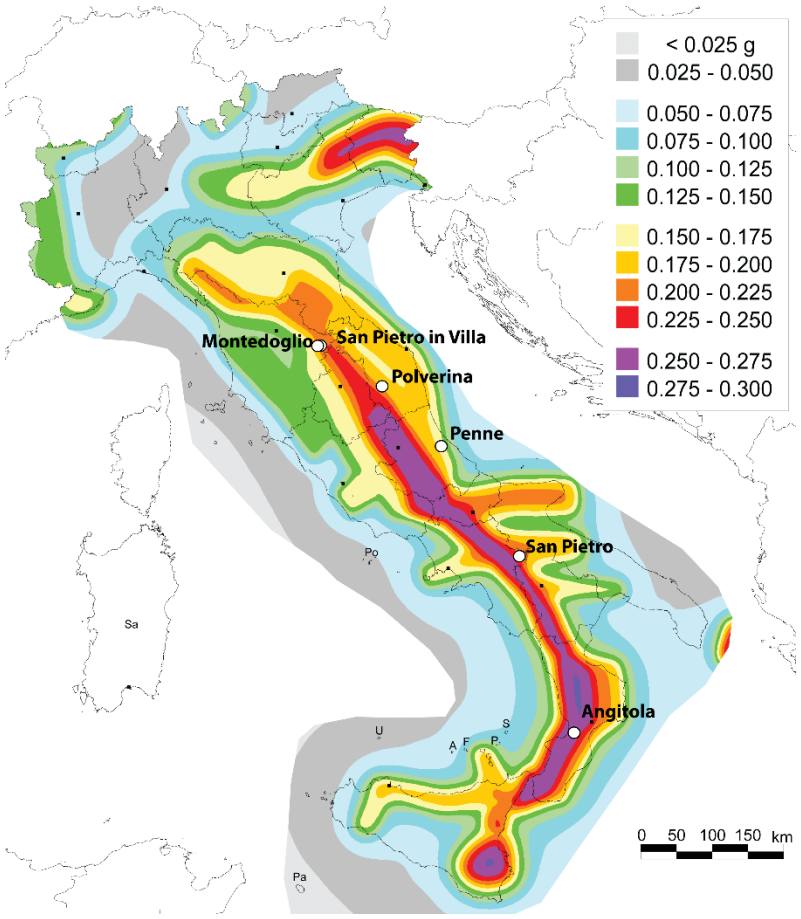

Figure 1: Location of the zoned dams examined, superimposed to the Seismic Hazard Map of Italy in terms of ground peak acceleration with 10% excess probability in 50 years, referred to rigid bedrock (Vs>800 m/s).

3 BASIC GEOTECHNICAL PROPERTIES OF CORE MATERIALS

Site investigations and geotechnical in-situ and laboratory tests were carried out to obtain the physical and mechanical properties of core materials of the six dams. In each dam boreholes were carried out, from the dam crest up to a maximum depth of 50 m, to evaluate the Vs profile in the core. Specifically, two boreholes were carried out at Montedoglio, Polverina, San Pietro and San Pietro in Villa dams (to perform cross-hole test) whereas at Angitola and Penne only one borehole was executed (to perform down-hole test).

In the following, only the physical properties as determined from laboratory tests carried out on the undisturbed samples retrieved from the cores are illustrated and discussed. Table 2 provides a summary of the main physical properties and state variables obtained on the samples subjected to cyclic and/or dynamic tests.

Grain size distributions, illustrated in Figure 2, indicate that core materials generally consist of silt, sand and clay in variable percentages; for Polverina sandy fraction is predominant, in the range 40-50%, in accordance to information from literature [4]. Clay fraction is always present for all tested materials, ranging between 20 and 40%. Figure 3 shows the profiles of unit weight (γ), water content (w), void ratio (e), degree of saturation (S_r) and clay fraction (CF) with depth. It can be noted that γ is about constant (20.1-21.3 kN/m^3) and also water content varies in a small range (w=15.2-23.3%) which is very close to the plastic limit (w_p) range (13.8-26.0%). Liquid limit can be found in the range 33-55% and plasticity index (PI) varies between 13 and 29. Degree of saturation (S_r) is between 90 and 100%. Consistency

index (I_C) is generally higher than 1, indicating a stiff material. According to the Casagrande chart (Figure 4a), the core materials can be classified as inorganic clays of low to medium plasticity whereas on the activity chart (Figure 4b) they correspond to soils with low activity.

Table 2: Physical properties and state variables of the tested samples

#	Dam name	Test	Depth (m)	γ (kN/m³)	w (%)	e_0 (-)	w_L (%)	PI (-)	CF (%)	I_C (-)	S_r (%)
1	Angitola	DSDSS	18.9	20.3	20.8	0.565	44	23	36	1.00	98.7
2a	Montedoglio	DSDSS	4.70	20.2	23.3	0.629	55	29	35	1.09	100.0
2b	Montedoglio	DSDSS	23.0	21.3	17.4	0.469	37	16	23	1.24	99.8
2c	Montedoglio	DSDSS	30.0	21.2	15.2	0.456	34	15	30	1.24	91.9
3	Penne	DSDSS	30.0	20.2	18.3	0.513	48.2	27.3	36	1.10	93.7
4a	Polverina	DSDSS	7.50	21.2	15.3	0.445	37.6	17.9	25	1.25	93.1
4b	Polverina	RC**	12.2	20.8	17.6	0.503	37.5	18.0	23	1.11	94.8
4c	Polverina	RC*	21.2	21.2	17.3	0.468	27.5	13.0	20	0.79	100.0
4d	Polverina	DSDSS	21.3	21.0	16.2	0.488	33.8	15.4	19	1.14	91.0
5	San Pietro	RC	15.0	20.1	23.0	-	42	22	32	0.9	-
6a	San Pietro in Villa	DSDSS	3.00	20.4	19.4	0.56	39	15	28	1.30	94.5
6b	San Pietro in Villa	DSDSS	6.00	20.7	18.4	0.56	33	14	11	1.00	94.5

*Sapienza Univ of Rome **ISMGEO laboratory

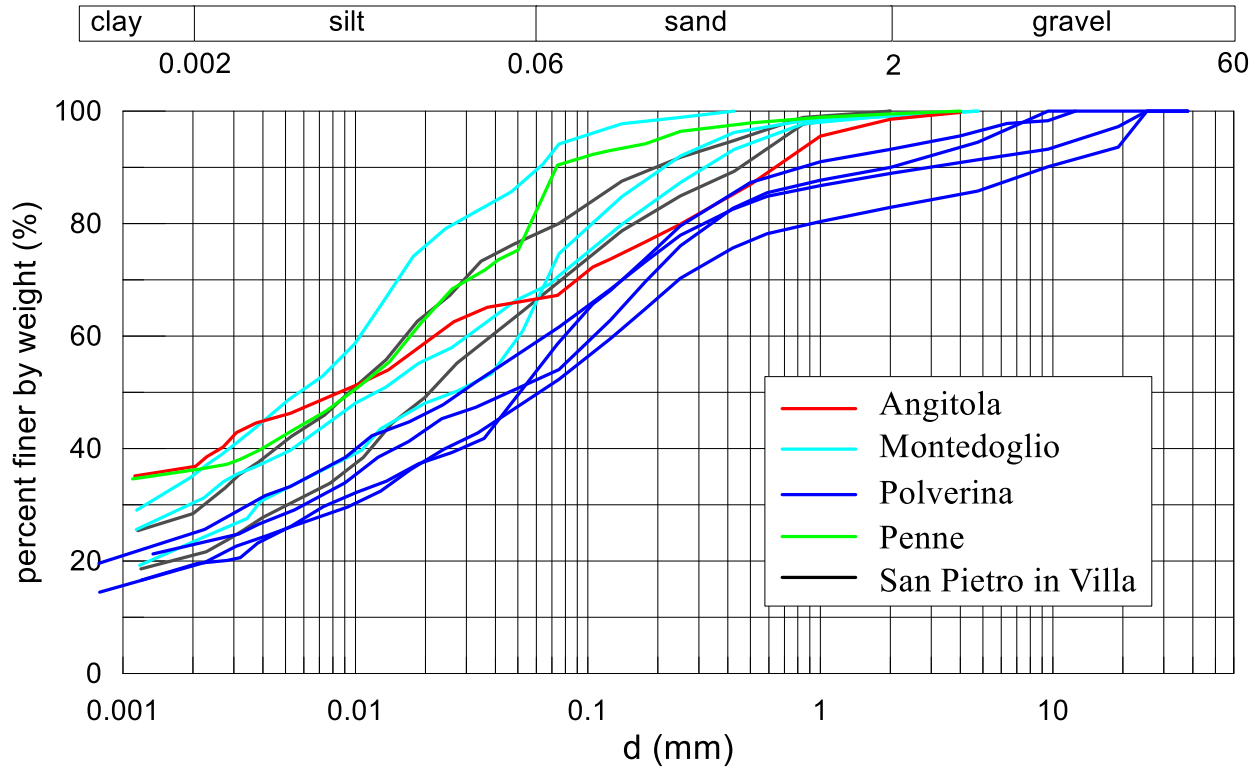

Figure 2: Grain size distributions of the core samples subjected to cyclic and dynamic tests

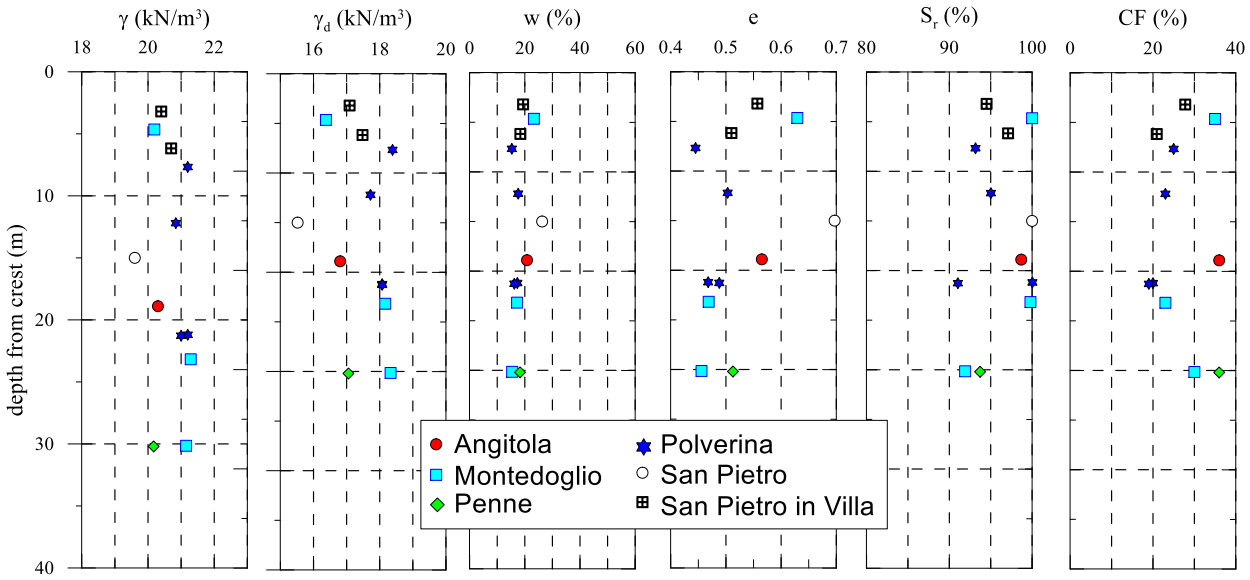

Figure 3: Variation of index and state properties of core samples with depth from the crest of the dams

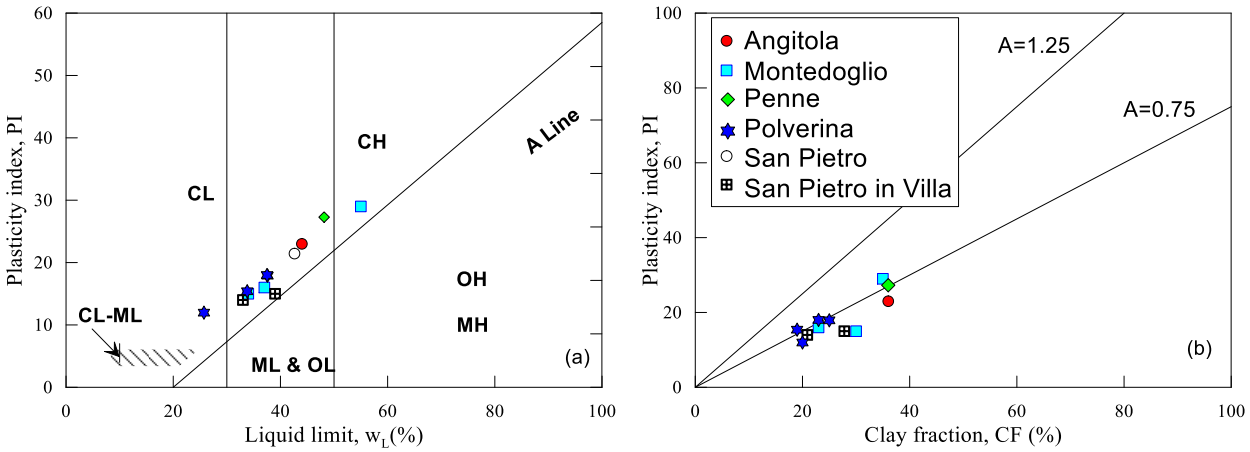

Figure 4: Casagrande and activity charts of core samples

4 CYCLIC AND DYNAMIC LABORATORY APPARATUSES

Deformation properties of core materials have been determined through laboratory cyclic and dynamic testing. As mentioned before, these properties are expressed in terms of normalized shear modulus reduction and damping ratio curves, that is G/G_0-γ_c and D-γ_c, respectively.

Most of the experimental investigations have been carried out at the Geotechnical Laboratory of the Department of Structural and Geotechnical Engineering of the Sapienza University of Rome (Faculty of Architecture). More specifically, cyclic simple shear tests have been conducted with a Double Specimen Direct Simple Shear (DSDSS) apparatus on Angitola, Montedoglio, Penne, San Pietro in Villa and Polverina dams (Table 3). For Polverina core material two RC tests have also executed, one at the Geotechnical Laboratory of the Department of Structural and Geotechnical Engineering of the Sapienza University of Rome (Faculty of Engineering) and the other by a private laboratory (ISMGEO). Finally, data from RC test have also been found in the literature on San Pietro dam. Usually the samples have been consolidated at the in-situ vertical or mean effective stress, variable between 50 and 500

kPa, but in some cases (e.g. Montedoglio and Polverina) very high confining pressure were also applied (up to 1500 kPa) in order to investigate the effect of confining stress

Table 3: Cyclic and dynamic tests carried out on core materials

#	Dam name	Depth (m)	Cyclic/Dynamic laboratory test	σ'_v (kPa)	σ'_m (kPa)
1	Angitola	18.9	DSDSS	250-500	166.7-333.3*
2a	Montedoglio	4.70	DSDSS	95-200	63.3-133.3*
2b	Montedoglio	23.0	DSDSS	430-800	286.7-533.3*
2c	Montedoglio	30.0	DSDSS	500-1000-1500	333.3-666.7-1000*
3	Penne	30.0	DSDSS	250-500	166.7-333.3*
4a	Polverina	7.50	DSDSS	150-300	100-200*
4b	Polverina	12.2	RC	-	125
4c	Polverina	21.2	RC	-	270-400
4d	Polverina	21.3	DSDSS	300-600-1200	200-400-800*
5	San Pietro	15.0	RC	-	150-300
6a	San Pietro in Villa	3.00	DSDSS	50-100	33.3-66.7*
6b	San Pietro in Villa	6.00	DSDSS	125-250	83.3-166.7*

* Estimated value

The DSDSS device was originally conceived, designed and constructed at the University of California at Los Angeles [5], specifically for investigating small-strain behaviour. In fact, due to its double specimen configuration, typical frictional problems that characterize the standard Norwegian Geotechnical Institute (NGI) direct simple shear device [6] were eliminated, thus allowing cyclic soil behaviour to be studied even at small strains. The DSDSS version used in this study is available at the Geotechnical Laboratory of the Faculty of Architecture, Sapienza University in Rome. A detailed description of this apparatus can be found in D'Elia et al. [7] and only a brief summary is provided hereafter. The layout of the apparatus is shown in Figure 5. Tests are carried out under constant volume conditions and a horizontal piston is used to apply the cyclic loading. The specimens are initially consolidated under anisotropic conditions. The mean effective stress σ'_m can be estimated under the assumption of oedometric conditions with a coefficient of earth pressure at rest (K_0) of 0.5. The anisotropic σ'_m is then evaluated as $\sigma'_m = (\sigma'_v + 2\sigma'_h)/3$. After the consolidation phase, cyclic loadings are applied with increasing cyclic shear strain amplitudes usually variable between 0.0004% and 1%. The test is performed under displacement control conditions. The secant shear modulus (G) and damping ratio (D) are directly measured from the cyclic stress-strain loop, according to the γ_c reached. The maximum shear modulus (G_0) can be estimated from the extrapolation of the experimental data at γ_c=0.0001%. For each step, 10 loading cycles are applied with a loading frequency of about 0.1 Hz. The apparatus is not instrumented for pore water pressure measurements.

As already mentioned, the device is capable of measuring the cyclic properties of soils in a very wide range of cyclic shear strain amplitudes, spanning from very small ($\gamma_c \cong 0.0004\%$) to very large ($\gamma_c \cong$3-4%) strains. As a matter of fact, the DSDSS device has been successfully used to investigate cyclic behaviour for a variety of soils and soft rocks (e.g. [8-10]. An example is shown in Figure 6 where the results of the DSDSS test carried out on the Penne core specimens (PI=27.3, σ'_v=500 kPa) are illustrated in terms of stress-strain loops, for increasing γ_c values from 0.0005% to about 3%, showing the large strain range investigated during the test.

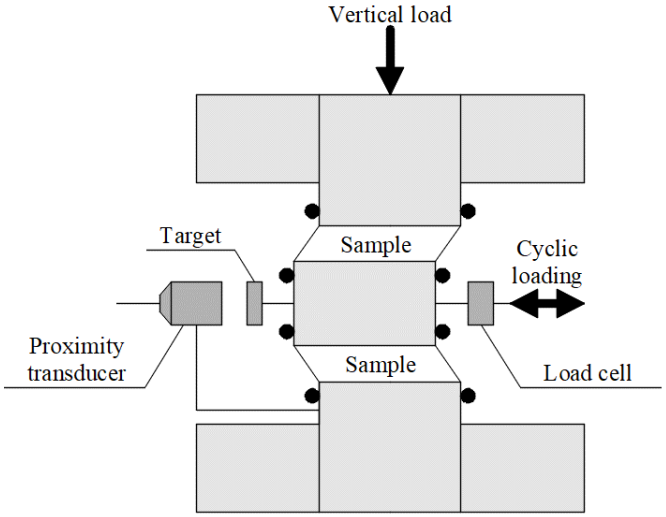

a)

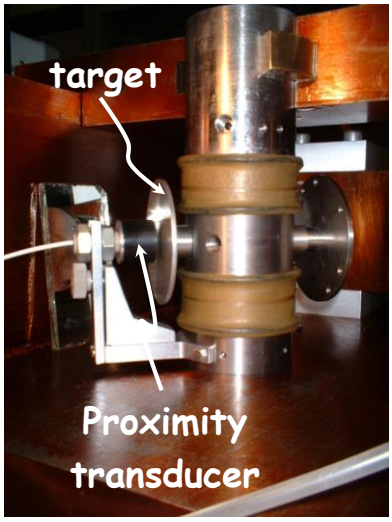

b)

Figure 5 a) Layout of the DSDSS apparatus available at the Geotechnical Laboratory (Faculty of Architecture) of the Sapienza University of Rome; b) picture of the DSDSS apparatus.

The RC apparatus made available by the Geotechnical Laboratory of the Sapienza University of Rome (Faculty of Engineering) is a modified version of the first free-fixed type machine designed at the University of Texas at Austin [11] and is equipped with an electro-pneumatic motor that allows closed-loop feedback control of torsional load or angular deformation, a signal conditioning unit and a data logger. The cylindrical soil specimen is fixed at the bottom base and excited at the top using an electrical motor able to generate a torsional moment, constituted by eight drive coils encircling four magnets attached to a drive plate. This device and the specimen are placed into the compressed air cell for the application of the isotropic total pressure, while a drainage system allows control of the pore water pressure. In the RC test the specimen is dynamically excited applying a torsional oscillation at the top base while varying the frequency of the input signal in a range that can go from 10 to 250 Hz. The response of the specimen in terms of motion amplitude (rotation angle) is measured either by an accelerometer or by proximity displacement transducers, so that the fundamental mode of vibration is found in correspondence of the maximum response. The shear modulus is calculated from the resonant frequency according to the elasticity theory, while material damping can be determined from the half power bandwidth or from the free-vibration decay curve observed after stopping the excitation at resonance.
It is important to note that the RC and DSDSS confinement states are different, isotropic for RC (K_0=1) and anisotropic for DSDSS (assumed K_0=0.5) tests.

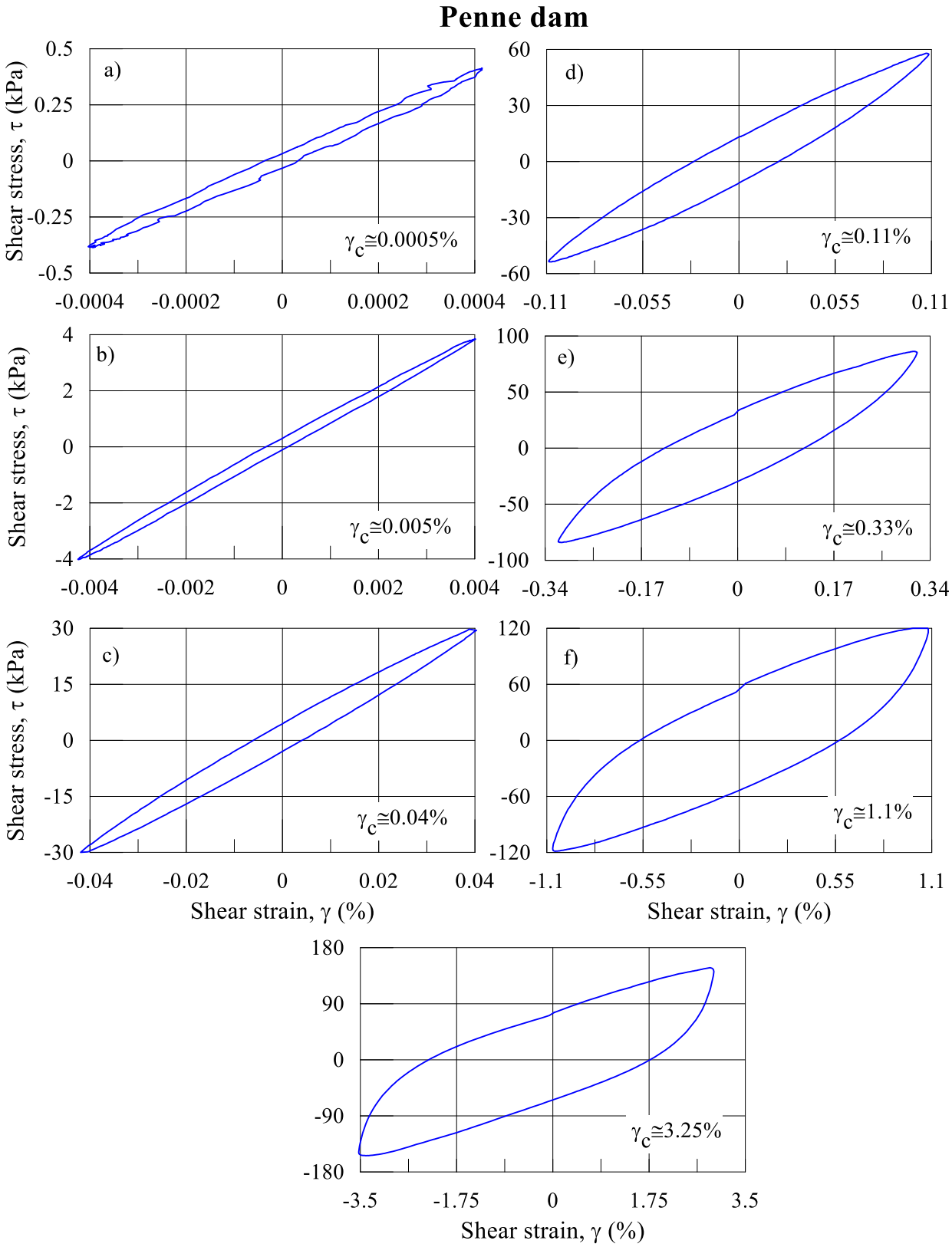

Figure 6 Cyclic stress-strain loops obtained from the Penne specimen (PI = 27.3) in DSDSS tests at σ'_v = 500 kPa for increasing levels of shear strain amplitude γ_c.

5 RESULTS OF CYCLIC AND DYNAMIC TESTS

The G/G_0-γ_c and D-γ_c data points of the tested core samples are illustrated in Figures 7 through 10. Specifically, Figure 7 and Figure 8 show the influence of effective confining stress and plasticity index for Angitola and Montedoglio dams, respectively. For Angitola (PI= 23) tests have been conducted at σ'_v=250 kPa and σ'_v=500 kPa and data points overlap almost completely; only a very small reduction of damping at small strains for increasing σ'_v can be noted. For Montedoglio, tests have been conducted on samples of different plasticity (PI=15, 16 and 29) effective confining stress (σ'_v=100-1500 kPa). It can be noted that all the curves describe a very narrow range, regardless of the different values of plasticity index in the range examined (PI=15-29). Also the effect of confining pressure is not very significant, considering the high σ'_v applied to the specimens; in particular the influence of confining pressure is negligible on the normalized stiffness curves, whereas some effect can be noted on damping ratio with D values shifting downwards as confining stress increases. To illustrate further the effect of PI and σ'_v on the G/G_0-γ_c and D-γ_c relationships, test results on Polverina dam are shown in Figure 9. These tests have been conducted on core samples with similar plasticity index (PI=13-18) consolidated at effective confining stresses variable in a wide range (σ'_m=100-800 kPa). Moreover, different apparatuses were used (i.e. DSDSS and RC), thus a comparison in terms of stiffness and damping ratio can also be made. In accordance with previous results it can be seen that the effect of effective confining stress is very limited on normalized stiffness whereas is more significant on damping ratio values, especially at smaller γ_c amplitudes. In fact, it can be seen from DSDSS tests that small-strain damping ratio varies between about 3.5% and 1% for σ'_v= 150-1200 kPa; small-strain damping ratio from RC tests are higher than those predicted by cyclic DSDSS tests. These differences can be presumably attributed to the different loading frequencies applied.

Figure 10 illustrates the experimental data obtained for all tested materials. It can be seen that the whole set of data fall in a narrow range and no clear trend with plasticity index can be identified, as commonly established for natural soils. Only for Polverina dam, the experimental trend shows a more nonlinear behavior in terms of stiffness reduction as compared the other materials. This is consistent with the grain size composition of Polverina core material which is characterized by a greater sandy fraction and the lowest values of plasticity index. However, damping ratio values fall within the range identified for the other core materials.

The above observations indicate that the effect of PI on the G/G_0-γ_c and D-γ_c of undisturbed core materials is not so evident and important as it is for natural fine-grained soils, at least in the range investigated (PI=13-29). Further, the effect of effective confining stress is also very limited. This behavior can be presumably due to the overconsolidation induced by compaction during construction. Similar kind of behavior has been recently observed also by Park and Kishida [12].

In Figure 10 the G/G_0-γ_c and D-γ_c data points are also compared with the V&D (Vucetic and Dobry) [13] empirical curves for similar PI. The V&D curves are not completely able to capture the variation of normalized stiffness with shear strains, at least up to about γ_c=0.05%, where the experimental data show a more linear behavior as compared to literature curves. Also for Polverina, which shows a slightly less linear behavior, the linear threshold is higher than that calculated by V&D curves. However, at larger shear strains experimental data fall within the band identified by V&D for soils of similar plasticity (PI=15-30). Comparison in terms of damping ratio shows that experimental data are lower than generic curves at small strains ($\gamma_c \cong 0.05\%$) whereas at moderate to large strains ($\gamma_c > 0.1\%$) experimental data are higher than V&D curves. In the damping ratio plot, experimental data from Polverina RC tests have not been included.

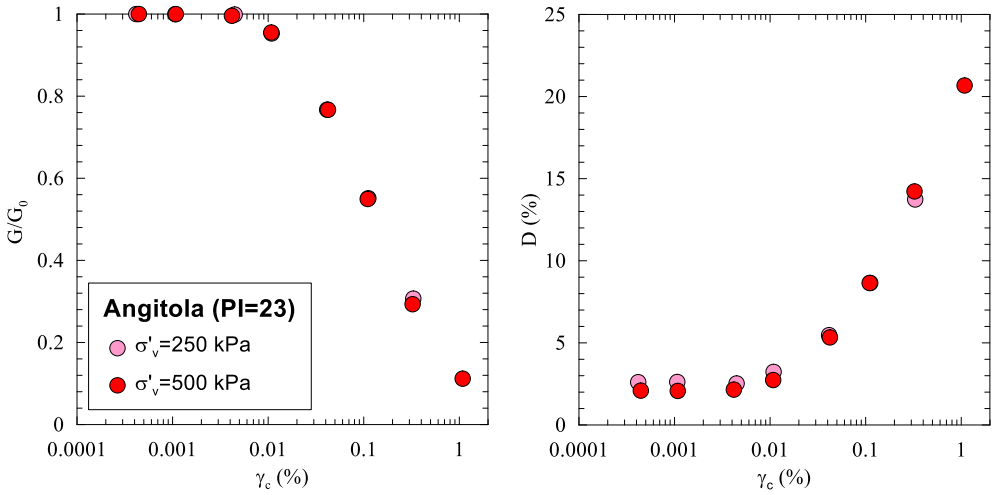

Figure 7 Modulus reduction and damping ratio data points of Angitola dam core from DSDSS tests..

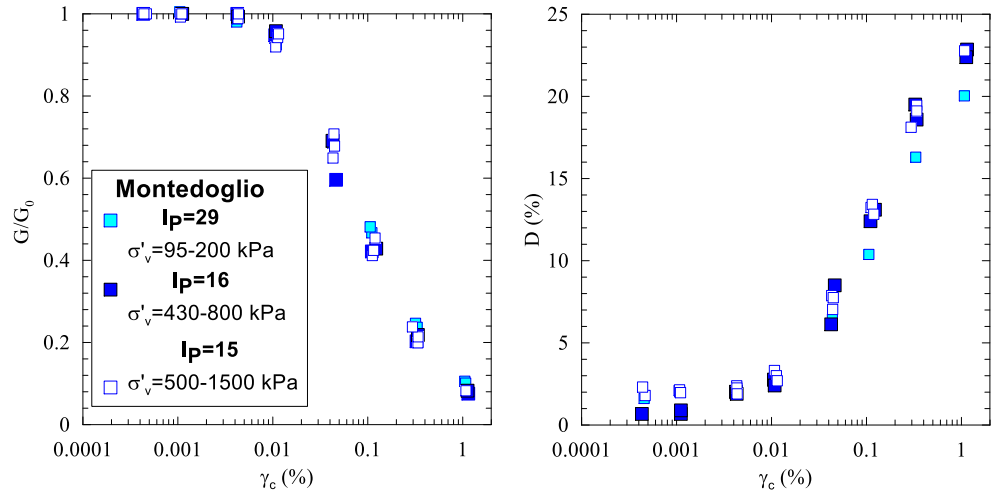

Figure 8 Modulus reduction and damping ratio data points of Montedoglio dam core from DSDSS tests.

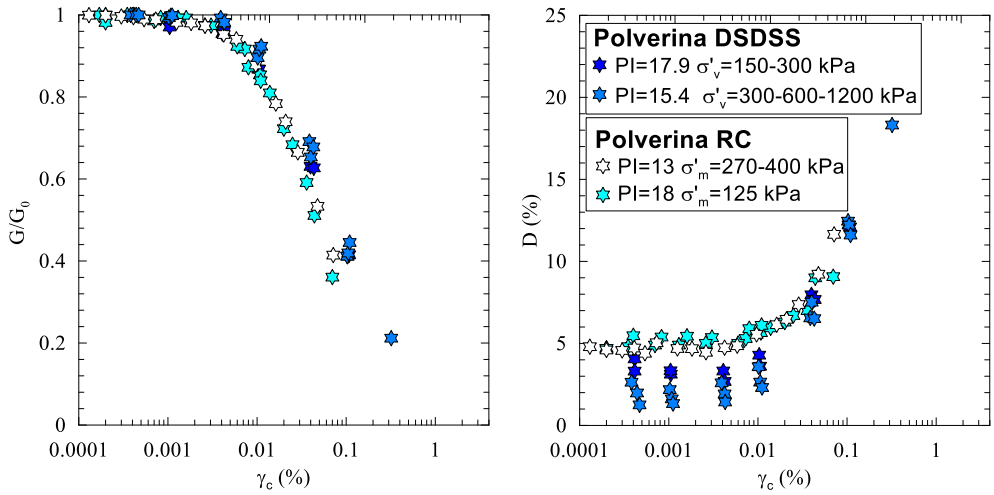

Figure 9 Modulus reduction and damping ratio data points of Polverina dam core from RC and DSDSS tests.

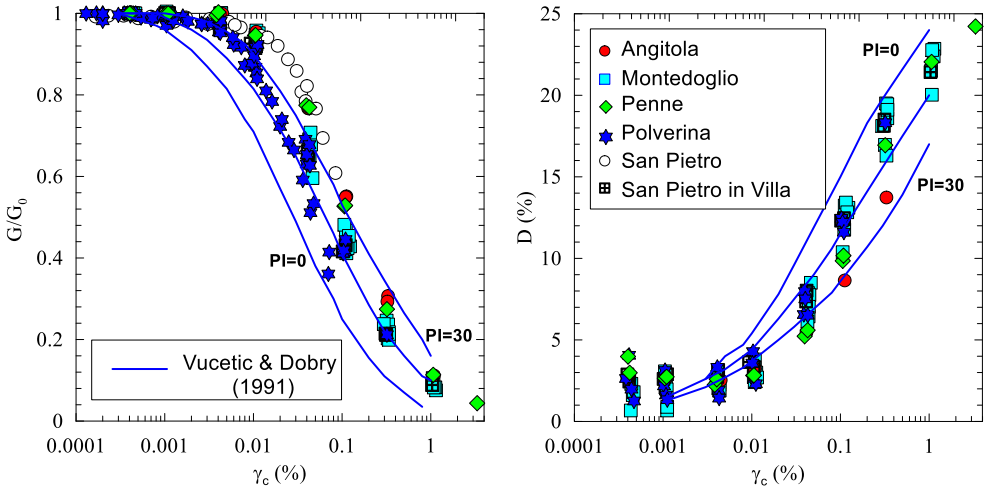

Figure 10 Modulus reduction and damping ratio data points of Italian core dam materials compared with empirical relations by Vucetic & Dobry (1991).

6 CONCLUSIONS

A series of laboratory tests have been illustrated aiming at investigating the main factors affecting the nonlinear stiffness and damping properties of undisturbed samples of core materials of six Italian zoned dams. The laboratory investigations comprised cyclic simple shear and resonant column tests. Based on the gathered experimental results, the importance of conducting site-specific measurements on dynamic properties of core materials, rather than using generic literature data to properly conducting numerical dynamic analyses, has emerged. More specifically, the following tentative conclusions can be drawn:

- normalized modulus reduction and damping ratio curves do not seem to follow the well-established trend for natural fine-grained soils in terms of plasticity index and confining stress, at least in the ranges investigated (PI=13-29 and σ'_m=100-800 kPa);
- it is speculated that this lack of clear shifting of the G/G_0-γ_c and D-γ_c curves as plasticity and effective confining stress incraese is due to the overconsolidation induced by compaction process during the construction of the dam;
- empirical correlations from literature (such as Vucetic and Dobry curves) are not completely capable to predict properly the G/G_0-γ_c and D-γ_c trend with PI and σ'_m, especially in the small-to-medium strain range; for this reason it is recommended conducting specific laboratoy tests to assess the nonlinear dynamic behaviour of core materials of embankment dams.

The above results have to be considered preliminary as more laboratory tests are needed to corroborate the indications that emerged from the study and to provide a greater generality to the results obtained.

ACKNOWLEDGMENTS

The writers want to express their gratitude to O&M Hydro (Engs. Rosella Caruana, Francesco Fornari, Alberto Frezza and Renzo Sparnacci) for allowing the publication of test results of Polverina dam. Eng. Stefano Cola of EAUT (*Ente Acque Umbre-Toscane*) is gratefully acknowledged for the permission to publish the data of Montedoglio and San Pietro in Villa dams. The permission to publish data for Angitola dam by Eng. Pasquale Cimbalo (*Consorzio di Bonifica "Tirreno Catanzarese"*) is also appreciated. Finally, Eng. Alessandro Masciotta of Studio Masciotta in Rome is gratefully acknowleged for having provided the undisturbed samples of the core of Penne dam.

REFERENCES

[1] Gruppo di Lavoro MPS. Redazione della Mappa di Pericolosità Sismica prevista dall'Ordinanza PCM del 20 marzo 2003, n. 3274, All. 1, Rapporto Conclusivo, INGV Milano/Roma, 2004. http://zonesismiche.mi.ingv.it/documenti/rapporto_conclusivo.pdf (in Italian)

[2] Ministero delle Infrastrutture e Trasporti. Verifiche sismiche delle grandi dighe, degli scarichi e delle opere complementari e accessorie. Istruzioni per l'applicazione della Normativa Tecnica di cui al D.M. 26.6.2014 (NTD14) e al D.M. 17.01.2018 (NTC18). Direzione Generale per le dighe e le infrastrutture idriche ed elettriche, Version 1 – July 2018 (in Italian).

[3] Calabresi G., Rampello S., Callisto L., Cascone E. (2004). Diga S. Pietro sul Fiume Osento. Verifica delle condizioni di stabilità e analisi del comportamento in condizioni sismiche. Contratto di Ricerca con il Consorzio per la Bonifica della Capitanata, Univ. di Roma "La Sapienza", Dip. Ing. Strutt. e Geotecnica, 2004.

[4] Jappelli R., Silvestri T. Rassegna dei materiali sciolti adoperati nelle dighe in Italia nel periodo 1950-1975. In ricordo di A. Pellegrino, Napoli, September 2005 (in Italian)

[5] Doroudian M, Vucetic M. A direct simple shear device for measuring small-strain behavior. Geotech Test J GTJODJ 18(1): 69–85, 1995.

[6] Bjerrum, L. & Landva, A Direct Simple-Shear Test on a Norwegian Quick Clay. Géotech, 16 (1): 1-20, 1966.

[7] D'Elia B., Lanzo G., Pagliaroli A. Small strain stiffness and damping of soils in a direct simple shear device. In: Pacific conference on earthquake engineering 2003, Christchurch, New Zealand, 2003.

[8] Lanzo G., Pagliaroli A., Tommasi P., Chiocci F.L. Simple shear testing of very soft offshore clay for wide strain range. Can Geotech J 46(11):1277–1288, 2009

[9] Pagliaroli A., Lanzo G., Tommasi P., Di Fiore V. Dynamic characterization of soils and soft rocks of the Central Archaeological Area of Rome. Bulletin of Earthquake Engineering, 12, pp. 1365-1381, 2014

[10] Verrucci L., Lanzo G., Tommasi P., Rotonda T. Cyclic and dynamic behaviour of a soft pyroclastic rock. Géotechnique 65(5): 359-373, 2015

[11] Isenhower W. M. 1979. Torsional simple shear/resonant column properties of San Francisco Bay mud. Thesis GT80-1, Geotech. Engrg Ctr. University of Texas at Austin, TX.

[12] Park D.S., Kishida T 2019. Shear modulus reduction and damping ratio curves for earth core materials of dams. Can. Geotech. J. 56: 14–22 (2019), dx.doi.org/10.1139/cgj-20

[13] Vucetic, M., Dobry, R. (1991). Effects of the soil plasticity on cyclic response. J. Geot. Eng. Div., 117(1): 89-107.

Application of SPT results on liquefaction phenomenon modeling of tailings dams

Ljupcho Petkovski[1] and Stevcho Mitovski[2]

University "Sts Cyril and Methodius", Civil Engineering Faculty
Blvd. Partizanski odredi 24, Skopje, Republic of Macedonia
E-mail: petkovski@gf.ukim.edu.mk

Keywords: Tailings dam, Liquefaction, Collapse surface concept

Abstract. *The tailings dams, due to the enormous volume of the waste lagoon, are earth-fill structures with highest potential hazard for the surrounding. However, the numerous reports of collapses of the tailings dams in the last three decades, all over the World, indicate that the structural (static and dynamic) safety and the liquefiable resistance was not controlled with the proper carefulness. In this research, the concept of collapse surface is used for liquefaction assessment, which is defined by two parameters, the angle of inclination of the collapse surface and steady-state strength. The steady-state strength of the different zones of the tailings dam is adopted from the results obtained from "In situ" investigations by Standard Penetration Test (SPT) and laboratory tests of fines. In this paper are presented results from the analysis of the dynamic response, the liquefaction assessment and the seismic resistance of the hydro tailings dam Topolnica, of the mine Buchim, Radovish. This tailings dam, in the east part of Republic of Macedonia, is formed by combination of downstream (in the first phase) and upstream (in the second phase) method of construction, with total height from the crest to the downstream toe of the dam of 141.2 m.*

1 INTRODUCTION

Tailings dams are complex engineering structures, composed of an initial dam, sand dam, waste lagoon, drainage system, outlet pipe for discharge of clear water, and structures for protection in case of inflow (external) water, [1] and [2]. The tailings, on one hand, due to the numerous structures of which are composed, should be checked on great number of safety cases at static loading, similar as for conventional fill dams [3], and on other hand, due to the enormous volume of the waste lagoon, they are fill structures with highest potential hazard for the surrounding [4]. Due to the great importance of the tailings dams, one of the ICOLD's Technical Committees is exactly for tailings dams and deposit lakes - ICOLD Committee on Tailings dams and Waste Lagoons, that has published several Bulletins, [5], [6], [7], [8] and [9].

Due to the long construction period, the approach for conventional dams (for creation of water reservoirs) for confirmation of proper accomplishment of the hydraulic structures – with full supervision of the construction and control of the first reservoir filling, as well and the assessment of the dam's proper behavior with construction parameters throughout comparison with monitoring data, at most cases is not applied fully in case of tailings dams. Unfortunately, such main difference between the conventional and tailings dams is amplified

[2] University "Sts Cyril and Methodius", Civil Engineering Faculty, smitovski@gf.ukim.edu.mk

in case of technical solutions with combined construction method [10] and heightening [11] thus providing increase of the deposit space of the tailings dams. The investigation of the settlements in tailings dams body upon service period of the waste lagoon [12] is necessary to plan the dam crest heightening and to estimate limit values for the displacements. These estimated limit values have to be compared with the measured values within monitoring process, so the proper conclusion can be drawn out for the regular behavior of the dam in the future period.

The purpose of this research is to apply the collapse surface concept (CSC) for liquefaction assessment. This concept is defined by two parameters, the angle of inclination of the collapse surface and steady-state strength. The steady-state strength of the different zones of the tailings dam is adopted from the results obtained from "In situ" investigations by Standard Penetration Test (SPT) and laboratory tests of fines. In the text below, the paper will be illustrated with data from the research of the dynamic response, the liquefaction assessment and the seismic resistance evaluation of the hydro tailings dam Topolnica, with combined construction method, of the mine Buchim, Radovish, Republic of Macedonia.

2 BASIC PARAMETERS OF THE TAILINGS DAM TOPOLNCA

Tailings dam Topolnica of mine Buchim, Radovish, commissioned in 1979, is created by deposition of the flotation pulp. By the method of pulp hydro-cycling, from the sand is created the downstream sand dam, and the spillway from the hydro-cyclones (sometimes, mud and water without hydrocycling) is released in the upstream waste lagoon. In such way in the waste lagoon is done mechanical deposition of the finest particles and chemical purification of the used reagents, present in the tailings. In the past period in tailings dam Topolnica is deposited tailings volume over 130 millions m^3 and water is stored in volume of approximately 9 millions m^3.

The tailings dam is characterized with stage construction and combined construction method, by downstream progressing in first stage and upstream progressing at heightening from second stage, in two phases. The construction started with the initial dam, with foundation elevation 518.5 m and crest elevation 558.5 m. The construction of the sand dam in first stage, up to elevation 610 m (I stage), was constructed in inclined layers, by progressing in downstream direction from the initial dam. Afterwards, the construction of the sand dam to elevation 630 m as (II stage, phase 1), due to the vicinity of village Topolnica to the downstream toe of the dam, was constructed by filling in upstream direction. At terminal stage is adopted sand dam crest at 654.0 m (II stage, phase 2), by progression in upstream direction.

The overall dimensions of the representative cross section for structural (static and dynamic) analysis are length 801.4 m and height 141.2 m. The tailings dam Topolnica, with height of dam no. 2-2 above the foundation of initial dam of H0 =654.0-518.5=135.5 m, is one of the highest tailings dams in Europe. The final height of the tailings dam no. 2-2, from crest to downstream toe, is H2 = 654.0 - 512.8 = 141.2 m, by what Topolnica tailings dam is highest dam in R. Macedonia. Namely, the highest conventional dam (for water reservoir), dam Kozjak, according to as built data from 2001, has height from dam crest to core foundation of 472.2 – 341.8 = 130.4 m. The enormous dimensions of the sand dam, heterogeneous composition of the geo-medium and combined construction method, downstream in stage I and upstream in stage II, obviously shows that dam Topolnica is one of the most complex and most important fill structures in R. Macedonia.

Regarding the geotechnical parameters of the local materials, from which the tailings dam is constructed certain approximations are foreseen, thus contributing to simplification of the numerical experiment and in same time does not decrease the safety analysis. The

simplification of the material parameters is provided by the following approximations: (1) the waste lagoon, possessing highly non-specified and heterogeneous composition, by finer grain size fractions in the upstream and coarser grain size particles in the downstream part of the sand dam, is represented with 3 different materials; (2) the filter transition zones in the initial dam are neglected, for which is estimated that they have small dimensions, compared to the geo-medium from interest in the analysis. In such a way is prepared idealized cross section for structural analysis (static and dynamic), and the heterogeneous composition of the tailings dam is modeled with number of segments by 6 different materials, (figure 1). The discretization of the tailings dam for structural analysis (figure 2) is done in order to model the stage construction, by development and dissipation of the consolidation pore pressure.

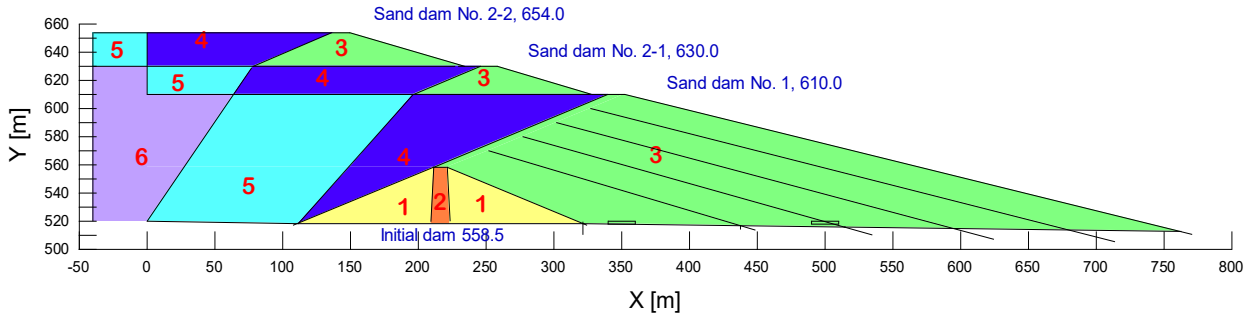

Figure 1: Segments by 6 different materials. 1 – gravel in initial dam body, 2 – clay in initial dam core, 3 – sand in tailings dam, 4 – sand silt in beach, 5 – sand silt between the beach and lagoon and 6 – silt in waste lagoon

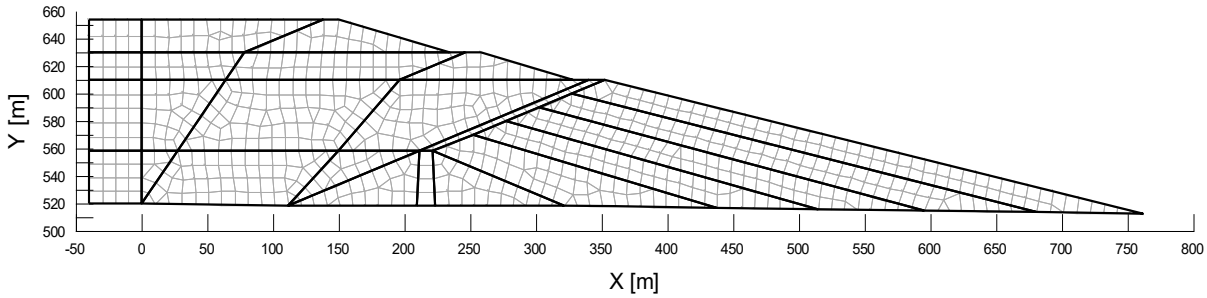

Figure 2: Discretization of the mediums for static analysis by FEM (Nodes=810, Elements=766)

3 MODELING OF THE INITIAL STRESS STATE, PRIOR TO THE EARTHQUAKE

By the model is simulated realistic progress of the tailings dam, i.e. filling of the waste lagoon is by appropriate time delay upon sand dam construction. The upstream water saturation of the tailings due to the existing water inflow from river Topolnica in the tailings dam during progressing of the waste lagoon is adopted to be 2.0 m lower then the deposited tailings. Such upstream non-steady hydraulic boundary condition is necessary for the analysis of the effective stresses for the alternative with upstream water saturation of the tailings during construction, which is the service period of the structure. In the consolidation analysis, by analyzing the effective stresses in drained conditions in realistic time domain [13] is adopted water filling function in the waste lagoon, as variable upstream boundary condition for analysis of the non-steady seepage [14]. In such complex and coupled analysis (by parallel mechanical and hydraulic response), in the same time are simulated: (a) stage construction, (b) development and dissipation of consolidation pore pressure, (c) change of the upstream hydrostatic pressure and (d) heterogeneous medium by irregular geometry. In the applied analysis, that simulates the tailings behavior most realistically, both the material

parameters and the time component, i.e. the realistic construction dynamics, have significant influence.

The state with maximal potential hazard of the hydro system on the downstream river valley is the critical or the most important state for assessment of the seismic resistance of the tailings dam no. 2-2 for crest elevation 654.0 m. It is a case when the waste lagoon is at maximal operating level (or normal water level at elevation 652.0 m) and when steady seepage in the tailings dam is established. Then, the maximal values of the pore pressure are generated (figure 3) and for appropriate total stresses (figure 4) the geo-medium has minimal effective normal stresses (figure 5), i.e. it possesses minimal tangential resistance or reduced stiffness.

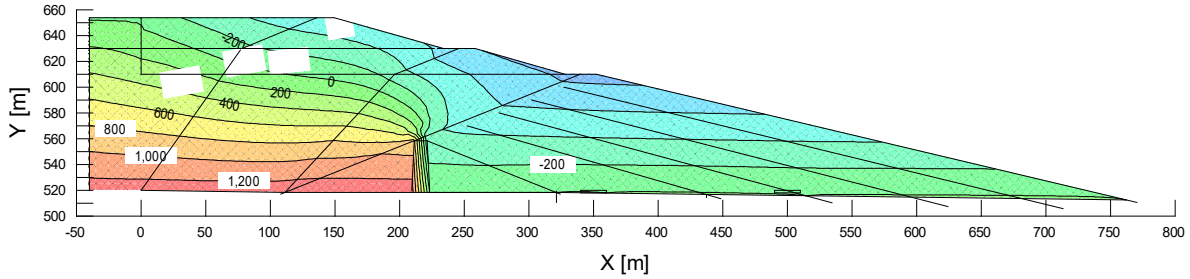

Figure 3: Pore pressure distribution in kPa, for steady seepage in the tailings dam, at upper water elevation at 652.0 m, Pw,max = 1,309.2 kPa

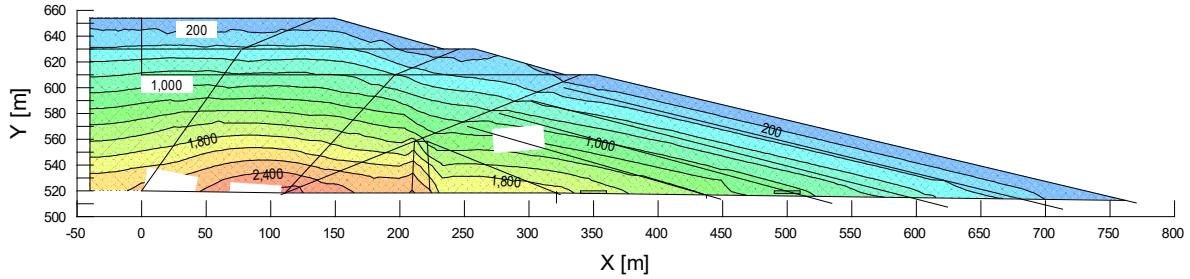

Figure 4: Maximal total stresses distribution, in kPa, for steady seepage in the tailings dam, at upper water elevation at 652.0 m, S1,max = 2,658.7 kPa

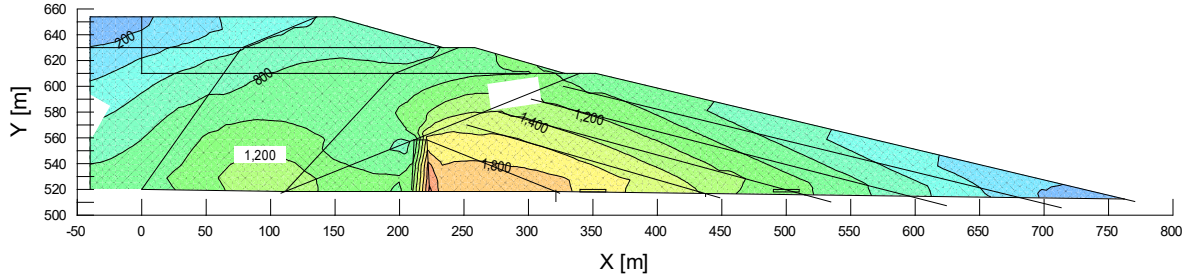

Figure 5: Maximal effective stresses distribution, in kPa, for steady seepage in the tailings dam, at upper water elevation at 652.0 m, S1`,max = 2,250.8 kPa

4 MODELING OF THE DAM RESPONSE AT ACTION OF A STRONG EARTHQUAKE - SEE

In the model for dynamic analysis of fill dams in time domain is applied program [15]. In the paper, having in mind the size and importance of dam Topolnica, as well and the available dynamic material parameters it is adopted the dynamic response of the dam to be determined by application of “Equivalent Linear Analysis” (ELA). The approach applied in the present analysis for determination of the permanent deformations during the seismic

excitation, not only for the potential sliding body, but also for any node within the fill dam, is the method of “Dynamic Deformation Analysis” (DDA), which is successive non-linear redistribution of the stresses. By such method, for geo-medium discretized by finite elements, are calculated deformations caused by forces in nodes, calculated by the incremental stresses in the elements. Thus, by application of non-linear model, for each time step of the dynamic response of the structure is obtained new state of the total stresses and pore pressure. By the differences of the effective stresses in two successive time steps are obtained incremental forces, resulting in deformations, in accordance with the chosen constitutive law for stress – strain dependence. So, for each loading case during the dam dynamic response elastic and eventual plastic strains are produced. If dynamic inertial forces cause plastic strains, then in the geo-medium will occur permanent deformations. The permanent displacements, at any point in the dam and at end of the seismic excitation, are cumulative sum of the plastic deformations.

In this analysis, for the assessment of the “Liquefaction Potential”, which is strongly influenced by the initial stress state, the "Collapse Surface Concept" (CSC) is applied. In this concept, the slope of the "Critical State Line" (CSL) in the q (p ') stress space is equal to:

$$M = (6 * \sin\varphi') / (3 - \sin\varphi') \quad (1)$$

Where:

$$q = (\sigma_1 - \sigma_3) \quad (2)$$

is a strain deviator and represents the shear of the soil material,

$$p' = (\sigma'_1 + \sigma'_2 + \sigma'_3) / 3 \quad (3)$$

is a mean effective stress, which is defined in terms of effective principal stress, and φ' is conventional peak effective strength parameter (angle of internal friction).

In the case of monotonic static loading in undrained conditions, increases in stresses occur up to the "collapse point" (CP), where the structure of the granules collapses. After the CP, a sudden increase in pore pressure occurs and the strength rapidly falls to point of "Steady State Strength" (SSS). Another way of describing this is that liquefaction is initiated at the CP. According to Sladen, D'Hollander and Krahn [16], the straight line from SSS point through the CP of a soil material at the same initial void ratio, but consolidated under different confining pressures, is called "Collapse Surface" (CS), or according to Vaid and Chern [17] and Kramer [18] is called "Flow Liquefaction Surface" (FLS).

A cyclic loading can also lead to liquefaction. With increasing of the pore-pressure (under earthquake), cyclic stress path intersects the CS. Then the material will liquefy, and the strength will suddenly fall to SSS point. The input parameters in the CSC are "steady state strength" (Css) in kPa and collapse surface angle (φ_L) in degrees, which determine the slope of the CS or FLS in the q-p' stress space, where the deviator stress for SSS is qss = 2 * Css.

According to Kramer, [18], $\varphi_L \approx 2/3\ \varphi'$. While the values for (Css) were adopted from the technical literature according to Fell [19] on the (Css) dependence of $(N1)_{60} + \Delta(N1)_{60FinesContent}$, using the method of Idriss and Boulanger [20], where corrections for fines content is based on Seed [21]. Using the data on the number of impacts N determined by the "Standard Penetration Test" (SPT) and Fines content, from the renewed geotechnical investigations, the values of (Css) for the materials in the waste lagoon were calculated and adopted in the interval of 10-20 kPa, table 1.

Table 1: Input parameters of liquefaction potential of the waste lagoon materials, according to the CSC

Number		1	2	3	4	5	6
material		gravel	clay	sand	sandy silt	silty sand	silt
Segment or region		initial dam	initial dam	tailings dam	beach	beach, lagoon	waste lagoon
φ	o	34.0	18.0	38.0	30.0	25.0	20.0
N1(60)						9.4	6.7
DN1(FC)						1.5	1.5
N1+DN1						10.9	8.2
Css	kPa				20.0	15.0	10.0
φ_L	o				18.0	15.0	12.0

With the values adopted (table 1), Critical State Line (CSL) and Collapse Surface (CS) are determined for potentially liquefied materials in the waste lagoon, and the values for the dimensionless parameter (q / p'), when the materials become liquefied, figure 6. Each zone with (q / p') above the CS is liquefied and possesses the steady state strength (SSS). Each zone with (q / p') under CS, but above SSS is potentially liquefied and can pass over CS with increasing of pore-pressure. Each zone with (q / p') under SSS is not potentially liquefiable, and when the pore pressure increases, the shear strength depends on φ' and c' - the peak effective strength parameters.

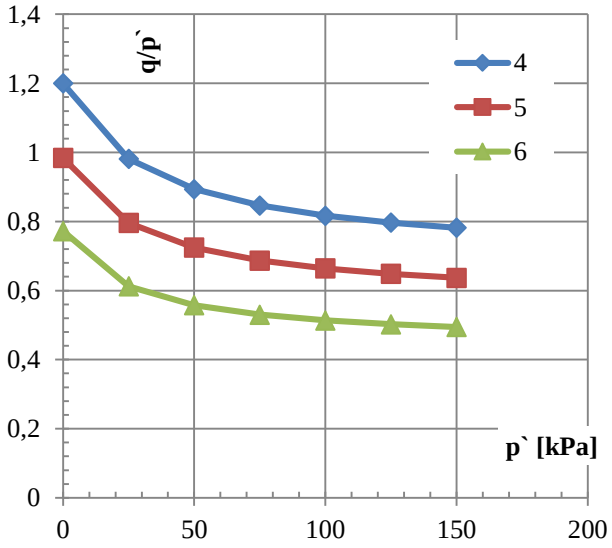

Figure 6: Values for the dimensionless parameter (q / p ') when the materials liquefied, Legend: 4 – sandy silt in beach, 5 – silty sand between the beach and lagoon and 6 – silt in waste lagoon

From figure 6, it can be concluded that the zones of the mixture of materials in the waste lagoon, with the values of the parameter (q / p ') in the interval from 0.5 to 1.2, are potentially liquefiable zones. That is, if the initial (or pre-earthquake) state yields values for (q / p ') close to 0.50 (for a silt), 0.64 (for silty sand) and 0.78 (for sandy silt), then in the event of strong earthquakes and generating an excess pore pressure, in these zones will develop the liquefaction, figure 7.

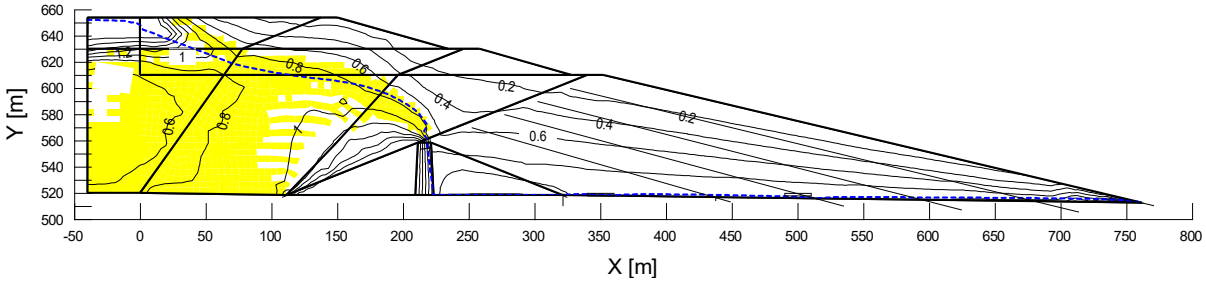

Figure 7: Distribution of the parameter q / p '[-] with the liquefaction zone, for the initial stress state and steady seepage for water level in the lagoon on 652.0 m

5 RESULTS FROM DYNAMIC BEHAVIOUR AND POST-EARTHQUAKE STABILITY ANALYSIS

Here below is presented the dam response at action of Maximum Credible Earthquake (MCE) or Safety Evaluation Earthquake (SEE) - or Synthetic earthquake Z2-EC81 (EuroCode8, type 1), with PGAx = 0.40 g, PGAy = 0.27 g, and duration of t=25 s. The dynamic response is analyzed in the crest edge of dam no. 2-2 at elevation 654.0 m, figures 8 and 9. The permanent displacement, obtained by Dynamic deformation analysis (figure 10), is key parameter for assessment of the seismic resistance of the embankment dam, and is studied in the critical point from where is possible uncontrolled emptying of the lagoon – upstream edge of the dam crest No. 2-2 at elevation 654.0 m.

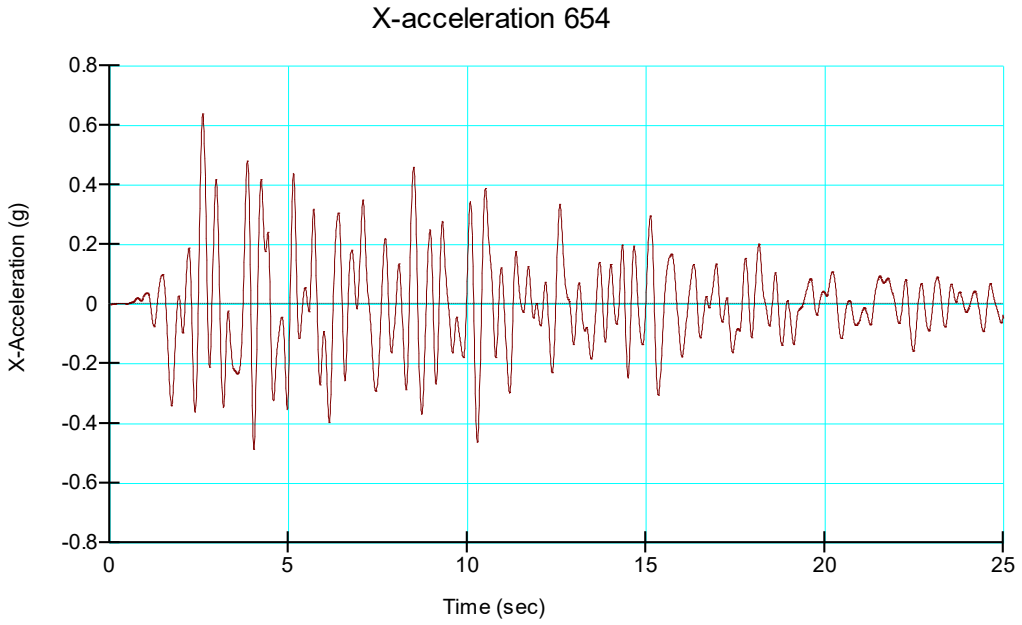

Figure 8: Absolute acceleration a [g] ÷ t [s] in a horizontal direction, dam 2-2, elevation 654.0 m

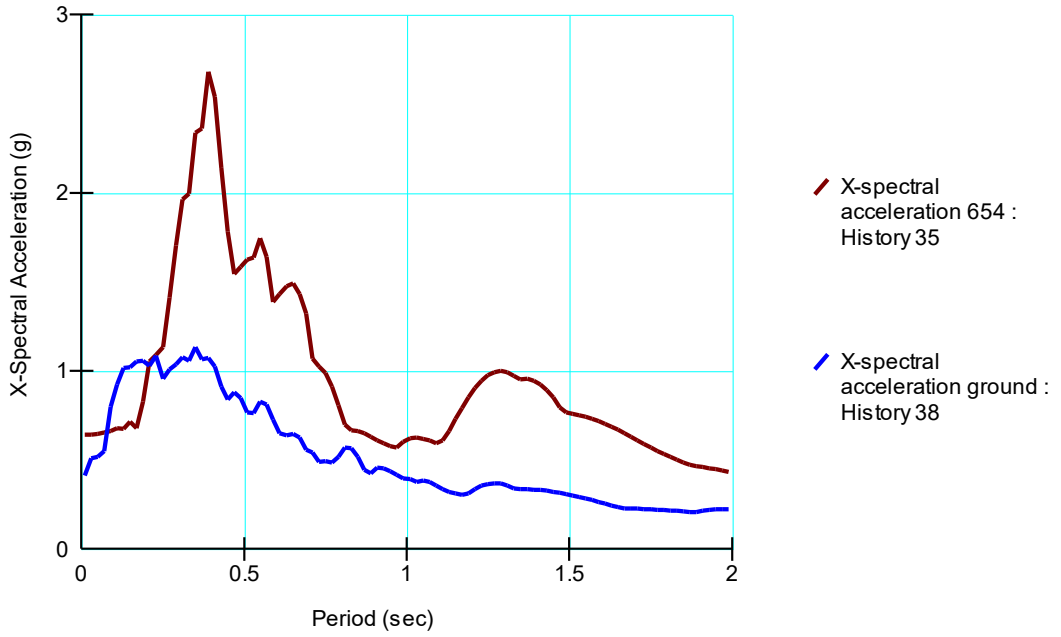

Figure 9: Spectrum of the acceleration response Sa [g] ÷ T [s] for DR = 0.05, in the rock base (excitation) and in the crown of dam 2-2 (response)

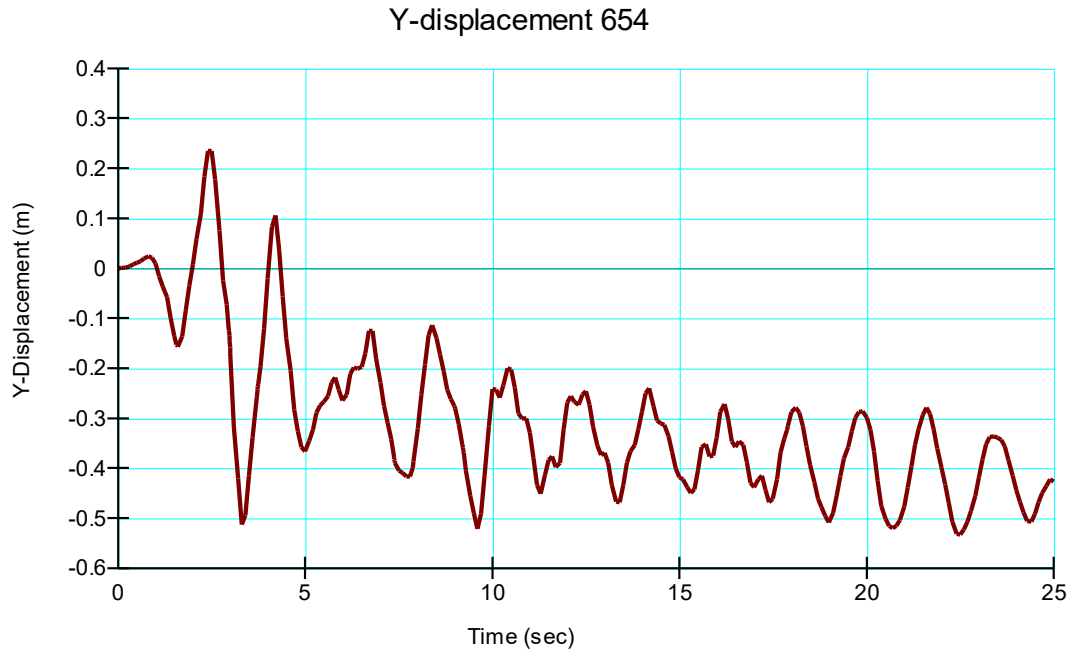

Figure 10: Permanent vertical displacements obtained by the dynamic deformation method, Y [m] ÷ t [s], in the upstream crest edge of the dam 2-2, at level 654.0 m

During the earthquake (MCE / SEE) there is an increase in the pore-pressure, creating a liquefaction zone, after the earthquake (figure 11). The appearance of liquefaction will cause redistribution of the effective stresses, which will result in post-earthquake displacements in the dam (figure 12). In order to assess the seismic resistance of the dam, the crown settlement is crucial due to the liquefaction phenomenon, estimated at about 20 cm.

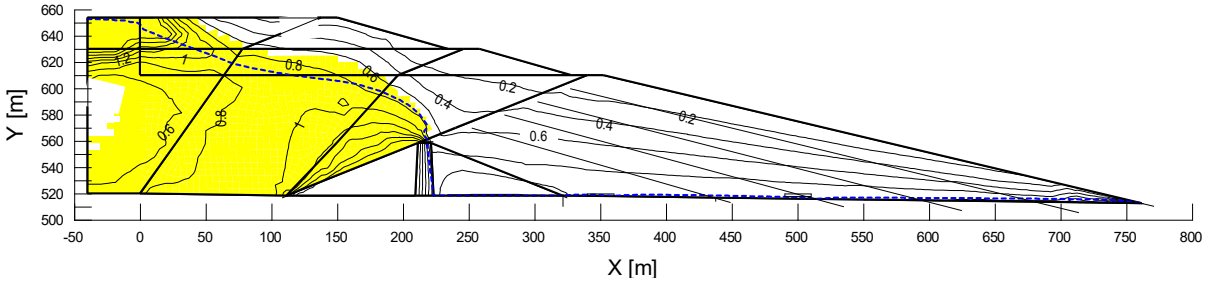

Figure 11: Distribution of the parameter q / p' [-] with the liquefaction zone after the strong earthquake

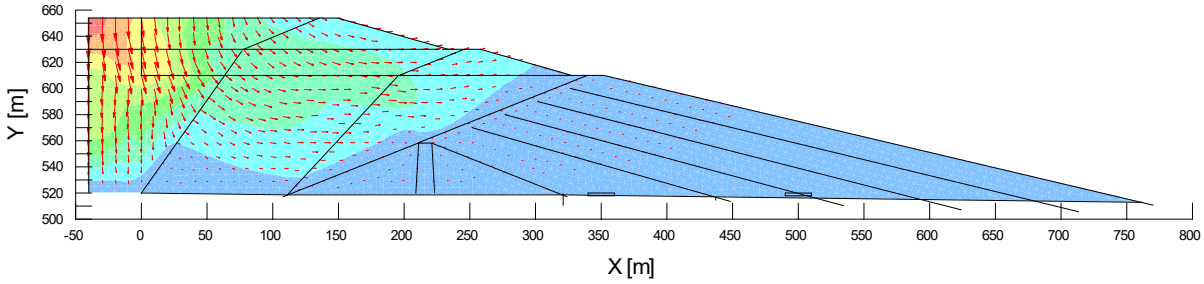

Figure 12: The direction and intensity of the resulting displacements XY, after the earthquake

The granules collapses of the liquefied materials in the waste lagoon cause change of the strength parameters (figure 13) along the critical slide surface. The increase of pore-pressure and the decrease steady state strength, after the earthquake, result to decrease of the stability of the slope [22] of the tailings sandy dam (figure 14).

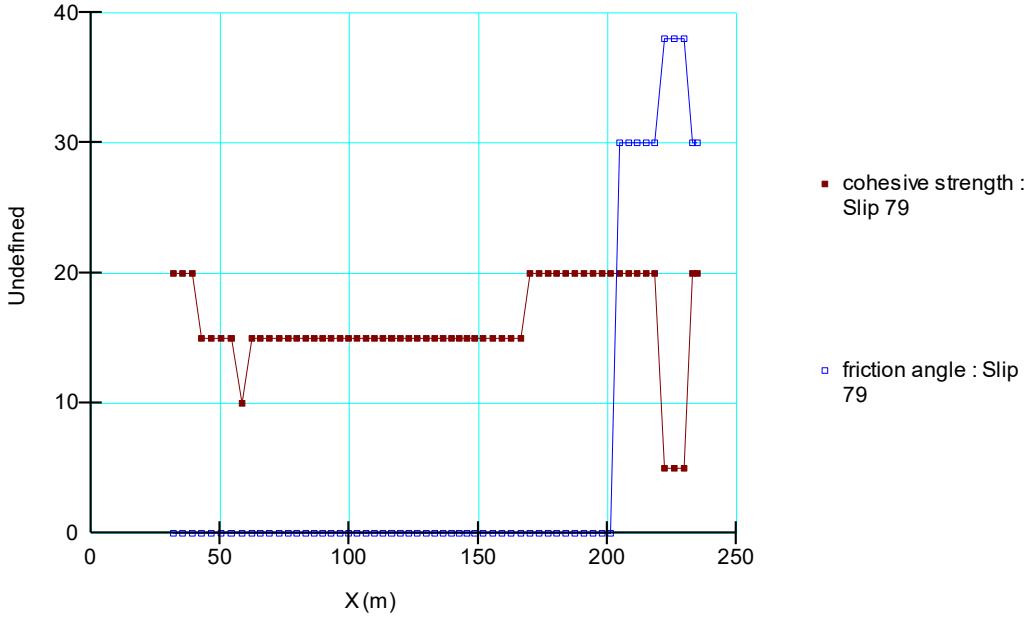

Figure 13: Distribution of strength parameters along the critical surface, cohesion in kPa and internal friction angle in degrees, after the strong earthquake

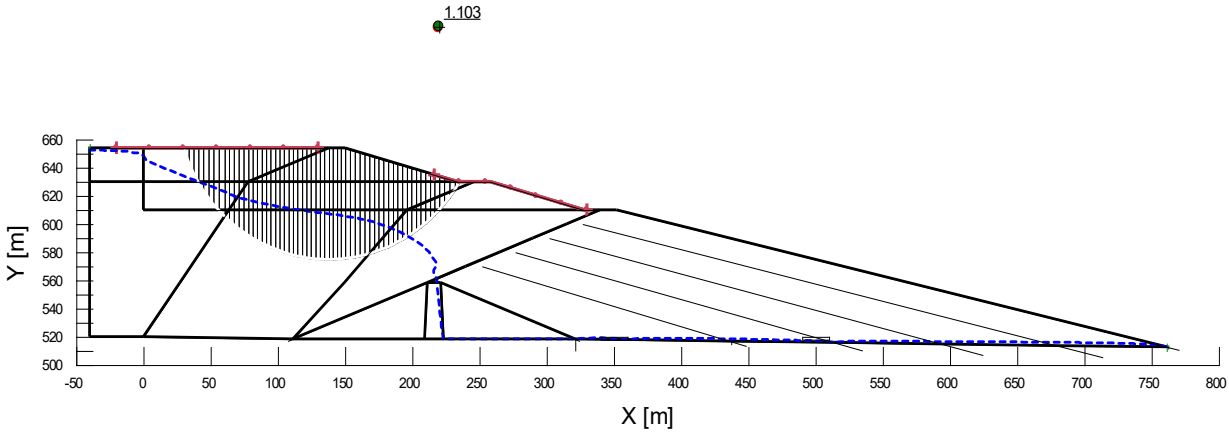

Figure 14: Critical sliding surface, in the post-earthquake phase, with a stability factor F = 1.103

6 CONCLUSIONS

The cumulative settlement in the crest at 654.0 m, caused by catastrophic earthquake, are sum of: (1) additional compaction and reduced stiffness at materials on cyclic action Y1 = 70.0 cm, calculated by previous approximate approach, (2) dissipation of the pore excessive pressure caused by the liquefaction phenomena Y2 = 20.0 cm, determined by this research, and (3) permanent displacements caused by dynamic inertial forces during earthquake Y3=50.0 cm, also determined by the present analysis. The cumulative settlements in the crest at 654.0 m are Ys =Y1+Y2+Y3=70.0+20.0+50.0 = 140.0 cm. So, the height of 2.0 m (from dam crest at 654.0 m to the highest level of tailings silt in the lagoon 652.0 mnv) is not reached, i.e. there is no danger of rapid (uncontrolled) flow of silt from the waste lagoon during action of catastrophic earthquake.

Stability factor of the downstream slope of the tailings sandy dam No. 2-2, in the post-earthquake state, with the steady-state strength in liquefied zones of the waste lagoon (according to the applied model with a water level on 652.0 m and about 150 m upstream from the crown of the dam), is 1.103. The calculated stability factor (FL) for the liquefaction event due to strong earthquake is approximately equal to the permitted value for incidentally and temporary loading (FL,per = 1.1). Therefore, the first measures to improve resistance against liquefaction, we recommend to be reduction of the normal water level elevation in the waste lagoon, from 652.0 to 649.0 m and distancing the upstream border filtration condition from 150 m to 700 m upstream from the crown of the dam no. 2-2. Our opinion is that these measures are the simplest and the most economical, and that will drawdown the steady seepage phreatic line in the foundation zone of the tailings sand dam No. 2-2 and could reduce the potential of liquefaction in the critical regions of the waste lagoon.

REFERENCES

[1] Petkovski L., Gocevski B., Mitovski S., *Comparative analysis on choice of most favorable method for tailings dam construction*, paper, IV Symposium of Macedonian Association of Geotechnics, June 25-28, Struga, R.Macedonia, Proceedings 293-300, (2014).

[2] Petkovski L., Peltechki D., Mitovski S., *Contribution to the methodology on choice of most favorable site and optimal dam type for creation of tailings*", paper, 10th Conference on water economy and hydrotechnics, Struga, R. Macedonia, Proceedings, p. 227-236, ISBN 978-608-65373-3-3, (2014).

[3] Petkovski L., Tančev L., Mitovski S., *A Contribution to the standardization of the modern approach to assessment of structural safety of embankment dams,* 75th ICOLD Annual Meeting, International Symposium "Dam Safety Management, Role of State, Private Companies and Public in Designing, Constructing and Operation of Large Dams", St. Petersbourg, Russia, Abstracts Proceedings p.66, CD-ROM (2007).
[4] Petkovski L., Mitovski S., *Creating of tailings space by stage construction of rockfill dam,* 25. Congress on Large Dams, ICOLD, Stavanger, Norway, CD Proceedings Q.98-R.4, p. 53-65, (2015)
[5] ICOLD, 1982, Bulletin 45, *Manual on tailings dams and dumps*. ICOLD, 1989, Bulletin 74: *Tailings Dam Safety Guidelines*. ICOLD, Bulletin 97: *Tailings Dam - Design of Drainage*, (1994).
[6] ICOLD, 1995, Bulletin 98: *Tailings Dams and Seismicity - Review and Recommendations*. ICOLD, 1995, Bulletin 101: *Tailings Dams, Transport, Placement and Decantation - Review and Recommendations*, (1995)
[7] ICOLD, 1996, Bulletin 103: *Tailings Dams And Environment - Review and Recommendations*. ICOLD, 1996, Bulletin 104: *Monitoring of Tailings Dams - Review and Recommendations*, ICOLD, 1996, Bulletin 106: *A Guide to Tailings Dams and Impoundments - Design, Construction, Use and Rehabilitation*, (1996)
[8] ICOLD, 2001, Bulletin 121: *Tailings Dams Risk of Dangerous Occurrences - Lessons Learnt From Practical Experiences*, (2001)
[9] ICOLD, 2011, Bulletin 139, *Improving tailings dam safety - Critical aspects of management, design, operation and closure*, (2011)
[10] Petkovski L., *Modified conventional dam in phase construction – an alternative to tailings dam*, UDK: 627.821, Original scientific paper, Watereconomy, ISSN 0350-0519, Vol. 47, No. 273-275, p. 41-50, Beograd, Serbia, (2015).
[11] Petkovski L., Mitovski S., *Structural safety of tailings dams at increasing of the deposit space,* Conference, Talinigs dams in Republic of Macedonia, MACOLD, Shtip, R.Macedonia, Proceedings, p. 89-100, (2012).
[12] Petkovski L., Mitovski S., *Numerical analysis of displacements in the post exploitation period of tailings dam with a combined construction method*, Topic - Tailings Dams, USSD 38th Annual Meeting and Conference, A balancing Act: Dams, Levees and Ecosystems, Miami, Florida, USA, CD Proceedings, (2018).
[13] Geo-Slope SIGMA/W v8, 2017. "*User's Guide for finite element stress/deformation analysis*", GEO-SLOPE International Ltd., Calgary, Alberta, Canada. (2017)
[14] Geo-Slope SEEP/W v8, 2017. "*User's Guide for finite element seepage analysis*", GEO-SLOPE International Ltd., Calgary, Alberta, Canada. (2017)
[15] Geo-Slope QUAKE/W v8, 2017."*Dynamic Modeling*", GEO-SLOPE International Ltd., Calgary, Alberta, Canada. (2017)
[16] Sladen, J.A., D'Hollander, R.D. and Krahn, J., The liquefaction of sands, a collapse surface approach, Canadian Geotechnical Journal Vol.22, pp.564-578. (1985)
[17] Vaid, Y.P. and Chern, J.C. The effect of static shear on resistance of liquefaction, Soils and Foundations, Vol. 23, pp. 47-60. (1983)
[18] Kramer S.L., *Geotechnical Earthquake Engineering*, Prentice Hall, New Jersey, USA, (1996)
[19] Fell R., et all, 2015, *Geotechnical Engineering of Dams*, 2nd edition, Taylor & Francis Group, London, UK, (2015)
[20] Idriss, I.M. and Boulanger, R.W., Soil liquefaction during earthquakes. Monograph MNO-12, Earthquake Engineering Research Institute, Oakland, Ca. (2008)
[21] Seed, H.B., Design problems in soil liquefaction. JASCE Geotechnical Engineering, Vol. 113, No. GT 8, 827–845. (1987)

[22] Geo-Slope SLOPE/W, v8, 2017. "*Stability modeling*", GEO-SLOPE International Ltd., Calgary, Alberta, Canada, (2017)

The effect of liquefaction-induced damage on an embankment: "virtual" laboratory tests

Christina Khalil[1] and Fernando Lopez-Caballero[2]

MSS-Mat CNRS UMR 8579 Laboratory, CentraleSupélec, Paris-Saclay University,
8-10 rue Joliot Curie, Gif-sur-Yvette, France
E-mail: christina.khalil@centralesupelec.fr

Keywords: liquefaction; virtual; laboratory tests; earthquake engineering practice

Abstract. *In earthquake engineering practice, the site effect simulation is evaluated based on the geometry and stratigraphy of the site, the characterization of the soil properties and the ground motions records. Usually, to identify the soil characterization, laboratory or in-situ tests take place (i.e. triaxial tests, direct shear tests, CPT or SPT …). In order to simulate these tests and in case of absence of experimental tools, numerical models can represent the response of the soil. Liquefaction, till our days, is considered as one of the most complex behaviors that happen to the soil due to sudden and severe shakings. The aim of this paper is to conduct "virtual" laboratory tests on soil samples extracted from the foundation of an embankment. They serve to a better representation of the realistic case of the soil taking into account complex input data and to a comparison with the laboratory tests for the purpose of understanding the global soil response. The numerical model used is an elasto-plastic multi-mechanism model to represent the soil behavior.*

1 INTRODUCTION

The site effects are known as the local ground response, basin effects, and surface topographic effects. In practice, either empirical models or wave propagation analysis are used to quantify these effects. It is also necessary to know i) the geometry and stratigraphy of the site; ii) the characterization of the soil properties from geotechnical or geophysical tests; iii) ground motions recorded at the site of interest (i.e. seismic hazard) and iv) the choice of soil material model [1,2, among others]. Laboratory and in-situ tests serve to characterize the soil properties. They collect data based on definite experimental or field conditions that in some cases could not reflect the realistic case. Hence, they represent a large range of uncertainties. For example, the cyclic stress-based liquefaction resistance is influenced by factors such as the soil fabric, the age, the stress-strain history [3]. These factors can be destroyed by sampling and are difficult to replicate in the laboratory [3]. In addition, in-situ tests collect data from sites that are gently sloped or not geographically complicated, so the data will be affected by site conditions or restrictions [4]. Therefore, numerical models not only help to understand the global response of the soil even if there exist a big number of input variables, but also, they serve to validate the laboratory or in-situ tests.

[2] MSS-Mat CNRS UMR 8579 Laboratory,CentraleSupélec Paris-Saclay University, E-mail: fernando.lopez-caballero@centralesupelec.fr

Otherwise, liquefaction is one of the most devastating and complex behaviors that affect the soil. When induced by seismic shakings, liquefaction is related to the volume change of the soil and to the buildup of the pore water pressure [5]. Under both static and cyclic loadings, it is considered as one of the major causes of damage for earth structures and foundations [6]. It is well known that not all the soil types are susceptible to liquefaction [3]. The soil gradation, the particle shape, the density, all are factors that influence the soil to be susceptible to liquefaction. In addition to the evaluation of the disturbance severity that initiated or triggered the liquefaction of the soil.

This paper aims to simulate virtual tests in order to find the behavior of the soil and identify the liquefaction apparition. At the beginning, a soil sample is extracted from the foundation of an embankment, and typical triaxial tests were simulated. They serve as the laboratory data input of this study. Consistency with the laboratory experiments was taking into consideration by the type of loading and experiments conditions applied. Hence, regular and irregular loading were simulated on the sample and the liquefaction resistance of the sample was identified. These ideas are developed in Sections 3 and 4. In Section 5, a study on a 1D soil column taken at free field is conducted in order to compare the behavior of the soil after the propagation of the earthquake. For this purpose, 447 real input ground motions were injected on the column and the soil behavior was tested in addition to the liquefaction resistance. Finally, an accuracy between the laboratory and the finite element methods is conducted based on statistical approach. The finite element calculations of this study were performed using the GEFDyn code [7].

2 NUMERICAL MODEL AND GEOMETRY

2.1 Numerical model

A constitutive model for soils should be able to well represent the volume change in case of drained conditions or the distribution of the excess pore water pressure in case of undrained conditions [7]. The use of numerical modelling best describes the non-linear soil behavior under cyclic loading. A good modelling takes into consideration essential properties: necessary data, an appropriate constitutive model and adequate parameters, in addition to the method that solves boundary value problems [8]. The *Ecole Centrale Paris ECP* elastoplastic multi-mechanism model (also known as Hujeux model) is the one chosen for this study and it deals with the effective stresses. The non-linearity of this model is represented by four coupled elementary plastic mechanism: three plane-strain deviatoric plastic strain mechanism in three orthogonal planes (*k* - planes) and an isotropic plane to take into account normal forces. For the sake of brevity, the details of this numerical model will not be developed, hence, more information are provided in [7] and [8].

2.2 Geometry

The geometry of the virtual model, as shown in Figure 1, consists of a soil foundation of 10 m. The shallow layer is composed of a contractive loose to medium sand of 4 m followed by a 6 m layer of a dense sand. The bedrock at the bottom of the dense sand is 5 m and has the shear wave velocity Vs = 1000 m/s. The water table is at 1 m below the ground surface. The "virtual" experimental laboratory tests were conducted first on a soil sample that has the same properties as the shallow saturated layer. Second, a model of 1D column at free field, is taken into consideration from which a soil sample extracted from the middle and bottom of this layer (i.e. 2.5 m and 4 m below the ground surface). The effect of the embankment is not taken into consideration in this paper.

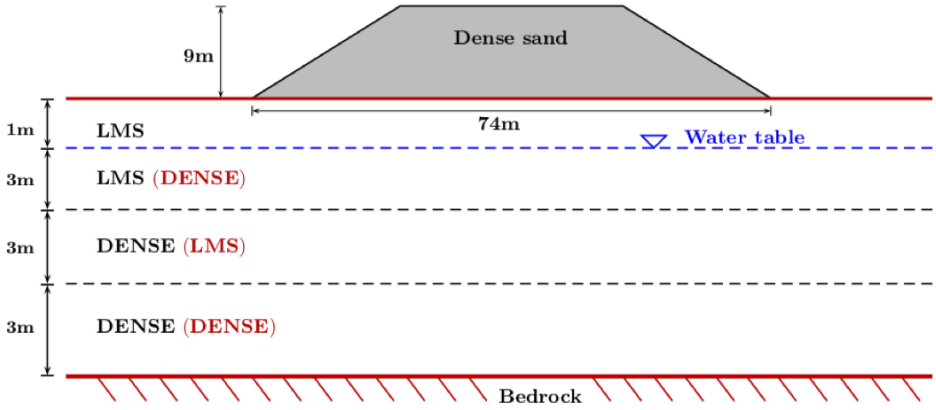

Figure 1: Model geometry

3 LABORATORY TESTS SIMULATIONS

In the development of the constitutive models, an identification of the effective stress path of the soil is important for analyzing its behavior. To do so, two approaches of liquefaction apparition are developed: the "Critical State" approach and the "Collapse Surface" approach; they are based on the effective stress path of the soil subjected to drained or undrained tests. In the drained tests, the separation between the compressive and dilative regions of the soil is called: "Characteristic Line" whereas in the undrained tests, it is called "Transformation Line" or "Critical State Line". The transformation phase of the soil occurs at the point where the stress path turns its direction in stress-strain space [9]. This point is considered critical because the soil sample has to go through at least once in order for it to reach a liquefied state. Nevertheless, different approaches have been conducted to quantify the liquefaction susceptibility. The Critical State approach is the cyclic resistance of the soil defined in terms of the required cyclic stress under which a specified amount of axial strain is developed in a given number of cycles [10]. Based on the study of [11], this amount is determined by the occurrence of 5% double-amplitude axial strain in which the state of liquefaction would be adopted. It should be mentioned that the occurrence of 2% or 3% double-amplitude axial strain is also acceptable based on other studies like [12, 10, among others]. Whereas, the second approach for liquefaction prediction is the Collapse Surface approach which defines the peak points of undrained effective stress paths surface in terms of the major and minor stresses [13]. This surface represents the limit of stability of the soil above which liquefaction will occur under load-controlled conditions, in some studies it is nominated as "Instability Line" [14,15, among others].

Similar to any common laboratory test, first, monotonic triaxial tests are conducted in order to understand the type of the material and estimate its behavior once subjected to different types of loading. Hence, drained and undrained monotonic triaxial tests were conducted (better saying, simulated) on the tested material. Notice that the triaxial test has been a preferred method to determine the soil parameters because its apparatus is widely available, and the sample behavior will always be determined because of the minimization of the non-uniformities in case of a contractive or dilative soil [13]. Different initial values of the mean effective stresses were chosen (p'_0 = 20, 50 and 70 kPa).

From the conducted test, the stress-strain path represented by the major and minor stresses (i.e. $s' = (\sigma'_1 + \sigma'_3)/2$ and $t = (\sigma'_1 - \sigma'_3)/2)$ from the undrained monotonic triaxial tests is shown in Figure 2(a), and the variation of the volumetric strain from drained monotonic triaxial tests is shown in Figure 2(b).

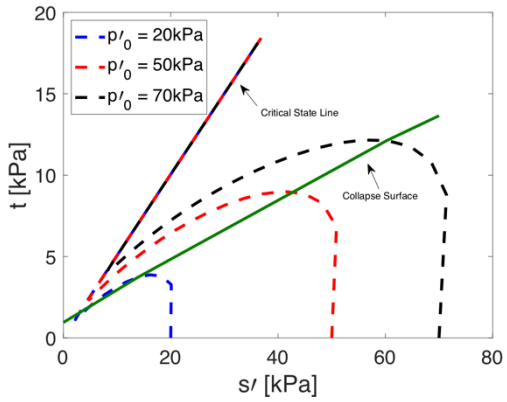

Figure 2(a): The stress path of the tested material with

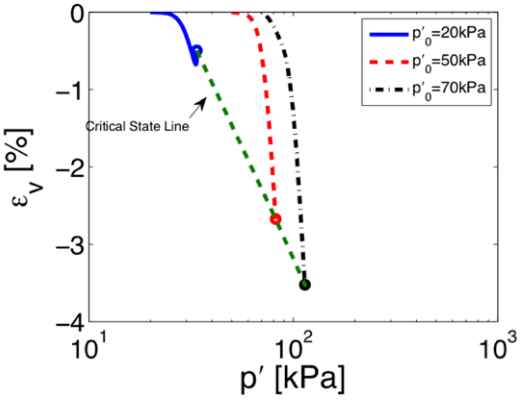

Figure 2(b): The variation of the volumetric strain respect to the mean effective stress

It can be seen from Figure 2(a) that the stress path shows a peak value until it reached the Critical State Line (CSL). From Figure 2(b), the volumetric strain decreases to reach the CSL. From these ``experimental" results, it can be viewed that the tested material is a ``normally consolidated" sand. It is true that the consolidation nomination is only applied for clay soils and is difficult to adopt for sands except for some cases [16] but in this study, the nomination of *loose* and *dense* sand refers to high or low relative density D_r as will be shown later in this section. In Figure 2(a), the collapse surface passes by the maximum stresses for each initial confining pressure. It designates the failure initiation state of the material; above this line, the material is not stable and may be subjected to liquefaction.

Moreover, in practice, the liquefaction charts are used to quantify the liquefaction apparition. These charts are characterized by the severity of the earthquake loading and the soil resistance for liquefaction [17]. The level of the loading is characterized by the cyclic stress ratio which is taken to be the ratio of the maximum cyclic shear stress to the initial effective confining pressure (i.e. $CSR = \frac{q_{cyc}}{2p'_0}$) [18,3, among others]. Whereas the soil resistance can be identified by field measurements (i.e. N-values of the SPT test, q-values of the CPT test and shear wave velocity) or laboratory tests (triaxial tests; monotonic or cyclic, drained or undrained). In the case of regular loading, which is best compatible with the laboratory experiments, different values of the cyclic shear stress were considered in order to find the soil resistance (i.e. 8, 9, 10, 11 and 12 kPa). For the sake of brevity only, one initial confining pressure is considered (p'_0 = 50 kPa). The cyclic resistance is represented in the graphs as the cyclic stress ratio versus the number of cycles N_f that generates an axial strain of 2% double-amplitude [11]. The results are shown in red curve in Figure 3.

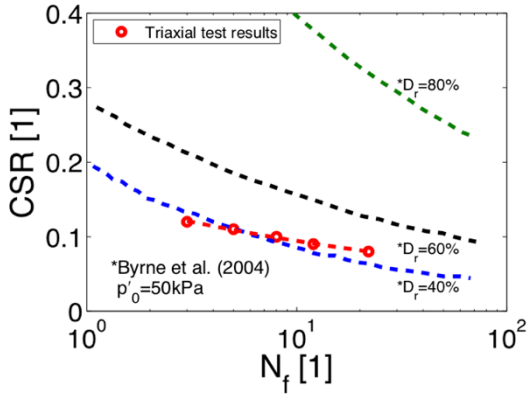

Figure 3: The Variation of the Cyclic Stress Ratio CSR as function of the number of cycles N_f

In Figure 3, a reference to an experimental study [19] conducted on Nevada sand for different values of relative densities is represented. Comparing their results to the ones simulated in this study, the cyclic resistance of the tested material lies approximately on the curve of D_r = 40%. Hence, the tested material is shown to behave as a loose sand, so it has a high tendency to generate liquefaction. The results of the cyclic resistance for regular loading will be used in the proceeding of this paper as a boundary between the combination of the loading parameter and the liquefaction resistance parameter in order to characterize the liquefaction apparition [3].

4 EFFECT OF IRREGULAR CYCLIC LOADING

Liquefaction happens due to strong shakings; therefore, the effect of the earthquakes is important to consider. Against the usual laboratory tests that only deal with sinusoidal loading, application of irregular loading represents more realistically the effect of earthquake motions by the use of ``virtual'' laboratory tests [21]. For this purpose, this section will develop the effect of irregular cyclic loading on the tested sand by conducting triaxial undrained tests and by applying different loading with earthquake shapes. An example of the used type of load is represented in Figure 4. In order to compare an irregular earthquake-induced loading with laboratory loading conditions, a conversion factor from a series of irregular cycles to uniform cycles is required. Hence, 60% of the maximum shear stress value are used in this case [13, 3, 4 among others]. The values of the shear stresses were chosen accordingly (i.e. 16, 17, 18, 19 and 20 kPa). Based on the theory, liquefaction happens due to the rapid increase of the pore water pressure [13, 3, 5, among others] or when the axial strain reaches 2% or 3% double amplitude (DA) [12, 10 among others]. Accordingly, a representation of the generation of the excess pore water pressure Δu and the variation of the axial strain $\varepsilon_1$was found as function of the number of cycles N_{cyc} of the regular loading applied (Figure 5). The initial confining pressure used for this case is also p'_0 = 50 kPa. For the sake of brevity, one tested motion will serve to analyze the soil behavior of this section and one value of the cyclic shear stress will be shown (q_{cyc} = 20 kPa).

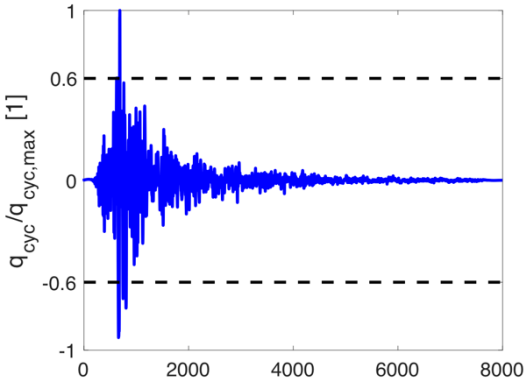

Figure 4: An example of an applied loading with earthquake shape

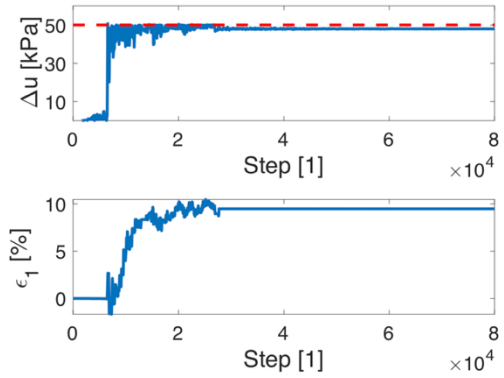

Figure 5: The variation of Δu (top) and ε_1(bottom) with respect to N_{cyc} of the irregular loading

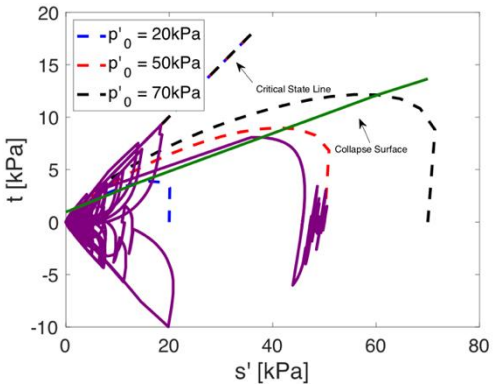

Figure 6: The stress path of the irregular loading

It can be seen from Figure 5 that the excess pore water pressure Δu increases at the beginning of the loading until it reaches the same value of the initial confining pressure of 50 kPa (i.e. the excess pore water pressure ratio r_u is equal to 1). As for the evolution of the axial strain, at the beginning of the loading, it was zero until it reaches a certain number of cycles where it shows values of 2% DA which corresponds also to the generation of the excess pore water pressure. Hence, the tested sand shows liquefaction for the presented value of cyclic shear stress and this is confirmed by the stress paths shown in Figure 6. This path shows clearly that the specimen enters an instability phase once it reaches the collapse line after which hysteretic loops starts to occur until failure is reached.

In order to identify the level of loading for all the tested motions, the cyclic stress ratio is represented in terms of the number of cycles. In the case of irregular loading, the number of cycles that generates liquefaction is different from that of regular loading (i.e. the one designated as N_f in the previous section). From the viewpoint of counting cycles in fatigue [21], the number of cycles of the irregular loading N_{equiv} is considered. Also in this case, the cyclic stress ratio becomes $CSR^*= \frac{q_{cyc}}{2p'_0}$ with $q_{cyc} = 0.6\ q_{cyc,max}$. The results are shown in Figure 7. The black dots designate the non-liquefied cases on the opposite of the blue dots that designate the liquefied cases. The red curve on Figure 7 is the boundary generated by the experimental data results developed in Section 3.

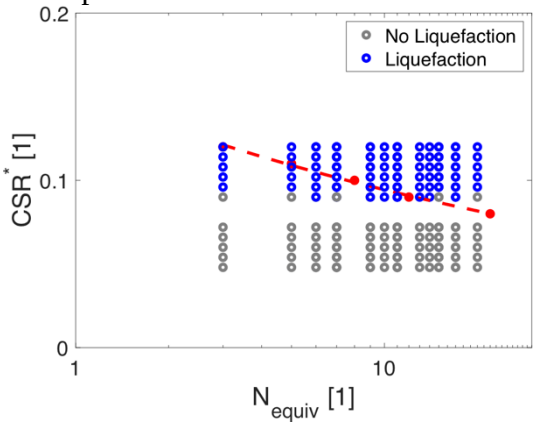

Figure 7: Cyclic stress ratio CSR* for the case of irregular loading

From Figure 7, it can be seen that the increase in the cyclic stress affects in the generation of the liquefaction in a way that the specimen tends to liquefy. The cases that are below the boundary did not liquefy, whereas for the ones above it: there are cases that liquefied and other did not.

It can be partially concluded that the laboratory tests under-estimate the soil response because the cases that were predicted to liquefy, did not do as such in the actual scenario. It should be noted that the experimental tests can also be complicated by the specimen non uniformity which causes large range of uncertainty [3]. To be more consistent with the realistic case, the behavior of the soil will be studied based simulated *in-situ* soil response. A study on a soil column will take place in the next section. Moreover, the soil response will be compared to the experimental and field data.

5 *IN-SITU* RESPONSE - STUDY ON A COLUMN

In the previous sections, the behavior of a soil sample was studied based on simulated laboratory experiments. The effect of irregular loading was taken into consideration in order to better approach the realistic case of a soil subjected to earthquake, and hence to characterize the liquefaction apparition. In this section, the behavior of the soil sample is simulated from a 1D wave propagation in a column. The finite element code used for the simulation is a 2D coupled modelling with GEFDyn Code [7] using a dynamic approach derived from the $u - p_w$ version of the Biot's generalized consolidation theory [22]. The FE element model is composed of quadrilateral isoparametric elements (0.5 m x 0.5 m). For the boundary condition of the dynamic phase, only vertically incident shear waves are introduced in the column. For the bedrock's boundary condition, paraxial elements simulating "deformable unbounded elastic bedrock" have been used [23]. To take into account the dynamic effect, 447 different ground motions were injected at the bottom of the column so that the waves will propagate all along the soil layers. For the sake of brevity only, the behavior of the soil will be studied for one tested ground motion as an example. The response of all the tested motions will be represented in the proceedings of this section. The tested soil sample was extracted from the bottom of the liquefied layer, so at 4m below the ground surface.

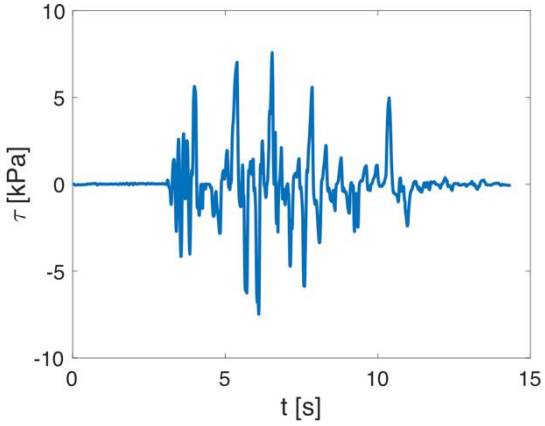

Figure 8: Obtained irregular time history of shear stress

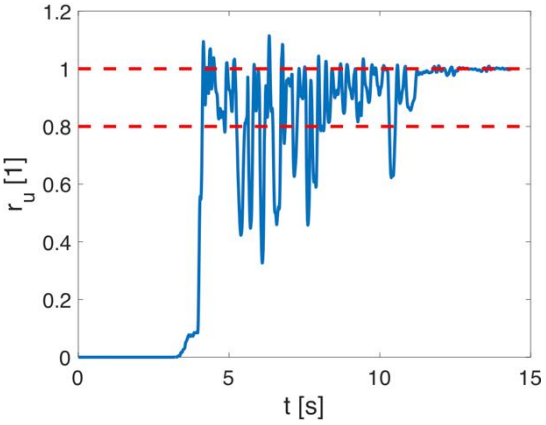

Figure 9: Excess pore water pressure time history

Figure 8 shows the variation of the obtained shear stress τ during the earthquake occurrence. It shows irregular behavior. Figure 9 shows the variation of the excess pore water pressure ratio r_u. To take into consideration the cyclic mobility and the true liquefaction, it is assumed that liquefaction appears when r_u > 0.8 [24]. For the ground motion taken as an example, it can be seen that liquefaction occurs.

Characterizing the liquefaction resistance of the soil and taking into account all the tested ground motions, the cyclic stress ratio approach is developed for this case as well. Laboratory tests show that the cyclic shear stress required to trigger liquefaction increases at high effective confining pressures [3]. [25] and [4] suggested correction factors that take into account the effect of the initial shear stress (i.e. K_α) and the effective overburden pressure (i.e. K_σ). The field corrected cyclic stress ratio for the case of this study is shown as a green curve in Figure

10. This curve will be considered as the new boundary for the coming tested cases. Studying the soil response at the bottom of the liquefied layer, the cyclic stress ratio was found for the 447 ground motions and is shown also in Figure 10. It was calculated similar to the case of irregular loading described in Section 4, in addition to the same definition of the number of cycles (i.e. N_{equiv}). Liquefaction apparition was identified based on the excess pore water pressure ratio. The motions that did not liquefy are represented in black and the ones that did, are shown in blue.

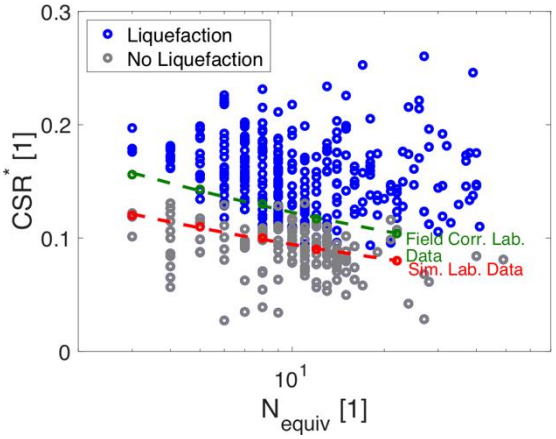

Figure 10: The cyclic stress ratio of the tested motions

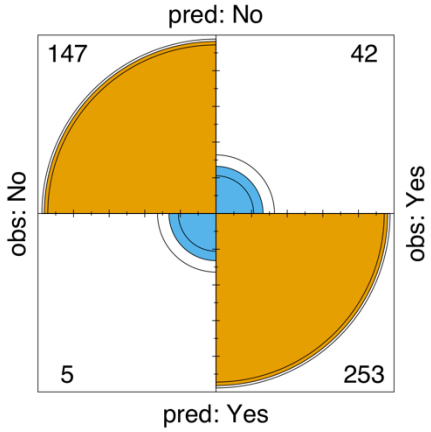

Figure 11: The confusion matrix of the tested motions

It can be seen from Figure 10 that there exist some cases where liquefaction did not occur above the field corrected boundary. In addition to some cases where liquefaction occurs below the boundary. Hence, accuracy of the laboratory tests cannot be confirmed. In order to better understand it, in addition to an understanding of the global response of the soil regarding the tested ground motions, confusion matrices were drawn and shown in Figure 11. The purpose of these matrices in the presented case of this paper, is to summarize the performance of the soil based on both the actual observations (i.e. finite element methods) and the predicted observations (i.e. laboratory tests). From Figure 11, 147 cases are not supposed to liquefy based on the predicted laboratory test and actually, they did not liquefy. These cases are called the True Negative (TN) results. Also, 253 cases are supposed to liquefy, and they liquefied based on the actual observations. Hence, they are the True Positive (TP). On the contrary, 5 cases located above the field corrected boundary did not liquefy based on the actual observations and they are called the False Positive (FP) data. And finally, the False Negative (FN) data (i.e. 42 cases) are the ones that were not supposed to liquefy since their cyclic stress ratio is below the field corrected boundary, but based on the actual observations, they liquefied. The FN data are considered as a dangerous case for the decision making. They under-estimated the response of the soil because the soil that did not liquefy in the laboratory, had a different behavior when being in-situ. The FP data are also not beneficial for the decision maker since in the laboratory the soil sample liquefied whereas when the wave propagated in the realistic case, the soil did not liquefy. This means that unnecessary precautions could be set in field if there was a reference to laboratory tests only.

Accuracy between the laboratory and the finite element method in this case, is 89.49% (i.e. (TN+TP)/(TN+TP+FN+FP)). This will lead to a partial conclusion that the laboratory tests, in some cases, under-estimate the response of the soil. This last one will be accurate when attached to numerical models for a better understanding of the soil global response.

6 CONCLUSIONS

Virtual laboratory tests were simulated in this paper via an elastoplastic multi-mechanism soil behavior model with the help of a 2D finite element code (GEFDyn). These

tests are helpful to validate the laboratory tests in order to better understand the global response of the soil.

At the beginning of this paper, the behavior of a soil sample extracted from the foundation of an embankment was found based on simulated triaxial tests. To be consistent with the realistic cases that the loading applied on the soil are not regular, loadings with earthquake shaped were simulated on the soil sample. Based on this case, the change in the behavior of the soil was analyzed. In the final section, in-situ tests were simulated on a 1D column after the propagation of 447 real input motions. The behavior of the soil at the bottom of the liquified layer was analyzed accordingly. At the end of this section an accuracy study between the laboratory and the finite element methods.

The results have shown that the studied soil sample is very loose and hence, it has an ability to liquefy rapidly. Subjected to regular loading, the cyclic resistance of the sample created a boundary that was used as a reference to characterize the liquefaction apparition. It was shown that based on irregular loading, liquefaction did not appear below the boundary whereas above it, the response depends on the severity of the irregular load.

Concerning the in-situ simulations, the results of the soil resistance show that below a field corrected boundary, the soil may liquefy whereas above it, the response will also depend on the severity of the earthquake.

As a conclusion, the laboratory tests in some cases, under-estimate the soil response but they are somehow accurate with the finite element models. Hence, for a decision making and to a good estimation of the soil response, experimental and numerical tests will be perfect.

7 ACKNOWLEDGMENT

This work, within the ISOLATE project, benefited from French state funding managed by the National Research Agency reference under program Mobility and Sustainable Urban Systems (DS06) 2017 reference No. ANR-17-CE22-0009. The research reported in this paper has been supported in part by the SEISM Paris Saclay Research Institute.

REFERENCES

[1] Lopez-Caballero, F., Razavi, A. M. F., & Modaressi, H. (2007). Nonlinear numerical method for earthquake site response analysis I—elastoplastic cyclic model and parameter identification strategy. *Bulletin of Earthquake Engineering*, *5*(3), 303.

[2] Foerster, E., & Modaressi, H. (2007). Nonlinear numerical method for earthquake site response analysis II—case studies. *Bulletin of Earthquake Engineering*, *5*(3), 325-345.

[3] Kramer, S. (2005). L.(1996). Geotechnical Earthquake Engineering. *Pren-tice Hall, New Jersey*.

[4] Youd, T. L., & Idriss, I. M. (2001). Liquefaction resistance of soils: summary report from the 1996 NCEER and 1998 NCEER/NSF workshops on evaluation of liquefaction resistance of soils. *Journal of geotechnical and geoenvironmental engineering*, *127*(4), 297-313.

[5] Ueng, T. S., Wu, M. C., Lin, C. Y., & Yu, R. Y. (2000, January). Pore water pressure changes in sands under earthquake loading. In *Proceedings of the 12th World Conference on Earthquake Engineering, Auckland, New Zealand* (Vol. 30).

[6] Papadopoulou, A. I., & Tika, T. M. (2016). The effect of fines plasticity on monotonic undrained shear strength and liquefaction resistance of sands. *Soil Dynamics and Earthquake Engineering*, *88*, 191-206.

[7] Aubry, D., Hujeux, J. C., Lassoudiere, F., & Meimon, Y. (1982, September). A double memory model with multiple mechanisms for cyclic soil behavior. In *Proceedings of the Int. Symp. Num. Mod. Geomech* (pp. 3-13).
[8] Lopez-Caballero, F., Modaressi, A., & Elmi, F. (2003). Identification of an elastoplastic model parameters using laboratory and in-situ tests. In *Deformation Characteristics of Geomaterials/Comportement Des Sols Et Des Roches Tendres* (pp. 1202-1209). CRC Press.
[9] Ishihara, K., Tatsuoka, F., & Yasuda, S. (1975). Undrained deformation and liquefaction of sand under cyclic stresses. *Soils and foundations*, *15*(1), 29-44.
[10] Pan, K., & Yang, Z. X. (2018). Effects of initial static shear on cyclic resistance and pore pressure generation of saturated sand. *Acta Geotechnica*, *13*(2), 473-487.
[11] Ishihara, K. (1993). Liquefaction and flow failure during earthquakes. *Geotechnique*, *43*(3), 351-451.
[12] Cubrinovski, M. (2011). Seismic effective stress analysis: Modelling and application.
[13] Sladen, J. A., D'hollander, R. D., & Krahn, J. (1985). The liquefaction of sands, a collapse surface approach. *Canadian Geotechnical Journal*, *22*(4), 564-578.
[14] Lade, P. V. (1994). Instability and liquefaction of granular materials. *Computers and Geotechnics*, *16*(2), 123-151.
[15] Lade, P. V., & Ibsen, L. B. (1997, October). A study of the phase transformation and the characteristic lines of sand behavior. In *Proc. Int. Symp. on Deformation and Progressive Failure in Geomechanics, Nagoya* (pp. 353-359).
[16] Biarez, J., & Hicher, P. Y. (1994). *Elementary mechanics of soil behavior: saturated remoulded soils*. AA Balkema.
[17] Sassa, S., & Yamazaki, H. (2016). Simplified liquefaction prediction and assessment method considering waveforms and durations of earthquakes. *Journal of Geotechnical and Geoenvironmental Engineering*, *143*(2), 04016091.
[18] Seed, H. B., & Idriss, I. M. (1971). Simplified procedure for evaluating soil liquefaction potential. *Journal of Soil Mechanics & Foundations Div*.
[19] Byrne, P. M., Park, S. S., Beaty, M., Sharp, M., Gonzalez, L., & Abdoun, T. (2004). Numerical modeling of liquefaction and comparison with centrifuge tests. *Canadian Geotechnical Journal*, *41*(2), 193-211.
[20] Kim, S. I., Park, K. B., Park, S. Y., Hwang, S. J., Lee, J. H., & Choi, J. S. (2005, December). Effects of irregular dynamic loads on soil liquefaction. In *16th International Conference on Soil Mechanics and Geotechnical Engineering: Geotechnology in Harmony with the Global Environment, ICSMGE 2005*.
[21] Niesłony, A. (2009). Determination of fragments of multiaxial service loading strongly influencing the fatigue of machine components. *Mechanical Systems and Signal Processing*, *23*(8), 2712-2721.
[22] ZIENKIEWICZ, C. (1991). The finite element method; solid adnd fluid mechanics. *Dynamics and non-linearity*, *2*, 219.
[23] Modaressi, H., & Benzenati, I. (1994). Paraxial approximation for poroelastic media. *Soil Dynamics and Earthquake Engineering*, *13*(2), 117-129.
[24] Rapti, I., Lopez-Caballero, F., Modaressi-Farahmand-Razavi, A., Foucault, A., & Voldoire, F. (2018). Liquefaction analysis and damage evaluation of embankment-type structures. *Acta Geotechnica*, *13*(5), 1041-1059.
[25] Seed, H. B. (1981). Earthquake-resistant design of earth dams.

Assessment of the seismic risk associated with small earth dams: a simplified approach

R.M. Cosentini[1], F. Passeri[2] and S. Foti[3]

Department of Structural, Geotechnical and Building Engineering (DISEG), Politecnico di Torino
Corso Duca degli Abruzzi, Turin, Italy
E-mail: renato.cosentini@polito.it

Keywords: Earth dam; Seismic risk; Seismic vulnerability, simplified method

Abstract. *Small earth dams are characterized by a reduced height of the retaining structure and by a limited reservoir volume of water. They are often located along slopes close to populated areas, therefore the risk associated with their potential rupture could be considerable. Also for this reason, the evaluation of their seismic vulnerability is of paramount importance for Civil Protection purposes. In addition, the usual lack of technical information represents a significant further challenge. In this regards, a simplified methodology based on a reduced number of parameters was required for vulnerability assessment studies. A simplified procedure was developed to systematically classify a large number of small earth dams. The proposed methodology is based on the compilation of data-sheets that lead to a preliminary classification of structures in terms of their associated seismic risk. The application of this procedure to about a hundred earth dams in the Piedmont region allowed identifying the most critical structures, which require a priority in the planning of further investigations and analyses.*

1 INTRODUCTION

The Italian Technical Code for Dams [1] classifies dams with respect to the maximum height of the retaining structures and the cubage of the reservoir volume of water. Dams over 15 m high or with a reservoir volume larger than 10^6 m^3 are defined "large dams", whereas dams up to 15 m high and a reservoir volume lower than 10^6 m^3 are defined "small dams". In addition, these structures can be classified according to the risk associated with their potential rupture as "strategic", "significant", and "normally relevant". These classification methods are adopted to select the parameters for their rigorous seismic analysis. In this respect, the current Italian Technical Code [2] introduces the concept of "gradualness" for seismic risk studies performed for existing structures. The choice of the analysis model to evaluate the seismic risk depends on the available information about the structure. The seismic risk assessment study can be conducted adopting models with increasing complexity, according to the level and quality of the available information. In this regards, "large dams" are characterized by a large quantity of information and data deriving from original design documents and long-time monitoring [3]. In these cases, the adoption of complex models is possible. On the contrary, the information about "small dams" are often limited and the use of simple models is usually

[2] Politecnico di Torino, federico.passeri@polito.it
[3] Politecnico di Torino, sebastiano.foti@polito.it

suggested in standard practice. The main goal of the "ReSba" (Resilienza degli Sbarramenti) project is to improve the knowledge regarding the risks of dams and the related resilience of the community. It is a project sponsored by the European fund for regional development (Interreg-ALCOTRA) for the French-Italian Alps. More than 900 dams [4] are located in the Piedmont region; approximately 100 of them are small earth dams located close to populated areas of the Alps region (Figure 1). Therefore, a criterion to identify the most critical structures that need a priority in planning further investigations and analyses is required. A simplified procedure was developed to systematically classify a high number of small earth dams. The proposed methodology is based on the compilation of data-sheets that lead to a preliminary classification of the earth dams in terms of their associated seismic risk. The present paper describes the procedure developed within the ReSba project and its application to a case study.

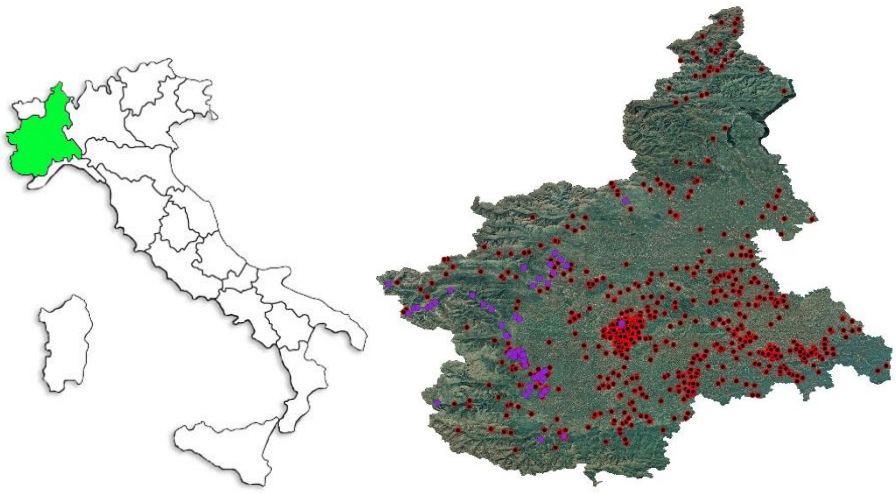

Figure 1: Localization of dams: purple dots are dams included in ReSba project.

2 SIMPLIFIED APPROACH TO EVALUATE THE SEISMIC VULNERABILITY

The most relevant earthquake-induced effects on earth dams were documented by [5] who reported the damages of these structures subjected to past seismic events. On the bases of this study, a seismic vulnerability analysis should require a deep knowledge of the structure (e.g., geometry, mechanical properties of the embankment and foundation, etc.). Therefore, a detailed analysis can be performed only for a few specific and well-characterized dams. On the contrary, when a large number of structures are under consideration, a simplified approach should be adopted.

The proposed approach is based on basic information that can be obtained through a direct survey and a collection of technical data from documents. Following this approach, the vulnerability of small earth dams is computed through an index $V_{structure}$ defined as the sum of four parameters:

$$V_{structure} = V_{condition} + V_{liquefaction} + V_{settlements} + V_{displacements} \quad (1)$$

where: $V_{condition}$ is the vulnerability of the dam due to its general state; $V_{liquefaction}$ is the vulnerability due to liquefaction phenomena; $V_{settlements}$ and $V_{displacements}$ are the vulnerability due to the potential crest settlements, and the possible slope displacements, respectively. Five classes were defined on the base of the vulnerability index of the structure (Table 1). The global seismic vulnerability (V) is then computed as the average of $V_{structure}$. This value is incremented of 0.1 if the dam is susceptible to potential hydro-geological instabilities.

Table 1: Seismic vulnerability classes of structure and levels of risk.

Vulnerability ($V_{structure}$)	Classes of vulnerability	Levels of vulnerability
≤ 1	A	Negligible
1 ÷ 2	B	Low (hydraulic leakage into the embankment)
2 ÷ 3	C	Moderate (internal erosion of the embankment)
3 ÷ 4	D	High (internal erosion of the foundation)
≥ 5	E	Maximum (freeboard reduction and overflow)

Each vulnerability parameter is evaluated as described in the following sections.

Global dam conditions. This vulnerability parameter is defined through a direct in situ inspection. Four classes have been defined on the base of deterioration phenomena affecting the body of the dam. The fifth class refers to the absence of in situ observations. Each class is linked to a value of vulnerability as indicated in Table 2.

Table 2: Value of the vulnerability due to global dam conditions.

Condition level			$V_{condition}$
1	Optimum	No crack evidence / good condition	0.2
2	Good	Small cracks but no superficial deformation	0.4
3	Discrete	Evident superficial degradation	0.6
4	Poor	Cracks, superficial deformation especially on layer lining	0.8
5	Unacceptable	No in situ observations	1.0

Liquefaction vulnerability. Generally, earth dams consist of cohesive soils that are usually not subjected to liquefaction phenomena. However, these types of soil can be subjected to shear strength and stiffness degradation under dynamic cyclic loads due to the accumulation of excess pore-pressure, with severe plastic deformation. An index related to the exclusion criteria proposed by [2] was used aiming at guaranteeing the simplicity in the evaluation of the liquefaction vulnerability. The maximum value for this vulnerability factor is adopted in case none of the previous were satisfied or in the absence of observations (Table 3).

Table 3: Value of the vulnerability due to liquefaction phenomena.

	Exclusion condition	$V_{liquefaction}$
1	Peak acceleration at the surface under free filed conditions < 0.1 g	0.0
2	Seasonal average depth of the water table in excess of 15 m below grade	0.0
3	Clean sand deposit with $(N_1)_{60} > 30$ or $q_{c1n} > 180$ (*)	0.0
4	Grain size distribution external to the zones shown in Figure 2	0.0
5	None of the previous or no in situ observations	1.0

(*) $(N_1)_{60}$ is the normalized value of N_{SPT}; q_{c1n} is the normalized cone penetration resistance (q_c).

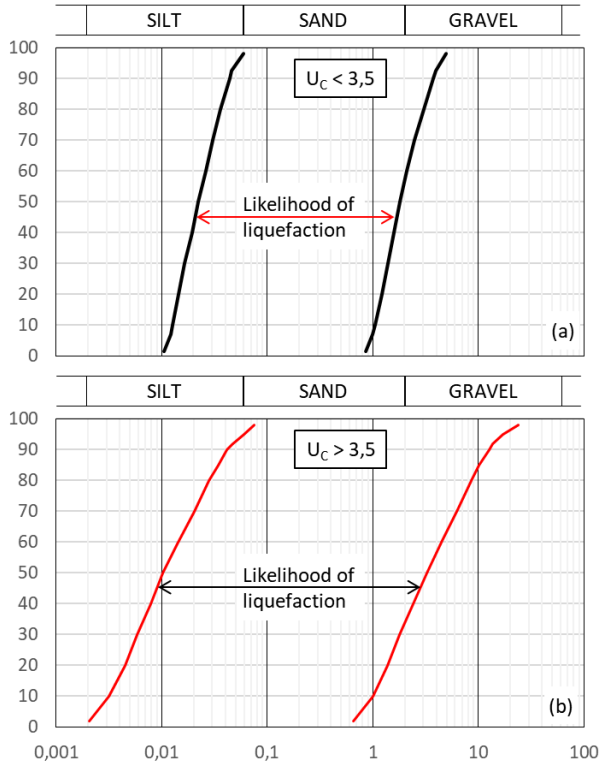

Figure 2: Grain sizes for preliminary assessment of the liquefaction susceptibility of a soil (soils of uniform grain size (a) and extended grain size (b)) [2].

Crest settlements. Two different approaches can be used to evaluate the settlements of dams under seismic loads: simplified and rigorous methods. The latter requires a very complex model and the knowledge of the mechanical properties of the soils. Due to the lack of technical information, a more simple empirical approach was here adopted for small earth dams.

The relationship (Eq. 2) proposed by [6] relates the crest settlements with the peak ground acceleration (*PGA*) and earthquake magnitude (*M*) that characterize the site:

$$w(\%) = e^{(6.07 \cdot PGA + 0.57 \cdot M - 8)} \quad (2)$$

The vulnerability due to the potential crest settlements was defined as the ratio between the predicted settlements and their admissible value. Admissible values of crest settlements have to be related to the degree of damage of dams. Following the study of [6], two values were here considered: 0.02% and 1% of the high of the dam plus the thickness of soil foundation, corresponding to moderate and serious levels of damage, respectively.

Slope displacements. Different approaches can be adopted to compute slope displacements. The simplest requires a dynamic analysis based on the well-known Newmark model [7]. This approach is commonly adopted in many empirical formulations, like the one proposed by [8]:

$$u_d = k_{max} \cdot D_{5-95} \cdot 10^{1.87 - 3.477 \frac{k_y}{k_{max}}} \quad (3)$$

where $D_{5\text{-}95}$ is the significant duration of shaking (i.e. 5-95% normalized Arias intensity), $k_{max}=PGA/g$ is the maximum acceleration and k_y is the yield acceleration of slope. This last parameter can be preliminarily estimated on the basis of the static factor of safety F_S as k_y =

(F_S – 1) sen(α), where α is the average angle of the failure surface with the horizontal. In the proposed method, $k_y = 0$ if no specific slope stability analyses are available, whereas $D_{5\text{-}95}$ is related to the magnitude (M) and the epicentral distance (r) of the earthquake through the Eq. (4) proposed by [9]

$$ln(D_{5-95}) = ln\left[\frac{\left(\frac{e^{5.04+0.851\cdot(M-6)}}{10^{1.5\cdot M-16.05}}\right)^{\frac{-1}{3}}}{15.7\cdot 10^{6}} + 0.063\cdot(r-10)\right] 0.8664 (r \geq 10km)$$

$$ln(D_{5-95}) = ln\left[\frac{\left(\frac{e^{5.04+0.851\cdot(M-6)}}{10^{1.5\cdot M-16.05}}\right)^{\frac{-1}{3}}}{15.7\cdot 10^{6}}\right] 0.8664 (r < 10km) \quad (4)$$

The vulnerability associated with the slope displacements was defined as the ratio between the predicted slope displacements and their admissible value. [8] proposed two admissible values of the slope displacements: 5 cm and 15 cm.

3 SEISMIC VULNERABILITY OF PIEDMONT EARTH SMALL DAMS: A PARAMETRIC STUDY

The proposed simplified approach was used to classify the small earth dams located in the Alps area of the Italian Piedmont Region (Figure 1). This area is included in the "ReSba" project. Initially, a parametric analysis was performed to check how the choice of admissible values of crest settlements and slope displacements influences the index of structural vulnerability. In this respect, three admissible value of crest settlements (0.02%, 0.1% and 1%) with the same amount of admissible slope displacements (5, 10 and 15 cm) were chosen.

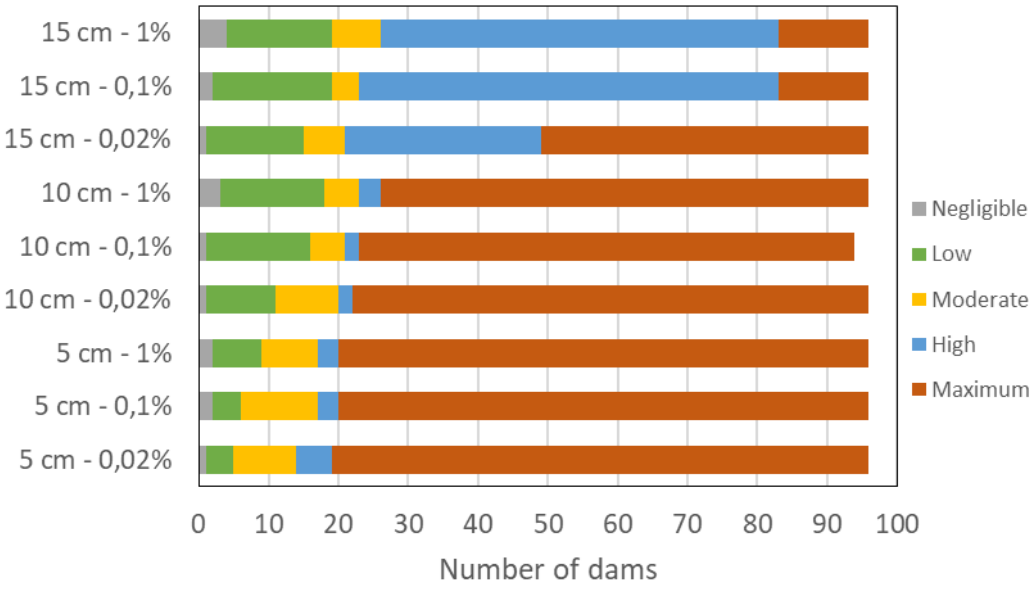

Figure 3: Comparison of risk vulnerability classification of dams assuming different admissible values of crest settlement and slope displacement.

Figure 3 shows how the classification of the seismic vulnerability of small earth dams changes with the different combination of the above admissible values. It shows that dams

within high-maximum range of vulnerability slightly decrease if the highest admissible values of crest settlement and slope displacement are assumed.

In particular, 85% of earth dams have a high/maximum level of associated risk if values of 0,02% and 5 cm are adopted as admissible values of crest settlements and slope displacements, respectively (Figure 4a). The percentage decreases to 76% (Figure 4b) if the previous admissible values are 1% and 15 cm. The percentage changes very slightly because of the lack of technical information on these dams. To guarantee cautionary analyses, lower admissible values of crest settlements and slope displacements should be adopted.

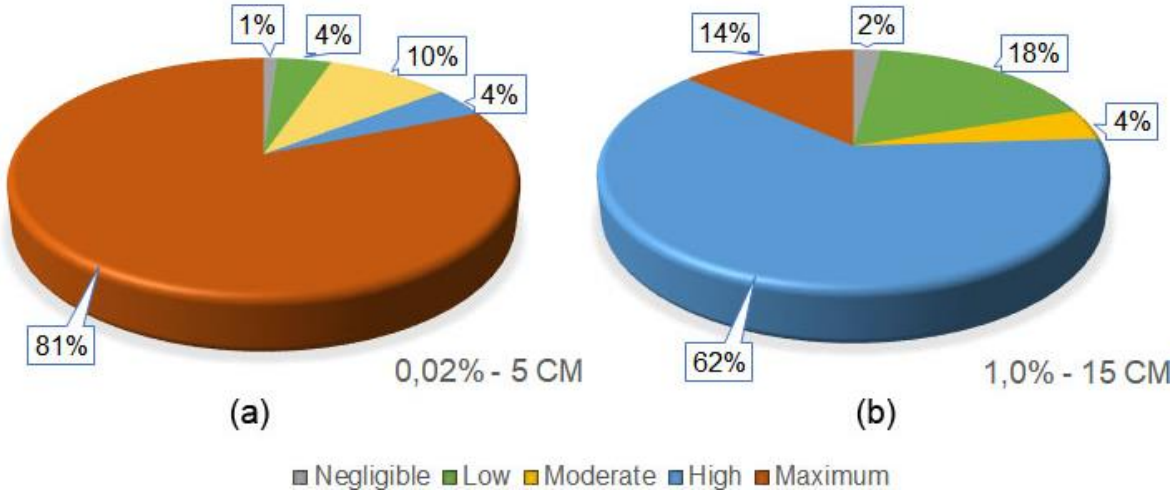

Figure 4: Comparison of risk vulnerability classification of dams assuming two different couples of an admissible value of crest settlement and slope displacement.

4 SEISMIC RISK ASSESSMENT

The seismic Risk (R) is defined as the probability of losses occurring due to earthquakes within a given period of time, and it is computed by the convolution ($\otimes$) of three quantities: $R=H \otimes V \otimes E$, where: H is the seismic Hazard; V is the seismic Vulnerability and E is the Exposure. Therefore, the seismic risk assessment of structure needs the independent evaluation of these three factors. The procedure previously described for the assessment of the seismic vulnerability assessment has been implemented in a simple data-sheet. This sheet collects all information obtained with a survey of direct observations and the analysis of the technical documents. The framework of this data-sheet is composed of four main sections:

- S1 – General information (localization and regional classification);
- S2 – Description (geometry, characteristics of the soil, exposure and seismic data);
- S3 – Calculation of the vulnerability;
- S4 – Conclusions.

Input data in sections S2 and S3 allow defining the seismic hazard, exposure and seismic vulnerability. In addition, seismic hazard and exposure are computed through simple approaches.

The hazard factor is computed as:

$$H = (4 - Z) + 1 \tag{5}$$

where Z is an integer number that represents the zone in which the earth small dam falls. Since 2003, the national territory has been classified in four seismic categories, according to the maximum outcrop acceleration with a probability of exceedance equal to 10% in 50 years

(zone 1=0.35 g, zone 2=0.25 g. zone 3=0.15 g, zone 4=0.05 g). Intermediate classes were added in 2015 when an update of this classification was released.

The exposure factor takes into account the consequences on the surrounding anthropic environment produced by potential damage or the complete collapse of the dam. Therefore, it can be defined through a simplified study of breakdown scenarios. For example, the Piedmont regional administration has defined three levels of exposure (Table 4) on the base of different scenarios [10].

Table 4: Exposure values.

Classes of exposure		E
Low	Negligible economic and environmental losses in downstream areas	1
Medium	Serious environmental consequences or significant economic losses and damage of commercial and/or industrial facilities, public services and/or structure in downstream areas (unlikely loss of life)	2
High	Losses of life and significant economic damage in downstream areas (urban areas with several inhabitants)	3

At the end of the data-sheet (section S4), the three factors that define the seismic risk are combined following a Multi-Criteria Decision Making (MCDM) protocol to evaluate the seismic criticality of the dam. In this respect, the following matrix is used:

	Vulnerability	Maximum			High			Moderate			Low			Negligible		
	Exposure	High	Medium	Low	High	Medium	Low	High	Medium	Low	High	Medium	Low	High	Medium	Low
Hazard	Zone 1	17	16	15	14	13	12	11	10	9	8	7	6	5	4	3
	Zone 2	16	15	14	13	12	11	10	9	8	7	6	5	4	3	2
	Zone 3	15	14	13	12	11	10	9	8	7	6	5	4	3	2	1
	Zone 4	14	13	12	11	10	9	8	7	6	5	4	3	2	1	0

On the base of this index, five degrees of criticality were defined (Table 5).

Table 5: Scale of seismic critical index.

Range of CS	Class of criticality	Degree of criticality
0 ÷ 4	A	Low
5 ÷ 7	B	Low – medium
8 ÷ 10	C	Medium
11 ÷ 13	D	Medium - high
14 ÷ 17	E	High

5 CASE HISTORY: EARTH DAM OF ENVIE (CN) - ITALY

The proposed approach is herein applied to a small earth dam located in the city of Envie (CN) – Italy (Figure 5).

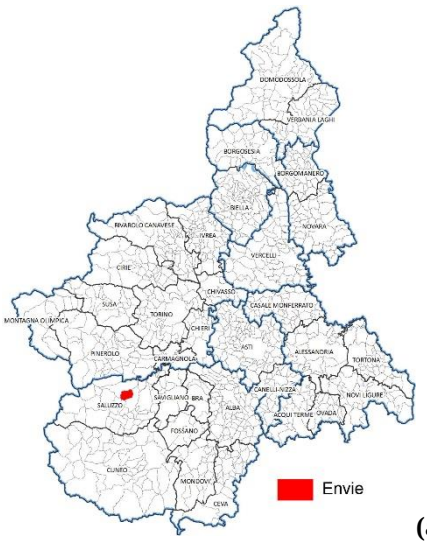

(a)

(b)

Figure 5: Earth dam of Envie: (a) Localization of dam in the regional map. (b) Overview of the dam.

The main characteristics of this dam are reported in Table 6:

Table 6: Characteristic of the dam.

Characteristics of the dam	
Crest length	155 m
Height of dam	15 m
Top width.	3.6 ÷ 13.6 m
Reservoir volume	22.000 m^3
Freeboard	1 m
Maximum top water level	349 m a.s.l.
Normal top water level	349 m a.s.l.
Soil of dam	Sandy silt

According to the Italian seismic hazard map (http://esse1.mi.ingv.it) reported here for the Piedmont region (Figure 6a), the maximum outcrop acceleration (return period of 475 years) is a_g = 0.132 g. Peak ground acceleration (*PGA*) was then computed through the simple approach proposed by [2]:

$$PGA = S_s \cdot S_T \cdot a_g \tag{6}$$

where S_S and S_T are the stratigraphic and topographical amplification factors, respectively. Considering the type of soil and the geometry of the dam (see Table 6), the values assumed for these amplification factors were: S_S = 1.6 and S_T = 1.0.

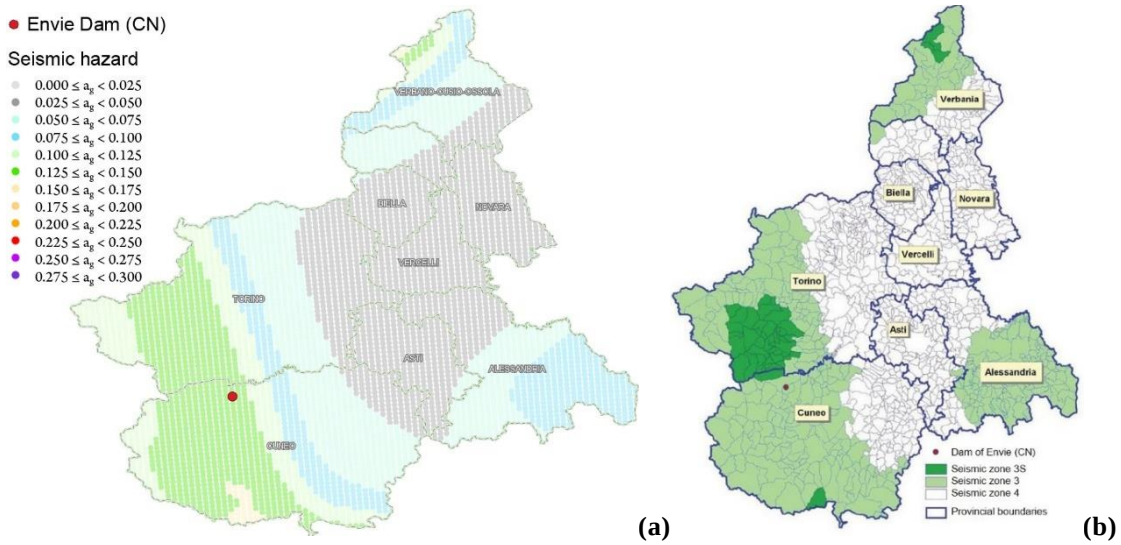

Figure 6: Localization of dam in the regional: (a) seismic hazard map and (b) seismic zonation map.

The earthquake magnitude (*M*) and the epicentral distance (*r*) were evaluated through a disaggregation analysis in accordance with the national probabilistic seismic hazard analysis (Figure 7) (http://esse1.mi.ingv.it). These average values were evaluated: M = 4.72, r = 8.23 km.

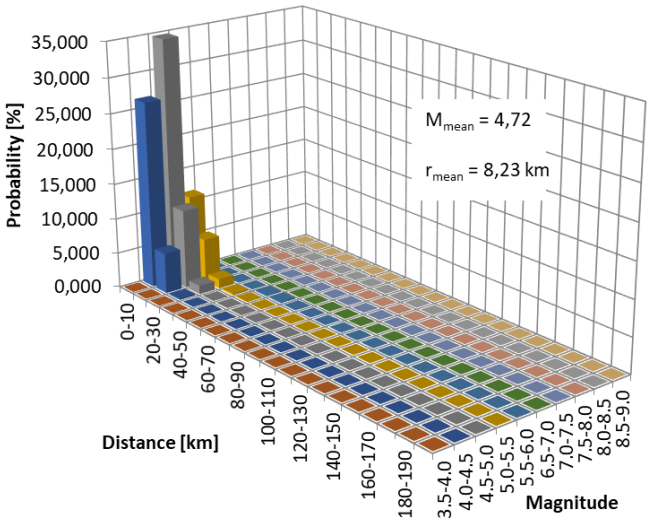

Figure 7: Disaggregation graphs referring to a return period of 475 years.

Following the above described procedure, the values of *PGA*, *M* and *r* were then used to evaluate the crest settlement (Eq. 2) and the slope displacement (Eq. 3). Assuming the most restrictive admissible values of crest settlement (0.02%) and the slope displacement (5 cm), the value of vulnerability parameters due to these aspects are $V_{settlements}$ = 0.881 and $V_{displacements}$ = 0.688. Since only small cracks without other surficial deformations were observed during a survey conducted in April 2014, the vulnerability of dam due to its general state is $V_{condition}$ = 0.4 (see Table 2). Finally, the vulnerability due to potential liquefaction phenomenon was evaluated equal to $V_{liquefaction}$ = 0.0, because the embankment was built with dense soils (q_{c1n} > 180 – see Table 3).

Therefore, the vulnerability of the dam given by Equation (1) is $V_{structure}$ = 1.97, i.e. the dam has a low level of vulnerability (Table 1). Since no potential hydrogeological instability was established, the global vulnerability is V = 0.5.

Since the whole municipality is included in seismic zone 3 (Figure 6b), the seismic hazard (E. 5) is H = 2. Instead, the level of exposure assigned to the dam is medium, due to some buildings very close to the dam (< 500m) that could be hit by the flood wave, how shown in a breakdown scenario reported in Figure 8.

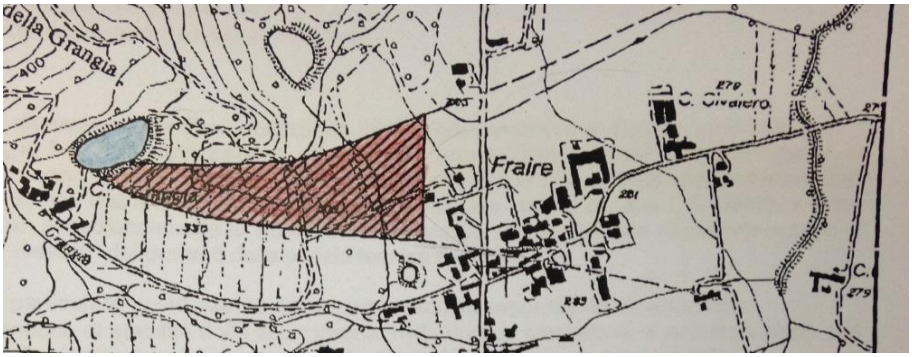

Figure 8: Breakdown scenario: the shadow zone represents the potential area hit by flood wave up to the first building.

Ultimately, following the Multi-Criteria Decision Making (MCDM) protocol, the dam of Envie is within the low-medium range of criticality.

6 CONCLUSIONS

In the present study, a simplified approach has been developed to evaluate the seismic risk of small earth dams. It is based on the quick compilation of data-sheets, where a reduced number of parameters deriving from in situ survey and documents are collected. The method allows a preliminary classification of small dams in terms of their associated seismic risk. It is very useful when a high number of structures have to be analyzed and the available technical information is lacking. The application of this procedure to about 100 earth dams in the Piedmont region allowed identifying the most critical structures that require a priority in planning further investigations.

Acknowledgments. The activity presented in the paper is part of the ReSba project sponsored by the European fund for regional development (Interreg-ALCOTRA) for the French-Italian Alps area.

REFERENCES

[1] Ministero delle Infrastrutture e Trasporti (2014). Norme Tecniche per la Progettazione e la Costruzione degli Sbarramenti di Ritenuta (dighe e traverse). Decreto 26/06/2014. Gazzetta Ufficiale Serie Gen. N. 156 del 08/07/2014.

[2] Ministero delle infrastrutture e Trasporti (2018). Aggiornamento delle «Norme tecniche per le costruzioni». Decreto 17/01/2018. Gazzetta Ufficiale Serie Gen. N. 42 del 20/02/2018.

[3] Russo, C., Costigliola R., Pagano, L. and Silvestri, F. (2017). Dighe in terra: meccanismi di danneggiamento e Stati Limiti in condizioni sismiche. XXVI Convegno Nazionale di

Geotecnica “La Geotecnica nella Conservazione e Tutela del Patrimonio Costruito”, Jun. 20-22, Roma, vol. 1, 323-333.
[4] Risba (2015) “Rischio degli Sbarramenti artificiali”. Progetto transfrontaliero Italia-Francia ALCOTRA. Regione Piemonte, Torino.
[5] Seed, H.B. (1979). Considerations in the earthquake-resistant design of earth and rockfill dams. Géotechnique 29(3), 215–263.
[6] Swaisgood, J. R. (2003). Embankment dam deformations caused by earthquakes. 7th Pacific Conference on Earthquake Engineering, Feb. 13-15, Christchurch, New Zealand.
[7] Newmark, N. (1965). Effects of earthquakes on dams and embankments. Géotechnique 15(3), 139–160.
[8] Blake, T., Hollingsworth, R. and Stewart, J. (2002). Recommended procedures for implementation of DMG. Special Publication 117 guidelines for analyzing and mitigating landslide hazards in California. ASCE Los Angeles Section Geotechnical Group. California Geological Survey.
[9] Abrahamson, N.A. and Silva, W.J. (1996). Empirical ground motion models. Report prepared for Brookhaven National Laboratory, New York, NY.
[10] Regional guidelines n.12 09/11/2004. "Regolamento regionale di attuazione della legge regionale 6 ottobre 2003, n. 25 (Norme in materia di sbarramenti fluviali di ritenuta e bacini di accumulo idrico di competenza regionale. Abrogazione delle leggi regionali 11 aprile 1995, n. 58 e 24 luglio 1996, n. 49). B.U. 11/11/2004 n. 45

Validation of the FR-JP simplified dynamic analysis

Moez Jellouli[1], Antoine des Garets[1] and Jean-Jacques Fry[2]

ISL Ingénierie
75 boulevard Mac Donald 75019 Paris, France
E-mail: jellouli@isl.fr

Keywords: Embankment dam; seismic modelling; simplified dynamic analysis, validation, CFBR, JCOLD

Abstract. *This paper presents the validation case studies of the new simplified dynamic calculation method FR-JP for embankment and rockfill dams. This method has been developed since 2014 thanks to the collaboration between CFBR and JCOLD. The main assumptions of this analysis are based on observations of the seismic performances of large dams under strong motion earthquakes and their interpretations. The feedback of Japanese dams having sustained strong earthquakes shows that four effects cannot be neglected in number of cases: (1) the damage coupled with pore pressure increase, (2) the loss of strength with shear displacement, (3) 3D vibration effects and (4) the assessment of max settlement. In comparison with usual simplified dynamic methods, this method specially includes all these four main phenomena in modeling. The validation of this analysis is based on the comparison between observed and predicted seismic performances of a large number of dams.*

1 INTRODUCTION

1.1 Interest of simplified dynamic analyses

With the periodic re-evaluation of seismic hazard assessment and the very large number of embankment dams in seismic areas over the world, it is of matter to make available to dams owners and their consulting engineers validated simplified seismic analysis methods. Here we call “simplified seismic analyse” or “simplified dynamic method”, a quick method to assess the seismic performance of embankment dams.

The pseudo-static method is a useful first step, but cannot give information on vibratory behaviour and dynamic performance of the embankment. The sophisticated effective stress analyse coupling hydraulic and mechanical behaviours in the time domain is the upmost way to simulate the dynamic behaviour of dam, however it is very time consuming, requires a lot of parameters and causes often convergence difficulties affecting the results.

Consequently, the simplified seismic analyses are widely used today. The main simplified analyses used in France are the methods of Seed & Makdisi (1978), Ambrasey & Menu (1983), Tardieu (1983) and Hyne, Griffith & Franklin (1984) derived from Sarma (1967).

[2] EDF CIH Le Bourget du Lac 73 373 Cedex, France, jean-jacques.fry@edf.fr

1.2 Limits of current simplified dynamic analyses

In 2014, with assistance of JCOLD, these methods were compared to the observed seismic performance of 2 zoned dams founded on rock:

- Aratozawa dam (H=74m) shaken by the 2008 Iwate-Miyagi Nairiku shock (M=6,9),
- Takami dam (H=120 m) shaken by shock occurring on September 26th, 2003 (M=8).

The comparison between calculated and observed performances leads to five conclusions:

1. The dynamic behaviour and the vibratory answer of the dam are highly influenced by the 3D effects, while current methods are based on 2D assumptions. The fundamental frequencies, calculated by the transfer function between recorded accelerations in gallery and those recorded on crest of the Aratozawa dam during the 2008 Iwate-Miyagi Nairiku earthquake, are consistent with 3D modal analysis (Table 1) and not with 2D analytical formulae like those proposed by Makdisi and Seed (1978).

Table 1: Comparison between calculated and measured period factors of the 3 first modes

Period	Formula	Takami dam			Aratozawa dam	
factor	Makdisi & Seed	Modal 2D	Modal 3D	Measured	Modal 3D	Measured
A1	2.6	3.1	2.1	2.1	2.7	2.7
A2	1.1	1.9	1.3	1.25	1.9	1.75
A3	0.7	1.45	1.2	unclear	1.7	unclear

2. The current methods do not predict the pore pressure generation and its impact on the performance of dams. This flaw leads to an overestimation of the dam rigidity and its accelerations under strong motion. For instance, the pore pressure generation was low at Takami and high at Aratozawa (PGA=1g), consequently the measured modulus was better predicted at Takami and overestimated at Aratozawa dam (Fig.1).

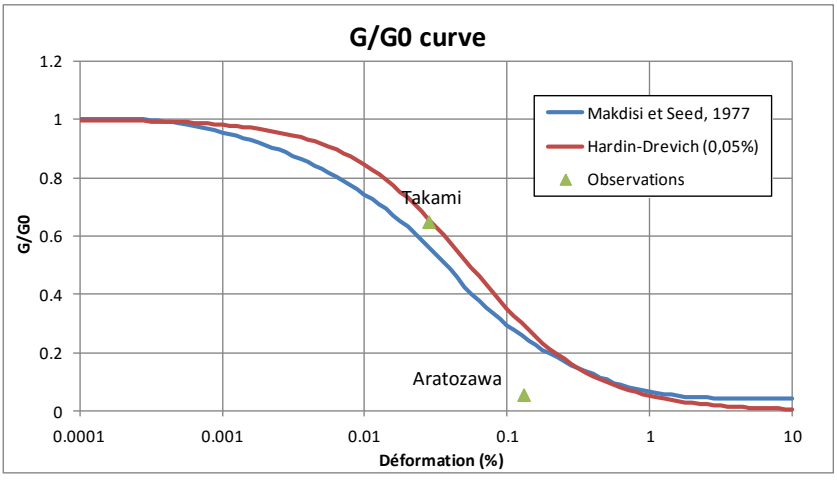

Figure 1: Measured modulus reduction compared to curves G/G0 =f(γ) from litterature

3. The current methods overestimate max permanent displacements or acceleration of zoned dams under strong motion earthquakes (Table 2).

Table 2: Calculated and measured max displacements at Aratozawa dam in 2008

Comparison	Crest acceleration (g)	Displacement along the most critical circle (cm)		
		Minimum	Medium	Maximum
Measured	0.5	0		4
Makdisi & Seed	1.18	10	26	44
Tardieu	0.54	0	2	7

4. The progressive loss of strength with shear displacement and pore pressure rise is the main hazard triggered the earthquakes. The simplified seismic analyses do not take in account this crucial phenomena.
5. Ishibuchi dam suffered large settlements (around 60 cm) shaken by the Iwate Miyagi earthquake in 2008 (M=7.0). Such settlement can cause overtopping and finally breaching of the dam, as it occurred at Fujinuma dam (2011). The simplified seismic analyses are focused on shear permanent displacements and not on large settlements.

1.3 The Fr-Jp method

Consequently, a new method was set up in order to improve the current simplified analyses by implementing the four previous phenomena. The new method is called Fr-Jp in respect to the French and Japanese Committees of Large Dams, which provide data and fruitful discussions to support its development. The new method has been described in a previous paper published in the proceedings of the first European symposium of the working group on Dams and Earthquakes [4]. This paper is an update of that article. The main concepts and equations are recalled. Emphasize will be put on the results of calibration tests on JCOLD database and on three cases studies used for validating the method.

2 DESCRIPTION OF THE FR-JP SIMPLIFIED DYNAMIC ANALYSIS

2.1 Basic assumptions of the new simplified seismic analysis

The main assumptions of this new method are:

1. The dam is a non linear elastic structure
2. The dam is founded on rock and data includes accelerogram at its base.
3. Accelerations at crest and in potential sliding mass are calculated in the time domain, by modal projection at the first fundamental modes.
4. Rigidity, damping, average shear strain and pore pressure are updated at each step.
5. Pore pressure generation and volume strain are calculated with Byrne method (1991).
6. Permanent sliding is calculated by double time integration.
7. Shear resistance decreases with pore pressure generation and permanent displacement.
8. Max permanent displacement includes sliding and compressibility settlement.

A quick and friendly tool has been developed to select quickly the input data and to use it in only some seconds.

2.2 Input data

The main input data are presented in Table 3.

Table 3: Main input data

Type	Parameter	Definition	unit
Earthquake data	a(t)	Accelerogram	m/s^2
Dam properties	G_0	Initial equivalent shear modulus of the dam	MPa
	ρ	Wet mass unit of the soil	kg/m^3
	H	Dam's height	m
	G/G_0 (γ)	Shear modulus reduction curve versus shear strain γ	-
	$\xi(\gamma)$	Plastic damping curve versus shear strain γ	%
	ξ_r	Added radiative damping	%
	A_i	Period factor of mode n°i	-
	FP_i	Participation factor of mode n°i at crest	-
	C1, C2	Byrne coefficients for pore pressure generation	-
	M	Constrained rebound tangent modulus (Byrne)	MPa
Sliding mass data	y/H	Relative depth of exit of potential sliding mass	-
	$FP_{mass\ i}$	Participation factor of mode n°i for sliding mas	-
	$k_c(L_u=0)$	Initial critical seismic coefficient k_c	-
	$k_c(L_u=0, d_{res})$	k_c at residual strength	-
	$k_c(L_u=1)$	k_c at liquefaction ratio $L_u=1$	-
	$k_c(L_u=1, d_{res})$	k_c at liquefaction ratio $L_u=1$ and at residual strength	-
	D_{res}	Permanent displacement leading to residual strength	m

2.3 Main equations

Fundamental period Ti of mode n°i is given by Equation & and notations of Table 3:

$$T_i = A_i\, H/[(G/\rho)^{0.5}] \quad (1)$$

Acceleration at crest is a_c depending on $OSC(T_i, \xi)$, the simple oscillator vibration at period T_i and damping ξ associated to the input accelerogram:

$$a_c = \Sigma\, FP_i \times OSC(T_i, \xi) \quad (2)$$

Volume strain increase $\Delta\varepsilon_v$ versus γ the average shear strain by cycle (Byrne, 1991):

$$\Delta\varepsilon_v = C1.\gamma.\exp(-C2.\ \varepsilon_v/\gamma) \quad (3)$$

Pore pressure generation Δu with M depending on the compressibility of the soil and the fluid:

$$\Delta u = M.\Delta\varepsilon_v \quad (4)$$

Shear modulus G update with L_u, the liquefaction ratio, which is equal to the generated pore pressure Δu divided by the initial effective stress σ'_0:

$$G = G[\gamma].(1-\Delta u/\sigma'_0)^{0,5} \quad (5)$$

Where G[γ] is the dam shear modulus, that depends on distortion γ and the elastic shear modulus G_0 (modulus reduction curves).

2.4 Main algorithm steps

The calculation is written in explicit numerical scheme. At each time step are calculated:

1- The first fundamental modes and frequencies (Eq. 1),
2- The participation of each mode combined to the acceleration at crest (Eq. 2),
3- The mean shear strain of the dam from displacement at crest,
4- The volume strain and pore pressure increase (Eqs. 3-4),
5- The shear modulus and the damping updating given Δu and γ at last cycle (Eq. 5),
6- The time step increment and return to step 1.

2.5 Sliding mass equilibrium

In the last step the average acceleration of the potential sliding mass is compared to its critical acceleration $k_c(L_u, d_{max})$, decreasing given the increase of liquefaction ratio L_u and the increase of permanent displacement (from peak to residual resistances of materials).

The average acceleration of the sliding mass is calculated in the same way that the acceleration at crest.

$$A_{mass} = \Sigma\ FP_{mass\_i} \times OSC(T_i, \xi) \quad (6)$$

Where OSC(Ti, ξ) is the simple oscillator vibration at period Ti and damping ξ shaken by the input accelerogram. The only difference with crest acceleration calculation stays in the values of the participation factors which can be taken from bibliography or from a finite element modal analysis. Here, the post-processing of the modal analysis gives both participation factors for acceleration at crest and for the average acceleration of a sliding mass.

2.6 Permanent displacement assessment

The components of the permanent displacement are calculated with:

1- Sliding displacement: explained just before.
2- Settlement due to volume strain: calculated as the product: $H.\varepsilon_v$ (equation 3).
3- Settlement due to deviatoric strain (still in progress).

The total settlement is the sum of the first term with the vertical component of the second and third terms.

2.7 Output data

The calculations described above lead to the time-history results of:

1. acceleration at crest ac(t) and acceleration of the given potential sliding mass, km(t)
2. liquefaction ratio Lu(t),
3. damping ξ(t),
4. shear modulus G(t) and first fundamental frequencies fn(t),
5. max permanent shear displacement dmax(t) and max settlement smax(t).

3 JUSTIFICATION PROCEDURE

3.1 First validation on JCOLD's accelerograms database

The JCOLD database (JCOLD 2015) provides recorded accelerograms on numerous dams in Japan. The accelerations, measured at several elevations of the dams' axis, are a unique opportunity to use and calibrate the new method with several seismic records. Out of the data base, 31 records on 15 dams were selected. The dam parameters are unknown.

3.2 Criteria of best fitting

The parameters of Anderson (2003), scored from 0 to 10, check the fitting of the computed accelerograms at crest to the observed ones. The parameters are (Figure 2):

C1: Arias Duration
C2: Energy Duration
C3: Arias Intensity
C4: Energy Integral
C5: Peak Acceleration
C6: Peak Velocity
C7: Peak Displacement
C8: Response Spectra (f<10Hz)
C9: Fourier Spectra (f<10Hz)
C10: Cross Correlation

Score	Verbal value
8-10	Excellent
6-8	Good
4-6	Fair
<4	Poor

Figure 2: Equivalence Score-Verbal value

The final ranking is quantified by the average score of the ten parameters and qualified (Figure 2) by the verbal scale of Kristekova (2009).

3.3 Results of the comparison

The calculated accelerograms at crest with the method are compared to the measured ones. As the material properties are unknown, they are determined with a loop.

- In the first step, the method is applied with initial assumed values of material characteristics: elastic shear modulus G_0 and radiative damping ξ.
- In the second step, these values are calibrated to improve the fitting.

The Table 3 sums up comparisons.

The calibration is from good to excellent (Figures 3 to 5). It is of matter to notice that the worst comparisons correspond in general to earthquakes with main direction bank to bank or to aftershocks.

Table 3: Score-Verbal values for all calculated earthquakes

		Goodness-of-fit		Scores detail									
Dam	**Re-cord**	**Score**	**Verbal appreciation**	**C1 DIA**	**C2 DIE**	**C3 IA**	**C4 IE**	**C5 Amax**	**C6 Vmax**	**C7 D_{max}**	**C8 SA**	**C9 FFT**	**C10 CC**
INAMURA	1	8.7	Excellent	8.0	7.7	9.7	9.9	9.6	9.1	8.9	9.5	9.0	6.0
IWAYA	1	7.6	Good	6.3	7.2	5.5	7.9	9.2	9.7	10.0	6.8	6.8	6.3
KASSA	1	9.1	Excellent	7.4	7.6	10.0	9.9	9.9	10.0	10.0	9.5	9.4	7.3
	2	7.7	Good	5.4	5.6	6.1	8.8	8.8	10.0	9.6	7.8	7.7	6.7
	3	9.0	Excellent	7.8	7.8	9.9	8.9	9.5	10.0	10.0	9.5	9.0	7.1
MIHO	4	7.4	Good	7.0	7.9	8.9	4.7	10.0	8.6	6.7	7.4	8.1	4.5
SHICHIKA-SHUKU	1	8.8	Excellent	7.7	7.5	9.2	9.1	10.0	9.9	9.7	9.7	9.5	6.1
	3	8.7	Excellent	8.2	7.3	9.7	10.0	7.4	10.0	10.0	8.8	9.0	6.7
TADAMI	1	8.8	Excellent	7.4	8.5	9.8	9.9	10.0	10.0	9.9	8.8	8.3	5.4
	2	8.4	Excellent	7.7	8.3	6.8	9.4	9.4	10.0	10.0	9.4	7.5	5.7
	3	8.4	Excellent	8.6	7.0	8.5	9.5	9.8	8.9	10.0	8.2	8.5	4.4
TAKAMI	1	8.7	Excellent	8.3	8.6	8.3	10.0	9.8	10.0	10.0	8.1	7.3	6.6
	2	8.4	Excellent	7.3	7.2	9.5	10.0	7.9	9.7	10.0	8.1	7.9	6.7
SHIMOYU	1	9.2	Excellent	8.0	8.7	9.9	10.0	10.0	10.0	9.9	9.6	8.7	7.4
TOKUYAMA	1	8.2	Excellent	7.3	8.1	7.4	7.3	8.6	9.6	9.4	8.4	8.6	7.1
NISHOUNAI	1	8.9	Excellent	7.3	7.8	10.0	9.7	9.4	10.0	9.3	9.7	8.2	7.2
TATARAGI	3	9.0	Excellent	8.4	8.3	9.9	9.5	10.0	10.0	9.8	9.5	9.3	5.2
	4	8.8	Excellent	7.7	7.3	10.0	9.9	9.8	9.8	10.0	9.7	9.6	4.7
ARATOZAWA	1	8.9	Excellent	8.4	8.3	9.9	9.3	9.8	10.0	9.9	8.8	8.7	5.4
	2	9.0	Excellent	8.4	8.4	9.9	10.0	9.9	9.8	10.0	9.7	9.0	5.0
	3	8.1	Excellent	6.9	7.0	9.1	10.0	9.1	9.6	10.0	9.4	9.5	0.1
	4	9.0	Excellent	8.8	8.6	9.5	9.9	8.4	9.8	9.9	9.8	9.3	6.4
	5	7.9	Good	6.4	7.0	9.0	8.4	9.9	9.9	10.0	6.8	8.5	3.5
	9	7.2	Good	6.1	7.1	8.4	8.1	9.8	7.8	8.1	6.0	8.4	1.8
	10	6.7	Good	3.4	4.2	9.8	6.2	9.5	10.0	9.7	6.9	6.6	0.9
	14	8.1	Excellent	7.1	5.7	9.8	9.9	9.5	9.6	9.5	9.6	8.3	1.7
	15	8.6	Excellent	8.1	8.4	10.0	8.8	10.0	9.5	9.2	9.2	9.3	3.7
	16	8.4	Excellent	6.9	7.4	7.6	10.0	10.0	9.4	10.0	9.6	8.4	5.0
	17	8.5	Excellent	6.5	6.7	7.2	9.7	9.9	10.0	10.0	9.8	8.8	6.6
	18	9.2	Excellent	8.7	8.8	9.9	9.5	10.0	10.0	9.6	9.3	9.4	6.5
	19	8.8	Excellent	8.3	9.0	10.0	9.2	9.0	9.7	9.8	9.0	9.3	5.0

Three examples of calibration are given in the figures 3 to 5.

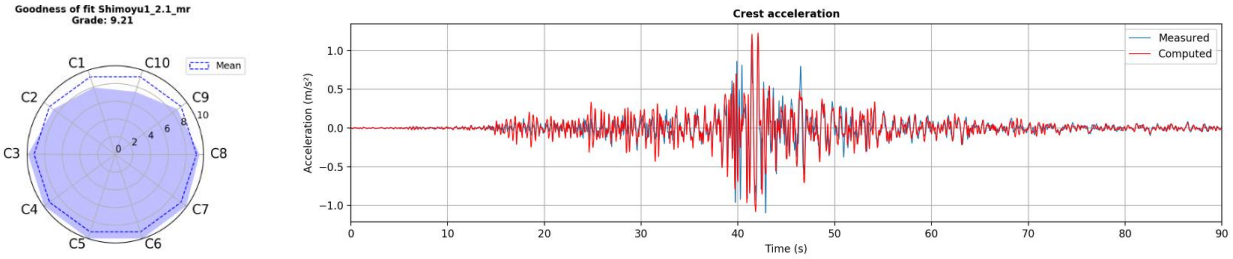

Figure 3: The best score with records of accelerogram at Shimoyu dam

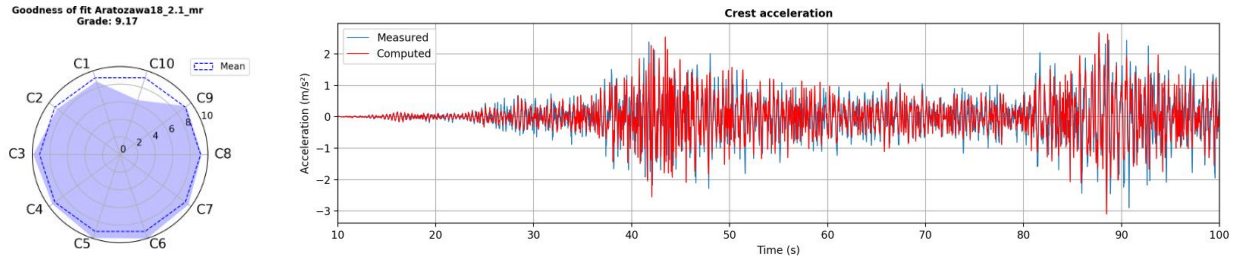

Figure 4: Excellent score with record 18 of Aratozawa dam

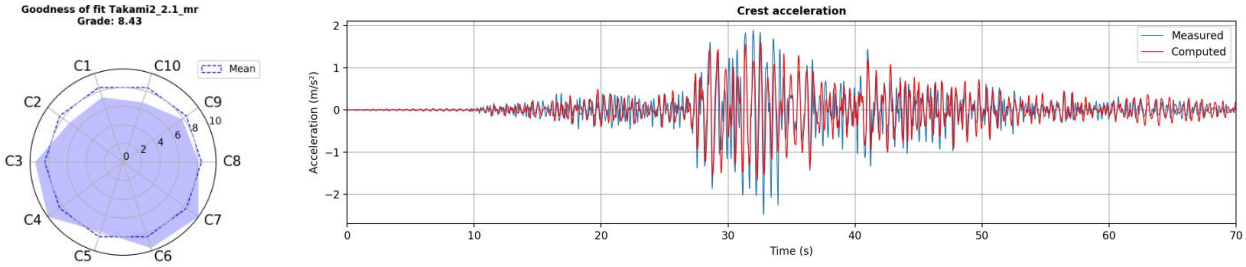

Figure 5 : Average score with record of accelerogram 2 at Takami dam

3.4 Results of calibration of dam shear modulus and radiative damping

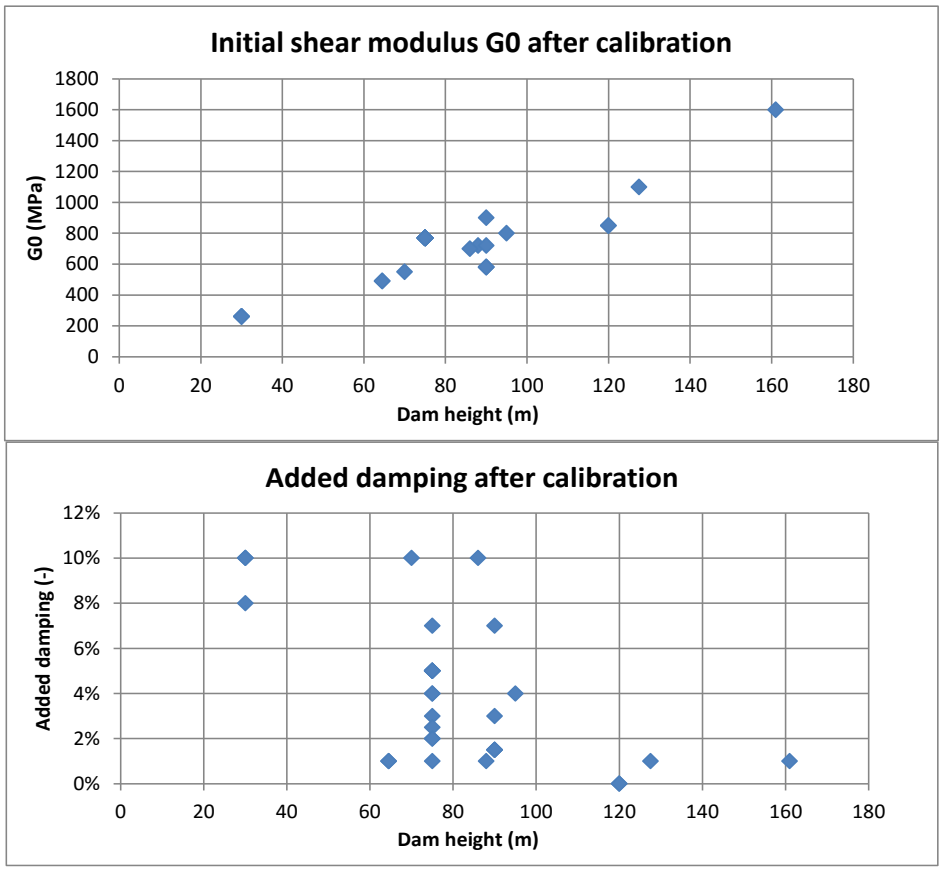

Figure 6 : Calibrated shear modulus G_0 (top) and radiative damping (bottom)

The calibrated elastic shear modulus G_0 looks proportional to the height of the dam. The calibrated added damping is between 1 and 10% of critical damping with an average of 4%.

4 VALIDATION ON THREE CASE STUDIES

4.1 Aratozawa dam, June 2008

Aratozawa dam (H=74 m) is a clay core dam with rockfill shells. It was shaken by the Iwate-Miyagi Nairiku shock (M=6,9 – $a_{U/S-D/S}$=10.2 m/s²). The stream acceleration at crest is a_c=5.25 m/s². The dam performed very well, on contrary of usual simplified analyses predictions. The max settlement of the shells crest was 20 cm. No sliding was observed. Max crest horizontal displacement was 4 cm. Calculations were carried out using this set of parameters hereunder. The main results are presented in Figures 15-19.

- G_0 = 750 MPa (corresponding to K=90 MPa)
- ρ = 2100 kg/m^3
- ξ_r = 5 %
- A1 = 2.7 ; FP1 = 2.5
- C1 = 0.5, C2 = 0.8, M = 350 MPa

Table 4: Strengths and critical accelerations

	Drained peak strength		Drained Residual strength		
	Cohesion (kPa)	Friction angle (°)	Cohesion (kPa)	Friction angle (°)	Displacement for residual strength (cm)
Shell material	0	45	0	40	20
Core material	10	30	0	27	20
k_c.g (L_u=0)	5.5 m/s²		4.5 m/s²		D_{res}=20 cm
k_c.g (L_u=1 $_{core}$)	5.0 m/s²		4.0 m/s²		D_{res}=20 cm

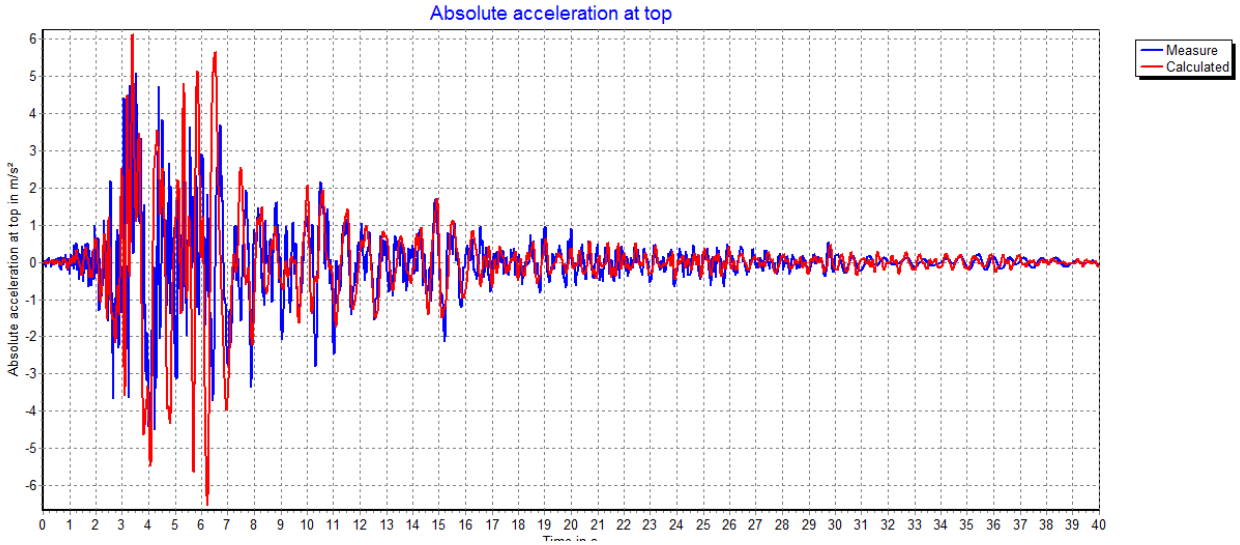

Figure 7 : Acceleration at the top and liquefaction rate

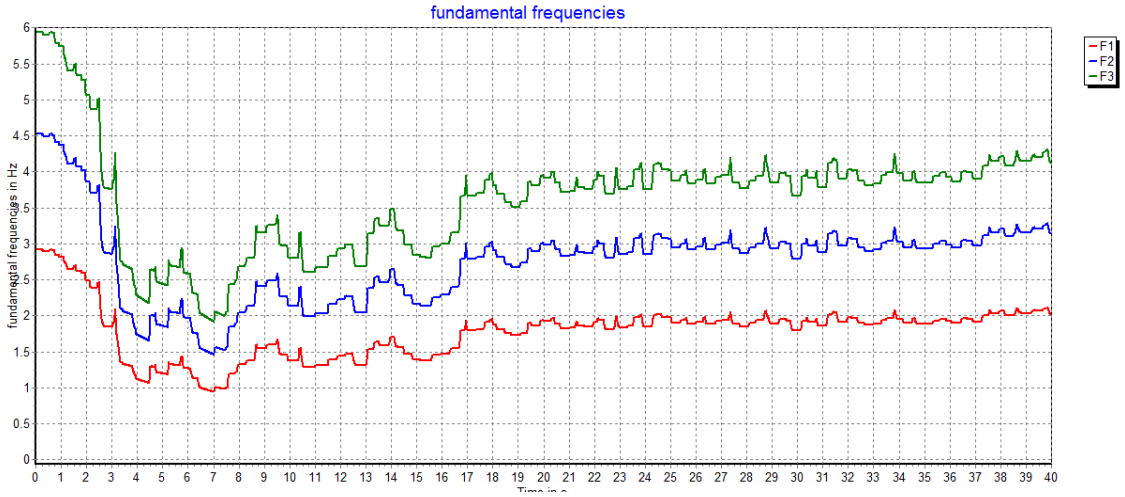

Figure 8 : First fundamental frequencies

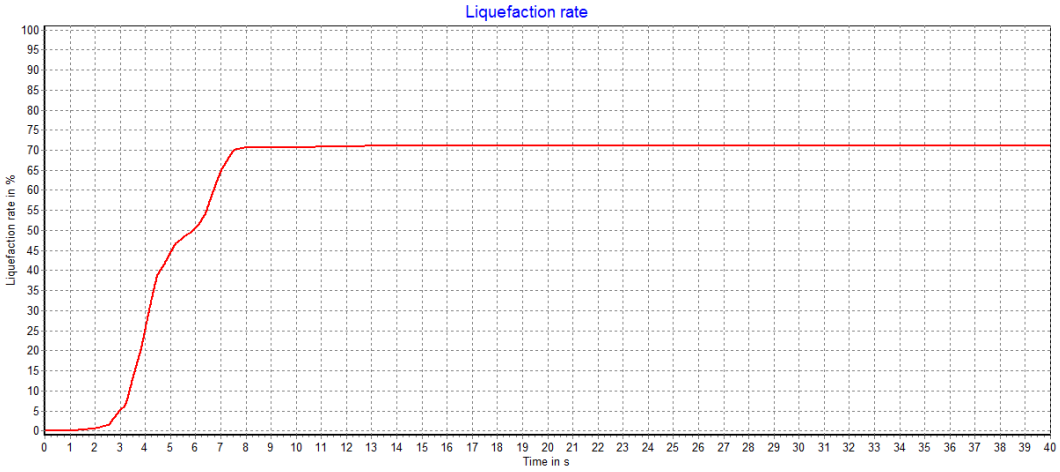

Figure 9 : Liquefaction rate evolution

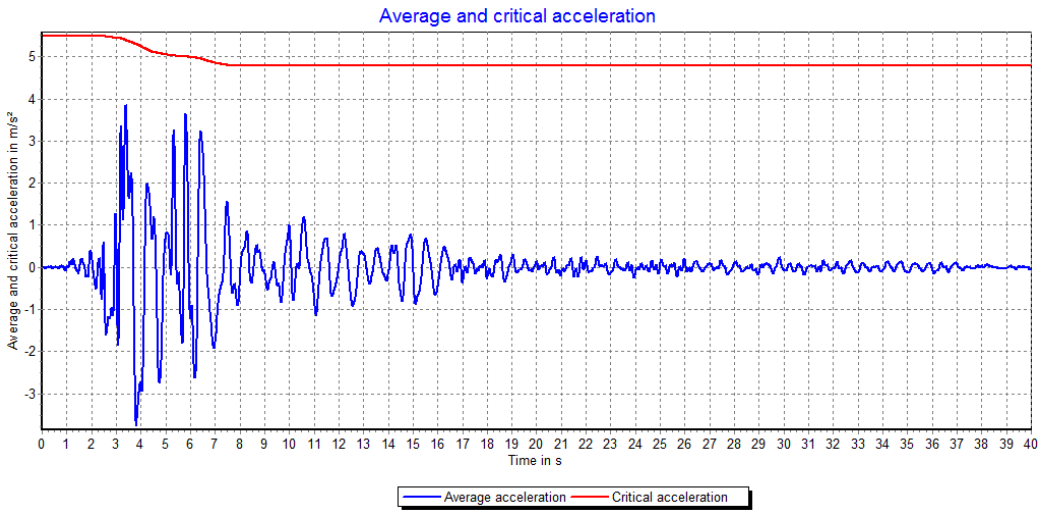

Figure 10: Average acceleration of the slipping mass and critical acceleration

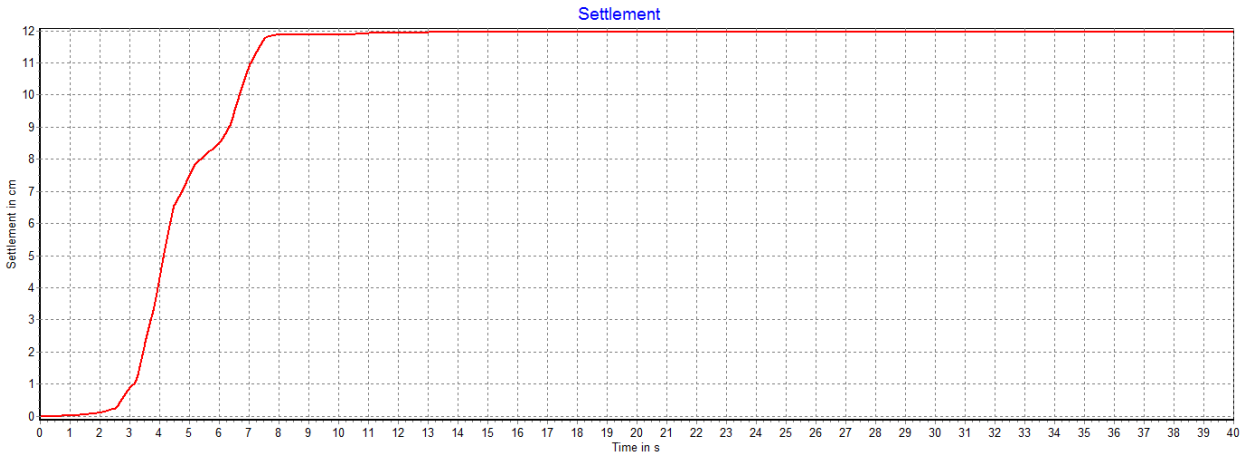

Figure 11 : Computed Settlement of the crest

There is agreement between results and observations:

- The method predicts the de-amplification of the stream acceleration at crest (all current simplified methods give computed acceleration at crest higher than the measured one).
- The fundamental frequencies are with a good agreement with those calculated from transfer function between the bottom and the top of the dam (see Table1).
- No sliding: the average acceleration of sliding mass is always under the critical acceleration.
- The settlement calculated is 12 cm. It is less than the observed one (20 cm). The deviatoric settlement, not calculated (work still in progress), could explain the gap.

4.2 Fujinuma dam

The second case study is the collapse of the Fujinuma dam (H=19m) during the Great Tohoku, M9.0, which lasts more than 100s on March 11 2011. Fujinuma dam is an unzoned earthfill dam. The construction, begun in 1937, was stopped during World War II and completed in 1949 with very poor compaction due to restrictions just after the war. It is made of three horizontal layers described below:

1. Top fill: sandy soils
2. Middle fill: silty soils
3. Bottom fill: fine sand and gravels.

The parameters taken for the calculations are presented hereunder:

- G_0=110 MPa (corresponding to K=25 MPa)
- ρ = 1600 kg/m3
- ξr = 5 %
- A1=2.7 ; FP1 = 2.5
- C1 = 0.5, C2 = 0.8, M = 60 MPa
- The modulus reduction curve G/G_0 and the damping curve related to the shear strain are taken from Tatsuoka (2016).
- The critical accelerations are assessed for initial state, damaged state (permanent displacement above 2 cm) and liquefaction state.

4. Table 6: Critical accelerations for Fujinuma dam.

State	Critical acceleration (g)
Initial	0.2
Damaged	0.1
Liquefaction	0

Unfortunately there is no records of this earthquake at the dam site. Data from the nearby station of the KiK-net database (FKSH10) was used (PGA~1g and t> 200 s).

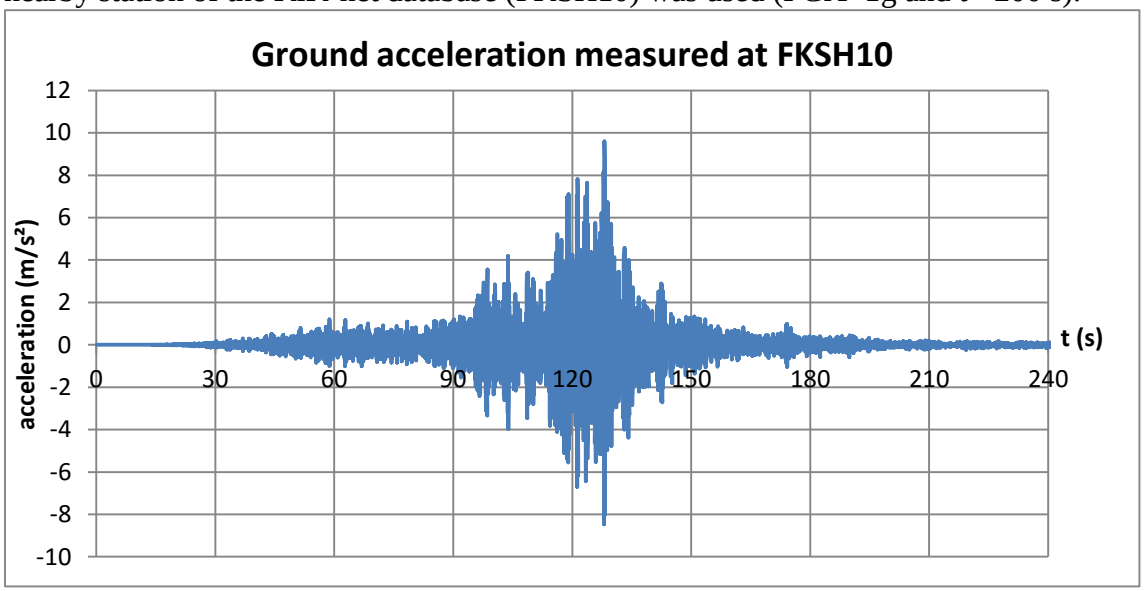

Figure 12 : Ground acceleration measured at station FKSH10 during the earthquake of 11th of march 2011

As Tasuoka and Duttine used another accelerogram, a sensitivity study is carried out on PGA by multiplying the previous time acceleration by a reduction coefficient.

4.2.1 Results with the FKSH accelerogram (PGA = 1g)

With FKSH accelerogram, calculation shows liquefaction 110 s after the beginning of the earthquake. This caused the drop of the critical acceleration, and the beginning of the slide. Settlement due mostly to the sliding leads to an overtopping and to dam breaching.

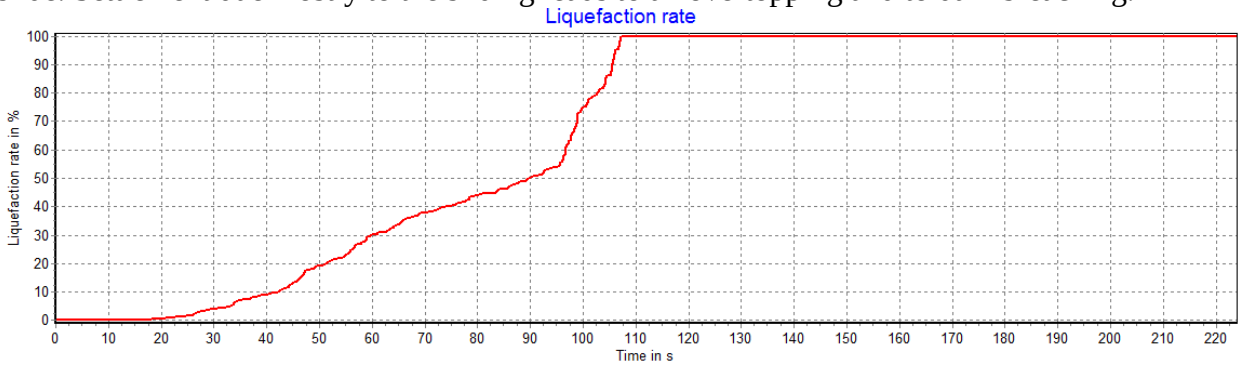

Figure 13 : Liquefaction rate calculated during the earthquake

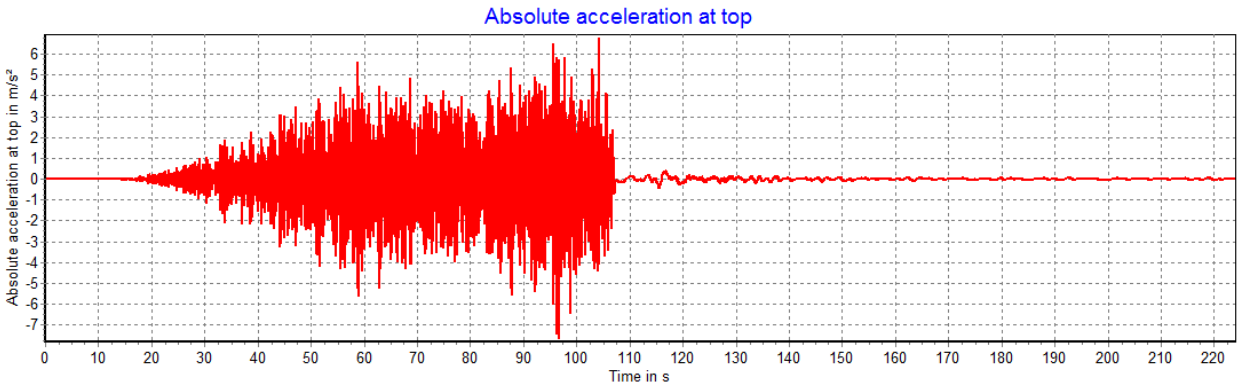

Figure 14 : Acceleration computed at the crest

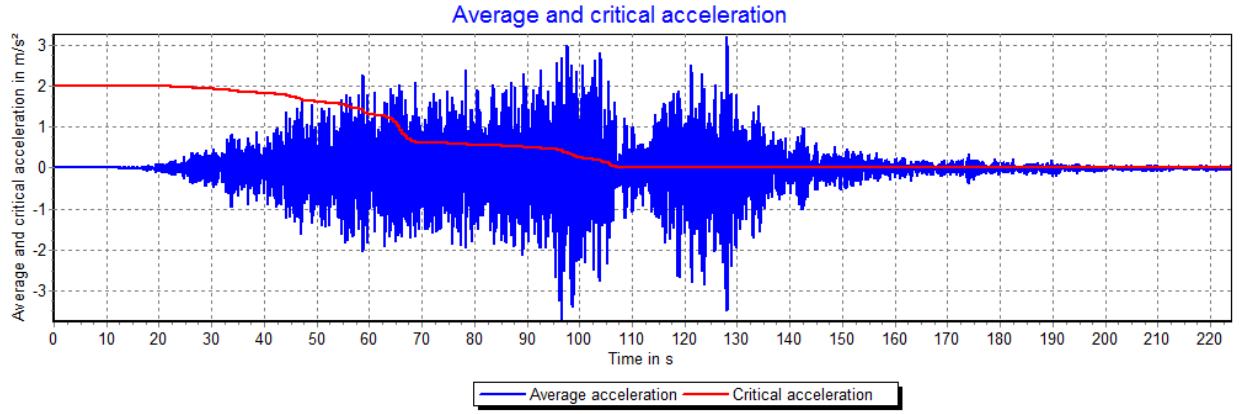

Figure 15 : Average acceleration of the slipping mass C1 and critical acceleration

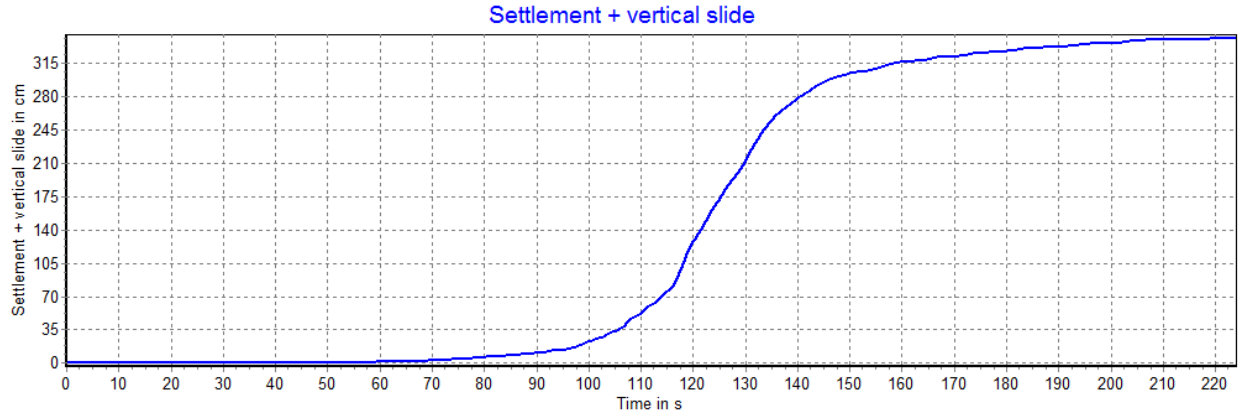

Figure 16 : Permanent sliding computed for the slipping mass C1

Maximum vertical displacement calculated for the sliding mass if 340 cm at the end of the earthquake. But this mass is still unstable at the end of the earthquake due to liquefaction and sliding can still occur after the main shock.

4.2.2 Results of the sensitivity study to PGA

In the sensitivity study, the measured accelerations at station FKSH10 are multiplied by a constant parameter varying from 0.05 to 2. The results of this study are summarized in the figures below in term of liquefaction ratio and maximum vertical settlement versus PGA.

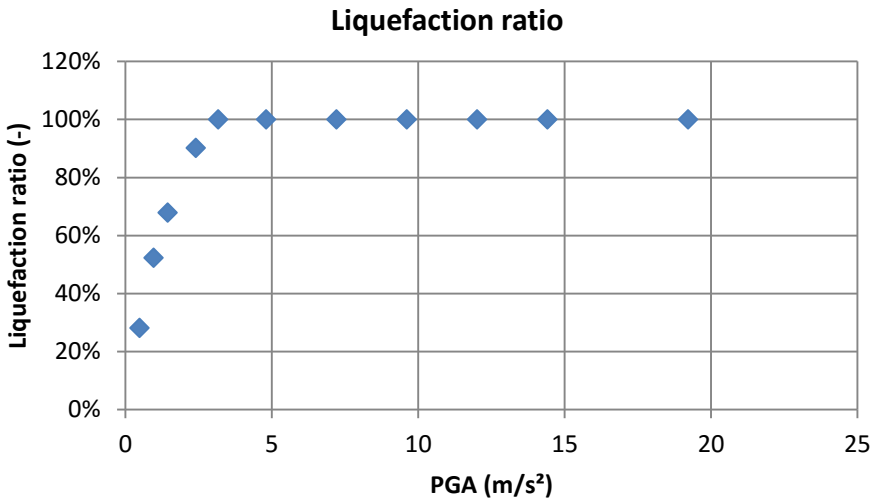

Figure 17 : Calculated liquefaction ratio versus PGA for Fujinuma dam, earthquake of 11th of march

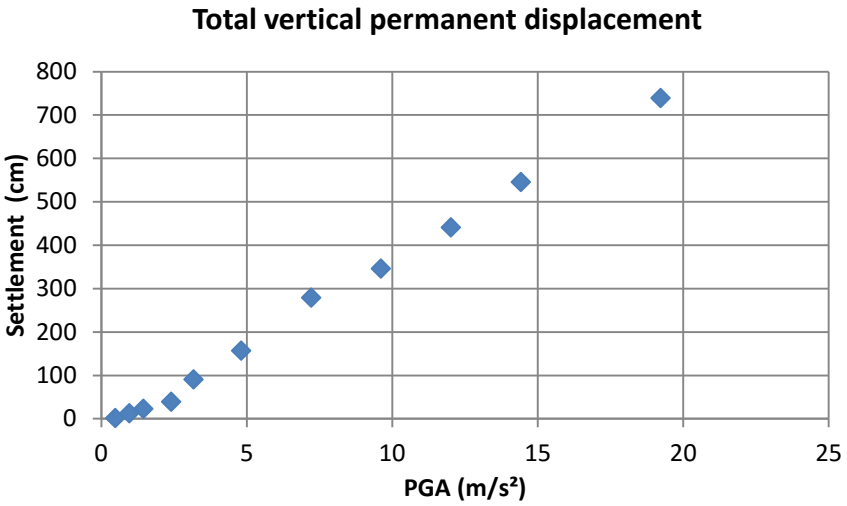

Figure 18 : Calculated settlement versus PGA for Fujinuma dam, earthquake of 11th of march

The last figures show evidence of liquefaction for PGA higher than 3 m/s². This is partially explained by the exceptional duration of the earthquake. The vertical permanent displacement begins for a PGA of 2 m/s² with a relative slow increase until PGA reaches 3 m/s² corresponding to the beginning of the liquefaction. For higher PGA, the vertical permanent displacement is very high and depends mostly on the residual shear strength after liquefaction which is almost zero in this case.

4.3 The collapse of San Fernando dam, February 1971

The third case is the collapse of San Fernando dam in February 1971. This 42m height dam is a hydraulic fill. The parameters used for calculation are the following:

- G_0 = 350 MPa (according to the calibration presented in Figure 6).
- Added damping: 5% (according to the calibration presented in Figure 6).
- Byrne parameters are taken from Byrne (1991) for a poorly compacted soil: C1 = 0.75; C2 = 0.53 and M = 260 MPa.
- A1=2.7; FP1 = 2.5.
- The critical accelerations assessed are presented in the table below:

Table 7: Critical accelerations for San Fernando dam.

State	Critical acceleration (g)
Initial	0.216
Damaged	0.150
Liquefaction	0

The acceleration was recorded at the station located at the Pacoima dam, located at 5 km from San Fernando Dam. The results are presented in the figures below.

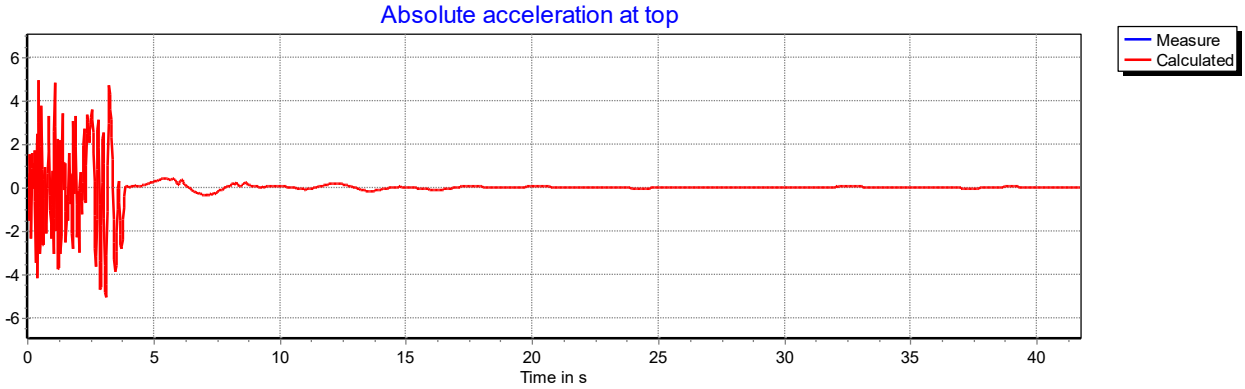

Figure 19 : Computed crest acceleration time history

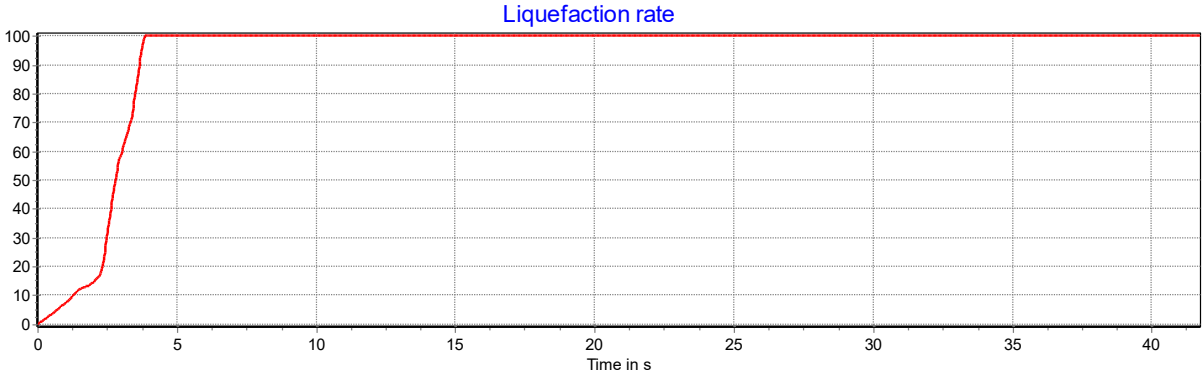

Figure 20 : liquefaction rate calculated during the earthquake

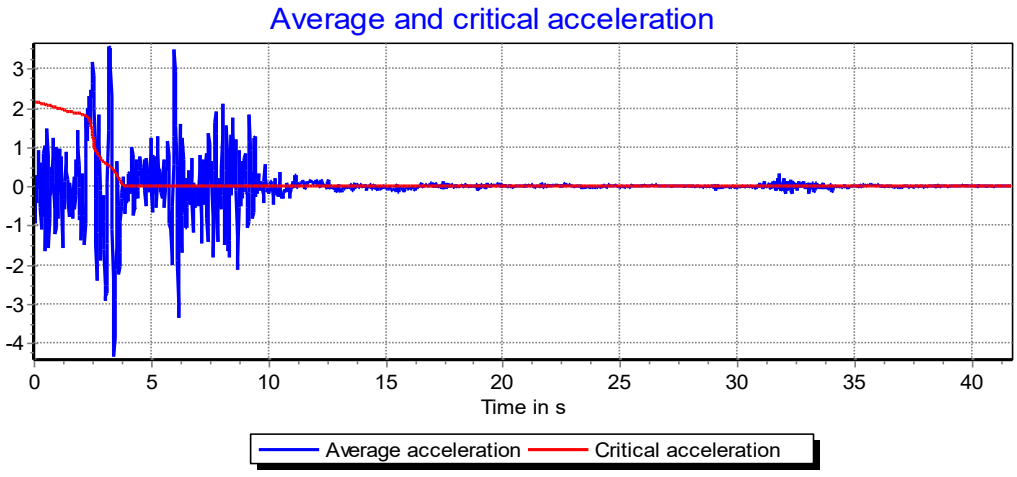

Figure 21 : Average acceleration of the slipping mass and critical acceleration

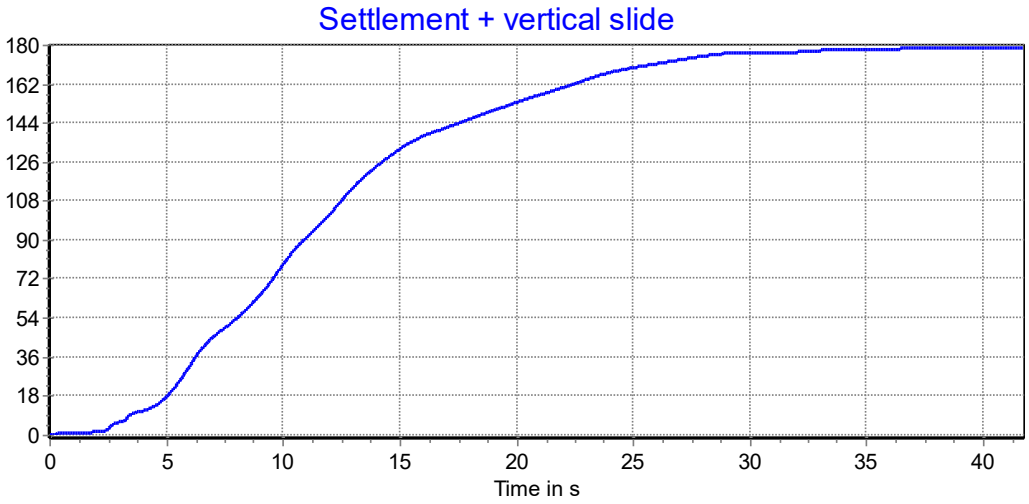

Figure 22 : Computed permanent displacements

The method predicts the liquefaction of the dam, which then leads to large permanent displacements. After liquefaction, the changes on the geometry of the dam are progressive. Although the computed vertical displacement are less than the observed one, the failure of the dam can be easily confirmed by these results.

5 CONCLUSIONS

The collaboration between JCOLD and CFBR has been a unique opportunity to develop a new simplified dynamic analysis. The main advantage of this method, compared to the previous simplified analyses, is the implementation of damage coupled with pore pressure increase, the loss of strength with shear displacement, the 3D vibration modes and the assessment of max settlement.

The method has been tested with reasonable success on 31 earthquake records given by JCOLD (2015) and can explain the observed performance of three case studies. The results are much more accurate than those obtained by other usual simplified dynamic approaches.

REFERENCES

[1] Anderson, J.G., (2004). *Quantitative measure of the goodness-of-fit of synthetic seismograms*, 13th World Conference on Earthquake Engineering Conference Proceedings, Vancouver, Canada, Paper 243.

[2] Kristekova, M., J. Kristek, and P. Moczo (2009), *Time-frequency misfit and goodness-of-fit criteria for quantitative comparison of time signals*, Geophysical Journal International, 178 (2), 813-825.

[3] Fry J-J & al. (2015) *Embankment dams: first assessment of a new simplified dynamic analysis*. 9° colloque AFPS, Marne-la-Vallée.

[4] Fry J-J, M. Jellouli, A. des Garets. (2017) *The FR-JP simplified Dynamic Analysis*. Proc. International Symposium on Qualification of dynamic analyses of dams and their equipment and of probabilistic assessment of seismic hazard in Europe, 31th August – 2nd September, Saint Malo, France (eds. Fry, J.-J. and Matsumoto, N.).

[5] Makdisi F, Seed H. (1978). *Simplified procedure for estimating dam and embankment earthquake-induced deformations*. Journal of Geotechnical Engineering, 104(7), 849–867.

[6] Ambraseys N. N., and Menu J. M. (1988). *Earthquake-induced ground displacements*. J. Earthquake Eng. 16, 985–1006.
[7] Ambraseys N. and Sarma S. (1967). *The response of earth dams to strong earthquakes*, *Geotechnique*, 17,181-213.
[8] Byrne, P. M. (1991). *A cyclic Shear-Volume Coupling and Pore Pressure Model for Sand* Proceeding. Second International Conference on Recent Advances in Geotechnical Earthquake Engineering and Soil Dynamics. March 11-15.St.Louis, Missouri, Paper No.1.24.
[9] Newmark, N.M. (1965). *Effects of earthquakes on dams and embankments*, Geothechnique, 15(2), 139-160.
[10] Tatsuoka, F., Tanaka, T., Ueno, K., Duttine, A., and Mohri, Y. 2016, *Soil properties and seismic stability of old and new Fujinuma dams*, Proc. International Symposium on Qualification of dynamic analyses of dams and their equipment and of probabilistic assessment of seismic hazard in Europe, 31th August – 2nd September, Saint Malo, France.

Deformations of rockfill dams under strong earthquake and nonlinear dynamic response analyses

Tadatsugu Tanaka [1] and Hiroshi Mori [2]

The Japan Association of Rural Resource Recycling Solutions, Tokyo 105-0004, Japan
E-mail: tad.tanaka@gmail.com

Keywords: Rockfill dam; Strong earthquake; Strain softening; Elasto-plastic analysis

Abstract. *An earthquake measuring 6.6 Mw on the moment magnitude scale struck Iburi Subprefecture in southern Hokkaido, Japan, on 6 September 2018. Mizuho Dam is located near the epicenter of this earthquake and strongly shaken. The recorded base peak accelerations in upstream and downstream directions was 491 Gal , and 937 Gal was recorded at dam crest. Maximum settlement of crest was about 12 cm and cracks attained about 2.0 m depth were observed around the crest. A simple strain softening elasto-plastic constitutive model is rather robust for application to a dynamic response analysis of structures. This material model is applied to Mizuho Dam with the features of non-associated flow characteristics, post-peak strain softening, and strain-localization into a shear band with a specific width. Also we computed earthquake induced accelerations and displacements of Aratozawa Dam which is 74.4 m high rockfill dam.*

1 INTRODUCTION

An earthquake measuring 6.6 Mw on the moment magnitude scale struck Iburi Subprefecture in southern Hokkaido, Japan, on 6 September 2018. The earthquake's epicenter was near Tomakomai and occurred at a depth of around 35.0 km. The earthquake caused many roads to become impassable. Some roads were blocked by debris from landslides.

Mizuho Dam located near the epicenter of this earthquake and strongly shaken. The recorded peak acceleration at base of Mizuho Dam in upstream and downstream direction was 491 Gal , and 937 Gal was recorded at crest of the dam. Maximum settlement of crest was 10 - 12 cm and cracks attained about 2.0 m depth were observed around the crest. Azuma Dam spillway was blocked by debris from landslides.

Recorded peak acceleration at base of this dam was 297 Gal and at crest 1293 Gal. The displacements of crest are not yet surveyed.

In a total stress analysis, the simulation of the loading conditions to which a geomaterial element will be subjected in the field is important. This is normally achieved by consolidated-undrained tri-axial test which represents the field condition. The advantage of the total stress analysis is that it is simple and numerically stable, and a strain softening elasto-plastic constitutive model can be applied to a dynamic response analysis of fill-type dam. The strain softening material model has features of non-associated flow characteristics and strain-localization into a shear band with a specific width.

[2]Faculty of Agriculture and Life Sciences, Hirosaki University, Hirosaki, Aomori Prefecture 036-8560, Japan, e-mail: hmori@hirosaki-u.ac.jp

We present mainly the dynamic response analysis of Mizuho Dam and the computed settlements are compared to observed ones. Also we computed earthquake induced accelerations and displacements of Aratozawa Dam which is 74.4 m high rockfill dam.

2 MATERIAL MODEL FOR BEHAXIOR OF GEOMATERIALS

The material model will be briefly described in this section[1,2]. The yield function (f) and the plastic potential function (Φ) are given by:

$$f = \alpha I_1 + \frac{\bar{\sigma}}{g(\theta_L)} - \gamma = 0 \tag{1}$$

$$\Phi = \alpha' I_1 + \bar{\sigma} - \gamma = 0 \tag{2}$$

where

$$\gamma = \frac{6c\cos\phi}{\sqrt{3}(3-\sin\phi)}, \alpha = \frac{2\sin\phi}{\sqrt{3}(3-\sin\phi)} \tag{3}$$

$$\alpha' = \frac{2\sin\psi}{\sqrt{3}(3-\sin\psi)} \tag{4}$$

$$\sin\psi = \frac{\sin\phi - \sin\phi_R'}{1-\sin\phi\sin\phi_R'} \tag{5}$$

where I_1 is the first invariant (positive in tension) of deviatoric stresses and $\bar{\sigma}$ is the second invariant of deviatoric stress. With the Mohr-Coulomb model, $g(\theta_L)$ takes the following form

$$g(\theta_L) = \frac{3-\sin\phi}{2\sqrt{3}\cos\theta_L - 2\sin\theta_L\sin\phi} \tag{6}$$

ϕ is the mobilized friction angle, c is the cohesion, ψ is the dilatancy angle and θ_L is the Lode angle.

In case of simple strain softening constitutive model, the frictional softening is given by next function.

$$\alpha(\kappa) = \alpha_P + \frac{\alpha_1\kappa}{B+\kappa} \quad \alpha_1 = -(\alpha_P - \alpha_R) \tag{7}$$

and cohesion softening is given by next function.

$$\gamma(\kappa) = \gamma_P + \frac{\gamma_1\kappa}{D+\kappa} \quad \gamma_1 = -(\gamma_P - \gamma_R) \tag{8}$$

The dilatancy is reduced by next function.

$$\alpha'(\kappa) = \alpha'_P\left(1 - \frac{\kappa}{C+\kappa}\right) \tag{9}$$

where κ is plastic parameter, *B, C, D* are constants for softening function. The suffices *P*, *R* represent the peak and residual state.

A more realistic frictional softening function is expressed as follows

$$\alpha(\kappa) = \alpha_R + (\alpha_P - \alpha_R)\exp\left\{-\left(\frac{\kappa}{C}\right)^2\right\} \tag{10}$$

$$\gamma(\kappa) = \frac{6c\cos\phi}{\sqrt{3}(3-\sin\phi)}\exp\left\{-\left(\frac{\kappa}{D}\right)^2\right\} \tag{11}$$

$$\phi_R^{'} = \phi_R\left\{1-\beta\exp\left\{-\left(\frac{\kappa}{E}\right)^2\right\}\right\} \tag{12}$$

where C, D, E and β are the material constants.

The residual friction angle (ϕ_R) and Poisson's ratio (ν) were chosen based on the data from the plane strain test or tri-axial test. The elastic moduli are estimated using the following equations.

$$G_0 = G_E\frac{(2.17-e)^2}{1+e}\sigma_m^{0.4} \tag{13}$$

$$K = \frac{2(1+\nu)}{3(1-2\nu)}G \tag{14}$$

The shear modulus is a function of confining pressure, initial void ratio e and G_E is empirical constant. This initial shear modulus G_0 may be fixed during dynamic analysis. The dilatancy angle (ψ) of clay cores under undrained condition may be zero and estimated from Rowe's stress-dilatancy relation for rock material. The shear banding in the numerical analysis was achieved by introducing a strain localization parameter s in the following additive decomposition of total strain increment as follows.

$$d\varepsilon_{ij} = d\varepsilon_{ij}^e + s d\varepsilon_{ij}^p \quad , \; s = F_b / F_e \tag{15}$$

where F_b is the area of a single shear band in each finite element and F_e is the area of the element.

3 DYNAMIC RESPONSE ANALYSIS OF MIZUHO ROCKFILL DAM

Mizuho Dam (Figure 1) is a rockfill dam used for irrigation completed 1998. It is 25.9 m high and 427.05 m long, impounding up to 4,300,000 cubic meters of water. An earthquake measuring 6.6 Mw on the moment magnitude scale struck Iburi Subprefecture in southern Hokkaido, Japan, on 6 September 2018. The seismic accelerations of measured at base and crest of Mizuho Dam are shown in Figure 3 and 4. The peak value at base is 491 Gal and at crest 937 Gal.

The simple elasto-plastic constitutive equations were applied to the impounded rockfill dam. Figure 1 shows Mizuho Dam cross section and Figure 3 shows finite element mesh used for dynamic response analysis. The core material is assumed undrained during the earthquake and elasto-plastic constitutive model (Eq.(7)-(9)) is applied. The strength of core material is obtained by isotropically consolidated and undrained tri-axial test. The peak cohesion and residual cohesion are 20 kPa . The peak friction angle is 20° and residual friction angle is assumed to be 18° . The shear band thickness is assumed to be 0.5 cm .The semi-permeable

zones are considered to be drained and the material constants of these zones used for the simple strain softening model (Eq. (10)-(12)) are as follows: φP = 33.0˚, φR = 30.0˚, β = 0.3, C = 0.1, D = 0.7, E = 0.05, peak cohesion = 15 kPa, residual cohesion = 0.0 and shear band thickness = 14 cm. The filter zone is assumed drained and the material constants of these zones used for simple strain softening model are as follows: φp = 39.0˚, φR = 34.0˚, β = 0.3, C = 0.1, D = 0.7, E = 0.05, peak and residual cohesion = 0.0 and shear band thickness = 5 cm. The Rayleigh damping is assumed 5.0%. Figure 3 shows the observed acceleration at the base of dam. Figure 4 shows observed acceleration at crest of the dam and Figure 5 shows computed acceleration at center of the dam crest. Figure 6 shows computed settlement at center of the crest. The surveyed crest settlement of this dam is about 10-12 cm, so we can say that the comparable result is obtained. The computed maximum shear strain is shown in Figures 7 and 8.

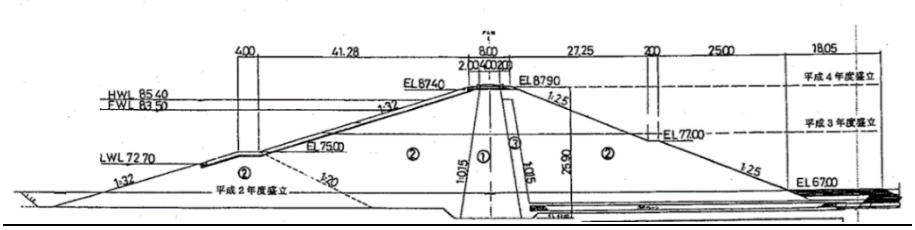

Figure 1: Cross section of Mizuho Dam

①Core zone ②Semi-permeable zones
③Filter zone

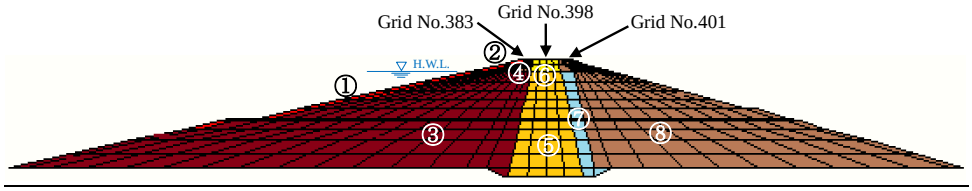

Figure 2: Finite element mesh of MIzuho Rockfill Dam

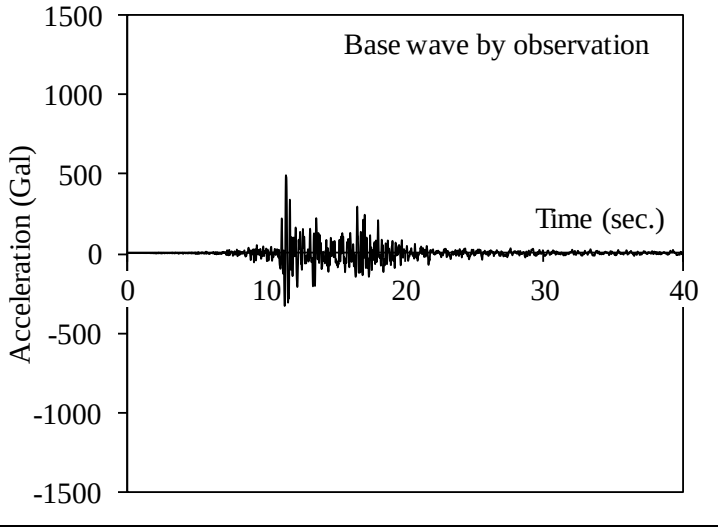

Figure 3: Observed acceleration at the base of Mizuho Dam

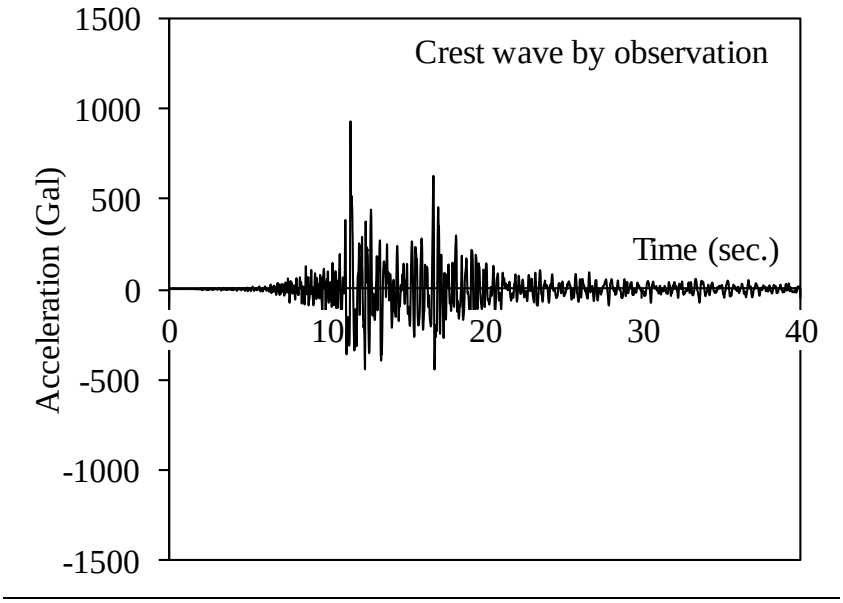

Figure 4: Observed acceleration at the crest of Mizuho Dam

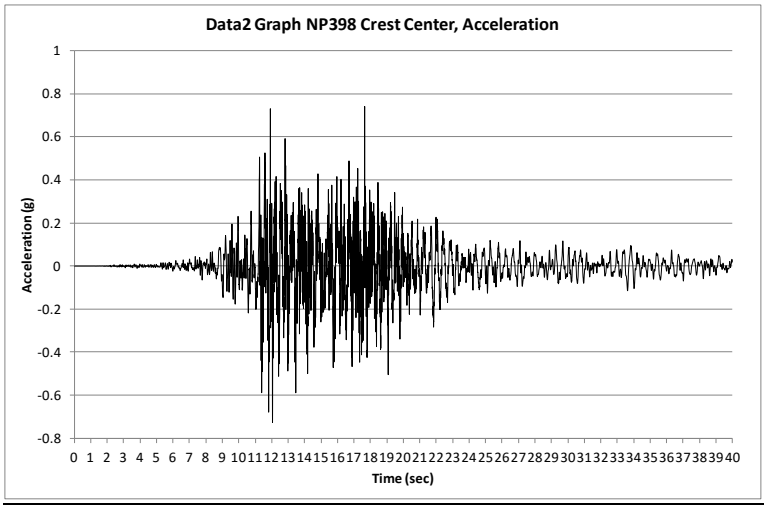

Figure 5: Computed acceleration at the crest center of Mizuho Dam

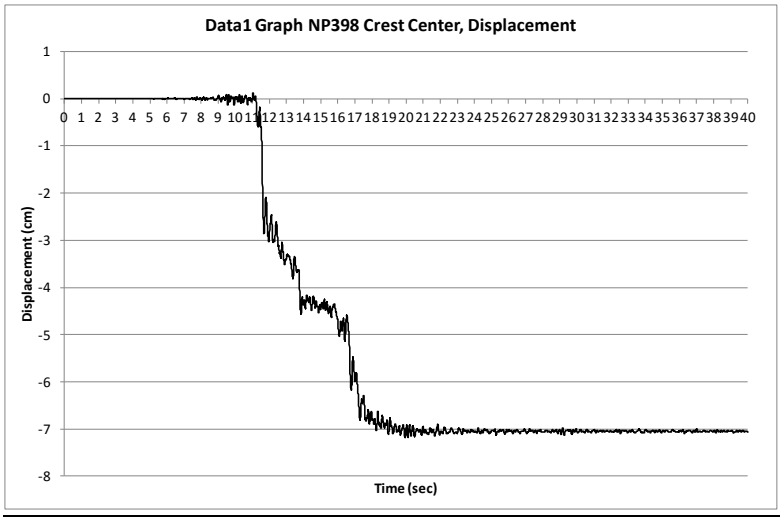

Figure 6: Computed settlement at the crest center of Mizuho Dam

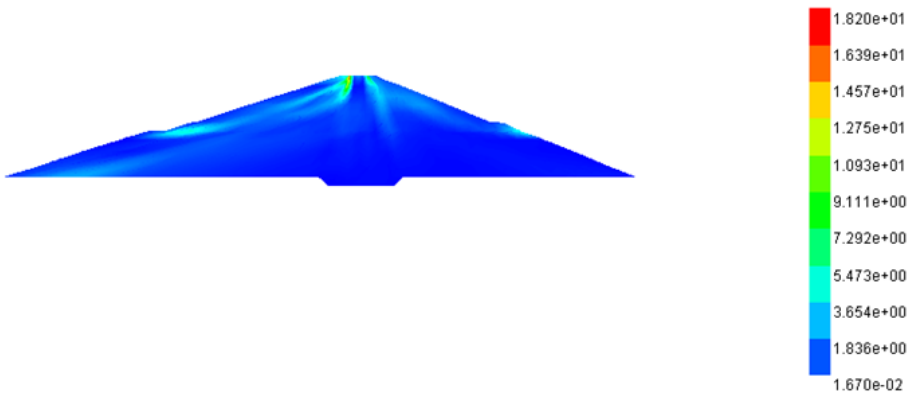

Figure 7: Computed maximum shear strain of Mizuho Dam

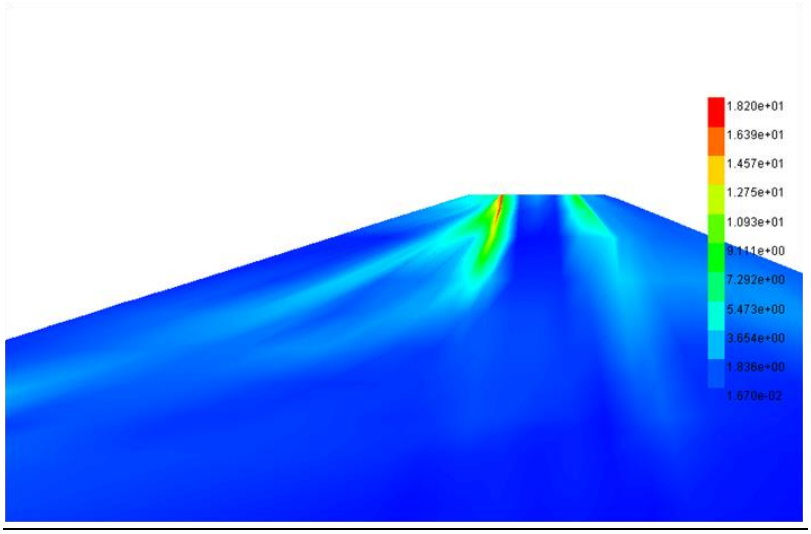

Figure 8: Computed maximum shear strain around the crest of Mizuho Dam

4 DYNAMIC RESPONSE ANAKYSIS OF ARATOZAWA ROCKFILL DAM

The Aratozawa Dam (Figure 9) is a rockfill dam used for irrigation, flood control and hydro-electric power generation completed 1998. It is 74.4 *m* high. On June 14 2008, the Iwate-Miyagi inland earthquake that had a magnitude of 7.2 hit the dam. The seismic acceleration measured at the base of Aratozawa Dam is shown in Figure 11.

The elasto-plastic dynamic analysis was also applied to the impounded rockfill dam using the same constitutive model as Mizuho Dam, that is, simple strain softening elasto-plastic constitutive model. Figure 9 shows Aratozawa dam cross section and Figure 10 shows rather coarse finite element mesh used for dynamic response analysis. The core material is assumed undrained and strain softening elasto-plastic constitutive model is applied. The peak cohesion is 60 *kPa* and the assumed residual cohesion is 30 *kPa*. The peak friction angle is 20° , residual friction angle is 18° and shear band thickness is 4.5 *cm*. The rock and transition zones are assumed drained and the material constants of these zones used for simple strain softening model are as follows: $\phi_p = 42.0^\circ$, $\phi_R = 34.0^\circ$, $\beta = 0.3$, $C = 0.1$, $D = 0.7$, $E = 0.05$, peak

cohesion = 20 *kPa* and residual cohesion = 0.0 and shear band thickness = 105 *cm*. Figure 11 shows the observed acceleration at the base of dam. The Rayleigh damping is assumed 5.0%. Figure 12 shows observed acceleration at the crest of dam and Figure 13 shows computed acceleration at center of the dam crest. Figure 14 shows computed settlement at center of the crest. The measured crest settlements of this dam are 25-30 *cm*, so we can say that the comparable result is obtained. The computed maximum shear strain is shown in Figure 15.

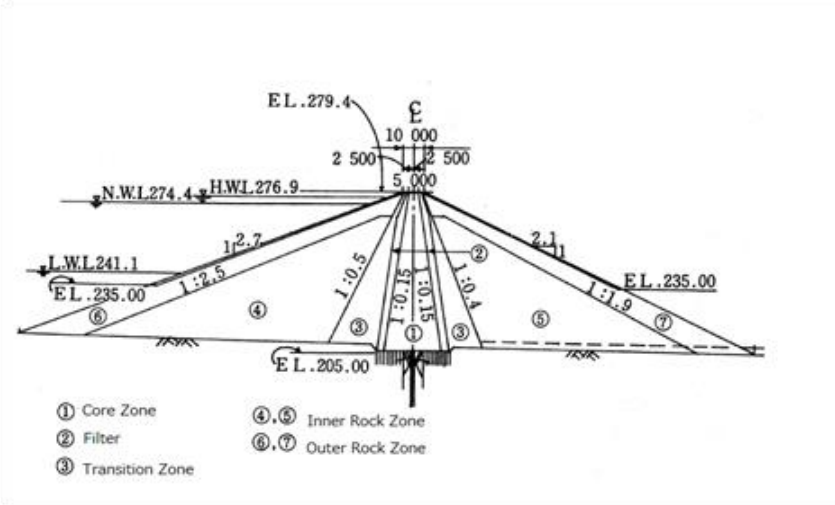

Figure 9: Cross section of Aratozawa Dam

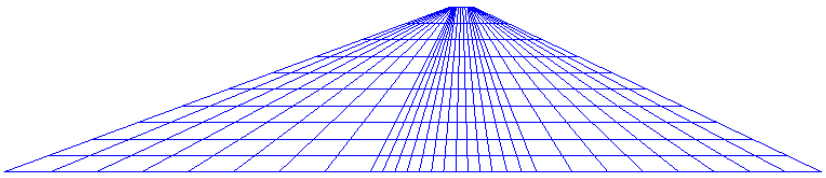

Figure 10: Finite element mesh of Aratozawa Dam

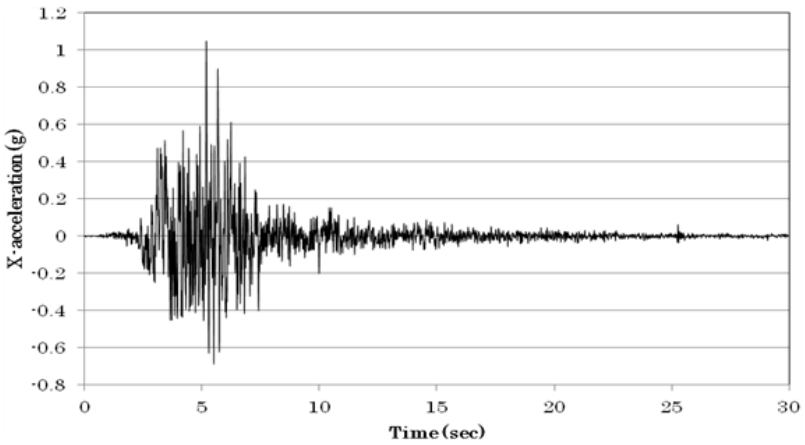

Figure 11: Observed acceleration at the base of Aratozawa

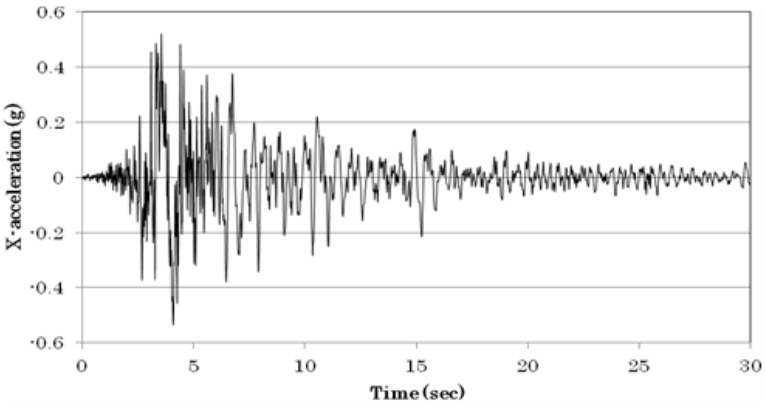

Figure 12: Observed acceleration at the crest of Aratozawa Dam

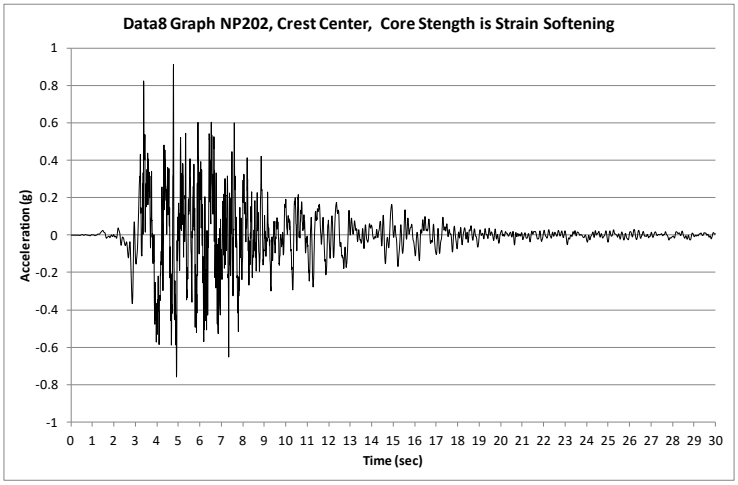

Figure 13: Computed acceleration at the crest of dam

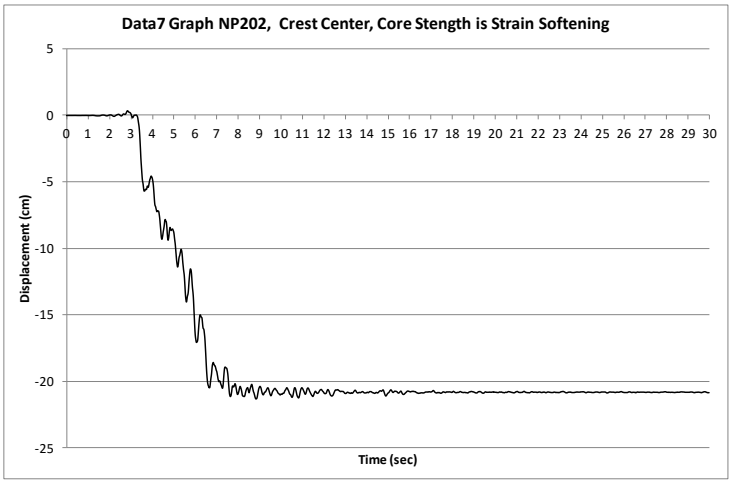

Figure 14: Computed settlement at the crest of dam

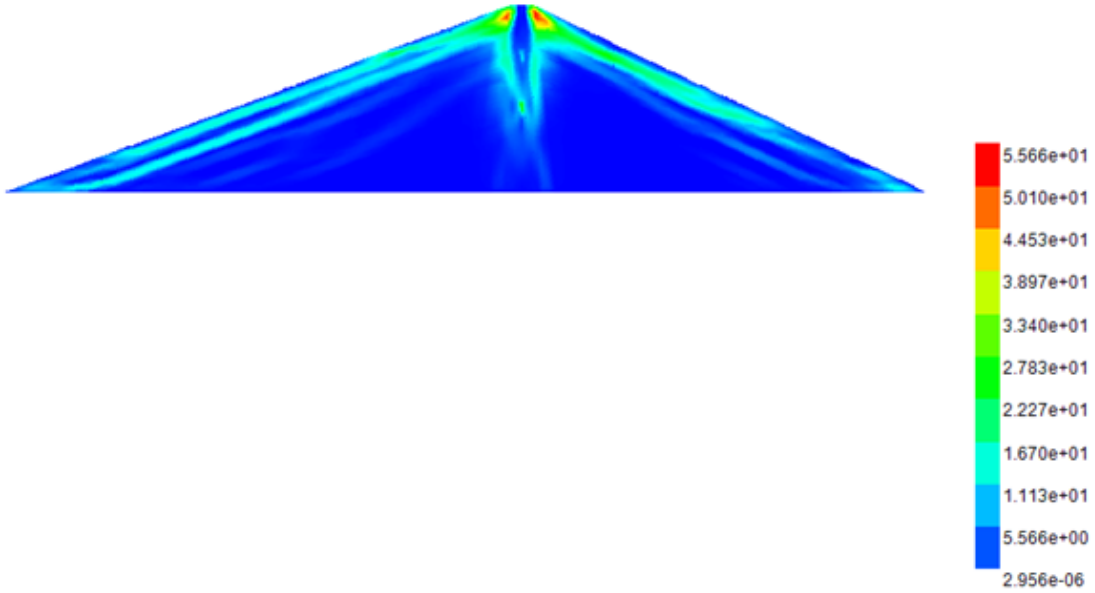

Figure 15: Computed maximum shear strain of dam

5 CONCLUSIONS

A simple strain softening material model for geomaterial is used with the features of post-peak strain softening, and strain-localization into a shear band with a specific width. This material model is applied to the computation of real rockfill dams. We obtained earthquake induced accelerations and displacements of Mizuho Dam which is 25.9 m high and Aratozawa Dam which is 74.4 m high. The computed accelerations at the crest of dams are compared to the observed ones and the computed displacements are also verified by the surveyed settlements. The simple strain softening constitutive model is applicable to the computation of a real fill-type dam.

REFERENCES

[1] T. Tanaka, *Elasto-plastic strain hardening-softening soil model with shear banding.* Proc. 15th ASCE Engineering Mechanics Conf., New York, p.8 (CD-ROM), (2002).

[2] T. Tanaka, *Cyclic behavior of soils and numerical analyses in cold regions and seismic zones*, Sciences in Cold and Arid Regions, Vol.7 Issue 5, pp.492-502(2015).

Seismic analysis of hardfill dams

Ioannis M. Siskos[1], Panos Dakoulas[2]
University of Thessaly
Pedion Areos, 383 34, Volos, Greece
E-mail: iosiskos@civ.uth.gr

Keywords: Dams; concrete; hardfill, seismic hazard; numerical analysis

Abstract. *Hardfill is a roller compacted lean concrete with a small percentage of cement (50-80 kg/m^3) and properties in between concrete and rockfill. In this study, the seismic behavior of hardfill dams is investigated numerically accounting for the dam – water – canyon dynamic interaction, using Abaqus. Two case studies are presented: (a) the 55m-high Filiatrinos hardfill dam (Greece) and (b) a 100m-high hardfill dam with geometry similar to Cindere dam (Turkey). The results demonstrate that for the 55 m dam subjected to a PGA of 0.28g, the tensile stresses are low. By contrast, for the case of a 100 m dam subjected to a PGA of 0.46g, the tensile stresses in the upstream and downstream faces reach the tensile strength, causing damage and local weakening of the material.*

1 INTRODUCTION

Over the last decades, new types of dams have been constructed based on empiricism, some basic concepts and relatively simple calculations. The methodology of construction, the geometry and the material specifications were adjusted after observations of their behaviour throughout the years. Introduction of more precise methods of determining the behaviour of dams under seismic forces, can allow design improvements regarding the material properties, the geometry and, possibly, the construction process of such structures.

The dynamic analysis of dams in general, including hardfill dams, is complicated because they are three dimensional nonlinear systems, which may be significantly affected by the dam-water-canyon interaction and the energy radiation through outgoing waves along the system boundaries. In this study, the seismic behaviour of hardfill dams is investigated by taking into account the dam-water-canyon interaction during seismic loading.

2 CHARACTERISTICS OF HARDFILL DAMS

The hardfill material can be defined as an intermediate material between embankment fill and concrete. It may be considered as Roller Compacted Concrete containing low cement content, with or without addition of pozzolan or fly ash and a high value of the water/cement ratio [1]. The average values are 60 kg/m^3 for cement, 13 kg/m^3 for pozzolan, 135 kg/m^3 for water, corresponding to a w/c ratio of 1.86 [2]. In numerical simulations, the hardfill material is usually modelled with adjusted concrete properties, although sometimes rockfill material properties with high cohesion are used.

Londe and Lino [3] calculated that compressive stress in a 100 m-high hardfill dam with upstream and downstream slopes 0.7:1 (h:v) is lower than 1.5 MPa. Thus, for a safety

[2] University of Thessaly, E-mail: dakoulas@uth.gr

factor in the range of 3 to 4, the required hardfill unconfined compressive strength is about 4.5 to 6 MPa [3]. Moreover, it was concluded that for an excitation with peak ground acceleration of 0.2g, no tensile strength is required.

In the following, two case studies referring to the seismic performance of hardfill dams are presented: (a) the 55m-high Filiatrinos dam (Greece) subjected to a seismic event with 0.28g PGA (Kalamata earthquake) and (b) a 100m-high hardfill dam with a geometry similar to that of Cindere dam (Turkey) subjected to a strong excitation of 0.46g PGA (Koyna earthquake). These case studies are developed to examine the response of the dams in seismic active areas, under big earthquakes.

3 CASE STUDY A: FILIATRINOS DAM

3.1 Filiatrinos Dam

Filiatrinos is a face symmetrical hardfill dam constructed in Peloponissos (Greece) in 2016. The dam has a height of 55 m, upstream/downstream slopes equal to 0.8:1, crest length 246 m, and was constructed using lean concrete. Fig. 1 illustrates the maximum cross-section of the dam.

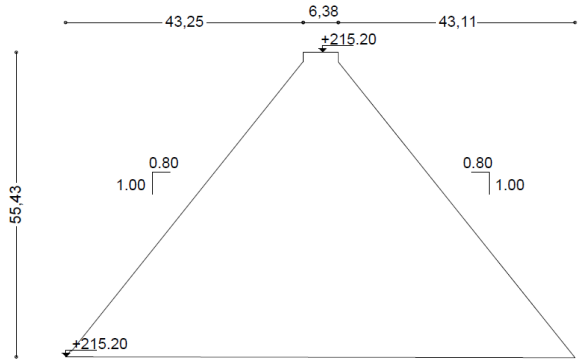

Figure 1: Maximum cross-section of Filiatrinos hardfill dam (units: meters)

In the original design of Filiatrinos dam, a concrete upstream face slab was considered as the waterproofing element. A subsequent revision replaced the slab with a PVC membrane as a waterproofing element [4]. Thus, the present numerical analysis considers the hardfill embankment covered with a membrane. The characteristics and composition of the materials used for the production of the hardfill are given in Table 1.

Table 1. Filiatrinos dam: characteristics of hardfill mixture [5]

Hardfill mixture characteristics	
Maximum aggregate grain size (mm)	75
Fraction passing sieve No. 200 (%)	15
Plasticity Index (%)	15
Cement content (kg/m^3)	51
Fly ash content (kg/m^3)	7–23

3.2 Numerical model

The finite element mesh used for the analysis consists of 26245 solid 8-node elements (C3D8R with reduced-integration and hourglass control) for the dam and canyon rock and 945 acoustic elements (AC3D8) for the reservoir water.

The dam–reservoir and canyon– reservoir dynamic interactions resulting from the transverse component of ground motion are modelled with acoustic elements. Such elements

account for the water compressibility, the wave absorption at the infinite end of the reservoir and the impedance of wave radiation at the reservoir sediments [6]. The various stages of analysis and the response of the dam in different loading conditions help understand how the dam-water interaction, reservoir boundary absorption, water compressibility, dam-foundation interaction and rock boundary absorption of energy influence the dam response.

3.3 Material properties

The mechanical behaviour of the hardfill material is modelled using the concrete damaged plasticity constitutive model by Lee and Fenves [7]. The model assumes that the main two failure mechanisms are tensile cracking and compressive crushing of concrete. The evolution of the yield (or failure) surface is controlled by two hardening variables, ε_t^{pl} and ε_c^{pl}, linked to failure mechanisms under tension and compression loading, respectively. We refer to ε_t^{pl} and ε_c^{pl} as tensile and compressive equivalent plastic strains, respectively [6].

The tensile strength is estimated approximately to be 10% of the ultimate compressive strength. The tensile post failure behaviour is given in terms of a fracture energy cracking criterion by specifying a stress/displacement curve instead of a stress-strain curve. This is accomplished with the post cracking stress/displacement curve. Tensile damage, d_t, is specified as a function of cracking displacement by using the post cracking damage displacement curve (Fig. 2). The stiffness degradation damage caused by compressive failure (crushing) of the concrete, d_c, is assumed to be zero. It should be mentioned that the compressive and tensile strength used in the simulation are already at the lower limits of the hardfill material strength.

Table 2: Filiatrinos Dam: Material properties of hardfill and canyon rock

Properties	**Hardfill**	**Canyon rock**
Density (kg/m^3)	2643	2400
Young's modulus (GPa)	11	27
Poisson's ratio	0.2	0.2
Dilation angle	36.3^o	–
Compressive strength (MPa)	5	–
Tensile strength (MPa)	0.5	–

It is generally accepted that concrete dams have damping ratios of about 2–5%. In this study the material damping is taken approximately 5% of the critical damping for the first mode of vibration of the dam. The first natural frequency of the dam is ω_1= 41 rad/s, whereas the selected values of Rayleigh damping parameters are α=2.84 s^{-1} and β=0.00746 s.

3.4 Seismic excitation

The transverse components of the ground accelerations recorded during Kalamata earthquake (PGA=0.28g), are used for this study. Fig. 2 plots the acceleration time history and the response spectra of the Kalamata record. Prior to the earthquake excitation, the dam is subjected to gravity loading due to its self-weight and to the hydrostatic pressure of the reservoir on the upstream face.

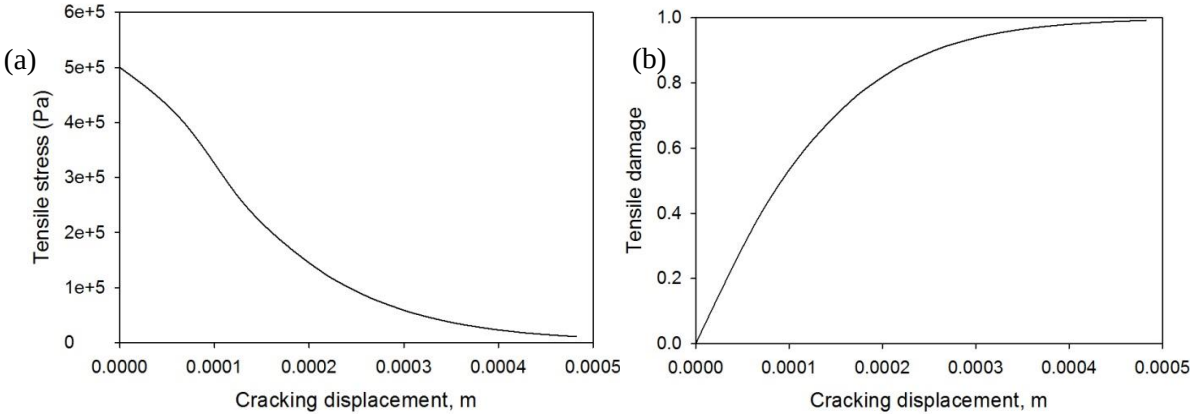

Figure 2: Damage plasticity model for hardfill (a) tensile strength reduction and (b) tensile damage factor

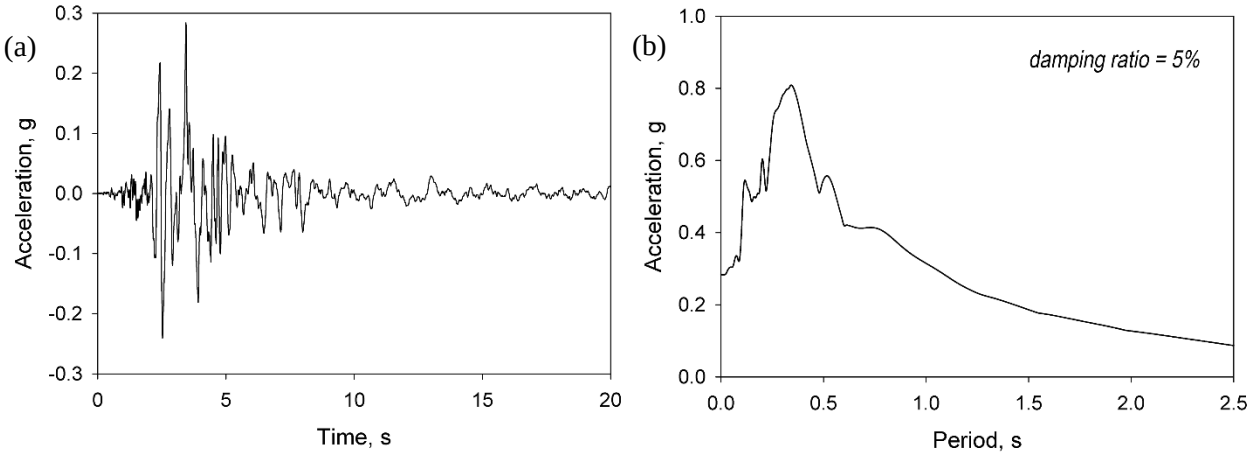

Figure 3: Kalamata record: (a) acceleration time history and (b) acceleration response spectra.

To account for the wave energy radiation at the canyon base, absorbing boundaries consisting of dashpots in the normal and shear directions are utilized. The earthquake excitation is imposed in terms of normal and shear tractions given by:

$$t_n = -\rho \cdot C_p \cdot v_n \tag{1}$$

$$t_s = -\rho \cdot C_s \cdot v_s \tag{2}$$

where: v_n and v_s are the normal and shear components of the excitation velocity at the boundary; ρ is the mass density and C_p and C_s are the *P* and *S*-wave velocity of the canyon rock.

3.5 Analysis and results

The staged construction of the dam is simulated using 10 layers. After gravity loading, hydrostatic pressure due to impoundment is imposed in three phases corresponding to 33%, 67% and 100% of the maximum water elevation. Subsequently, the displacement boundary conditions are replaced with reaction forces at the base nodes, allowing the activation of the dashpots during seismic shaking.

Fig. 4 plots the acceleration time history at the dam crest due to the Kalamata excitation. Its peak value is almost twice as high compared to the peak values at the dam toe.

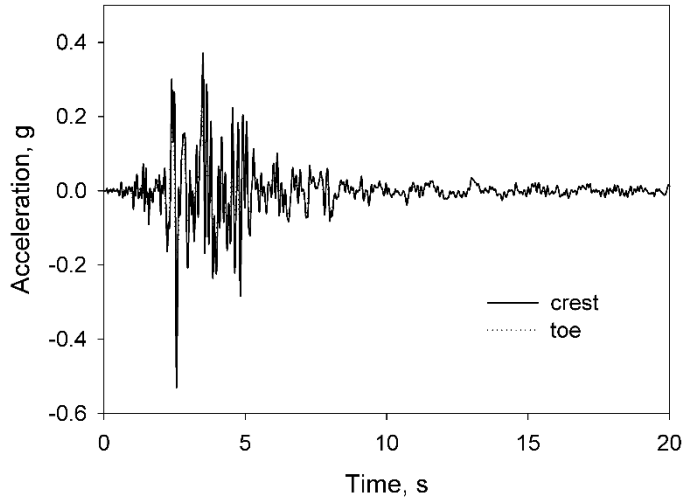

Figure 4: Acceleration time history at the dam crest and toe due to Kalamata excitation.

The maximum and minimum principal stresses developing at the dam face during seismic shaking are within the limits of operational safety levels (see Fig. 5). Fig. 6 plots the maximum and minimum principal stresses along the height of the upstream and downstream faces. The maximum compression is less than 1.33 MPa, which is a much lower value than the compressive strength of hardfill (5 MPa). Moreover, the maximum tension is lower than 0.27 MPa, which is also much lower than the tensile strength of hardfill (0.5 MPa).

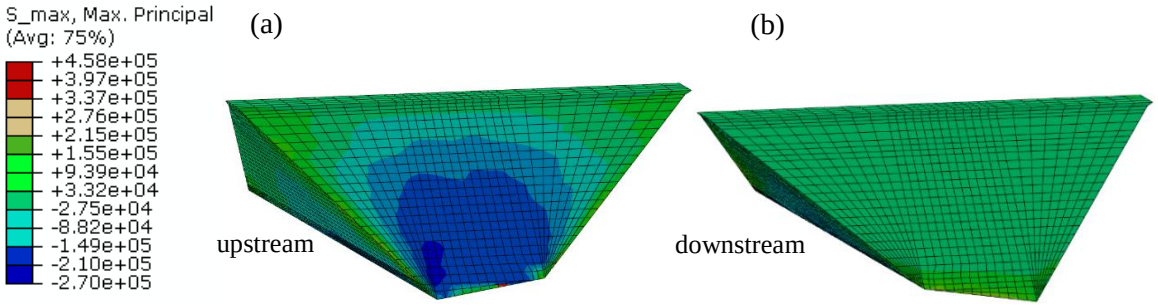

Figure 5: Maximum principal stress at the (a) upstream side and (b) downstream side (tensile stresses are positive)

Tensile stresses appear only near the toe of the dam. The maximum compressive stress occurs also at the dam toe. The stress values are progressively reduced in the direction towards the dam crest. The results for the downstream face of the dam are similar to those in the upstream face (Fig. 6), except that the compression by the reservoir water reduces the tensile stresses at the upstream surface.

The maximum permanent horizontal displacement of the dam at the end of shaking are very small (in the range of 2.5 cm) and concentrated in the mid-crest region, as shown in Fig. 7. Thus, the hardfill embankment is behaving almost as a stiff elastic body. The upstream face of the dam shows only small damage due to tensile stress near its toe (see Fig. 8).

The numerical results for this 55m-high hardfill dam, subjected to PGA values of 0.28g, confirm the conclusions of Londe and Lino [3] for this category of hardfill dams.

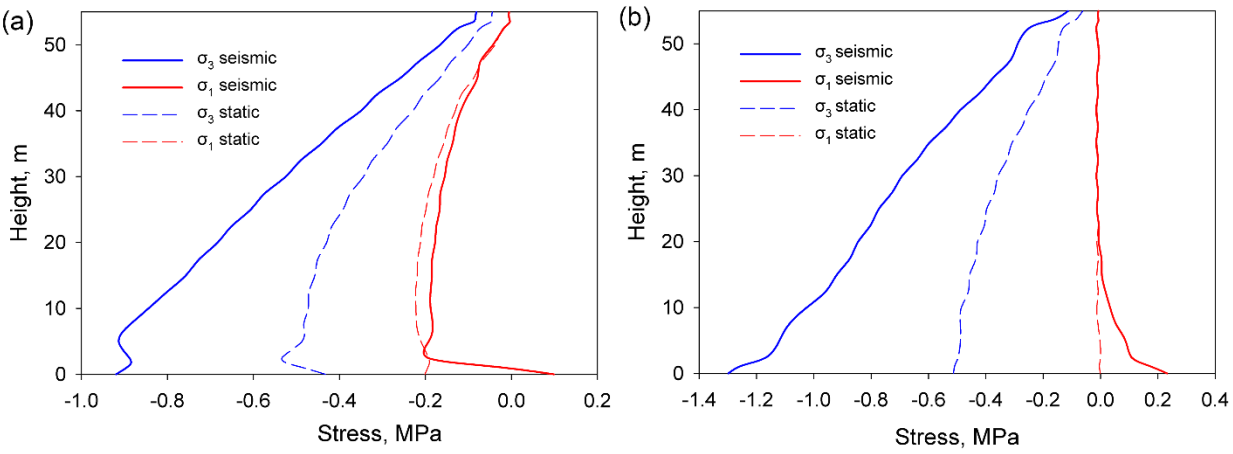

Figure 6: Maximum and minimum principal stresses along the height (a) upstream face and (b) downstream face

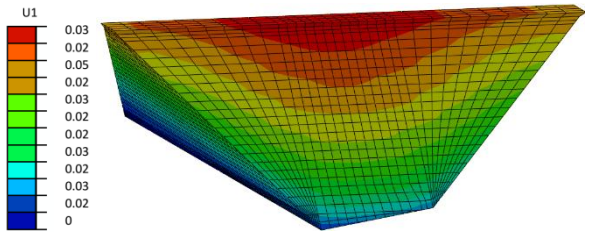

Figure 7: Horizontal displacements at the end of shaking (upstream face)

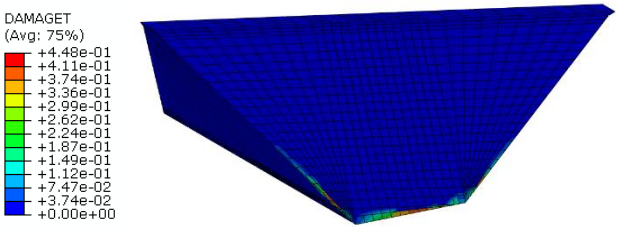

Figure 8: Damage factor due to tensile stress at the end of shaking (upstream face)

In the following, a 100m-high dam with steeper slopes, subjected to a stronger excitation, is investigated.

4 CASE STUDY B: 100M TALL HARDFILL DAM

4.1 Hardfill dam description

A hypothetical 100 m tall hardfill dam is considered, having symmetric slope inclinations equal to 0.7:1 and crest length equal to 250 m. This dam is similar to Cindere dam (Turkey), which has a height of 107 m and is the tallest hardfill dam to date. A cross-section of Cidere dam is shown in Fig. 9 [8]. This model was created to examine the validity of the assumption by Londe and Lino [3] for dams having a height of about 100 m. In this case study the behaviour of this model into strong excitation (earthquake of PGA=0,46g) is examined.

In this case, the upstream face of the dam is covered with a concrete slab used as a waterproofing element. The face slab consists of 16 concrete panels, having width of 15 m and thickness of 0.5 m.

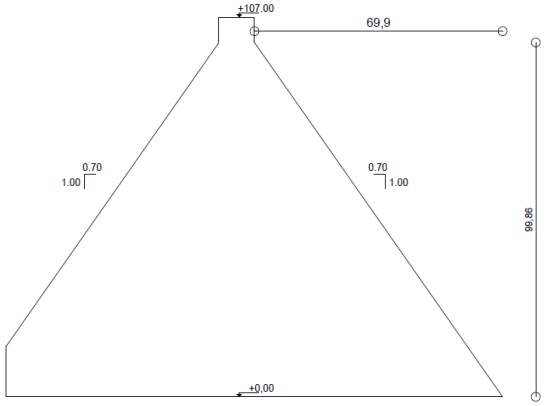

Figure 9: Maximum cross-section of Cindere hardfill dam

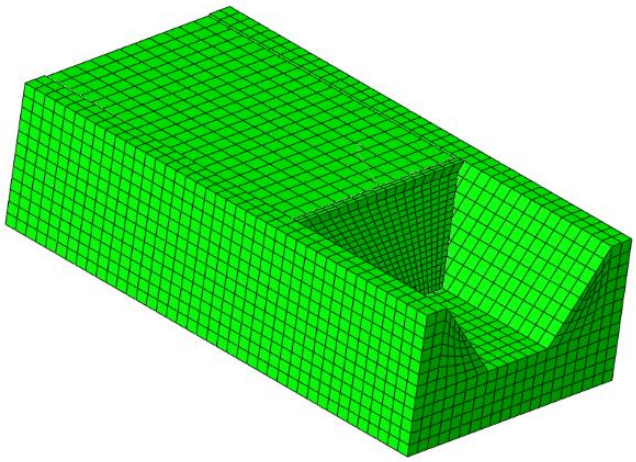

Figure 10: Numerical model of the studied 100m tall hardfill dam

4.2 Numerical model

The numerical model consists from the following parts: hardfill embankment, 16 concrete slabs resting on the upstream face, the canyon and the reservoir water (Fig. 10). The canyon geometry has a length of 600 m, width of 310 m and depth of 170 m. The model consists of 16108 solid 8-node elements (C3D8R with reduced-integration and hourglass control) for the dam, slabs and canyon rock and 2178 acoustic elements (AC3D8) for the reservoir water. The slabs are placed at the upstream surface with contact interaction allowing frictional behaviour and separation. The base nodes of the slab panels are properly supported in order to simulate the connection of the slabs to the plinth. Finally, the acoustic elements of water are tied at the slabs. The boundary conditions and the sequence of loading is the same with the previous example.

4.3 Material properties

As in the previous case, the mechanical behaviour of the hardfill material is modelled using the concrete damaged plasticity constitutive model by Lee and Fenves [7]. The material properties for the hardfill, slab concrete and the canyon rock used in the analysis are

presented in Table 3. For the hardfill material, a 5% damping ratio is assumed, corresponding to Rayleigh parameters α=1.4145 s and β=0.001 s^{-1}.

Table 3: Material properties of hardfill, slab concrete and canyon rock

Properties	**Hardfill**	**Slab concrete**	**Canyon rock**
Density (kg/m^3)	2643	2400	2400
Young's modulus (GPa)	11	29	27
Poisson's ratio	0.2	0.2	0.2
Dilation angle	36.3º	36.3º	–
Compressive strength (MPa)	6	42	–
Tensile strength (MPa)	0.6	4.6	–

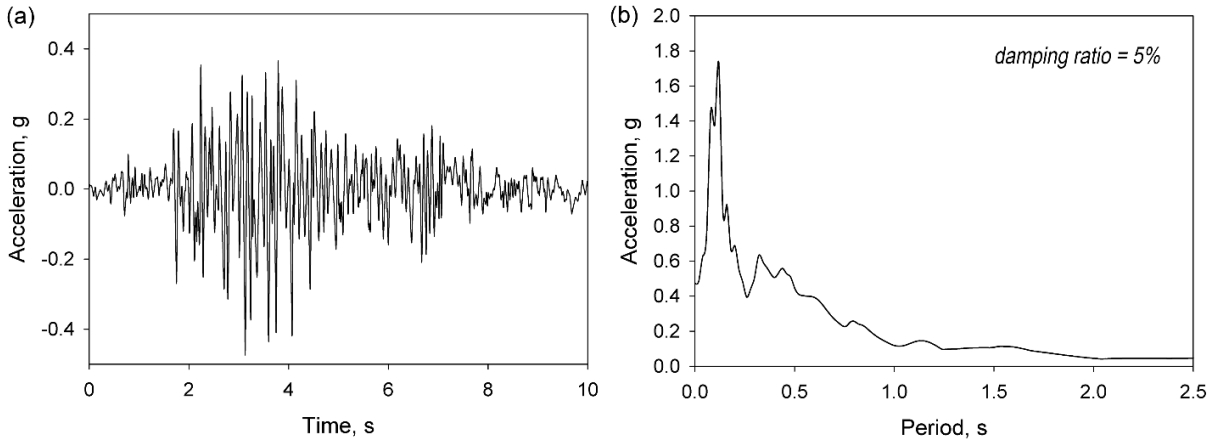

Figure 11: Koyna record: (a) acceleration time history and (b) acceleration response spectra.

4.4 Analyses and results

Prior to the earthquake excitation, the dam is subjected to gravity loading due to its self-weight and the reservoir pressure on the upstream face. During static analysis, tensile stresses do not develop within the dam body, while compressive stresses remain very low (<1.1 MPa).

The horizontal component of the ground acceleration recorded during 1967 Koyna earthquake (PGA=0.46g) is used for this study. Fig. 11 plots the acceleration time history and the response spectra of the Koyna record.

Fig. 12 plots the acceleration at the crest of the dam having a peak value of about 1.8g. During seismic shaking, the maximum compressive stress (2.09 MPa) shown in Fig. 13 is lower than the compressive strength of hardfill at the whole body of the dam (6 MPa). By contrast, the tensile stresses reach the tensile strength locally, leading to tensile cracking (Fig. 14). The tensile stresses are becoming critical at the upper middle part of the downstream face and near the abutments at the upstream face (Fig. 14).

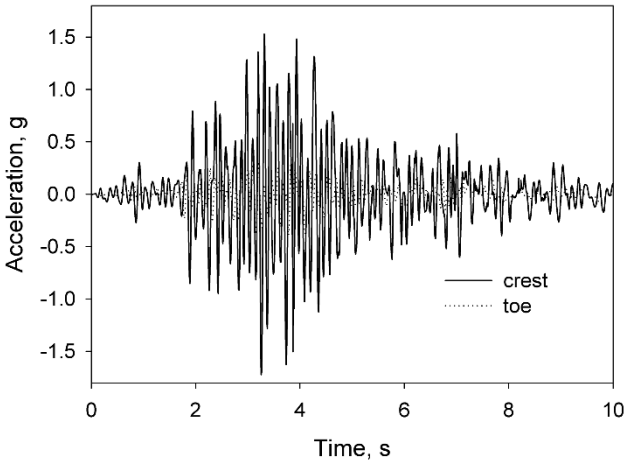

Figure 12: Acceleration time history at the crest and toe of the dam due to Koyna earthquake.

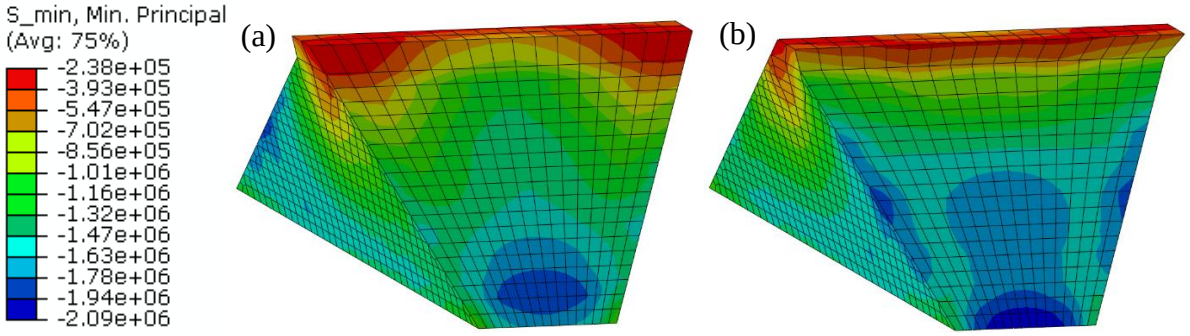

Figure 13: Distribution of minimum principal stresses at the (a) upstream face and (b) downstream face

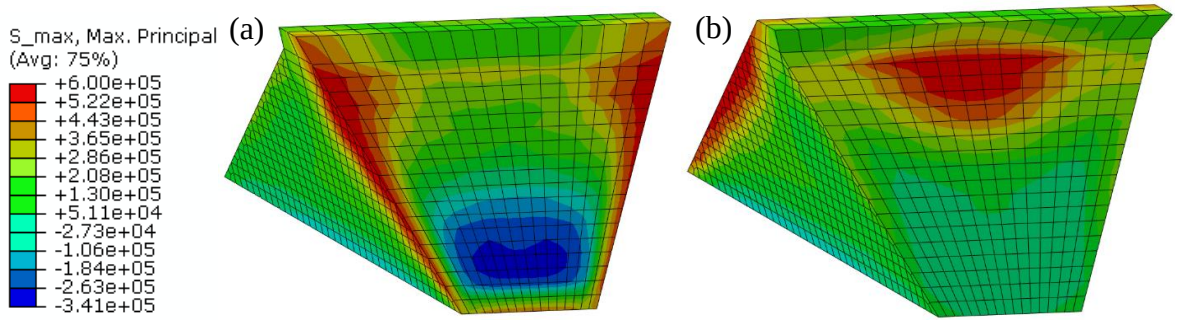

Figure 14: Distribution of maximum principal stresses at the (a) upstream face and (b) downstream face

Fig. 15 plots (with solid lines) the distribution of the maximum and minimum principal stresses along the height at mid-section in the upstream and downstream face. Also plotted in the figure (with dashed lines) are the corresponding values due to static loads.

The damage factor, shown in Fig. 16, is caused at areas where the tensile stresses exceed the tensile strength of the material. This is happening locally near the abutments in the upstream face and at the middle top part of the dam in the downstream face. The stiffness degradation variables shown in Fig. 17 indicates stiffness reduction in the downstream face, whereas such reduction does not appear in the upstream face.

The residual deformations at the dam body shown in Figs. 18 and 20b are acceptable, with maximum values about 3.5 cm in the horizontal and 4.5 cm in the vertical direction.

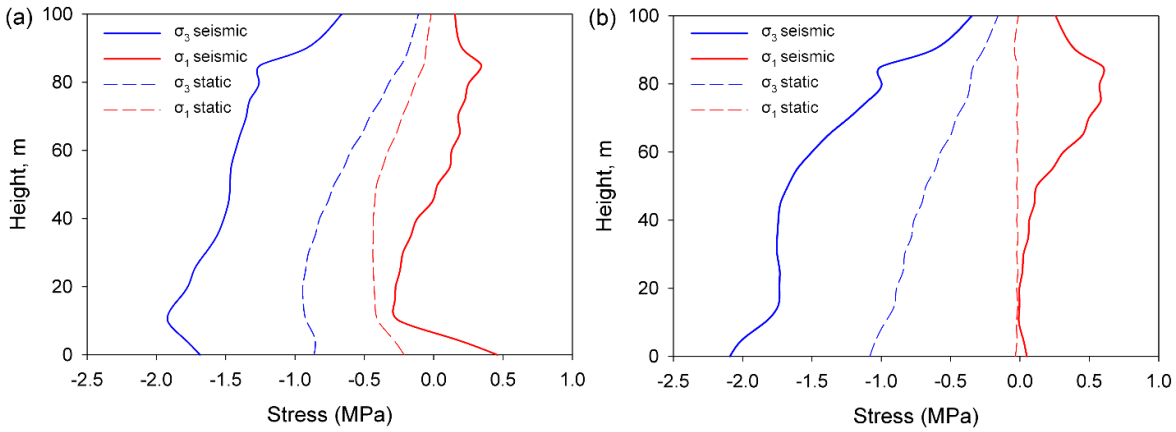

Figure 15: Maximum and minimum principal stresses along the height (a) upstream face and (b) downstream face

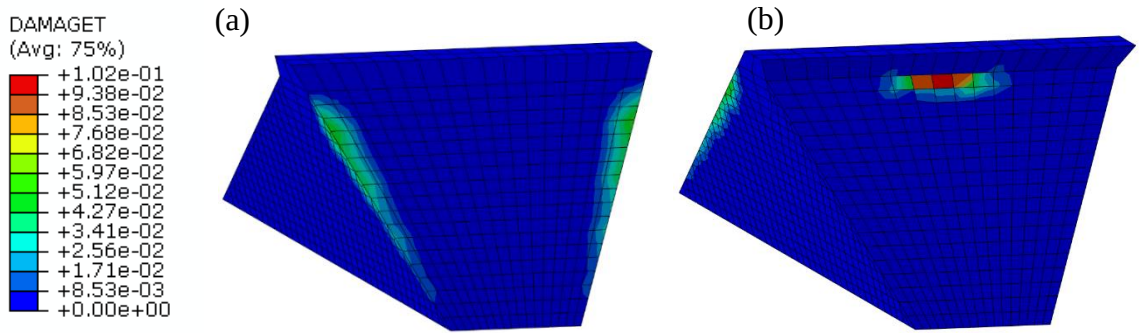

Figure 16: Damage factor due to tension at the (a) upstream face and (b) downstream face

The behaviour of the concrete slabs under seismic loading, considering the fluid – structure interaction, shows that tensile damage develops at the upper half of the slabs.

The hydrodynamic pressures that develop at the upstream face during the strong ground shaking by the Koyna excitation increase dramatically the stresses at the top 30 m of the dam. As a result, damage develops in the slabs at the middle part of the structure (see Figure 19). Moreover, the slabs tend to detach from the dam body in the region near the dam crest. This damage affects only the slabs and is not transferred at the dam body.

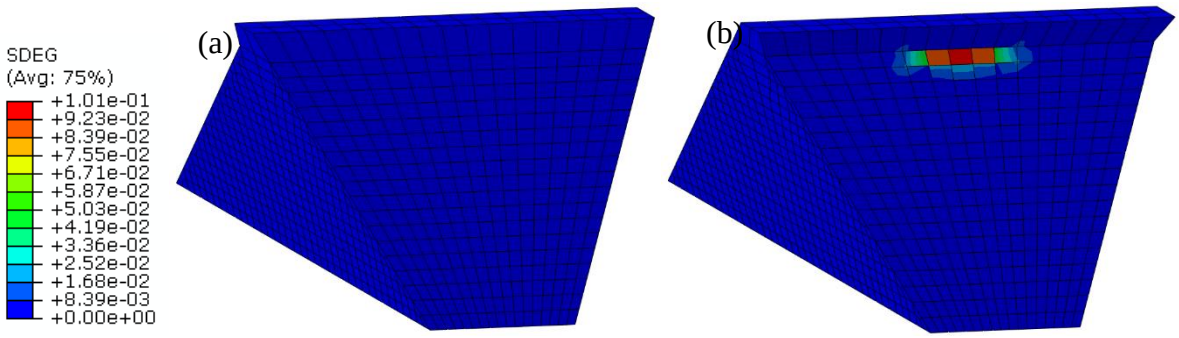

Figure 17: Stiffness degradation parameter at the (a) upstream face and (b) downstream face

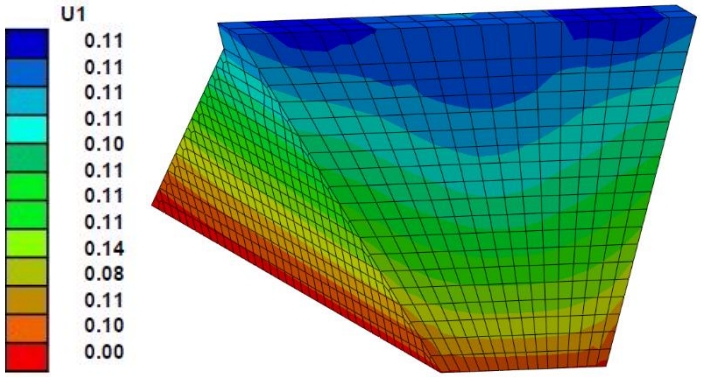

Figure 18: Horizontal displacements of the dam at the end of the earthquake

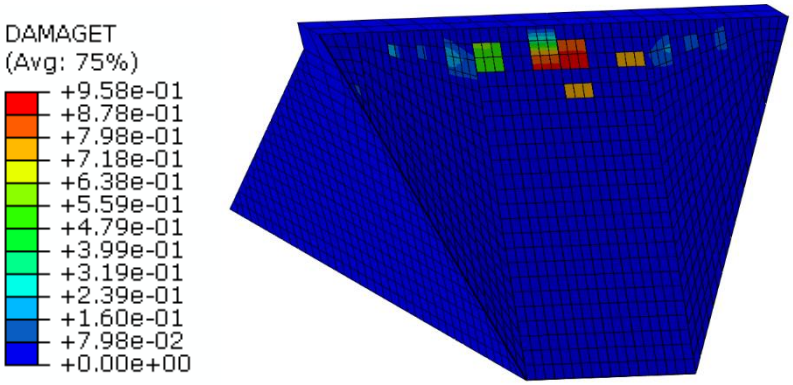

Figure 19: Damage factor due to tensile stresses at the upstream face slab panels

From the above, it is noticed that while the values of the compressive stresses are not critical, providing the necessary factor of safety for the material, the tensile stresses that develop during strong seismic incidents, such as the Koyna earthquake, could lead to local material failure.

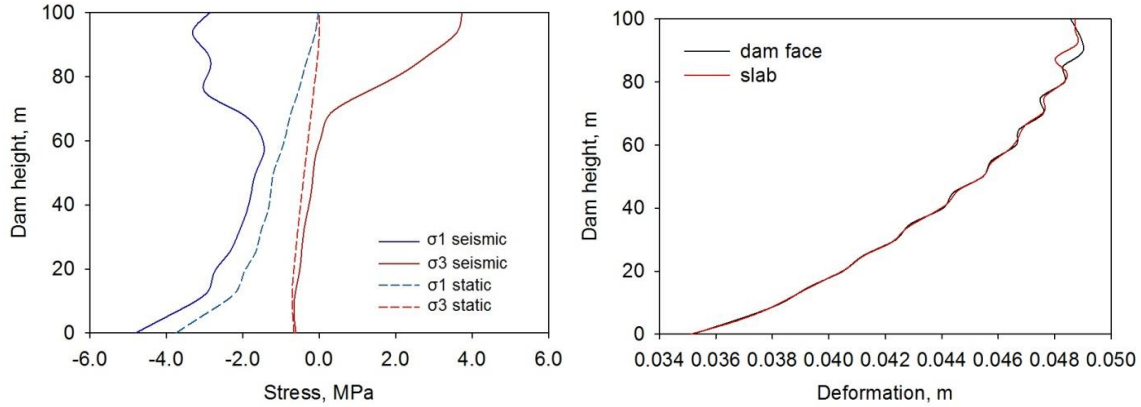

Figure 20: Middle slab panel: (a) Maximum and minimum principal stress versus depth and (b) Relative displacements versus depth

5 CONCLUSIONS

The results of the analyses confirm that the theory of Londe and Lino for dams up to 50 m, even for higher PGA values than 0.2g, where both the maximum and the minimum principal stresses are lower than the material strength. For the case of a 100 m dam and a peak ground acceleration of 0.46g, the values of tensile stresses in the upstream and downstream faces of the dam reach the tensile strength, causing damage and local weakening of the material. In such cases, the seismic behaviour of the hardfill could be improved by flattening the inclination of the slopes and increasing slightly the tensile strength of the hardfill material. Additional analyses, not shown here, have also confirmed that for the case of the 100 m dam subjected to a PGA up to 0.2g, the hypothesis of Londe & Lino remains valid. Additional studies could help produce guidelines for the design of this kind of dam.

REFERENCES

[1] Commitee on Concrete Dams, Roller compacted concrete dams, state of the art and case histories, ICOLD, (2003)
[2] L. Tanchev, *Dams and appurtenand hydraulic structures.* Taylor & Francis Group, London, UK. (2014).
[3] P. Londe, M. Lino, *The faced symmetrical hardfill dam: A new concept for RCC.* Water Power and Dam Construction, (1992).
[4] Y. Thanopoulos, N. Moutafis, *The geomembrane faced hardfill dam, ANCOLD (2017)*
[5] H. Gouvas, P. Orphanos, *Determination of Factors Affecting Compressive Strength of Lean RCC Mixtures: The experience of Filiatrinos Dam*, Geotech Geol Eng, (2014).
[6] ABAQUS, *Users manual*. Simulia, (2012).
[7] J. Lee, G. Fenves, *Plastic-Damage Model for Cyclic Loading of Concrete Structures*, Journal of engineering mechanics, (1998).
[8] S. Batmaz, *Cindere dam – 107m high Roller Compacted Hardfill Dam in Turkey*, RCC Dams - Roller Compacted Concrete Dams: Proceedings of the IV International Symposium on Roller Compacted Concrete Dams (2018).

Site effect study of a large rockfill dam: Denis-Perron Dam

Daniel Verret[1], **Denis LeBoeuf**[2], **Éric Péloquin**[3], **Annick Bigras**[4]

Hydro-Québec - Montréal, QC, Canada.
Geotechnical Eng., M. A. Sc., Dam Expertise,
Verret.daniel@hydro.qc.ca

Keywords: Rockfill Dam, Seismic, Ambient noise, Dynamic analysis, Natural Frequencies.

Abstract. *The In this paper, analyses of strong-motion and ambient noise measurements at the Denis-Perron (SM-3) dam were carried out to evaluate possible site effects and the actual frequency of resonance (FN) of this earth structure. The Denis-Perron Dam is a rockfill embankment dam standing 171 meters high and 378 meters long. It is the highest earthfill dam in Québec. The dam is built in a narrow valley. Three-component digital strong-motion stations were installed on the dam's crest and on bedrock, on the left abutment. The fundamental vibration frequency in each direction is estimated from a series of three small earthquakes that occurred in 1999 and 2002. The site response is also evaluated with the ambient noise records. Ten sets of ambient noise measurements were conducted using six «Tromino» velocimeters on the dam. A modal analysis regrouping a set of these measurements synchronized together is presented. Vibration modes calculated from the ambient noise measurements in comparison to those obtained for the earthquakes confirm that ambient noise offers a great potential to accurately determine the vibration modes of a large dam. Finally, a 3D numerical modal analysis made it possible to estimate a profile of the average stiffness of the embankment fill taking into account the characteristics of the site and the vibration modes of the dam.*

1 INTRODUCTION

The seismic analysis of an embankment dam requires dynamic parameters of the structure. The dam's vibration modes and the stiffness of the fill materials are essential data. The vibration modes can be obtained from earthquakes recorded on instrumented dams. However, there is very little instrumented dam and the occurrence of seismic events in eastern Canada is relatively low due to the seismic activity of this region. Obtaining seismic data is even more rarely for large dams built in a steep valley.

This article discusses the use of ambient noise to determine the vibration patterns of a large dam built in a steep valley in Quebec. The modal analysis of the ambient noise is performed by synchronizing experimental measurements obtained with each individual velocimeters. The occurrence of 3 microseisms measured on this same dam allows a rigorous validation of analyzes carried out with the experimental ambient noise

[2]Geotechnical Eng., Ph. D., Department of Civil Engineering and Water Engineering, Université Laval, Québec, Canada, Denis.LeBoeuf@gci.ulaval.ca
[3] Manager, Dam Safety Reviews, Hydro-Québec - Montréal, QC, Canada, Peloquin.Eric@hydro.qc.ca
[4] Manager, Dam Expertise, Hydro-Québec - Montréal, QC, Canada, Bigras.Annick@hydro.qc.ca

measurements. Lastly, a 3D modal analysis of the dam and its valley also validates the dam's vibration modes by iteratively adjusting the average stiffness of the embankment.

2 DENIS-PERRON DAM SITE DESCRIPTION

Denis-Perron Dam is a rockfill embankment 171 m high with a central till core and a crest length of 378 m. It closes the river in a very steep valley. It is built on coarse alluvium at the bottom of the valley except for the core, filters and transitions that are based on remodeled bedrock or concrete. On the banks, the fills are based on the bedrock or colluviums on the right bank downstream side.

Figure 1a) illustrates the plan view of the valley and the dam while figure 1b) shows a section of the valley in the longitudinal axis of the structure. The site area has rugged terrain formed by narrow valleys between rock masses that peak at an average elevation of about 500 m. The region is located in the Grenville Geological Province of the Canadian Shield; it is a tectonically stable zone of crystalline, igneous and metamorphic rocks of the Precambrian age. The bedrock is usually composed by a series of migmatized gneisses and, more rarely, gneisses. Locally, these series are interspersed with intrusive masses consisting of anorthosite, granite and pegmatite.

This dam was instrumented with two accelerometers between 1998 and 2002. An instrument was located on the crest of the embankment while the second station was positioned at the mid-height of the dam on the craggy rock support. The approximate position of the accelerometers is shown (red dots) in figure 1a).

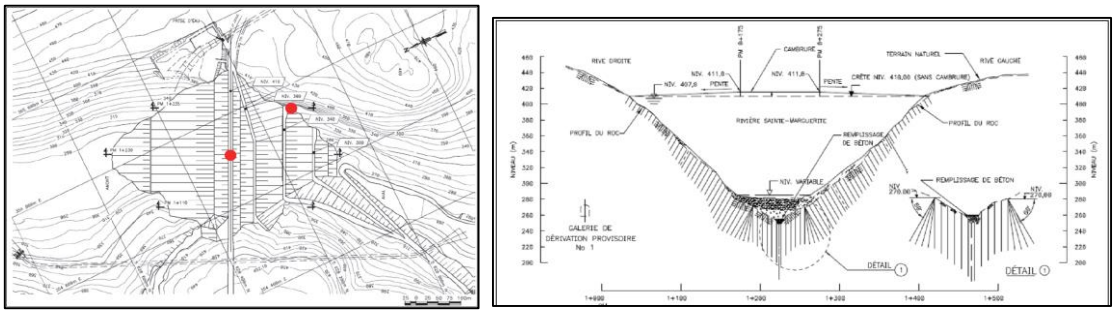

Figure 1.a) Plan view of the Denis-Perron dam, 1b) Longitudinal section of the valley in the central dam axis

3 EARTHQUAKES EVENTS

3.1 Signals processing

The accelerometers were of Altus K2 Kinemetrics type, recording signals in three directions, longitudinal, transverse and vertical with respect to the dam axis. They were instruments equipped with an acquisition system and an analog-digital converter, with a resonant frequency specific to each instrument around 50 Hz. The two instruments were synchronized in time.

This section presents an analysis of transfer functions from signals to estimate the fundamental vibration frequency. A more detailed analysis of these signals is presented by [1].

Between 1998 and 2002, these instruments recorded close to 671 sets of instrumental data. The vast majority of these events were related to blasting activities in the area of this hydro-electric facility. Although blasting activities are suitable for triggering such instruments, the large amount of non-earthquake instrumental data is derived from the fact that instruments were programmed to trigger at a low acceleration of 0.1% g (1 cm/s^2). A detailed analysis of seismic events identified by the Geological Survey of Canada (GSC) has allowed three sets of signals to be related to actual earthquakes. Table 1 lists these events and their main characteristics. The magnitude de Nuttli (M_N) of these earthquakes varies between 4.0 and 5.1.

Table 1: Earthquakes measured at the Denis-Perron dam site

Date	MN	Epicentral distance (km)	Latitude (°)	Longitude (°)
March 16, 1999	5.1	129.2	49.615	– 66.344
January 20, 2002	4.1	146.4	49.487	– 66.954
July 23, 2002	4.0	134.5	49.594	– 66.953

Signals in table 1 were processed according a bandpass filter between 0.3 and 40 Hz and a baseline correction. **Error! Reference source not found.**Figure 2 shows the temporal functions of the three earthquakes studied. Table 2 presents peak accelerations for each earthquake. These are earthquakes of very low amplitude. It is interesting to note that for the first two earthquakes, peak acceleration in the vertical direction exceeds horizontal peak accelerations and that for the third earthquake, the vertical acceleration remains also significant compare to horizontal directions. This is contrary to what is normally observed for free field land condition. In our understanding, this is a 3D effect (called site effect) resulting from the geometry of the steep valley. Elgamal [2] made the same observation for seismological data measured on the La Villita dam, particularly for the weakest earthquake.

Table 2: Peak acceleration of each earthquake

Earthquake	Acc. max Transversal direction			Acc. max Longitudinal direction			Acc. max Vertical direction		
	Rock (g)	Crest (g)	Ratio	Rock (g)	Crest (g)	Ratio	Rock (g)	Crest (g)	Ratio
March 16, 1999	0.0021	0.0118	5.6	0.0022	0.0105	4.7	0.0019	0.0178	9.4
January 20, 2002	0.0004	0.002	5	0.0006	0.0017	2.8	0.0004	0.0045	11.3
July 23, 2002	0.0002	0.0037	18.5	0.0002	0.0039	19.5	0.0002	0.0026	13

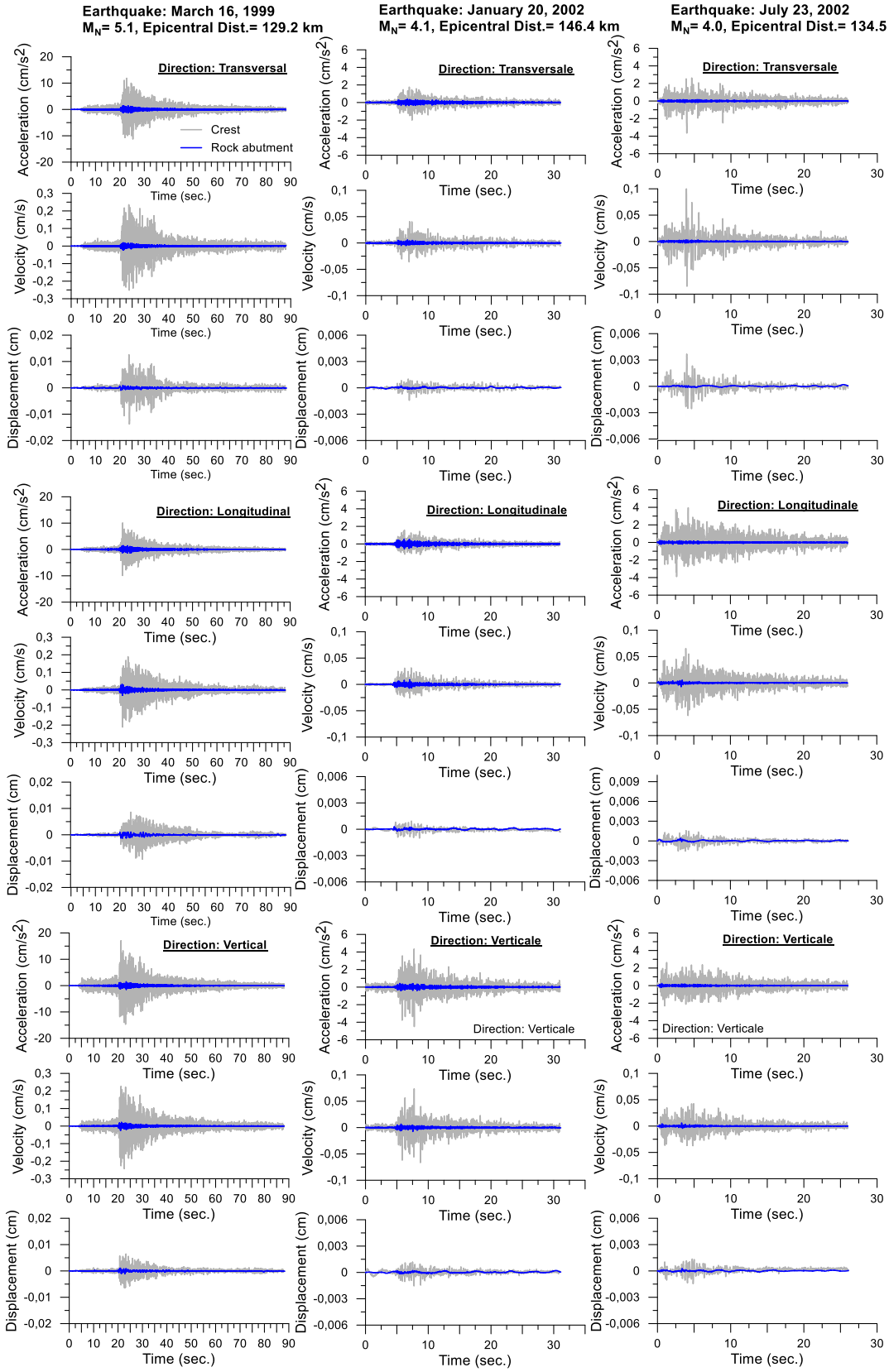

Figure 2.Temporal functions of the three recorded earthquakes on the Denis-Perron dam crest

3.2 Analysis of the fundamental vibration frequencies

For each direction of the earthquakes studied, the transfer function and the fundamental vibration frequency (F_N) were calculated by a comparison of the Fast Fourier Transform of

the signal on the crest of the dam compared to the one at the bedrock abutment (FFTcrest / FFTrock), calculated by averaging the ratios over a moving range. For each FFT value, it is an average of the Parzen window type defined over a range of frequencies centered on the FFT value. In the present analysis, the selected frequency range is 0.1 Hz (0.05 Hz on both sides of the FFT value).

Figure 3 show the transfer functions and the fundamental vibration frequency according to each direction of the three earthquakes. Transfer functions are similar for each earthquake event.The March 16, 1999 event, with the highest magnitude, has slightly higher fundamental vibration frequency values in the horizontal direction that one could be associated with slightly more nonlinear deformations. These small differences between the fundamental vibration frequencies can also be affected by various factors as winter conditions, level of the reservoir, uncertainties of the instruments, etc. Overall, these results from three different events are consistent. These signals, although of small amplitudes, offer the possibility to establish fundamental vibration frequency in each direction and to validate the behavior laws at very small deformations.

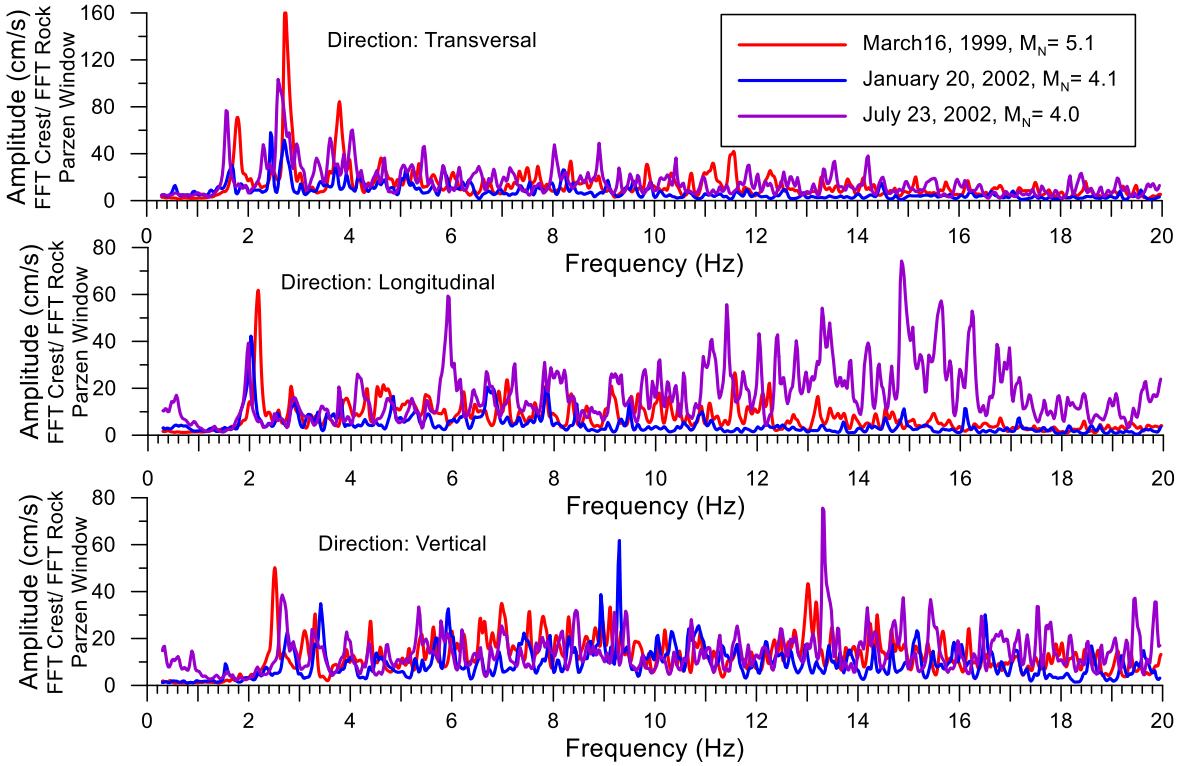

Figure 3: Transfer functions according to the three directions of the three earthquakes

Table 3 summarize fundamental vibration frequency range for each direction of the three earthquakes components.

Table 3: Fundamental vibration frequency range of the three earthquakes components

Direction	Fundamental vibration frequency (Hz)
Transversal	1.55-1.82
Longitudinal	2.00-2.20
Vertical	2.45-2.80

4 AMBIENT NOISE STUDY

4.1 Experimental ambient noise measurements

Ambient noise measurements were carried out on the Denis-Perron dam using six three-components Tromino-type velocimeters. The experimental program consisted of 10 sets of test measurements (T1 to T10) with the 6 instrument devices, 5 sets of measurements which were completed entirely on the dam crest (T1 to T5). For each series of measurements, a master identified instrument (M1) remained stationary at the same location and the other 5 Tromino devices (IN2 to IN5) were moved to various locations and synchronized with this master instrument (M1).

For the measurement series on the downstream face, additional master instruments (IN2, IN3 and IN4) remained stationary. Thus, with these stationary additional master instruments (IN1 to IN4), it became possible to synchronize all the individual series of measurements. Figure 4 illustrates the position of the test experimental measurements on the dam. As part of this project, the experimental data were acquired at a sampling rate of 1024 Hz over a period of 30 minutes with the exception of the last serie (number 10), which was acquired on a period of 20 minutes. As presented by[3], measurements with Tromino devices were conducted using the rigid plate support including 3 rods custom steel stems developed for this project and powerful antennas (TP-Link 2.4GHz 8dBi) connected to 6 m long cables were used to allow communication and achieve synchronization between each instrument.

5 MODAL ANALYSIS

5.1 Modal analysis by processing synchronized ambient noise measurements

The Artemis Modal Pro code [4], a software for modal analysis, was used to analyse synchronized ambient noise measurements. Artemis Modal Pro offers the advantage of selecting different modal analysis techniques in both frequency and time domains. The ability to use techniques in these two areas offers the advantageous option of comparing the calculated vibration modes with very different resolution methods. Analyses of the present study were carried out with two recent developed methods: the "Enhanced Frequency Domain Decomposition - EFDD" in the frequency domain and the "Stochastic Subspace Identification Extended Unweighted Main Component - SSI-UPCX" in the time domain. EFDD method provides estimates of damping ratios as well as improved estimates of natural frequencies and mode shapes.

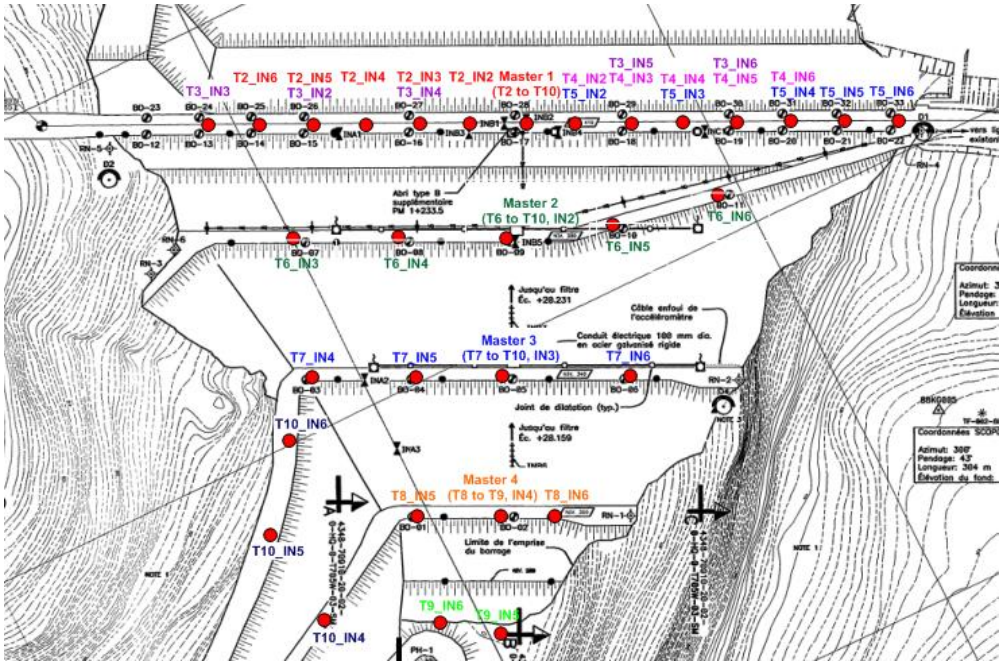

Figure 4: Position of the experimental ambient noise measurements

Figure 5 shows a compilation of vibration modes shape obtained with EFDD and SSI-UPCX estimation technics tested. Artemis provides an option called Modal Assurance Criterion (MAC) diagrams for mode shapes comparison between same or different estimation technics. A very good consistency is observed between the results of these two methods.

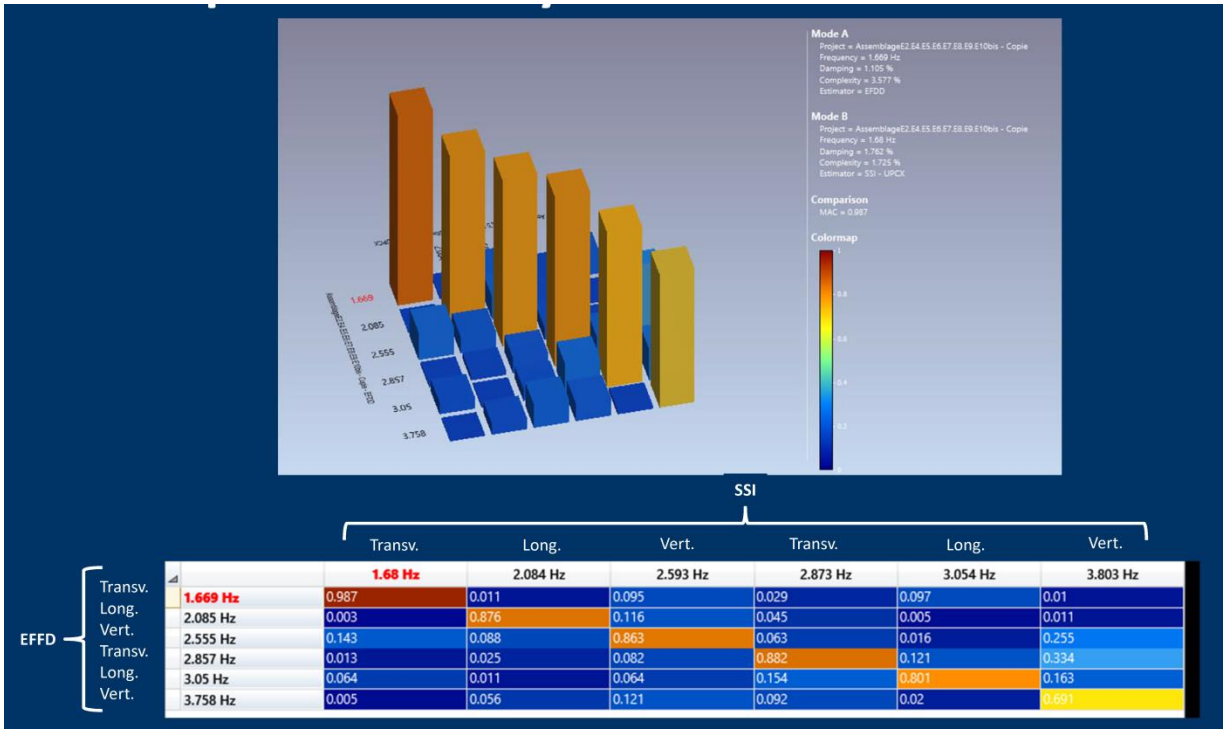

SSI

EFFD	SSI: Transv.	SSI: Long.	SSI: Vert.	SSI: Transv.	SSI: Long.	SSI: Vert.
	1.68 Hz	2.084 Hz	2.593 Hz	2.873 Hz	3.054 Hz	3.803 Hz
Transv. 1.669 Hz	0.987	0.011	0.095	0.029	0.097	0.01
Long. 2.085 Hz	0.003	0.876	0.116	0.045	0.005	0.011
Vert. 2.555 Hz	0.143	0.088	0.863	0.063	0.016	0.255
Transv. 2.857 Hz	0.013	0.025	0.082	0.882	0.121	0.334
Long. 3.05 Hz	0.064	0.011	0.064	0.154	0.801	0.163
Vert. 3.758 Hz	0.005	0.056	0.121	0.092	0.02	0.691

Figure 5: Compilation of vibration modes calculated with EFDD and SSI-UPCX methods

Fundamental vibration frequencies determined from a modal analysis by processing synchronized ambient noise measurements on the dam crest are within the range of fundamental vibration frequencies determined from the earthquakes event data.

Artemis Modal Pro provides also the advantage of visualizing modal deformed animations. These animations are very consistent with the individual results obtained with the software Grilla to the effect that the upper portion of the dam (berm at level 380 m to the dam crest) is much more excited in comparison to the lower portion of the dam confined in the valley, associated with a site effect.

5.2 Modal analysis by numerical retrofit calculation of the 3D valley-dam system

A numerical modal analysis was carried out in order to provide a second validation of the vibration modes obtained from the experimental ambient noise measurements. A three dimensional model of the Denis-Perron valley and dam was developed using the Rhinoceros 3D modeling software [4] and the ANSYS ICEM CFD Meshing software [6]. The modal analysis was performed with the ANSYS software [7] using the Finite Element Method (FEM). The geometry of the dam was modeled with mean uniform slopes incorporating the berms. Embankments fill were represented by only one material. Alluvium and colluvium left in place in the narrow furrow at the bottom of the valley were not represented in the numerical model at this stage of analysis. Despite these simplifications, the three dimensional model allows to take into account the geometric effects of the valley. Figure 6 illustrates the three dimensional model of the valley-dam system.

The modal analysis performed is a linear analysis and the foundation model is assumed to be massless. By considering a massless foundation, only its flexibility is taken into account. The modal analysis is affected by the rigidity of the dam-foundation system, the dam mass and the three dimensional geometry dam-valley system. The reservoir has not been taken into account for this modal analysis.

As reported by [8], this method has been used extensively for two and three dimensional dynamic analysis of concrete dams. In the present study, this method is applied for a three dimensional large rockfill dam. The stiffness of the embankments was gradually adjusted following a prismatic shear beam model as described in [9]. Figure 7 illustrates the schema of this model. The dam stiffness was also related to the parameter $K_{2\ max}$ computed with the standard relation (1) proposed by [10] (modified to be adimensional), whose stiffness is related with the effective mean stress (σ'_m) and the atmospheric pressure (P_{atm}). For this analysis, K_{2max} was increased iteratively until the fundamental vibration frequencies computed with Ansys coincided as closely as possible with those computed with earthquake events and by processing ambient noise data.

$$G_{max} = P_{atm} \cdot 21.7 \cdot K_{2max} \cdot \sqrt{\frac{\sigma'_m}{P_{atm}}} \quad (1)$$

Table 4 presents the three dimensional modal analysis results of the Denis-Perron Dam. The best retrofit of the fundamental vibration frequencies during the modal analysis is obtained using a K_{2max} of 130 (figure 8a)). Although this stiffness is an average value representative of an entire horizontal fill layer, as illustrated on the figure 8b), this K_{2max} value compares relatively well with published test results conducted on Oroville dam fill materials [10]. The fundamental vibration frequency presented in the table 1 for each direction is very close to the results obtained with earthquake events and by processing ambient noise measurements. Modal analyses indicate also than more than 80 % of the dam

mass is mobilized for the fundamental vibration frequency and almost the entire mass (more than 98 %) is mobilized when the second vibration mode is included.

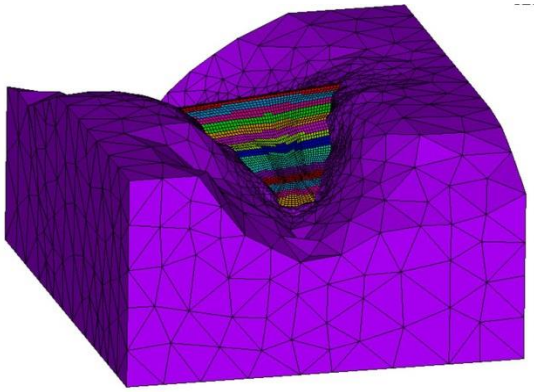

Figure 6: 3D model of the dam-valley system

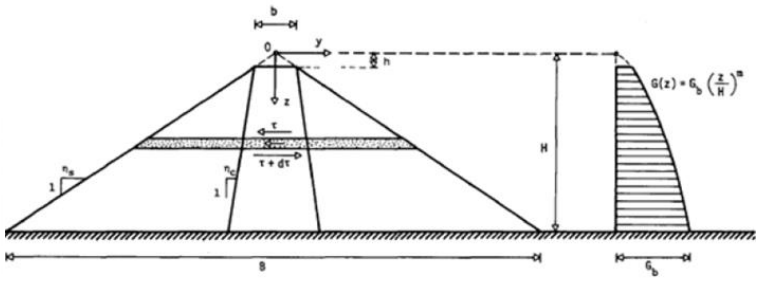

Figure 7: Prismatic shear beam mode, [9]

Table 4: 3D Denis-Perron dam modal analysis results with ANSYS

Mode	Frequency	Mass Contribution		
		Transversal	Longitudinal	Vertical
1	1.83	80.8	0.00	0.1
2	2.16	0.0	94.2	0.1
3	2.34	0.0	0.35	0.1
4	2.44	0.0	0.01	91.6
5	2.79	0.8	0.05	0.0
6	2.86	0.1	5.08	0.0
7	2.96	17.4	0.00	0.3
8	3.06	0.2	0.00	4.7
9	3.14	0.0	0.01	0.2
10	3.34	0.7	0.35	2.9

6 VIBRATION MODES RESULTS COMPARISON

Table 5 compiles vibration frequencies of the Denis-Perron dam calculated according to different methods. The similarity of frequencies between the different methods is impressive.

In comparison to values established from real earthquakes which are considered reference values or verification values, based on these results, ambient noise measurements appear very promising to determine vibration frequencies. Ambient noise measurements are easy, relatively inexpensive and quick to perform and do not present any risk of damage to the dam. But above

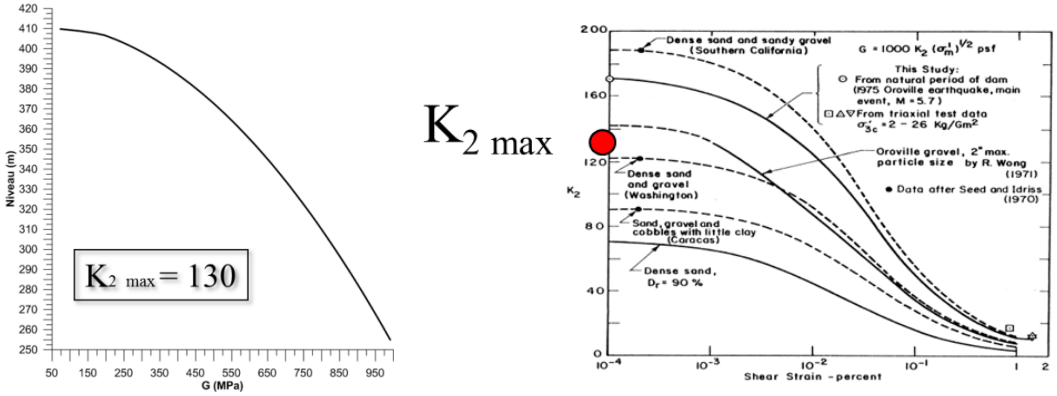

Figure 8:. a) Stiffness evaluation of the embankment dam, b) K2max comparison based on [11]

all it takes into account the site effects, i.e. geometry of the valley and the dam, foundation and stiffness of embankment fills. Second vibration mode could be only estimated after completing modal analysis with Artemis Pro software. From the earthquake data analyses or analyses of each ambient noise individual measurements data with Grilla software, it is very difficult to establish with certainty the second mode of vibration. The modal analysis with the software Artemis Pro offers analyzes that determine the higher modes taking into account a set of ambient noise measurements on a dam with its own characteristics (height, geometry, zoning, fill materials rigidity, shape of the valley, etc.).

The numerical modal analysis with a simplified 3D model in ANSYS also makes it possible to check the coherence between the estimation of the materials stiffness and the fundamental and superior dam modes of vibration confirmed with the analyses of real earthquakes and ambient noise measurements.

Table 5: Summary of vibration frequencies of the Denis-Perron dam

Direction	Fundamentals vibration frequency (Hz)				Second mode of vibration (Hz)			
	Earthquakes	Ambient Noise (Grilla) by[3]	Ambient Noise Modal analysis (Artemis Pro)	Modal analysis (Ansys)	Earthquakes[1]	Ambient Noise[1] (Grilla) by [3]	Ambient Noise Modal analysis (Artemis Pro)	Modal analysis (Ansys)
Long.	1.55 - 1.82	1.79 - 1.82	1.67 - 1.68	1.83	2.33 – 2.74	2.7 – 2.9	2.86 - 2.87	2.96
Trans.	2.00 - 2.20	2.07 - 2.10	2.08 - 2.09	2.16	2.84 – 2.92	3.1	3.05	2.86
Vert.	2.45 - 2.80	2.59	2.56 - 2.59	2.43	3.10 – 3.45	3.6 – 3.8	3.76 - 3.80	3.86

Note 1: Second vibration mode estimated after completing modal analysis with Artemis Pro software.

The comparison of the fundamental vibration frequencies results between seismic and ambient noise measurements for a large dam, as presented in Table 5, demonstrates the consistency of these two types of measurements in establishing the fundamental vibration modes for this type of earth structure.

7 CONCLUSION

It has been possible to measure ambient noise on a large rockfill dam in a steep valley. Processing of these signals made it possible to study the Denis-Perron 3D dam site effects and to determine the modes of vibration of this structure. The study of 3 real earthquakes makes it possible to validate analyses results obtained with the experimental ambient noise measurements. The study of 3 real earthquakes measured on the dam in 1999 and 2002 makes it possible to validate analyses results obtained with the experimental ambient noise measurements as well as those of the numerical 3D modal analysis.

This first validation of the potential for using ambient noise to establish the dynamic parameters of a large dam with real earthquakes by Hydro-Québec shows that this technology can be applied to embankment dams. Results of this work offer a very promising alternative for establishing dynamic parameters of an embankment dam without the need for a more conventional practice, namely the costly installation and maintenance of accelerometers in areas of low occurrence of seismic events as in eastern Canada.

8 ACKNOWLEDGMENTS

The authors wish to thank NSERC Canada and Hydro-Québec for funding this research project. The authors also wish to thank Hydro-Québec for sharing the instrumental data of the accelerometers installed on the Denis-Perron dam and authorizing this publication.

In order to share these results with the scientific community, the content of this paper was also published for the annual meeting of the 87th International Commission on Large Dams (ICOLD, 2019) [10] and the 12th Canadian Conference on Earthquake Engineering (CCEE, 2019) [10].

REFERENCES

[1] Verret, D., LeBoeuf, D. and Péloquin, É., (2015), Effets de Site du Barrage en Enrochement Denis-Perron (SM-3), Québec, Annual conference of Canadian Geotechnical Society, Québec, Canada
[2] Elgamal, A.W., (1992), Three-Dimensional Seismic Analysis of La Villita Dam. Journal of Geotechnical Engineering 118(12), 22.
[3] Miquel, B. and Verret D., (2019), The use of ambient vibration instrumentation for dams at Hydro-Québec, 12th Canadian Conference on Earthquake Engineering, Québec, Canada
[4] Artemis Modal Pro Software, Structural Vibration solutions, www.svibs.com
[5] Rhinoceros 3D Software, www.rhino3d.com
[6] ANSYS ICEM CFD Meshing software, www.ansys.com
[7] ANSYS Software, www.ansys.com
[8] Léger, P. and Boughoufalah, M., (1989), Earthquake input mechanisms for time-domain analysis of dam-foundation systems. Engineering Structures, 11(1), 37-46.
[9] Dakoulas, P., and Gazetas, G., (1985), A Class of Inhomogeneous Shear Models for Seismic Response of Dams and Embankments, Soil Dynamics and Earthquake Engineering, Vol. 4, No. 4, pp. 166-182.
[10] Seed, H.B. and Idriss, I.M. 1970. Soil moduli and damping factors for dynamic response analysis. Report No. UCB/EERCB-70-10, Earthquake Engineering Research Center, University of California, Berkeley

[11] Banerjee, N. G., Seed, H.B., Chan and C. K., (1979), Cyclic Behavior of Dense Coarse Materials in Relation to the Seismic Stability of Dams, Report No. UCB/EERC-79 /13, Earthquake Engineering Research Center, University of California, Berkeley
[12] Verret D., LeBoeuf D, and Péloquin É., (2019), Site effect study of Denis-Perron Rockfill Dam, 87th International Commission on Large Dams annual meeting, Canadian Dam Association, Ottawa, Canada
[13] Verret D., LeBoeuf D., Péloquin É. and Bigras A., (2019), Site effect study of a large rockfill dam: Denis-Perron Dam, 12th Canadian Conference on Earthquake Engineering, Québec, Canada

Performance of Darbandikhan Dam during a major earthquake on November 12, 2017

Omed S. Q. Yousif[1], Kawa Zaidn[2], Younis Alshkane[3], Abdulrahman Khani[4], Salar Kareem Hama[5]

[1]PhD, Irrigation Engineering, University of Sulaimani, Al- Sulaimaniyiah, Iraq
E-mail: omed.qadir@univsul.edu.iq

Keywords: Earthquake; Rockfill Dams; Failure; Deformation; Transverse Cracks; Longitudinal Cracks; probability

Abstract. *Darbandikhan Dam, a 128-meter-high rockfill dam with a vertical earth core and dumped rockfill shells, was struck by a strong earthquake (M 7.3) on November 12, 2017. The focal depth and distance of the earthquake from the dam were 23.4 km and 32 km respectively. Based on the magnitude and effect classifications, the earthquake was classified as a major earthquake with serious damage effects. The earthquake, therefore, caused remarkable deformation in the dam body. Several minor and major cracks, both transverse and longitudinal cracks, were developed in the crest pavement near the abutments and the center of the dam as well as along the dam axis at both u/s and d/s sides of the crest. In addition, the embankment settlement was notable along the axis of the dam with the maximum value near the maximum cross-section of the embankment. In this paper, the impacts of the earthquake on the dam body and its appurtenant structures were evaluated. From the results, it was observed that although the dam was strongly shaken, in general, its performance was satisfactory. This finding is fairly promising, however, this observation is influenced by the fact that the reservoir was low at the time of the earthquake. Thus, the November 12, 2017 Earthquake cannot be considered as the critical condition of the dam.*

1 INTRODUCTION

During earthquakes, the earth crust vibrates in all directions, both horizontally and vertically [1]. For embankment dams, the earthquakes may cause lateral and longitudinal deformation in the dams which in turn may cause settlements, and form longitudinal and transverse cracks [2,3]. The damages and deformations occurred due to the earthquakes may lead to near-failure or even full failure [4]. The settlement may cause freeboard reduction which in turn may lead to overtopping risks. The longitudinal cracks may lead to dam slope instability. The transverse cracks may cause initiation of internal erosion and then dam failure due to piping depending on whether there are adequate filter zones to stop the erosion [2]. Accordingly, one of the most serious problems worried dam engineers and the public is dam safety under strong earthquakes [5, 4, and 6]. For that reason, the designers seek for developing more convincing design approaches. In addition, the regulatory agencies started

[2]Professor, Irrigation Engineering, University of Sulaimani, Al- Sulaimaniyiah, Iraq, e-mail: kawa.abed@univsul.edu.iq

[3] PhD, Civil Engineering, University of Sulaimani, Al- Sulaimaniyiah, Iraq, e-mail: younis.ali@univsul.edu.iq

[4] Geologist, Director, Darbandikhan Dam Directorate, Al- Sulaimaniyiah, Iraq, e-mail: rahmankhany@gmail.com

[5] Civil Engineer, Darbandikhan Dam Directorate, Al- Sulaimaniyiah, Iraq, e-mail: salar.kariem@gmail.com

asking for more strict requirements pertaining to dam safety under seismic activities. Therefore, dam performance during earthquakes is considered in both national and international design codes [7].

Monitoring the behaviour of embankment dams during and/or after earthquakes occurrence is useful in predicting the behaviour of the dams in the future. This in turn can be useful tools in developing damage-seismic intensity relationships for predicting the occurrence of deformation in dams; settlements and cracks (longitudinal and transverse cracks).

According to Swaisgood [8], since 1990, the behaviours of embankment dams subjected to earthquakes has been under evaluation in order to obtain (1) an immediate assessment tool for the structure that has undergone seismic loading and (2) a method for estimating how much an embankment dam will deform based on actual dam behaviour during past earthquakes. The objectives of the study were evaluating the damages and deformation of a rockfill dam with central clay core subjected to a strong earthquake. This can be a useful tool to find the factors that have effects on the damages and deformation dams incurred during earthquakes. In other words, the evaluation can provide a valuable insight into earthquake – resistant design of dams and to verify the mathematical models used in design stage for a better prediction of dam performance in the future.

2 DARBANDIKHAN DAM AND RESERVOIR

Darbandikhan dam (see Figure 1) is a multi-purpose rockfill dam located on the Diyala-Sirwan river approximately 65 km south-east of Sulaimaniyah city and 230 km north-east of Baghdad city (Iraq); at Latitude 35.1128° N, and Longitude 45.7053° E. The dams' dimensions are 128 m height, 445 crest length, and 17 m crest width at elevation 495 m.

Figure 1 Darbandikhan Dam/ Iraq (Darbandikhan Dam Directorate).

The construction was begun in 1956 and completed in summer 1961. The design total capacity of Darbandikhan reservoir is 3 km³ at normal pool level (El. 485.00 m); 2.5 km² live storage and 0.5 km³ dead storage. However, due to 57 years of sedimentation, the current total storage volume is less than the design one (now it is about 2.5 km³). The reservoir is controlled by a gated ogee spillway having three 15m x 15m tainter gates. The spillway is located on the right abutment adjacent to the dam embankment. Two outlet conduits, 6 m and 9 m in diameter, feed three large turbines in a power house located at the dam's toe. A concrete intake tower for the outlets is located between the spillway approach channel and dam embankment, see Figure (1). In the intake tower houses, there are three vertical lift

gates, each 4.75m x 9.5m – one of the three gates serves the 6m diameter outlet conduit, the other two gates serve the 9m diameter outlet conduit.

3 FOUNDATION GEOLOGY AND CONSTRUCTION MATERIALS

Darbandikhan dam is located at the end of a narrow steep-sided canyon cut through an anticline by Diyala/Sirwan River. It lies in a folded nappe zone to the southwest of the plate boundary where the Arabian plate is being subducted beneath the Persian plate. At the dam site, the rocks dip downstream towards the southwest; about 45 degree. The dam's foundation comprises a series of sedimentary rocks including marls, sandstones, and conglomerates.

The dam body is composed of a thin vertical clay core with side slopes of 1:0.3 (v:h), upstream and downstream transition zones (two-stage chimney drain upstream consists of a finer-grained filter layer and a coarser grained drain layer each of width of 3 m, with an identical three stage drain at the d/s), and upstream and downstream dumped rockfill shells with side slopes of 1:1.5 and 1:1.35, respectively. The core and filters were compacted, while the outer rockfill shells were dumped. There is no alluvial layer present under the dam. Figures (2) and (3) show the cross-section (maximum cross section) and the longitudinal of the dam; respectively.

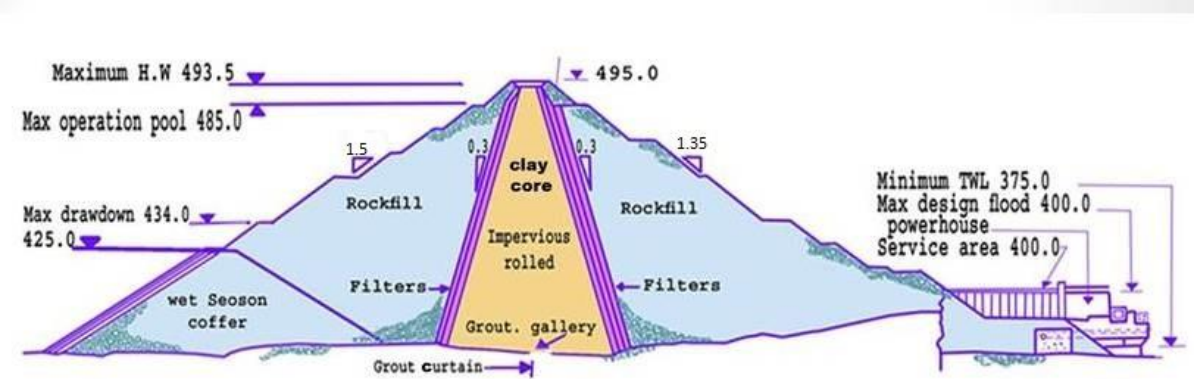

Figure 2 Maximum Cross Section of Darbandikhan Dam (Darbandikhan Dam Directorate).

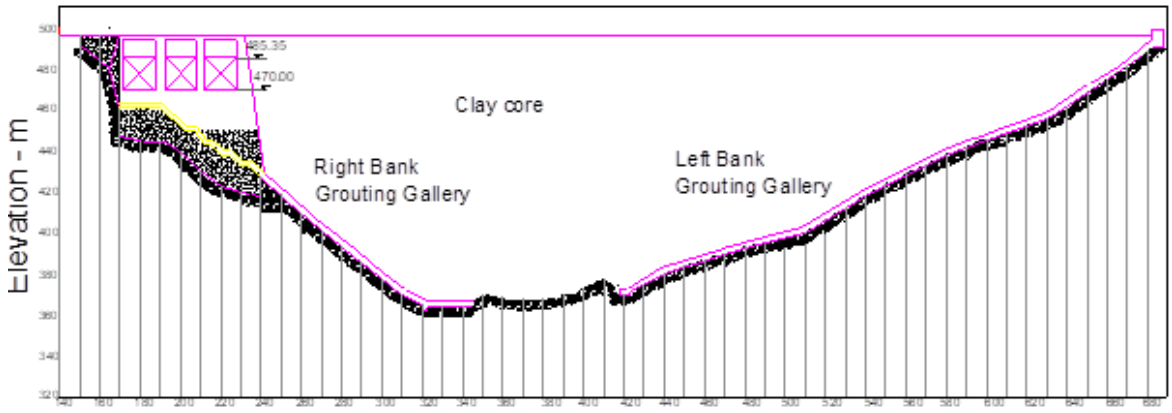

Figure 3 Profile of the Darbandikhan Dam - Looking Upstream (Darbandikhan Dam Directorate).

4 SEISMIC FEATURES

A large earthquake with a moment magnitude of 7.3 (Mw = 7.3) occurred on November 12, 2017, near the Iran-Iraq border (220 km northeast of Baghdad, Iraq) [9]. According to USGS [9], the earthquake occurred as the result of oblique-thrust faulting at mid-crustal depth (~25 km). Preliminary focal mechanism solutions for the event indicate rupture occurred on a fault dipping shallowly to the east-northeast, or on a fault dipping steeply to the southwest. The epicentre of the main shock of the event was located near Ezgeleh town (5 km from Ezgeleh and 43 km from Sarapul-e Zahab, see Figure 4; at latitude 34.77 N and longitude 45.76 E. The focal depth and distance of the earthquake from Darbandikhan dam were 23.4 km and 32 km respectively. The event, commonly referred to as the Ezgeleh Earthquake, was among the most disastrous earthquakes that have affected Iraq/Iran border since 1909 like the Sialkhor earthquake with Mw 7.4 in the central Zagros region USGS [9]. The earthquake resulted in 500 victims and about 12 000 homeless.

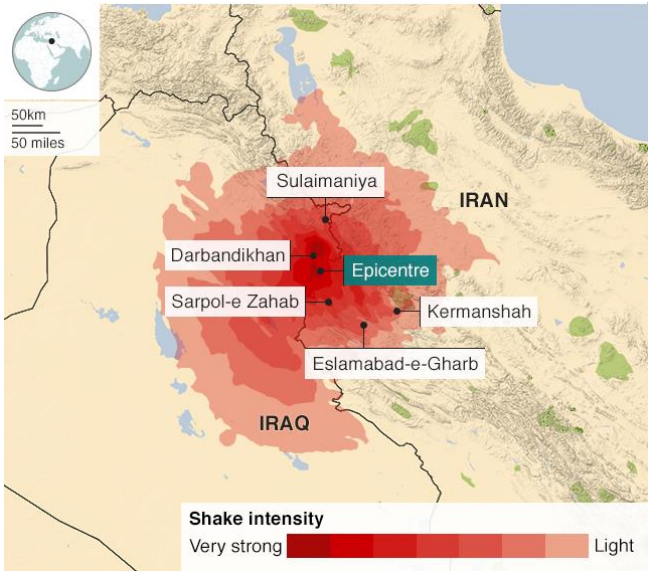

Figure 4 Earthquake intensity and extent (adapted from USGS, 2017)

4.1 Peak Ground Acceleration

Peak ground acceleration (*PGA*) is the maximum earthquake-induced ground acceleration at the dam foundation. These values are given as a fraction of the acceleration due to gravity. An estimation of the peak ground acceleration at the foundation can be predicted by using the formula of Esteva and Rosenblueth [10], as reported by Fell et al. [3]. The calculation requires knowledge of the magnitude (*M*), focal depth in km (*FD*) and epicentral distance in km (*ED*). The formula of Esteva and Rosenblueth [10], as cited in Pells and Fell, [2], is as follows:

$$PGA = \frac{20000}{9810} e^{0.8M} \left(\sqrt{ED^2 + FD^2 + 400}\right)^{-2} \quad (1)$$

Accordingly, for the earthquake occurred on November 12, 2017, with *FD* = 23.4 km and *FD* = 32 km, the peak ground acceleration at Darbandikhan dam site is 0.3555g.

4.2 Duration

A major feature of the observed earthquake besides its high magnitude is its long duration. The Ezgala earthquake duration was about 30 seconds [9]. Long durations of earthquakes may have more impact on embankment dams than short period earthquakes having the same peak acceleration or even less peak acceleration [11].

4.3 Effects of the Earthquake

At the time of the earthquake, the water level in the reservoir was at elevation 471.92 m; about 13 m below the normal operation level (about 23 m below the crest). Furthermore, the reservoir level had been low for about six months prior to the earthquake. Therefore, the upper embankment materials can be considered as non-saturated part at the time of the earthquake. However, the embankment experienced notable deformation at the crest. There were transverse cracks in the crest pavement near the abutments as well as longitudinal cracks along the whole dam length at both u/s and d/s sides of the crest. Settlements along the length of the dam have occurred. In addition, due to the earthquake, many rock boulders have fallen from the high steep mountains surrounding the dam. The sizes of the rocks ranged from a few centimetres to more than 2.5 m in diameter.
After the earthquake, many experts have immediately visited the dam to check its safety and to provide instructions for dealing with the new situation of the dam. As an instant safety measure, the reservoir water level was gradually reduced during one week (about 1.9 m).

5 SETTLEMENTS AND DEFORMATION

Soon after first filling of the Darbandikhan reservoir, 1961-1962, unexpected large settlement occurred in the contact zone with the concrete intake/spillway structure. A report of the commission of experts from 1973 indicates settlement of 1.08m [12]. A further report of experts from December 1976 concluded that the settlements resulted from the consolidation process of the core material in that zone. The remedial works undertaken in 1980 and further reconstruction works of the crest were required in 2001 which were undertaken by the Dam Directorate included the construction of an asphalt crest road with kerbs and safety barriers [12].

According to the geodetic survey conducted immediately after the earthquake, the dam has experienced non-recoverable earthquake-induced deformations; about 22 cm horizontally in the upstream/downstream direction, 13 cm horizontally in the right abutment to the left abutment direction. In addition, the maximum vertical displacement was about 48 cm as shown in Figure (5). The displacements of dam were measured basing on the movements of benchmarks installed along the dam axis.

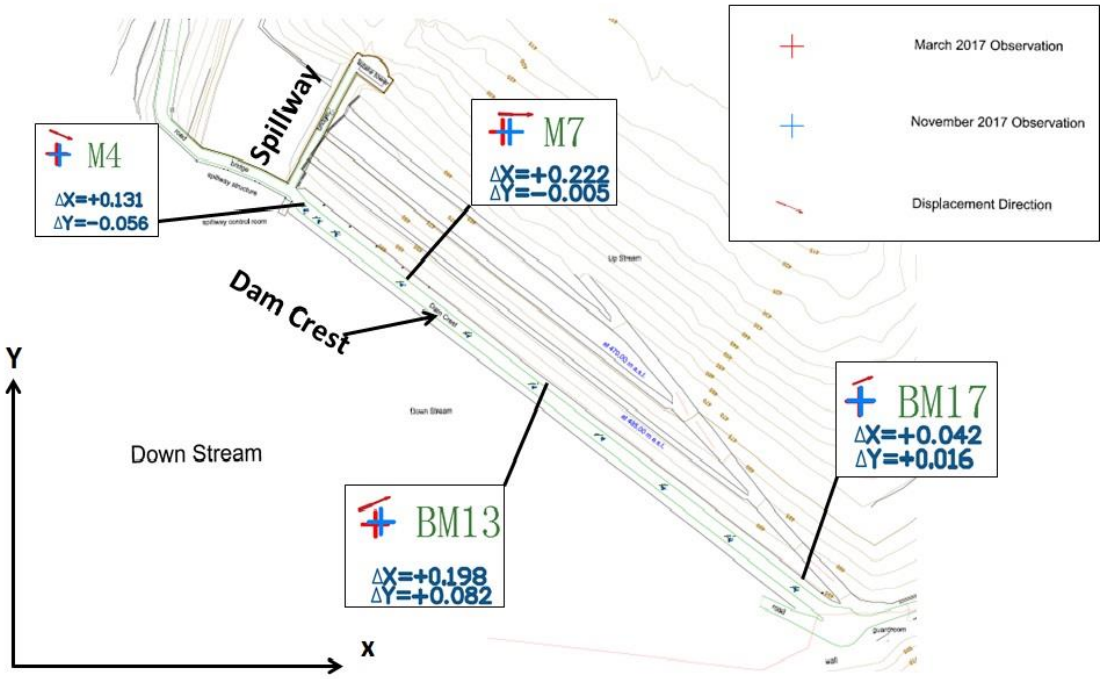

Figure 5 Displacement on the surface of the dam (Darbandikhan dam Directorate)

Regarding dam settlement, Figure 6 shows the settlements occurred over the crest of the embankment dam as a result of the earthquake. The figure shows that settlement of up to 48 cm was occurred over crest length with slightly greater settlements near the maximum cross section.

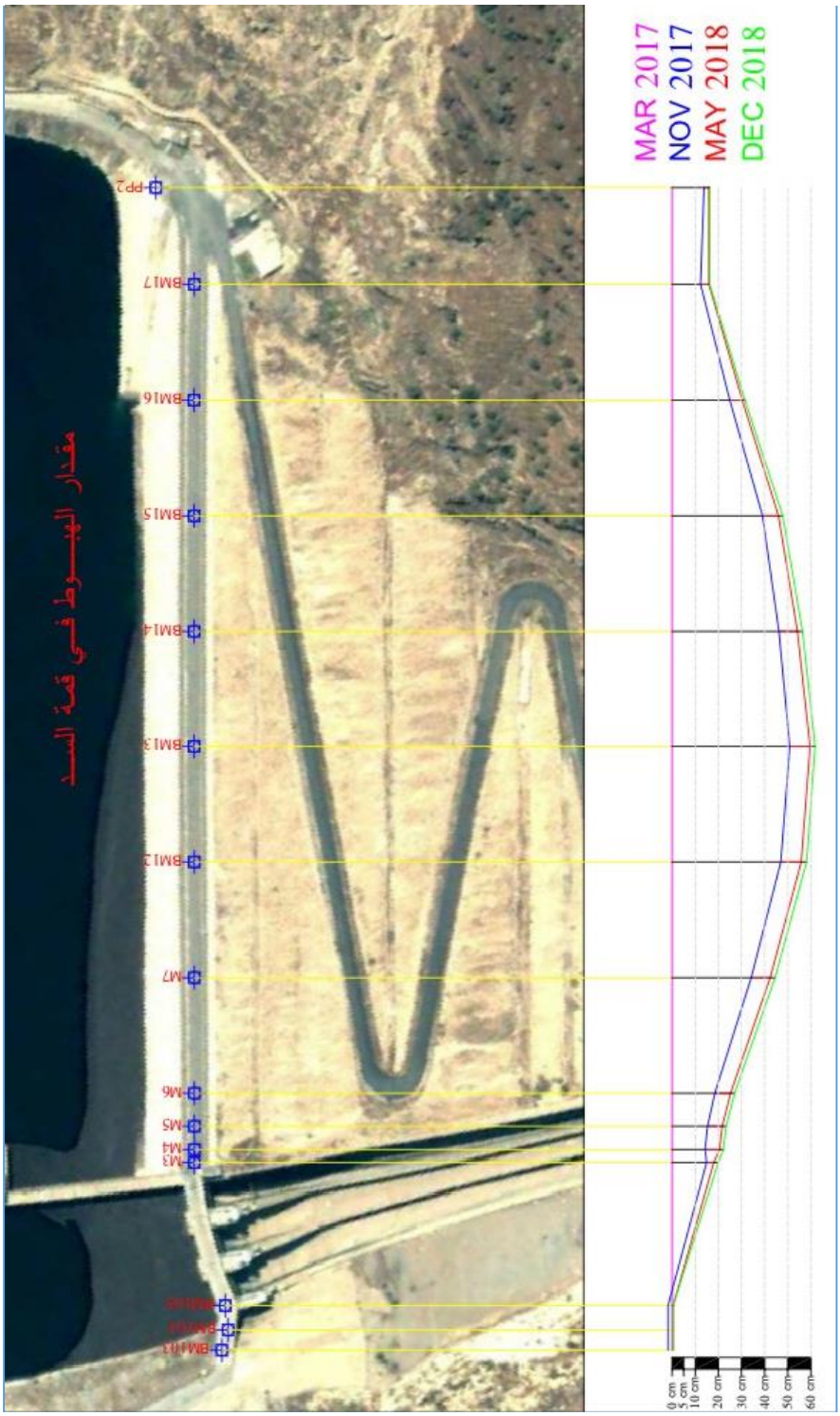

Figure 6 Vertical settlements occurred over the crest of the embankment dam as a result of the earthquake and after the earthquake (Darbandikhan Dam Directorate).

The mathematical model provided by Swaisgood [8] was used to estimate the crest settlement. The model, for the dams not subjected to liquefaction, can be expressed as:

$$\%Settlement = e^{(6.07PGA+0.57M-8.00)} \quad (2)$$

Where % Settlement = the amount of settlement of the crest of the dam (in meters) divided by the height of the dam plus the thickness of the alluvium (in meters) times 100; *PGA* = peak horizontal ground acceleration of the foundation rock (in g) recorded or estimated at the dam site; and *M* = earthquake magnitude (in surface-wave scale: *MS*).

The estimated earthquake-induced crest settlement for Darbandikhan dam using Swaisgood [8] mathematical expression is 0.19% [M = 7.3; PGA = 0.355]. The actual average and maximum crest settlements are 28 and 48 cm respectively. Therefore, the actual average and maximum % settlements for the crest are 0.22% [0.28/128)*100] and 0.375% [(0.48/128)*100] respectively. From the results, it seems that Swaisgood [8] formulae predictions are optimistic, perhaps more suitable to describe the average settlement.

Cracks, along with settlements, are the most regular feature occurs in dams under seismic loading [2, 11, 13, and 14]. Although they occur in various kinds, cracking in dams subject to earthquake can be classified in two main forms; longitudinal cracking and transverse cracking. The longitudinal cracking of embankments is cracking that is oriented parallel to the crest (axis) of the dam. While the transverse cracks of embankments are cracking that is oriented perpendicular to the crest of the dam. Although, according to Swaisgood [15], the longitudinal cracking on the upstream slope, is the most common type in dams subject to earthquake, the transverse cracks are the most dangerous ones which pose a greater threat to the safety of the dam.

5.1 Longitudinal cracks

The longitudinal cracks of Darbandikhan dam, occurred due to the November 12, 2017 earthquake, were mostly on both upstream and downstream slopes near the crest. The two main longitudinal cracks were occurred at both sides of the asphalt road, see Figure (7), and run over the entire length of the dam (445 m). Shorter longitudinal cracks were also formed at other locations down the slopes. However, no longitudinal cracks were observed along the middle of the road. The width and the depth of these cracks were variable and the largest longitudinal crack has been seen at the downstream side, opening a gap of about 15 cm as shown in Figure (8). The longitudinal crack width decrease near the abutments where the height of the dam is lower. In addition, the walkways beside the pavement on the dam crest, at both d/s & u/s sides, were deformed and sloped and the lighting poles were tilted at angles between 20 to 40 degrees, see Figure (8). The inclination of the walkways and the separation of the pavement and curbs on the crest of the dam, without any longitudinal cracks in the middle, indicate that the shells have deformed much more than the core. The deformations are attributed to the rearrangement of the aggregates and stones in the dumped rockfill shells. This can be affirmed by the fact that the main two longitudinal cracks are aligned with the interfaces between the compacted clay core and filter layers and the dumped rockfill shells.

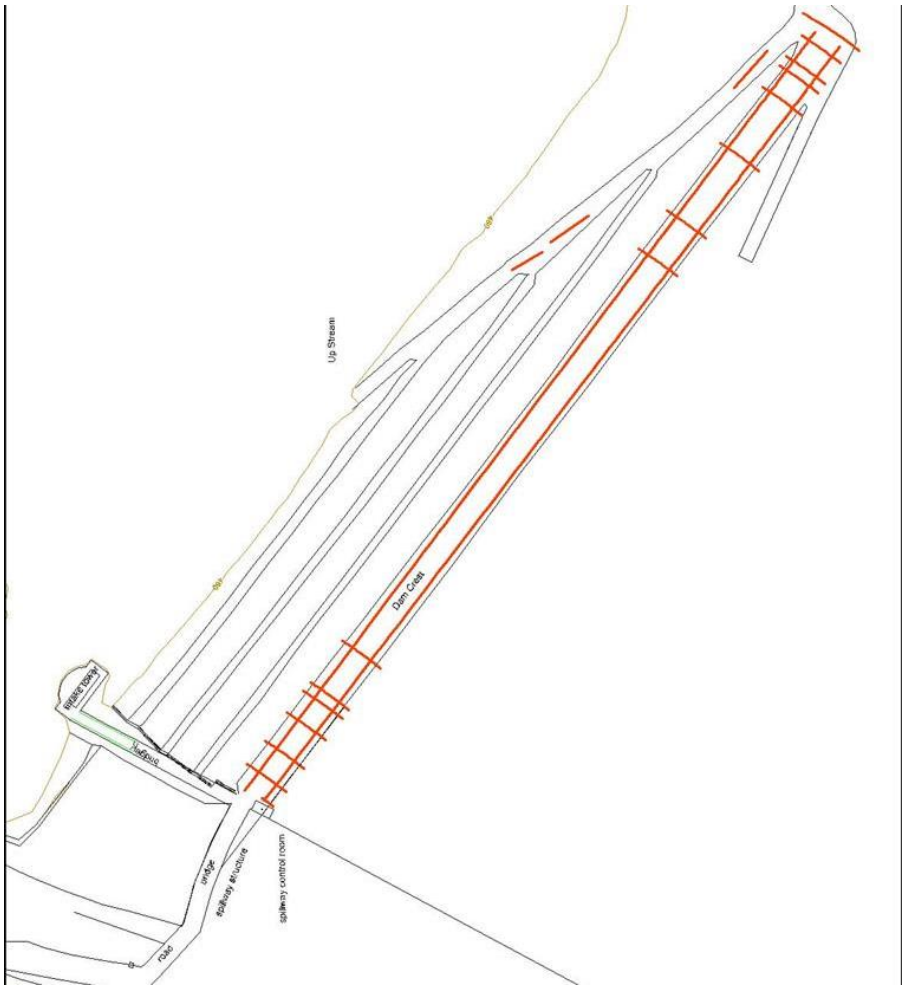

Figure 7 Cracks pattern, the red lines are transverse and longitudinal cracks as a result of the recent earthquake

In order to check the extent of the longitudinal cracks and existence of any sliding scarps, several test pits have been excavated. It was found that the cracks are limited to the top two meters of the gravelly protection materials above the clay core. Regarding sliding, no sliding traces have been observed.

Figure 8 Longitudinal cracks and walkway deformation at the d/s side (looking to the left of the dam (Darbandikhan dam Directorate).

5.2 Transverse Cracks

The earthquake caused several transverse cracks in Darbandikhan dam. The cracks distributed along the length of the dam at the crest. However, the transverse cracks are mainly close to the abutments as shown in Figure (9A). From the pits, it was found that most of the transverse cracks, except one, are superficial minor cracks with depths less than two meters and widths less than 3 cm in general. One transverse crack, located next to the concrete spillway, was major crack. This kind of transverse crack, called separation crack, is common in embankment dams close to a concrete structure, or built on a very steep abutment, under both seismic and static loads [2, 16]. The embankment of Darbandikhan dam is leaning to a concrete spillway structure constructed on the right abutment. The maximum crack width was 16 cm, but its depth could not be found. From Figure (9A), it appeared that the crack formed a wedge at this location. The maximum width of the wedge was 74 cm.

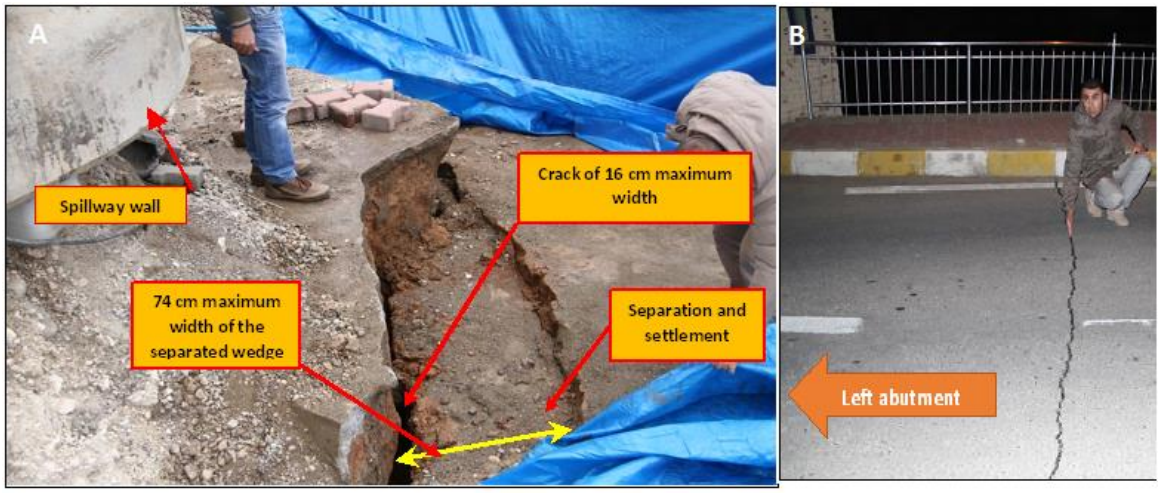

Figure 9(A) The crack at the contact between the spillway and the embankment, (B) Transverse crack near the left abutment

6 SLIDING

Although it is a well-recognized phenomenon, sliding of embankment dams and their foundations due to earthquakes is few, or not reported by the previous authors [16]. However, according to Swaisgood [15], the earthquake induced slides are shallow, sloughing type slides located mostly in the outer portion of the slopes. Therefore, sliding with large displacement is typically attributed to liquefaction. Furthermore, some authors believe that often longitudinal cracking represent the top of the slide scrap [2]. Regarding Darbandikhan dam, although several longitudinal cracks occurred, no sliding traces have been observed.

However, landslides near the dam have been reported at the left and the right banks of the reservoir **(see Figure 10)**. The right bank sliding is more dangerous compared to the left one because it is near the spillway and the bottom outlet intake. The maximum movement recorded at the right side due to the earthquake was **26 cm towards the reservoir.** It should be noted that the right bank already has sliding problem and historically many treatment measures have been carried out to minimize the sliding at this zone.

Figure 10 Sliding at the left abutment (adapted from directorate of Darbandikhan Dam).

7 THE EFFECT OF THE EARTHQUAKE ON THE DAM FOUNDATION, GALLERIES AND SPILLWAY

The grouting gallery in Darbandikhan dam consists of two parts; right side part (right gallery) and left side part (left gallery). The right gallery of the Darbandikhan dam was constructed at the base of the clay core, along the dam axis, following the bedrock surface. The upper part of the gallery, ends at about elevation 366 m, is merged into the spillway concrete structure and extends to 175 m from the right abutment. Similarly, the left gallery of the dam was constructed at the base of the clay core, along the dam axis, following the bedrock surface. It ends at about elevation 373 m and extends about 250 m from the left abutment. The two galleries have not been linked to each other; therefore there is a 75 m gap between them under the middle part of the dam. Figure (3) shows the profile of the Darbandikhan dam. The galleries are found to be generally in a good condition after the earthquake. Seepage flows into the gallery were mainly observed at construction joints in the concrete walls and vault, although some leakage water was also observed at points where no joint is located.

The spillway experienced shaking under the earthquake. From the visual inspections it was found that the spillway structure was not damaged. Cracks have not been observed. Although, the spillway displaced 11 cm in the downstream direction, to the southwest, no damages have been observed; the spillway itself and the radial gates on the spillway ogee crest are operating normally.

Regarding the intake structure, the tower and the gates, no damages have been observed as well.

7.1 Seepage condition

In Darbandikhan dam, there are 28 piezometers in the grouting galleries; 13 in the right gallery and 15 in the left one. In addition, there are 9 pressures cells, installed in 1976, in the clay core close to the spillway (6 m to 17 m away from the spillway) with different depths from 22 m to 54 m. Furthermore, two small weirs, placed at the bottom of the two galleries (one placed in the left gallery and the other weir in the right one) are regularly used to measure the total flow in the galleries. Regarding the seepage from the dam core into the downstream filter layers, since the toe drain is covered by the buildings of the hydropower station, no information can be obtained. Therefore, the only collectible data regarding seepage are those collected by the small weirs in the galleries.

From the data collected in the day after the earthquake, the seepage amounts in the galleries were increased; from 1.0 l/min to 2.1 l/min and from 1.47 l/min to 5.44 l/min for the

left and the right galleries respectively. In addition, some of the piezometers in the left gallery showed water surface elevation increases; up to 9 meters. However, the other piezometers showed a little or no increasing in water pressure. The piezometers in the right gallery showed little or no increase as well. Regarding the pressure cells, although four of them are not functional, in the remaining five pore water pressure cells indicate that the water pressure increased up to 6 meters one day after the earthquake. The cause of water rise is debatable. However, the increased pressure in the piezometers and cell pressures can be attributed to the earthquake-induced consolidation of the clay core in the dam.

8 THE EFFECT OF AFTER SHOCK EARTHQUAKES ON THE DAM.

Typically, there will be a rise in water pressure within the embankment dams after the earthquakes. However, the increased pressure will normally dissipate over time. In addition, the possibility of activation or reactivation of internal erosion by seismic loading is a long-recognized phenomenon [17]. It is also known that most of the changes in seepage conditions returned to pre-earthquake conditions within a month after the event [2]. Regarding Darbandikhan dam, the increased seepage in the grouting galleries have not returned to their normal values so far; more than a year after the earthquake. However, the increases in the pressure cell and piezometers started to go back towards the normal levels in about one week. Regarding the settlements in Darbandikhan dam after the earthquake, their values increased. This means the settlement of the dam is continuous; the maximum crest settlement increased from 48 cm immediately after the earthquake to 61 cm after 13 months; from November 12, 2017, to March 2019 (see Figure 6). The increased values in the settlement can be attributed to either dissipation of the increased pore water pressure due to the earthquake, or due to the post shocks. Regarding the crack widths, after 13 months, little changes have been observed.

9 DAMAGE CLASSIFICATION

Since the actual maximum crest settlement for the dam due to the earthquake is 0.375%, according to Swaisgood [15, 18] damage classification system, the Darbandikhan dam has suffered minor to moderate damage. However, according to the damage classification system developed by Pells and Fell [2], since the maximum width of the longitudinal cracks is 140 mm, the dam has suffered major damage. From the excavated pits, it was found that the longitudinal cracks were in the top layer of the dam (top granular layer of the dam); they only penetrated upper two meters of the road subbase on the top of the dam. The cracks have not penetrated the core. Therefore, the later system cannot be used for Darbandikhan dam. Accordingly, the damages occurred in the Darbandikhan dam is considered as minor to moderate.

10 PROBABLITY OF FAILURE OF THE DAM

The safety of Darbandikhan dam becomes a crucial issue after the earthquake for the managers of the dam, the major concern was about the crack close to the spillway whether it has deep extension or not. That is why the dam directorate kept the water level below 470 m (25 m below the crest of the dam) for more than a year.

Internal erosion problems are often difficult to identify and to estimate. However, clayey materials may not be likely to erode until cracks reach 2.5 or 5 centimeters in width and hydraulic gradients approach 0.5 or more, cracks in clays may be closed upon swelling by wetting process, Fell et al. [3]. Darbandikhan dam may be considered at low risk providing the high plasticity clay core and the upstream and downstream filters which restrict

internal erosion processes. The objectives of this paragraph are to give a quantitative risk assessment and guidance for persons in charge to assessing the safety of the dam.

Foster et al. [19] developed a method at the University of New South Wales (UNSW) to calculate the probability of failure of embankment dams due to piping. UNSW method relies upon the assumption that the performance of embankment dams in the past is a guide to their performance in the future. This method estimates the likelihood of piping failure of a dam by adjusting the historical frequency of piping failure by weighting factors which take into account the dam zoning, filters, age of the dam, core soil types, compaction, foundation geology, dam performance, and monitoring and surveillance [20].

UNSW method considers three modes of piping failures namely; piping through the embankment, foundation and from embankment to the foundation. The annual probability of failure by piping, P_p, is obtained by summing the weighted likelihoods of each of the modes as shown in the following expression:

$$P_p = w_E P_e + w_F P_f + w_{EF} P_{ef} \quad (3)$$

Where

w_E, w_F and w_{EF} are weighting factors for piping through the embankment, foundation and from the embankment to the foundation, P_e, P_f and P_{ef} are annual frequency of failure through the embankment, foundation and from embankment to the foundation.

The probability of failure due to piping 1.65×10^{-7} so, the risk of piping is low in Darbandikhan dam, this low value of probability of failure is attributed to the proper measures adopted in the construction of the dam such as multi stage filters and the high plasticity clay core.

11 CONCLUSIONS

Darbandikhan dam, rockfill embankment dam with a central clay core, was struck by a strong earthquake on November 12, 2017. The dam has experienced several damages and deformations. The deformation of the dam's crest caused by the earthquake is principally settlement and cracks; apparently, there is no slide failure along the longitudinal cracks. Differential settlement and the cracks in the dam are related to changes in geometry and compressibility of material in the embankment zones; core, shells and foundation slope discontinuities. Basing on the deformations caused by the earthquake, the dam suffered minor to moderate damages. In addition, basing on the UNSW method for assessing the probability of piping failure, since it was designed and constructed adequately, Darbandikhan dam has low chance to fail by piping under static condition. Furthermore, at the time of the earthquake the water level in the reservoir was low. Therefore the dam performed satisfactorily and survived from the earthquake occurred on November 12, 2017, with a magnitude of 7.3.

Acknowledgement

The authors are very grateful to the Darbandikhan Dam Directorate and the supervisory committee for evaluating of Darbandikhan Rockfill dam from the General Directorate of Dams and Reservoirs in Iraq especially Consultant Engineer Tareq Albatal for providing data and graphs. Also we would like to acknowledge the Surveying Engineer Omed Fakhrulddin for pr.oviding the details of the deformatan due to the earthquake.

References

[1] Newmark, N. M. Effects of earthquakes on dams and embankments. Geotechnique, 15(2), 139-160, (1965).

[2] Pells, S., & Fell, R. Damage and Cracking of Embankment Dams by Earthquakes and the Implications for Internal Erosion and Piping. University of New South Wales, School of Civil and Environmental Engineering, (2002).

[3] Fell, R., Foster, M. A., Cyganiewicz, J., Sills, G. L., Vroman, N. D., Davidson, R. R. Risk Analysis for Dam Safety: A Unified Method for Estimating Probabilities of Failure of Embankment Dams by Internal Erosion and Piping, URS Australia, New South Wales, Sydney, Australia, (2008).

[4] Davoodi, M., Sakhi, M. A., & Jafari, M. K. Comparing Recorded Earthquake Signals of MS Embankment Dam with Numerical Modeling Results. In Paper of "China Day", 14th World Conference on Earthquake Engineering, Beijing, China, October (pp. 12-17), (2008).

[5] Seed, H. Bolton, "Earthquake-Resistant Design of Earth Dams" International Conferences on Recent Advances in Geotechnical Earthquake Engineering and Soil Dynamics. 23, (1981).

[6] Houqun, C. Consideration of dam safety after Wenchuan earthquake in China. In Paper of "China Day", (2008).

[7] Sêco e Pinto and Pedro Simão Understanding seismic embankment dam behaviour through case histories. In Proc. V Int. Conference on Recent Advances in Geotechnical Earthquake Engineering and Soil Dynamics, San Diego, paper n. SOAP (Vol. 2), (2010).

[8] Swaisgood, J. R. Embankment dam deformations caused by earthquakes. In Pacific conference on earthquake engineering, 14th World Conference on Earthquake Engineering, Beijing, China, October (pp. 12-17), (2003).

[9] USGS. https://earthquake.usgs.gov/earthquakes/eventpage/us2000bmcg/executive,(2017).

[10] Esteva, L. and Rosenbluth , E. Espectros de temblores a distancias moderadas y grandes. Bol. Soc. Mex. Sism.,2: 1-18, (1964)

[11] Yamaguchin Y., Kondo M., Kobori T. Safety inspections and seismic behavior of embankment dams during the 2011off the Pacific Coast of Tohoku earthquake. Soils andFoundations, 52(5), 949-955, (2012).

[12] Cordell, M.C. Dokan and Derbendikhan Dam Inspections; SMEC International Pty. Ltd.: Malvern East, Australia, (2006).

[13] Singh R., Roy D., Jain K. S. Analysis of earth dams affected by the 2001 Bhuj Earthquake. Engineering Geology, 80, 282-291, (2005).

[14] Bardee J. P. and Davis C. A. Performance of San Fernando dams during 1994 Northridge earthquake. Journal of Geotechnical Engineering, 122(7), 554-564, (1996).

[15] Swaisgood J. R. Seismically-induced deformation of embankment dams. In proceedings of sixth national conference on earthquake engineering. Seattle, Washington, U. S. A. May 31 – June 4 (1998).

[16] Sherard, J. L., Woodward, R. J., Gizienski, S. F. & Clevenger, W. A, Earth and earth rock dams. John Wiley & Sons, (1963).

[17] Vick, S.G. Effect of Seismic Shaking on Internal Erosion of Embankment Dams. Report prepared to BC Hydro, (1993).

[18] Swaisgood, J. R. "Estimating deformation of embankment dams caused by earthquakes." ASDSO Western Regional Conf. (1995).

[19] Foster, Mark, Robin Fell, and Matt Spannagle. "A method for assessing the relative likelihood of failure of embankment dams by piping." *Canadian Geotechnical Journal* 37.5 (2000): 1025-1061.

Dynamic behavior of a large earth dam located in a severe seismic area

Dariush Belashi

Mahab Ghodss Consulting Engineer
Iran
E-mail: dbelashi@yahoo.com

Keywords: Seismic design; Dynamic analysis; Permanent deformation; Equivalent linear; nonlinear

Abstract. *Equivalent-linear analysis of earth dams is an acceptable approach in order to determine the dynamic behavior of earth structures. Nevertheless, with significant progress in nonlinear material modeling and testing, the embankment dams are increasingly being studied by finite element and finite difference methods with advanced nonlinear material models. In order to better understand the difference between results of two approaches for high dams located in sever seismic areas, a 150 meter height mixed clay earth fill dam located in severe seismic area near some major faults is analyzed using both the equivalent-linear and the nonlinear approach. The results of different methods for estimation of permanent deformation of the dam during earthquake are compared and the effects of geometry of the designed dam are also studied on the estimated earthquake induced displacements.*

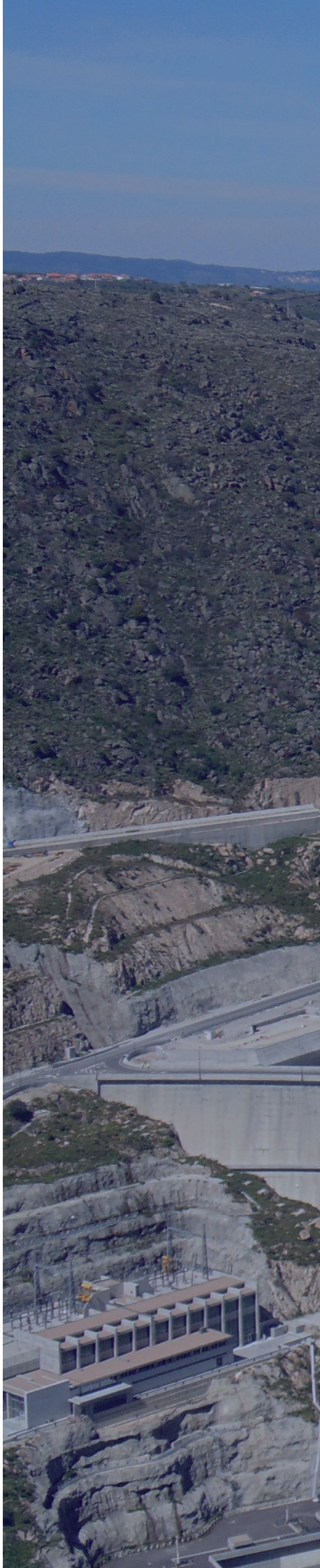

http://ewg2019.lnec.pt

ISBN 978-972-49-2308-6

AV DO BRASIL 101 • 1700-066 LISBOA • PORTUGAL
tel. (+351) 21 844 30 00 • fax (+351) 21 844 30 11
lnec@lnec.pt **www.lnec.pt**